THE PETROLOGICAL EVOLUTION AND TECTONIC ASSOCIATIONS OF THE BOM JARDIM COMPLEX, PERNAMBUCO STATE, NE. BRAZIL

by

Ignez de Pinho Guimaraes

A thesis submitted for the degree of Doctor of Philosophy of the University of London

Department of Geology
Royal School of Mines
Imperial College
London SW7 2BP

November 1989

ABSTRACT

The Bom Jardim complex is a multi phase intrusion emplaced within the boundary zone between the Pernambuco Alagoas median massif and the Pajeu Paraiba fold belt during the Pan African orogeny, 600 Ma ago.

The present investigation deals with the petrological and geochemical characterisation of the complex, together with a less detailed study of the adjoining Toritama complex, which, based on both petrographic and geochemical evidence is believed to represent an extension of the Bom Jardim complex.

The Bom Jardim complex is composed primarily of monzonites and syenites with subordinate granites. A combination of field mapping, detailed petrography and mineral chemistry has established six major facies within the complex. A series of fine grained mafic enclaves varying in composition from diorite, monzonite to syenite have also been studied. They appear to show a cogenetic relationship with the host monzonite-syenite suite. In addition, field and geochemical evidence also suggest that such enclaves represent synplutonic disrupted dykes. The boundaries of the complex appear to be thrust-fault controlled, although a later overprinting of strike slip movement has occurred.

The major and trace elements geochemistry has established a shoshonitic affinity for the monzonite-syenite assemblages, whereas the granites are clearly of a high-K calc-alkaline character. Detailed mineral chemistry coupled with whole-rock data has enabled the author to establish that the main geochemical trends determined for the complex are the result of fractionation of mainly amphibole, biotite, alkali feldspar $\pm$ clinopyroxene within the developing magmas. The presence of partially digested metasedimentary xenoliths indicates a crustal contribution during the emplacement of the complex.

The enrichment in transition metal elements, large ion lithophile elements (LILEs) and high LILE/HFSE ratios, coupled with an initial Sr^{87}/Sr^{86} ratio of 0.70709,

are considered to be consistent with a magma source from within a metasomatized lithospheric mantle below a subduction zone.

Based on the evidence from a number of tectonically related geochemical discriminant functions, field observations and published geophysical data, the author considers that both the Bom Jardim and Toritama complexes represent a late phase of magmatism, which occurred during the period of transition between collisional and post-collisional phases in the evolution of an active continental margin, now represented by the Pernambuco Alagoas median massif.

ACKNOWLEDGEMENTS

My special thanks go to Dr Jack Nolan and Dr Robert Thompson in the early stages, for their supervision of this project.

Special thanks are also due to Mr Peter Watkins for his constant help and advice, regarding the analytical work undertaken during the course of this project.

To Dr Terry Williams and Dr Francis Wall (Natural History - British Museum) for making available, and helping with, Neutron Activation counting facilities and micropobe analyses of accessory minerals.

Strontium isotopic work was carried out at the RHBNC, thanks to the co-operation and advice of Dr Mathew Thirlwall and Gerry Ingrid.

Thanks are also due to all technical staff of the Imperial College.

Dr Joao Batista (UFPA) for his scientific advice during the early stages of this project.

My colleagues geologists Evenildo Bezerra and Sheila who participated in my field work.

The late Dr Adejardo Silva and Eurideces Silva for their kindness in giving me accomodation during my field trips.

My brother Jorge Guimaraes and my late sister Elizabeth Guimaraes who helped me with the sample crushing.

My friend Marcelo R. da Silva who supplied me with Brazilian references throughout my research at Imperial College.

My colleagues from the Mineralogy and Petrology section; we all shared happy and difficult moments.

My friends Maria Azevedo and Luis Menezes for their helping to correct this thesis.

My relatives and friends who carried out the representative duties in Brazil.

Lastly, special thanks to my parents and my husband for putting up with me during the difficult moments. This work is dedicated to them.

LIST OF CONTENTS

Chapter	Title	Page
CHAPTER 1	**INTRODUCTION**	**24**
1.1	Regional Geology	24
1.1.1	Borborema province concept	24
1.1.2	Lithological assemblages	29
1.1.3	Structural framework	32
1.2	Plate tectonics and the Borborema province	33
1.3	Geophysical data	40
1.4	Summary of the regional geology	40
1.5	Previous works in the area	41
1.6	Objective of this study	42
CHAPTER 2	**THE FIELD AREA**	**43**
2.1	Introduction	43
2.1.1	Location and access	43
2.1.2	Physiographic aspects of the area	43
2.1.3	Mapping and map preparation	45
2.2	Aspects of field geology	45
2.3	Classification of the Bom Jardim rocks	49
2.3.1	Pyroxene biotite amphibole mafic syenites and monzonites	56
2.3.2	Pyroxene biotite bearing monzonites	58
2.3.3	Medium grained pyroxene biotite amphibole syenites	58
2.3.4	Pyroxene biotite bearing leucocratic alkali feldspar syenites	59
2.3.5	Very coarse grained brown alkali feldspar syenites	59
2.3.6	Pink granites	59
2.3.7	Minor facies	61
2.3.7.1	Mafic dykes	61
2.3.7.2	Enclaves	64
2.3.7.3	Pegmatites and aplites	68
2.4	Summary and conclusions	70
CHAPTER 3	**PETROGRAPHIC CHARACTERIZATION OF THE BOM JARDIM COMPLEX**	**72**
3.1	Petrographic descriptions of the major facies	73

3.1.1 The coarse grained pyroxene biotite amphibole mafic syenites and monzonites (PBAMS)..... 73
3.1.2 The pyroxene biotite monzonites (PBM)..... 81
3.1.3 The medium grained pyroxene biotite amphibole syenites (MPBAS)..... 83
3.1.4 The pyroxene biotite alkali feldspar leuco syenites (PBLS)..... 85
3.1.5 The very coarse grained brown alkali feldspar syenites (CS)..... 88
3.1.6 The pink granites..... 90
3.2 The minor facies..... 91
3.2.1 Igneous enclaves..... 91
3.2.1.1 Group 1 enclaves..... 92
3.2.1.2 Group 2 enclaves..... 92
3.2.1.3 Group 3 enclaves..... 94
3.2.1.4 Group 4 enclaves..... 95
3.2.2 Dykes..... 95
3.2.2.1 Monzonites and monzodiorites..... 96
3.2.2.2 Mafic syenites..... 97
3.2.2.3 Gabbro norites..... 97
3.3 Summary and conclusions..... 97
CHAPTER 4 MINERAL CHEMISTRY..... 99
4.1 Introduction..... 99
4.2 Mineral chemistries of the major facies..... 99
4.2.1 Clinopyroxenes..... 99
4.2.2 Amphiboles..... 105
4.2.2.1 Amphibole geobarometry..... 110
4.2.3 Biotite..... 113
4.2.4 Plagioclase feldspars..... 118
4.2.5 Alkali feldspars..... 120
4.2.6 Minor phases..... 124
4.2.7 Opaque minerals..... 132
4.3 Mineral chemistry of the minor facies..... 134
4.3.1 Pyroxenes..... 134
4.3.2 Amphiboles..... 136
4.3.3 Biotite..... 136
4.3.4 Feldspars..... 139
4.3.5 Minor phases..... 139
4.4 Summary and conclusions..... 142
CHAPTER 5 GEOCHEMISTRY OF THE BOM JARDIM MAJOR FACIES.. 143

5.1 Introduction..... 143
5.2 Major element geochemistry..... 143
5.2.1 Normative data..... 143
5.2.2 Chemical characterization and classification of the Bom Jardim magma series..... 145
5.2.3 Major element variations..... 157
5.2.4 Major element modelling..... 162
5.3 Trace element geochemistry..... 164
5.3.1 Introduction..... 164
5.3.2 Partition coefficients and compatibility of the elements..... 165
5.3.3 Trace element modelling..... 167
5.3.4 Large ion litophile elements (LILE)..... 168
5.3.4.1 Barium..... 168
5.3.4.2 Strontium..... 174
5.3.4.3 Rubidium and caesium..... 175
5.3.4.4 Thorium, uranium and lead..... 180
5.3.5 Transition elements..... 184
5.3.5.1 Nickel..... 184
5.3.5.2 Chromium..... 184
5.3.5.3 Vanadium..... 188
5.3.5.4 Copper..... 190
5.3.6 High field strength elements (HFSE)..... 190
5.3.6.1 Zirconium..... 193
5.3.6.2 Hafnium..... 196
5.3.6.3 Yttrium and scandium..... 196
5.3.6.4 Niobium and Tantalum..... 199
5.3.7 Rare earth elements (REE)..... 200
5.3.8 Chondrite normalized incompatible element diagram (spidergrams)..... 214
5.4 Geochemical interactions during the intrusion of the complex; fenitisation and contamination..... 216
5.5 Summary and conclusions..... 228
CHAPTER 6 GEOCHEMISTRY OF THE MAFIC DYKES AND ENCLAVES. 230
6.1 Major element geochemistry..... 230
6.2 Trace element geochemistry..... 235
6.3 Rare earth elements..... 240
6.4 Chondrite normalized incompatible element diagrams (spidergrams)..... 244

6.5 Genesis of the enclaves..... 247
6.6 Summary and conclusions..... 249
CHAPTER 7 A COMPARATIVE STUDY OF THE BOM JARDIM AND TORITAMA COMPLEXES..... 251
7.1 Introduction..... 251
7.2 Petrography and mineral chemistry..... 251
7.3 Geochemical considerations of the Toritama complex..... 265
7.3.1 Introduction..... 265
7.3.2 Major element geochemistry..... 265
7.3.3 Trace element geochemistry..... 270
7.4 Summary and conclusions..... 280
CHAPTER 8 TECTONIC SETTING..... 281
8.1 Introduction..... 281
8.2 Strontium isotope ratios and the magma source..... 285
8.3 The tectonic settings of the shoshonitic rock series..... 286
8.4 Geochemical discriminants and tectonic setting; their implications..... 287
8.5 Discussion and conclusions..... 297
CHAPTER 9 MAGMA GENESIS, CONSIDERATIONS AND FINAL CONCLUSIONS..... 300

REFERENCES..... 306

Appendices..... 323
Appendix A Analytical techniques..... 323
Appendix B Major element oxides, CIPW norm and modal data..... 334
Appendix C Trace element Data..... 354
C.1 Trace elements..... 354
C.2 REE elements..... 362
Appendix D Mineral chemistry data..... 368

LIST OF FIGURES

Figure	Title	Page
Figure 1.1	The structural provinces of Brazil after Almeida et al., (1981).....	25
Figure 1.2	The geological map of the Borborema province after Brito Neves (1983).....	26
Figure 1.2.1	The regional map of the Bom Jardim area...	27
Figure 1.3	The geological map of the Borborema province after Jardim de Sa (1984).....	28
Figure 1.4	A paleo-reconstruction of the West Africa and N.E. Brazil after Jardim de Sa (1984).....	34
Figure 1.5	Granitoids of Brasiliano age in the the Borborema province. After Santos et al. (1984).....	35
Figure 1.6	Diagrammatic cross sections showing the evolution of the Borborem province, after Jardim de Sa (1984).....	36
Figure 1.7	Distribution of Bouger gravity anomalies for the Pernambuco-Alagoas massif.....	39
Figure 2.1	Geological map of the Bom Jardim complex..	46
Figure 2.2	a) Modal composition of the Bom Jardim complex rocks in the QAP triangle diagram after Streckeisen (1976), b) the modal composition of mafic phases versus alkali feldspar and plagioclase.....	50
Figure 2.2.A	Location of samples with modal analyses plotted in figure 2.2.....	51
Figure 2.3	The distribution and classification of the Bom Jardim rocks after the scheme of Debon and Le Fort (1983).....	52
Figure 2.3.A	Location of chemically analysed samples plotted in figure 2.3.....	53
Figure 4.1	Plot of pyroxene compositions from the Bom Jardim complex.....	100
Figure 4.2	The Bom Jardim pyroxene trend compared with pyroxene trends from the literature.....	100
Figure 4.3	Individual micropobe analyses of the Bom	

Jardim complex pyroxenes expressed in terms of atom percent Na^{+}, Mg^{2+} and Fe^{2+} + Mn^{2+}..... 102
Figure 4.4 Bulk rock Na/Na+ Ca ratios versus Na contents of pyroxenes from the Bom Jardim complex..... 103
Figure 4.5 Variation of atomic Al versus Fe/Fe+Mg in pyroxenes from the Bom Jardim complex..... 104
Figure 4.6 Variation of atomic Mn versus Fe/Fe+Mg in pyroxenes from the Bom Jardim complex..... 104
Figure 4.7 Composition and classification of the amphiboles from the major facies of the Bom Jardim complex..... 106
Figure 4.8 A) Variation of Al^{4} in T site versus Na+K in A site, B) Al^{6} in T site versus Al^{6}+ Fe^{3+}+2Ti in M1-M2-M3 sites..... 107
Figure 4.9 Variation of total atomic Fe (expressed as Fe^{2+}) with Al^{4} in amphiboles from the major facies of the Bom Jardim complex.... 109
Figure 4.10 Variation of atomic Ti with Al^{4} in amphiboles from the Bom Jardim complex.... 109
Figure 4.11 Plot of Al^{t} versus Al^{4} for amphiboles from the Bom Jardim complex..... 112
Figure 4.12 Individual micropobe analyses of biotites from the Bom Jardim complex expressed in terms of atomic proportions of Ti-Mg-Fe..... 115
Figure 4.13 Composition of biotites from the Bom Jardim complex plotted in terms of Al_2O_3-FeOt-MgO..... 117
Figure 4.14 Variation in the composition of plagioclase feldspars from the major facies of the Bom Jardim complex..... 119
Figure 4.15 Variation in composition of alkali feldspars within the Bom Jardim complex... 122
Figure 4.16 Variation in the BaO content across two alkali feldspar megacrysts from the mafic syenite..... 123
Figure 4.17 Chondrite normalized REE plots for two

keilhauite grains from the PBLS..... 131
Figure 4.18 Variation in Cr_2O_3 contents of magnetites as a function of D.I. for members of the major facies of the Bom jardim complex..... 133
Figure 4.19 A) Composition of pyroxenes from members of the minor facies of the Bom Jardim complex. B) composition of Ca-rich and Ca-poor pyroxenes from the two pyroxene diorite..... 135
Figure 4.20 Composition and classification of amphiboles from the minor facies of the Bom Jardim complex (after Leake, 1978).... 137
Figure 4.21 A) Variation of MgO content with Fe/Fe+Mg and B) variation of Al_2O_3 content with Fe/Fe+Mg ratio for biotites from the minor facies of the Bom Jardim complex.... 138
Figure 4.22 Individual micropobe analyses of feldspars from the minor facies of the Bom Jardim complex..... 140
Figure 5.1 Normative data for the Bom Jardim granitoids projected in terms of Qz-Ab-Or-Ne..... 144
Figure 5.2 Data from the Bom Jardim complex, plotted in terms of molecular $CaO-Al_2O_3-(K_2O+Na_2O)$ (after Loiselle and Wones, 1979)..... 146
Figure 5.3 Variation of Na+K/Al versus D.I.for rocks from the Bom Jardim complex..... 148
Figure 5.4 AFM plot of rocks from the Bom Jardim complex..... 149
Figure 5.5 Classification of the rocks from the Bom Jardim complex after Wright (1969)..... 150
Figure 5.6 Classification of the rocks from the Bom Jardim complex after Rogers and Greenberg (1981)..... 151
Figure 5.7 Diagram showing the alkali-lime index for the Bom Jardim suite (after Peacock, 1931)..... 152
Figure 5.8 Plot of K_2O versus SiO_2 for the major

facies of the Bom Jardim complex (after Peccerillo and Taylor, 1976)..... 154
Figure 5.9 Enrichment/depletion patterns for the major elements in the PBAMS (A), and (PBLS) (B), compared with calc-alkaline and shoshonite suites from the literature..... 155
Figure 5.10 Variation of log CaO/Na_2O+K_2O with silica for rocks of the Bom Jardim complex and other geochemically similar rock suites..... 156
Figure 5.11 Plot of log K_2O+Na_2O versus SiO_2 for the Bom Jardim granitoids..... 158
Figure 5.12 Major element oxide variation diagrams.... 159
Figure 5.13 Schematic diagram illustrating the method of modelling trace element variations in terms of Rayleigh fractionation. (After MacCarthy and Hasty, 1976)..... 169
Figure 5.14 Bivariant plot of Ba(ppm) versus K_2O (wt %) for rocks of the Bom Jardim complex..... 170
Figure 5.15 Plots of LIL elements versus D.I. for rocks of the Bom Jardim complex..... 171
Figure 5.16 LogRb-logSr diagram showing the distribution of the Bom Jardim granitoids..... 177
Figure 5.17 Variation of the Rb/Sr ratio with the D.I. for the Bom Jardim granitoids..... 178
Figure 5.18 Variation of the Ba/Rb ratio with Rb/Sr for the Bom Jardim granitoids..... 179
Figure 5.19 Scatter diagrams for selected trace elements in the Bom Jardim complex..... 182
Figure 5.20 Variation of the transition elements with D.I. for the Bom Jardim granitoids..... 185
Figure 5.21 Logarithmic, bivariant plot of Ni versus Cr for the Bom Jardim complex..... 187
Figure 5.22 Logarithmic, bivariant plot of V versus Cr for the Bom Jardim granitoids..... 189
Figure 5.23 HFS elements versus D.I. for the Bom Jardim granitoids..... 191

Figure 5.24 Zr(wt %)/TiO_2 versus SiO_2 for the Bom Jardim granitoids..... 194
Figure 5.25 Bivariant plots of Hf-Th, Hf-TiO_2 and Hf-Zr for the Bom Jardim granitoids... 195
Figure 5.26 Variation of Y with CaO contents in the granitoids of the Bom Jardim complex..... 198
Figure 5.27 Plot of selected REE contents versus D.I. for members of the Bom Jardim complex..... 201
Figure 5.28 Chondrite normalized REE plots for the different lithologies of the Bom Jardim complex..... 203
Figure 5.29 Variation of total REE content with silica for the Bom Jardim granitoids..... 210
Figure 5.30 Whole rock normalized REE patterns of amphibole, clinopyroxene and biotite from the Bom Jardim complex..... 211
Figure 5.31 Logarithmic, bivariant plot of Hf versus Ce for the Bom Jardim complex..... 212
Figure 5.32 Logarithmic, bivariant plot of Ce versus Yb for the Bom Jardim granitoids..... 213
Figure 5.33 Chondrite normalized incompatible element patterns of the different facies of the Bom Jardim complex..... 217
Figure 5.34 A comparison of the chondrite normalized incompatible element patterns for the PBAMS, MPBAS and PBLS facies of the Bom Jardim complex..... 223
Figure 5.35 Chondrite normalized REE patterns of metasediments around the Bom Jardim complex, granite from the fenitisation zone, a metasedimentary enclave within the complex, "uncontaminated" syenite and, contaminated syenite..... 226
Figure 6.1 Variation of K_2O as a function of MgO for enclaves and dykes from the Bom Jardim complex..... 231
Figure 6.2 Normative data for Bom Jardim enclaves and dykes projected onto the Qz-Ab-Or-Feldspatoid quaternary diagram..... 231
Figure 6.3 Variation of the major element oxides

as a function of D.I. for the dykes and enclaves of the Bom Jardim complex..... 232
Figure 6.4 Plots of the Bom Jardim enclaves and dykes in the diagram of Peccerillo and Taylor (1976)..... 236
Figure 6.5 Variation diagrams of analysed trace elements versus D.I..... 237
Figure 6.6 Chondrite normalized REE plots for the different enclaves and dykes lithologies..... 241
Figure 6.7 Chondrite normalized incompatible elements plots of Bom Jardim enclaves and dykes..... 245
Figure 7.1 Geological sketch map of the Toritama complex..... 252
Figure 7.2 Al^4 and Al^t contents of amphiboles from the Toritama complex..... 260
Figure 7.3 Pyroxene compositions from the Toritama complex..... 260
Figure 7.4 Whole rock normalized REE patterns of sphene from the Toritama complex..... 264
Figure 7.5 Variation of K_2O with SiO_2 content for the rocks of the Toritama complex..... 271
Figure 7.6 AFM diagram of the Toritama granitoids.... 272
Figure 7.7 Major element oxide variation diagram..... 273
Figure 7.8 Enrichment/depletion pattern for PBAMS facies of both the Toritama and Bom Jardim complexes..... 275
Figure 7.9 LogRb - logSr diagram showing the distribution of the Toritama granitoids...
Figure 7.10 Chondrite normalized REE plots for the different lithologies of the Toritama complex..... 278
Figure 7.11 Chondrite normalized incompatible element patterns of the different lithologies recorded in the Toritama complex..... 279
Figure 8.1 Rb-Sr whole rock and clinopyroxene isochron..... 283
Figure 8.2 The ranges of Sr isotope ratios for

intrusive suites from Mesozoic and Tertiary magmatic arcs, compared to those recorded in the Bom Jardim and Toritama complexes..... 286

Figure 8.3 R1 versus R2 discriminant function diagram (Batchelor and Bowden, 1985) for the Bom Jardim and Toritama complexes..... 289

Figure 8.4 Variation of Nb versus Y for rocks from the Bom Jardim and Toritama complexes..... 290

Figure 8.5 Rb versus (Nb+Y) discriminant diagram, after Pearce et al., (1984)..... 291

Figure 8.6 Rb/Zr ratios plotted versus SiO_2 for rocks from the Bom Jardim and Toritama complexes. (After Harris et al., 1986).... 292

Figure 8.7 Rb-Hf-Ta plot for acid-intermediate intrusive magmatism. (After Harris et al., 1986)..... 293

Figure 8.8 Variation of Nb versus Zr for Bom Jardim and Toritama rocks with less than 60% SiO_2. (After Leat et al., 1986)..... 295

Figure 8.9 Variation of Th/Yb versus Ta/Yb for the Bom Jardim and Toritama complexes..... 296

Figure 9.1 Chondrite normalized incompatible element plot comparing rocks from the PBAMS facies of the Toritama and Bom Jardim complexes with samples from the Lorne plateau lavas and a shoshonite picrite.... 301

Figure 9.2 Chondrite normalized incompatible element plot comparing Bom Jardim granites and country rocks..... 304

LIST OF TABLES

Table	Title	Page
Table 3.1	Average modal analyses of the Bom Jardim major facies	72
Table 3.2	Average modal analyses of the Bom Jardim enclaves	91
Table 3.3	Average modal analyses of the Bom Jardim mafic dykes	96
Table 4.1	Representative analyses of pyroxenes from the Bom Jardim major facies	101
Table 4.2	Representative analyses of amphiboles from the Bom Jardim major facies	108
Table 4.3	Representative analyses of biotite from the Bom Jardim major facies	113
Table 4.4	Representative INAA data for biotite, amphibole, pyroxene and sphene from the Bom Jardim complex	114
Table 4.5	Representative analyses of plagioclase feldspars from the major facies of the Bom Jardim complex	118
Table 4.6	Representative analyses of alkali feldspars from the Bom Jardim complex	121
Table 4.7	Average analyses of minor phases from the Bom Jardim major facies	124
Table 4.8	Electron microprobe analyses of two Th LREE rich sphene	129
Table 4.9	Representative analyses of pyroxenes from the two pyroxene diorite	134
Table 4.10	Analyses of minor phases from the Bom Jardim minor facies	141
Table 5.1	Average whole rock analyses for the different major facies of the Bom Jardim complex	145
Table 5.2	Results of the least squares mixing solutions for the modelling of the variations in major element concentrations within the Bom Jardim complex	163
Table 5.3	Partition coefficients used in this work	166

Table 5.4 Selected trace element analyses of metasediments, fenitised rock, and both contaminated and uncontaminated syenites..... 225
Table 5.5 Analyses of granite and syenite host rocks from the Bom Jardim complex..... 227
Table 6.1 A comparison of the compositions of elongated and rounded enclaves from the MPBAS facies..... 248
Table 7.1 Equivalent rock types of the Toritama and Bom Jardim complexes..... 253
Table 7.2 Representative micropobe analyses of the alkali feldspars from the Toritama complex..... 258
Table 7.3 Representative micropobe analyses of the plagioclase from the Toritama complex..... 258
Table 7.4 Representative micropobe analyses of the amphiboles from the Toritama complex..... 259
Table 7.5 Representative micropobe analyses of the pyroxenes from the Toritama complex..... 261
Table 7.6 Representative micropobe analyses of biotites from the Toritama complex..... 262
Table 7.7 INAA data for sphene from the PBAMS facies from the Toritama complex..... 263
Table 7.8 Chemical analyses of the Toritama major facies..... 266
Table 7.9 Chemical analyses of the Toritama enclaves..... 268
Table 8.1 Granite types in Northeast Brazil. After Almeida et al. (1967)..... 282
Table 8.2 Rb-Sr data for the Bom Jardim and Toritama complexes..... 284
Table 8.3 Mineral-whole rock and mineral-mineral Rb-Sr ages for the Bom Jardim complex..... 284
Table A.1 Precision of major element analysis by ICP-AES..... 329
Table A.2 Accuracy of major element analysis by ICP-AES..... 330
Table A.3 Precision of trace element analysis by ICP-AES..... 330

Table A.4 Accuracy of trace element analysis by ICP-AES..... 331
Table A.5 Comparison of trace element data for 5 samples analysed by XRF and ICP-AES..... 331
Table A.6 Comparison of Rb data for 5 samples analysed by XRF and flame emission spectrometry..... 332
Table A.7 Comparison of REE data for 3 samples analysed by INAA and ICP-AES..... 332
Table A.8 Accuracy of trace element analysis by INAA..... 333
Table A.9 Analyses of jadeite and olivine by electron micropobe..... 333
Table B.1 Major element data from PBAMS facies..... 334
Table B.2 Major element data from PBM faacies..... 337
Table B.3 Major element data from MPBAS facies..... 338
Table B.4 Major element data from PBLS facies..... 341
Table B.5 Major element data from CS facies..... 342
Table B.6 Major element data from pink granites..... 343
Table B.7 Major element data from igneous enclaves... 344
Table B.8 Major element data from mafic dykes..... 346
Table B.9 Major element data from country rocks..... 347
Table B.10 Modal data from PBAMS facies..... 348
Table B.11 Modal data from PBM facies..... 349
Table B.12 Modal data from MPBAS facies..... 350
Table B.13 Modal data from PBLS facies..... 350
Table B.14 Modal data from pink granites..... 351
Table B.15 Modal data from igneous enclaves..... 352
Table B.16 Modal data from mafic dykes..... 353
Table C.1.1 Trace element data from PBMAS facies..... 354
Table C.1.2 Trace element data from PBM facies..... 355
Table C.1.3 Trace element data from MPBAS facies..... 356
Table C.1.4 Trace element data from PBLS facies..... 358
Table C.1.5 Trace element data from CS facies..... 359
Table C.1.6 Trace element data from pink granites..... 359
Table C.1.7 Trace element data from igneous enclaves... 360
Table C.1.8 Trace element data from mafic dykes..... 361
Table C.2.1 REE data from PBAMS facies..... 362
Table C.2.2 REE data from PBM facies..... 363
Table C.2.3 REE data from MPBAS facies..... 363

Table C.2.4 REE data from PBLS facies..... 364
Table C.2.5 REE data from CS facies..... 364
Table C.2.6 REE data from pegmatites..... 365
Table C.2.7 REE data from pink granites..... 365
Table C.2.8 REE data from igneous enclaves..... 366
Table C.2.9 REE data from mafic dykes..... 366
TableC.2.10 REE data from country rocks..... 367
Table D.1.1 Mineral chemistry of pyroxenes (PBAMS)..... 368
Table D.1.2 Mineral chemistry of pyroxenes (PBM)..... 370
Table D.1.3 Mineral chemistry of pyroxenes (MPABS)..... 371
Table D.1.4 Mineral chemistry of pyroxenes (PBLS)..... 373
Table D.1.5 Mineral chemistry of pyroxenes (CS)..... 375
Table D.1.6 Mineral chemistry of pyroxenes (enclaves).. 376
Table D.1.7 Mineral chemistry of pyroxenes (mafic dykes)..... 378
Table D.2.1 Mineral chemistry of amphiboles (PBAMS).... 380
Table D.2.2 Mineral chemistry of amphiboles (MPBAS).... 383
Table D.2.3 Mineral chemistry of amphiboles (enclaves). 385
Table D.2.4 Mineral chemistry of amphiboles (mafic dykes)..... 387
Table D.3.1 Mineral chemistry of biotites (PBAMS)..... 388
Table D.3.2 Mineral chemistry of biotites (PBM)..... 390
Table D.3.3 Mineral chemistry of biotites (MPBAS)..... 391
Table D.3.4 Mineral chemistry of biotites (PBLS)..... 392
Table D.3.5 Mineral chemistry of biotites (CS)..... 393
Table D.3.6 Mineral chemistry of biotites (pink granites)..... 394
Table D.3.7 Mineral chemistry of biotites (igneous enclaves)..... 395
Table D.3.8 Mineral chemistry of biotites (mafic dykes)..... 397
Table D.3.9 Mineral chemistry of biotites country rocks..... 399
Table D.4.1 Mineral chemistry of plagioclases (PBAMS).. 401
Table D.4.2 Mineral chemistry of plagioclases (PBM).... 403
Table D.4.3 Mineral chemistry of plagioclases (MPBAS).. 404
Table D.4.4 Mineral chemistry of plagioclases (PBLS)... 406
Table D.4.5 Mineral chemistry of plagioclases (igneous enclaves)..... 407
Table D.4.6 Mineral chemistry of plagioclases (mafic

dykes)..... 409
Table D.5.1 Mineral chemistry of alkali feldspars (PBAMS)..... 411
Table D.5.2 Mineral chemistry of alkali feldspars (MPBAS)..... 413
Table D.5.3 Mineral chemistry of alkali feldspars (PBLS)..... 415
Table D.5.4 Mineral chemistry of alkali feldspars (CS). 416
Table D.5.5 Mineral chemistry of alkali feldspars (igneous enclaves)..... 417
Table D.5.6 Mineral chemistry of alkali feldspar (mafic dykes)..... 419
Table D.6.1 Mineral chemistry of magnetites (PBAMS).... 420
Table D.6.2 Mineral chemistry of magnetites (MPBAS).... 421
Table D.6.3 Mineral chemistry of magnetites (PBLS)..... 422
Table D.7 Mineral chemistry of minor phases..... 423

LIST OF PLATES

Plate	Title	Page
Plate 2.1	The Bom Jardim complex viewed from the N.E.	44
Plate 2.2	Syenite with elongated enclaves, near the contact with the metasediments	44
Plate 2.3	Post emplacement deformation within the Bom Jardim complex	48
Plate 2.4	Evidence of multiple injection within the mafic syenite massif of the Bom Jardim complex	55
Plate 2.5	The contact between the MPBAS and the PBLS	57
Plate 2.6	Field characteristics of the mineralogy and texture of the MPBAS	57
Plate 2.7	Field characteristics of the PBLS	60
Plate 2.8	Field characteristics of the texture and mineralogy of the CS	60
Plate 2.9	A non disruptive dyke with minimum deformation cutting the mafic syenite	62
Plate 2.10	Examples of syn-plutonic disrupted dykes within the Bom Jardim complex	63
Plate 2.11	"Pillowing" enclaves of diorite, surrounded by aplite, the whole enclosed within the mafic syenite	65
Plate 2.12	Extremely elongated enclaves within the mafic syenite, close to its contact with the metasediment	66
Plate 2.13	Enclaves resulting from the dismemberment of a mafic dyke	66
Plate 2.14	Metasedimentary enclaves showing different degrees of reaction with the mafic syenite	67
Plate 2.15	Pegmatites within the Bom Jardim complex	69
Plate 3.1	Replacement of plagioclase by alkali feldspar (PBAMS)	74
Plate 3.2	Oval shaped alkali feldspar crystal surrounded by plagioclase within the PBAMS facies	74

Plate 3.3 Zoned plagioclase phenocryst within the PBAMS facies..... 75
Plate 3.4 Primary amphibole within the PBAMS facies... 75
Plate 3.5 Relicts of pyroxene within amphibole in the PBAMS facies..... 77
Plate 3.6 Secondary sphene developed along the amphibole cleavage (PBAMS)..... 77
Plate 3.7 Allanite surrounded by epidote (PBAMS)..... 79
Plate 3.8 Oval shaped monazite developing pleochroic haloes in the host biotite (PBAMS)..... 79
Plate 3.9 Localized clots of alkali feldspar and plagioclase in a fine grained variation of the PBAMS facies..... 80
Plate 3.10 Globular masses of fine grained mafic syenite within the PBAMS facies..... 80
Plate 3.11 Micro textural features within the PBM facies..... 84
Plate 3.12 Amphibole enclosing apatite and plagioclase. Sphene is clearly later..... 84
Plate 3.13 Reaction between biotite and a later crystallised alkali feldspar..... 86
Plate 3.14 Sphene developed as a reaction rim around Fe-Ti oxide (PBLS)..... 86
Plate 3.15 Th and LREE rich sphene, enclosing apatite (PBLS)..... 89
Plate 3.16 Zoned alkali feldspar, showing a distinct alternating zonal distribution of coarse and fine perphite (CS)..... 89
Plate 3.17 Contact between a mafic enclave and the host leuco syenite..... 93
Plate 3.18 Monazite hosted by biotite within an enclave..... 93
Plate 4.1 S.E.M. back-scattered images showing the distribution of P, Ce and Ti in a grain of monazite from the PBLS facies..... 126
Plate 4.2 S.E.M back-scattered images of Th-LREE rich sphenes from the PBLS facies..... 128
Plate 7.1 Mafic igneous enclave containing aligned alkali feldspar phenocrysts (PBAMS)..... 254
Plate 7.2 A boudin shaped syn-plutonic dyke intruded

into PBAMS..... 254
Plate 7.3 Typical surface exposure of the medium grained syenite (MPBAS)..... 255
Plate 7.4 Coarse grained syenites (CS) cut by a thin aplite vein..... 255
Plate 7.5 Contact between aplite and the CS facies within the Toritama complex..... 256

CHAPTER 1
INTRODUCTION

1.1 REGIONAL GEOLOGY

1.1.1 Borborema province concept

The Bom Jardim complex is located within the Atlantic shield of the South American platform. The Atlantic shield can be further subdivided into three major provinces (see fig 1.1) i.e., 1) Sao Francisco, 2) Mantiqueira and 3) Borborema province (Almeida et al., 1981). The field area is located within this latter province.

The Borborema province occupies an area of approximately 450.000 sq Kms and, is composed of two fundamentally different terrains: i) the gneiss-migmatite-granite terrains or massifs of Archaean to Middle Proterozoic age (up to 1300 Ma.) and ii) the metasedimentary and metavolcanic terrains or fold belts of Upper Proterozoic age (700-500 Ma.) (Brito Neves 1975, 1983 and Almeida et al., 1981) (see figure 1.2).

The southern limit of the province is dominated by the Sao Francisco craton, which formed a very stable geological unit during the Upper Proterozoic (Almeida et al., 1981).

Jardim de Sa (1984) concluded on the basis of field and geochronological studies, that most of the supracrustals (fold belts) in the province, were deformed during the Lower Proterozoic (2100 to 1300 Ma.) and secondly that the fold belts of Upper Proterozoic age, are far more restricted in area than proposed by Brito Neves (1975, 1983) and Almeida et al. (1977, 1981). Figure 1.3 shows the geology of the Borborema Province after Jardim de Sa (1984).

As previously mentioned the Bom Jardim complex forms part of the Borborema Province and, intrudes both the Pernambuco-Alagoas median massif and Pajeu Paraiba fold belt (Brito Neves, 1983) (see figure 1.2), and according to Jardim de Sa (1984) also intrudes the Leste de Pernambuco

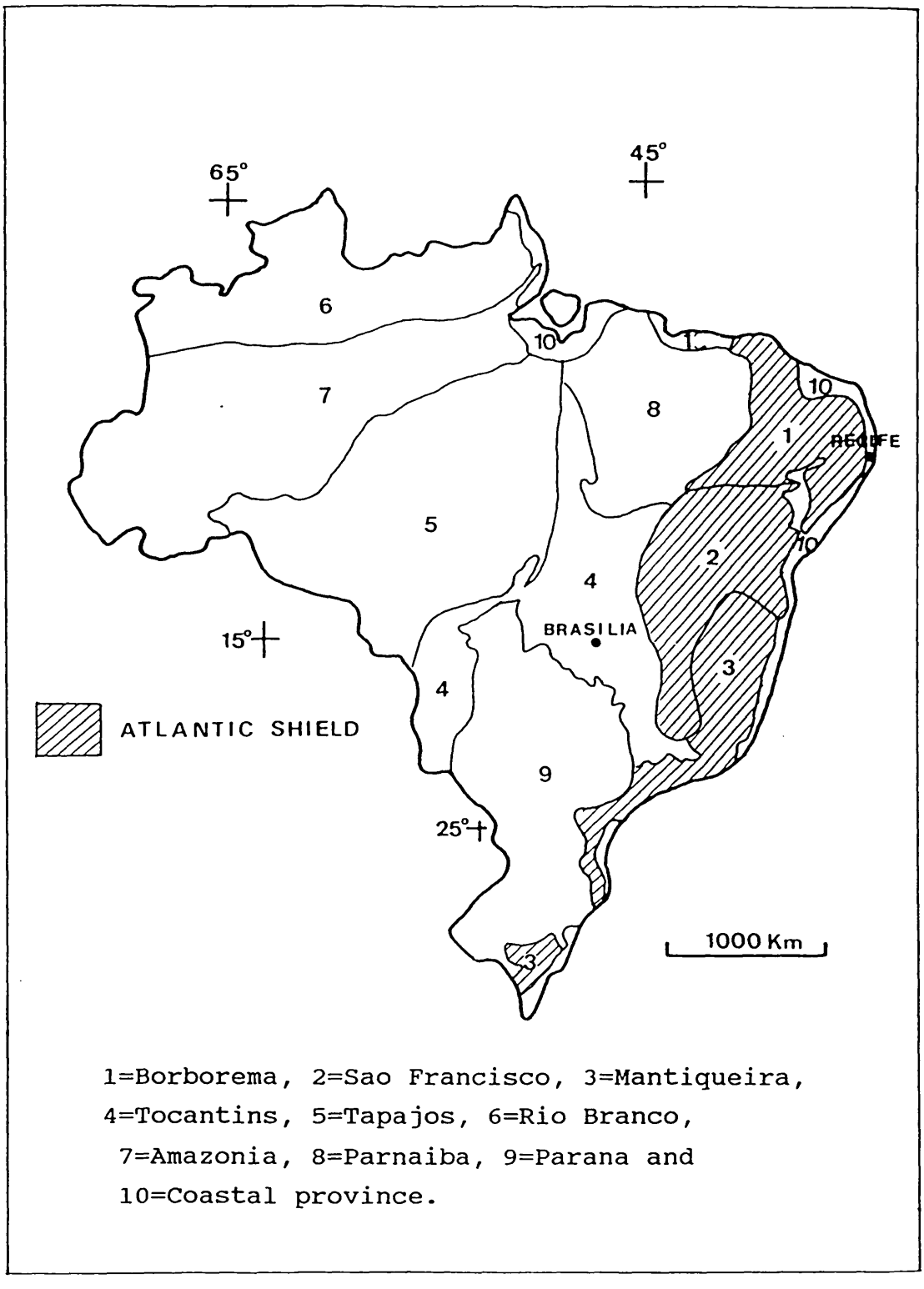


Figure 1.1 The structural provinces of Brazil after Almeida et al. (1981).

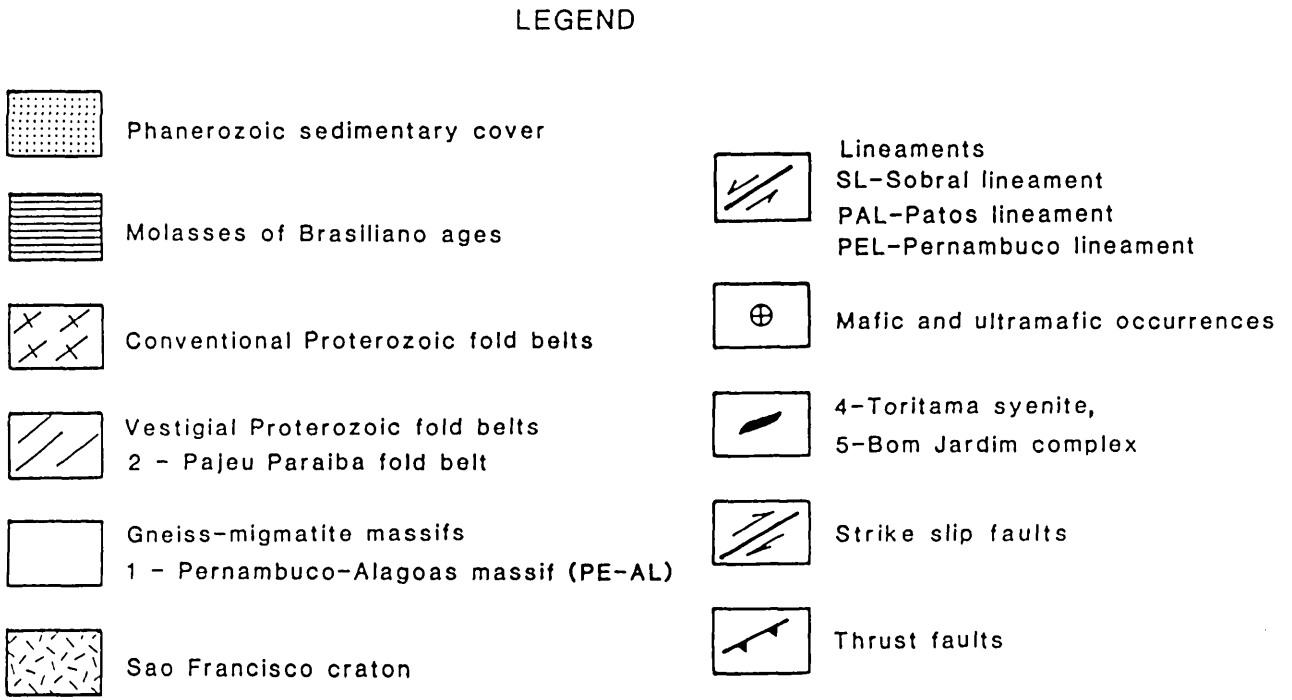
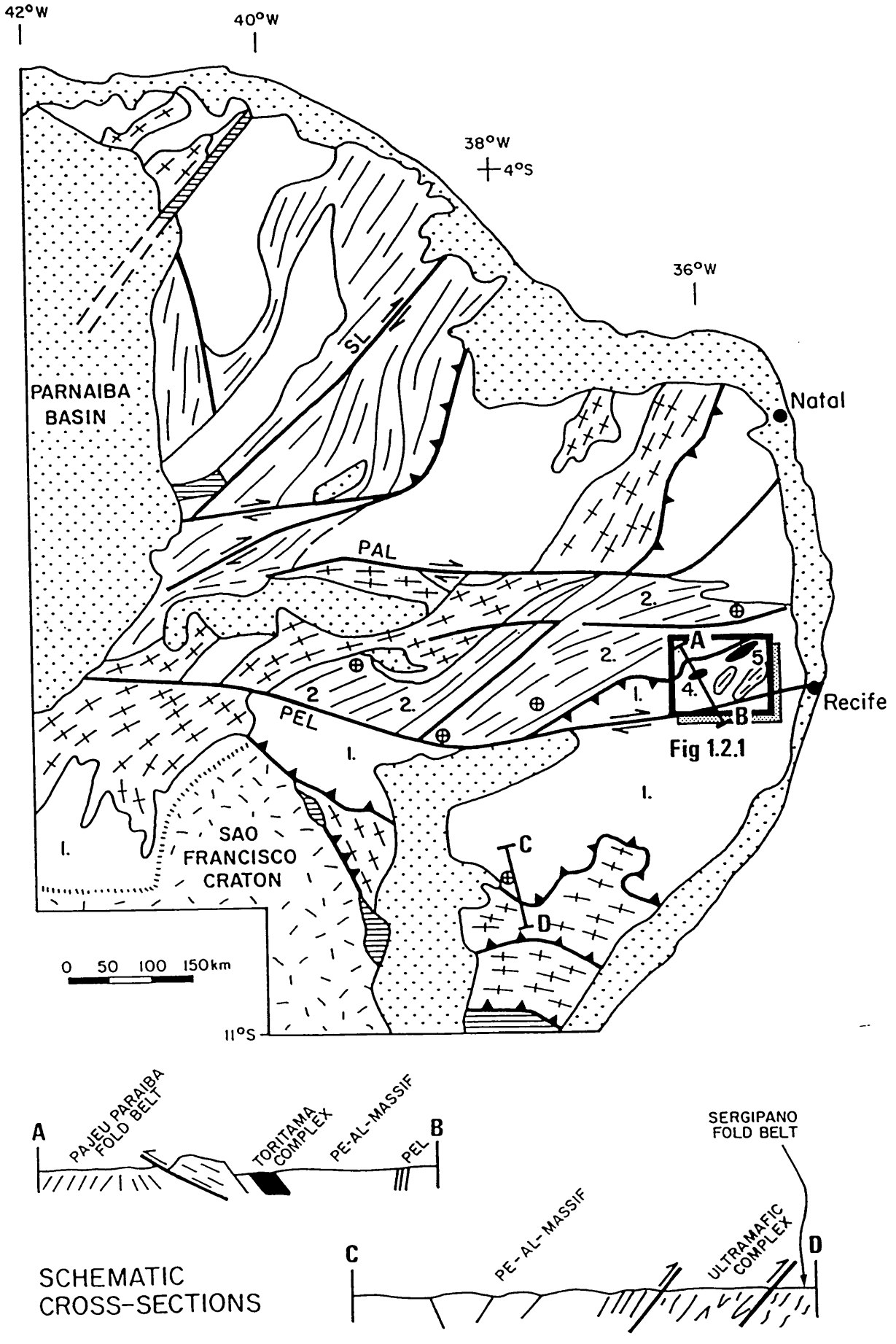


Figure 1.2 Geological map of the Borborema province after Brito Neves (1983). The schematic cross sections are from Brito Neves et al. (1982).


42°W
40°W
38°W
4°S
36°W
PARNAIBA BASIN
SL
PAL
PEL
Natal
Recife
A
B
C
D
Fig 1.2.1
SAO FRANCISCO CRATON
0 50 100 150km
11°S
PAJEU PARAIBA FOLD BELT
TORITAMA COMPLEX
PE-AL-MASSIF
SERGIPANO FOLD BELT
ULTRAMAFIC COMPLEX
SCHEMATIC CROSS-SECTIONS

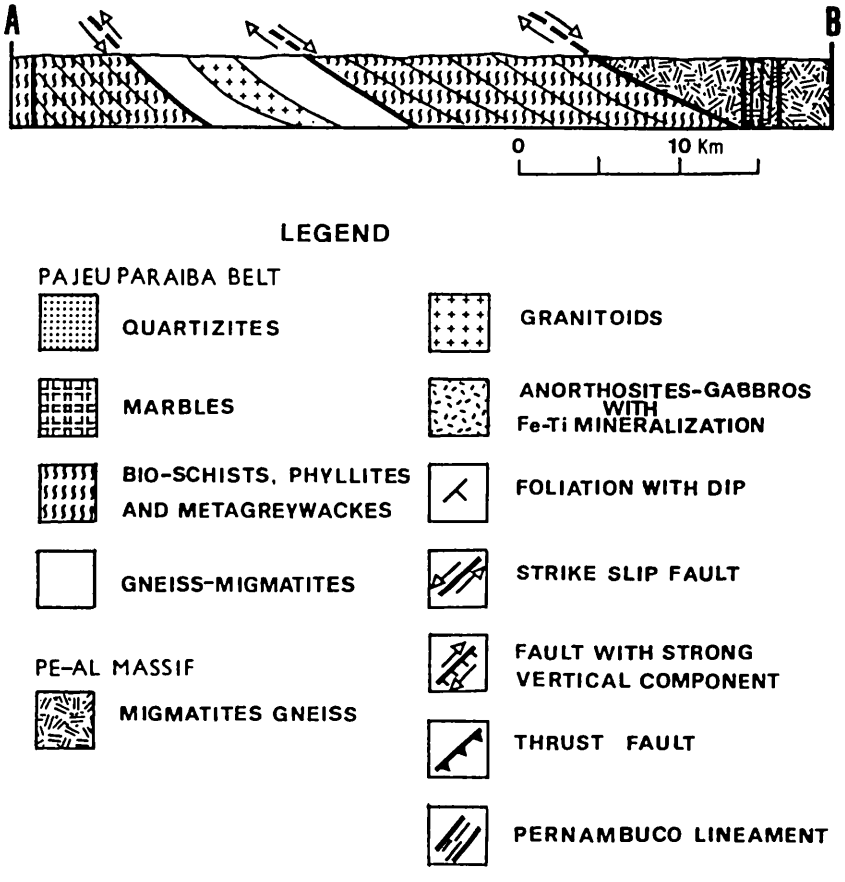
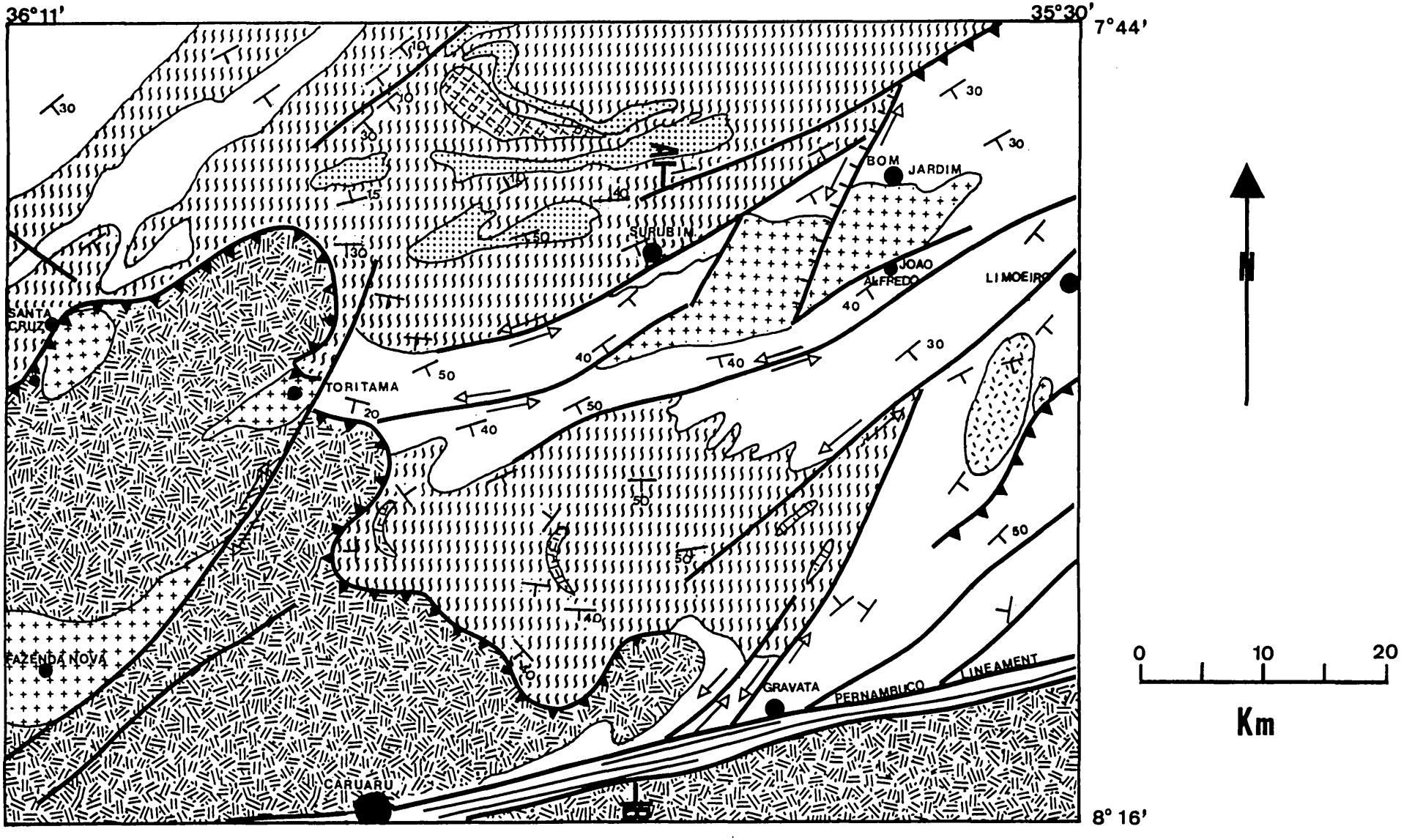


Figure 1.2.1 Simplified regional geological map of the Bom Jardim area. See text for detail.


36°11'
35°30'
7°44'
8°16'
BOM JARDIM
SURUBIM
JOAO ALFREDO
LIMOEIRO
SANTA CRUZ
TORITAMA
FAZENDA NOVA
CARUARU
GRAVATA
PERNAMBUCO LINEAMENT
N
0
10
20
Km

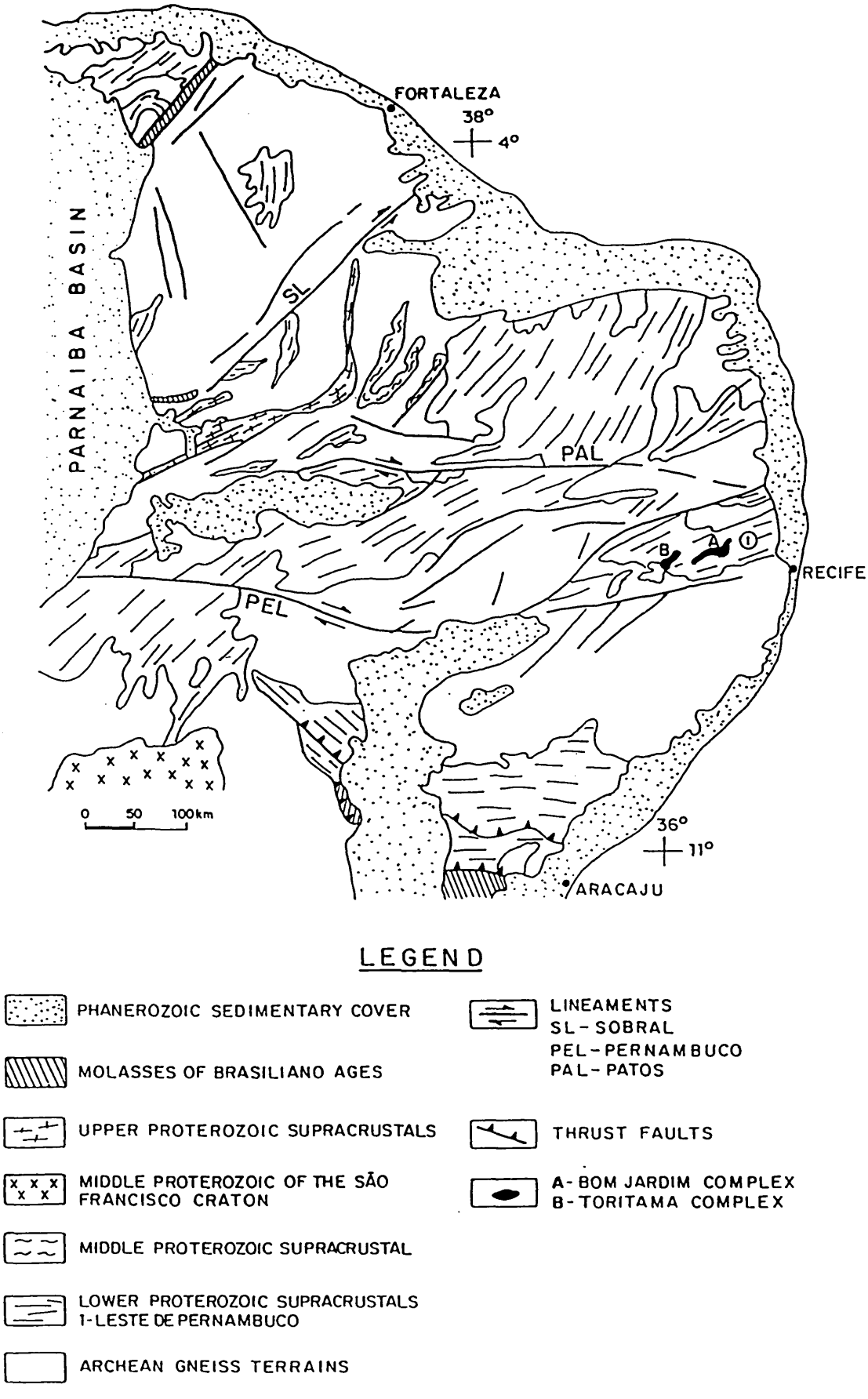


Figure 1.3 Geological map of the Borborema province, after Jardim de Sa (1984).

supracrustal (see figure 1.3). In this present study the geotectonic units proposed by Brito Neves (1983) for the Borborema Province will be used, however, this does not mean that the present author agrees with the tectonic interpretation of Brito Neves (1983) for the Borborema Province.

The regional geological map, compiled by the author and shown in figure 1.2.1, was based on the CPRM (1979) regional map, schematic cross sections from Brito Neves et al. (1982), Sial and Menor (1969), Mello (1971), Dantas and Brito Neves (1980) and data collected during the present field investigation. The present author interprets the Bom Jardim complex as being emplaced in an area already deeply affected by the Pan-African orogeny, and that the migmatites surrounding the complex, are not part of the Pernambuco Alagoas massif as proposed by Brito Neves (1983), but probably represent slabs of the basement of the Pajeu Paraiba fold belt, placed in contact with the higher crustal metasediments by thrust faults (figure 1.2.1.).

1.1.2 Lithological assemblages

The Pernambuco-Alagoas massif was previously defined as a cratogenic area by Mello et al. (1977). It comprises an area of about 70.000 sq Km, triangular in shape and, located in the states of Pernambuco and Alagoas, NE Brazil. The lithological constitution of the massif shows a variety of rock types i.e., i) migmatite-gneiss terrains associated with metamorphosed mafic and ultramafic rocks, ii) large polydiapiric batholiths of granite and granodiorite and, iii) supracrustal terrains representing folded cover. The grade of metamorphism is generally within the amphibolite facies, reaching granulite P-T conditions in certain areas. The massif itself is both cut and surrounded by Brasiliano\Pan African granitoids (650-550 Ma).

The best exposures of the mafic and ultramafic rocks in the massif have been reported: i) in the lower reaches of the Sao Francisco river between the states of Alagoas and Sergipe, ii) in the Floresta area iii) in the

Custodia area and, iv) in the Limoeiro-Passira area (figure 1.2).

The occurrence of the mafic and ultramafic rocks in the Sao Francisco river section, along the southern border of the massif, was identified and mapped by Silva Filho et al. (1981). It comprises a largely metavolcanic-metasedimentary sequence, including acid, basic and ultrabasic rocks, alternating with clastic and chemical sediments. The whole sequence has been folded, metamorphosed and cut by late granites and syenites.

The Limoeiro-Passira occurrence is located near the northern border of the massif. Sial and Menor (1973), Da Silva Filho and Guimaraes (1979) and Farina et al. (1981) have described this occurrence as a suite of metamorphosed anorthosites, amphibolites and gabbros associated with Fe-Ti-V mineralization and, related to thrust faults. Conventional Rb-Sr ages for two amphibolites from this area gave Archaean ages of 2.9 and 2.6 Ga. (Dantas and Brito Neves, 1980). However, Transamazonico\Ebournean ages (1800-700 Ma.) have also been obtained from the suite (Brito Neves et al., 1982).

Angel and Riera(1959), Dantas (1971) and Veroness (1985), decribed a sequence of mafic and ultramafic rocks along the northwestern contact between the Pernambuco-Alagoas massif and the Pajeu Paraiba fold belt. The rocks comprise a suite of meta- anorthosites, meta-gabbros, meta-gabbros with garnet and amphibolites associated with Fe-Ti-V mineralization. Beurlen (1988) has recently established the presence of eclogites in the Floresta area.

Santos (1977) described another mafic and ultramafic suite in the Custodia area, coincident with the northern contact between Pernambuco-Alagoas massif and Pajeu-Paraiba fold belt. It consists of metamorphosed gabbros, norites, diorites and anorthosites associated with Fe-Ti mineralization.

The supracrustal terrains are best exposed in the central area of the massif and also, along its northern border. The metasediments along this margin consist mainly of mica shists, quartzites with some limestone

intercalations and metagreywackes, all of which have been metamorphosed within the amphibolite-greenshist facies. According to Brito Neves et al. (1982), these metasediments are intensively tectonized along their basement, making it difficult to precisely determine their extent in relation to the metasediments of the Pajeu-Paraiba fold belt. At present there are insufficient data to precisely define the northern limit to this terrain, which forms a boundary between the Pernambuco-Alagoas massif and the Pajeu Paraiba fold belt.

The Pajeu Paraiba fold belt is generally oval in shape, with its long axis trending NE and is considered to be of Transamazonico age (1800-700 Ma), according to Jardim de Sa (1984). Lithologically, it comprises biotite gneiss, garnet biotite schists (with almandine and sillimanite), metagrewackes, phyllites, chlorite schists together with some quartzites and marbles. The metamorphic grade is again within the amphibolite facies. According to Brito Neves (1975), the Pajeu Paraiba fold belt is characterized by episodes of intensive magmatism, reflecting different stages of evolution i.e.,i) stocks of gabbros and diorites, dykes and lenses of ortho amphibolites and meta orthopyroxenites marking an early phase of magmatism, ii) syn orogenic granitoids and, iii) late stocks of syenite and quartz-syenite (540 Ma.).

Costa et al. (1979) identified a suite of metamorphosed gabbros, gabbros with garnet, anorthosites with Fe-Ti mineralization, pyroxenites and eclogites, 45 Km north of the The Bom Jardim complex. The eclogites form lenses in the granulite grade terrain, concordant with the NE-SW structural trend of the massif. A similar occurrence was reported by Angel and Riera (1959) along the western border of The Pajeu Paraiba fold belt with the Pianco Alto Brigida fold belt. Beurlen (1988) has described eclogites related to this particular sequence.

The anorthosites associated with mafic and ultramafic rocks including eclogites, also form a belt oriented in the same NE-SW trends as mentioned above. They occur near the contact between the Pernambuco -Alagoas massif and Pajeu Paraiba fold belt.

The Pre-Brasiliano magmatism in the Borborema Province was mainly mafic to ultramafic in nature and limited in occurrence as discussed above. In contrast, the plutonism associated with the Brasiliano orogeny was more active and widespread, being characterized by numerous stocks and batholiths of granitoid rocks with ages of about 610 Ma.. The late Brasiliano magmatism in the province is often associated with large faults and took place about 540 Ma.. This latter episode is mainly represented by batholiths, small intrusions, dyke swarms of an alkaline ultrapotassic nature (Da Silva Filho et al., 1987) and pegmatites with and without mineralization.

1.1.3 Structural framework

The Borborema Province is structurally characterized by a complex and large NE-SW trending fault system, that divides the fold system of the province into a series of blocks. According to Almeida et al. (1981) and Jardim de Sa (1984), this NE-SW fold system is very old, deep, and has been reactivated at different times with a different character. The transcurrent character of this fault system (see figure 1.2), reflects only the late stages of the Brasiliano orogeny (Almeida et al., 1981). The NE-SW faults seem to have suffered deviations and inflections by later E-W fault systems. Two of these E-W faults, namely the lineaments of Pernambuco and Paraiba (or Patos), clearly show their late character in relation to the NE-SW fault system (see figure 1.2). The thrust faults seem to be restricted (or best preserved ?) along the contact between the median massif and the fold belts.

The boundary between the Pernambuco Alagoas massif and Pajeu Paraiba fold belt, is marked by NE-SW thrust faults, dipping towards the SE. A simplified geological cross-section across the massif (see figure 1.2), shows that the Pernambuco- Alagoas massif represents a typical "Pop-Up" structure with the fold belts showing a general schistosity dipping towards the massif.

1.2 PLATE TECTONICS AND THE BORBOREMA PROVINCE

According to Jardim de Sa (1984) the reconstruction of the Gondwana continent (see figure 1.4) shows that the pattern of folding and major lineaments of Brasiliano age in the Borborema Province, can be traced into the Nigerian shield. Caby et al. (1981) using geophysical evidence have suggested that these structures can be traced under the Phanerozoic cover outcropping again in the Hoggar shield, some 1500 km from the proposed Brazilian-African boundary. In spite of the large distances involved, Jardim de Sa (1984) argues that the similarity of chronological evolution and the continuity of the structural trends, allows such an extrapolation to be made between the two continents.

The 4^{o} 50'E Hoggar lineament divides the Hoggar shield into two distinct domains. If, this lineament is projected to the south, up to the Dohomey region, where it has been identified by geophysical data (Caby et al., 1981), it appears to have continuity with the Sobral lineament within the Borborema Province. The Hoggar lineament is dextral in nature, allowing the geology of the NW region of the Ceara state in Brazil, to be correlated with the E part of Hoggar shield (Jardim de Sa, 1984).

A complete evolution of a Wilson's cycle (opening and closing of an ocean - Wilson, 1968) has been recognized in the E part of the Hoggar (Caby, 1978; Bertrand and Caby, 1978; Caby, 1987; Caby et al., 1981 and Black, 1980) i.e., starting with the opening of an oceanic basin during Ebournean time (at least 800 Ma.), then followed by continental collision between the West African craton and the Hoggar shield, during the Upper Pan African (640-610 Ma.). The end of the cycle was marked by deposition of the molasse and post-orogenic plutonism including mafic, rhyolitic and alkaline dykes swarm with ages of around 590 Ma.. The Pan African event in Africa as in the Borborema Province, is characterized by an episode of granitic plutonism, with ages ranging from 650 to 510 Ma. (see figure 1.5).

In the NW region of the state of Ceara, no

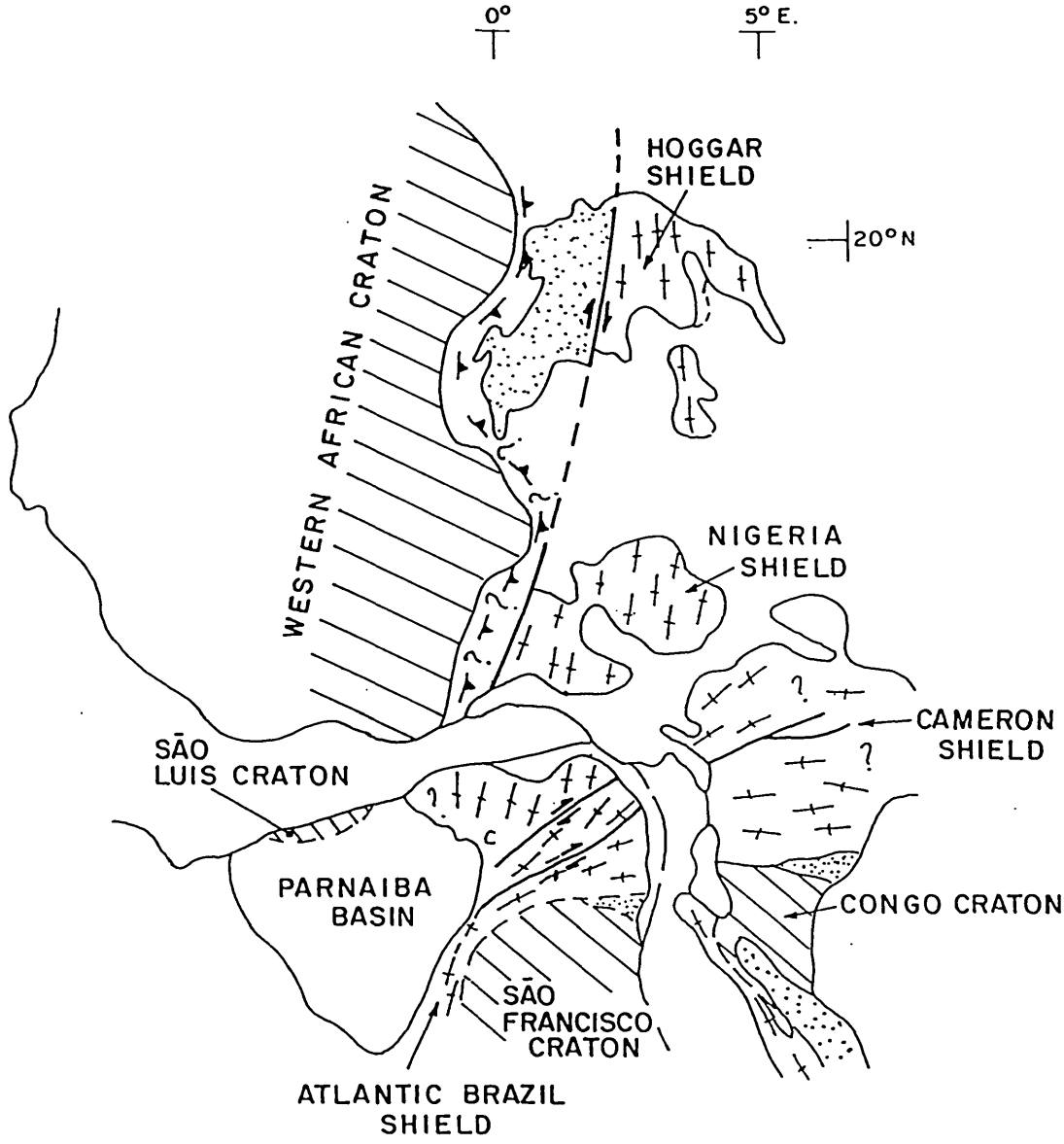


Figure 1.4 A paleo-reconstruction of the West African and NE Brazil during the Proterozoic (after Jardim de Sa, 1984).

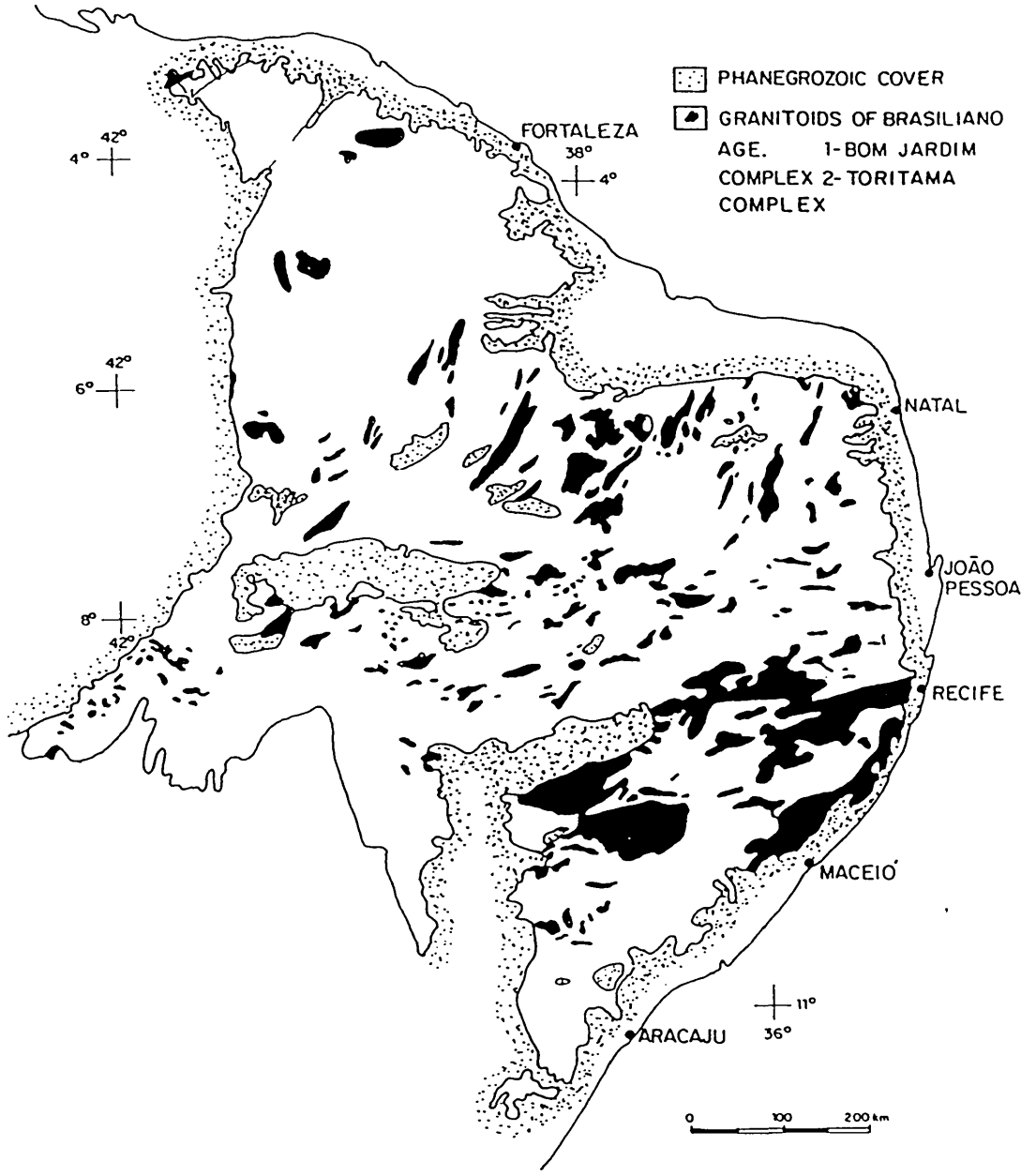


Figure 1.5 Granitoids of Brasiliano age in the Borborema province. After Santos et al. (1984).

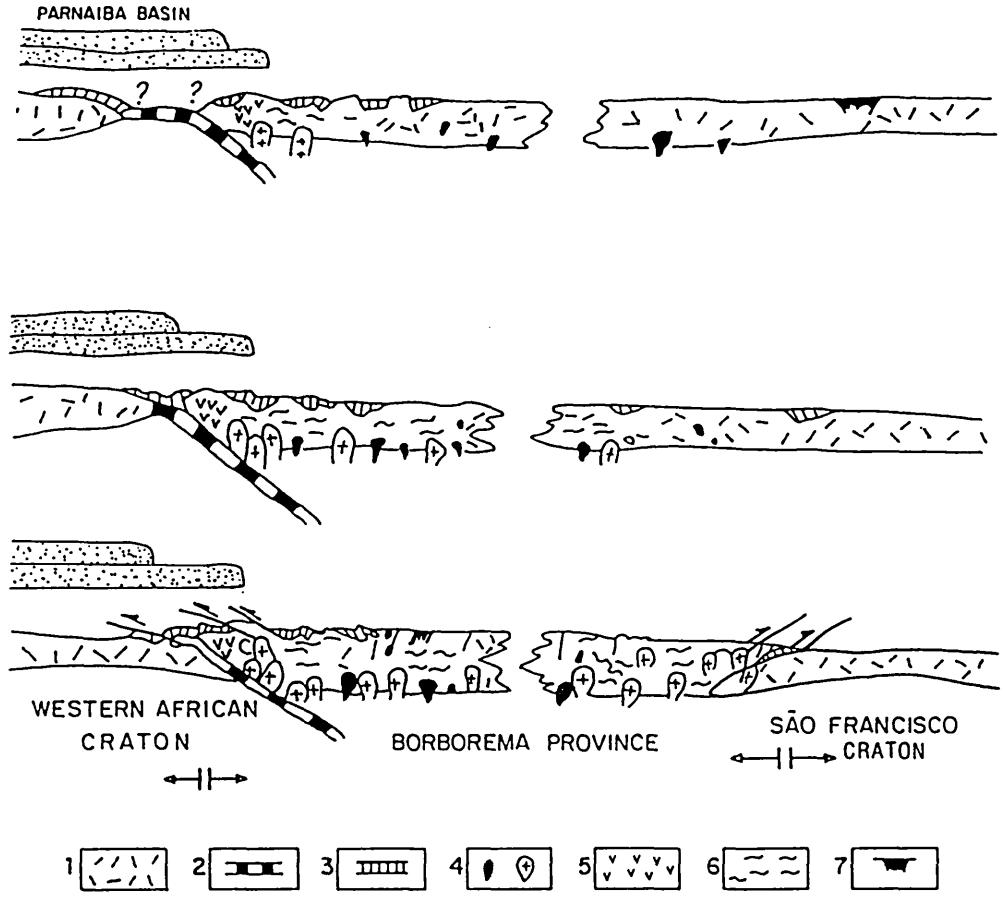


Figure 1.6 Diagrammatic cross sections showing the evolution of the Borborema province, after Jardim de Sa (1984). See text for details.
(1=continental crust, Archaean embasement and lower and middle Proterozoic supracrustals; 2=Oceanic crust; 3=Upper Proterozoic supracrustals; 4=Granites and mafic to intermediate rocks of Brasiliano ages; 5=Upper Proterozoic volcanic rocks; 6=Deformation of Brasiliano ages and 7=Molasses of the Brasiliano cycle).

corresponding mafic and ultramafic rocks, volcano-sedimentary terrains and paired metamorphic belts observed in the suture zone of the Hoggar have been found. Jardim de Sa (1984), suggested that : if the suture zone was continuous in Brazil, it could lie under the Phanerozoic sediments of the Parnaiba basin or, the suture could be at a deeper level than that observed in the Hoggar, with superposition of nappes, including basement and supracrustal rocks.

According to Jardim de Sa (1984), in spite of the lack of evidence at the present time, for the existence of a suture in the Borborema Province, the continuity of the lineaments between the NW region of the Borborema Province and the African platform and also, the correlation of the Brasiliano cycle between Brazil and Africa, does appear to suggest the development of a Wilson's cycle in the NW part of the Borborema Province. However to the South of the Borborema Province the field data shows no evidence for the existence of a suture zone. This latter observation is partially supported by the existence of a gradational contact between the Sao Francisco craton and the Sergipano fold belt and the fact that both units have been affected by deformation associated with the Brasiliano orogeny and there is no geophysical evidence to substantiate a major structural division between the two (Jardim de Sa, 1984).

Using the A-type subduction model of Kroner (1982), Jardim de Sa (1984) suggests an ensialic evolution for the province, whereby you have the initial development of a continental margin "Andean type" tectonic setting (Ubajara group in Ceara state could possibly represent this phase of evolution ?), later evolving to an "A-type" subduction situation or, to a Tibetan plateau type, the magmatic of which could be represented by the Brasiliano granites . The geodynamic model proposed by Jardim de Sa (1984) is presented in figure 1.6.

Burke and Dewey (1973) in keeping with many others interpretations of collisional tectonics have suggested that a cryptic suture exists along the boundary of the West African-Sao Luis craton. They based their interpretation on the fact that along strike from Dohomey

(Hoggar) to Brazil, parts of the suture are characterized by the lack of any exposure of eugeosyclinal material and the fact that both reactivated and unreactivated crustal material can be found in contact with each other. The same authors also claim there is evidence of a completely different earlier tectonic regime (pre 2.5 Ga.) and that the transition between these two different regimes is characterized by an exceptional suite of rocks, including aulacogens and thick sequences of supra-crustal sedimentary and volcanic material.

The geodynamic models proposed for the evolution of the Borborema Province hardly if ever take into account the presence of the median massifs and the belt of mafic and ultramafic rocks with their associated Fe-Ti mineralization. Neither, have these aspects been considered in terms of the wider plate tectonic tectonic setting for the province.

The origin of anorthosites associated with the gabbros and Fe-Ti mineralization also presents some problems (Wiebe, 1980), not only in terms of their composition but also in regard to their rather limited age span (1600-1100 Ma.). Sawkins (1984) has suggested that the anorthosites represent products of mid-Proterozoic hotspot activity rather than normal products of deep crustal processes in collision orogens as proposed by Dewey and Burke (1973). If the Transamazonico to Archaean ages obtained for the anorthosites in the Borborema Province can be confirmed, then, adopting the ideas of Sawkins (1984), the belt of anorthosites in the Borborema Province could probably represent the early products of rifting in a supercontinent comprising the West African and Sao Francisco cratons plus the median massifs, which later breaks up into several micro plates. If this is so, the Brasiliano compression in the province certainly involved more than the two plates in the model proposed by Jardim de Sa (1984). On the other hand, if the ages obtained by the Rb-Sr and K-Ar methods (Beurlen, 1988) are incorrect, and the anorthosites associated with gabbros and ultramafic rocks have Upper Transamazonico to Brasiliano ages (about 700 Ma.), these rocks could be interpreted as a "pseudo-

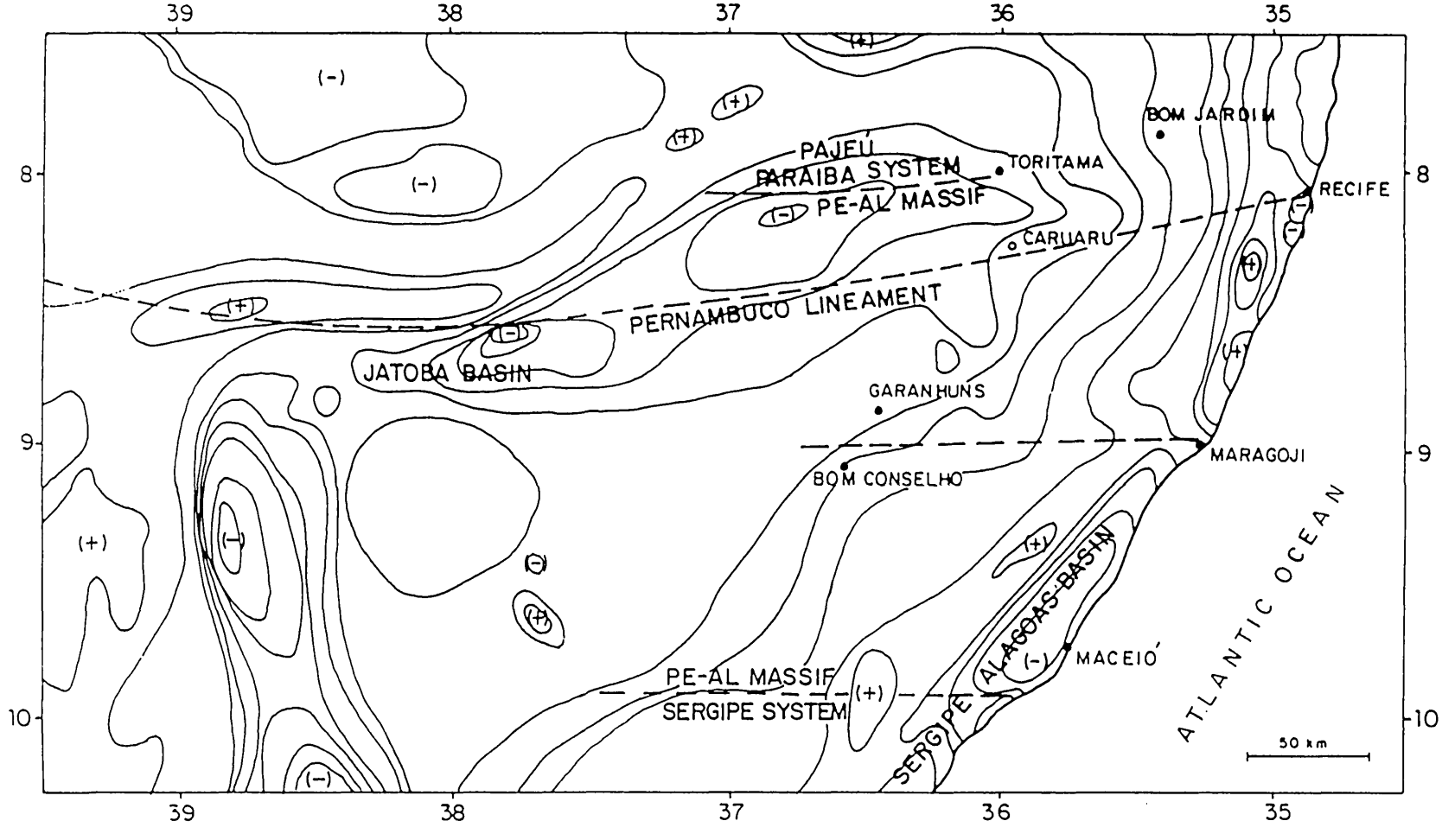


Figure 1.7 Distribution of Bouger gravity anomalies for the Pernambuco-Alagoas massif. Anomalies are shown by (+) and (-) signs. After Brito Neves et al. (1982).

ophiolites suite" as suggested by Caby (1987), marking a suture zone, during the Brasiliano compression.

1.3 GEOPHYSICAL DATA

Geophysical data presented by Brito Neves et al. (1982) and Ussami et al. (1986), shows a negative Bouger anomaly coincident with the northern boundary of the Pernambuco-Alagoas massif (see figure 1.7). This zone of negative anomaly associated with thrust faulting, suggests a down folding of the crust probably to the depth of the Moho, rather than a graben and horst system as proposed by Brito Neves et al. (1982).

1.4 SUMMARY OF THE REGIONAL GEOLOGY

A combination of factors including geophysical evidence, the spread of Archaean ages (Dantas and Brito Neves, 1980) and the distribution of the Brasiliano plutonism, associated with thrust faults restricted to the border of the massif, suggest that the Pernambuco Alagoas massif is a cratonic segment which was partially preserved during the later Brasiliano orogeny.

The present author agrees in part with the general continent-continent collision model proposed by Jardim de Sa (1984) to explain the Brasiliano orogeny within the Borborema province. However, when one looks in detail at the complex structural configuration of the interior of the province, a much more complex plate tectonic model must be considered. The present author is of the opinion that the median massifs (Brito Neves, 1975) represent micro continents involved in the Brasiliano collision event.

In order to evaluate any plate tectonic model proposed for the evolution of the interior of the province two factors must be taken into account viz; the lack of any evidence of volcanic activity of Brasiliano age and, secondly the location of the inferred suture zone (or

zones). The absence of Brasiliano volcanism could be simply due to the high present level of erosion in the province, or the consequence of subduction at a low angle as discussed by Thorpe (1987). The suture zone in many examples of continent - continent collision has not easily been recognised because the structure can often be further complicated and obscured by the involvement of pieces of crust, separated as flakes during the collision, thus leaving very litle trace of any original ocean floor material in the observed stratigraphic recorded.

1.5 PREVIOUS WORK IN THE AREA

The earliest description of syenitic rocks along the northern boundary of the Pernambuco-Alagoas massif was given by Mello and Mello (1969) for the Toritama complex, which probably represents an southwestern extension of the Bom Jardim complex. In a later and more detailed investigation of the Toritama complex by Mello (1971), both the high potassic character of the suite and its high modal mafic minerals content were established. Based on the presence of mafic enclaves of clinopyroxene bearing hornblendite, Mello suggested that the rocks of the Toritama complex were the products of a regional metasomatic transformation of mafic igneous rocks (clinopyroxenites). However, field evidence presented in this investigation, clearly shows that the contacts between the enclaves and host syenites within the Bom Jardim intrusion are sharp and not diffuse or gradational as one might expect from a metasomatic replacement origin. This interpretation of Mello (1971 and 1972) was clearly influenced by the "metasomatic school of thought" prevalent at that time and, reflects a general lack of knowledge concerning the Precambrian tectonic regime present within the province.

The general form of the Bom Jardim complex was first established as a result of the regional mapping project "Projeto extremo Nordeste do Brasil" carried out in 1979 by the CPRM (Mineral Research Company). The complex

was described as being composed of porphyritic syenites, monzonites and mangerites. The latter rock-types were regarded as being the unmetasomatised relicts of an original mafic igneous rock. In 1983 further exploratory mapping was carried out by the Minerios de Pernambuco (Pernambuco Ore Company) and specifically concerned with determining the extent of the coarse grained syenite within the complex (Maranhao,1983).

1.6 OBJECTIVE OF THIS STUDY

The use of geochemical discriminant functions has become one of the major tools in determining the different tectonic regimes of both volcanic and plutonic suites of rocks . With this in mind the Bom Jardim complex was chosen to see if a detailed mineralogical and geochemical study could shed some light on the tectonic evolution of part of the Borborema province.

The Bom Jardim complex is the largest multiply intruded syenite body within province and is clearly intimately related to the tectonic evolution of the area. Combining field evidence with a carefully integrated geochemical and mineralogical programme of research it is hoped that both the tectonic regime and the particular stage of magmatic evolution can be established for the complex, as well as the main processes which have led to the continuum of rock compositions found within it.

To this end, major and trace element analyses have been carried out on all the major rock types including a systematic determination of the rare earth elements, and $Sr^{87}\backslash Sr^{86}$ isotopic ratios. In addition most of the mineral phases have been analysed by both electron microprobe and\or I.N.A.A. techniques.

It is hoped that such an integrated investigation as presented here will provide the necessary basis for the future work required before the collision tectonics in N.E. Brazil can be more fully understood.

CHAPTER 2
THE FIELD AREA

2.1 INTRODUCTION

2.1.1 Location and access

The field area is located near the village of Bom Jardim approximately 90 Km due NW of Recife, within the state of Pernambuco-NE Brazil (see figure 1.1). The main access to the field area is by road, the PE 90 from Recife to the village of Surubim, a series of dirt roads cut the area in a N-S direction. Apart from the extreme western part of the complex which has no roads at all, most parts of the complex are reasonable accessible.

2.1.2 Physiographic aspects of the area

The topography within the field area is clearly controlled by the distribution of the different rock types and the major faults. Generally, the area of the complex is fairly flat lying, apart from where the granite and coarse grained syenitic rocks form low hills (see plate 2.1).

The area has a relatively high rural population density for the state of Pernambuco, and as a consequence there are small quarries located throughout the complex which are used for local building stone. As a consequence, access to fresh material is generally good.

Drainage within the complex is characterized by both temporary and perennial streams whose courses are again largely controlled by the fracture patterns within the area. The majority of the streams are tributaries of the Capibaribe river which runs from West to East across the complex and is one of the few water supplies within the Pernambuco state.

The climate is tropical, semi-arid type, with two well marked seasons, the dry season occurring between October and April and the rainy season from May to September; during these latter months many of the dirt



Plate 2.1 The Bom Jardim complex viewed from the NE. Sy, very coarse grained syenite and Gr, granite.



Plate 2.2 Syenite with elongated enclaves, near the contact with the metasediments. The deformation is related to crystal plastic strain (see text for details).

roads become impossible making access to the complex very difficult.

Average maximum and minimum temperatures are 34° C (95° F) and 18° C (64° F) respectively with an average rainfall of 200 cm per year, most of that falling in June and July.

2.1.3 Mapping and map preparation

The field work was carried out in three stages:
1) A ten day reconnaissance trip in January 1985.
2) Ten days were spent in the least accessible western part of the complex in August 1985.
3) Over three months from October to January 1986\1987 were spent carrying out the final field mapping and more detailed sample collecting in certain areas of the complex.

The mapping itself was carried out using base maps compiled from 1:30.000 aerial photographs and plannimetric maps, enlarged from 1:100.000 plannimetric maps based on radar imagery and aerial photographs produced by RADAM BRAZIL in 1984. The lack of any ordnance datum points, meant that all the maps produced were without contours or even spot heights. Thus all cross sections produced have arbitrary vertical scales.

The geological map of the Bom Jardim complex produced by the author can be seen in figure 2.1.

2.2 ASPECTS OF FIELD GEOLOGY

The Bom Jardim complex forms an elongate multipli-injected intrusive covering an area of approximately 200 sq Km. Its principal axis is generally parallel to the main foliation in the area. The regional foliation trending NE-SW and dipping to the SE is picked out by an alignment of euhedral alkali feldspar phenocrysts and the mafic biotite and amphibole. Neither field observation nor microscopic examination shows any indicator

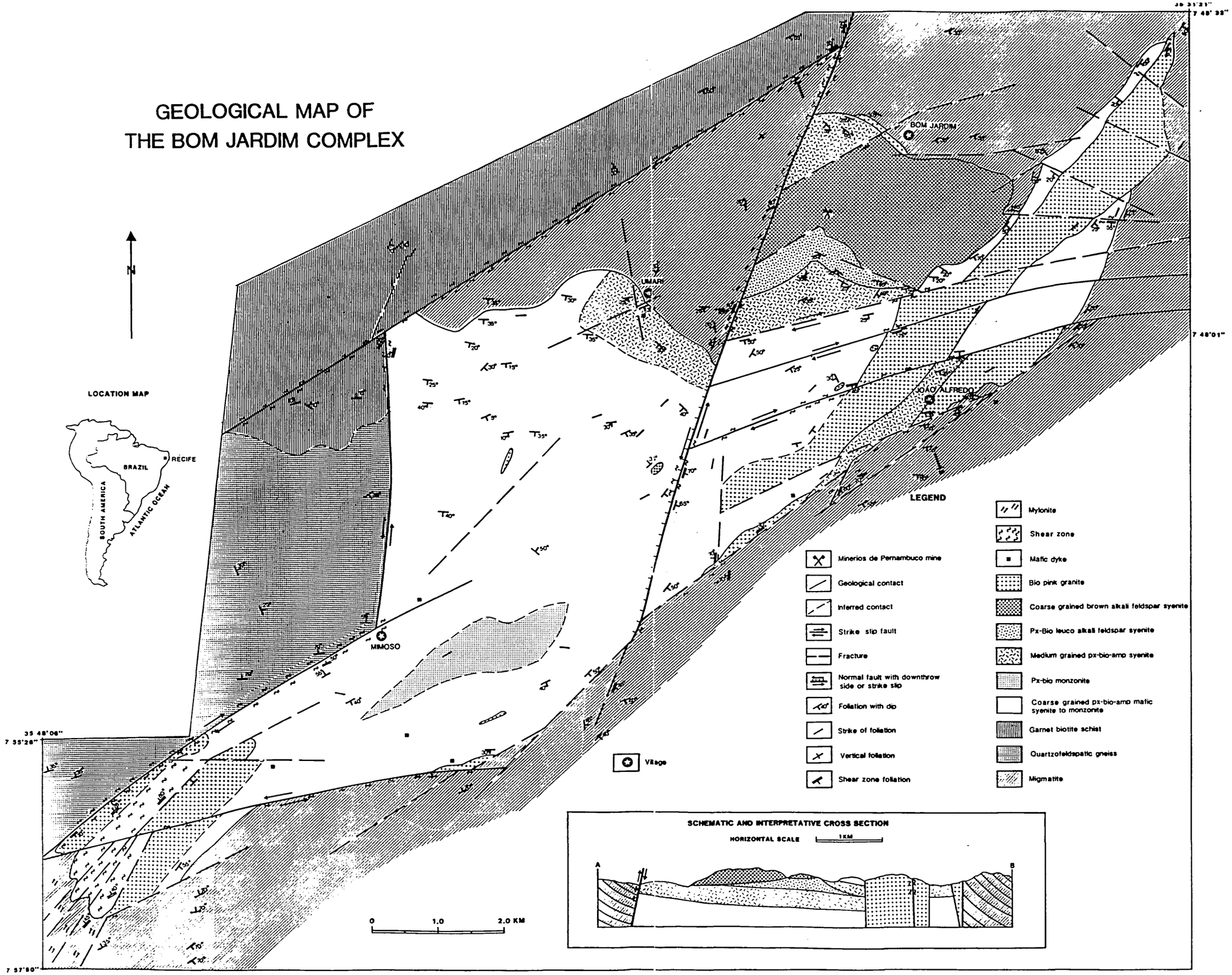


Figure 2.1 Geological map of the Bom Jardim complex.

of brittle deformation within this same foliation direction.

The general euhedral shape of the alkali feldspars phenocrystals and the presence of unaltered biotite has led Berthe et al. (1979) to conclude that such deformation took place at temperatures in excess of 450^{o}C. According to Hutton (1987), syn-kinematic plutons (those emplaced synchronously with the regional deformation) show many of the aspects of deformation of melt plus crystal assemblages (normally with more than 30% melt). Many of the characteristics described by Hutton (1987) have been recorded within the Bom Jardim complex and will be discussed later. As a consequence it could be argued that the complex represents either a syn or late kinematic intrusive.

The low angle foliation within the complex generally runs parallel to the main thrust faults within the region. This suggests that the emplacement of the complex could be related to thrust tectonics, with the NE-SW foliation imposed whilst the rocks were still predominantly in the plastic state.

Shear zones with a strike-slip displacement cut the whole complex and on a regional scale could be linked with shear zones of much larger continental dimensions, eg. the Pernambuco lineament. Some very localised examples of brittle deformation were found along the shear zones (see plate 2.2). Generally however, the majority of deformation recorded along the strike slip shear zones appears to be related to crystal plastic strain. According to Hutton (1987) this would indicate less than 30% melt remaining and both the main phenocrystals phases and the late crystallising phases showing deformation of their respective crystalline structures. Post emplacement brittle deformation was mainly observed along the west and northwestern boundaries and locally in the center of the complex. The post emplacement deformation observed within the complex probably reflects the reactivation of the major Pernambuco lineament, during either the late or post tectonic stages of the Brasiliano orogeny which partially overprinted the thrust tectonics (see plate 2.3).



Plate 2.3 Post emplacement deformation within the Bom Jardim complex.

A relatively large N-S trending fault virtually cuts the complex in two. The folded migmatites exposed along this fault display folding with axial planes dipping at high angles towards the west and generally parallel to the line of the fault. The fault shows a strong vertical displacement in that it is not possible to trace the boundaries of the different facies across the fault. Field evidence suggests that the western side of the fault has been uplifted exposing much deeper seated members of the complex. The sinistral displacement of the units around the fault indicate some component of horizontal displacement. The lack of any significant evidence of brittle deformation along this fault, suggests an interplay between this fault system and the strike slip faulting previously discussed.

The contacts between the Bom Jardim intrusion and the country rocks are mainly faulted as are the contacts between the different facies within the complex; these latter faults have been interpreted as low angle thrust faults. Along the southern contacts of the complex there is clear evidence of metasediment digestion and incorporation by the syenitic magma.

2.3 CLASSIFICATION OF THE BOM JARDIM ROCKS.

The recommended I.U.G.S. rock classification (Streckeisen, 1976) has been used to classify all the rocks of the Bom Jardim complex. This classification, based on modal proportion of quartz, plagioclase and alkali feldspar indicates a continuum of major rock types present in the complex ranging from monzonites to quartz alkali syenites (see figure 2.2), with the associated granites clearly plotting away from the main trend. This continuum of rock types from monzonites to quartz alkali syenites is equivalent to the alkaline series proposed by Lameyre and Bowden (1982). The minor facies within the complex range from diorites to syenites. Modal compositions were determined in 44 different samples within the complex (see table B.10 in the appendix B) and represent all the different facies variations found within the complex.

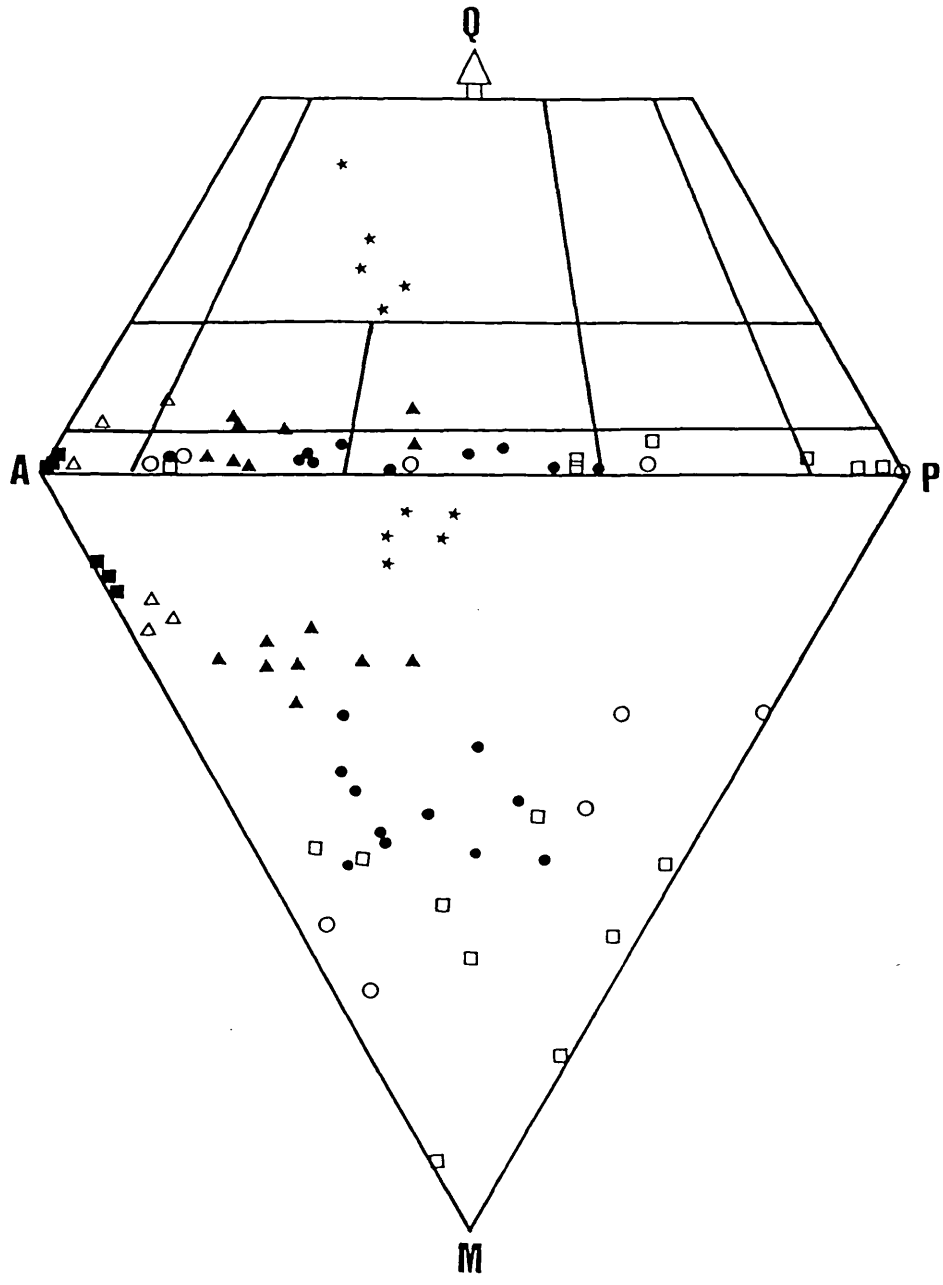


Figure 2.2 a) Modal composition of the Bom Jardim complex rocks in the QAP triangle diagram after Streckeisen (1976) b) the modal composition of mafic phases versus alkali feldspar and plagioclase. (Closed circles = PBAMS plus PBM, closed triangles = MPBAS, open triangles = PBLS, closed squares = CS, stars = pink granites, open circles = dykes and open squares = enclaves).

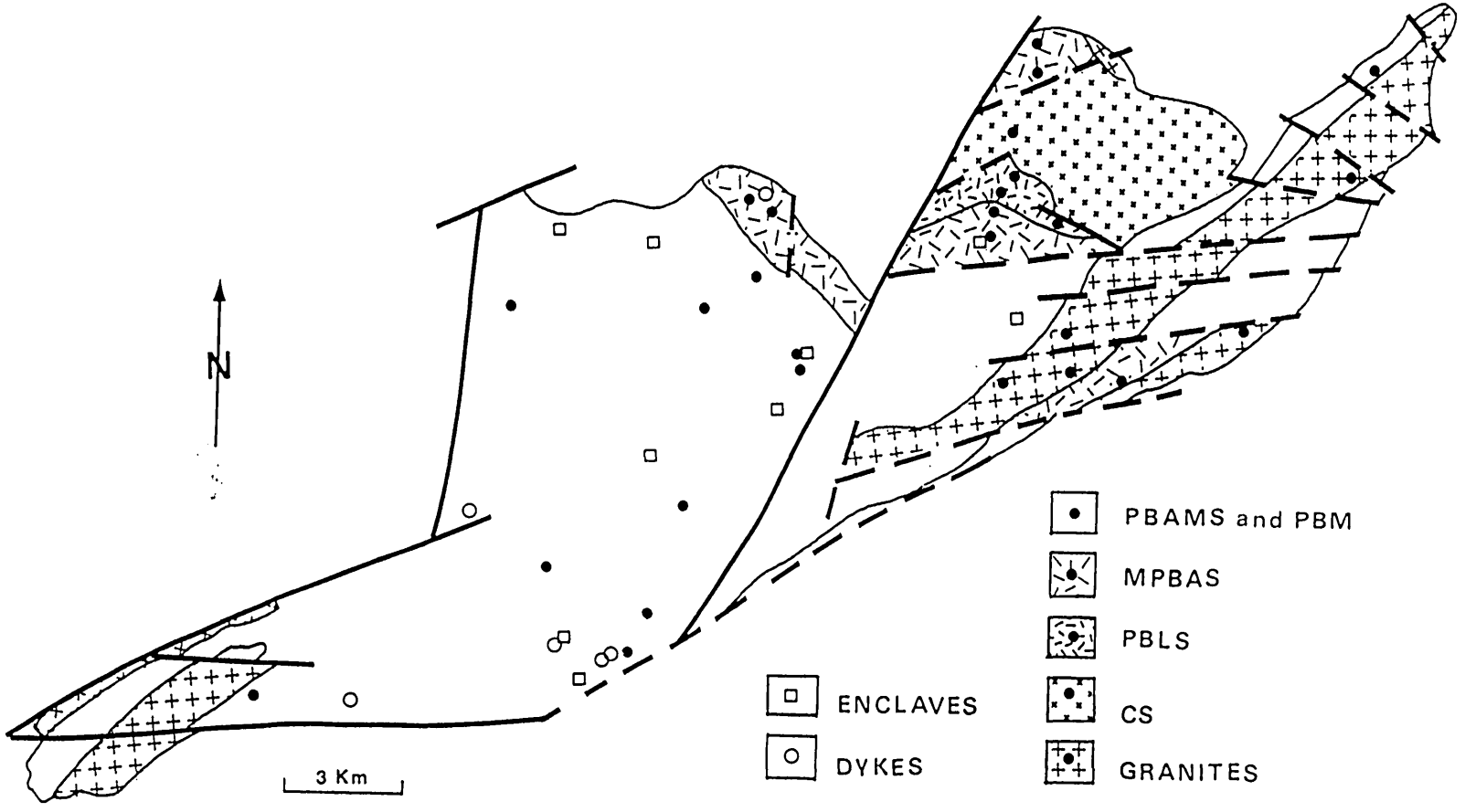


Figure 2.2.A Location of samples with modal analyses plotted in figure 2.1.

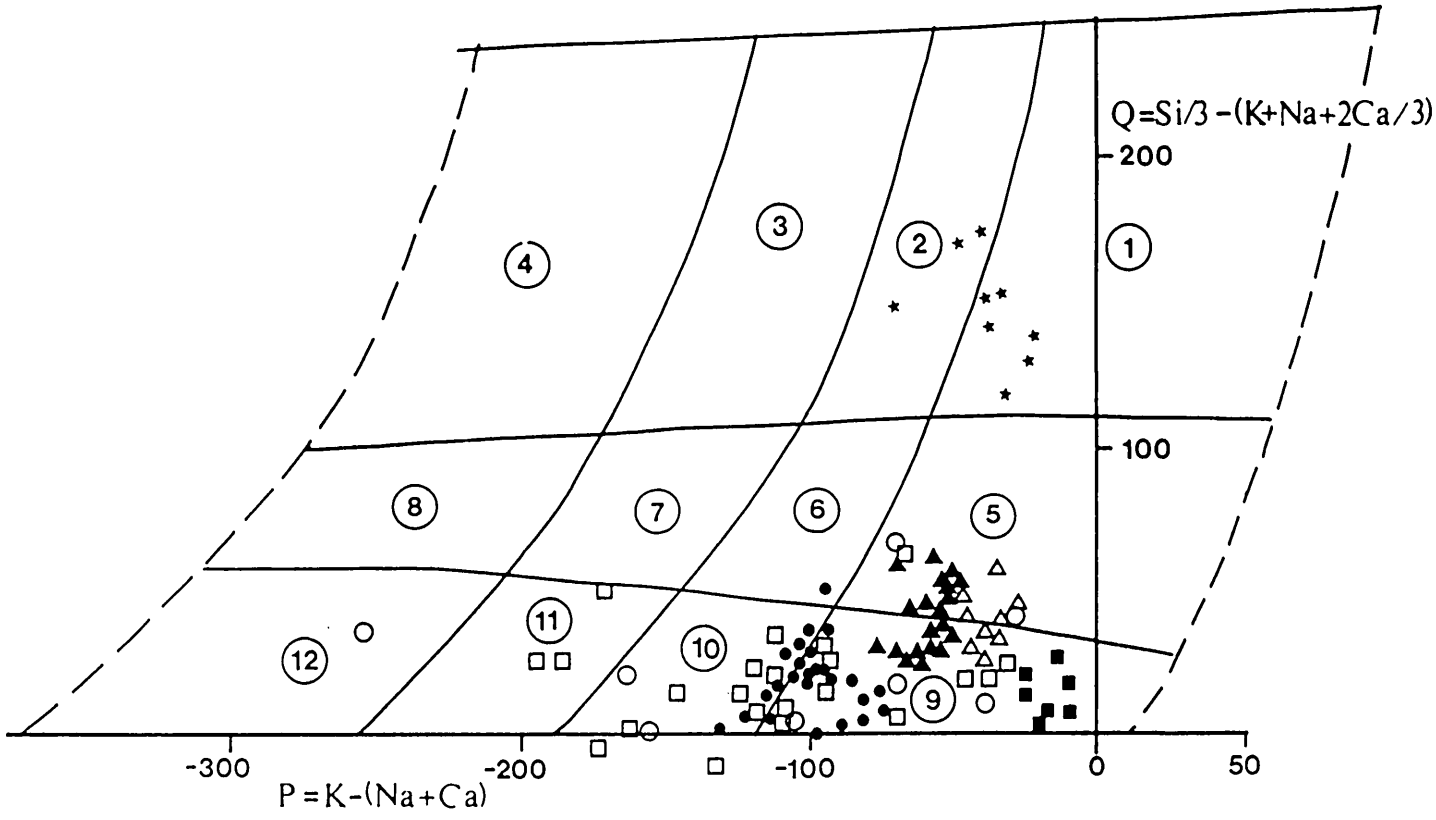


Figure 2.3 The distribution and classification of the Bom Jardim rocks after the scheme of Debon and Le Fort (1983). (1, granite; 2, adamellite; 3, granodiorite; 4, tonalite; 5, quartz-syenite; 6, quartz-monzonite; 7, monzodiorite; 8, quartz-diorite; 9, syenite; 10, monzonite; 11, monzogabbro and 12, gabbro). Symbols as in figure 2.1.

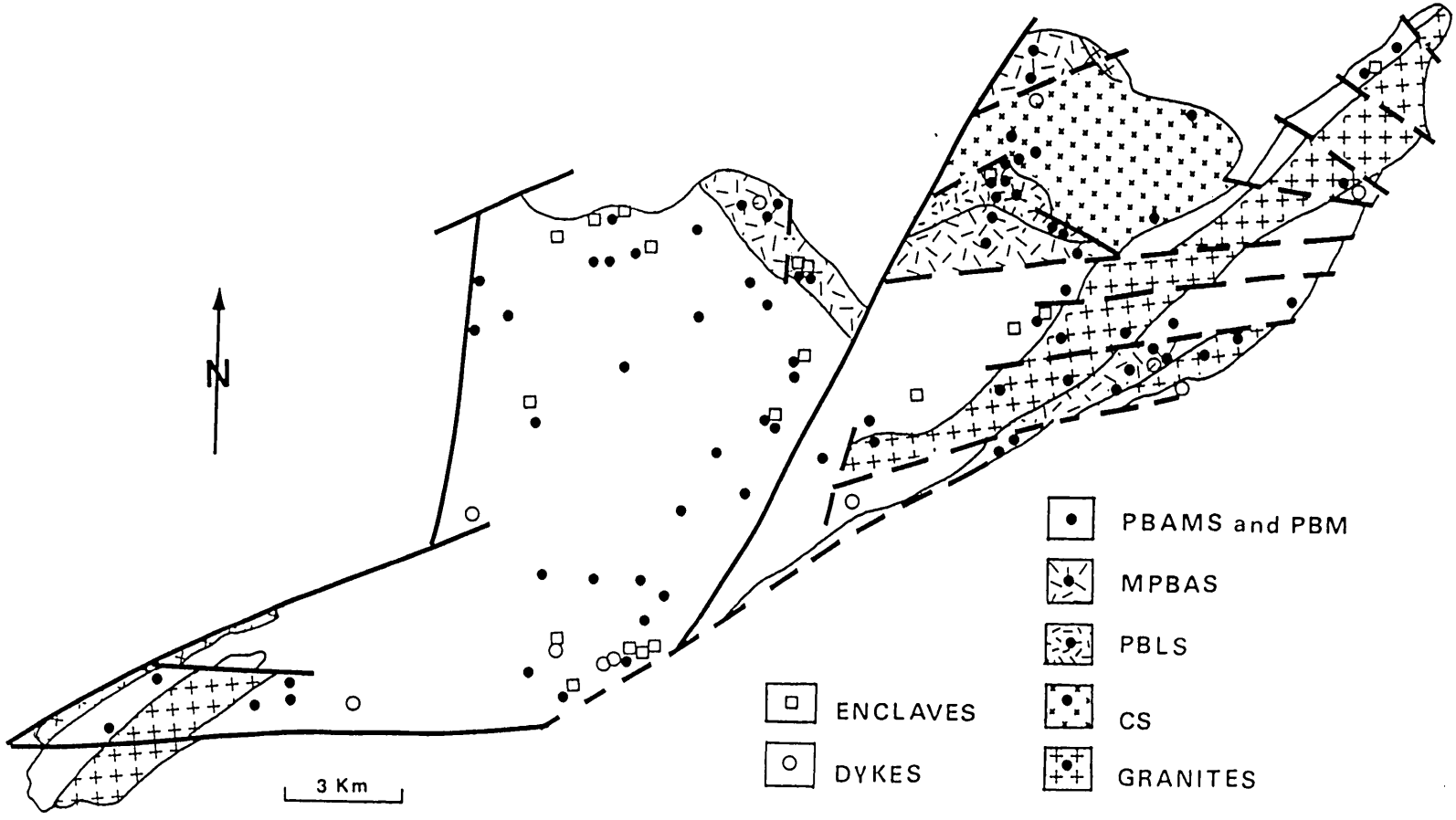


Figure 2.3.A Location of all chemically analysed samples plotted in figure 2.3 (after Debon and Le Fort, 1983).

The IUGS classification however does not discriminate between mafic and leucosyenites. The lower part of the figure 2.2 shows a plot of the modal distribution of mafic minerals (biotite + amphibole + pyroxene), together with plagioclase and alkali feldspar, for the different facies of the Bom Jardim complex. As can be seen, the major facies show a trend from mafic members to those containing less than 15% modal mafic phases; in all five subpopulations can be identified. The minor facies on the other hand, are made up of only two populations: one characterized by low modal abundances of alkali feldspar, the other with much greater abundances of the same phase.

The classification of Debon and Le Fort (1983) was initially tested and compared to that of Streckeisen (1976). This classification is based on parameters calculated from major element analyses and expressed as 1 gm equal to 1000 atoms of each element per 100g of rock. The figure 2.3 shows the classification of the Bom Jardim rocks using this procedure, where Q = Si/3 - (K + Na + 2Ca/3 and P = K - (Na + Ca). Both the IUGS and the Debon and Le Fort classifications give similar classification groupings for the major facies types. However, when one considers the members of the minor facies, negative Q values sometimes occur, i.e. the rocks will plot in the feldspathoid field even though they contain no modal feldspathoid. As might be expected this result is very common in rocks containing high proportions of modal biotite.

Considering the problems encountered by both the classifications, the author opted to use a compromise scheme, using the general terms of the rock groups from the IUGS classification, the general texture of the rocks and the modal amount of mafic minerals. Based on this classification the Bom Jardim complex is composed of six major facies:

1) Coarse grained porphyritic mafic syenites and monzonites, containing clinopyroxene, biotite and amphibole (PBAMS)

2) Medium grained porphyritic clinopyroxene and biotite bearing monzonites (PBM)

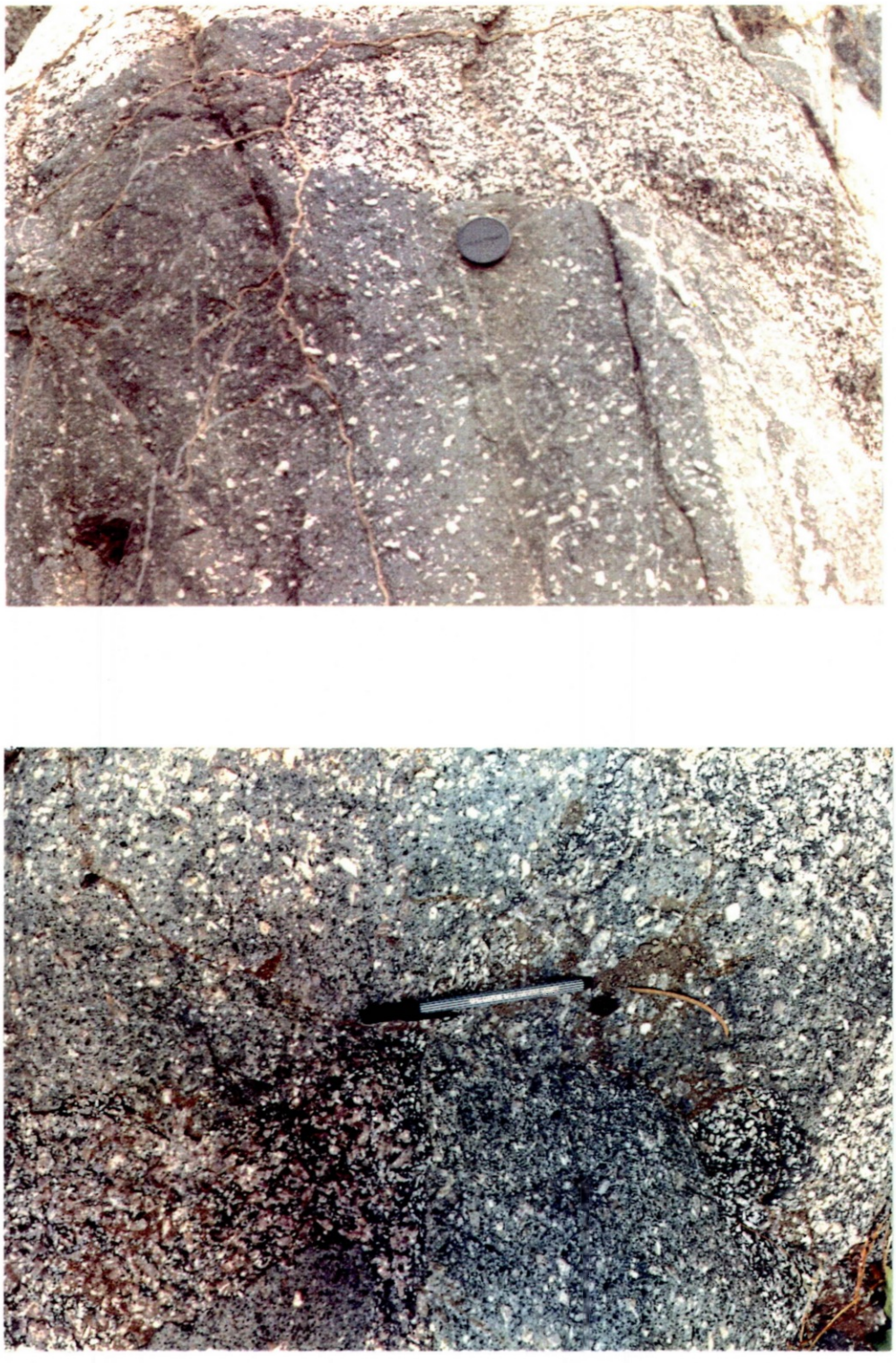


Plate 2.4 Evidence of multiple injection within the mafic syenite massif of the Bom Jardim complex.

3) Medium grained porphyritic syenites containing clinopyroxene, amphibole and biotite (MPABS)
4) Medium grained biotite and clinopyroxene bearing leucocratic alkali feldspar syenites (PBLS)
5) Very coarse grained brown alkali feldspar syenites (CS)
6) Biotite bearing pink granites

2.3.1 Pyroxene biotite amphibole mafic syenites and monzonites

The mafic syenites and monzonites outcrop in two main areas, in the west and south eastern parts of the complex and between them make up an area of approximately 135 sq Km. Both rock types occur together and in practice can only be separately classified by microscopic inspection. In handspecimen, they are both porphyritic with phenocrysts of pink alkali feldspar and occasionally plagioclase. The groundmass is generally dark in colour and is largely composed of biotite and amphibole. The phenocrysts do exhibit a range in grain size but generally show an average length of 1.5 cm. No clear systematic spatial distribution of different grain sizes has been found, apart from the general tendency to find finer average grain sizes towards the contacts with the metasedimentary country rocks.

Inside the massif there is clear evidence of more than one pulse of magma (see plate 2.4). For example, within the western part of the intrusion, a syenite with a distinct rapakivi texture outcrops in an area of approximately 400 sq metres with sharp and irregular contacts with the host mafic syenite. Near the contact with the metasediments, discontinuous small bodies of a glomeroporphyritic monzonite (less than 40 sq m) have been found with phenocrysts of both alkali feldspar and plagioclase. Their contact with the host mafic syenite is very sharp (see plate 2.4).

The mafic syenites and monzonites have clearly intruded the surrounding migmatites, and the major contacts between the intrusives and the country rocks appear to be fault bounded. Syenitic orthogneisses have also been

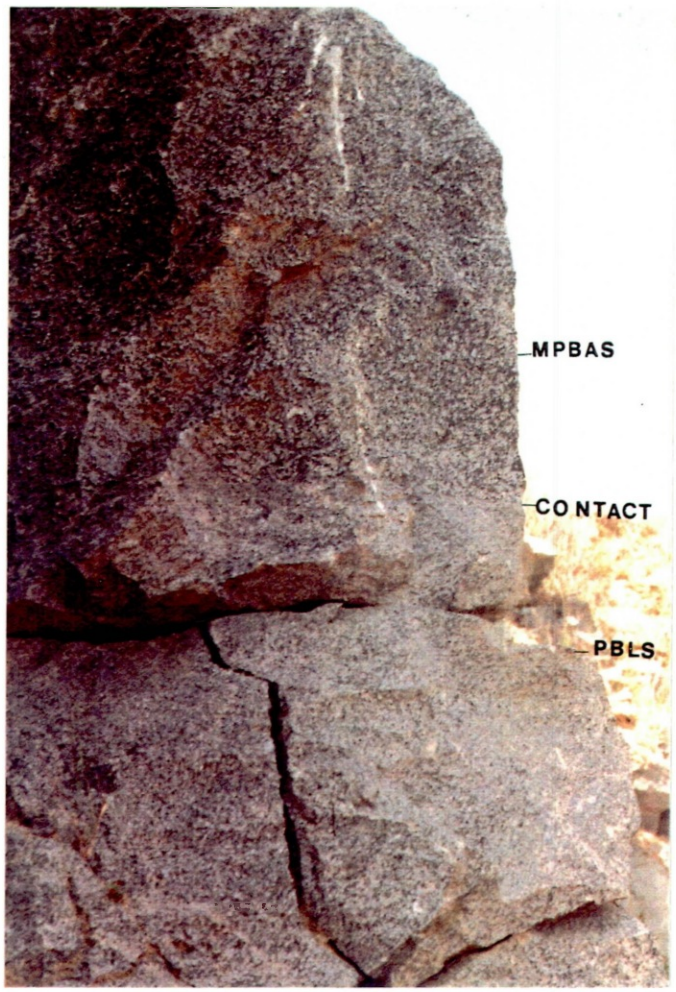


Plate 2.5 The contact between the medium grained syenite (MPBAS) and the leuco-syenite (PBLS).



Plate 2.6 Field characteristics of the mineralogy and texture of the medium grained syenite (MPBAS).

recorded near the contacts reflecting a moderate solid state deformation. Along the southern boundary of the complex there is clear evidence of relationships between the metasedimentary wall rocks and the mafic syenite.

2.3.2 Pyroxene biotite bearing monzonites

This facies is characterised in the field by the presence of phenocrysts of red feldspar, with a fairly uniform grain size of approximately 5 mm, set in a groundmass composed mainly of pale green clinopyroxene and biotite. In the field, members of this facies occur as small densely packed bodies within the host mafic syenite, rather than as a single intrusive body. The contacts with the host syenite are less sharp.

2.3.3 Medium grained pyroxene biotite amphibole syenites

The members of this facies outcrop in four isolated bodies, one to the west of the main N-S fault and three to the east. Petrographically, the rocks are characterised by phenocrysts of pink alkali feldspar, set in a mesocratic groundmass (see plate 2.6).

The contacts between this facies and the surrounding rock types show quite a wide variation in style. For instance, the contacts with the migmatites in the north are generally subhorizontal, whereas against the mafic syenite the contacts are mainly faulted. In contrast, those contacts with the very coarse grained alkali syenite are subhorizontal and have been overprinted by strike slip fractures. The contacts between the leucocratic alkali feldspar syenite and the medium grained syenite are subhorizontal and sharp (see plate 2.5). The disposition of the four different masses of the medium grained syenite, together with the adjoining rock types has led the author to propose that originally this facies formed a single subhorizontal body which later became disrupted by faulting. The outcrop of medium grained syenite near the village of Umari probably belongs to the same unit as found near the village of Bom Jardim, but represents a slightly

deeper part of the unit.

2.3.4 Pyroxene biotite bearing leucocratic alkali feldspar syenites

This facies is mainly medium grained (average grain size of 0.5 cm), essentially equigranular with an occasional subordinate porphyritic texture (see plate 2.7). In handspecimen it consists largely of light pink alkali feldspar, with up to a maximum of 15 modal % of biotite plus pyroxene and sphene. Quartz occurs in some samples. The leucocratic syenites generally occur as small sheets, cutting the mafic syenite (often too small to be recorded on the scale mapped); only one relatively large body (about 4 sq km) was found in the NW part of the complex.

2.3.5 Very coarse grained brown alkali feldspar syenites

This facies is characterized by large phenocrysts of brown alkali feldspar varying in length from 1 to 10 cm, they occasionally show a rim of pink alkali feldspar. The groundmass is generally dark in colour and constitutes less than 20% of the rock (see plate 2.8).

This facies forms a major intrusive unit with an area of 50 sq km in the NW of the complex and also three much smaller bodies (usually less than 0.5 sq km) in the center of the complex. The outcrops are generally restricted to the top of hills, although in a valley near the Minerios de Pernambuco mine, a subhorizontal contact with the pyroxene-biotite leucocratic alkali feldspar syenite was observed.

2.3.6 Pink granites

The granites are fine grained, equigranular pink in colour and leucocratic, with less than 10% mafic minerals (mainly biotite). One of the most significant characteristics of this rock type is the large amounts of metamictic material, which usually takes the form of a yellowish powder.

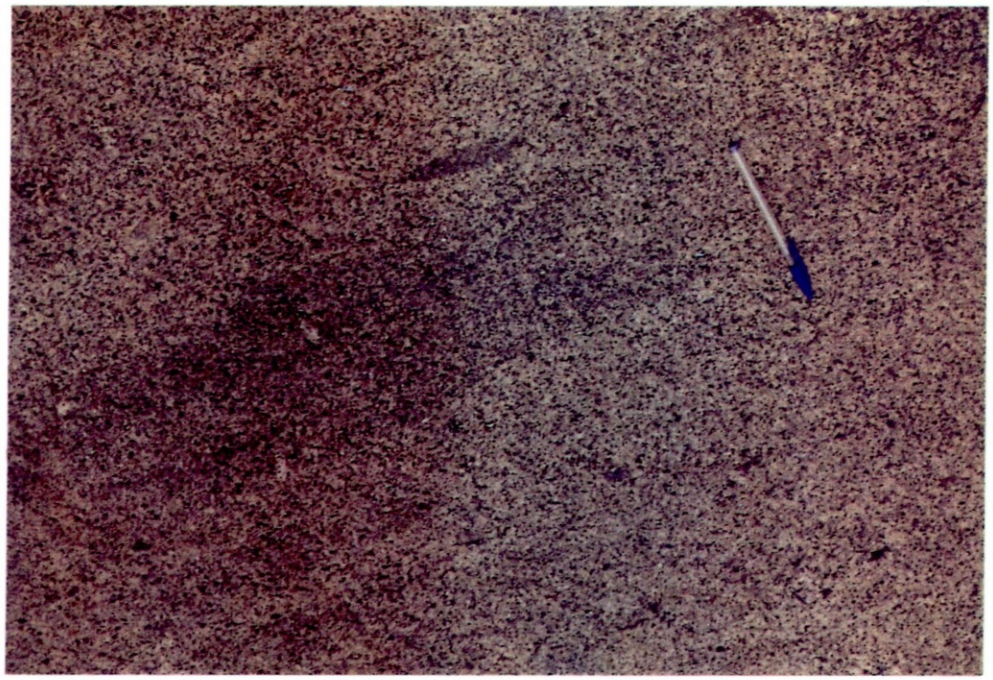


Plate 2.7 Field characteristics of the leuco-syenite (PBLS).



Plate 2.8 Field characteristics of the texture and mineralogy of the very coarse grained syenite (CS).

The granites form a rather large (30 sq km) elongate body trending NE- SW in the southern part of the complex. They are found intruding both the mafic and medium grained syenites where the contacts are both nearly vertical and sharp. The same granites have also been found as much smaller bodies cutting the mafic syenites and also in the contact zone between syenite and metassediments. These granites clearly represent the last major intrusive episode in the evolution of the Bom Jardim complex.

2.3.7 Minor facies

2.3.7.1. Mafic dykes

The dykes are fine grained and dark in colour, and occur as both disrupted and non-disrupted intrusives. Eleven non-disrupted dykes have been recorded. They are generally thin ranging from 30 cm to 60 cm in width with a lateral extension seldom greater than about 6m. They are mainly located near the margins of the complex, and all show a foliation which parallels that of the host syenite. The contacts are generally sharp and well defined. A number of the dykes have been intruded by late pegmatites and aplites. The non-disrupted dykes (see plate 2.9) lack any evidence of enclaves from the host syenite.

Several disrupted dykes have been recorded mainly towards the center of the complex. These dykes show a range of deformation from hardly deformed examples (see plate 2.10) to those with a highly deformed fabric (S>L), dismemberment by pinch and swell was commonly observed (see plate 2.13). Dykes cut by late stage aplites and pegmatites or preferentially deformed recrystallized or dismembered, within a granitoid host were the common features used by Roddick and Armstrong (1959) to define syn-plutonic dykes.

Synplutonic dykes are ubiquitous in granitoid terrains as is clearly shown by a survey of the literature. For example they have been described in the Coast Mountains of British Columbia (Roddick and Armstrong, 1959), Donegal (Pitcher and Read, 1960), Sierra Nevada (Moore and Hopson, 1961), in the Coastal Batholith of Peru (Pitcher and



Plate 2.9 A non disruptive dyke with minimum deformation cutting the mafic syenite.





Plate 2.10 Examples of syn-plutonic disrupted dykes within the Bom Jardim complex.

Bussell, 1985), the Idaho batholith (Toth, 1987) and in the Southern Patagonian Batholith (Suarez et al., 1985).

All of the above authors record very similar features for the syn-plutonic dykes, the only differences relate to the angularity of disruption, intensity of the foliation and degree of dismemberment. Such differences are related to the relative ductility contrast between the dyke and its host and the variable intensity of deformation at the time of the dyke injection (Pitcher and Bussell, 1985). The ductility contrast can also help to explain the preferential disposition of the non-disrupted dykes near the margins of the Bom Jardim complex, i.e., the ductility contrast between the dyke and the syenite would be high near the margins of the complex due to heat loss to the surrounding country rocks, while towards the centre of the complex retention of the heat content of the intrusion would result in a much lower ductility contrast.

2.3.7.2. Enclaves

The term enclave defined by Didier (1973) as follows: " Bodies of material totally enclosed within and differing in some way from the otherwise fairly homogeneous igneous rock in which it is found", is preferred by the author rather than the terms xenolith or inclusion and will be used throughout the present work. The term enclave has long been used by many geologists including Read (1957), Diddier (1973), Vernon (1983), Pitcher (1985), and Cook (1988). It is generally preferred on account of its more generic connotation and lack of genetic implications.

Enclaves are widespread throughout the Bom Jardim complex and can clearly be divided into igneous and metasedimentary types. The former shows a range in both composition and form. Field evidence indicates that some of the igneous enclaves are actually mafic disrupted mafic dykes.

The igneous enclaves can be subdivided into three compositional groups, viz:

1) Medium to fine grained biotite pyroxenites
2) Microsyenitic enclaves within the leuco alkali feldspar

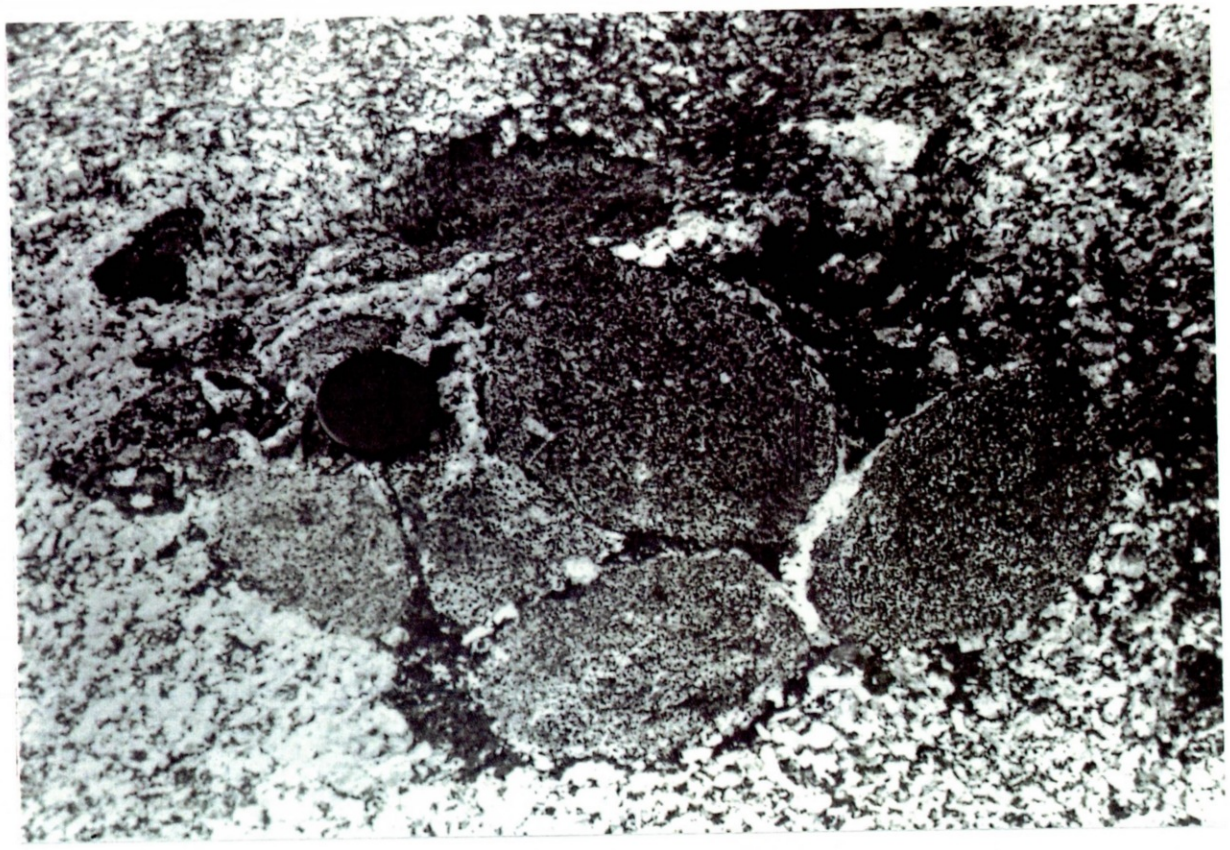


Plate 2.11 "Pillowing" enclaves of diorite, surrounded by aplite, the whole enclosed within mafic syenite.

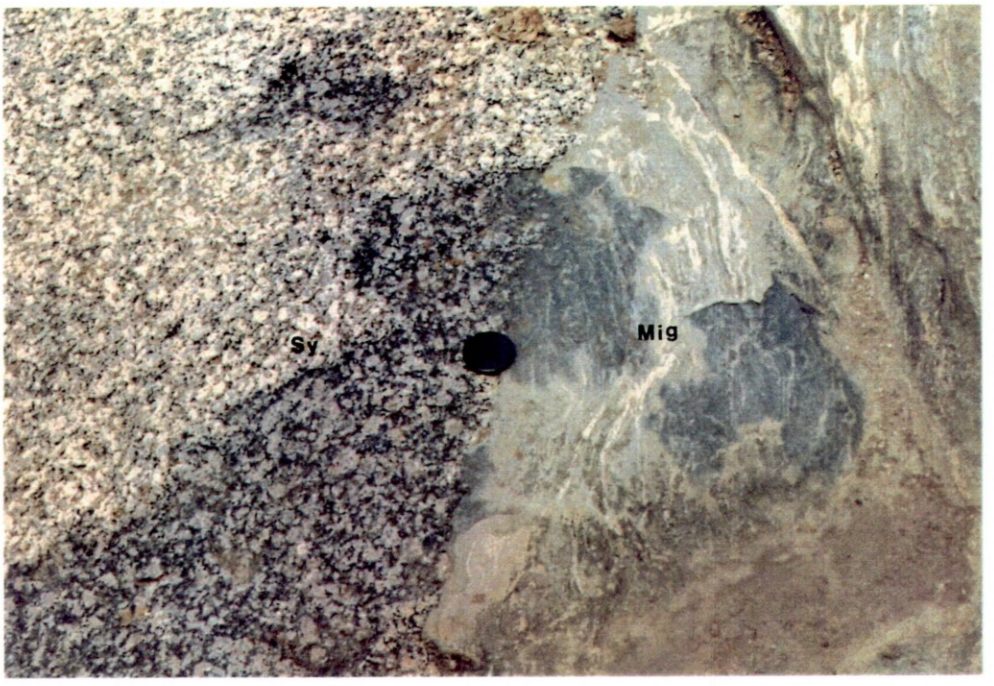


Plate 2.12 Extremely elongated enclaves within the mafic syenite, close to its contact with the metasediments.



Plate 2.13 Enclaves resulting from the dismemberment of a mafic dyke.

A)



B)

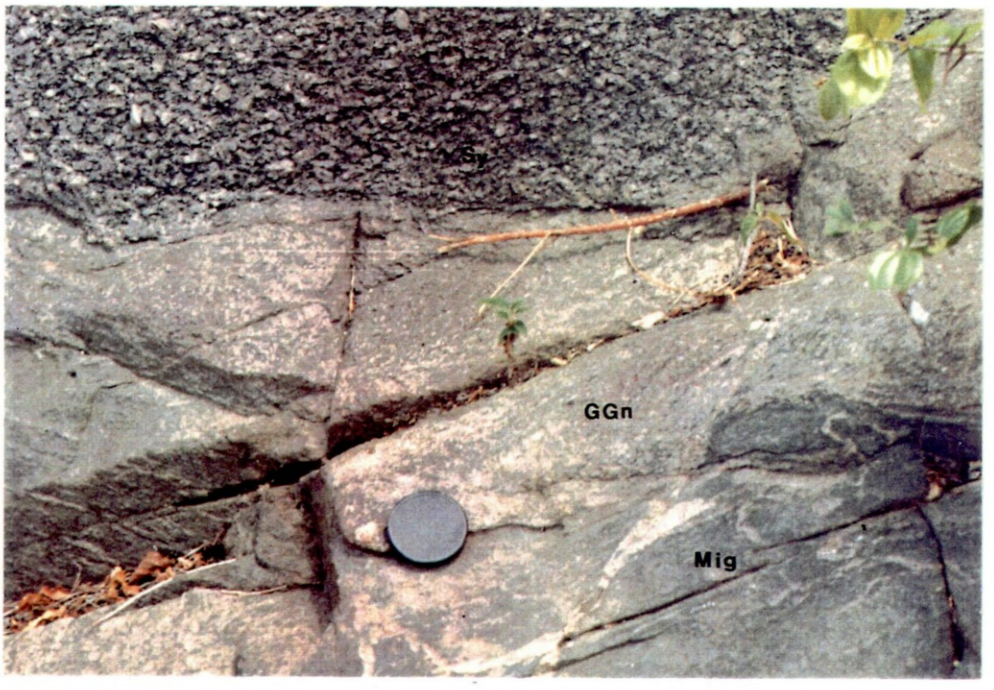


Plate 2.14 Metasedimentary enclaves showing different degrees of reaction with the mafic syenite. A) No clear reaction border is observed, B) the granite gneiss (GGr) appears to have result from the reaction between the syenite (Sy) and the enclave of migmatite (Mig).

syenite and probably representing part of the early crystallized fraction of the leuco- syenite magma

3) The most abundant fine grained to weakly porphyritic mafic enclaves.

All the igneous enclaves show sharp contacts with the enclosing syenite. A rather unusual occurrence of pillow-form dioritic enclaves, surrounded by aplitic material, has been observed in the center of the complex (see plate 2.11). Zoning within the enclaves has not been found, but near the contact with the enclosing syenites, enclaves do show a tendency to concentrated coarse amphibole crystals on their margins.

Elongation of the enclaves is quite common with aspect ratios varying between 2:1 and 5:1. Extreme elongation with aspect ratios up to 40:1 have been recorded within the mafic syenite close to its contact with the metasedimentary rocks (see plate 2.12). The foliation measured within the enclaves is generally parallel to that in the host syenite. Solid state deformation is not particularly in evidence in the more elongate types.

Metasedimentary enclaves have also been recorded within the mafic syenite, showing different degrees of reaction with the host syenite (see plate 2.14).

2.3.7.3 Pegmatites and aplites

Scattered and minor granite pegmatite dykes have been recorded mainly intruding the mafic syenite. Pegmatite veins were also observed cutting the coarse grained alkali feldspar syenite. The pegmatite dykes are more abundant along the contact between the mafic syenite and the metasediments. They are commonly quite massive, the contacts are very sharp and the width of the dykes range from 10 to 60 cm.

The pegmatites consist of K-feldspar, quartz, with small amounts of plagioclase and biotite. Minor amphibole was observed in some dykes emplaced very close to the contact with the metasediments. The dykes are generally homogeneous in composition, but a few are zoned, with feldspar concentrated at the margins and grey quartz in the

A)



B)

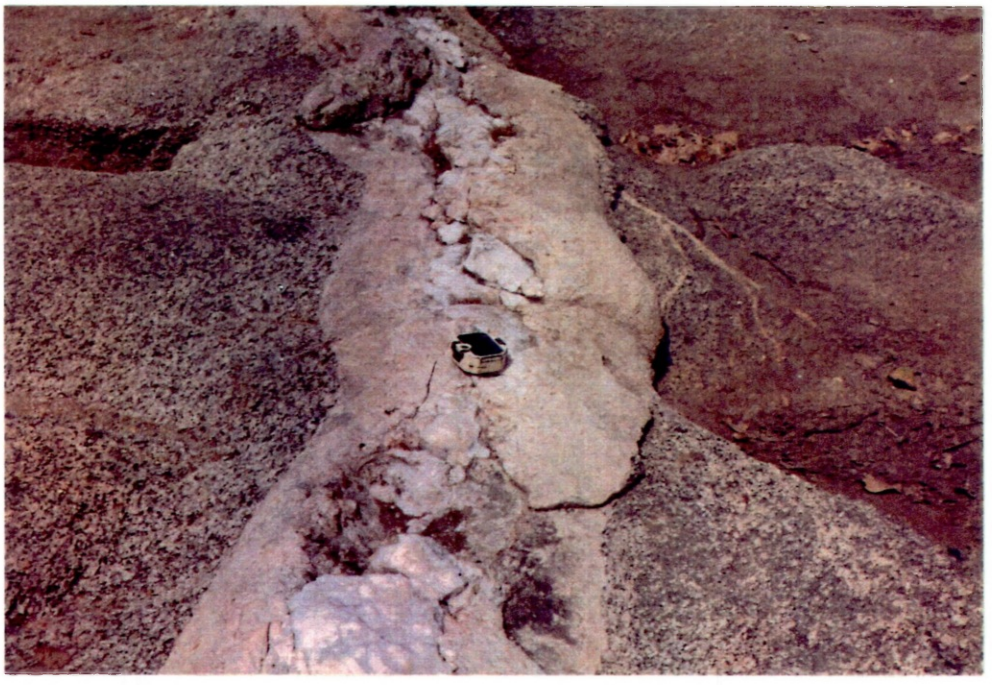


Plate 2.15 Pegmatites within the Bom Jardim complex. A) A homogeneous pegmatite dyke, B) zoned pegmatite dyke with feldspar concentrated at the margins and grey quartz at the center.

core (see plate 2.15). The grain size averages are 1-4 cm.

A small number of aplite dykes also intrude the syenite, close to the contact between syenite and pink granite. They are discordant with the foliation of syenite and, are probably related to the intrusion of the pink granite.

2.4 SUMMARY AND CONCLUSIONS

The field evidence suggests that the Bom Jardim complex crystallised from more than one pulse of magma. Mafic syenite to monzonite was the first rock type to crystallise and, this was followed by a more alkaline batch of magma which was the source of the medium grained pyroxene biotite amphibole syenite, the pyroxene biotite leuco alkali feldspar syenite and the very coarse grained brown syenite. Differentiation in situ appears to be involved in the evolution of this more alkaline magma and the coarse grained brown alkali feldspar syenite probably represents a cumulitic phase of this diferentiation process.

The fine grained monzonite with a glomero porphyritic texture seems to be contemporaneous with the intrusion of the mafic dykes and appears to represent the same batch of magma. The field relationships show clearly that these rocks are synplutonic with the mafic syenite.

The presence of vertical and sharp contacts between the syenite and pink granite suggests that the latter was the product of a late intrusive episode in the magmatic evolution of the complex.

The presence of metasedimentary enclaves partially digested by the syenite, and also reaction between the syenite and the metasedimentary wall rocks along the contact indicate that some crustal contamination has taken place.

Although the present details data of the regional geology within the province are still rather scant, the field relationships within the Bom Jardim complex together with its shape and relationship to the country rocks, suggest that the emplacement of the complex

is syn to late-kinematic with respect to the thrust tectonics associated with the Brasiliano orogeny in the Borborema province.

Chapter 3

PETROGRAPHIC CHARACTERIZATION OF THE BOM JARDIM COMPLEX ROCKS

The petrographic characterization of the Bom Jardim complex has been based on 92 thin sections. The petrographic classification of these different lithologies has been carried out using a combination of the modal amounts of quartz, alkali feldspar and plagioclase (the Q.A.P. classification of Streckeisen, 1976), the texture of the rocks and the modal percentages of the mafic phases as discussed in the previous chapter.

Modal compositions were determinated in 44 thin sections, 29 from the major facies, 6 dykes and 9 enclaves. The average modal contents of the different facies are given in table 3.1, table 3.2 and table 3.3. Individual modal analyses can be found in tables B.10 to B.16, appendix B. Microcline, perthite and albite occurring as either isolate grains or as reaction rims between plagioclase and K-feldspar have been recorded as alkali feldspar.

Table 3.1 Average modal analyses of the Bom Jardim major facies

	PBAMS	PBM	MPBAS	LPBS	GRANITES
Quartz	1.3	0.9	4.3	6.3	23.7
Alkali feldspar	33.7	27.4	54.0	71.1	44.5
Plagioclase	20.7	21.1	16.1	3.9	23.6
Biotite	18.5	27.6	12.8	9.9	5.4
Amphibole	19.3	3.2	5.5	0.5	-
Clinopyroxene	2.4	16.9	5.4	5.6	-
Zircon	0.3	0.2	0.1	0.05	0.2
Sphene	1.2	-	0.6	0.2	0.8
Apatite	1.5	1.6	0.8	0.6	0.5
Opaques	0.06	1.3	0.8	1.8	1.0

3.1 PETROGRAPHIC DESCRIPTIONS OF THE MAJOR FACIES

3.1.1 The coarse grained pyroxene biotite amphibole mafic syenites and monzonites.

This lithology is characterized by a hypidiomorphic porphyritic texture with megacrysts of alkali feldspar and less frequently plagioclase. The determined modal analyses of members of this facies shows quite a variation in petrography, especially the relative proportions of modal plagioclase and alkali feldspar.

The alkali feldspars are predominantly microcline macro and micro perthites according to Smith (1974), however mesoperthites (Michot, 1961) have also been found. Microcline without perthitic exsolution lamellae also occur as anhedral crystals restricted to the groundmass. The microcline perthite phenocrysts range in size from 0.5 cm to 2.0 cm, and usually occur as subhedral, normally zoned crystals. Inclusions of plagioclase feldspar, amphibole, biotite and opaque minerals occur in localised bands parallel to the zoning and crystal faces of the alkali feldspar. The plagioclase enclosed in many of the megacrysts of microcline perthite shows a compositional range of (An_{24} to An_{18}) and is frequently surrounded by a rim of albite (both with and without the development of myrmekite). Many of these included plagioclase grains which are clearly not in crystallographic continuity with the host microcline. In some samples, alkali feldspar has been observed replacing plagioclase (see plate 3.1). Carlsbad type twinning has also been recorded in microcline perthite phenocrysts, probably indicating crystallization as orthoclase followed by an inversion to microcline on cooling.

Some of the microcline perthite phenocrystals show ovoid cores sporadically mantled by an oligoclase rim, similar to rapakivi texture (see plate 3.2).

The plagioclase feldspar in this facies is mainly oligoclase in composition (An_{25} to An_{18}), subhedral to anhedral in shape, with some grains showing either normal or oscillatory zoning (see plate 3.3). The average

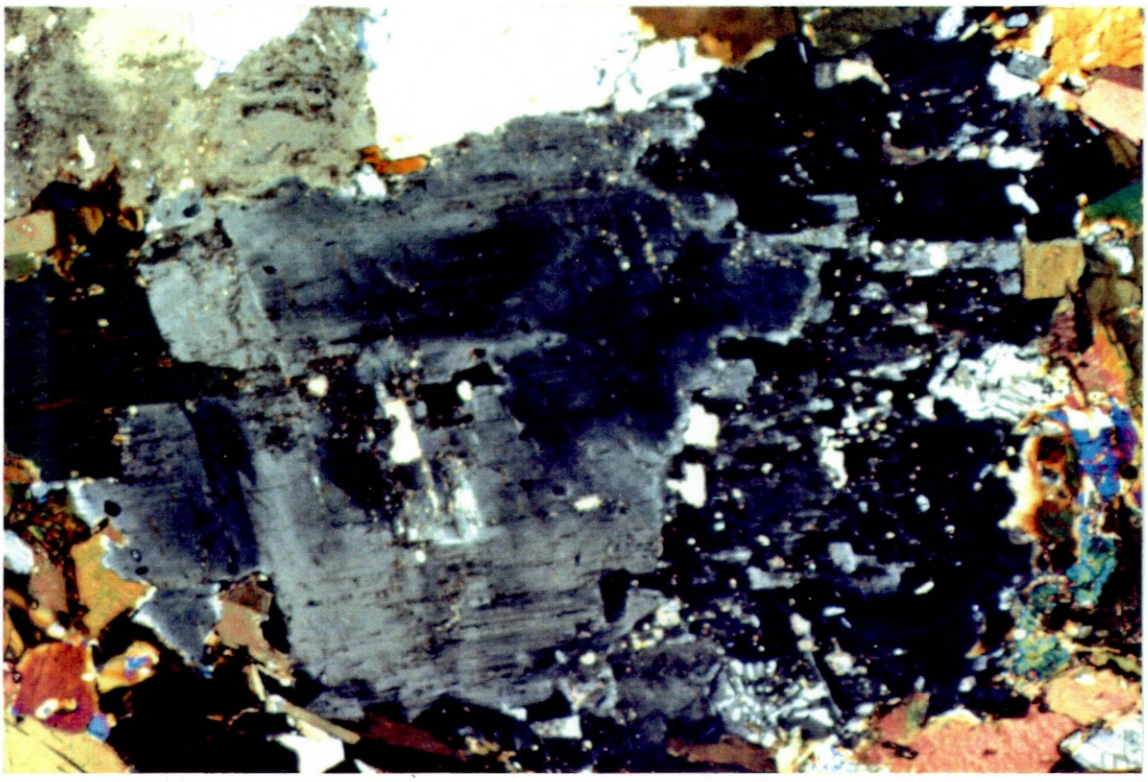


Plate 3.1 Replacement of plagioclase by alkali feldspar (microcline perthite) (PBAMS facies). Magnification X40.

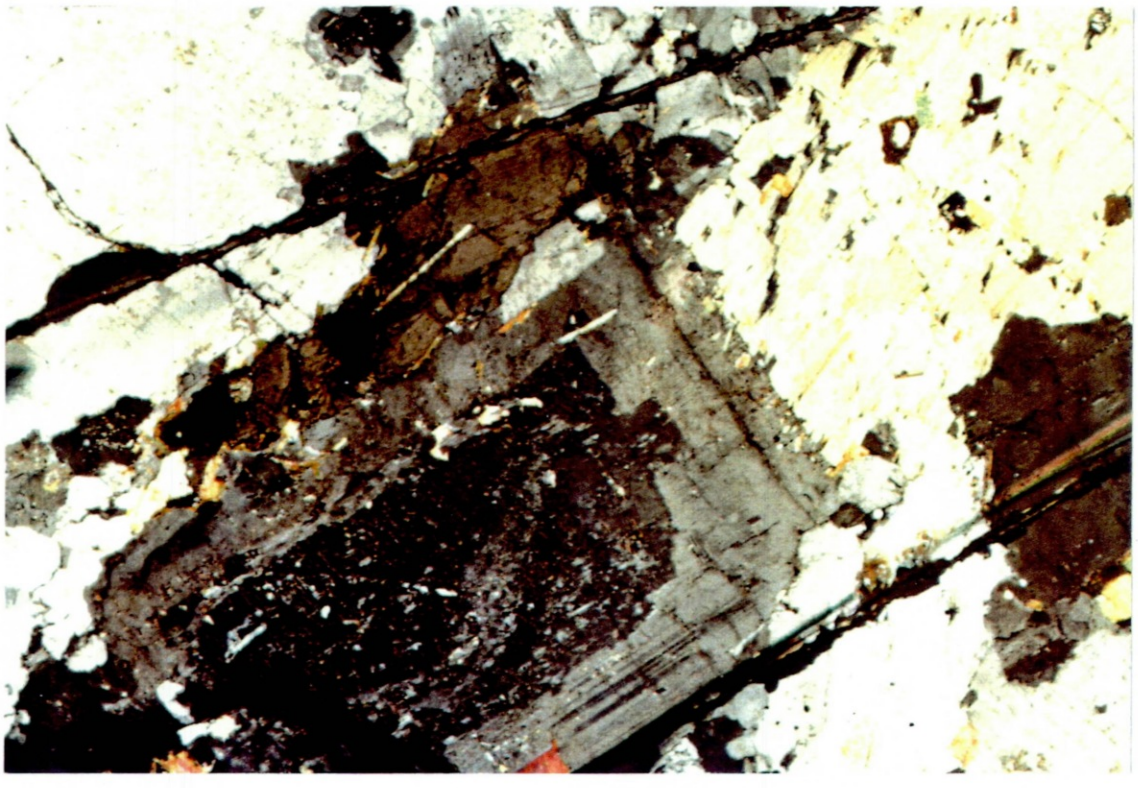


Plate 3.2 Oval shaped alkali feldspar crystal surrounded by plagioclase (rapakivi texture) within the PBAMS facies. Black parallels lines are artefacts due to thin sectioning. Magnification X20.



Plate 3.3 Zoned plagioclase phenocrysts within the PBAMS facies. Magnification X40.

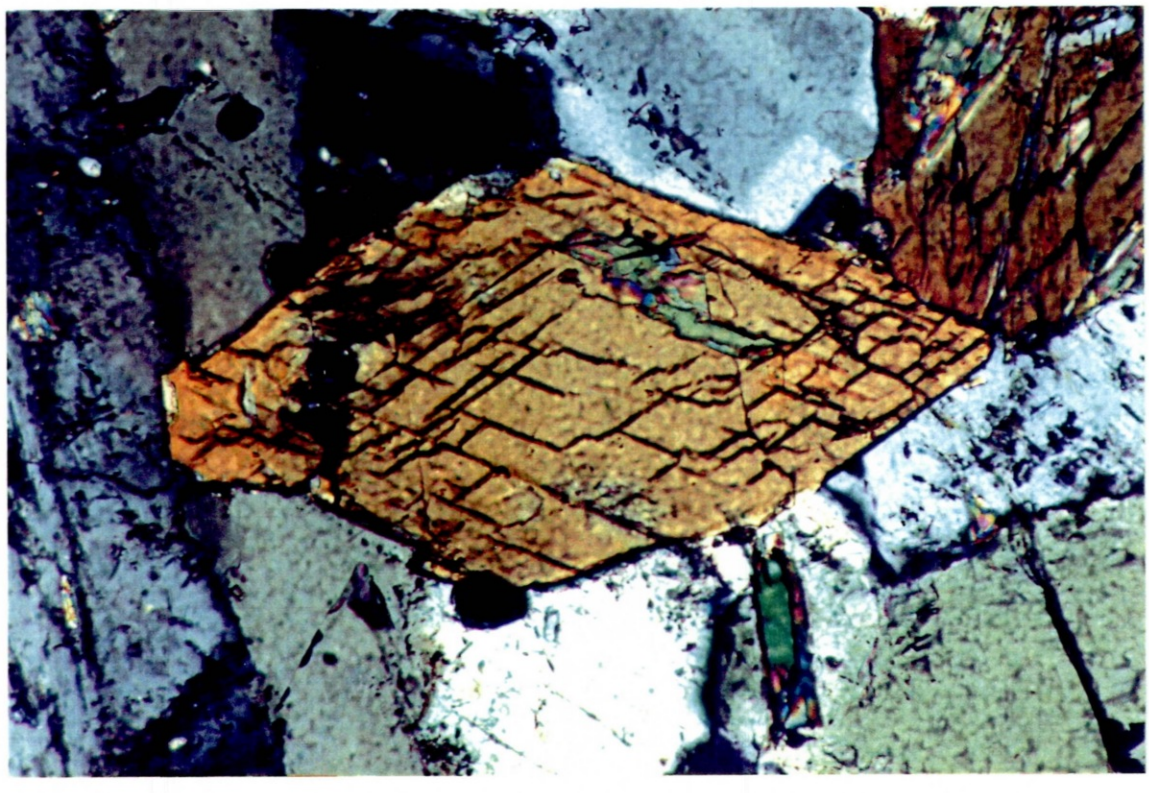


Plate 3.4 Primary amphibole within the PBAMS facies, showing secondary replacement by biotite. Magnification X160.

grain size is normally 1 to 3 mm, however in some samples the plagioclase achieves phenocrystals of size up to 1 cm. As discussed earlier some plagioclase is found as included grains in the alkali feldspar phenocrysts where it usually shows a corroded outline with the host mineral. Plagioclase associated with the myrmekitic intergrowths occurs mainly around the alkali feldspar phenocrysts. The different habits of plagioclase found within this facies suggests a fairly long crystallisation interval for this mineral. Sericitization has been observed in some grains.

Small modal percentages of quartz (usually less than 5%) are present (see table 3.1). The quartz usually occurs as small anhedral grains in the groundmass and frequently displays undulose extinction. Occasionally, small drop-like inclusions of quartz have been observed with the alkali feldspar phenocrysts.

The amphiboles present in these rocks are mainly hornblendes, magnesio hornblende to edenite in composition (Deer et al., 1980). However some actinolitic hornblende has been observed replacing pyroxene, and is obviously the product of a sub-solidus reaction. The igneous amphiboles occur both as anhedral to subhedral grains either intimately associated with clinopyroxene or as isolated grains with no obvious relationship with the later mineral (see plate 3.4). Clearly from the textural relationships the amphibole crystallised after the pyroxene. The isolated amphibole grains are frequently poikilitic with inclusions of apatite and zircon. Some members of this facies show a localised development of a simplectic intergrowth of amphibole and quartz replacing the earlier pyroxene.

The clinopyroxenes are dominantly of salite composition (Wo_{46} En_{41} Fs_{13} to Wo_{48} En_{38} Fs_{14}) and occur mainly as slightly zoned subhedral grains. Inclusions of magnetite are quite common. Corona-type textures with pyroxene mantled by amphibole are also quite common, as discussed above. This reaction relationship frequently goes almost to completion (see plate 3.5), resulting in a tiny relict core of pyroxene within the amphibole (see MacKenzie et al., 1982). According to Ernst (1966), amphibole reaction rims around pyroxenes occur mainly in response to

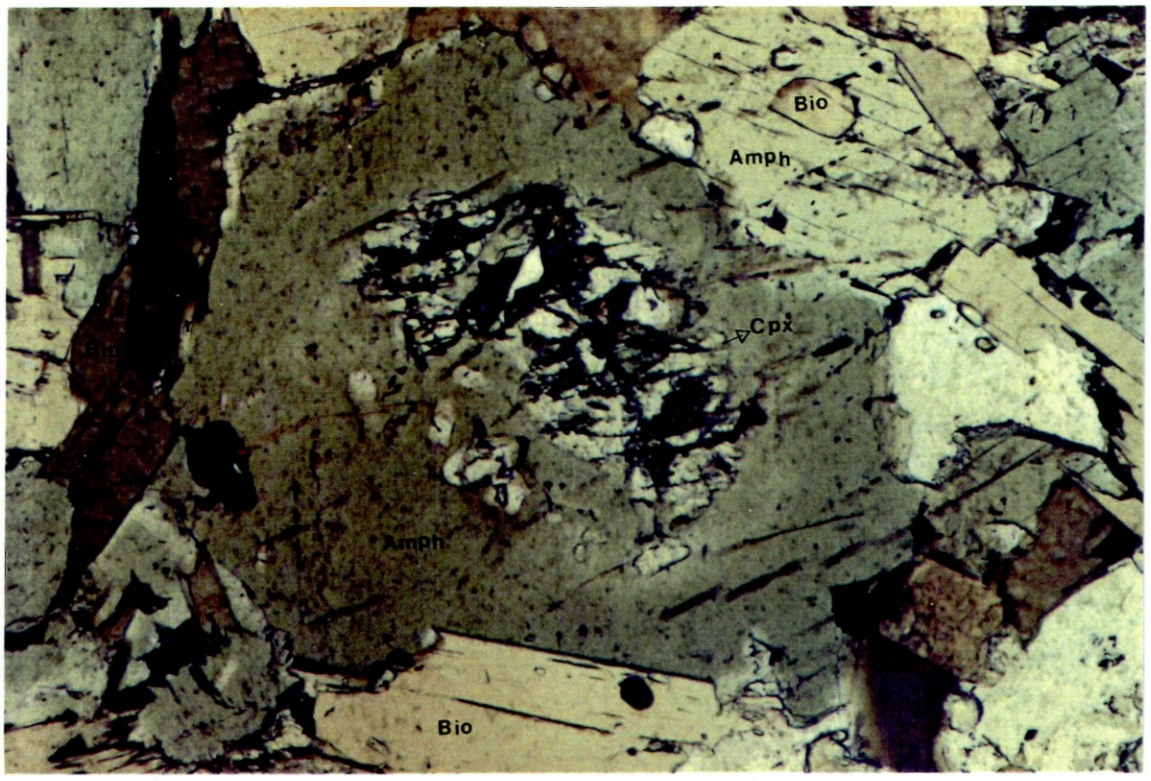


Plate 3.5 Relicts of clinopyroxene within amphibole, in the PBAMS facies. Magnification X40.

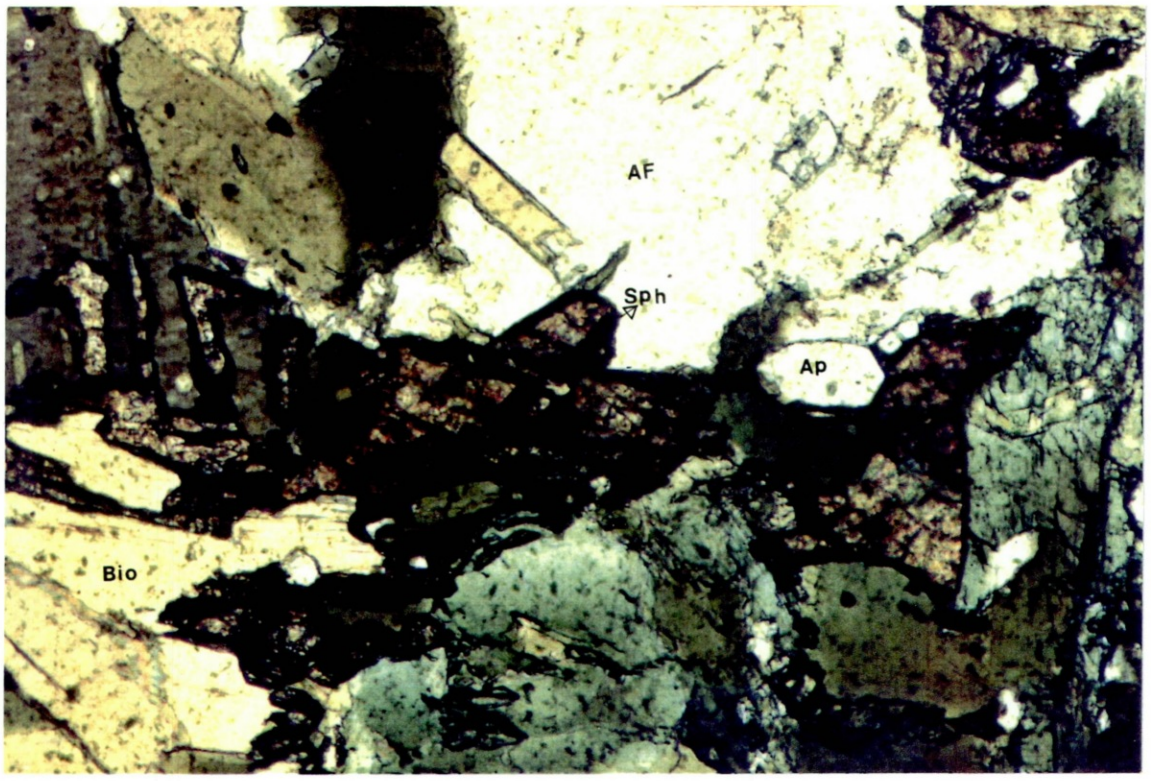


Plate 3.6 Secondary sphene developed along the amphibole cleavage (PBAMS facies). Magnification X128.

falling temperature and fO_2 and rising of PH_2O in the liquid, usually following a prolonged history of anhydrous phase crystallization.

Biotite commonly occurs as subhedral plates scattered throughout the rock and occasionally as a replacement product after both pyroxene and amphibole. It is strongly pleochroic, varying in colour from pale to dark brown. In some samples the biotites tend to show a rather corroded outline when found in contact with the alkali feldspar. Pleochroic haloes around both zircon and monazite have also been observed. Of the accessory minerals apatite is by far the most abundant. It is usually present as early formed small euhedral crystals. Other apatites with a very high aspect ratio of greater than 10:1 have been found as inclusions in both pyroxene and biotite. Wyllie et al. (1962), Spry (1969) and Nedelec and Paquet (1981) have interpreted such a habit as possibly indicative of a fairly rapid early cooling of a magma.

Both primary and what appears to be secondary sphene (see plate 3.6) have been observed in the rocks of this unit. From textural evidence the primary sphene appears to form late in the crystallisation interval. Zircon is present in low modal abundance (less than 0.6%). It is usually very well shaped, without any evidence of zoning and almost always found as inclusions in both biotite and amphibole. Allanite has been recorded within this facies but it is not particularly widespread in occurrence. It is found both as metamictic and non-metamictic subhedral to anhedral grains in the groundmass and is sometimes found surrounded by epidote (see plate 3.7). The accessory mineral monazite has also been observed, it has both a low modal abundance and a very localised occurrence, most frequently occurring as rounded inclusions in biotite (see plate 3.8).

The presence of monazite in granitoids, has been regarded by many authors to signify an "S"-type origin (Chappell and White, 1974) for the suite. However, the typical mineral assemblage of such granitoids normally comprises ilmenite+ biotite + muscovite $\pm$ cordierite $\pm$ garnet $\pm$ monazite (Chappell and White, 1974; White and

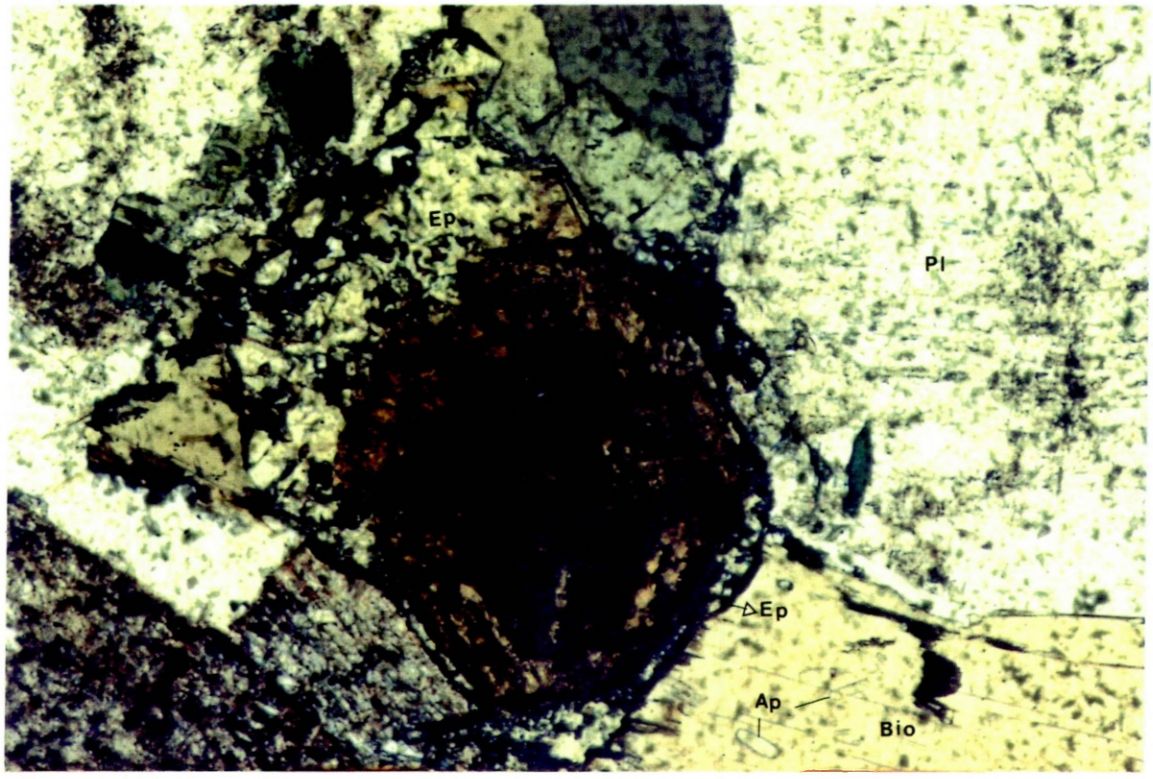


Plate 3.7 Allanite surrounded by epidote (Ep) (PBAMS facies). Magnification X128.

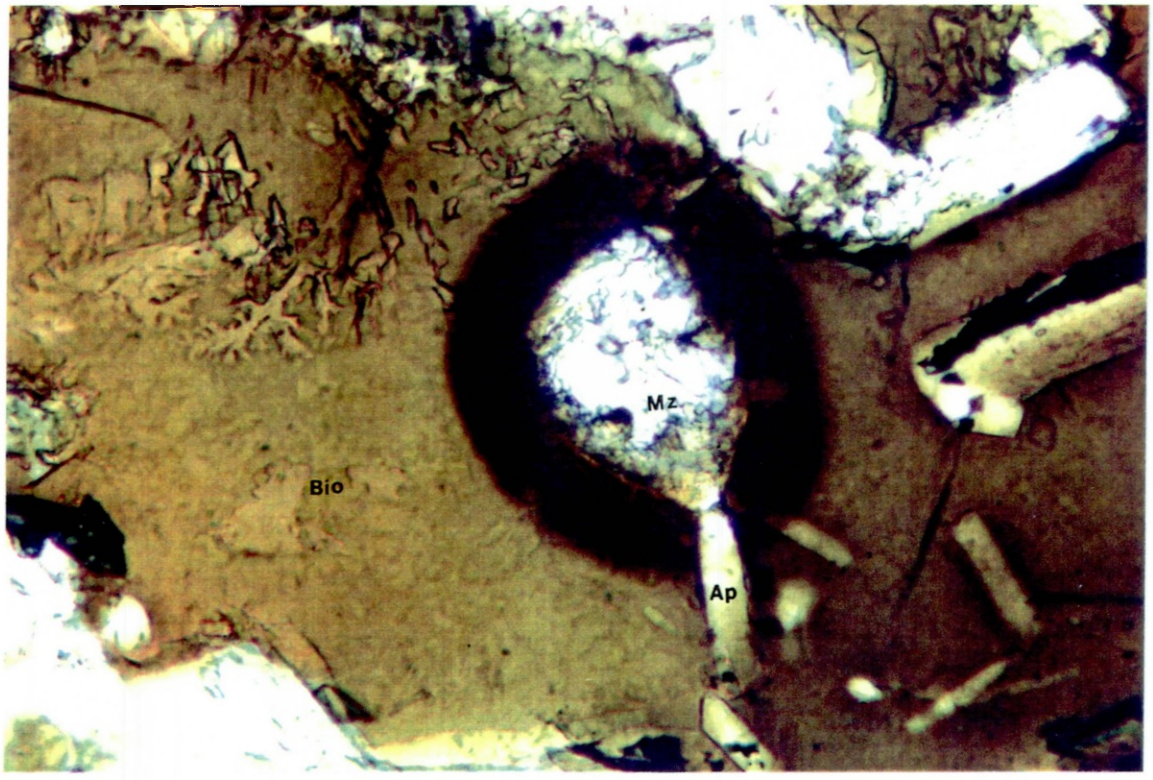


Plate 3.8 Oval shaped monazite (Mz) (PBAMS facies) developing pleochroic haloes in the host biotite. Magnification X252.

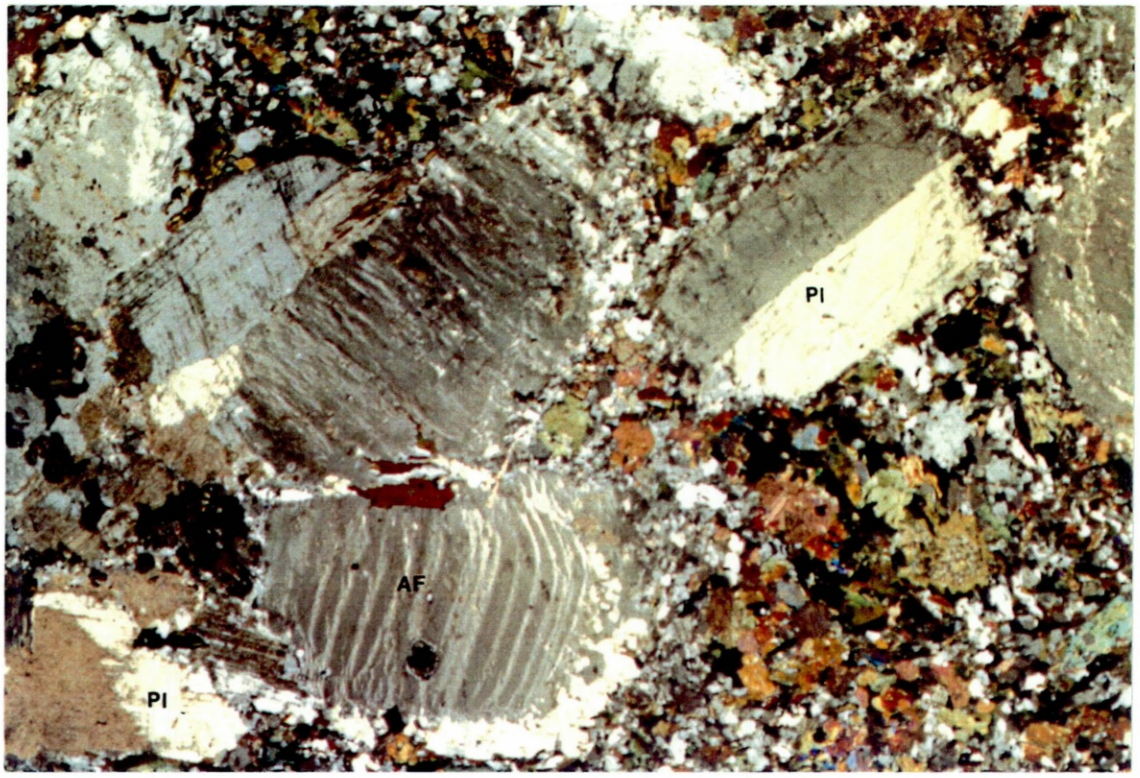


Plate 3.9 Localized clots of alkali feldspar and plagioclase in a fine grained variation of the PBAMS facies. Magnification X12.

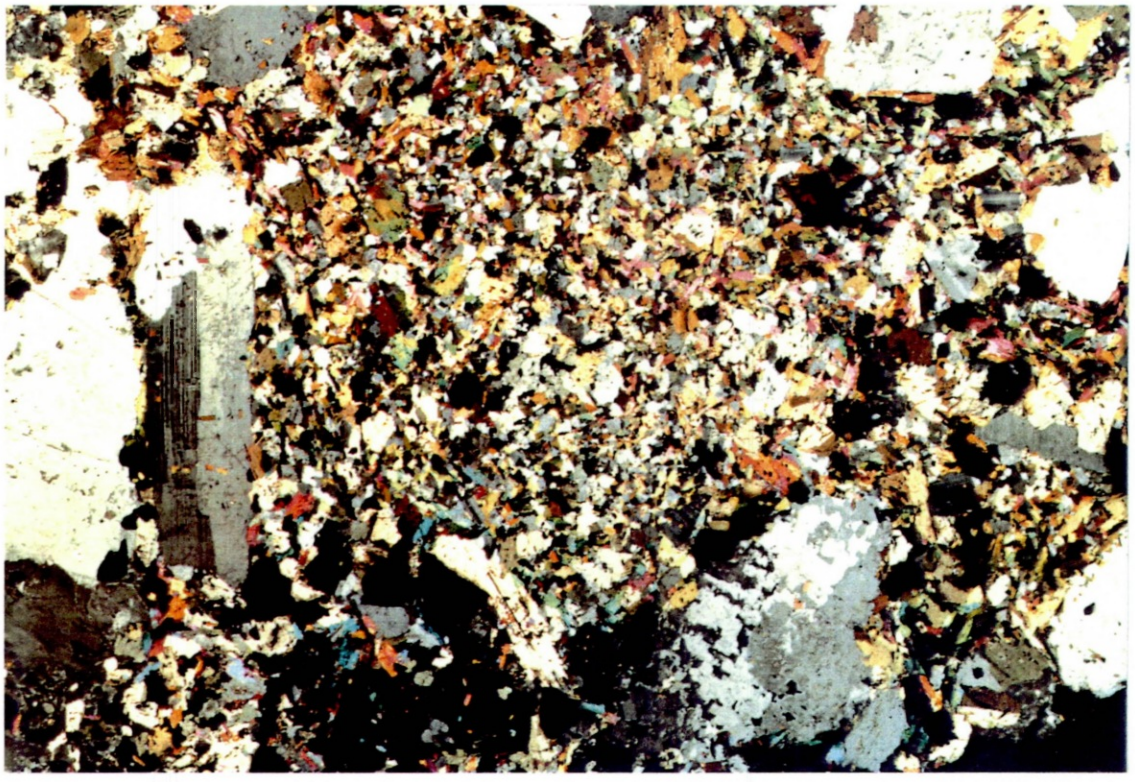


Plate 3.10 Globular masses of fine grained mafic syenite within the PBAMS facies. Magnification X6.

Chappell, 1977 and Pitcher, 1983). In contrast, the mineral assemblage recorded in the mafic syenites and monzonites of the Bom Jardim complex, consists of amphibole + biotite + pyroxene + magnetite ± allanite ± monazite, which is more typical of "I"- type cordilleran granitoids (Pitcher, 1983). The presence of rounded monazites within the Bom Jardim complex is interpreted by the present author as evidence of crustal contamination rather than an origin based primarily on the partial melting of a metasedimentary source.

The major opaque phase in these rocks is magnetite, although some crystals of pyrite have occasionally been observed as inclusions in amphibole.

Epidote is very rare and when present usually occurs as anhedral crystals associated with plagioclase. Only one grain has been recorded as an inclusion in biotite. The textural evidence indicates that this mineral is not a magmatic phase.

In certain members of this facies, clots of alkali feldspar and plagioclase have been observed enclosed in a more mafic fine grained syenite (see plate 3.9); at the interface there is clear evidence of a reaction rim. Globular masses of a very fine grained mafic syenite have also been observed within the PBAMS (see plate 3.10). Such features could indicate a limited amount of hybridisation between the PBAMS and a more mafic syenite magma.

3.1.2 The pyroxene biotite monzonites (PBM)

This rock type was distinguished from the monzonites described in the previous section by the absence of primary amphibole and a larger modal content of clinopyroxene. The lithology shows a hypidiomorphic porphyritic texture with subhedral phenocrysts of microcline perthite and plagioclase feldspar.

The alkali feldspar in this rock is predominantly made up of microcline perthite phenocrysts, often attaining a size of 1 cm. In the groundmass both microcline and microcline microperthite can be found. The phenocrysts of microcline perthites always show inclusions

of biotite and/or opaque minerals. The plagioclase feldspar is again of oligoclase composition varying from An_{24} to An_{18}. The crystals are generally subhedral and normally zoned, with sizes varying from 5mm to 1mm. Myrmekite is very occasionally observed in the margins of the alkali feldspar phenocrysts. The modal quartz content in these rocks is usually less than 1.0 percent and occurs as interstitial xenomorphic crystals showing undulose extinction.

The clinopyroxene is the second most abundant mafic phase in the rocks after biotite and averages about 18.7%. It is salitic in composition (Wo_{48} En_{39} Fs_{13} to Wo_{42} En_{42} Fs_{16}) and, subhedral to anhedral in shape. The pyroxene undergoes two types of late replacement: biotite can be seen replacing the pyroxene both within and along the margins of the grains (see plate 3.11) and secondly a pale green actinolitic amphibole has been observed replacing the pyroxenes in a small number of specimens.

Biotite is often the most abundant phase in these rocks averaging approximately 28 modal percent. It is strongly pleochroic and commonly contains inclusions of pyroxene, apatite, zircon and opaque minerals. In some samples the boundaries with alkali feldspar are often very irregular giving an almost corroded appearance.

Apatite is by far the most commonly occurring and abundant accessory mineral, and usually occurs as euhedral crystals included in both biotite and pyroxene. Zircon is present usually as small euhedral crystals, although occasionally very rounded grains have been observed. The most commonly occurring opaque mineral is magnetite. It is normally found in close association with both biotite and clinopyroxene, although as previously mentioned it does also appear as inclusions in the alkali feldspar. Trace amounts of allanite have also been observed in some rocks but its distribution is very sporadic. Rounded crystals of monazite have also been observed, they normally contain large pleochroic haloes and are found either partially or totally enclosed by biotite.

3.1.3 The medium grained pyroxene biotite amphibole syenites (MPBAS)

This lithology normally displays a medium grained xenomorphic to hypidiomorphic fabric with an occasional tendency towards a slightly porphyritic texture. The average grain size is approximately 4.0 mm. The apparent porphyritic texture occasionally observed in handspecimen, is actually produced by localised clots of alkali feldspar, plagioclase and sometimes quartz when viewed under the microscope, although very rarely true single phenocrysts of alkali feldspar have been observed.

Modal analyses have shown that the alkali feldspar varies in modal content from 47% to 63% and plagioclase from 9% to 14%. However samples collected from the village of Joao Alfredo (IG-62 and IG-65) show modal plagioclase contents varying from 23% to 29%. The phenocrysts are predominantly microcline perthite, subhedral to anhedral in shape. Large crystals of plagioclase are not common. The larger tablets of perthite usually contain quite a number of matrix grains. Microcline without any perthitic exsolution is restricted to the groundmass.

The plagioclase feldspar (An_{19} to An_{11}) occurs as subhedral grains with a weakly developed normal zoning pattern. Albitic rims are frequently observed along the grain boundaries with the microcline perthite, and such rims are always in crystallographic continuity with the plagioclase. According to Smith (1974) these rims are commonly the result of subsolidus reequilibration. Myrmekite is usually found near the edges of the perthite phenocrysts, but inclusions of myrmekite actually within the phenocrysts are not uncommon.

Quartz always occurs as an interstitial phase, amounting to about 6% modal percent.

Salitic pyroxene (Wo_{48} En_{38} Fs_{14} to Wo_{41} En_{41} Fs_{16}) is present as subhedral slight zoned crystals amounting to about 14% modal percent. The pyroxenes often show replacement by both biotite and amphibole. The majority of the amphibole present however, is not

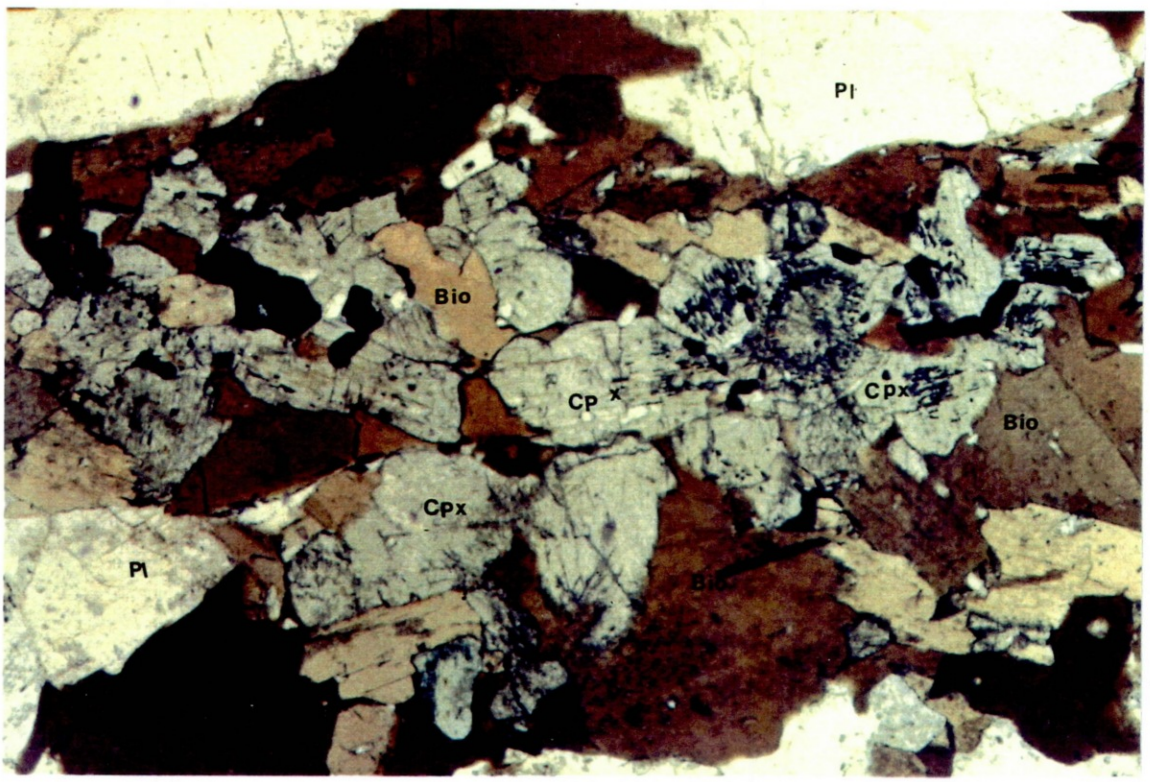


Plate 3.11 Micro textural features within the PBM facies. Clinopyroxene (Cpx) and plagioclase (Pl) surrounded by biotite (Bio). Magnification X12.

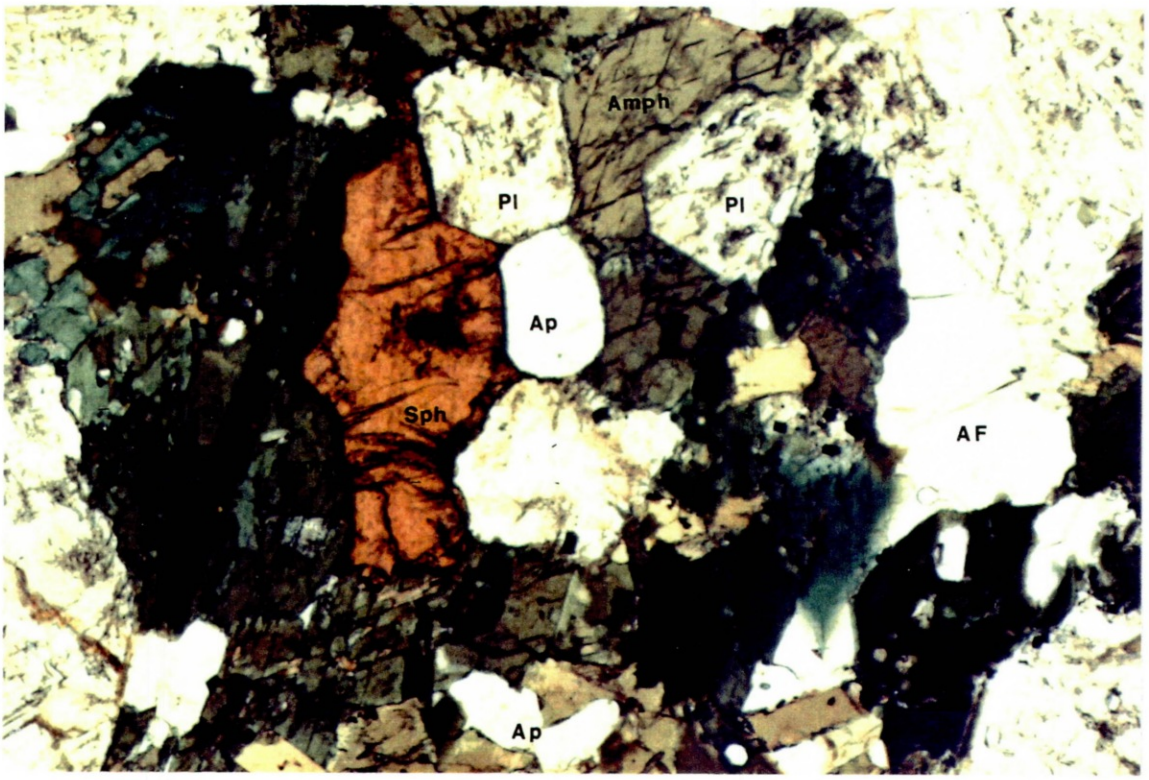


Plate 3.12 Amphibole enclosing apatite (Ap) and plagioclase (Pl). Sphene is clearly later and related to the amphibole. (MPBAS facies). Magnification X40.

associated with pyroxene and occurs as brown pleochroic isolate subhedral grains. The amphiboles present in samples from the villages of Umari and Joao Alfredo have all the features of a primary igneous phase.

Biotite normally constitutes about 10.0 modal percent in the rocks. It occurs as subhedral brown poikilitic plates containing inclusions of euhedral apatite and zircon. Mafic clots of biotite and amphibole containing apatite inclusions have also been observed.

Both primary and secondary sphene occurs in these assemblages, their colour varies from almost colourless to a deep orange (see plate 3.12). The euhedral primary sphene contains inclusions of both apatite and amphibole. Sphene has also been observed forming rims around the Fe-Ti oxides. Fowler (1985) considers this particular association to be due to the reaction of a late stage circulating fluid carrying incompatible elements with the opaque phase.

Apatite and zircon are both normally present as euhedral inclusions in the constituent phases suggesting an early magmatic crystallization. Rounded monazites and subhedral to anhedral thorium minerals, including thorite, have also been observed but tend to have a very localized occurrence. The accessory mineral allanite is also present as xenomorphic to subidiomorphic metamictic crystals occurring as both inclusions in amphibole and as isolated groundmass grains.

The opaque minerals are mainly magnetite with occasional localised Fe-Ti oxide.

3.1.4 The pyroxene biotite alkali feldspar leuco syenites (PBLS)

This lithology contains less than 20.0% modal percent of the mafic minerals biotite and pyroxene. It generally shows an equigranular medium grained hypidiomorphic texture, however locally some porphyritic varieties have been found showing a preferred orientation of prismatic subhedral phenocrysts (up to 5 mm) of

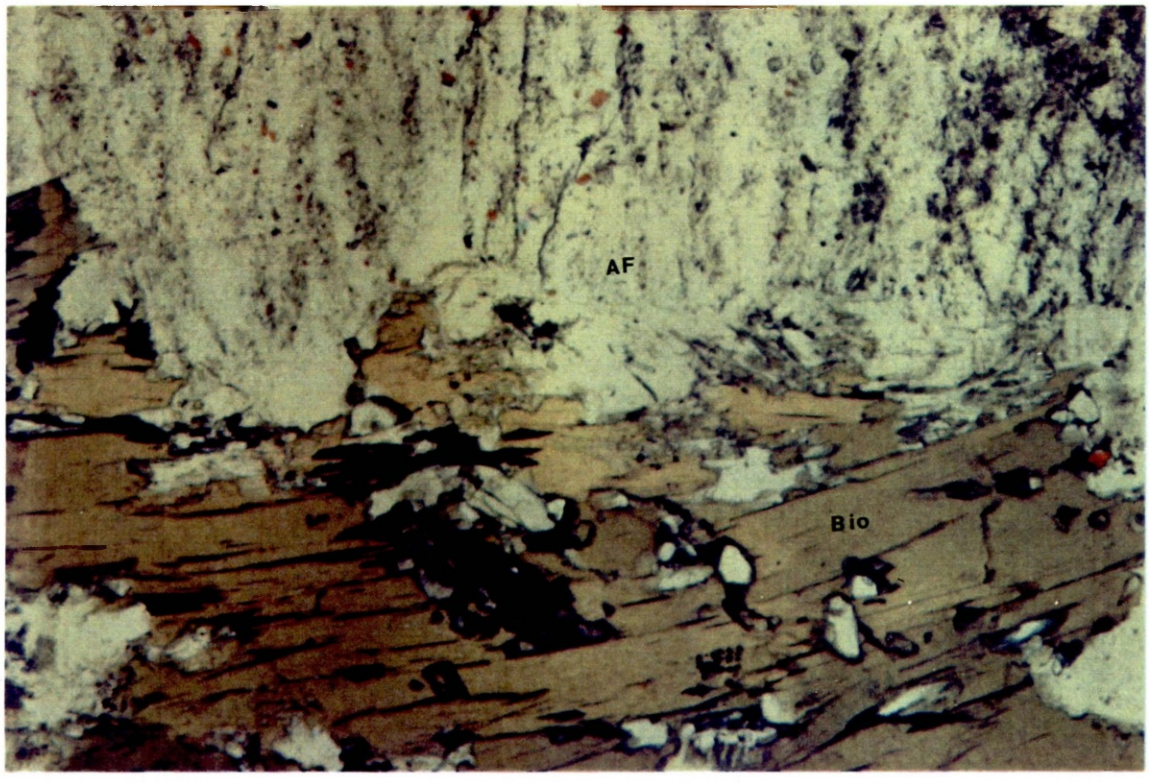


Plate 3.13 Reaction between biotite and a later crystallised Alkali feldspar (PBLS facies). Magnification X64.

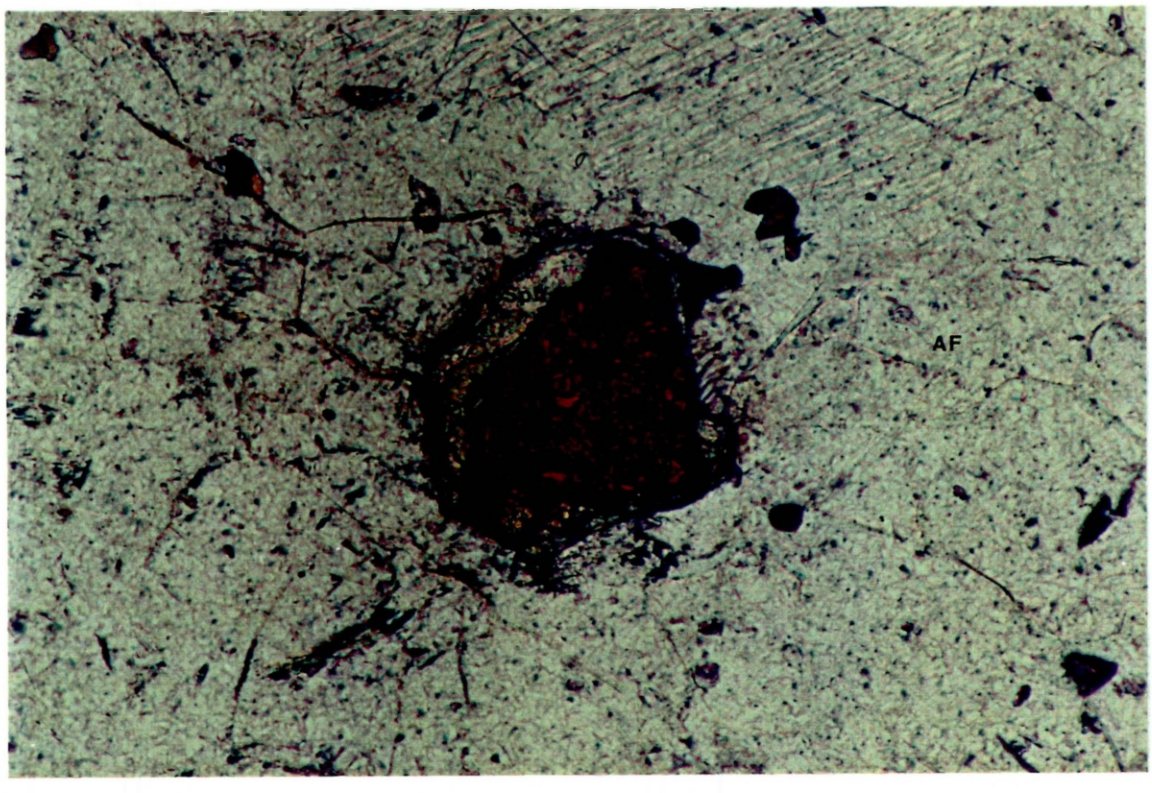


Plate 3.14 Sphene developed as a reaction rim around Fe-Ti oxide. (PBLS facies). Magnification X16.

microcline perthite.

The predominant mineral in this facies is alkali feldspar (microcline perthite) with modal contents ranging up to 74.0%. It always has a "dusty" appearance with inclusions of a translucent red mineral (probably hematite) lying along (010) together with magnetite, apatite, pyroxene and biotite. Zoning of the feldspar is quite common throughout this lithology. Large (2cm in average) rectangular crystals of alkali feldspar have been observed concentrated near the contact with the coarse grained brown alkali feldspar syenite.

Albitic plagioclase (An_{10} to An_0) occurs as small (0.5 to 1.0 mm) subhedral clear unzoned crystals, occasionally associated with a myrmekitic intergrowth.

Quartz is again restricted to the matrix, where it occurs as anhedral grains showing undulose extinction. Modally quartz makes up about 7.0 percent of the rock.

The mafic phases in this lithology are mainly biotite and salitic pyroxene (Wo_{48} En_{35} Fs_{17} to Wo_{43} En_{37} Fs_{19}). The biotite occurs as subhedral to anhedral poikilitic plates with numerous inclusions of pyroxene. Reaction between biotite and later crystallized alkali feldspar are quite common (see plate 3.13). A pale green secondary actinolite amphibole has also been observed replacing the pyroxene. A much deeper green variety of amphibole has also been found locally again mantling the pyroxene.

The most abundant accessory mineral is apatite. (normally making up 1.5 modal percent of the rock). It occurs both as euhedral inclusions in biotite, pyroxene and alkali feldspar and as well shaped grains in the groundmass. Much rarer apatites showing high aspect ratio (up to 8:1) have again been observed locally as inclusions in some of the mafic phases.

Deep orange sphene occurs both as euhedral single grains in the groundmass and occasionally as rims to Fe-Ti oxides (see plate 3.14). They are clearly one of the latest phases to crystallise.

Distinctly metamictic thorium rich minerals with subhedral to anhedral outlines and colours ranging from

deep yellow to brown have been recorded in all samples studied (see plate 3.15). Anhedral crystals of allanite are present, but have a very sporadic occurrence.

3.1.5 The coarse grained brown alkali feldspar syenites (CS).

This rock type is characterized by a porphyritic texture with large phenocrysts of alkali feldspar (3cm in average). The estimated modal compositions determined at outcrop indicate that the phenocryst contents vary from 60 to 90 percent of the total rock. There is also a strong tendency for the percentage of phenocrysts to decrease from the centre to the margins of the body. Maranhao (1980) observed a similar decrease in the modal content of alkali feldspar phenocryst with depth from a bore hole at the Minerios de Pernambuco Mine.

In thin section, the phenocrysts are composed of zoned microcline perthite with irregular outline (see plate 3.16). They have a "dusty" appearance brought about by numerous inclusions of acicular opaque minerals. Inclusions of subhedral amphibole, biotite, pyroxene and opaque minerals tend to form a concentric zonal arrangement within the grains. There does not appear to be any relationship however between the elongation of the inclusions and the faces of the host phenocryst.

The groundmass mainly consists of subhedral to anhedral albitic plagioclase often showing a relationship with myrmekite when it borders onto the alkali feldspar phenocrysts. Anhedral quartz together with plates of biotite and anhedral pyroxene and amphibole are also present.

Pyroxene is the most modally abundant mafic phase in this lithology and has a salitic composition (Wo_{45} En_{32} Fs_{23} to Wo_{46} En_{34} Fs_{20}). Simplectic intergrowths of amphibole and quartz have been observed locally replacing the pyroxene. In a number of samples biotite has also been observed replacing pyroxene both within and on the margins of the pyroxene grains. Primary amphibole is not a common constituent in the members of this lithology.

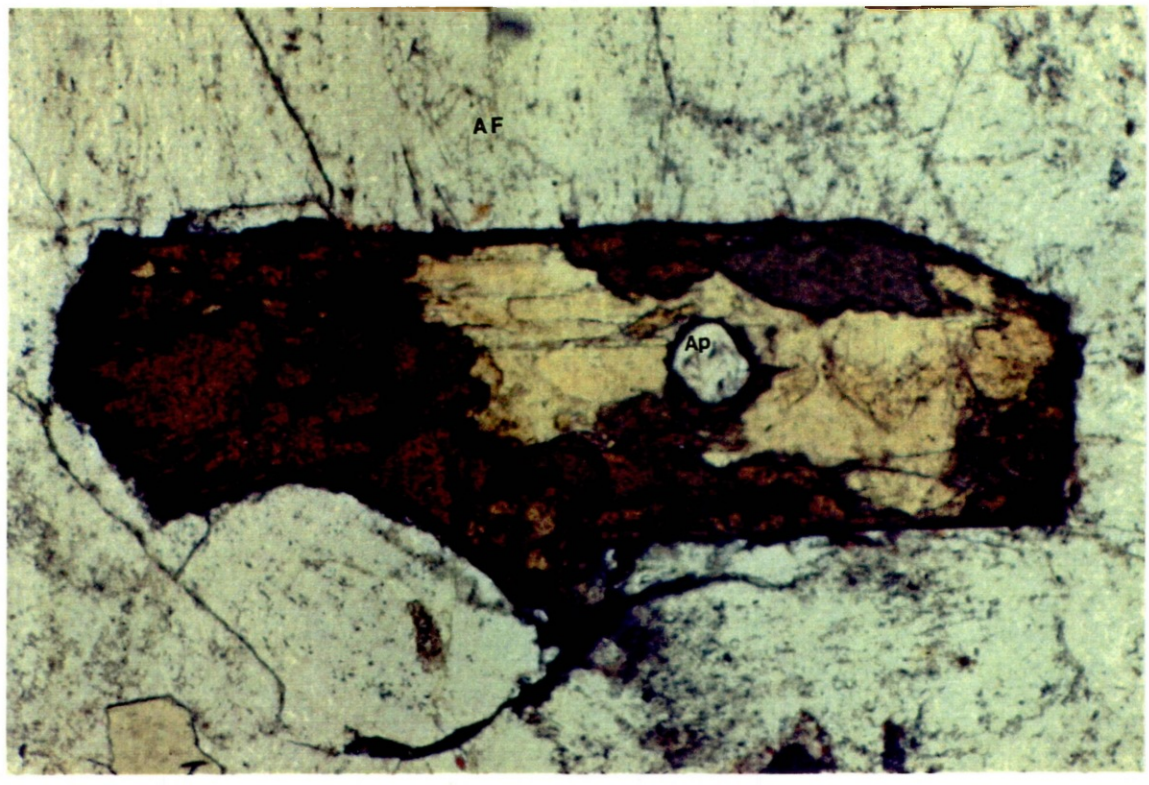


Plate 3.15 Th and LREE rich sphene enclosing apatite (PBLS facies). Magnification X100.



Plate 3.16 Zoned alkali feldspar, showing a distinct alternating zonal distribution of coarse and fine perthite. (CS facies). Magnification X12.

Euhedral apatite and zircon occur both as inclusions in biotite, amphibole and alkali feldspar and as isolate grains in the groundmass. Both primary and secondary occurences of sphene have been recorded, the mineral also occurs as rims around Fe-Ti oxides associated with biotite. Euhedral grains of magnetite are the main opaque phase present, usually found as small inclusions in the phenocrysts as well as in the groundmass.

3.1.6 The pink granites

The granites are generally leucocratic medium to fine grained rocks (average grain size 2mm) with a xenomorphic equigranular texture. The main mafic phase is biotite which usually makes up approximately 9.0 modal percent of the rock.

The alkali feldspar is modally the most abundant phase in the rocks (averaging 44.5%). It is mainly represented by anhedral crystals of microcline and microcline perthite. The alkali feldspars frequently show inclusions of plagioclase feldspar which have developed an albite rim at the interface with the host crystal, inclusions of biotite and zircon are common as is the association with myrmekite.

The modal abundance of quartz is quite variable, ranging from 17.0 to 33.0 percent, it is usually xenomorphic in shape and shows undulose extinction. Inclusions of euhedral zircon are not uncommon.

Plagioclase feldspar is approximately equal in modal abundance to quartz (approximately 23.6%), and shows a narrow compositional range of oligoclase composition (An_{19} to An_{17}). The subhedral to anhedral shaped grains frequently contain inclusions of both allanite and sphene. Alteration to sericite and epidote is noticeable in many of the samples.

A green-brown biotite is the only major mafic phase in this lithology (averaging 5.4 modal percent). The anhedral flakes of biotite often exhibit rather corroded boundaries when in contact with the alkali feldspar. Inclusions of euhedral zircon are quite common but apatites

are quite rare, and are usually only recorded as inclusion phases in the felsic minerals. Sphene is usually present as deep orange euhedral isolate crystals, as well as rims around Fe-Ti oxides as previously described. Allanite occurs in trace amounts. It is very sporadic in distribution, and is occasionally rimmed by epidote. Trace amounts of thorium rich minerals are common throughout this lithology.

3.2 The minor facies

3.2.1 Igneous enclaves

Petrographically four groups of igneous enclaves have been recognized within the Bom Jardim complex;
Group 1 - Diorites with less than 3 modal percent pyroxene.
Group 2 - Monzodiorites and monzonites with modal percentages of amphibole and pyroxene consistently greater than biotite.
Group 3 - Mafic syenites.
Group 4 - Pyroxene biotitites.

The average modal contents of each enclave group are given in table 3.2.

Table 3.2 Average modal analyses of the Bom Jardim enclaves

	GROUP 1	GROUP2	GROUP 3	GROUP 4
Quartz	0.5	-	-	1.3
Alkali-feldspar	3.0	36.6	23.5	8.2
Plagioclase	40.6	15.0	22.6	0.1
Amphibole	24.0	11.6	19.0	5.1
Biotite	29.5	26.4	25.3	58.1
Clinopyroxene	1.1	9.1	5.3	26.0
Sphene	0.4	0.1	1.9	-
Apatite	0.5	0.3	0.4	1.1
Opaques	0.3	0.4	0.1	-
Zircon	0.05	0.1	0.1	-

3.2.1.1 Group 1 enclaves

The enclaves from this group have only been observed within the PBAMS lithology. They are always fine grained (with grain sizes of 1mm on average), equigranular hypidiomorphic to xenomorphic in texture. Crystals of microcline perthite are fairly rare and when they do occur they tend to be poikilitic with inclusions of biotite and apatite.

Plagioclase (An_{33} to An_{21}) occurs as subhedral to anhedral crystals with inclusions of apatite and biotite. Zoning has been observed but it is not common.

The ferromagnesian minerals are mainly biotite and amphibole with average modal contents of 26 and 24 percent respectively. Zoned clinopyroxene (Wo_{46} En_{42} Fs_{12} to Wo_{45} En_{41} Fs_{13}) was observed showing a partial replacement by a secondary actinolitic amphibole.

Apatite and sphene are the most common accessory minerals, extremely acicular apatite is however rare. Anhedral sphene mainly occurs along the cleavage traces of biotite. Euhedral crystals of zircon are found as inclusions in biotite often associated with large pleochroic haloes. Allanite has also been observed as subhedral metamictic grains occasionally surrounded by epidote.

Magnetite is the only opaque phase and normally occurs as euhedral to subhedral grains in the matrix.

3.2.1.2 Group 2 enclaves

The second group of igneous enclaves and the most abundant have been found in all facies except in the granites. The contacts between the enclave and host syenite are generally sharp and show no signs of a reaction (see plate 3.17). They display a micro porphyritic texture with phenocrysts of plagioclase (An_{27} to An_{23}) 3mm to 5mm in size, containing frequent inclusions of biotite, concentrically arranged and parallel to the crystal faces of the host plagioclase. Occasional inclusions of microcline perthite have also been observed. In some

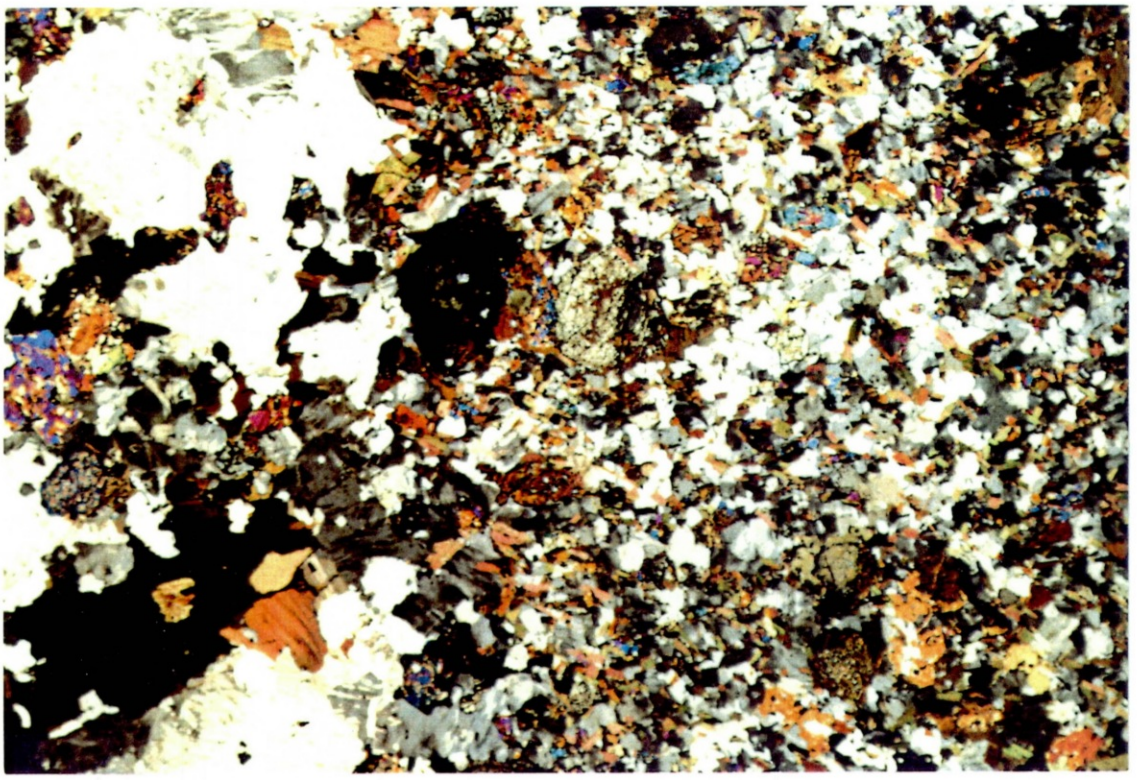


Plate 3.17 Contact between a mafic enclave (right) and the host leuco syenite (PBLS). Notice the lack of any significant reaction zone between the two. Magnification X12.

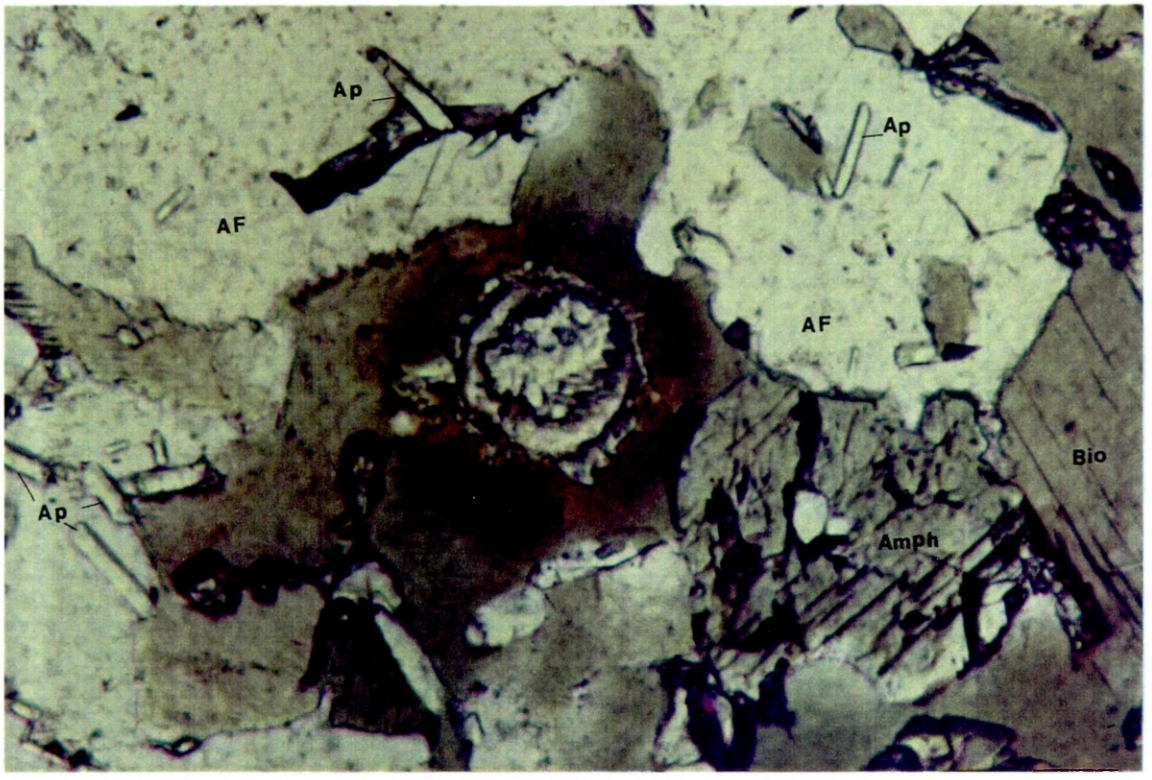


Plate 3.18 Monazite hosted by biotite within an enclave. Note the elongate crystals of apatite (Ap) enclosed by alkali feldspar (AF) and secondary sphene (Sph). Magnification X252.

samples micro phenocrysts of euhedral pyroxene (Wo_{47} En_{41} Fs_{12} to Wo_{42} En_{46} Fs_{12}) have been found showing a partial replacement by both biotite and amphibole.

The matrix with an average grain size of 0.4mm consists of microcline and microcline microperthite, subhedral unzoned plagioclase feldspar varying in composition from An_{19} to An_{22}, and small flakes of a green - brown biotite (showing a preferred orientation), together with subhedral pyroxene and amphibole.

The amphibole ferro hornblende occurs as a magmatic replacement of pyroxene and also as large poikilitic crystals forming localised clots often in association with biotite. Relict cores of pyroxene within amphibole are quite common.

Apatite is present as euhedral inclusions within both the biotite and amphibole. Acicular apatites with aspect ratios greater than 10:1 are mainly found as inclusions in the felsic phases. Sphene is present predominantly as anhedral grains which display a wide range colour; colourless grains are usually observed along the cleavage traces in biotites, whilst the light orange sphene usually occurs as isolate grains associated with the felsic components of the matrix.

Zircon occurs as small subhedral inclusions in biotite and also as isolate grains within the matrix; rounded zircons are not uncommon. Metamictic allanite and rounded monazite (see plate 3.18) have both been found as inclusions within biotite. Magnetite is generally the main opaque phase present, although disseminated chalcopyrite has been found in sample 323A and euhedral to subhedral grains of pyrite in sample 28A.

3.2.1.3 Group 3 enclaves

The third group of enclaves have been found in both the PBAMS and MPBAS facies. They are characterized by amphibole (19 modal average percent) together with both microcline and microcline perthite as the main felsic phase, with a combined modal percentage of 38 (37-40). Poikilitic microcline perthites are very frequent. Pyroxene

occurs as euhedral grains sometimes mantled by amphibole (2 modal average percent). Biotite is ubiquitous throughout the group with a modal average percentage of 25 (20-31), and occurs both as isolated flakes and as a late stage replacement of pyroxene. Plagioclase usually makes up less than 12 modal percent of rocks within this group.

The accessory minerals are mainly made of apatite, sphene and zircon. The former phase occurs as accicular inclusions in all the major constituent phases of the rocks. Sphene is largely anhedral, light brown to colourless, and occurs interstitially, commonly associated with biotite. Zircon is found as subhedral to rounded inclusions in biotite.

3.2.1.4 Group 4 enclaves

The more mafic enclaves of group 4 have a more restricted occurence, only three examples have been found. They consist mainly of colourless subhedral zoned pyroxene (26 average modal percent), commonly associated with a deep brown biotite, and an interstitial mesoperthite which makes up less than 10 modal percent of the rocks.

Amphibole occurs both as a secondary subsolidus reaction product replacing pyroxene and also more rarely, as a primary phase which in turn shows a replacement by biotite and the secondary actinolitic hornblende.

Apatite is by far the most abundant accessory mineral. It occurs mainly as acicular crystals with very high aspect ratios (up to 30:1) and also as small euhedral crystals. There is a tendency for such acicular apatites to be concentrated within the felsic phases. Zircon has been observed sporadically as inclusions in biotite but is extremely rare.

3.2.2 Dykes

The dykes mapped in the Bom Jardim area can be subdivided into three petrographic groups:

1. Monzonites and monzodiorites

2. Mafic syenites
3. Gabbro norites.

The average modal contents of the different groups of dykes are given in table 3.3.

Table 3.3 Average modal analyses of the Bom Jardim mafic dykes.

	Mafic syenites	**Monzonites**	**Gabbro-norite**
Quartz	0.8	1.1	0.5
Alkali feldspar	29.0	13.4	-
Plagioclase	3.8	35.9	66.1
Amphibole	27.8	13.4	-
Biotite	33.3	28.7	5.9
Clinopyroxene	-	3.4	16.2
Orthopyroxene	-	-	9.5
Sphene + allanite	3.7	1.1	-
Apatite	1.1	0.8	0.2
Opaques	-	1.9	2.2
Zircon	trace	trace	-

3.2.2.1 Monzonites and monzodiorites

The monzonites to monzodiorites are fine grained rocks with a xenomorphic equigranular texture and petrographically similar to the monzonitic (group 2) enclaves. They consist of subhedral zoned plagioclase feldspar (An_{21} to An_{33}) together with anhedral and sometimes poikilitic microcline perthite. The mafic minerals are mainly represented by subhedral clinopyroxene and biotite. Quartz has been observed in some dykes belonging to this group. Amphibole replacing pyroxene has also been recorded. Apatite is the chief accessory mineral, commonly occuring as accicular inclusions in the alkali feldspar. They are fine grained rocks with xenomorphic equigranular texture. This lithology is petrographically

similar to the monzonitic enclaves.

3.2.2.2 Mafic syenites

The mafic syenites can be further subdivided into: a) porphyritic types with phenocrysts of clinopyroxene, petrographically similar to the mafic syenitic (group 3) enclaves, apart from the alkali feldspar which is now dominantly microcline, and b) fine grained equigranular xenomorphic types, containing both primary and secondary amphibole (after pyroxene). Sample 205 belongs to this category of dyke and shows quite a large modal percentage of subhedral metamictic allanite together with anhedral light orange sphene.

3.2.2.3 Gabbro norites

The third group of dykes have a much more localized occurence. Sample 272A is an example from this group. It shows a hypidiomorphic equigranular texture with subhedral crystals of ortho pyroxene (Wo1 En59 Fs40 to Wo1 En60 Fs39) and clinopyroxene (Wo_{47} En_{39} Fs_{14} to Wo_{45} En_{39} Fs_{16}). Plagioclase is also present, the crystals are generally subhedral to anhedral in shape with a compositional range of An_{34} to An_{48} and therefore, strictly speaking adopting the IUGS classification should be termed diorites. A very deep brown biotite and opaque minerals can also be found replacing pyroxene.

3.3 SUMMARY AND CONCLUSIONS

Several important features have been established from the petrographic studies made on the rocks from the Bom Jardim complex.

a) Sphene was observed in all the magmatic rocks from the complex except in the PBS lithology. The sphenes show quite a wide range in colour, those displaying the deepest orange tend to be in the MPBAS facies. The lack of ilmenite in the rocks of the Bom Jardim complex suggests that sphene

might be the major phase controlling the variation of TiO_2 contents during magmatic differentiation.

b) Amphibole occurs as primary magmatic phase in the PBAMS and MPBS, but rarely in both the CS and PBLS and is totally absent in the PBM and granites. Clinopyroxene has been observed in all facies apart from the granites, although in some facies it is represented solely by small relict cores within amphibole (e.g. PBAMS).

c) Thorium minerals were not recorded from any of the early evolved facies, e.g., PBM, PBAMS, however, there is a clear evidence that their modal abundance increases from the MPBAS facies to the PBLS facies and granites.

d) The chief opaque mineral is magnetite. Ilmenite was observed (in low modal abundance) in the px-bio leuco alkali feldspar syenite (PBLS) and granites but was always rimmed by sphene. The presence of magnetite instead of ilmenite is generally regarded to be characteritic of "I-Type" granitoids (White and Chappell, 1977; Ishihara, 1977 and Pitcher, 1983).

e) The presence of monazite has been regarded by many petrologists as indicative of a S-type origin. However the main mineral assemblages in the Bom Jardim complex do not support this conclusion, they would indicate a far close affinity to I-type cordilleran granitoids. The presence of monazite has been interpreted by the present investigator as evidence of crustal contamination.

f) The localized clots of alkali feldspar and plagioclase hosted by the fine grained mafic syenites, together with the globules of fine grained syenite within the PBAMS, and the sporadic development of rapakivi type texture, indicates that some degree of hybridization between the PBAMS magma and a more mafic syenitic magma probably took place during the evolution of the Bom Jardim complex.

CHAPTER 4
MINERAL CHEMISTRY

4.1 INTRODUCTION

All the major mineral phases occurring within the rocks of the Bom Jardim complex together with the accessory minerals, sphene, apatite, allanite, monazite and some specific thorium minerals were analysed using a Cambridge Instruments mark 5 electron microprobe, equipped with a Link Systems energy dispersive detector, analytical details of which can be found in the appendix A. In addition five grains of thorium rich minerals were kindly analysed by Dr Terry Williams at the British Museum, Natural History using a Cambridge Instruments Microscan 9 electron wavelength dispersive electron microprobe.

In addition, several of the mineral phases were analysed by INAA techniques after careful separation and purification. All the samples were irradiated at the Imperial College Reactor, Silwood Park and counted at the Natural History Museum. Analytical details are given in the appendix A.

4.2 MINERAL CHEMISTRIES OF THE MAJOR FACIES

4.2.1 Clinopyroxenes

A total of over 60 pyroxenes from the different lithologies within the complex have been analysed, representative analyses can be found in the table 4.1, individual analyses are listed in appendix D, tables D.1.1 to D.1.5. Fe^{3+} values were calculated assuming Fe^{3+} = Na per formula units, based on 6 oxygens (see Parsons, 1981 and Stephenson and Upton,1982).

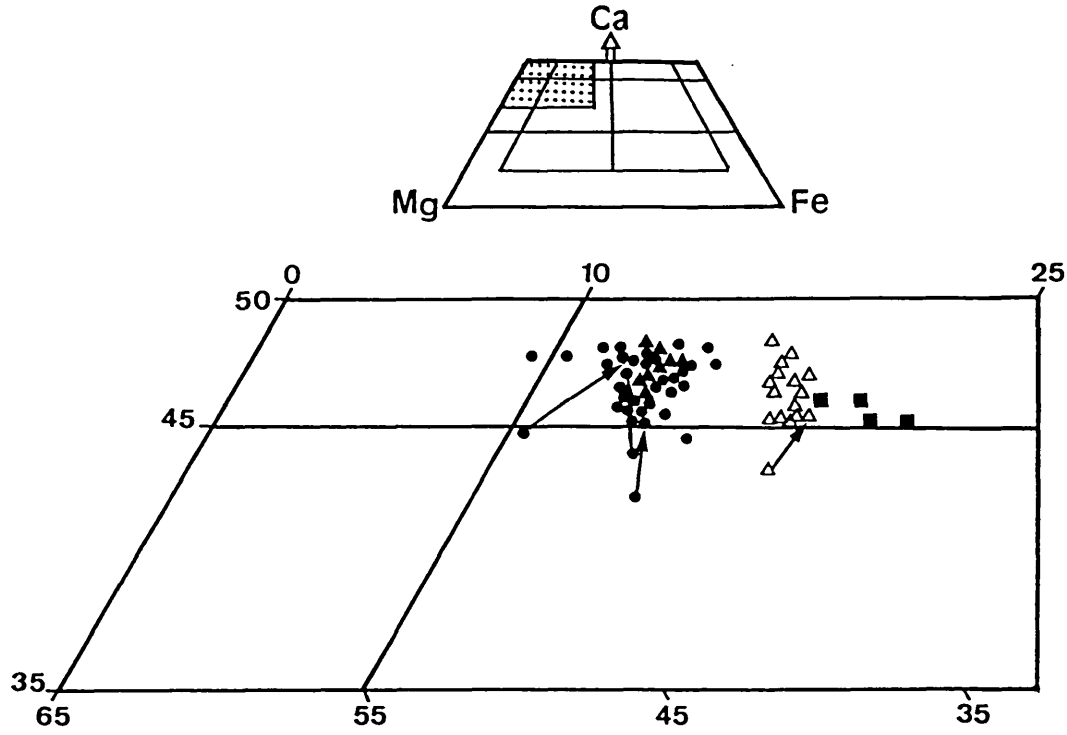


Figure 4.1 Plot of pyroxene compositions from the Bom Jardim complex. Filled circles represent pyroxenes from the mafic syenites and monzonites, filled triangles pyroxenes from the medium grained syenites; open triangles from the leuco syenites and filled squares pyroxenes from the coarse grained syenites. Arrows indicate core to rim variations within single pyroxenes.

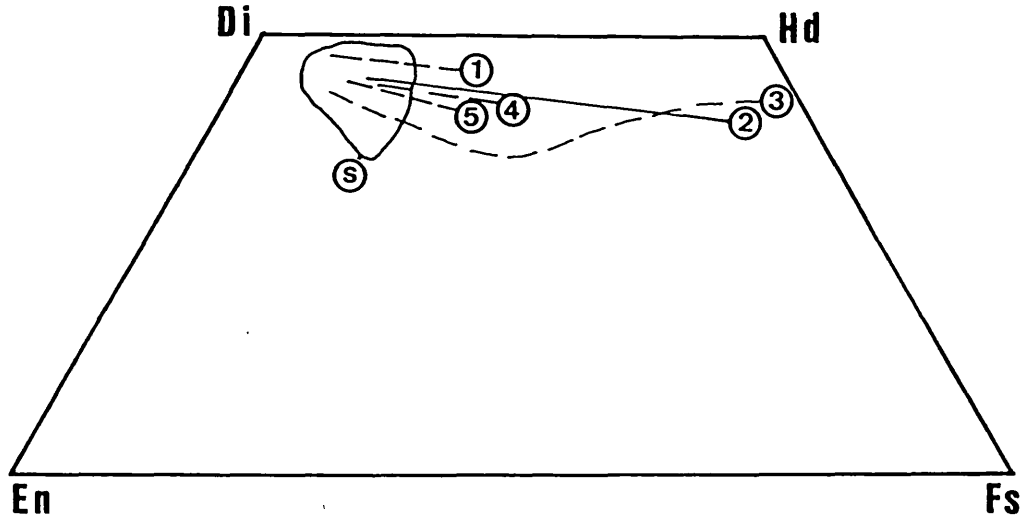


Figure 4.2 The Bom Jardim pyroxene trend (1) compared with Ca-rich pyroxene trends from: (2) Japanese alkali basalts, (3) Skaergaard, (4) Guadalupe complex, (5) Gough island alkaline series and, (S) field of pyroxenes from rocks rocks of shoshonitic associations. See text for references.

Table 4.1 Representative analyses of pyroxenes from the Bom Jardim major facies.

	200	**249**	**258**	**07**	**10**	**23**
SiO_2	53.13	52.40	52.60	53.22	52.25	51.47
TiO_2	0.00	0.32	0.00	0.00	0.27	0.20
Al_2O_3	0.77	0.98	1.01	1.02	1.07	0.51
FeO	8.01	8.80	7.30	7.98	11.12	13.19
MnO	0.51	0.22	0.47	0.42	0.47	0.43
MgO	13.55	12.75	13.97	13.22	11.84	10.53
CaO	22.99	22.21	22.69	22.72	21.92	20.75
Na_2O	1.05	0.90	1.19	1.20	1.27	1.98
TOTAL	100.01	99.15	99.23	99.79	100.21	99.35
Wo	48	47	47	48	46	46
En	39	38	41	39	35	32
Fs	13	15	12	13	19	22

Total iron expressed as FeO.

Zoning is quite common in the pyroxenes, although the compositional range displayed is not particularly great, commonly Ca increases from core to rim without a significant change in the Fe/Mg ratio. The compositions of the pyroxenes from the different lithologies in the Bom Jardim complex have been plotted in terms of Ca-Fe-Mg and are shown in the figure 4.1. The majority of the pyroxenes fall within the salite compositional field, with only the occasional core composition falling in the field of augite.

The pyroxenes do show a rather limited increase in the hedenbergite molecule, especially in the more evolved members of the complex. Figure 4.2 shows a comparison of Bom Jardim pyroxene trend with other documented trends from the literature. The limited Fe enrichment of the present pyroxene trend is similar to that displayed by the Ca-rich pyroxenes from the Guadalupe complex, in California (Best and Mercy, 1967) and those from Coastal batholith in Peru (Mason, 1985).

Best and Mercý (1967) have suggested that a

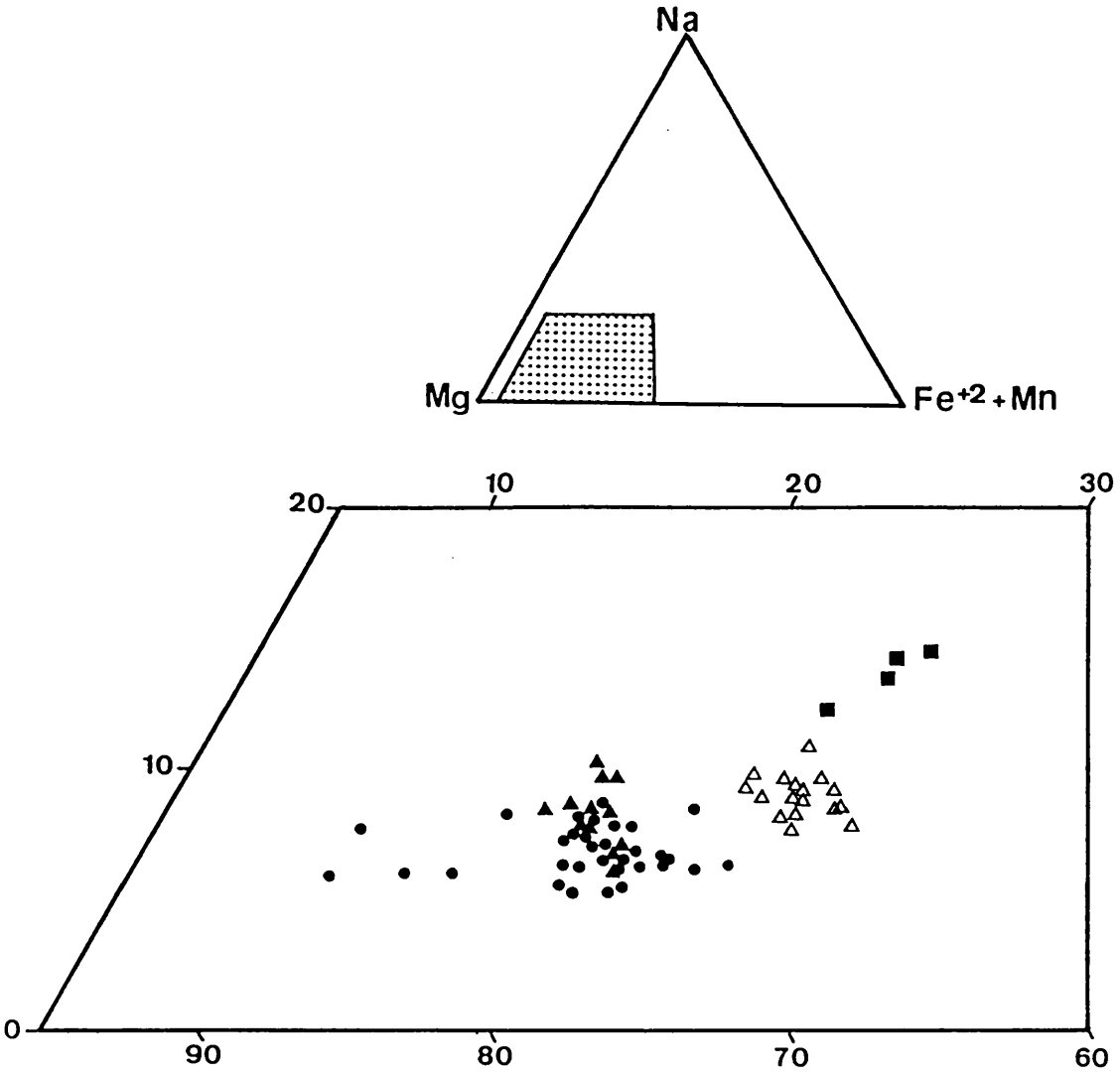


Figure 4.3 Individual micropobe analyses of the Bom Jardim complex pyroxenes expressed in terms of atom percent Na^{+}, Mg^{2+} and Fe^{2+} + Mn^{2+}. Symbols as in figure 4.1.

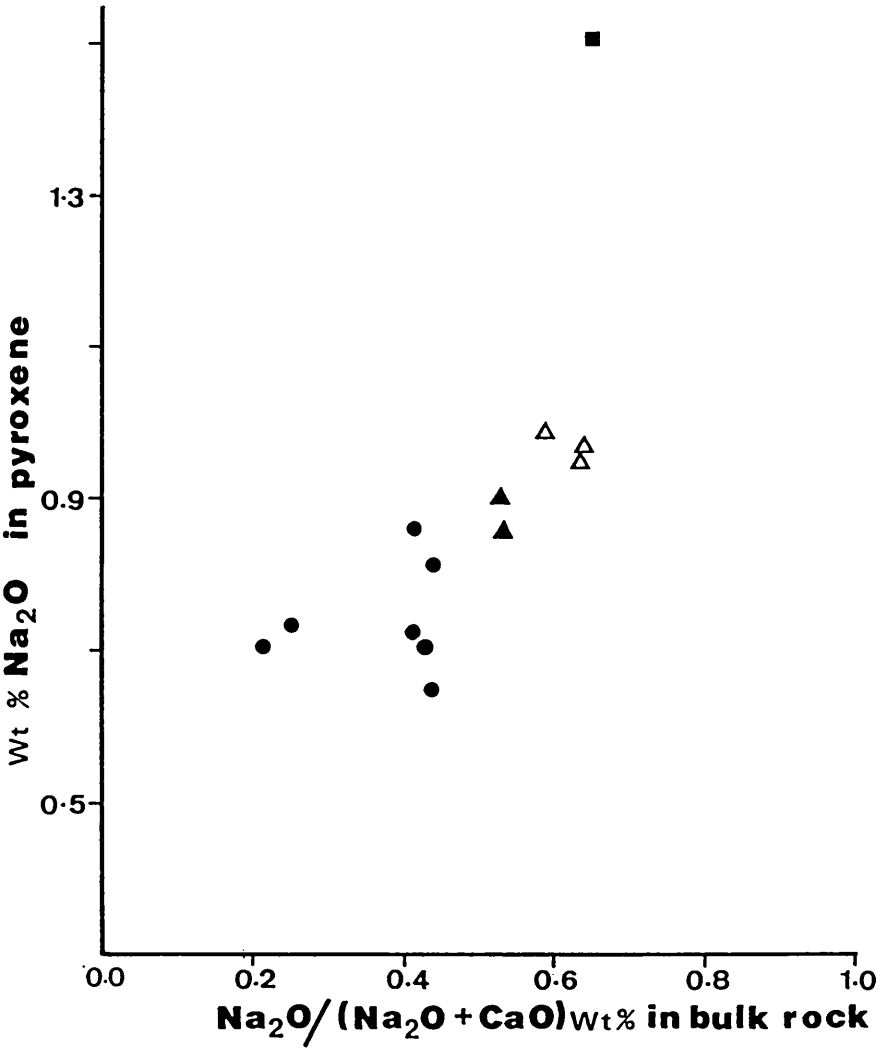


Figure 4.4 Bulk rock Na/Na+Ca ratios versus Na contents of pyroxenes from the Bom Jardim complex. Symbols as in figure 4.1.

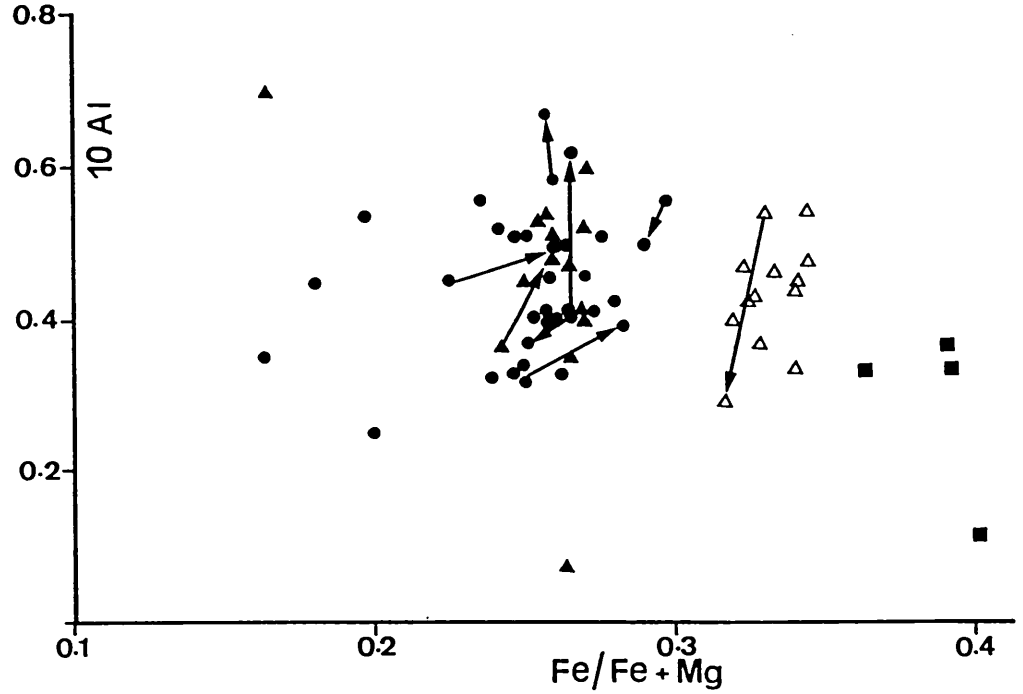


Figure 4.5 Variation of atomic Al versus Fe/Fe+Mg in pyroxenes from the Bom Jardim complex. (based on atoms to six oxygens, all Fe quoted as Fe^{2+}). Symbols as in figure 4.1. Arrows indicate core to rim variations within single grains.

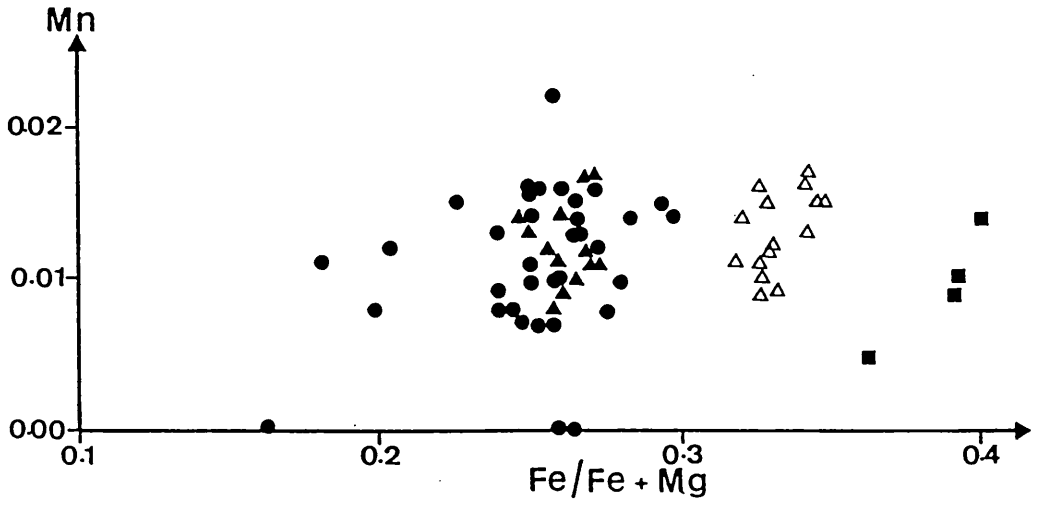


Figure 4.6 Variation of atomic Mn versus Fe/Fe+Mg in pyroxenes from the Bom Jardim complex. (based on atoms to six oxygens, all Fe quoted as Fe^{2+}). Symbols as in figure 4.1.

magma crystallising under relatively high fH2O conditions could lead to the early precipitation of amphibole and the depression of pyroxene stability field, forcing the magma to leave the pyroxene field before any appreciable Fe enrichment has taken place within the pyroxene. Biotite and amphibole would then replace pyroxene as the main ferromagnesian minerals.

Unlike the Guadalupe complex (Best and Merci, 1967) no Ca-poor pyroxenes have been observed within the Bom Jardim complex. Morrison (1980) has also commented on the fact that many of the shoshonitic complexes also display a limited Fs enrichment (see figure 4.2).

The pyroxenes within the Bom Jardim complex also display a slight enrichment in the acmite molecule with increasing differentiation as shown in figure 4.3. Early in the pyroxene evolution the main chemical substitutions are essentially Ca^{2+} Mg^{2+} being replaced by Ca^{2+} Fe^{2+}, however in both the leuco syenites (PBLS) and the very coarse grained syenites (CS) there is an increase in both Fe^{3+} and Na^{+}. Mitchell and Platt (1978) commented on the relationship between Na^{+} enrichment in pyroxenes and the alkalinity of the host magma. In the present investigation, there is a sharp correlation between the amount Na_2O in the pyroxenes and the ratio $Na_2O\backslash Na_2O+CaO$ in the host rocks (see figure 4.4).

Minor element substitutions within the pyroxenes show very little variation during the differentiation of the magma. The data for Al^{3+} and Mn^{2+} are shown in the figures 4.5 and 4.6 respectively.

4.2.2 Amphiboles

Over 70 amphibole analyses have been determined from 18 samples representing all the major rock types of the Bom Jardim complex. Representative analyses can be seen listed in table 4.2. Individual analyses are listed in tables D.2.1 and D.2.2, appendix D. Both the classification and nomenclature used in this investigation are after Leake (1978). Fe^{3+} and Fe^{2+} per units formula, based on 23 oxygens, were calculated using a basic

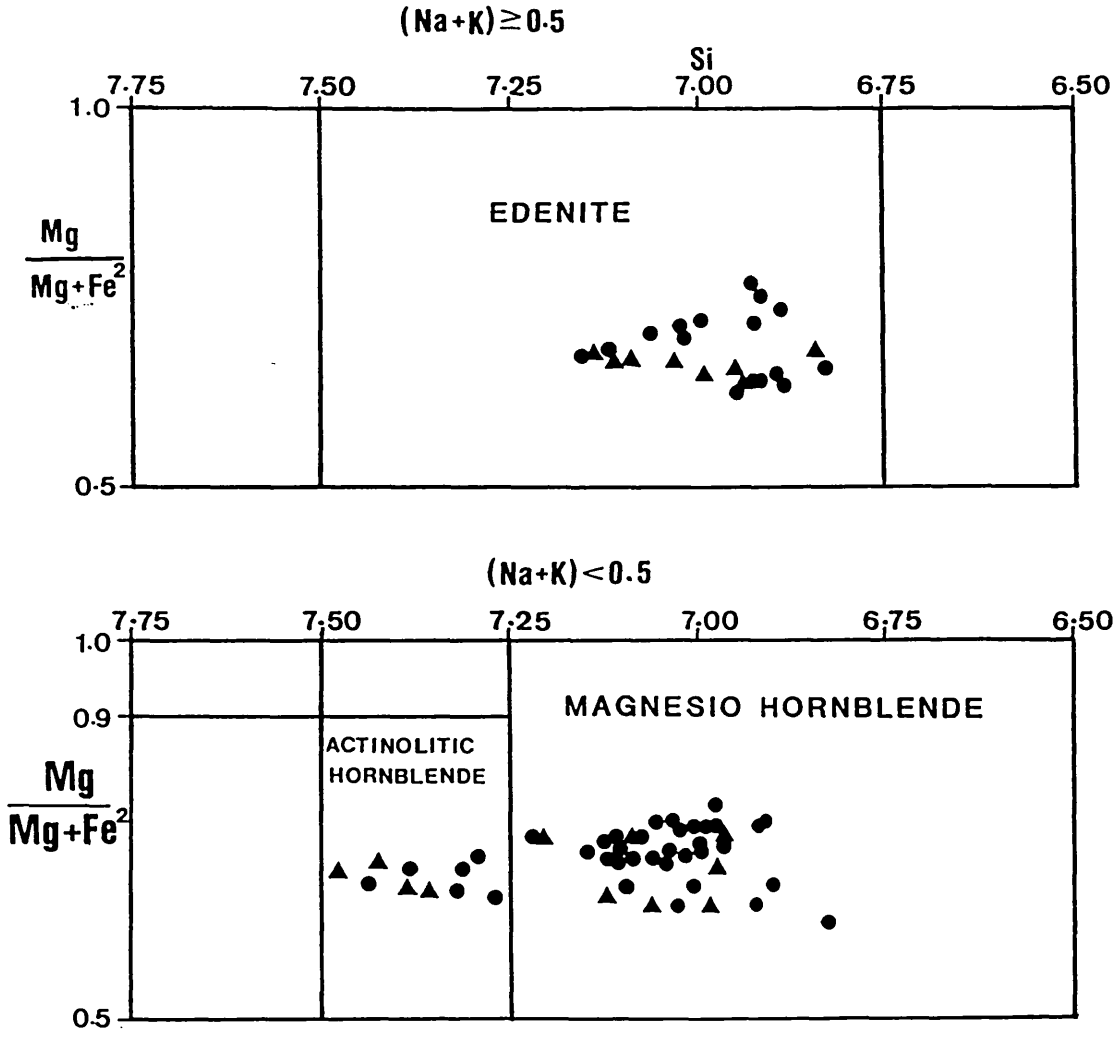


Figure 4.7 Composition and classification of the calcic amphiboles from the major facies of the Bom Jardim complex. (After Leake 1978). Symbols as in previous diagrams.

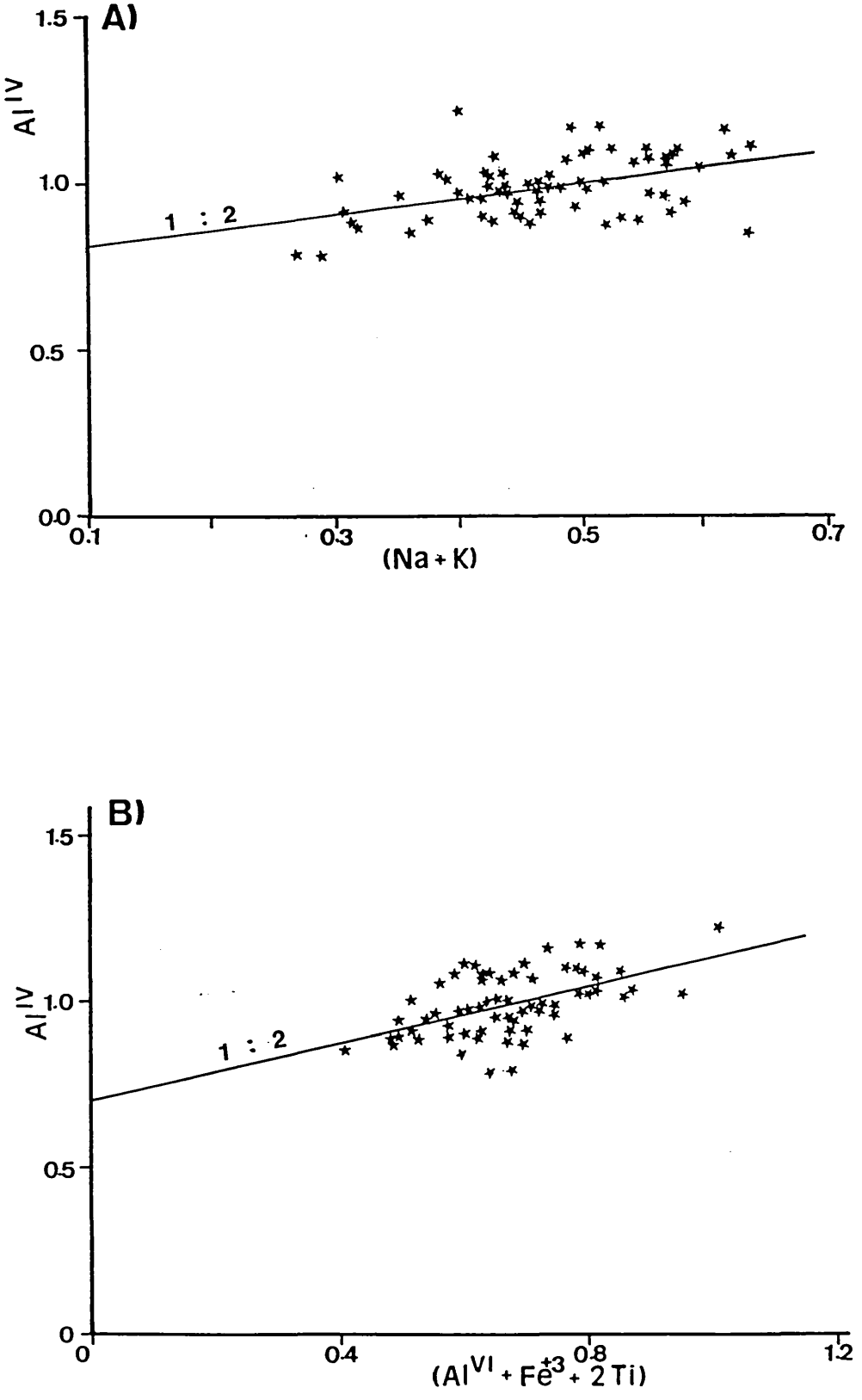


Figure 4.8 (A) Variation of Al^4 in T site versus Na+K in A site. (B) Al^4 in T site versus $Al^6 + Fe^{3+} + 2Ti$ in M_1-M_2-M_3 sites for amphiboles from the major facies of the Bom Jardim complex. (All calculations based on 23 oxygens).

programme "ANFIFICH".

Table 4.2 Representative analyses of amphiboles from the Bom Jardim major facies.

	EDENITE			MAGNESIO-HORNBLENDE		
	112	**86**	**27**	**28**	**29**	**268**
SiO_2	46.71	46.29	46.39	47.48	48.01	47.04
Al_2O_3	6.73	7.27	6.77	6.11	6.13	5.67
TiO_2	1.54	1.42	1.46	0.98	1.08	0.95
FeO	13.52	12.95	12.16	10.28	9.01	11.71
Fe_2O_3	0.77	1.02	1.69	2.86	3.35	2.97
MgO	13.04	13.07	13.26	13.87	15.23	12.94
MnO	0.31	0.36	0.20	0.30	0.00	0.00
CaO	11.87	11.68	11.57	11.89	11.58	11.39
Na_2O	1.92	2.19	1.82	0.90	1.77	1.00
K_2O	0.81	0.78	0.82	0.77	0.77	0.90
Total	97.22	97.03	96.14	95.44	96.93	94.57
$Mg/Mg+Fe^{2+}$	0.63	0.64	0.66	0.71	0.75	0.66

The amphiboles show a very much restricted range in composition, varying between magnesio hornblende and edenite (see figure 4.7). Actinolitic hornblendes with low aluminium contents (Al_2O_3 < 5.0%) are observed replacing clinopyroxene as the product of subsolidus reaction.

Figures 4.8A and 4.8B show the variation of Al[4] with both [A]site content and $[Al^{VI} + Fe^{3+} + 2Ti]$ respectively for the igneous amphiboles of the Bom Jardim complex. The data indicate the relative importance of the edenite and tschermakite type substitutions, i.e., for every two $Al[^4]$ ions occupying the tetrahedral position there is one Na and\or K ion in the [A] site and one $[Al^4 + Fe^{3+} + 2Ti]$ ion in the M_1-M_2, and M_3 sites.

Amphiboles from typical calc-alkaline granitoid complexes such as the Sierra Nevada batholith (Dodge, 1969) and Coastal batholith, Peru (Mason, 1985) are mainly magnesio or ferro-hornblendes, although edenites have been reported from calc alkaline granitic rocks, eg. the Guichon

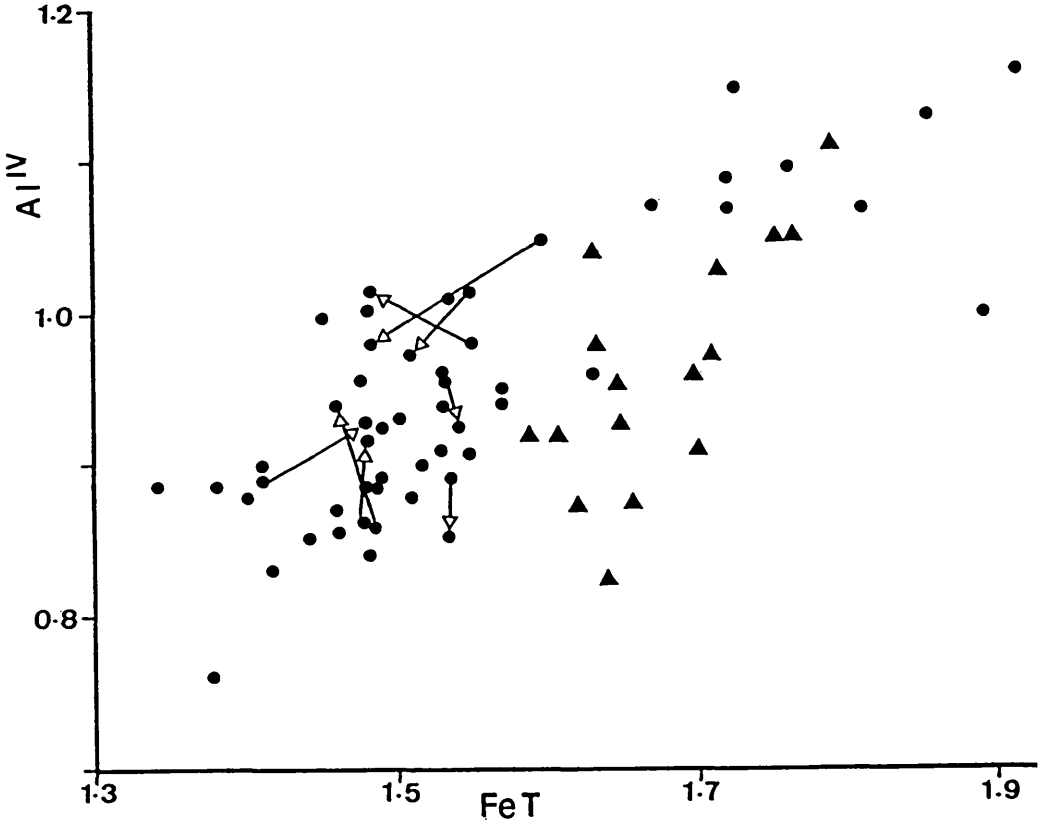


Figure 4.9 Variation of total atomic Fe (expressed as Fe^{2+}) with Al^4 in amphiboles from the major facies of the Bom Jardim complex (based on 23 oxygens). Arrows indicate core to rim variations within single grains.

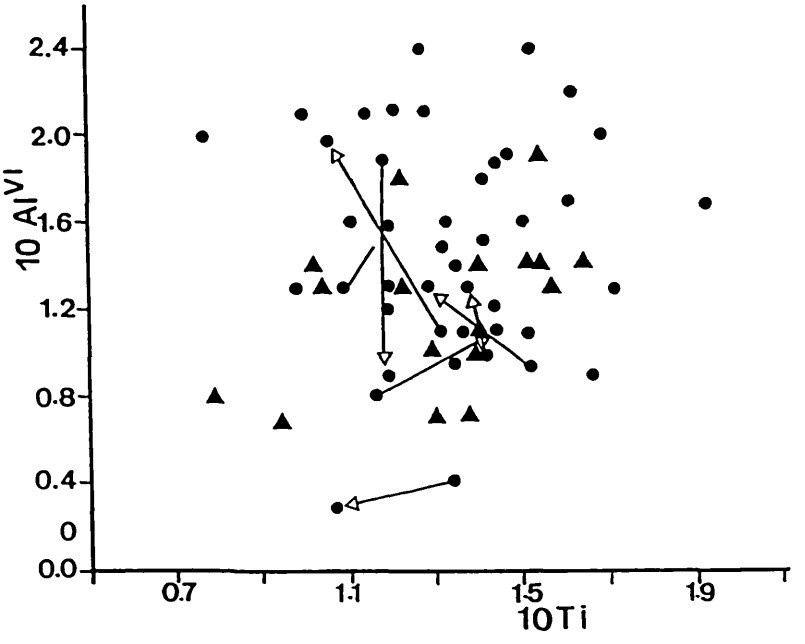


Figure 4.10 Variation of atomic Ti with Al^6 in amphiboles from the Bom Jardim complex (based on 23 oxygens). Arrows indicate core to rim variations within single grains.

Creek and La Caldera granitic intrusions of Canada (Johan, 1980).

The $Mg/Mg+Fe^{2+}$ ratio varies from 0.60 to 0.78, values very similar to those of typical amphiboles from calc-alkaline granitoids. Figure 4.9 shows a strong positive correlation between total Fe (expressed as Fe^{2+}) and Al^4, a similar trend has been observed by Mason (1978) for the mineralized calc-alkaline intrusives of the Western highlands, Papua-New Guinea.

The Al^4 contents of the amphiboles from the Bom Jardim complex vary from 0.064 to 0.276 cations per 23 oxygens. Figure 4.10 shows the variation of Al^6 with Ti contents.

4.2.2.1 Amphibole Geobarometry

The Al contents in amphiboles have been used by Leake (1965), Raase (1974), Hammarstron and Zen (1983, 1986), and Hollister et al. (1987) as an indicator of the pressure of crystallisation. However according to Mason (1985), the Al^6 contents of magmatic amphiboles reflect a change in silica activity (which change with pressure) and also in the state of polymerisation of the melt. Helz (1973) and Spear (1981) have investigated the effects of fO_2 on the composition of amphiboles under controlled P-T conditions. Their experimental findings indicate that differences in composition due to changes in fO_2 are small to negligible compared to the differences as a result of changes in pressure.

Hammarstron and Zen (1986) studied the composition of amphiboles from two shallow intrusives and from three plutons with evidence of deeper levels of emplacement within the crust. The amphiboles in all complexes are calcic but they show essential differences in composition, particulary in Al content. Hammarstrom and Zen (1986) have suggested that differences in Al content of calcic amphiboles are directly related to the depth of emplacement of granitic plutons and can therefore be used as a geobarometer. Data from experimental investigations provide an opportunity to study the control of intensive

variables on the composition of calcic amphiboles, and in particular the role of pressure in determining the Al content of hornblende. Helz (1982) summarized these relationships in detail and concluded that SiO_2 and Al_2O_3 in hornblende do not vary systematically with bulk composition and that when pressure alone is considered, the Al^6 content in hornblende increases with increasing pressure. Hammarstrom and Zen (1986) also showed that hornblendes formed at 3 Kb pressure or less have Al^t values < 2.1, whereas in hornblendes formed at 8 Kb pressure or higher the Al^t values were > 2.0. The authors do emphasize the fact that it is an empirical method and that certain pre-requisites should be met before applying their data to other plutons. Since the Al^4 content of hornblende is negatively correlated with silica content, the amphiboles should coexist with quartz to eliminate the activity of SiO_2 (a_{SiO2}) as a variable. The other stipulation is that the assemblage should include plagioclase (andesine-oligoclase), K-feldspar, quartz, hornblende, magnetite and\or ilmenite in addition to the hornblende and quartz in order to adequately buffer the system from changes in chemistry of the individual phases. All these conditions are met by the assemblages from the Bom Jardim complex.

Figure 4.11 shows the plot of Al^t versus Al^4 for the amphiboles of the Bom Jardim complex. They plot within the low pressure field of Hammarstron and Zen (1986). Using their best fit linear regression equation:
$P = -3.92 + 5.03Al^t$, the calculated pressure range for the Bom Jardim complex has been determined at 1.1 to 3.2 Kb. These values of pressure are very similar to those estimated for the Sierra Nevada batholith and Guadalupe complex (Hollister et al., 1987). The above lower pressure estimate of 1.1 Kb does not agree with the probable geological setting of the complex. Late stage subsolidus reequilibration and reaction commonly results in the growth of amphiboles with increased magnesium and lower aluminium contents. It is therefore quite likely that the lower pressure estimates discussed above are the result of such secondary subsolidus processes.

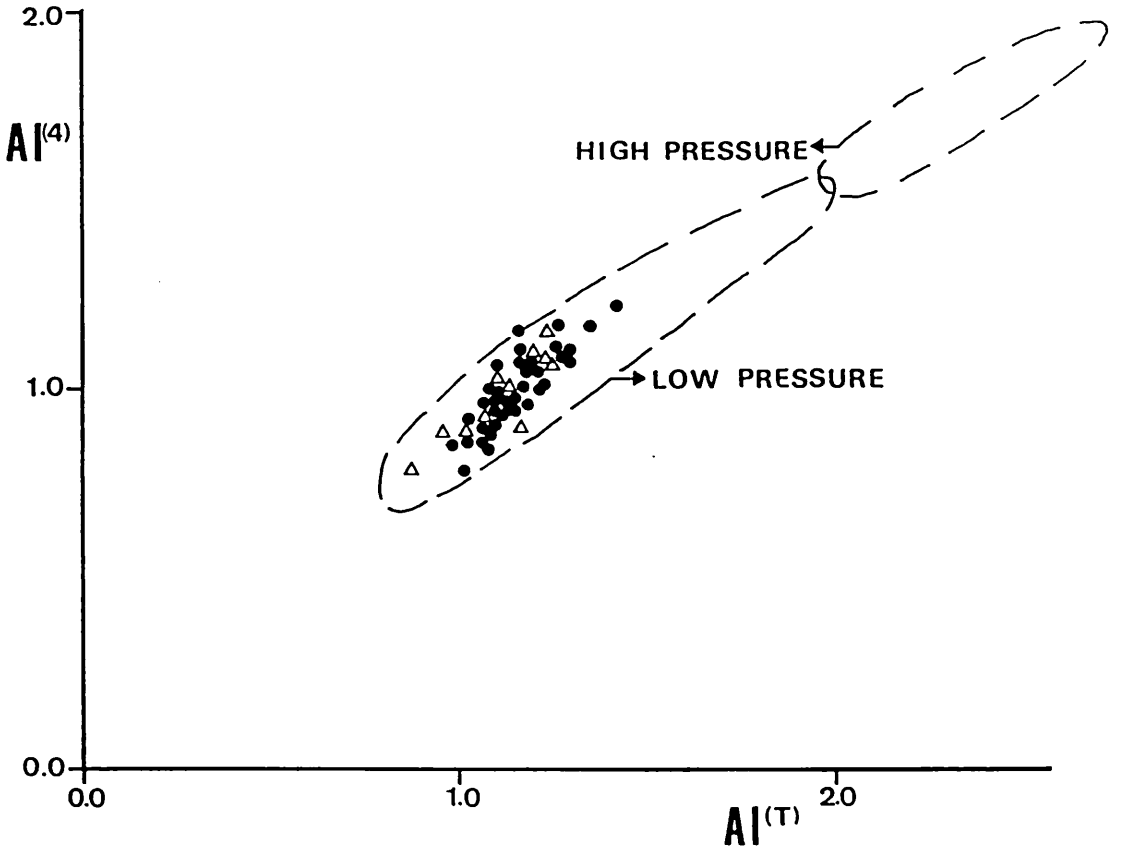


Figure 4.11 Plot of Al^t versus Al^4 for amphiboles from the Bom Jardim complex. Open triangles = amphiboles from MPBAS and closed triangles = amphiboles from PBAMS. Fields are from Hammarstron and Zen (1986).

4.3.2 Biotite

Nearly 70 individual analyses of biotites have been determinated in 29 samples from the main facies of the complex. Representative biotite analyses from the major rock types are given in table 4.3. Individual analyses and unit cell contents are given in appendix D (tables D.3.1 to D.3.6). Biotites were also separated from the pyroxene biotite monzonites (PBM), and the pyroxene biotite leuco alkali feldspar syenites (PBLS). The separated biotites were carefully handpicked, checked that they were inclusion free and analysed for by INAA. The results are given in table 4.4.

Table 4.3 Representative analyses of biotites from the major facies of the Bom Jardim complex.

	29	**119**	**252**	**48**	**49A**	**49B**	**23**
SiO_2	38.01	37.49	37.58	38.10	38.83	38.46	39.20
TiO_2	2.04	2.94	3.81	3.63	3.64	3.46	3.66
Al_2O_3	14.16	14.47	13.63	12.67	12.90	12.90	11.43
FeO	15.88	16.63	15.34	16.42	16.17	16.64	17.58
MnO	0.00	0.26	0.00	0.00	0.00	0.00	0.00
MgO	15.85	13.07	14.55	13.57	14.19	14.38	13.73
Na_2O	0.45	0.44	0.50	0.00	0.00	0.00	0.44
K_2O	10.42	9.82	9.90	10.04	10.12	10.00	11.43
BaO	0.47	0.00	0.29	0.42	0.79	0.00	0.00
Cr_2O_3	0.24	0.00	0.00	0.26	0.00	0.00	0.00
Total	97.68	95.12	95.60	95.12	96.65	96.39	96.31
FM	0.36	0.42	0.37	0.40	0.39	0.39	0.38

Total iron expressed as FeO

FM = Fe\Fe+Mg

Table 4.4 Representative INAA data for biotite (BIO), amphibole (AMPH), clinopyroxene (CPX) and sphene (SPH) from the Bom Jardim complex. MMAMPH represents an amphibole analysis from the McMurry Meadows pluton, California (Sawka, 1988).

	25BIO	90BIO	86AMPH	MMAMPH	86CPX	114SPH
Sc	5.8	8.6	54	146.0	72.3	6.8
Cr	247	628	369	35	423	18
Co	79	80	52	49	37	1.7
Ni	290	477	223	n.d	88	0
Rb	1022	465	13	n.d	0	0
Cs	66	9.0	0.6	n.d	0.6	0
Ba	1638	2910	0	55	0	0
Hf	3.3	1.2	7.4	0	3.4	33.3
Ta	3.3	1.9	1.3	1.8	0	153.6
Th	2.0	0.3	2.0	5.7	1.0	633
U	0.5	0.2	0.6	1.7	0.6	159.6
La	12.0	10.2	83.8	62.8	29.4	2106.8
Ce	17.0	18.6	250.4	214.0	81.8	6686.9
Nd	6.3	7.7	172.5	158.0	55.7	3611.5
Sm	1.3	1.5	33.7	38.0	12.1	636.7
Eu	0.3	0.3	6.9	3.3	2.3	191.6
Gd	2.2	1.7	27.9	36.9	8.4	352.1
Tb	0.1	0.1	3.2	4.6	1.2	59.0
Tm	0.1	0.1	1.3	n.d	0.5	19.6
Yb	0.2	0.2	4.9	18.1	1.9	124.6
Lu	0.06	0.02	0.57	2.74	0.30	14.5

n.d = not determined

In general, the biotites show moderately low Ti contents and, their Fe\Fe+Mg ratios are low ranging from 0.33 to 0.43, in contrast to the biotites from the metasedimentary country rocks with ratios from 0.47 to 0.51. Figure 4.12 shows a plot of the biotites from the Bom Jardim complex expressed in terms of Ti-Mg-Fe, they are

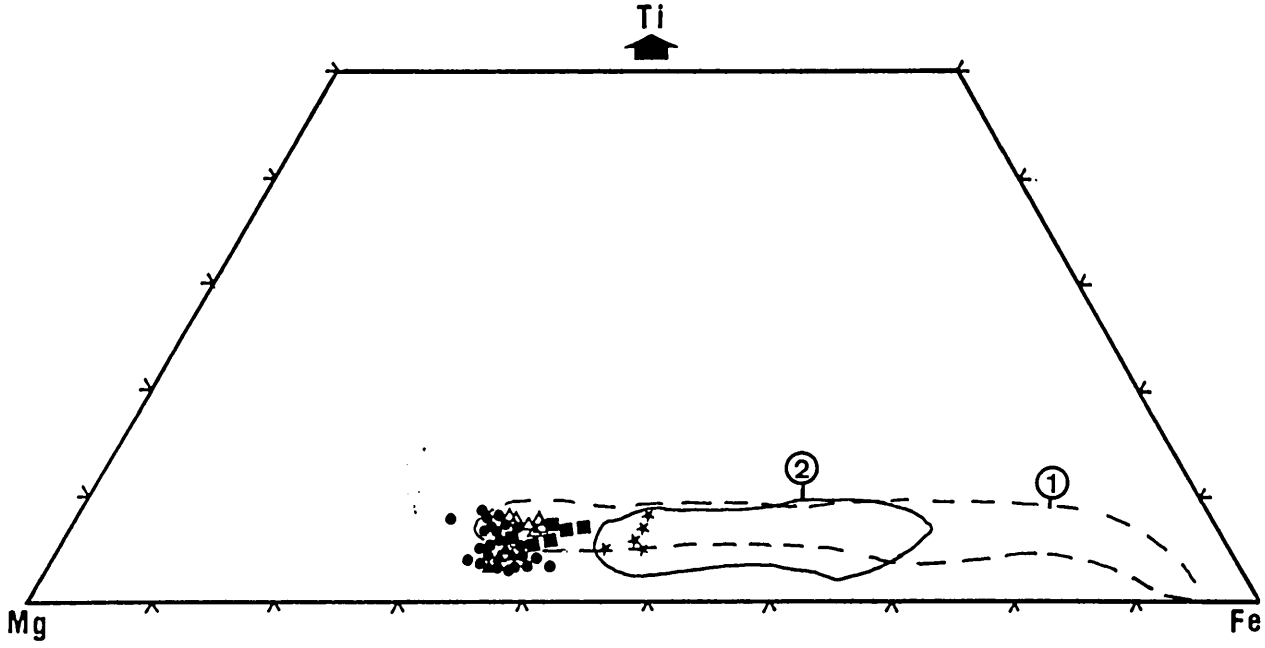


Figure 4.12 Individual micropobe analyses of biotites from the Bom Jardim complex expressed in terms of atomic proportions of Ti-Mg-Fe (all iron expressed as Fe^{2+}). Filled circles represent biotites from the mafic syenites and monzonites, filled triangles biotites from the medium grained syenites, open triangles from the leuco syenites, filled squares from the very coarse grained syenites and stars represent biotites from the granites. (1) - field of biotites from the japanese granitoids (Czamanske et al., 1981), and (2) - biotites from the Sierra Nevada Batholith (Dodge, 1969).

generally more Mg rich than the biotites from the Sierra Nevada batholith (Dodge, 1969) and cluster towards the Mg end of the trend displayed by biotites from the Japanese granitoids (Czamanske et al., 1981).

One method of expressing both the chemical variations and different parageneses of igneous biotite bearing assemblages is by the use of the ternary plot MgO-FeOt-Al_2O_3 (Nockolds, 1947 and Albuquerque, 1973); such a plot is shown in figure 4.13. The bulk of the Bom Jardim biotites fall within the field originally designated as biotites coexisting with amphibole (Nockolds, 1947). This paragenetic association is generally true for the Bom Jardim complex, however in both the pyroxene biotite monzonites and the pyroxene biotite leuco alkali feldspar syenites igneous amphiboles have not been found. It would therefore seem necessary in the present case to redefine field I, (see figure 4.13) as biotites coexisting with amphibole and\or pyroxene. Biotites from the pink granites plot either within or very close to field II designated as biotites unaccompanied by other ferro-magnesian minerals. This agrees with the petrographic data recorded for this facies.

Although there is not a clearly defined correlation between total Al and alkali content, the biotites with the lowest values of Al_{TOTAL} (generally found in the more evolved rocks) do tend to show the highest alkali contents. The unit cell contents of Al are always found to exceed Na+K in the biotites analysed.

The barium content of the biotites from the complex show some interesting trends when viewed in conjunction with their associated phases. Biotites which, from textural evidence are believed to have crystallised before the alkali feldspar show much higher BaO contents when compared to the smaller interstitial flakes. For example compare biotite analyses 49A and 49B, (see table 4.3), the former being typical of early formed biotites and the later a late stage interstitial flake. The two INAA analyses listed in table 4.4 also show that biotites from the less differentiated facies of the complex (90BIO) are more enriched in BaO as well as both Ni and Cr and depleted

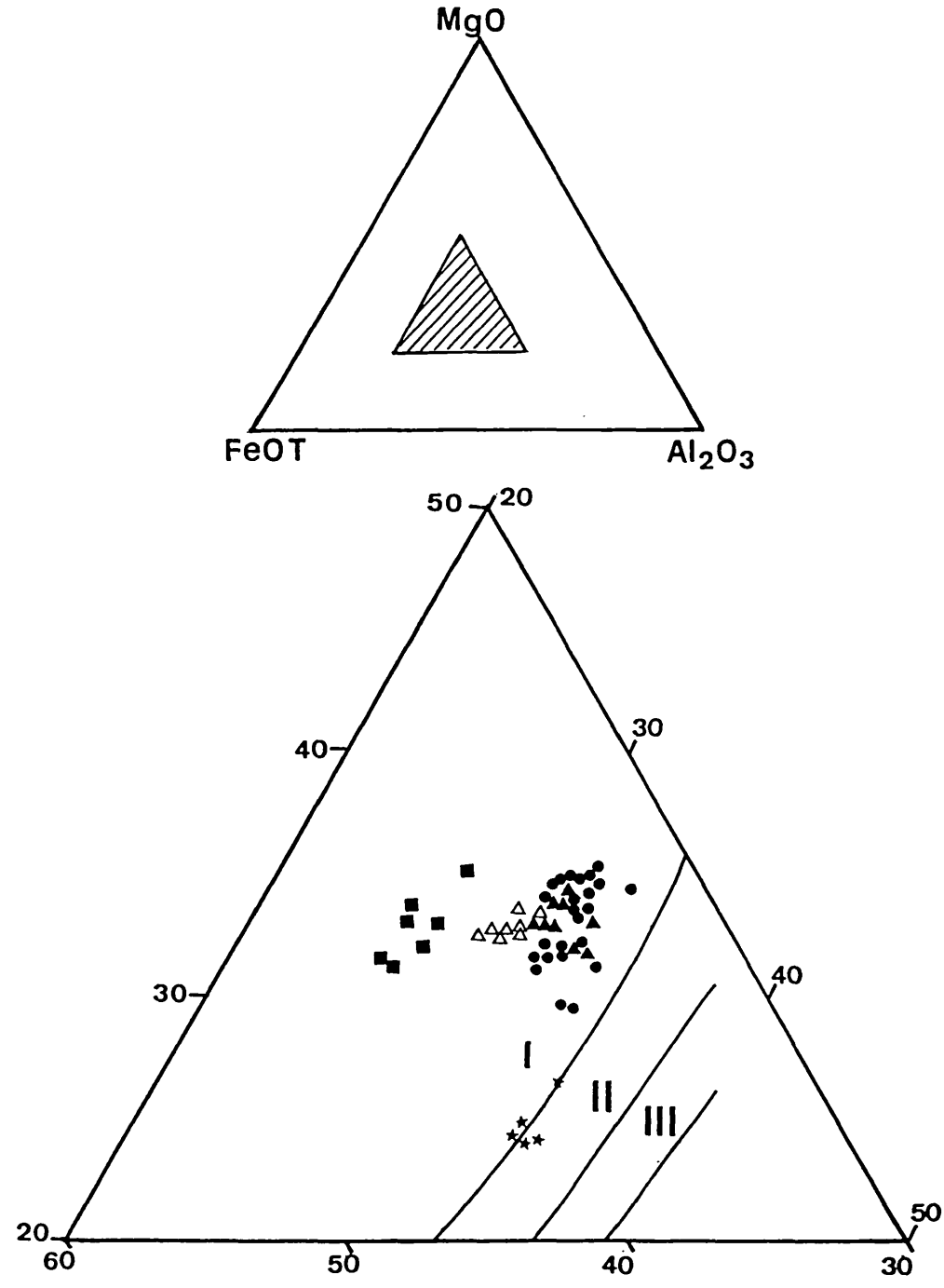


Figure 4.13 Composition of biotites from the Bom Jardim complex plotted in terms of Al_2O_3-FeO_T-MgO. (I) Field of biotites coexisting with amphiboles, (II) field of biotites unaccompanied by other ferromagnesian minerals and (III) field of biotites coexisting with muscovite (Fields after Nockolds, 1947). Symbols as in figure 4.11.

in Rb and Cs than the biotites from the more evolved rock types (25BIO). There is obviously a marked competition for Ba among the crystallising phases, especially biotite and alkali feldspar, and this aspect of the mineral chemistry will be dealt with in conjuction with whole rock geochemical trends in the next chapter.

4.2.4 Plagioclase feldspars

Plagioclase compositions were determined in 26 samples representing the major rock types in the complex. Over 160 individual analyses were carried out including core and rim compositions in many of the plagioclases displaying zoning. Representative plagioclase compositions for the major rock types are given in table 4.5. Individual plagioclase analyses are listed in the appendix D (table D.4.1 to table D.4.4).

Table 4.5 Representative analyses of plagioclase feldspars from the major facies of the Bom Jardim complex.

	144	**29**	**88**	**27**	**49**	**23**
SiO_2	60.79	61.97	63.08	64.47	66.39	68.58
Al_2O_3	24.98	23.58	22.80	21.48	20.58	18.99
CaO	5.96	4.78	4.26	3.19	1.63	0.00
Na_2O	8.21	8.52	8.54	9.56	10.41	11.44
K_2O	0.16	0.25	0.49	0.34	0.30	0.10
Total	99.98	99.10	99.19	99.04	99.31	99.11
Ab	71	75	76	83	90	99
An	28	23	21	16	8	0
Or	1	2	3	1	2	1

Figure 4.14 illustrates the compositional ranges of the plagioclase feldspars within each of the major

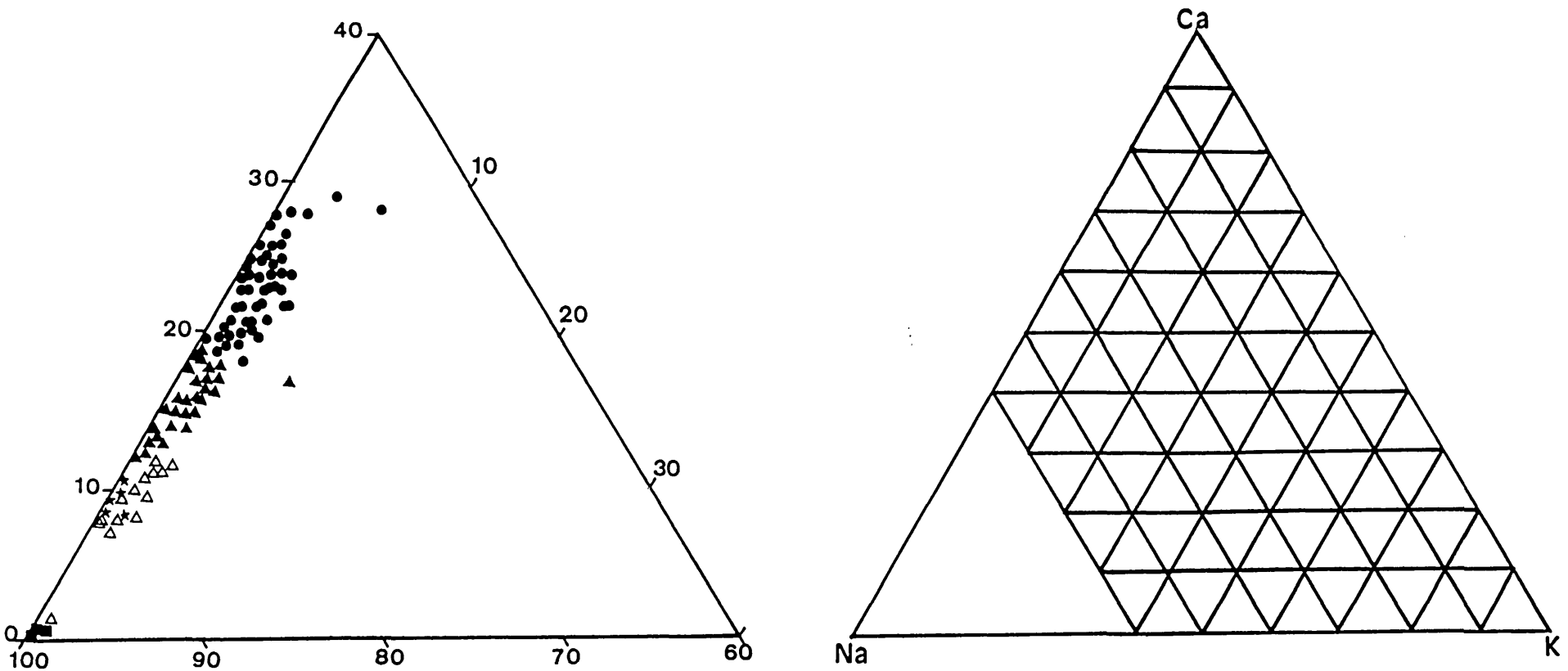


Figure 4.14 Variation in the composition of plagioclase feldspars from the major facies of the Bom Jardim complex. (Symbols as in previous figures.)

facies of the Bom Jardim complex. The feldspars in question form a continuous trend from approximately An_{30} to An_7, with the feldspars from the very coarse grained alkali syenites forming an isolated cluster close to Ab_{100}. Each major type can be defined by a tightly constrained group of plagioclase compositions.

Plagioclases from the monzonites and mafic syenites are oligoclase with compositions ranging from Ab_{71} An_{29} Or_3 to Ab_{80} An_{19} Or_1. The plagioclase phenocrysts do show some normal zoning with the maximum difference in An content core and rim compositions observed in a single crystal being An_4.

The plagioclase feldspars from the medium grained px-bio-amph syenites show a compositional range from Ab_{76} An_{17} Or_7 to Ab_{87} An_{13} Or_0. Normal zoning has been observed in all samples within this facies, although in general the compositional differences between cores and rims are quite small.

The plagioclase feldspars in the pyroxene biotite leuco alkali feldspar syenites vary in composition from Ab_{87} An_{11} Or_2 to Ab_{98} An_1 Or_1. Zoning was not detected. The granites also contain unzoned plagioclase feldspars which show a range in composition from Ab_{80} An_{19} Or_1 to Ab_{91} An_9 Or_0. In contrast the very coarse grained alkali syenites contain essentially pure albite Ab_{99} An_0 Or_1.

4.2.5 Alkali feldspars

Alkali feldspars have been analysed in a representative set of samples from the main facies of the Bom Jardim complex. Representative analyses from the main rock types are given in table 4.6, individual analyses are listed in the appendix D (tables D.5.1 to table D.5.4). Figure 4.15 shows the compositional range of alkali feldspars from the complex (Or_{48} Ab_{51} An_{10} to Or_{93} Ab7 An_0). Zoning is common amongst the alkali feldspars and usually takes the form of an enrichment in the An molecule in the core related to the rim.

Table 4.6 Representative analyses of alkali feldspar from the major facies of the Bom Jardim complex.

	31	**35**	**268**	**48**	**10**	**23**
SiO_2	64.25	64.04	63.48	64.14	64.97	64.18
Al_2O_3	18.44	19.12	19.37	18.02	18.63	18.17
CaO	0.00	0.29	0.22	0.00	0.22	0.00
K_2O	15.78	12.07	13.05	15.35	14.45	16.27
Na_2O	0.69	3.04	2.42	0.81	1.82	0.51
BaO	0.60	0.77	1.22	1.41	0.27	0.38
Total	99.76	99.33	99.76	99.72	100.37	99.51
Or	93	71	77	92	83	95
Ab	7	27	22	8	16	5
An	0	2	1	0	1	0

A series of core to rim transverses were made across two alkali feldspar phenocrysts with the individual spot analyses being carried out at the approximately 100 micron intervals. The results for BaO contents are shown in figure 4.16. The phenocryst from sample 29 (px-bio-amph mafic syenite), is clearly zoned with respect to barium; the core showing a marked enrichment in that element relative to the rim. The other phenocryst studied, (sample 35) from the same facies is again zoned with respect to barium but in this case the core shows a depletion in BaO with respect to the rim.

Experimental data from Long and Luth (1986) have indicated that when K-feldspar crystallises alone from a granitic melt it tends to be normally zoned with respect to barium. However the crystallisation of plagioclase, amphibole, pyroxene and any other phase with a Kd for Ba less than 1.0 will tend to cause an increase of Ba in the residual melt and consequently the K-feldspar will tend to be enriched in Ba towards the rim. Since both the above samples 29 and 35 are representatives of the same facies, it suggests that either alkali feldspar crystallised episodically or that it had a long crystallisation interval

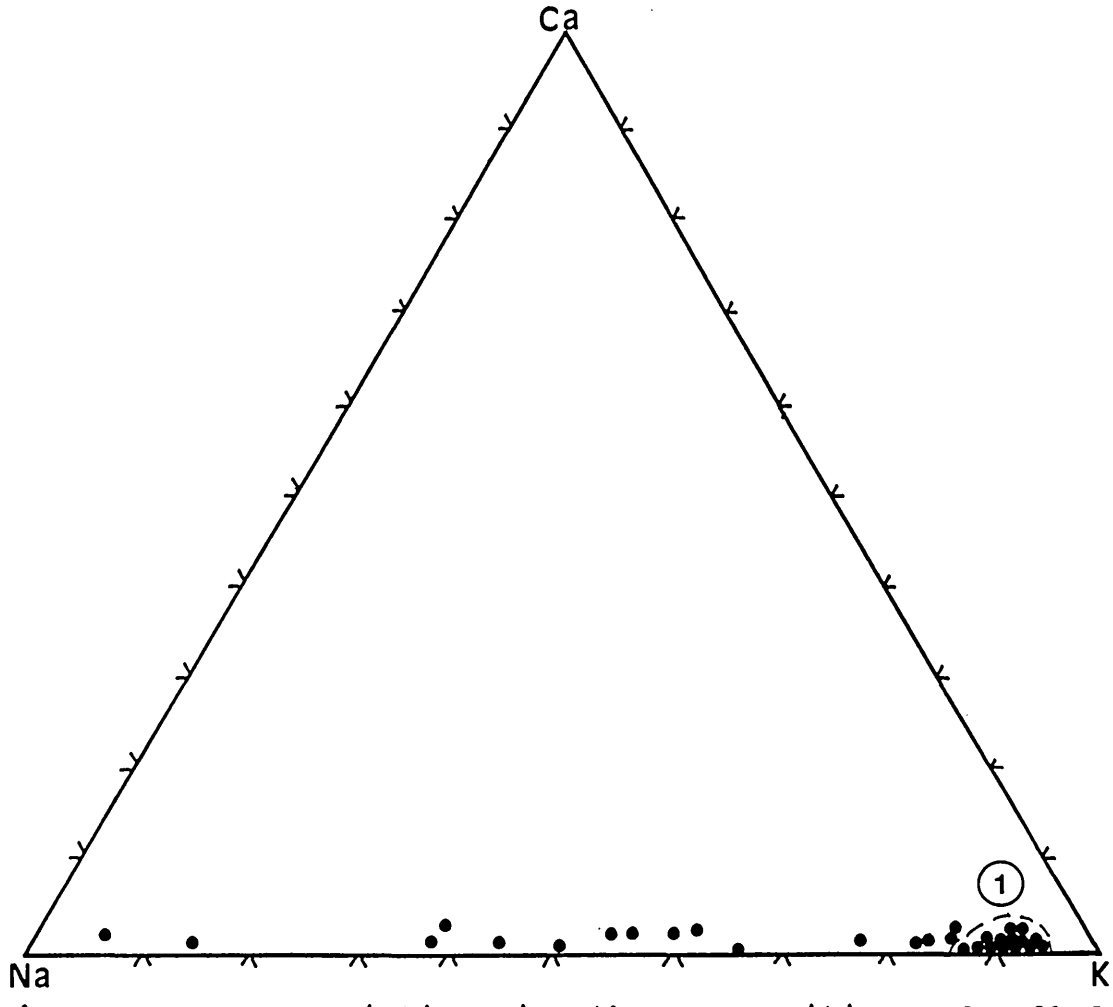


Figure 4.15 Variation in the composition of alkali feldspars within the Bom Jardim complex. Field denoted (1) represents the composition of 53 individual micropobe analyses.

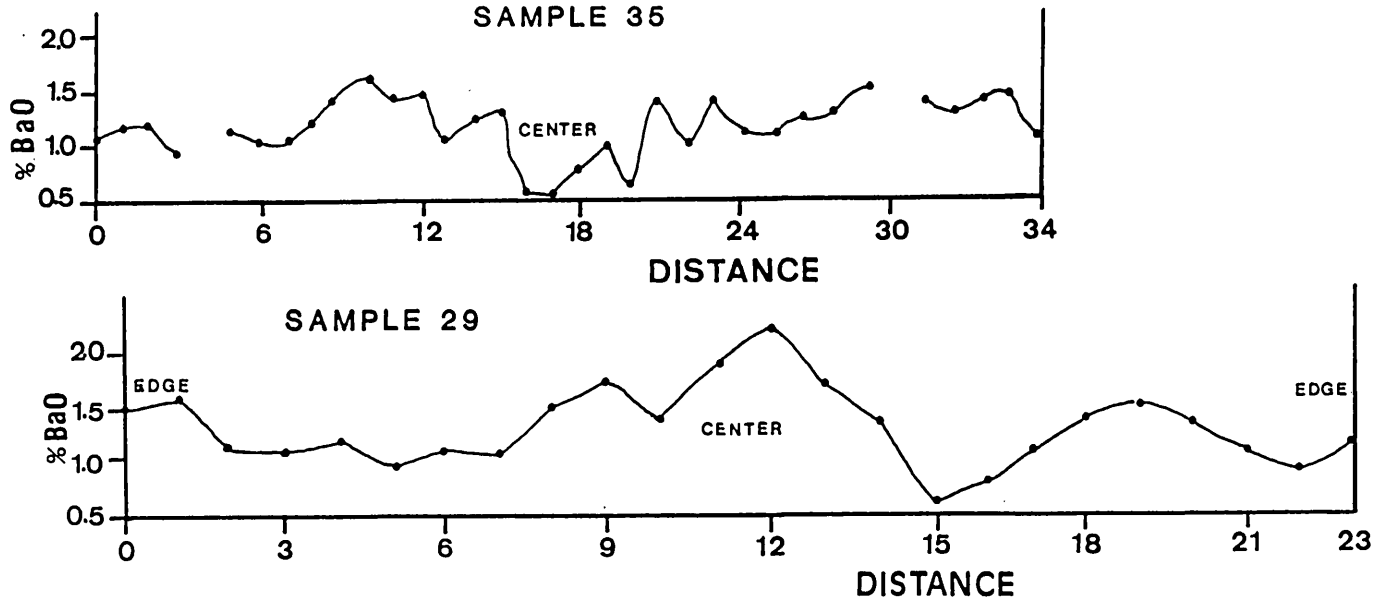


Figure 4.16 Variation in the BaO content across two alkali feldspar megacrysts from the mafic syenites. Gaps in the traverse for sample 35 represent plagioclase inclusions. Distance in microns $X10^2$

during the evolution of this particular magma sequence. This behaviour of Ba in alkali feldspars can also be seen occurring in other facies. The iron contents (expressed as FeO in all analyses) of the alkali feldspars from the complex are generally lower than 0.22 wt% and, this is usually taken to indicate relatively slow cooling conditions (Smith, 1974).

4.2.6 Minor phases

Apatite, zircon, sphene, allanite, monazite, thorite, together with some rarer varieties of thorium rich minerals were analysed by electron microprobe. Individual analyses can be found in table D.7, appendix D. Average analyses can be seen listed in table 4.7.

Zircon and apatite which are found in all the main facies of the complex have REE contents below the detection limits of the electron microprobe.

Table 4.7 Average analyses of minor phases from the major facies of the Bom Jardim complex.

Apatite		Monazite		Allanite		Sphene	
	(4)		(5)		(5)		(8)
CaO	54.73	La_2O_3	22.82	SiO_2	31.90	SiO_2	29.65
P_2O_5	44.10	Ce_2O_3	29.02	Al_2O_3	14.74	Al_2O_3	0.97
SiO_2	0.50	Nd_2O_3	6.02	FeO*	11.56	FeO*	1.90
Na_2O	0.11	PbO	0.88	MgO	0.72	TiO_2	36.00
Total	99.44	ThO_2	9.34	CaO	11.46	CaO	27.29
		CaO	0.84	TiO_2	1.09	Ce_2O_3	1.53
Zircon		P_2O_5	27.41	La_2O_3	7.80	Nd_2O_3	0.54
		Total	96.33	Ce_2O_3	10.07	Total	97.88
	(2)			Nd_2O_3	1.53		
ZrO_2	66.35			ThO_2	0.69		
SiO_2	32.69			Total	91.96		
Total	99.04			* Total Fe expressed as FeO			

In the larger grains of allanite zoning of ThO_2 and the LREEs has been detected, such elements are found in much higher concentration in the cores of the grains than in the rims. In all cases the allanite grains are surrounded by epidote with REE contents below the detection limit. Epidote appears to replace allanite in the crystallisation sequence of the complex, the latter mineral is absent from the more evolved leuco syenites.

The monazites show a wide range of ThO_2 contents ranging from 2.98 to 19.13 wt%. Zoning has again been detected with both ThO_2 and the LREEs being enriched in the cores relative to the rims. The smaller grain size of monazites from the monzonites and mafic syenites prevented the determination of core and rim analyses. However single spot analyses from these smaller grains showed ThO_2 and LREEs very similar to the cores of the monazites from the medium grained pyroxene biotite amphibole syenites. Careful examination of some of the monazite grains has shown a very complex mineral chemistry. One grain in particular from the pyroxene biotite leuco syenite appears to be a member of the thorite-monazite series, but within it are exsolved blobs of phosphorus rich minerals. The whole grain is in turn surrounded by a sphene with abnormally high ThO_2 values. The distribution of the various phases within this particular composite grain can be seen in a series of S.E.M. back-scattered images in plate 4.1.

A group of minerals with the approximate formula of $Th(SiO_4)$ have also been observed within the MPBAS, PBLS and granites of the complex. The chief minerals are thorite (tetragonal), huttonite (monoclinic). Huttonite is isostructural with monazite $REE(PO_4)$ and brabanite $CaTh(PO_4)_2$ (Speer, 1980), whereas thorite is isostructural with zircon, and generally contains greater than 4.0 wt% P_2O_5.

Up to 15 wt% water has been reported in thorite. It is generally thought to be present as essential structural molecular water, rather than simply being absorbed by the metamictic mineral, i.e. they are hydroxyl thorites (thorogummite) with the formula $Th(SiO_4)_{1-x}(OH)_x$. Huttonite has a denser structure and is generally believed

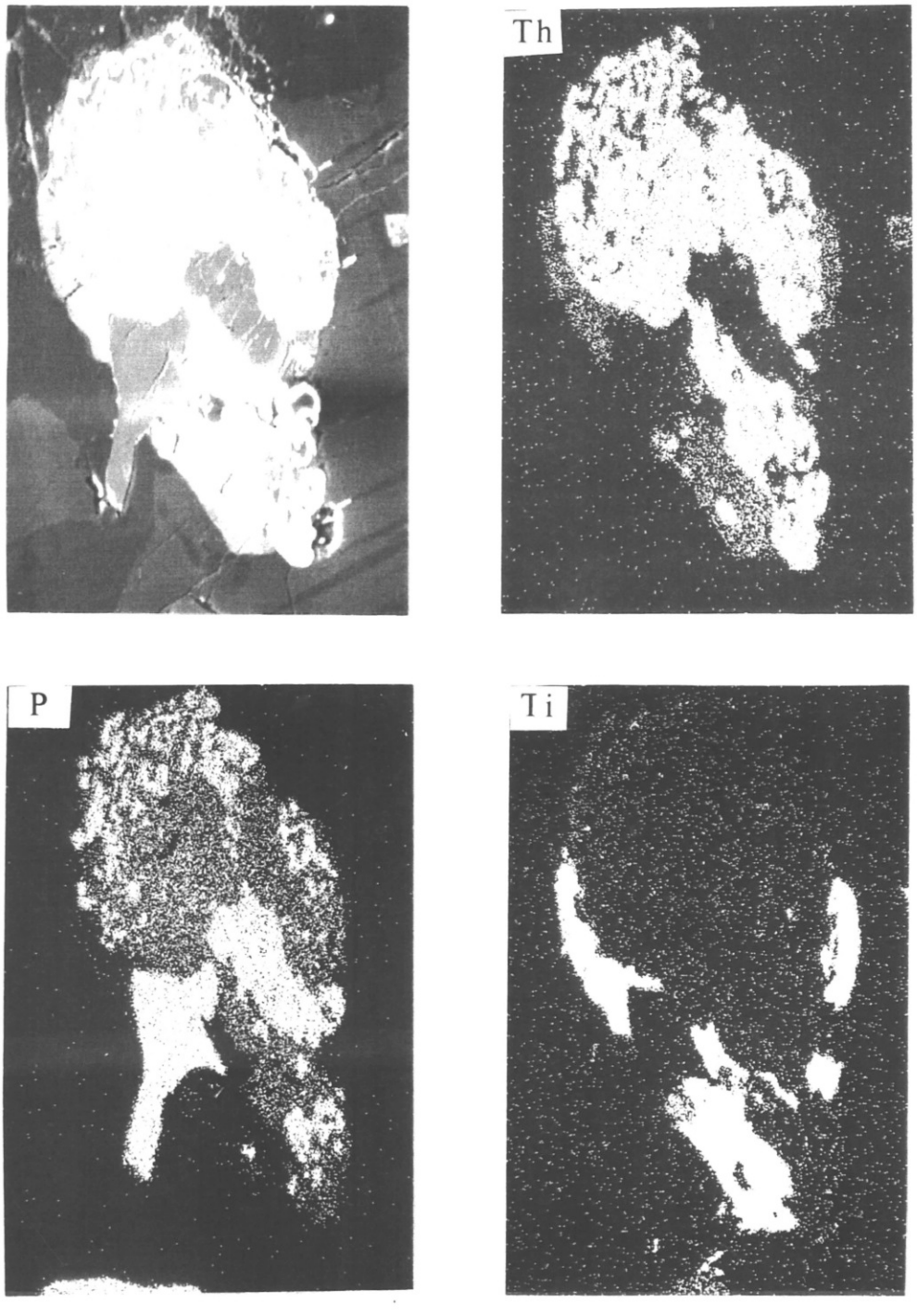


Plate 4.1 S.E.M. back-scattered images showing the distribution of P, Th and Ti in a grain of monazite from the PBLS facies. Magnification X300.

to be unable to accomodate molecular water. Over 45 elements have been reported occurring in a wide range of abundances within this group of minerals (Speer, 1980) as a consequence the number of possible substitutions within the series is vast. In general there are two kinds of substitutions, those for Si^{4+} and Th^{4+}. Such substitutions can not be treated separately as often coupled substitutions are required to satisfy charge balance. For thorites with low REE contents, small amount of P^{5+} substituing for Si^{+4} could provide the necessary charge balance eg, $Th^{+4} + Si^{+4} \rightleftharpoons REE^{+3} + P^{+5}$. The present data indicates that all the minerals within this group have P_2O_5 contents greater4.0 wt%. If the REE contents exceed those of P, then U^{6+} substitutions could provide the required charge balancing mechanism eg. $2REE^{3+} + U^{6+} \rightleftharpoons 3Th^{4+}$. Inspection of table 4.8 shows that values of UO_3 up to 2.7 wt% have been determined in some specimens. The total REE contents for the Thorite- huttonite group of minerals varies from 1.5 to 63.4 wt%. Staatz et al. (1976) after reviewing available thorite analyses in literature concluded that the mineral does not selectively accommodate one specific group of REE in preference to another, but simply incorporates what is available at the time of crystallisation. In the case of the Bom Jardim complex it would appear that the LREE are the most abundant.

Within the PBLS a distinctly different group of Th-rich minerals have been observed (see plate 4.2). These are normally titanium silicates containing ThO_2 (1.63 to 17.27 wt%), PbO (1.95 to 12.6 wt%) and a wide range of REE contents varying from 3.78 to 57.82 wt%. Individual electron microprobe analyses of the different phases shown in plate 4.2 can be seen listed in table 4.8. The dominance of the LREE enrichment within this group of minerals can be seen in figure 4.17.

The range of probable substitutions shown within this group of minerals is rather unusual. Normally the REE are expected to substitute for calcium within sphene-type minerals, however in the present case it would appear that the REE group tends to replace Ti^{4+}, and the calcium is in fact replaced by Th^{4+} (and possibly PbO which is generally

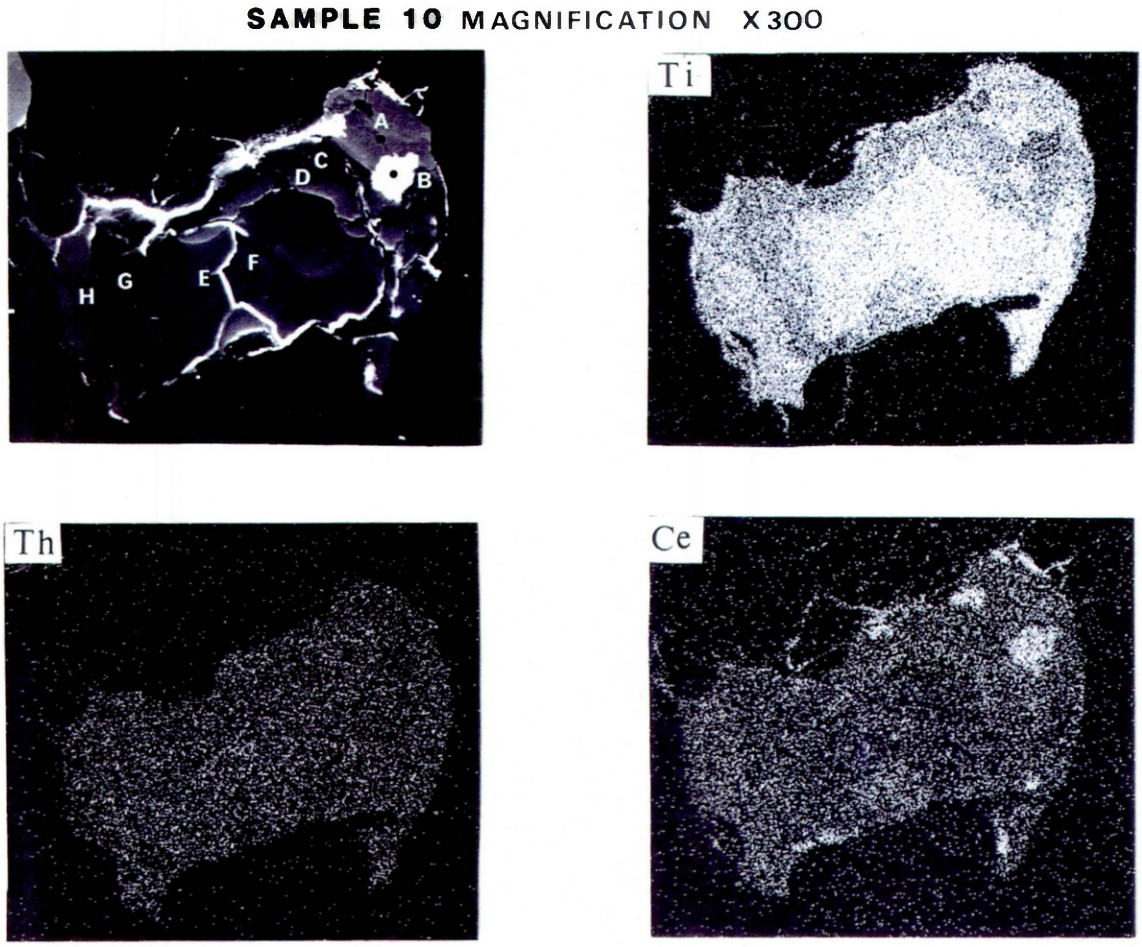


Plate 4.2 S.E.M back-scattered images of LREE, Th rich sphenes from the PBLS facies.

Table 4.8 Electron microprobe analyses of two Th LREE rich Sphene (keilhauite).

SAMPLE 10

	A	B	C	D	E	F	G	H
SiO_2	15.68	9.36	18.63	19.37	10.92	10.90	20.43	21.04
Al_2O_3	0.89	0.52	1.67	1.37	0.70	0.68	1.15	1.19
TiO_2	1.09	11.59	29.24	25.32	45.76	49.69	36.65	36.66
MgO	1.49	0.10	0.37	0.29	1.00	1.08	0.53	0.45
FeO	2.49	0.43	3.02	2.07	7.00	6.85	3.97	3.53
CaO	4.16	3.74	4.19	2.29	2.65	2.43	5.57	5.96
K_2O	0.22	0.09	1.51	0.46	1.28	1.32	0.37	0.04
MnO	0.00	0.00	0.00	0.03	0.03	0.01	0.02	0.06
La_2O_3	24.35	11.09	2.30	1.98	1.54	1.45	2.36	2.28
Ce_2O_3	23.64	21.14	4.48	4.28	2.98	2.92	5.91	5.77
Pr_2O_3	1.80	1.92	0.66	0.42	0.44	0.23	0.51	0.51
Nd_2O_3	5.97	6.62	1.53	1.55	0.81	0.76	1.72	1.76
Sm_2O_3	0.77	0.93	0.32	0.17	0.26	0.18	0.24	0.32
Gd_2O_3	1.29	1.05	0.19	0.23	0.17	0.33	0.35	0.11
UO_2	0.16	0.36	0.64	0.64	0.87	1.05	0.85	0.65
ThO_2	0.00	2.68	7.18	6.55	6.89	7.66	6.47	6.18
PbO	0.00	0.92	2.20	1.90	1.72	1.80	2.57	2.54
Y_2O_3	0.05	0.12	0.11	0.07	0.10	0.01	0.13	0.12
Nb_2O_5	0.00	0.14	0.44	0.34	0.69	0.66	0.37	0.47
ZrO_2	0.00	0.25	0.98	0.84	1.21	1.07	0.89	0.86
Total	84.01	73.05	79.66	70.17	87.02	91.08	91.06	90.50

Total iron expressed as FeO

To be continued

Table 4.8 (continued)

	SAMPLE 159	
	RIM	CORE
SiO_2	5.83	17.34
Al_2O_3	0.11	1.51
TiO_2	13.13	40.72
MgO	0.09	0.42
FeO	0.53	3.28
CaO	4.73	3.8
K_2O	0.07	0.35
MnO	0.03	0.28
La_2O_3	14.90	0.62
Ce_2O_3	25.84	4.65
Pr_2O_3	1.48	0.56
Nd_2O_3	6.05	0.71
Sm_2O_3	0.44	0.16
Gd_2O_3	0.84	0.15
UO_2	0.35	0.34
ThO_2	2.64	6.62
PbO	2.84	8.81
Nb_2O_5	0.12	0.30
ZrO_2	0.35	1.06
Y_2O_3	0.17	0.03
Total	80.54	91.72

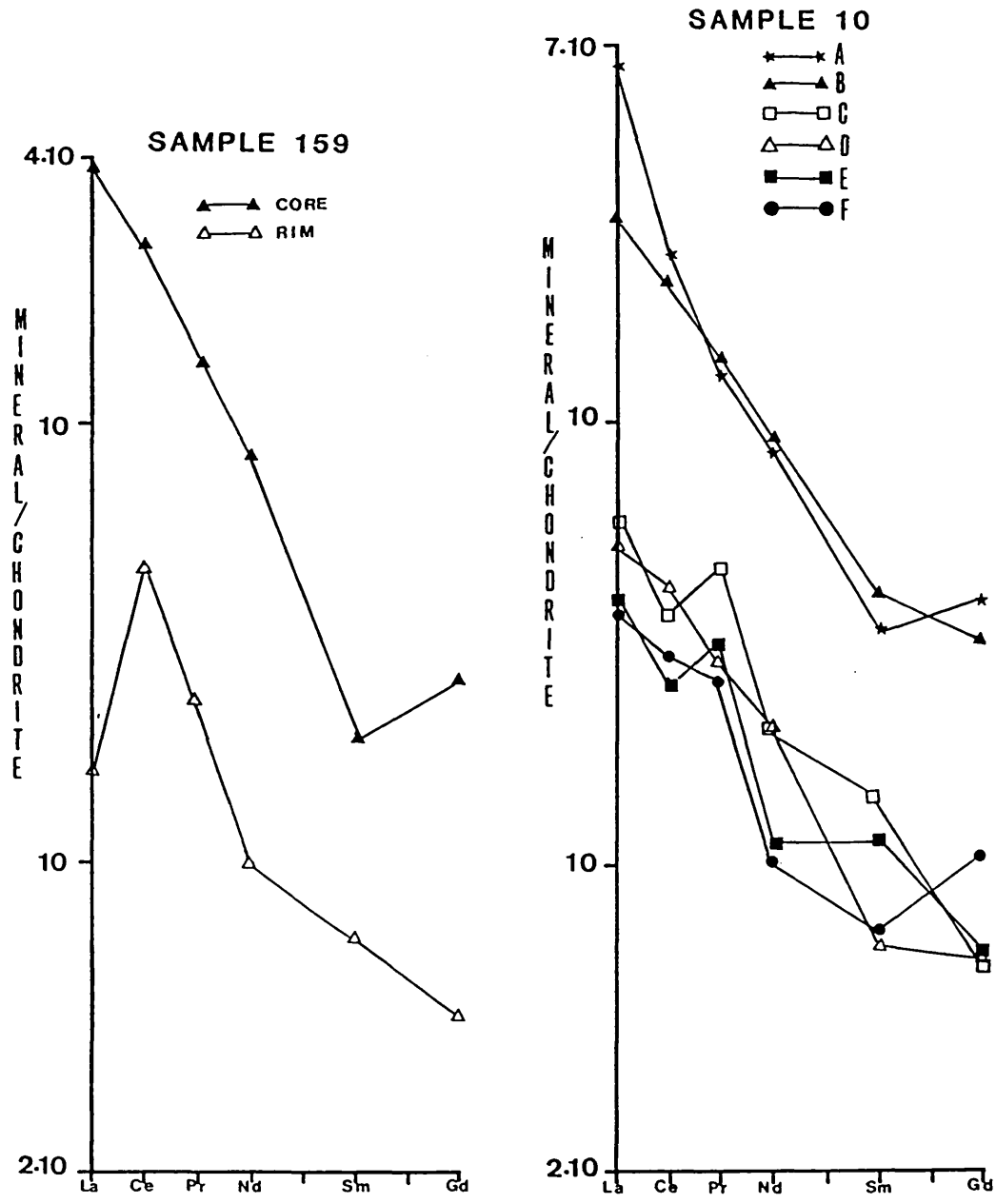


Figure 4.17 Chondrite normalized REE plots for two Th-LREE enriched sphene (keilhauite) grains from the leuco syenites (samples 10 and 159). The locations of the points analysed in sample 10 are shown in plate 4.2.

considered to be a decay product).

The author has found it extremely difficult to find comparable minerals within the literature. The only published data showing roughly comparable substitutions but with far lower REE contents, are keilhauites (Kubach and Wolgang, 1984). These are sphenes with > 3.0 wt% Of RE_2O_3.

These thorium rich minerals in the Bom Jardim complex are frequently zoned with a marked increase in total REE content towards the rim (see table 4.9 sample 159, and figure 4.17). Marked increases in the REE content within the rims of sphene grains has been reported by Gromet and Silver (1983). They indicate that this zonal distribution of the REEs is commonly found when their contents within a crystallising magma remains essentially constant.

Sphene is a commonly occurring accessory phase in most members of the Bom Jardim complex. Individual analyses of sphene can be found in table D.7, appendix D. The majority of primary sphenes show LREEs contents (La_2O_3 + Ce_2O_3 + Nd_2O_3) greater than 1 wt%, coupled with their ubiquitous appearance (far more abundant than keilhauite) makes sphene the major mineral control during the fractionation of the LREEs within the complex.

4.2.7 Opaque minerals

Magnetite is by far the most dominant opaque phase within the rocks of the Bom Jardim complex, ilmenite has only been recorded as a secondary phase in members of the leuco syenite facies. Individual magnetite analyses are listed in table 6.1 to 6.3, appendix D. TiO_2 contents are generally low (<0.25 wt%) as is MnO (<0.26 wt%). The Cr_2O_3 contents generally show a marked negative correlation with the differentiation index (see figure 4.18); the absolute values ranging from 4.02 wt% Cr_2O_3 in the mafic syenites to < 0.36 wt% in the leuco syenites.

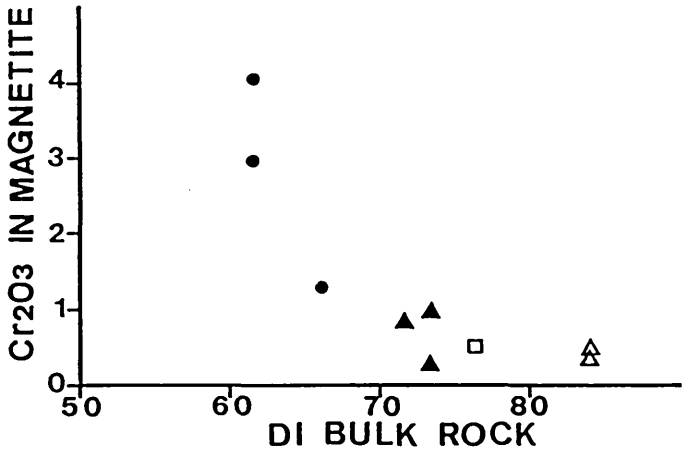


Figure 4.18 Variation in the Cr_2O_3 contents of magnetites as a function of the differentiation index for members of the major rock facies within the Bom Jardim complex. Filled circles represent magnetites from the mafic syenites and monzonites, filled triangles from the medium grained syenites, open squares from the very coarse grained syenites and open triangles from the leuco syenites.

4.3 MINERAL CHEMISTRY OF THE MINOR FACIES

4.3.1 Pyroxenes

Pyroxene from five dykes and six enclaves have been analysed. The individual analyses are listed in appendix D, tables D.1.6 and D.1.7 and the data plotted in the pyroxene quadrilateral shown in figure 4.19A and 4.19B.

The majority of the pyroxene compositions fall within the field defined by the major facies discussed previously and hence are mainly salites. In general the pyroxenes from the dykes and enclaves contain less of the hedenbergite molecule than those from the major facies. The pyroxene data from the two pyroxene diorite (see table 4.9) have been plotted separately in figure 4.19B. This particular unit is unique within the Bom Jardim complex and will be discussed in a later chapter.

Table 4.9 Representative analyses of pyroxenes from the two pyroxene diorite.

	SAMPLE 272A					
SiO_2	52.30	52.00	51.89	52.29	52.98	52.30
TiO_2	0.00	0.00	0.00	0.00	0.00	0.00
Al_2O_3	0.67	0.70	0.68	1.08	0.94	1.15
FeO	25.12	25.45	25.14	9.44	9.52	9.85
MnO	0.70	0.52	0.48	0.00	0.00	0.35
MgO	19.71	20.74	20.68	13.87	13.60	13.53
CaO	0.78	0.63	0.84	22.53	22.46	22.25
Na_2O	0.49	0.54	0.62	0.79	0.62	0.87
Total	99.77	100.58	100.33	100.00	100.12	100.30
Wo	2	1	2	46	46	46
En	57	59	58	39	39	38
Fs	41	40	40	15	15	16

Total iron expressed as FeO.

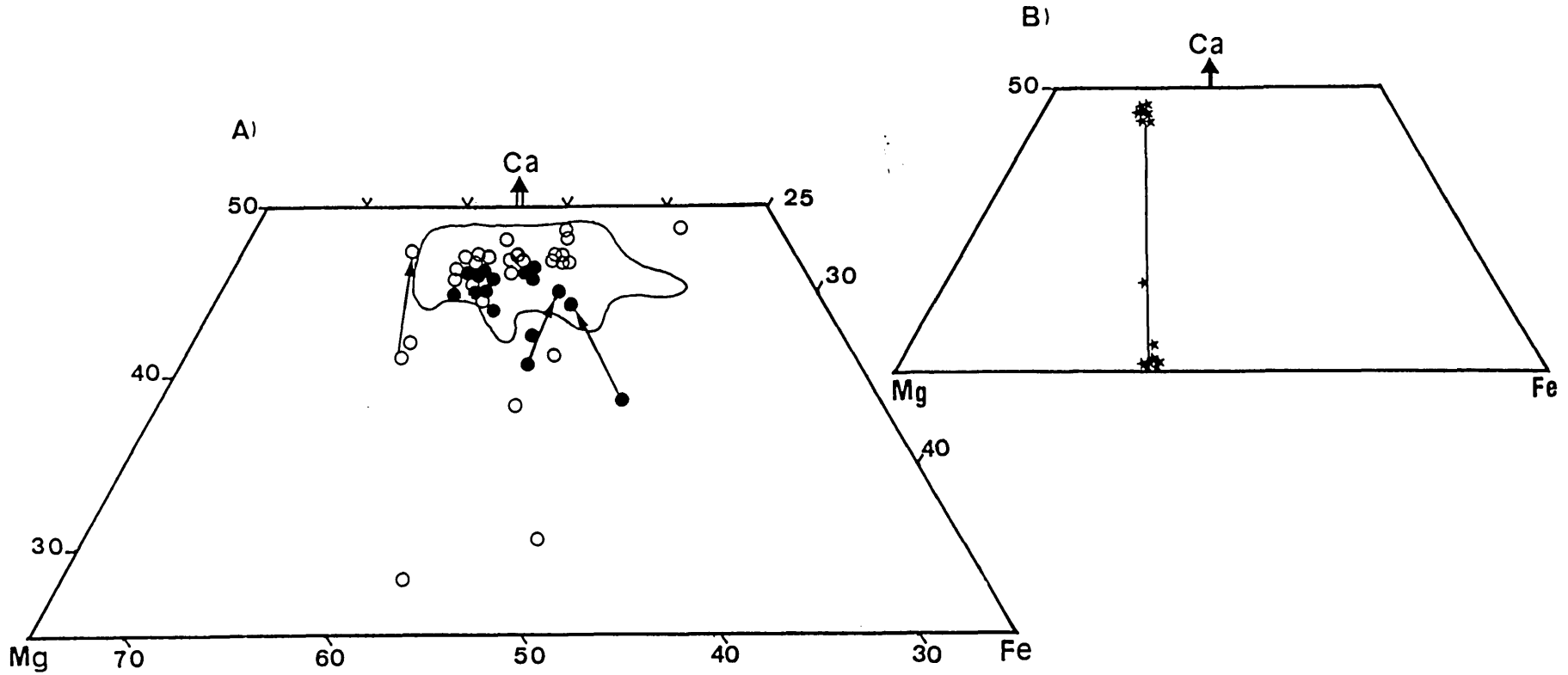


Figure 4.19 (A) Composition of clinopyroxenes from members of the minor facies within the Bom Jardim complex. Open circles represent pyroxenes from enclaves, and closed circles pyroxene from dyke rocks. Arrows indicate variations in composition from core to rim within individual pyroxene grains. The field enclosed by a continuous line indicates the range of pyroxene compositions from the major facies of the complex. (B)- Composition of calcium rich and calcium poor pyroxenes from the two pyroxene diorite (see text for details).

4.3.2 Amphiboles

Thirty amphiboles analyses have been determined from three dyke and five enclave samples. The individual analyses can be seen in appendix D, tables D.2.3 and D.2.4. Again both the classification and nomenclature used for the amphiboles are after Leake (1978). The magmatic amphiboles from the minor facies of the complex range in composition from magnesio-hornblende, edenite and tchermakitic-hornblende (see figure 4.20). Secondary actinolitic hornblendes are also present usually replacing clinopyroxene. Within some of the enclaves magnesio-cummingtonite has been identified replacing crystals of calcium poor pyroxene. Analyses of these amphiboles are listed in table D.2.3 (sample 265B) appendix D.

4.3.3 Biotites

Biotites have been analysed in nine enclaves, and six dyke rocks, including the two pyroxene diorite. The individual analyses are listed in tables D.3.6 and D.3.7, appendix D. The biotites generally show a range in the Fe\Fe+Mg ratio from 0.24 to 0.44, which are similar to the values quoted for biotites from the major facies i.e., 0.33 to 0.43. Figure 4.21A shows a plot of MgO versus Fe\Fe+Mg for biotites from the minor facies of the complex. The small field (labelled 1 in figure 4.21A) are from the more mafic enclaves which occasionally contain cummingtonite, as expected they have much lower Fe\Fe+Mg ratio. Also included in this diagram are the data for the country rock biotites which have higher Fe\Fe+Mg ratios. Figure 4.21B shows the variation of Al_2O_3 contents as a function of the Fe\Fe+Mg ratio again, three distinct biotite populations can be identified: those with low alumina and Fe\Fe+Mg ratios from the more mafic inclusions (associated with cummingtonite); a field of biotites from the metasedimentary country rocks with both high Fe\Fe+Mg ratios and alumina contents; and finally a field making up the majority of biotites from the enclaves and dykes. Within this latter field there is total overlap of data from the two rock types.

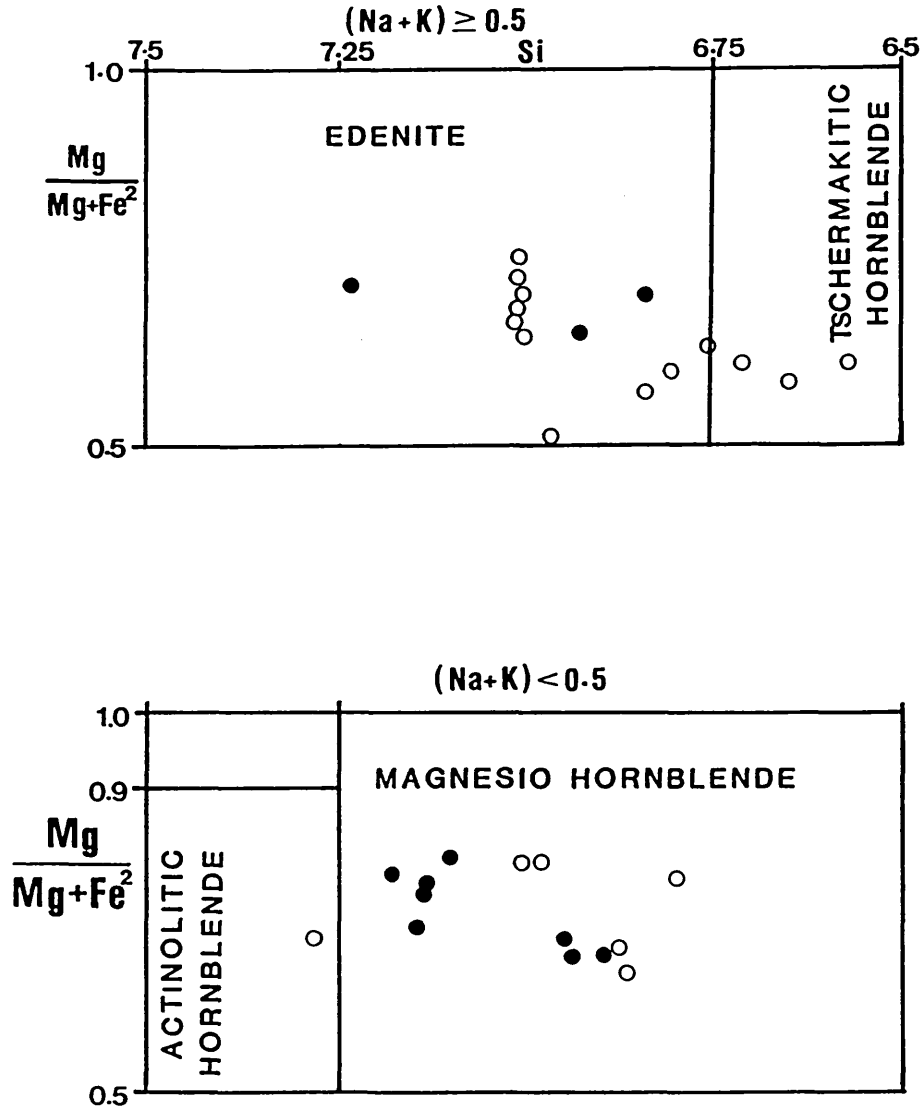


Figure 4.20 Composition and classification of amphiboles from the minor facies of the Bom Jardim complex (After Leak, 1978). Open circles represent amphiboles from the enclaves and closed circles amphiboles from the dyke rocks.

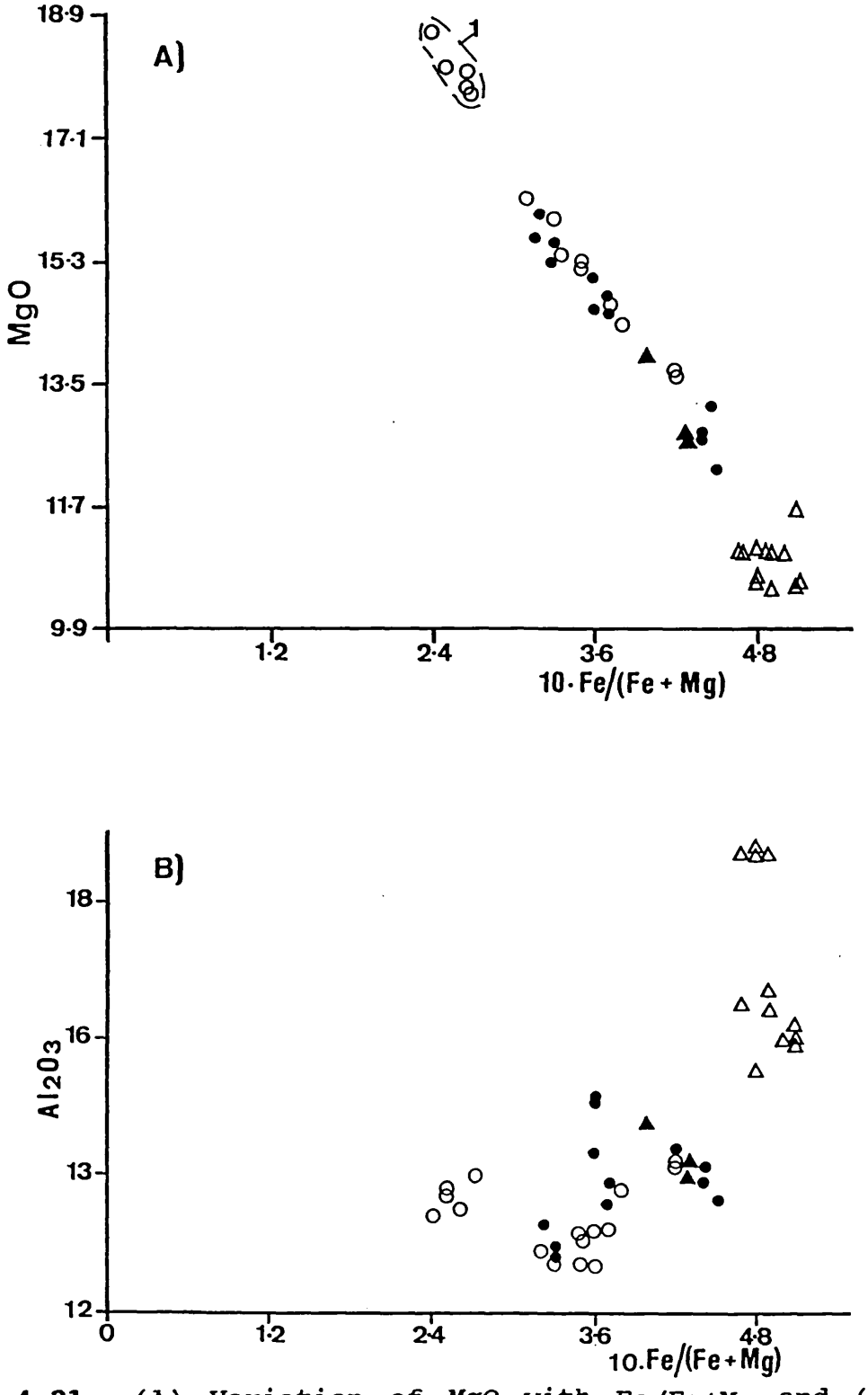


Figure 4.21 (A) Variation of MgO with Fe/Fe+Mg and (B) variation of Al_2O_3 content with Fe/Fe+Mg ratio for biotites from the minor facies of the Bom Jardim complex. Closed circles represent biotites from the enclaves, open circles biotites from the dykes, closed triangles biotites from the two pyroxene diorite. Open triangles represent biotites from the metasedimentary country rocks. The field denoted (1) represents those biotites coexisting with cummingtonite.

The biotite analyses from minor facies in which plagioclase is dominant over alkali feldspar show much higher barium contents than biotites in which alkali feldspar is dominant over plagioclase, again indicating a competition for barium between K-feldspar and biotite.

4.3.4 Feldspars

Plagioclase feldspars have been analysed from all the minor facies rock types. Individual analyses can be found in tables D.4.5 and D.4.6, appendix D. The data is plotted in figure 4.22. The plagioclase feldspars do show some normal and oscillatory zoning, varying in composition from Ab_{47} An_{52} Or_1 to Ab_{90} An_9 Or_1. There is considerable overlap in plagioclase compositions from the dykes and enclaves, and as expected the plagioclase feldspars from the two pyroxene diorite generally show the highest anorthite contents. Overall the spectrum of plagioclase composition is very similar to those from the mafic syenites and monzonites.

The individual analyses of alkali feldspars are listed in tables D.5.5 and D.5.6, appendix D, and the data is shown in figure 4.22. Their compositions range from Or_{95} Ab_5 An_0 to Or_{14} Ab_{82} An_4, with the greatest number clustering around Or_{92} Ab_8 An_0. Zoning is fairly common, but the range in core\rim compositions is quite small. The pattern of chemical zoning with respect to barium is very similar to that displayed by the alkali feldspars of the host syenites.

4.3.5 Minor phases

Sphene, allanite, monazite, together with some opaque phases have also been analysed from different members of the minor facies of the Bom Jardim complex, the data is listed in table 4.10.

Sphene analysed from a dyke rock (sample 205) has a LREE content (Ce_2O_3 + Nd_2O_3 + La_2O_3) great than 1.5 wt%. Allanites from both dyke rocks and enclaves have also

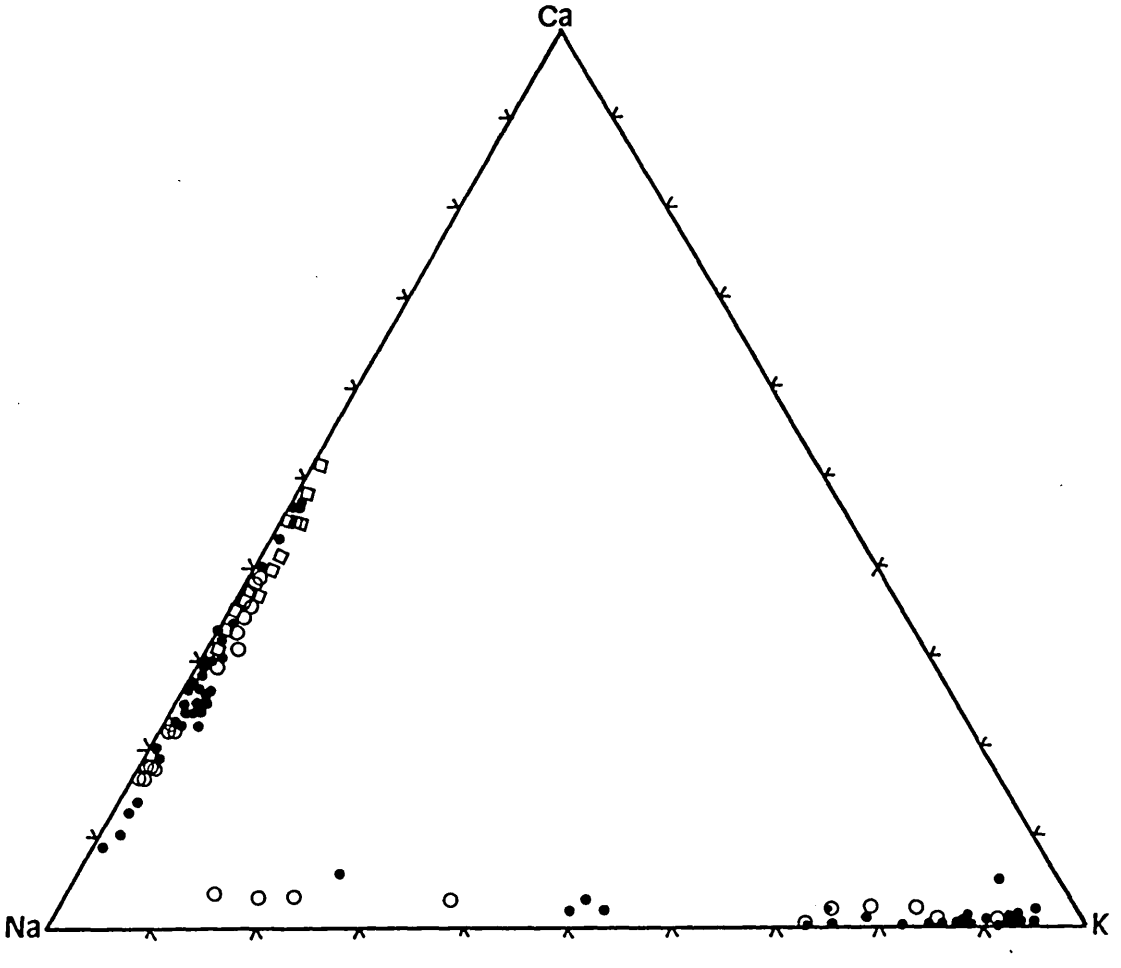


Figure 4.22 Individual micropobe analyses of feldspars from the minor facies of the complex. Open squares represent feldspars from the two pyroxene diorite, closed circles from the enclaves and open circles represent feldspars from the dyke rocks.

been analysed. Members of the thorite-monazite series with exsolved blobs of phosphoros rich minerals in the rims were recorded in one enclave sample.

The opaque minerals are mainly magnetite. However, chalcopyrite and pyrite were identified in some enclave specimens. Cr, Mn and Ti contents in the minor facies magnetites are always lower than the detection limit of the electron microprobe. In the sample 323-A the only opaque mineral is chalcopyrite, justifying the high Cu contents recorded in the whole rock.

Table 4.10 Minor phases analyses from the dykes and enclaves from the Bom Jardim complex.

	ALLANITES				MONAZITES	
	292A	292A	128A		28A	28A
SiO_2	34.50	32.87	33.27		core	rim
TiO_2	1.65	2.54	0.95	La_2O_3	24.44	6.94
Al_2O_3	15.93	13.01	14.96	Ce_2O_3	30.83	8.93
La_2O_3	3.80	3.32	7.57	Nd_2O_3	6.66	1.78
Ce_2O_3	6.39	6.72	11.16	ThO_2	3.57	3.15
ND_2O_3	1.58	1.57	2.44	UO_2	nd	nd
FeO	9.29	11.19	14.05	PbO	1.35	0.00
MgO	0.42	0.40	1.54	CaO	1.17	39.62
CaO	8.67	7.76	12.64	P_2O_5	29.74	38.64
ThO_2	2.14	1.63	0.00	SiO_2	1.47	1.21
Total	85.59	82.46	98.58	Total	99.23	100.27

	SPHENES	
	205	205
SiO_2	29.22	29.12
CaO	26.81	27.17
TiO_2	35.71	36.48
Al_2O_3	0.44	0.50
FeO	2.83	2.87
Ce_2O_3	1.08	1.28
Nd_2O_3	0.82	0.00
Total	96.91	97.42

nd = Not determined
Total iron expressed as FeO

4.4 SUMMARY AND CONCLUSIONS

The mineral chemistries of the essential minerals within the Bom Jardim complex, all indicate trends compatible with a fractionating magma, thereby add further support to the initial findings of the petrographic observations that the fractionation of such mineral phases could largely be responsible for the evolution of the Bom Jardim complex.

Both the compositions and trends of many of the ferro-magnesian minerals determined in the complex are similar to many calc-alkaline examples cited in the literature. In particular, the trend of the clinopyroxenes observed in the present investigation is very similar to those from shoshonitic associations (Morrison, 1980).

In general two conclusions can be drawn when one compares the mineral chemistries of the host rocks (major facies) with the dykes and enclaves. Firstly, many of the enclaves show mineralogies very similar to their host rocks; this could lead one to suppose that some of the enclaves could represent early more mafic products of the crystallising magma, which have been reabsorbed and transformed by reaction with the evolving magma. Secondly, in all the mineral groups studied, there was always a complete overlap in chemistries between the dykes and enclaves, which would seem to support the field observations that at least some of the enclaves could in fact be disrupted dykes.

The quantitative analysis of both the major and minor phases within the Bom Jardim complex will enable the author to quantitatively model the most likely fractionation processes responsible for its evolution. Such data is especially important when one considers the trends in evolution for the REEs, Th and U, and the roles played by such phases as allanite, monazite and sphene.

CHAPTER 5
GEOCHEMISTRY OF THE BOM JARDIM MAJOR FACIES

5.1 INTRODUCTION

Over eighty samples representing the major facies of the complex have been analysed by Inductively Coupled Plasma atomic emission spectroscopy (ICP-AES) for the major elements plus the following trace elements, V, Ba, Zr, Cu, Ni, Cr, Be, Sc and Y. Subsets of the same samples were also analysed by instrumental neutron activation (INAA) for the elements Hf, Ta, Th, U, Cs, La, Ce, Nd, Gd, Tb, Ho, Tm, Yb and Lu at the Natural History Museum after irradiation at the Silwood Park Reactor Center (Imperial College). In addition 32 samples were also analysed for REE and Y plus Sc by ICP-AES at RHBNC (London University). Nb and Pb were determined by wavelength dispersive XRF (Nb at Imperial College and Pb in the Department of Geology, Durham University). Rb was determined by atomic absorption (AA).

Details of the analytical techniques used, together with the assessment of accuracy, precision and detection limits can be found in appendix A. Full major and trace element data are listed in tables B.1 to B.6, C.1.1 to C.1.6 and C.2.1 to C.2.7, appendices B and C, together with the calculated CIPW norms. Average analyses for the different facies are presented in the table 5.1.

5.2 MAJOR ELEMENT GEOCHEMISTRY

5.2.1 Normative data

The CIPW norms have been calculated for the rocks of the Bom Jardim complex, using the computer programme "CIPWM07" (Dr P. Henderson pers comm.). The normative data has been recalculated and plotted in terms of Qz-Ab-Or-Ne (where Ne = Ne+Ks) in figure 5.1. The data points for the syenites and monzonites show a fairly tight cluster defining a field which straddles the Ab-Or join. The majority of rocks are Qz normative, and some (PBM and PBAMS) are Ne normative. For comparative purposes a suite

of Californian granitoids (Sylvester et al., 1978) has also been plotted; as can be seen the field defining the normative data for the Bom Jardim complex is generally more potassic with higher values of normative Or. The field defining the normative data for the Glen Dessary Syenites (Fowler, 1985) shows a very close similarity with the present normative distribution. Normative hypersthene has been recorded in almost all the syenite samples, but is absent in the monzonites. According to Morrison (1980) the presence of normative hypersthene is one of the features which help to distinguish the shoshonitic rock series from those belonging to the tholeiitic and calc-alkaline associations.

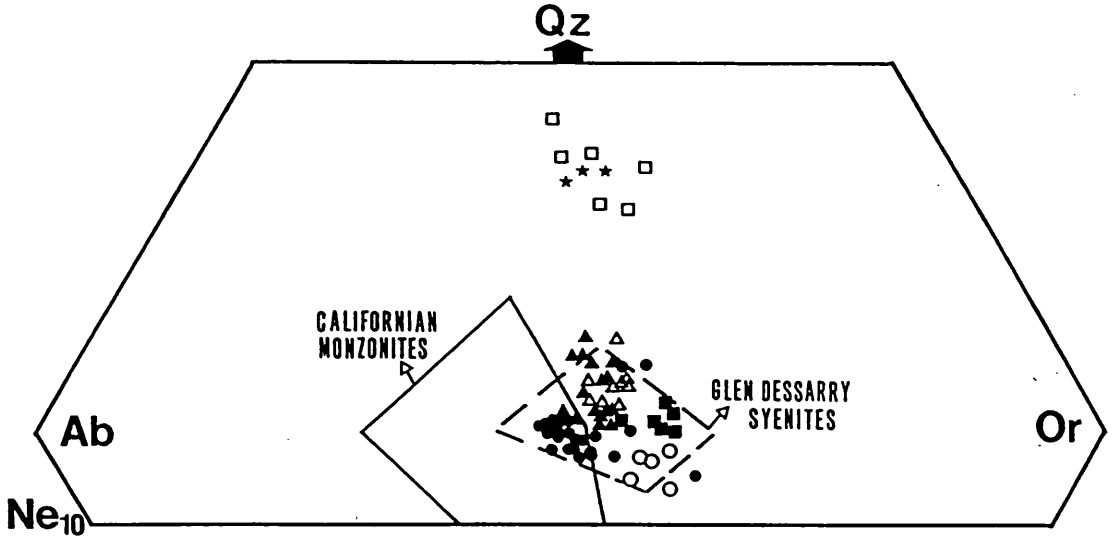


Figure 5.1 Normative data for Bom Jardim granitoids projected in terms of Qz-Ab-Or-Ne (where Ne=normative Ne+Ks).
(open circle = PBM, closed circle = PBAMS, closed triangle = MPBAS, open triangle = PBLS, closed square = CS, open square = pink granites and stars = pink granites from the contact zone between the syenites and country rocks.

Table 5.1 Average whole - rock analyses of the Bom Jardim complex.

	PBM (5)	PBAMS (24)	MPBAS (19)	PBLS (9)	CS (6)	PG (9)
SiO_2	53.77	55.72	60.47	61.76	59.96	73.55
Al_2O_3	15.28	15.18	15.28	15.21	15.88	14.17
Fe_2O_3t	6.64	6.07	4.70	4.71	4.89	1.39
MgO	6.08	5.89	3.86	2.70	2.66	0.43
CaO	5.43	5.52	3.52	2.48	2.93	1.25
Na_2O	3.59	3.64	3.85	4.04	3.85	3.78
K_2O	5.47	5.05	6.06	6.67	7.51	5.02
P_2O_5	0.71	0.61	0.45	0.44	0.47	0.09
TiO_2	1.04	0.94	0.73	0.77	0.94	0.24
MnO	0.09	0.09	0.07	0.06	0.07	0.02
LOI	0.64	0.68	0.60	0.22	0.49	0.36
TOTAL	98.74	99.39	99.59	99.06	99.65	100.30
Cr	288	260	175	90	90	20
Ni	150	140	95	40	30	7
V	110	100	70	70	90	9
Sr	1681	1676	1391	1187	1274	540
Ba	3563	3201	2879	2494	2753	1263
Rb	148	145	190	254	169	176
Zr	300	270	330	500	600	132

Total Fe as Fe_2O_3. Trace elements in ppm

5.2.2 Chemical characterization and classification of the Bom Jardim magma series

The rocks making up the major facies of the Bom Jardim complex cover a wide spectrum of chemical composition, for example silica contents range from 52 to 74 wt%. They are essentially peraluminous with only a minority being metaluminous, as shown by the molecular plot of $CaO - Al_2O_3 - (Na_2O + K_2O)$ in figure 5.2 (after Loiselle and Wones, 1979). The syenites and monzonites define a trend which parallels the peraluminous/metaluminous boundary. The granites are clearly more aluminous relative to both the syenites and monzonites. The modal phases recorded in all rock types of the Bom Jardim complex however are more characteristic of metaluminous granitoids (Shand, 1951).

The K_2O contents of the syenites and monzonites are consistently greater than those of Na_2O, and typically

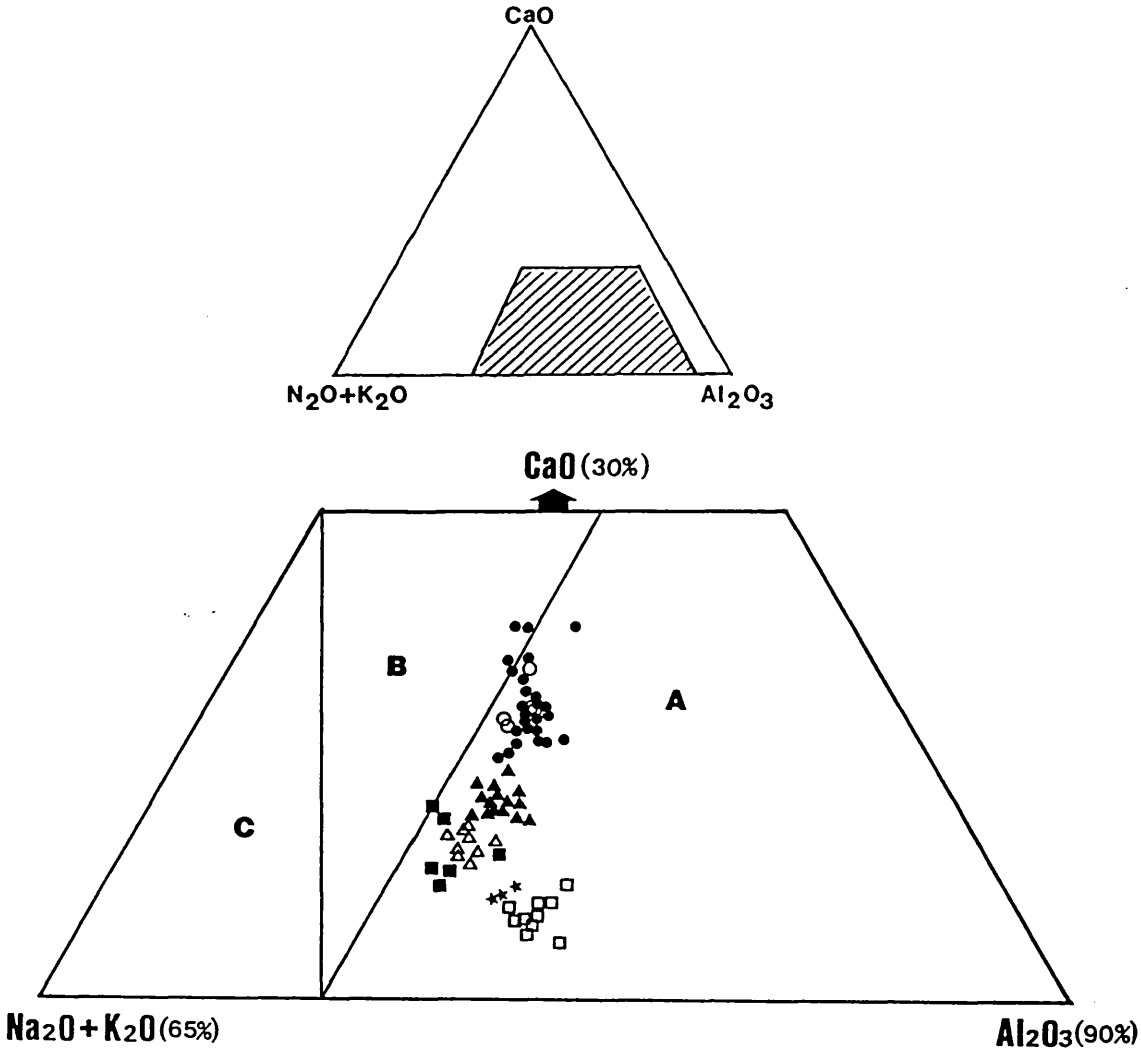


Figure 5.2 Data from the Bom Jardim complex, plotted in terms of molecular $CaO-Al_2O_3-(K_2O + Na_2O)$ (after Loiselle and Wones, 1979). **A** = peraluminous field, **B** = metaluminous field and **C** = peralkaline field. Symbols as indicated in the figure 5.1.

range from 4.6 to 6.9 wt% however, values greater than 7 wt% are found in the coarse grained brown alkali feldspar syenites (CS). Such high values probably reflect some form of alkali-feldspar cumulative process most likely involved in the origin of this particular facies. The (Na+K)/Al cation ratios (agpaitic index) range from 0.66 to 0.92, values of 0.96 have been obtained for the coarse grained brown alkali feldspar syenites (CS). A plot of the above ratios versus the Thornton-Tuttle differentiation index, D.I., (Thornton and Tuttle, 1960) can be seen in figure 5.3. The plot shows a continuous trend of values from the pyroxene biotite amphibole mafic syenites and monzonites (PBAMS) to the pyroxene biotite alkali feldspar leuco syenites (PBLS). Within this overall continuous trend, three distinct populations of the major facies can be identified and it is also clear that the granites within the complex plot off this trend.

In the AFM diagram shown in figure 5.4 the rocks from the Bom Jardim complex define a typical calc-alkaline high K trend (Morrison, 1980). However in figure 5.5 (after Wright, 1969), they clearly fall in the alkaline field. Rogers and Greenberg (1981) used a plot of $\log(K_2O/MgO)$ versus SiO_2 to distinguish between calc-alkaline and alkaline suites; this is shown in figure 5.6, where it can be seen that the majority of the data points fall between the two fields except for the granites which fall within the alkaline field. The alkali lime index (Peacock, 1931) for the rocks of the complex is 51 making the rocks alkalic (see figure 5.7), in all cases $K_2O + Na_2O$ are always greater than CaO.

This apparent confusion of the chemical classification is typical of many of the shoshonitic suites, where they fall in either the alkaline or calc-alkaline fields depending on the discriminant functions used (Smith, 1972; Morrison, 1980; Pagel and Leterrier, 1980; Thompson and Fowler, 1986 and Zhou, 1987). According to Baker (1982), the shoshonitic series shows very similar abundances of the major elements to those of the calc-alkaline series with two major exceptions: the K_2O contents are much higher and the Al_2O_3 values are much lower in the

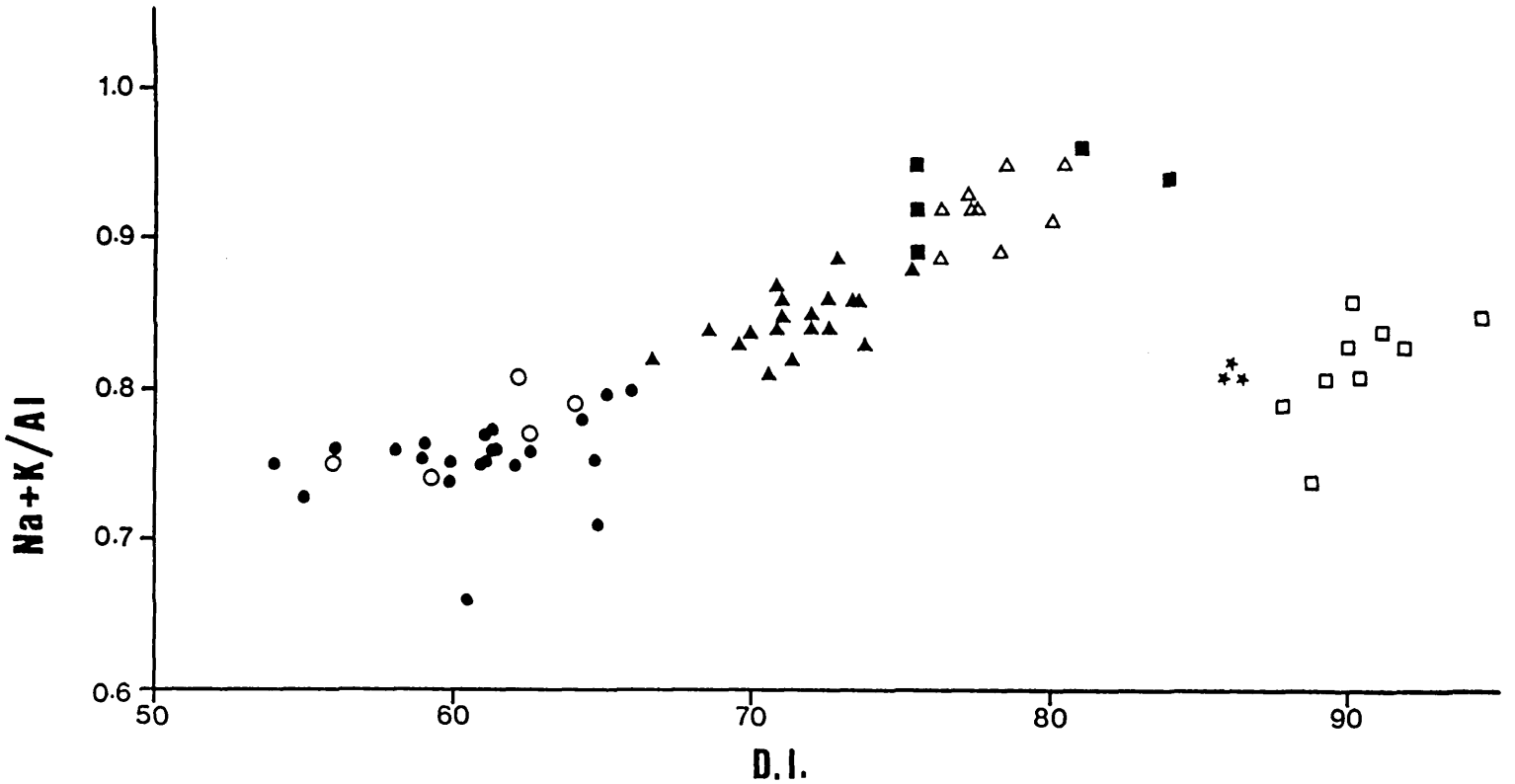


Figure 5.3 Variation of (Na + K) / Al versus DI for rocks from the Bom Jardim complex. Symbols as in figure 5.1.

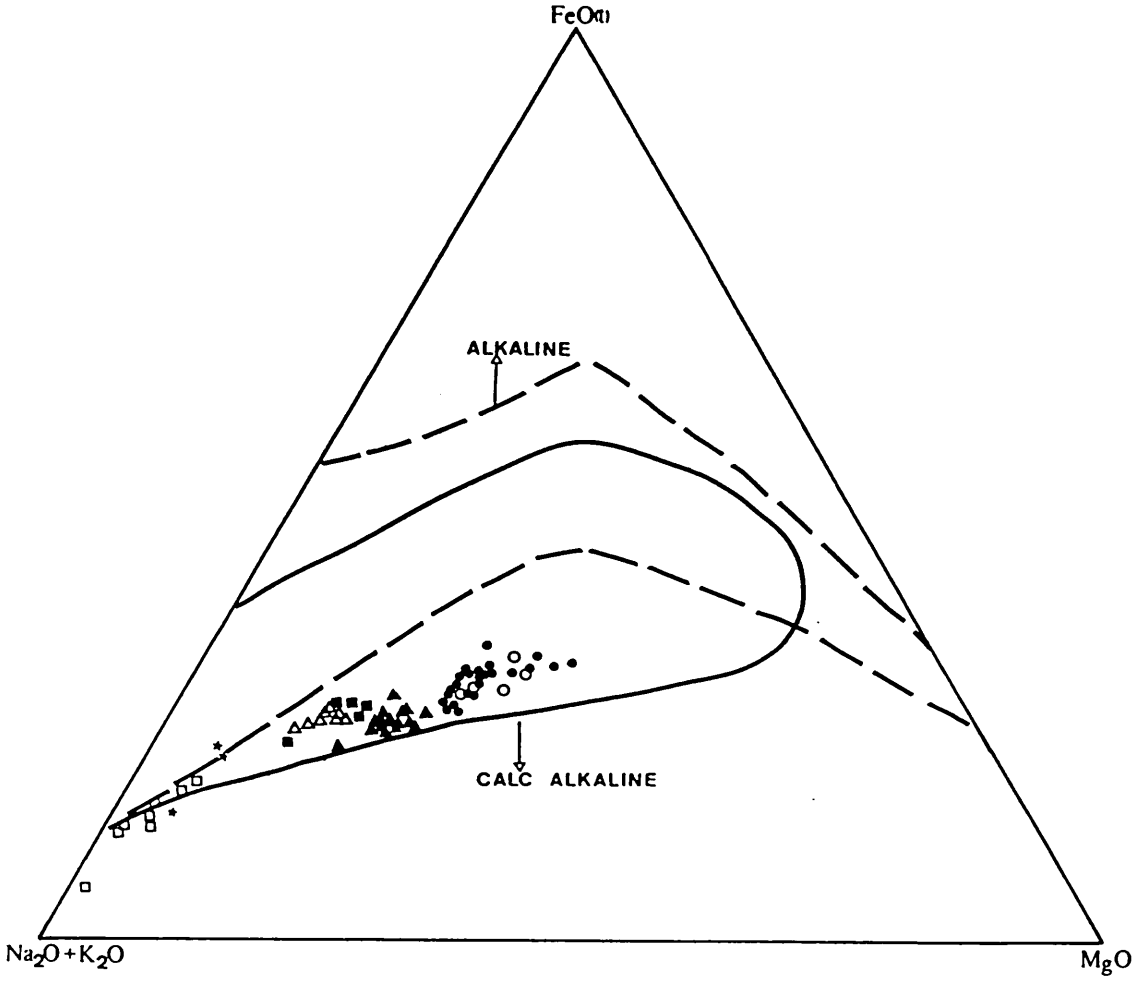


Figure 5.4 AFM plot of rocks from the Bom Jardim complex. Fields are from Morrison (1980). Symbols as shown in figure 5.1.

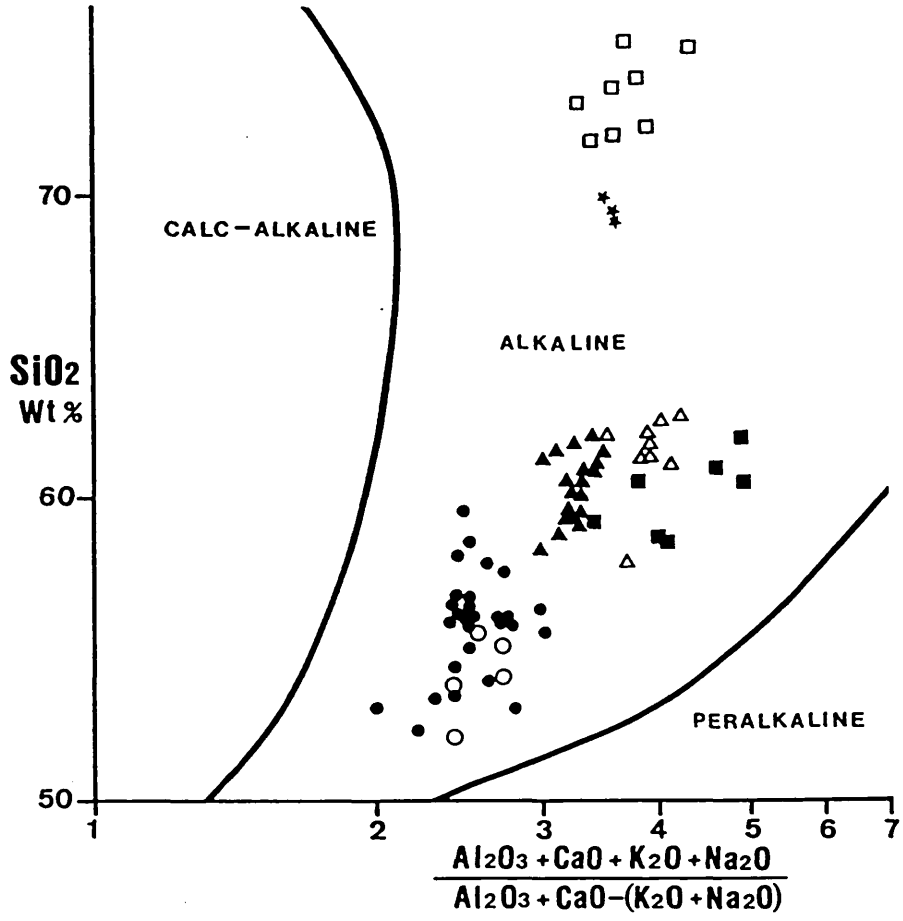


Figure 5.5 Classification of the rocks from the Bom Jardim complex after Wright (1969). Symbols as in figure 5.1.

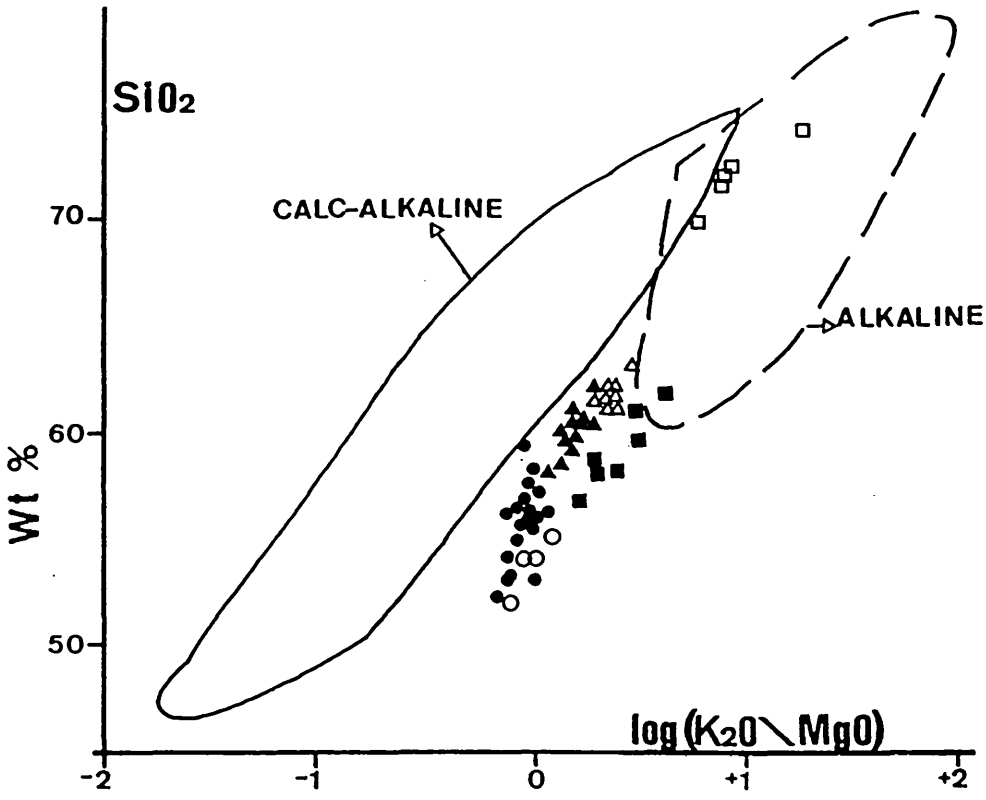


Figure 5.6 Classification of the rocks of the Bom Jardim complex after Rogers and Greenberg (1981). Symbols as in figure 5.1.

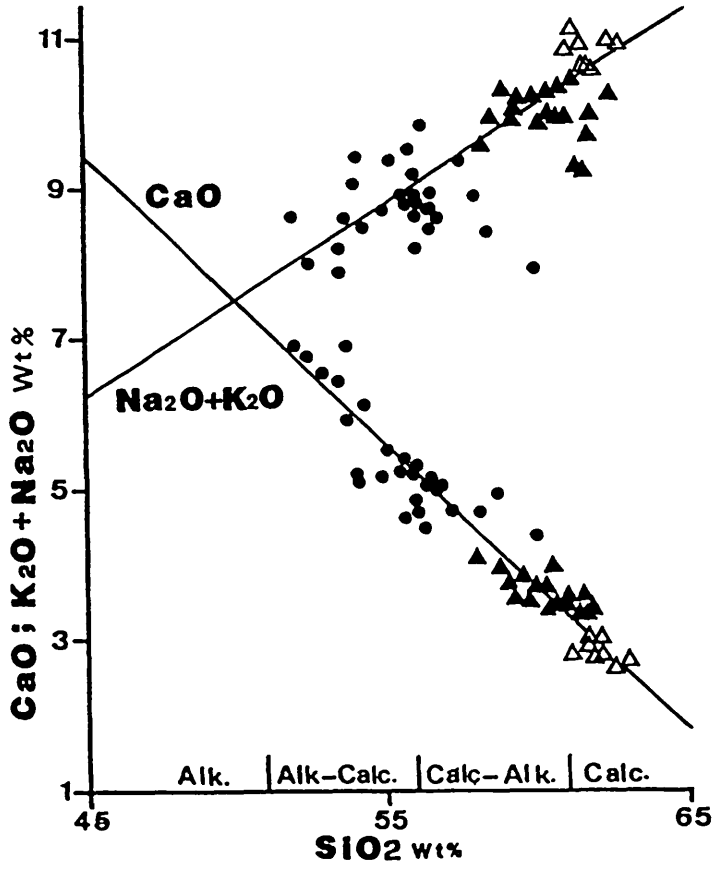


Figure 5.7 Diagram showing the alkali-lime index for the Bom Jardim suite (after Peacock, 1931). Symbols as in figure 5.1.

shoshonitic suites.

Peccerillo and Taylor (1976) used the variation of K_2O with silica to discriminate between tholeitic, calc-alkaline, high K calc-alkaline and the shoshonitic series. Figure 5.8 shows such a plot for the rocks of the Bom Jardim complex, and clearly all the rocks apart from the granites fall within the shoshonitic field.

Figures 5.9A and 5.9B illustrate a simple way of comparing the major element chemistry of the Bom Jardim complex with other well documented suites of calc-alkaline and shoshonotic affinities in the literature. Calc-alkaline rocks with similar SiO_2 contents from the Peruvian Coastal batholith (Mason, 1985), Guichon Creek batholith (Olade, 1976), and the Sierra Nevada batholith (Bateman et al., 1963) are compared with the rocks from the Bom Jardim complex. The members of the PBAMS suite generally show an enrichment in MgO, total iron (expressed as Fe_2O_3) and K_2O, and a depletion in MnO and CaO relative to the above suites (figure 5.9A). The PBLS suite shows depletion patterns in Al_2O_3, Fe_2O_3 (total iron), MnO and CaO, and enrichment in P_2O_5 and K_2O (figure 5.9B). When compared with the shoshonitic rocks from Papua-New Guinea (Smith, 1972) the Bom Jardim rocks show TiO_2 enrichment and CaO and MnO depletion in both PBAMS and PBLS suites. In comparison with the syenites from the Glen Dessary complex (Thompson and Fowler, 1986), the PBAMS suite in the Bom Jardim complex is enriched in MgO and total iron, and depleted in MnO, whilst the PBLS suite shows an enrichment in both MgO and P_2O_5 and a depletion in MnO and Na_2O.

According to Brown (1982) the ratio $CaO/(Na_2O+K_2O)$ decreases with increasing arc maturity, i.e., increasing distance from the active subduction margin. Using this ratio as a function of wt% of SiO_2 (see figure 5.10) one can see that the trend defined by the data from the Bom Jardim complex is very similar to that of the New Guinea continental arc (Brown, 1982), the Ballons massif, France (Pagel and Leterrier, 1980) and, the Scottish Caledonide granitoids (Thompson and Fowler, 1986 and Zhou,1987). The similarity between the alkali content between the Bom Jardim rocks and the New Guinea continental

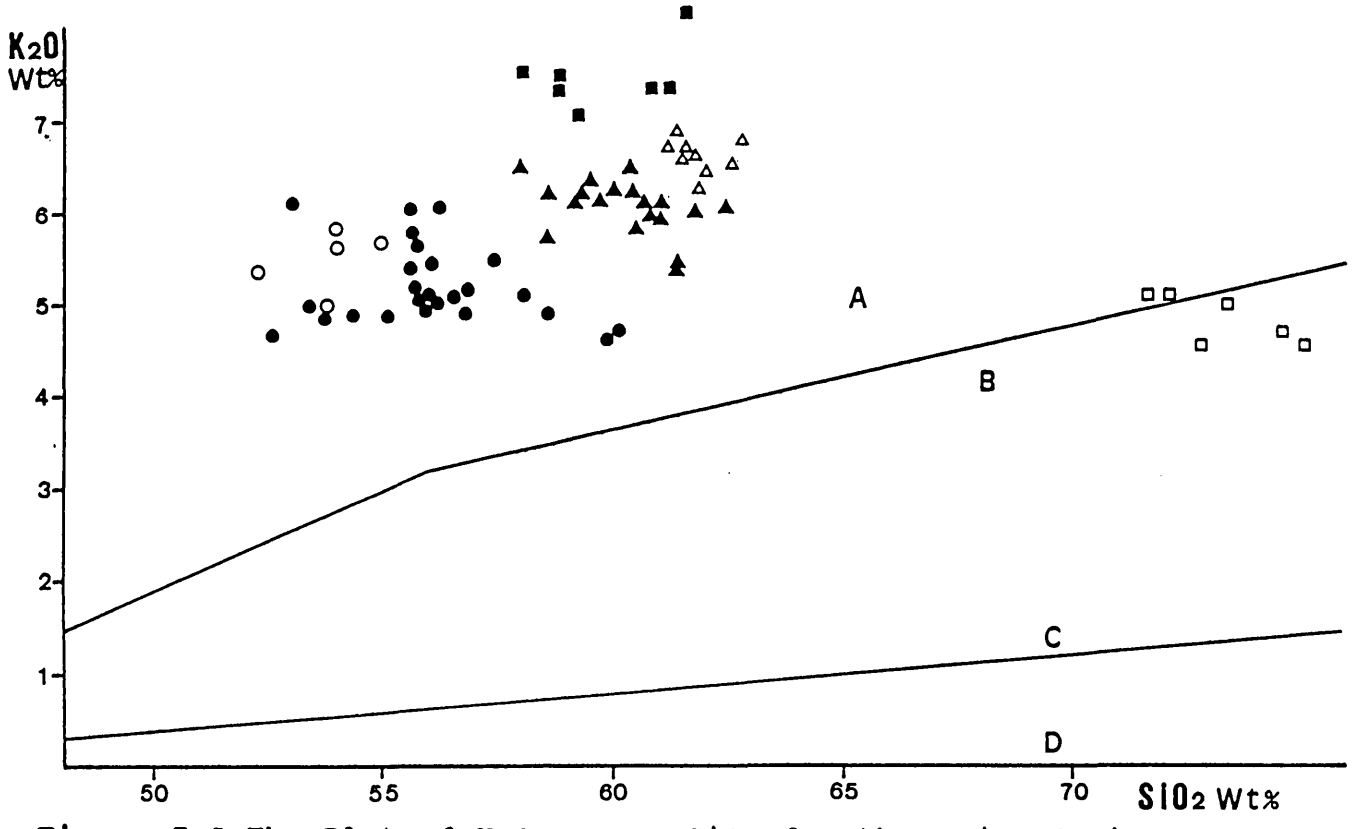


Figure 5.8 The Plot of K_2O versus SiO_2 for the major facies of the Bom Jardim complex (Peccerillo and Taylor, 1976). (closed circles = PBAMS, open circles = PBM, closed triangles = MPBAS, open triangles = PBLS and open square = pink granites. A = shoshonitic series, B = high-K calc-alkaline series, C = calc-alkaline series and D = tholeiitic series.

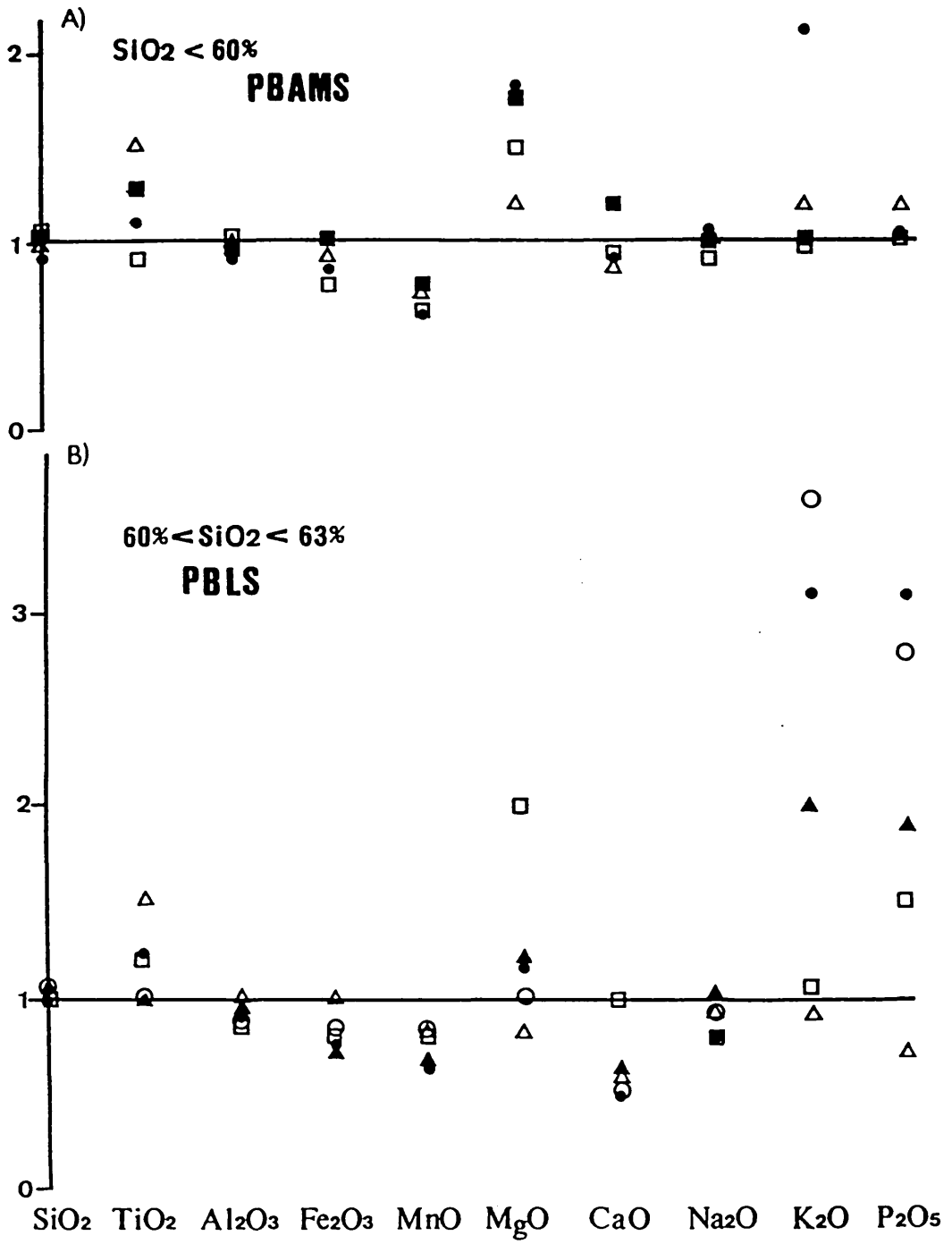


Figure 5.9 Enrichment\depletion patterns for the major elements in the mafic syenites (PBAMS) (A), and leuco syenites (PBLS) (B), compared to the Ballon massif (closed square), Coastal batholith (closed circle), Sierra Nevada batholith (closed triangle), Glen Dessarry syenites (open square), granitoids from Papua- New Guinea (open triangle) and Creek batholith (open circle)

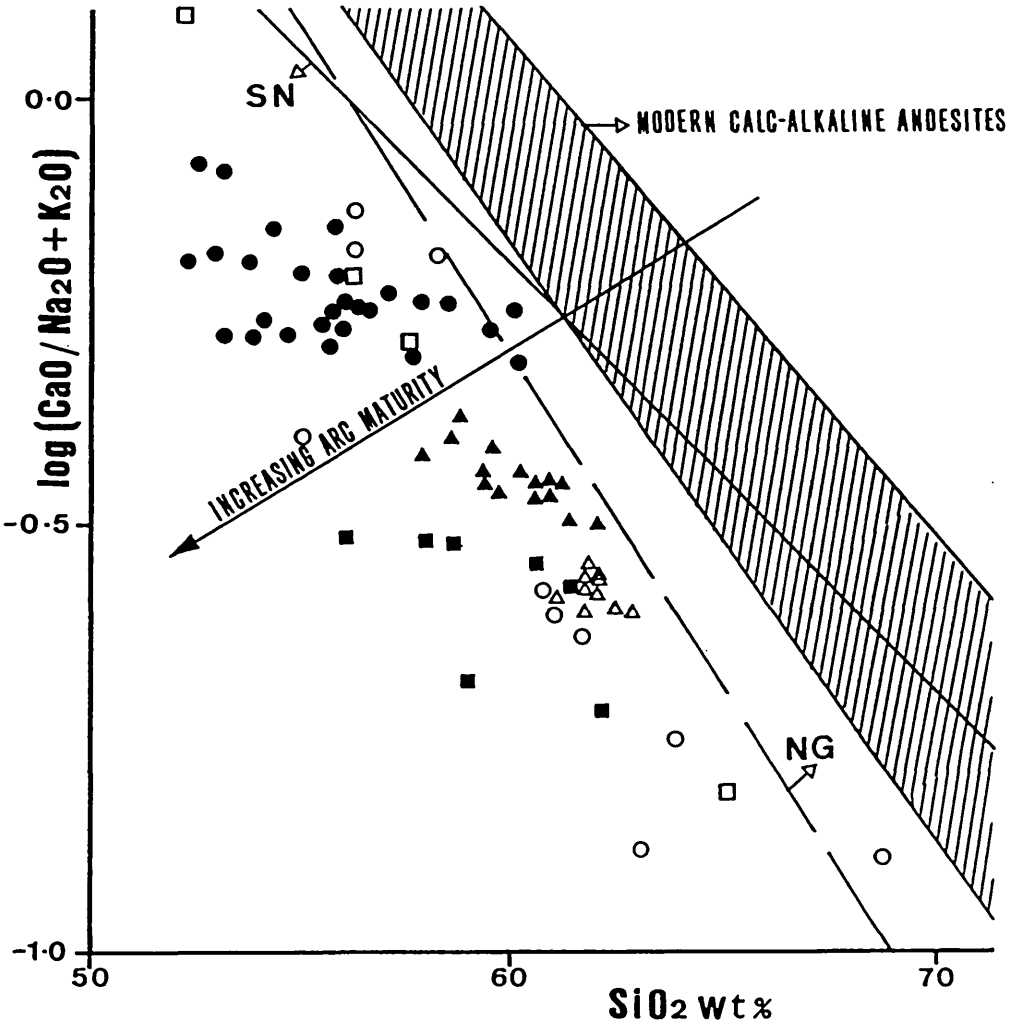


Figure 5.10 Variation of log $CaO/(Na_2O+K_2O)$ with silica for rocks of the Bom Jardim complex and other geochemically similar rock suites (after Brown, 1982). SN = Sierra Nevada trend, NG = New Guinea continental arc trend. (closed circles = PBM and PBAMS, closed triangles = MPBAS, open triangles = PBLS, open circles = Caledonide granitoids (Thompson and Fowler, 1986 and Zhou, 1987) and open square = Ballon massif, France (Pagel and Leterrier, 1980)

arc is even better displayed using a $\log(K_2O/Na_2O)$ versus SiO_2 diagram shown in figure 5.11 (Brown, 1981).

5.2.3 Major element variations

Variations of the major element concentrations have been displayed as a series of covariant diagrams in figure 5.12. The major element oxides of selected samples have been plotted against the Thornton and Tuttle Differentiation index D.I. (Thornton and Tuttle, 1960) where D.I. = normative Qz+Ab+Or+Lc+Ne. This differentiation index was preferred to the more conventional Harker type plot using wt percent SiO_2 as the abscissa, due to the rather restricted range in the latter oxide in the syenite - monzonite group of rocks within the Bom Jardim complex. The relevant features of the individual element oxide plots are given below.

The members of the syenite-monzonite facies display a continuum of compositions with D.I. ranging from 54 to 84. The granites tend to form a discrete cluster of D.I. values from 85 to 94. The major oxide component silica shows a marked three component trend; SiO_2 shows an early positive correlation up to values of DI of approximately 70; between 70 and 84, the trend flattens quite appreciably, then from DI values of 85 to 94 there is again a strong positive correlation, with a major discontinuity in SiO_2 values between 63 and 69 wt%.

Alumina also shows major discontinuities in its variation with DI. Again there is an early positive correlation, with Al_2O_3 values increasing up to DI values of 70, then a sudden flattening off, followed abruptly by a sudden decrease at a DI value of approximately 84. Titania shows less pronounced discontinuities in its trend but the inflexion points do occur at the values of DI as previously discussed,i.e. TiO_2 is negatively correlated with DI up to about 70, then flattens off and continues on a more pronounced negatively correlated trend between DI values of 84 to 94.

The alkalis K_2O and Na_2O both show a positive

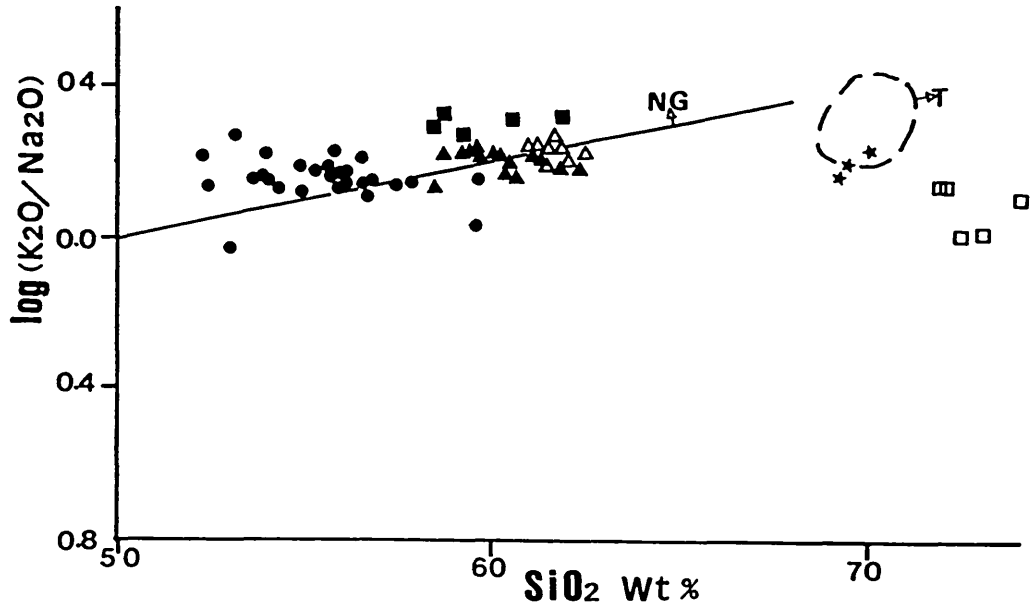


Figure 5.11 Plot of log (K_2O/Na_2O) versus SiO_2 for the Bom Jardim granitoids. NG = trend of the New Guinea continental arc, T = field of the granitoids from Thailand.
(closed circles = PBMAS, closed triangles = MPBAS, open triangles = PBLS, closed square = CS, open square = pink granites and stars = granites from the contact zone syenites - country rocks.

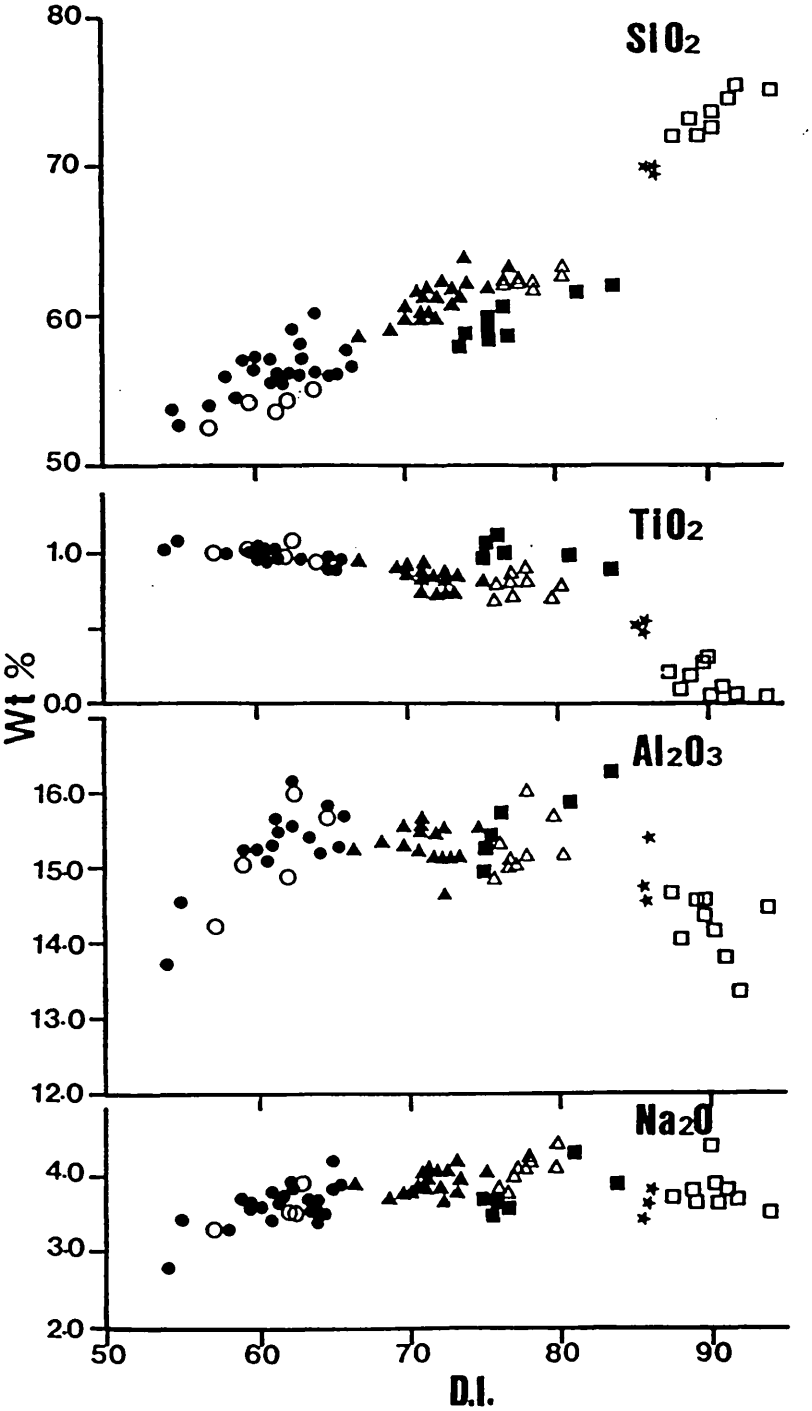


Figure 5.12 Major element oxide variation diagrams. DI. = The Thornton and Tuttle differentiation index. (Open circles = PBM, closed circles = PBAMS, closed triangles = MPBAS, open triangles = PBLS, closed square = CS, open square= pink granites and stars= granites from the contact syenites - country rocks.

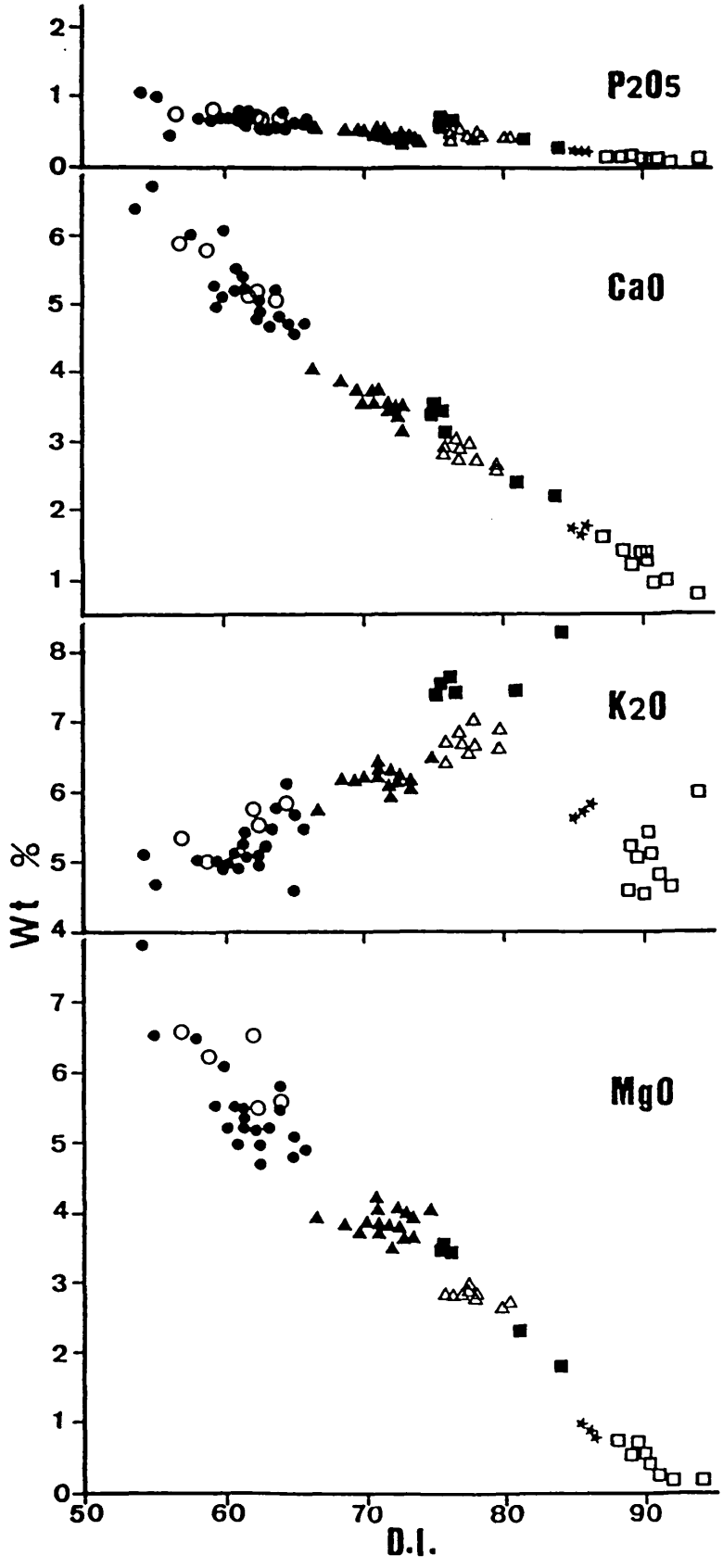


Figure 5.12 Continued

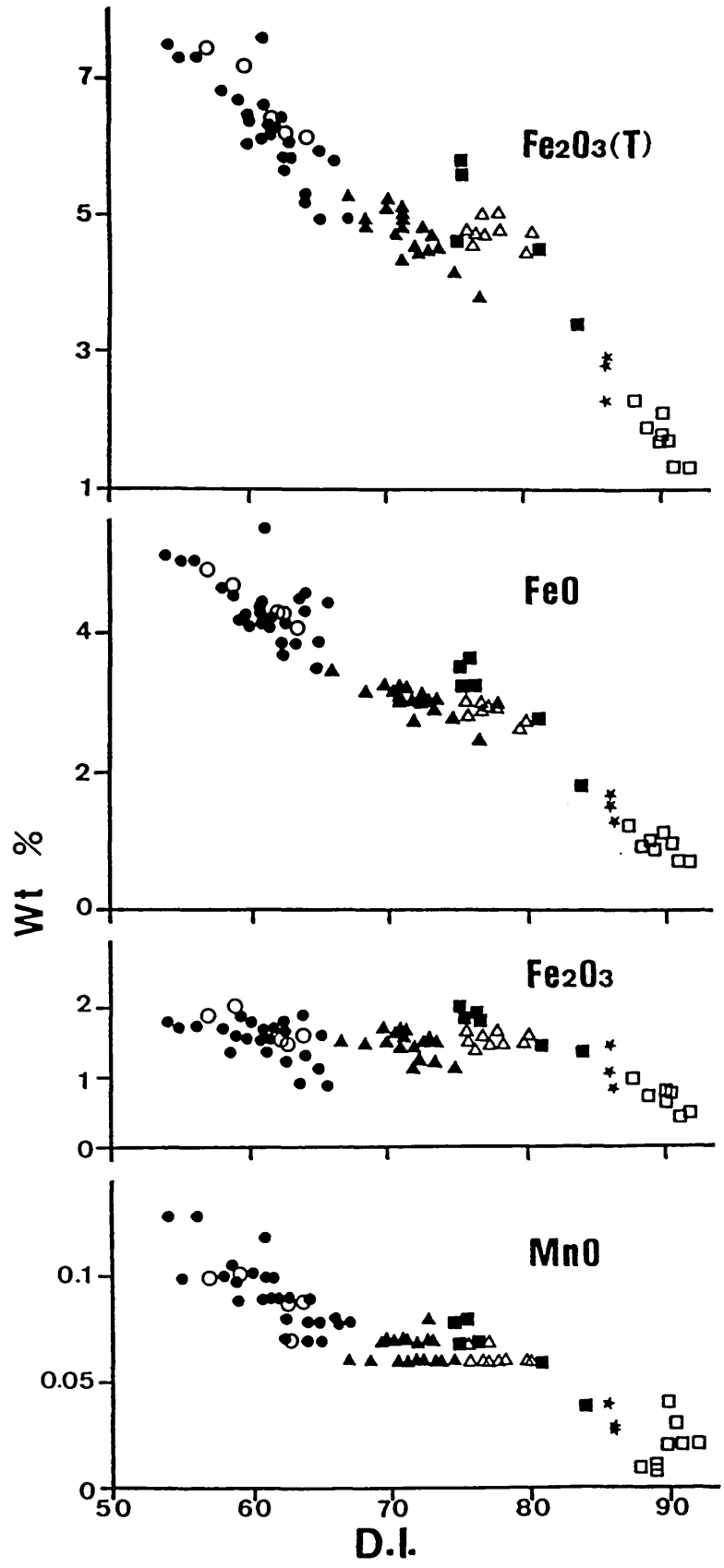


Figure 5.12 Continued

correlation with the differentiation index for the syenite and monzonite group of rocks (DI values of 53 to 70), with the former oxide showing a much stronger increase with DI. In both plots, the suite of granites are clearly displaced off the main trends.

The oxides MgO, CaO and P_2O_5 all show well defined negative correlations with the differentiation index. There is very little evidence of the major discontinuities displayed by the other oxides. The variation of iron oxides (total iron as Fe_2O_3 and FeO) and MnO with DI all show strong negative correlations (the plot of Fe_2O_3 is much flatter). Closer inspection of the trends does again indicate a discontinuity in the trends between values of 70 and 84 of the differentiation index.

The variation diagrams for the major element oxides SiO_2, TiO_2, Al_2O_3, Na_2O and K_2O (shown in figure 5.12), show that the population of granites from the Bom Jardim complex clearly does not lie on the main monzonite-syenite trend. The field evidence indicates that the different granite intrusions are related to zones of weakness within the main syenitic body of the complex. The evidence from the variation diagrams plus the inability to develop granitic liquids by fractionation processes involving the major modal phases observed in the complex, would suggest that the monzonite-syenite members and the later granites are not co-magmatic. This conclusion will be amplified later in the chapter with additional evidence from the trace element geochemistry.

5.2.4 Major element modelling

It is possible to model the observed variations in the major element concentrations in a co-magmatic suite of rocks by using simple least squares mixing solutions. This computational method utilizes the following simple relationship:

Composition of parental magma = extracted liquidus phases + composition of Residual melt.

Therefore providing that the mineral chemistries

of the fractionating phases are known, together with both melt compositions, the relative proportions of the extracted phases and the amount of residual melt can be calculated.

The mixing program used is a simplified version of the "Genmix" program (Le Maitre, 1981). The program allows a maximum of 10 component oxides and 9 extracted mineral phases to be treated simultaneously. Four intermediate stages of fractionation within the monzonite-syenite trend were chosen. Stage 1 (53.02 to 56.59 wt% SiO_2), stage 2 (56.59 to 59.63 wt% SiO_2), stage 3 (59.63 to 61.69 wt% SiO_2) and stage 4 (61.69 to 62.71 wt% SiO_2). A summary of the results is given in table 5.2, together with an indication of the quality of the fit (given by R^2, sum of squares of the residuals).

Table 5.2 Results of the least squares mixing solutions for the modelling of the variations in major element concentrations within the Bom Jardim complex.

STAGE 1

Parent Magma	Fractionating minerals (% Weight)							% Resid.L PBAMS	R^2
PBAMS (144)	Cpx 1.1	Amp 25.1	Bio 15.6	Pl 21.3	Kf -	Mt -	Sh -	(81) 41.6	0.0002

STAGE 2

Parent Magma	Fractionating minerals (% Weight)							% Resid.L MPBAS	R^2
PBMAS (81)	Cpx -	Amp 31.5	Bio 3.4	Pl 27.3	Kf 29.0	Mt 0.3	Sh 1.1	(7) 12.0	0.0002

STAGE 3

Parent Magma	Fractionating minerals (% Weight)							% Resid.L MPBAS	R^2
MPBAS (7)	Cpx 1.5	Amp 4.1	Bio 4.9	Pl 11.6	Kf 11.8	Mt 0.3	Sh 0.3	(47) 64.7	0.002

STAGE 4

Parent Magma	Fractionating minerals (% Weight)							% Resid.L LPBS	R^2
MPBAS (47)	Cpx 4.8	Amp -	Bio 7.4	Pl 5.4	Kf -	Mt -	Sh -	(163) 86.1	0.297

Cpx=clinopyroxene, Amp=amphibole, Bio=biotite, Pl=plagioclase, Kf= alkali feldspar, Mt=magnetite and Sh=sphene.

The results of the modelling show that during stage 1 of the fractionation process (evolution of the PBM and PBAMS facies) the major minerals extracted are the two silica poor phases, amphibole and biotite. The combined amounts of these two minerals is almost twice the amount of the next most important phase extracted, namely plagioclase. No K-feldspar is extracted during the early phaes of fractionation.

The starting liquid composition for stage 2 was carefully chosen to coincide with the point of inflexion (DI = 70) on the variation diagrams shown in figure 5.12. During stage 2 both amphibole and plagioclase remain as important fractionated phases, biotite decreases significantly and K-feldspar appears for the first time in amounts equal to amphibole and plagioclase. The most significant difference between stages 2 and 3 is the decrease in the total solids extracted. The feldspars now become the dominant fractionated phases in stage 3 with smaller amounts of clinopyroxene, amphibole and biotite. This trend of decreasing solid extract continues into the final stage. Clinopyroxene biotite and plagioclase are the only minerals fractionated. The quality of fit for the solution of the final stage is much poorer than the preceding ones, and a good deal of caution should be applied when interpreting the results. The difference in compositions is now much smaller, this together with the possibility that one may be dealing with a "crystal mush", rather than a discrete liquid phase as one of the products of fractionation could account for the increasing poor quality of fit for the mixing model.

5.3 TRACE ELEMENT GEOCHEMISTRY

5.3.1 Introduction

The term "trace element" is normally used for those elements present in rocks in concentrations of a few thousand parts per million, ppm (Cox et al., 1979). The trace element terminology used in this work, mainly follows

that of Saunders et al. (1979). The elements Cs, Rb, Ba, Sr, Ba, Th, Pb and U which have low field strength ionic states are termed "large ion lithophile elements" (LILEs), whereas Ti, P, Zr, Hf, Nb and Ta which have low radius / charge ratios are "termed high field strength elements" (HFSE); Pearce and Norry (1979) have also included Y in this group. The element scandium (Sc) displays a high ionic radius similar to those of Nb and Hf (Henderson, 1982), and for that reason it has also been included within the HFSE group. The rare earth elements (REEs) will be treated as a separate group although Cox et al. (1979) have grouped La and Ce with the LIL group of elements.Cr, Ni, V and Cu are grouped together as transition elements.

5.3.2 Partition coefficients and compatibility of the elements

The partition or distribution coefficients (Kds) express the extent to which elements are partitioned between mineral phases crystallising in chemical equilibrium with a magma, and can be expressed by the following relationship:

$$Kd = Co\backslash Cl$$

where Co is the element concentration in the mineral phase and Cl the element concentration in the melt. Partition coefficients have been measured both by synthetic equilibrium crystallisation experiments (see Irving, 1978 and Watson, 1976) and from natural phenocrysts/matrix pairs in glassy volcanic rocks. There is now a large data base of mineral/melt Kd values for the common rock-forming minerals available in the literature. The same cannot be said for the accessory minerals, where the data is very scant indeed. An inspection of the available data shows that the Kd values are strongly dependent on the magma composition and for this reason the andesitic data base of Gill (1978) has largely been used for the purposes of modelling in this investigation. In addition, both the temperature and the oxidation potential of the assemblages are variables which also control Kd values (see Drake and Weill, 1975 and Drake, 1975). There is also some evidence which suggests

Table 5.3 Partition coefficients used in this work.

Gill (1978), 1-Pearce and Norry (1979), 2-Villemant (1981)

	Rb	Sr	Ba	Ni	Cr	V	Sc	Y[1]	Nb[1]	Zr[1]
Pl	.07	1.8	.16	-	-	-	-	-	-	-
Bio	3.3	.12	6.4	13.0	17.0	50.0	8.3	1.2*	1.8*	1.2*
Hbl	.05	.23	.09	8.0	30.0	32.0	12.5	2.5	1.3	1.4
Cpx	.02	.08	.02	6.0	30.0	1.1	3.0	1.5	.3	.25
Mg	-	-	-	5.0	32.0	30.0	2.0	.5	1.0	.20
Ap	-	-	-	-	-	-		20.0	-	-
KF[2]	.30	10	3.6	-	-	-		-	-	-

* = Biotite + Zircon

Hanson (1980)

	Ce	Nd	Sm	Eu	Gd	Dy	Er	Yb
Clinopx	.30	.65	.95	.68	1.35	1.46	1.33	1.30
Hornblende	.90	2.8	4.0	3.4	5.5	6.2	5.9	4.9
Biotite	.32	.29	.26	.24	.28	.29	.35	.44

Wormer et al (1983)[1], Villemant (1981)[2] and Henderson (1982)[3]

	Th[1]	U[1]	Ta[1]	Hf[1]	Ce	Yb
Sphene	8.0	2.1	113.0	14.2	80.0[2]	72.0[2]
Apatite	1.2	0.0	-	-	31.0[3]	21.0[3]

Marhood and Hildreth (1983)

	Th	U	Ta	Hf	Ce	Yb
Zircon	91.2	383.0	40.2	3742.0	10.0	564.0
Allanite	548.0	17.0	4.4	28.0	2494.0	37.0

that pressure may also be a dependent variable, but the effects are generally small. The partition coefficients used in the present investigation together with their sources are listed in table 5.3.

In order to model the evolution of a magmatic liquid it is necessary to consider the bulk partition coefficient (D) of an element; this is calculated according to the relationship:

$$D = \sum_{i=1}^{n} Wi\ Kdi$$

Where Wi is the weight fraction of each mineral and Kdi is the partition coefficient of the relevant phase. Elements with D values > 1.0 will be depleted in the residual liquid, such elements are termed compatible. Elements with D < 1.0 will tend to be concentrated in the liquid phase during crystallisation; such elements are termed incompatible. However, it should be remembered that the compatibility of certain elements may change during the evolution of natural melts as phases appear and disappear in response to changing pressure, temperature and liquid composition.

5.3.3 Trace element modelling

Two basic equations are normally used to describe the extremes of trace element behaviour during the crystallisation of melts:

1) Closed system Rayleigh fractional crystallisation (Pearce and Norry,1979)

$$C1/C0 = F^{(Dx-1)}$$

and

2) Closed system Rayleigh equilibrium crystallisation

$$C1/C0 = 1 / [F + Dx\ (1 - F)]$$

Where:

C0 = Concentration of the element X in the original melt

C1 = Concentration of the element X in the residual melt

Dx = Bulk partition coefficient of element X

F = Weight fraction of melt remaining

The underlying rationale and application of the Rayleigh equations can be seen represented in schematic form in figure 5.13 (after MacCarthy and Hasty, 1976). This diagram also attempts to show the probable behaviour of granitic melts acting more as "crystal mushes" rather than as discrete melts and fractionated "cumulate" phases. During the Rayleigh fractionation the liquidus and solidus compositions will change along BE and AD respectively, the first solid phase to crystallise from liquid B will have a composition A. The composition of crystal mushes may also change in the same direction, but, according to MacCarthy and Hasty (1976) they may also change along mixing lines joining the cumulate and liquid compositional paths.

The use of such Rayleigh fractionation models in igneous petrology can in certain circumstances only give a semi-quantitative evaluation of the fractionated mineral assemblage capable of producing the observed trends. This is because the effects of contamination, and the proportion of fractionated phases to crystallised melt cannot be defined. In addition, the influence of accessory mineral phases may be crucial in understanding a particular set of trends, but because of their very low modal abundances and the general lack of reliable Kd values for such phases, their use may be severely minimized.

5.3.4 Large ion lithophile elements (LILE)

5.3.4.1 Barium

The variation of Ba contents within the different members of the Bom Jardim complex can be seen plotted against the differentiation index DI, in figure 5.15A. Although the trend does show scatter especially in the less evolved rocks, the syenite and monzonite members generally display a weak negative correlation. The granites are clearly not part of the same trend. Rocks belonging to the different facies within the complex generally display a restricted range of Ba values, although in some cases overlaps between the facies can be seen. The ranges of

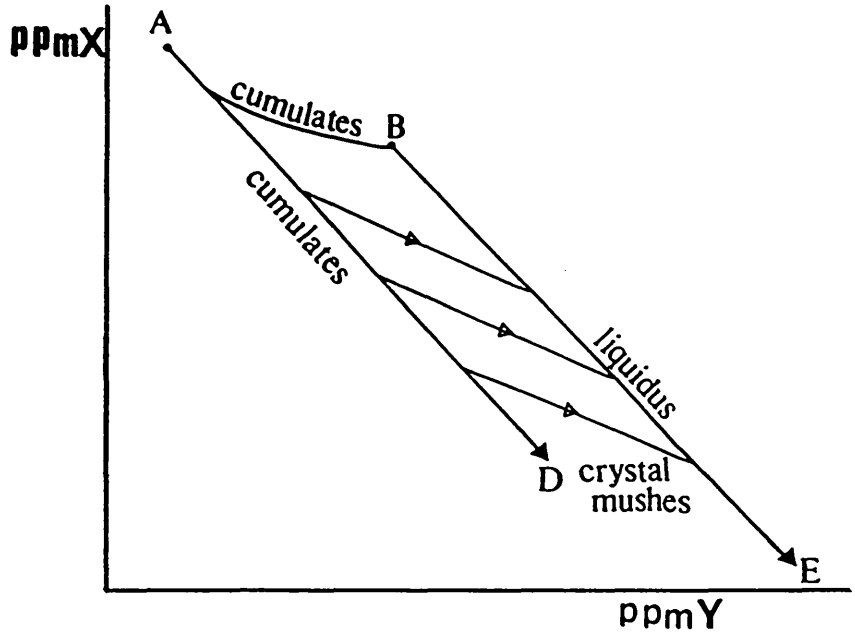


Figure 5.13 Schematic diagram illustrating the method of modelling trace element variations in terms of Rayleigh fractionation. (After MacCarthy and Hasty, 1976).

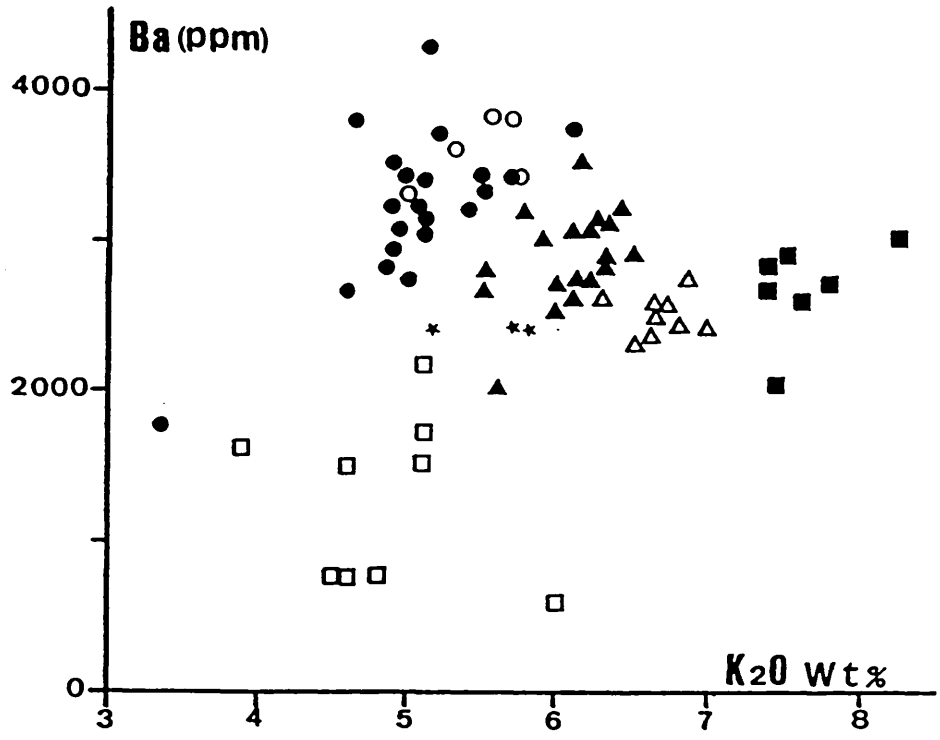


Figure 5.14 Bivariant plot of Ba (ppm) versus K_2O (wt%) for rocks of the Bom Jardim complex. Symbols as indicate in figure 5.12.

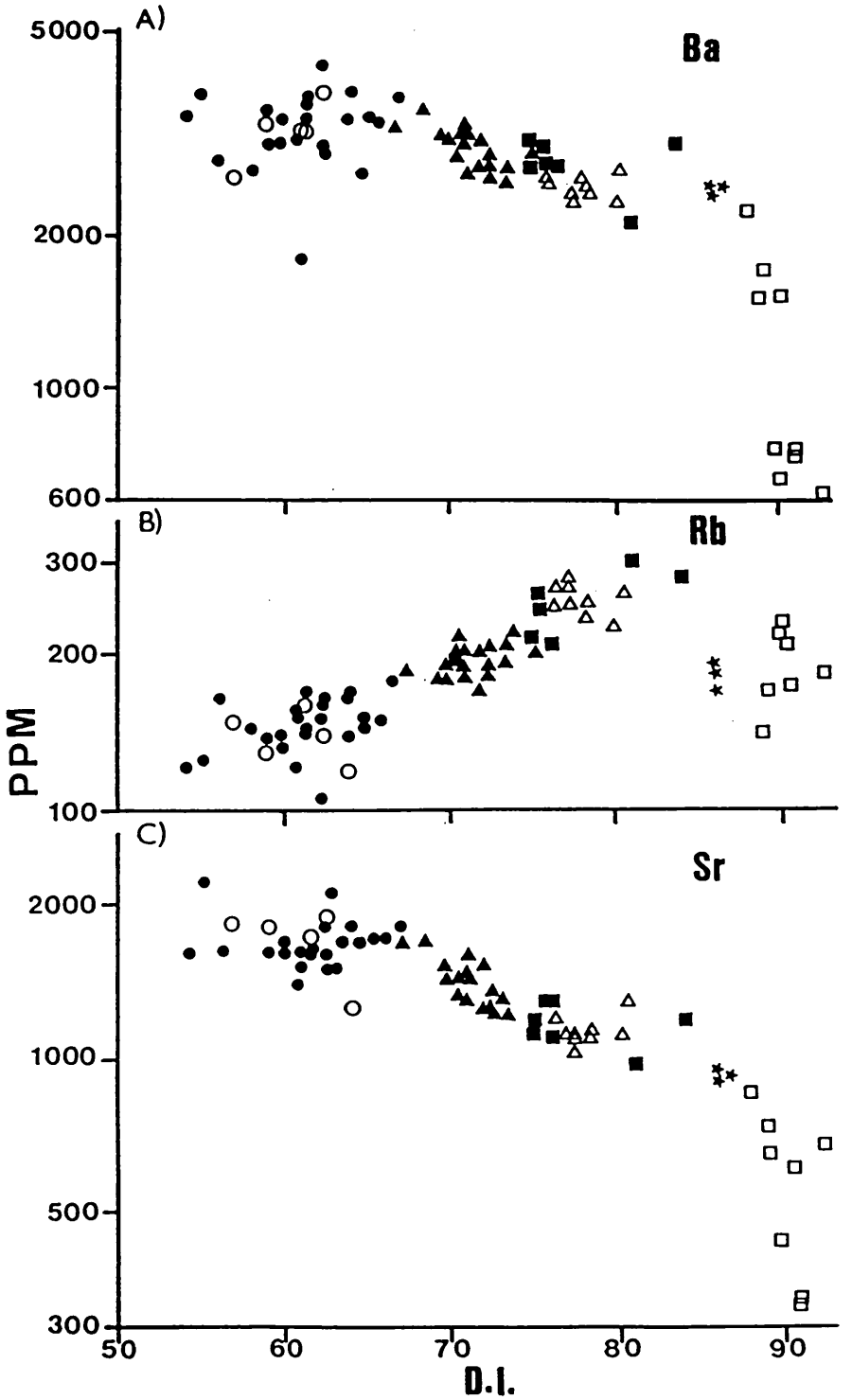


Figure 5.15 Plots of LIL elements versus DI for rocks of the Bom Jardim complex. Simbols as shown in figure 5.12.

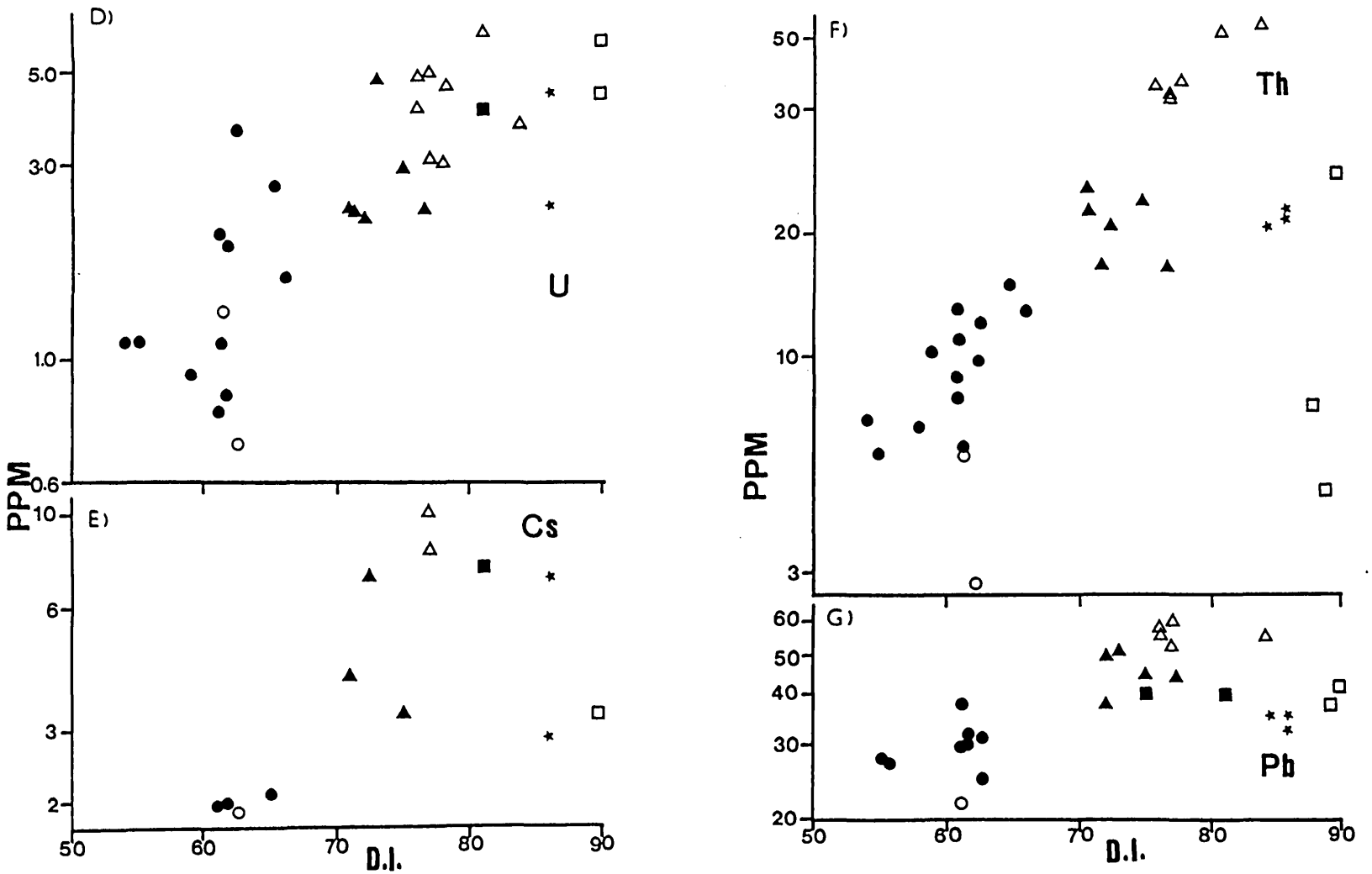


Figure 5.15 Continued.

barium contents for the different members of the complex are given below.

FACIES	RANGE OF BARIUM IN PPM
PBAMS	2597 - 4389
MPBAS	2507 - 3225
PBLS	2239 - 2776
CS	2060 - 2418
GRANITES	716 - 2418

The granites containing Ba values > 1000 ppm are generally restricted to bodies either within the contact zone between the syenites and the country rocks or from the main granite body, where it borders the syenites in the centre of the complex.

Figure 5.14 shows the variation of BaO with K_2O contents. Normally barium follows the same general trend as potassium during magmatic differentiation - both are commonly found enriched in the late acid differentiates. The generally accepted high incompatibility of Ba is clearly not shown during the evolution of the rocks in the Bom Jardim Complex. On the contrary, barium decreases with both differentiation index (DI) and K_2O.

The distribution coefficients for Ba in melts of intermediate composition are usually less than 1.0, with the exception of biotite and K-feldspar (see table 5.3). Barium obviously behaved in a compatible manner during the crystallisation of biotite and alkali feldspar. However, the observed variations in the barium contents within the complex are probably controlled by the competition between the crystallisation of alkali feldspar and biotite, which result in the decrease of Ba in the melt and the crystallisation of pyroxene and amphibole (with Ba Kd values < 1.0) which result in Ba increasing in the melt. The slight negative correlation of Ba with DI (figure 5.15A) would tend to rule out any significant fractionation of biotite.

5.3.4.2 Strontium

The variation of strontium with the differentiation index is shown in figure 5.15C. The trend appears to be subdivided into 4 components. The syenites and monzonites included in the PBM and PBAMS facies (DI varying from 53 to 67) display a fairly flat trend, whereas the rocks from the MPBAS facies (closed triangles in figure 5.15C) show a distinct negative correlation with the DI. The leuco syenites and very coarse syenites (DI varying from 75 to 85) again show a rather flat trend. As in the case of Ba, the variation in strontium for the granites defines a totally separate group which appears to be unconnected with the previously described trends. The strontium contents within the different facies are given below.

FACIES	**RANGE OF Sr (PPM)**
PBAMS	1099 to 2198
MPBAS	1184 to 1691
PBLS	1099 to 1353
Cs	1015 to 1353
GRANITES	380 to 980

The flat trend observed for the PBM and PBAMS facies has probably been brought about by the off-setting action of the crystallisation on the one hand of biotite and amphibole (with Kds < 1.0), and the alkali feldspar and plagioclase (with Kds > 1.0) on the other. This explanation is largely borne out by the modal analyses of the rocks in both these facies. The negative correlation observed for the MPBAS syenites is largely controlled by the compatible behaviour of Sr in such phases as alkali feldspar and plagioclase. In this facies the mafic phases are greatly reduced, thereby virtually negating any off setting action previously described. The main cause of the decrease in Sr with increasing values of DI must be largely due to the fractionation of alkali feldspar, as the modal contents of plagioclase in those facies are low. The flat trend shown for the rocks of the CS and PBLS facies (see

figure 5.15C) is far more difficult to interpret. The rocks within the very coarse syenite facies (CS) show quite large variations in the phenocrysts/matrix ratios, and it is possible that such variations have caused this flat trend.

5.3.4.3 Rubidium and Caesium

During fractional crystallisation of intermediate magmas, Rb acts in a highly incompatible manner, except when biotite is the phase being extracted (see table 5.3). This behaviour is clearly seen in the positive correlation shown by this element in figure 5.15B. The Rb contents within the different facies are given below.

FACIES	**Rb (PPM)**	**Rb/Sr**
PBAMS	120 (average)	0.05 - 0.11
MPBAS	190 (average)	0.11 - 0.17
PBLS	270 (average)	0.19 - 0.25
CS	300 (average)	0.18 - 0.30
GRANITES	140 - 226	0.12 - 0.49

Although biotite has been identified as a fractionating phase during the evolution of the Bom Jardim complex, its modal contents are much lower than the total for amphibole + pyroxene + plagioclase + alkali feldspar (all with Kd values < 1.0), and therefore the net result would be an increase in Rb with differentiation.

The Rb/Sr ratios in the Bom Jardim complex are comparable to those determined for the shoshonitic monzonites of the White - Inyo Range batholith, California (Sylvester et al., 1978), and the pre to mid Silurian granitoids of N. Scotland (Brown et al., 1981). However, they are lower than typical calc-alkaline suites with similar SiO_2 contents, for example the Sierra Nevada batholith (Bateman and Dodge, 1970) and the Coastal batholith (Atherton and Sanderson, 1985).

According to Condie (1973) the Rb and Sr

contents of igneous rock suites can be correlated with crustal thickness. Figure 5.16 shows the Rb and Sr data for the Bom Jardim complex plotted along with Codie's estimates for crustal thicknesses; as can be seen, the data clearly indicates a source greater than 30 Km.

Hanson (1978), and Hart and Allegre (1980) have suggested that the Rb/Sr ratios can also be influenced by fractionation. Using the available partition coefficient data from table 5.3, one can show that with fractionation of amphibole, clinopyroxene, plagioclase and K-feldspar (with Kd values for Rb < 1.0 and Sr Kd values for plagioclase and K-feldspar > 1.0) the Rb/Sr ratio should increase with differentiation. The Rb/Sr ratios for the complex substantiate this prediction (see figure 5.17); again the granites do not follow the syenite - monzonite trend. Clearly the Rb/Sr ratios in this case are not solely dependent on the depth of the source, but even taking this into consideration, the least evolved members of the suite still reflect a source greater than 30 Km.

Olade (1976) concluded that the Rb/Sr ratio does reflect the source of granitic rocks more so than the effects of mineral fractionation, and that rocks with Rb/Sr ratios less than 0.1 are normally associated with mantle sources and ratios greater than 0.25 with rock generated by crustal melting. However, one should point out the very significant fact that crustal Rb/Sr ratios have in fact increased since the Archaean. According to Taylor and MacLennan (1981) the Rb/Sr ratio for the upper crust has increased from 0.08 to 0.3 from the Archaean to the present day.

The Ba/Rb ratio has been used as effective differentiation index by several authors. The Ba/Rb ratios in the Bom Jardim complex show a marked reduction from the PBAMS (20.0 - 40.9) to the PBLS facies (8.8 - 10.7); the granites show a range in values from 3.5 to 22.4. The range of Ba/Rb ratios quoted above are comparable with those recorded for the Caledonian granitoids from Scotland (Thompson and Fowler, 1986 and Zhou, 1987), but much higher when compared with the shoshonitic monzonites from White-Inyo Range, California (Sylvester et al., 1978) and the

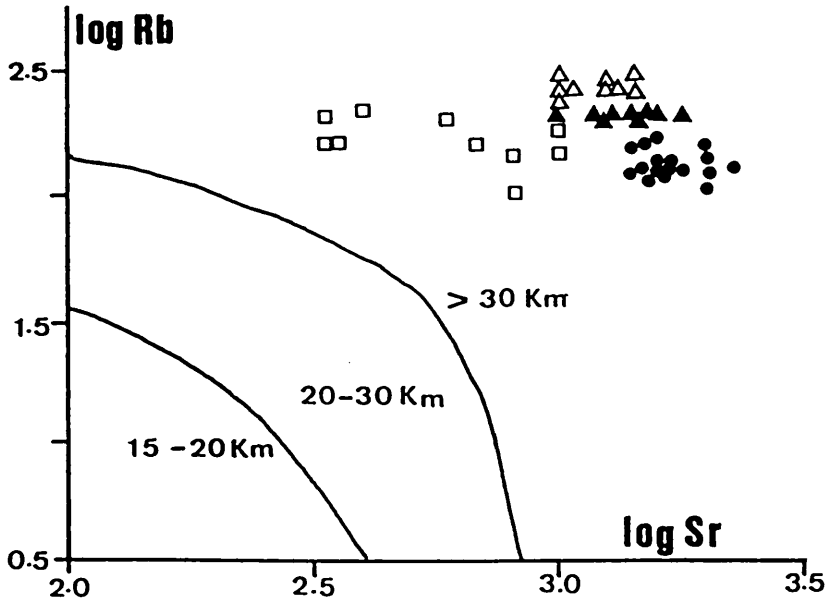


Figure 5.16 LogRb - logSr diagram showing the distribution of the Bom Jardim granitoids. Numbers in kilometers refer to crustal thickness (Condie, 1973). Symbols as in figure 5.12.

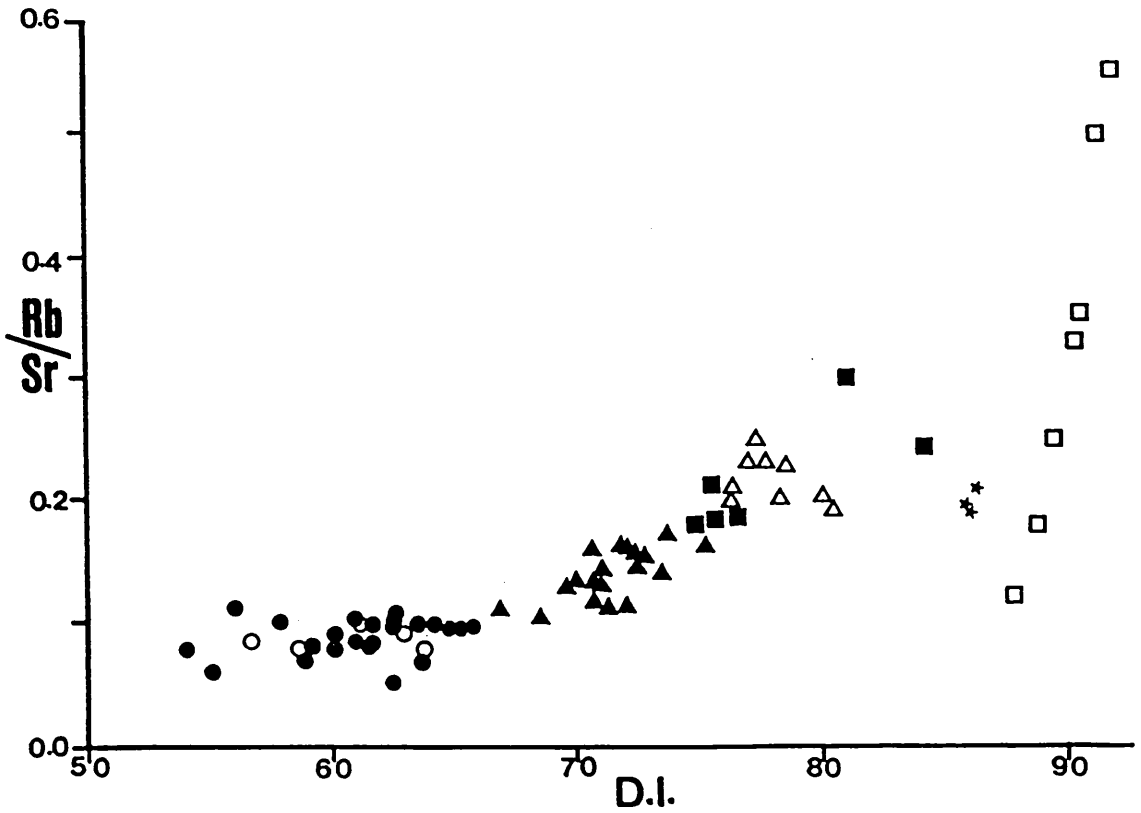


Figure 5.17 Variation of the (Rb/Sr) ratio with D.I. for the Bom Jardim granitoids. Symbols as indicate in figure 5.12.

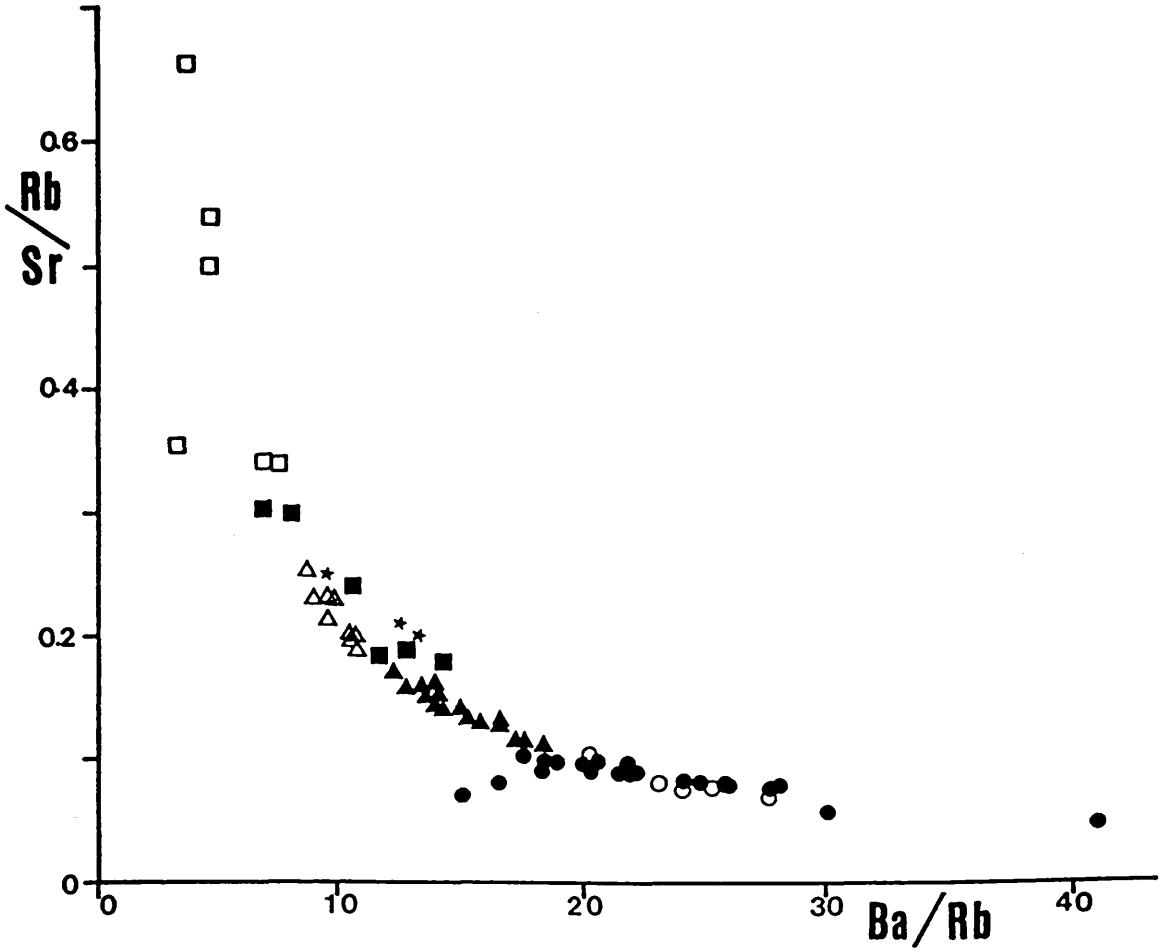


Figure 5.18 Variation of the Ba/Rb ratio with Rb/Sr for the Bom Jardim granitoids. Symbols as in figure 5.12.

Ballon massif, France (Pagel and Leterrier, 1980). Figure 5.18 shows the variation of the Ba/Rb ratio with that of Rb/Sr. There is a clearly defined asymptotic negative correlation between the two, with distinct clusterings of the different facies along the trend.

The caesium contents within the complex range from 1.9 (PBM facies) to 10.1ppm in the PBLS facies, with the granites showing a range from 2.9 to 7.2. Figure 5.15E shows the variation of Cs with increasing differentiation and, although the data are markedly scattered they do show a positive correlation. This enrichment in Cs is also borne out in the mineral chemistries, in that the Cs contents of biotites are significantly higher in the more evolved leuco syenites (PBLS) than in the biotites from the earlier monzonitic members.

5.3.4.4 Thorium, uranium and lead

The individual concentrations of Th, U and Pb are shown in figures 5.15 F,D and G respectively, plotted as a function of the variation in the differetiation index (DI). In each case, although the data is somewhat scattered, they all show an overall positive correlation with the DI. The ranges in concentration of the individual elements in the major rock types of the complex are given below.

Rock type	**Concentration range in ppm**		
	Th	U	Pb
Monzonites and syenites	2.8-61.4	0.6-6.0	22.0-60.0
Granites	4.8-29.0	2.4-6.0	37.0-45.0

The abundances of all three elements in the Bom Jardim complex are high when compared to the estimates for the average of bulk continental crust, 3.5ppm Th, 0.9ppm U and 8ppm Pb (Taylor and MacLennan, 1985). Leat et al. (1987), concluded that the high Th and U contents of rocks from the potassic suite in SW. England could only be explained by an influx of mantle derived magma strongly

enriched in Th, U and K.

Petrographic studies have shown that sphene (REE,Th enriched sphene - keilhauite), zircon and apatite are the most abundant accessory phases (with smaller contribution from monazite and thorite) in the main facies of the complex. Several different approaches have been made to examine the role that such minerals have played in the evolution and distribution of these three elements in the complex. Unfortunately they have not been altogether successful. It is very difficult to totally isolate each minerals contribution, when there are so many inter-element relationships possible between the phases. Figure 5.19 (A-H) shows one such attempt. TiO_2 and P_2O_5 are among the major constituents of sphene and apatite respectively; however, TiO_2 also occurs as a minor element constituent in the more modally important mafic phases, biotite, amphibole and pyroxene, and P_2O_5 also occurs in monazite.

The changes in the concentrations of U, Th and Pb with the variation in both TiO_2 and P_2O_5 are shown in figures 5.19 A-C and E-G respectively. All show a negative correlation for the differentiation interval between the PBAMS and MPBAS facies. This is then followed either by a sudden increase at constant TiO_2 and P_2O_5 contents or by a positive correlation between the MPBAS and PBLS facies. With the mafic mineral constituents decreasing in the latter differentiation interval, the relationship between TiO_2 and U, Th and Pb could be explained by an increase in sphene. The presence of apatite and monazite during the same differentiation interval could also explain the variations in U, Th and Pb with P_2O_5 contents.

These rather tentative observations simply reinforce the conclusions based on the mineral chemistries of the accessory phases discussed in chapter 4. Thorium distribution is mainly controlled by variations in modal amounts of apatite and members of the thorite - monazite group of minerals, with additional competition for Th from the modally subordinate REE, Th enriched sphene (keilhauite). The distribution of U is largely controlled by the modal variations in the thorite-monazite mineral group. Lead appears to follow Th in the REE, Th enriched

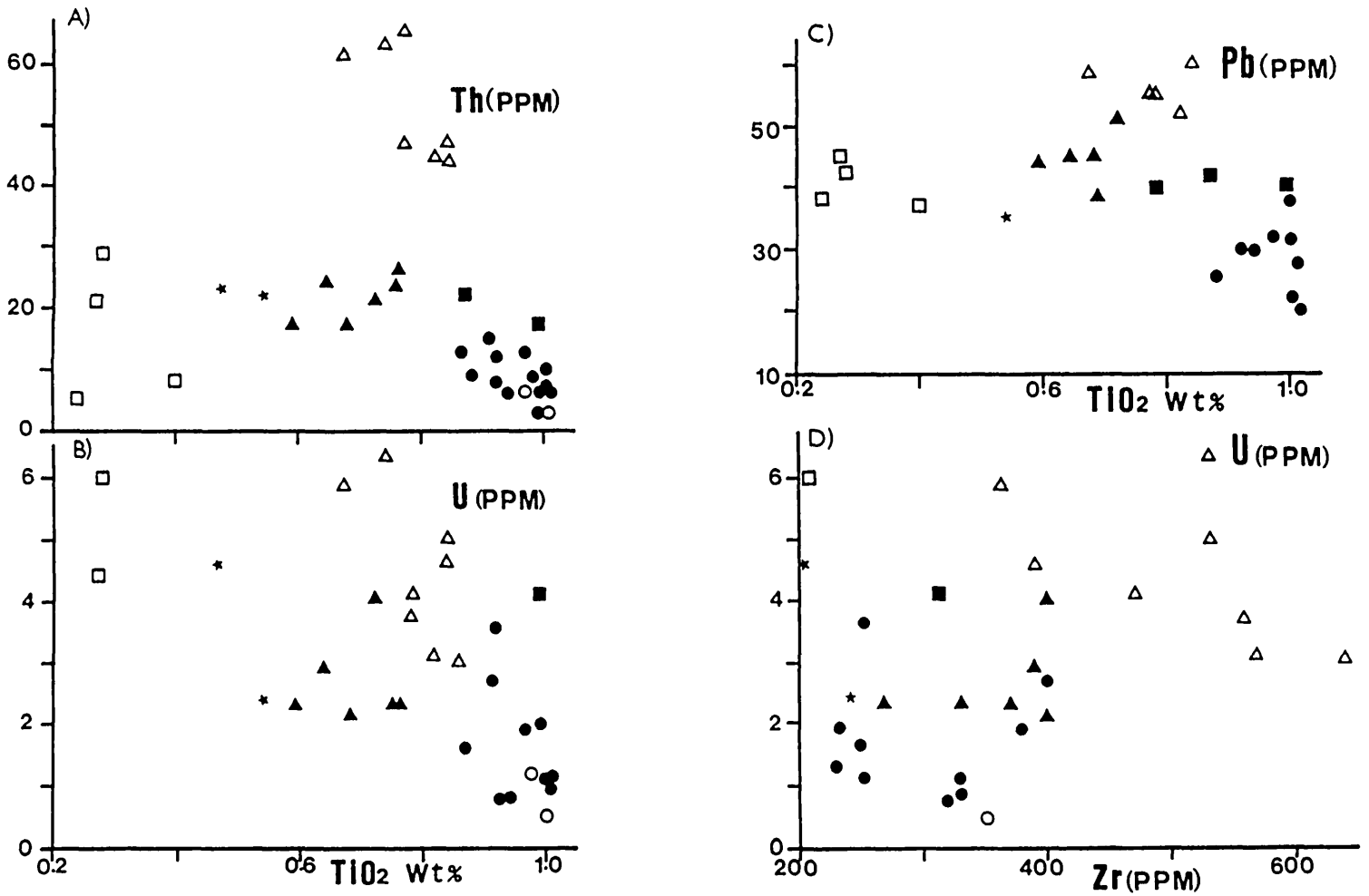


Figure 5.19 Scatter diagrams for selected trace elements in the Bom Jardim complex. Symbols as in figure 5.12.

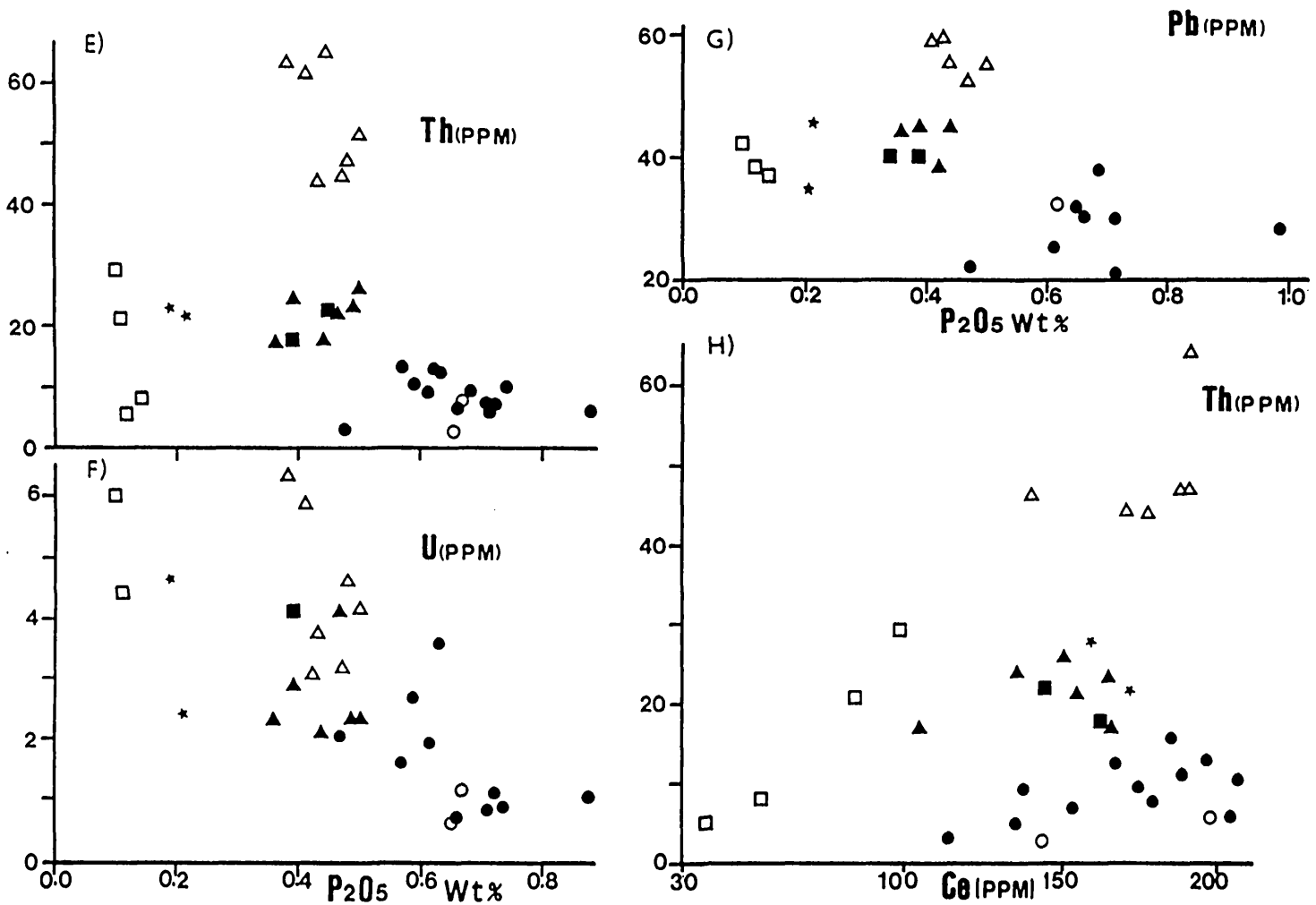


Figure 5.19 Continued

sphene (keilhauite).

5.3.5 Transition elements

5.3.5.1 Nickel

The individual Ni contents of rocks from the Bom Jardim complex are listed in the appendices and plotted as a function of the differentiation index in figure 5.20B. Overall, Ni shows a negative correlation with the DI, a trend which is characteristic of many intermediate rock suites (Olade, 1976). The Ni contents of members of the Bom Jardim complex are generally high, ranging from 30 to 250 ppm in the monzonites and syenites and less than 20 ppm in the granites. Nickel partitions strongly into pyroxene, amphibole, biotite and magnetite in magmas of intermediate compositions (see table 5.3). Using the available Kd data it can be shown that the fractionation of 12.5% amphibole, 17% clinopyroxene, 7.7% of biotite (and 20% magnetite) can each achieve the desired depletion shown in figure 5.20B. Modal analysis of the mafic members of the Bom Jardim complex have shown that the ferromagnesian phases (amphibole + biotite + pyroxene) make up more than 50% of the rocks, sufficient to account for the observed variations. The data shown in figure 5.20B also indicates a fairly constant depletion of Ni during the fractionation processes.

5.3.5.2 Chromium

The variation of Cr during the evolution of the complex is shown in figure 5.20A. Again, the transition element shows a marked negative correlation with differentiation. The Cr contents in the granites are generally less than 30 ppm. An inspection of the Kd values in table 5.3, indicates that Cr will behave in a more compatible manner than Ni during the crystallisation of the ferromagnesian phases (substantiated by the steeper Cr trend in figure 5.20A). Using the Kd values of Gill (1978)

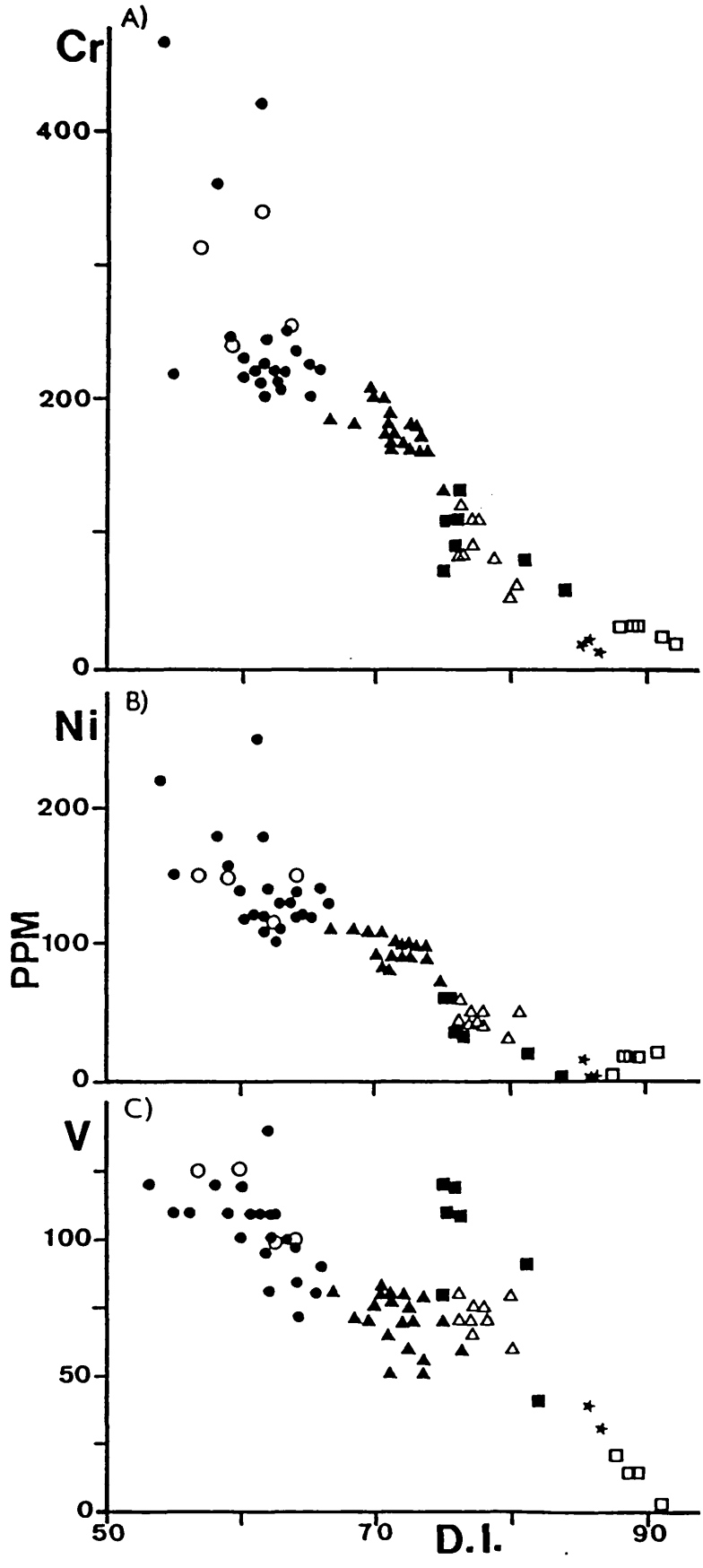


Figure 5.20 Variation of the transition elements with D.I. for the Bom Jardim granitoids. Symbols as in figure 5.12.

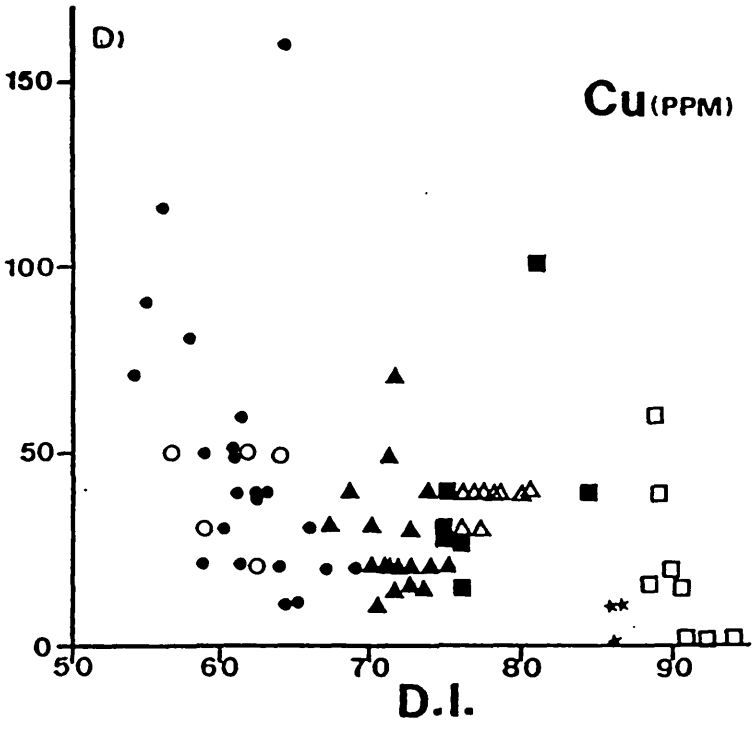


Figure 5.20 Continued

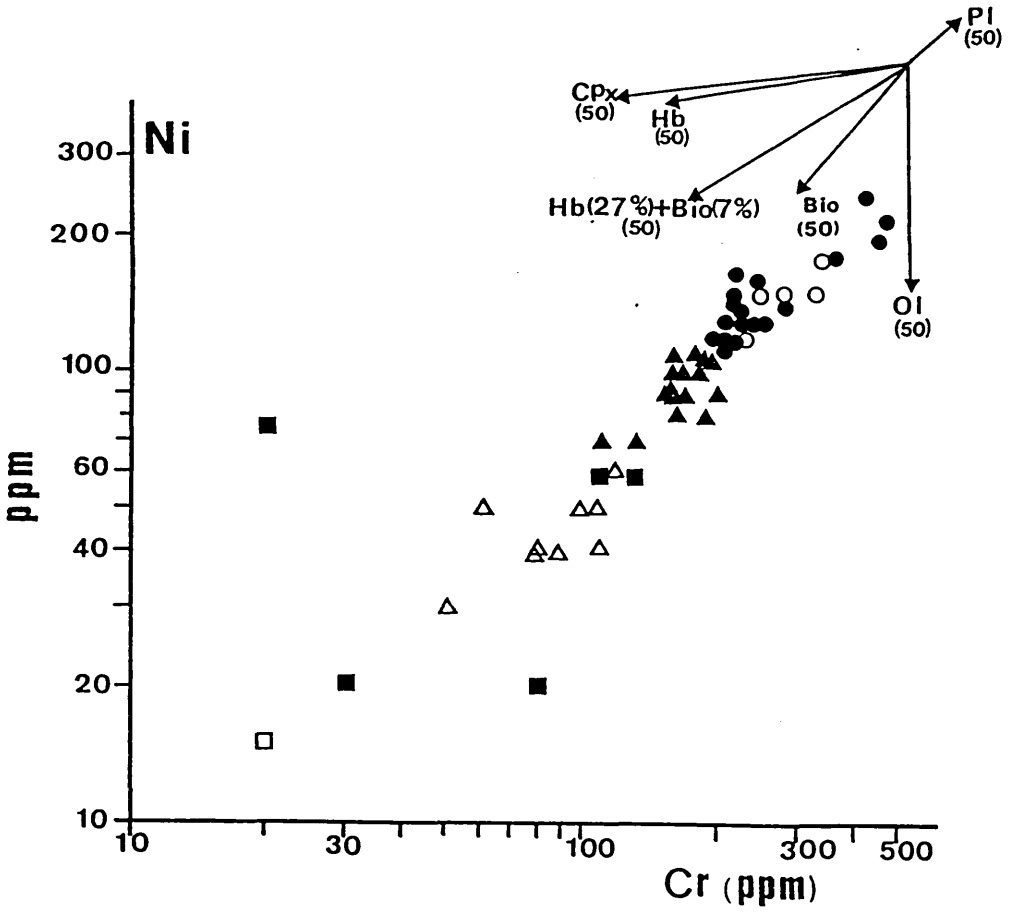


Figure 5.21 Logarithmic, bivariant plot of Ni versus Cr for the Bom Jardim complex. Mineral vectors calculated using the Kd values in table 5.3. Symbols as in figure 5.12.

listed in table 5.3, it can be shown that 5.6% amphibole, 3.3% clinopyroxene, or 5.6% biotite (10% magnetite) can achieve the desired depletion of Cr, during the evolution of the Bom Jardim complex. Figure 5.21 shows a plot of Cr versus Ni contents for the major facies of the Bom Jardim complex. The trend shows a strongly positive correlation between the two elements. The calculated mineral vectors also displayed in the diagram, indicate that a combination of approximately 27% hornblende plus 7% biotite could account for the trend shown. The modal data supports this conclusion.

5.3.5.3 Vanadium

The variation of V contents within the complex is expressed as a function of the differentiation index in figure 5.20C. There is quite a marked negative correlation during the early periods of differentiation (PBAMS to MPBAS) followed by a much flatter trend in the interval of the MPBAS to PBLS facies. Overall the V contents in the Bom Jardim complex are high, varying from 50 to 125 ppm in the syenites and monzonites, and 15 to 40 ppm in the granitic compositions.

The partition coefficients for V in amphibole, biotite and magnetite are > 30, the Kd for clinopyroxene is substantially less (1.1). As a consequence, it would appear that amphibole and biotite are the main fractionating phases responsible for the observed V trend.

Miyashiro and Shido (1975) used a plot of V versus Cr as a method of discriminating between rocks belonging to the common tectonically controlled rock suites. The majority of the samples from the Bom Jardim complex fall within the calc-alkaline field (see figure 5.22).

The Ni, Cr and V contents in the rocks of the Bom Jardim complex are very similar to the values recorded for the arc island shoshonitic suites (Morrison, 1980). Whereas when compared to the granitoids of the Scottish Caledonites (Thompson and Fowler, 1986 and Zhou, 1987), the Bom Jardim rocks have higher Cr and Ni contents, but are

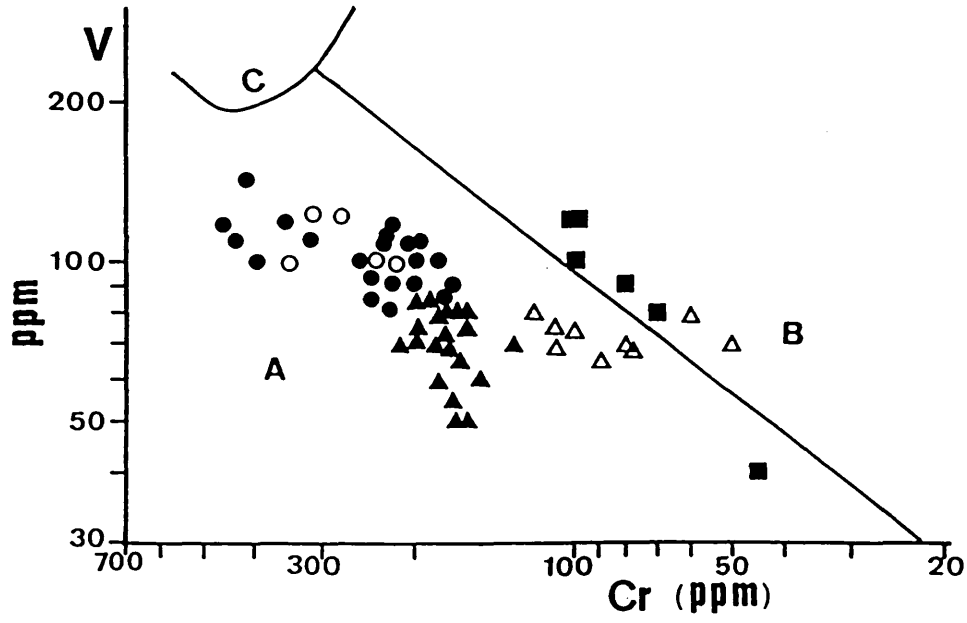


Figure 5.22 Logarithmic, bivariant plot of V versus Cr contents for the Bom Jardim granitoids. **A** = Field of typical calc alkaline series, **B** = field of calc alkaline and tholeiitic series, and **C** = abyssal tholeiite field. The fields are from Miyashiro and Shido (1975). Symbols as in figure 5.12.

generally depleted in V.

5.3.5.4 Copper

The Cu contents in the Bom Jardim complex are generally high, ranging from 10 to 160 ppm in the syenites and monzonites, and just greater than 60ppm in the granites. However the variation of Cu content with differentiation shown in figure 5.20D shows a great deal of scatter with no obvious trend. Even within rocks of the same facies type, there is a wide range of Cu values (eg. 10 - 160 ppm within PBAMS facies).

The geochemical behaviour of Cu in silicate melts is not particularly well understood (Al-Hashimi and Brownlow, 1970) and as a consequence Kds for Cu are not available in the literature. Cu is a strongly chalcophile element and would normally combine with sulphur in the formation of sulphides. Such sulphides are commonly found as inclusions in minerals, especially biotite (Olade, 1976). The behaviour of Cu during the evolution of the Bom Jardim complex could be related to the formation of such a Cu rich immiscible sulphide melt, which later formed sulphide inclusions within the major mafic phases. However, any attempt to use a mafic phase as the fractionated host for the Cu has failed to explain the distribution of that element within the complex. In keeping with the behaviour of the other transition elements in the complex, the range of Cu contents are similar to those recorded in suites of intermediate composition with shoshonitic affinities (Morrison, 1980).

5.3.6 High field strength elements (HFSE)

Saunders et al. (1980) grouped together the elements Ti, P, Zr, Hf, Nb and Ta on the basis of their high charge/radius ratios and termed them the high field strength elements (HFSE). Yttrium has also been included in this group, and for the purpose of the present

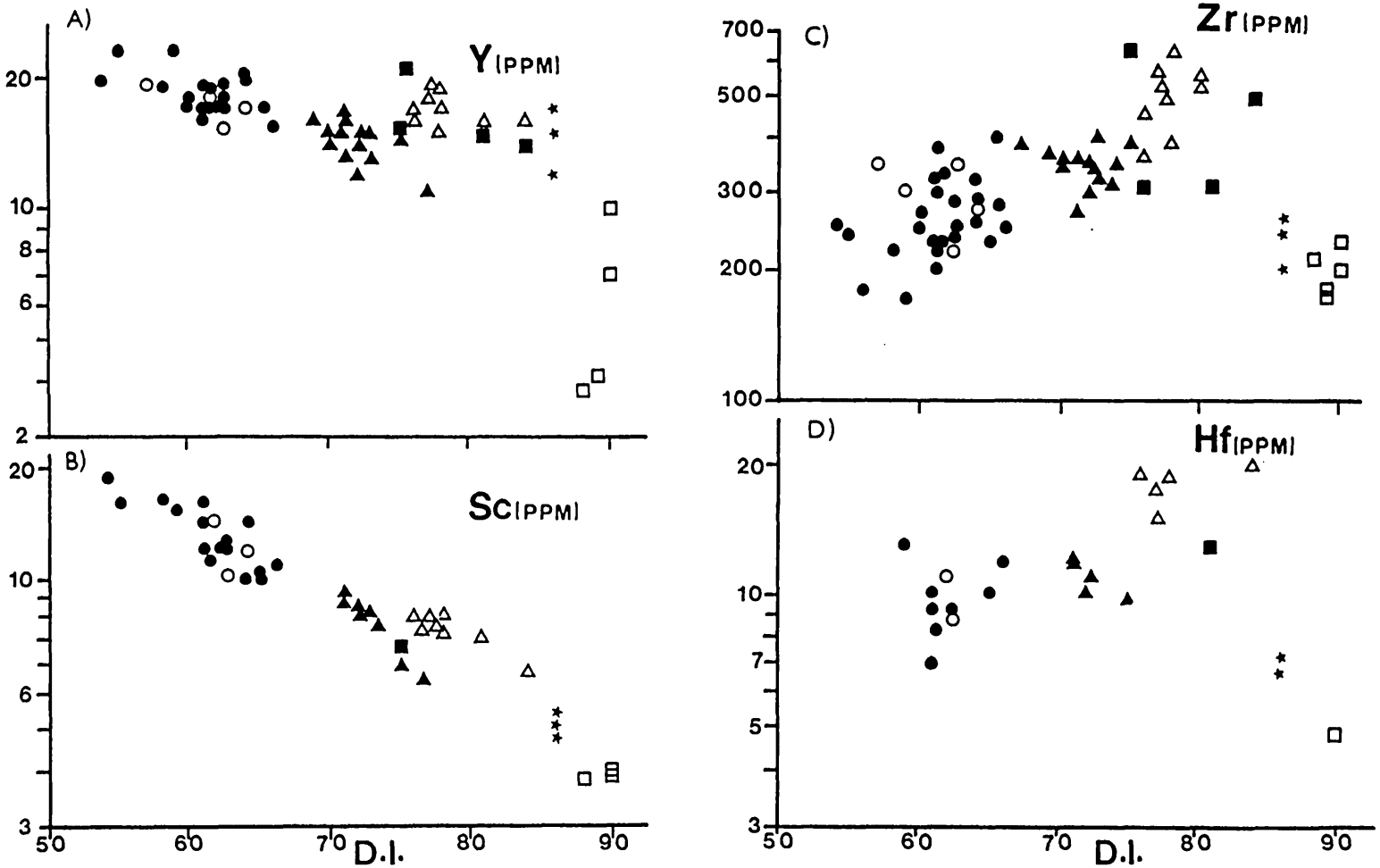


Figure 5.23 HFS elements versus DI for the Bom Jardim granitoids. Symbols as in figure 5.12.

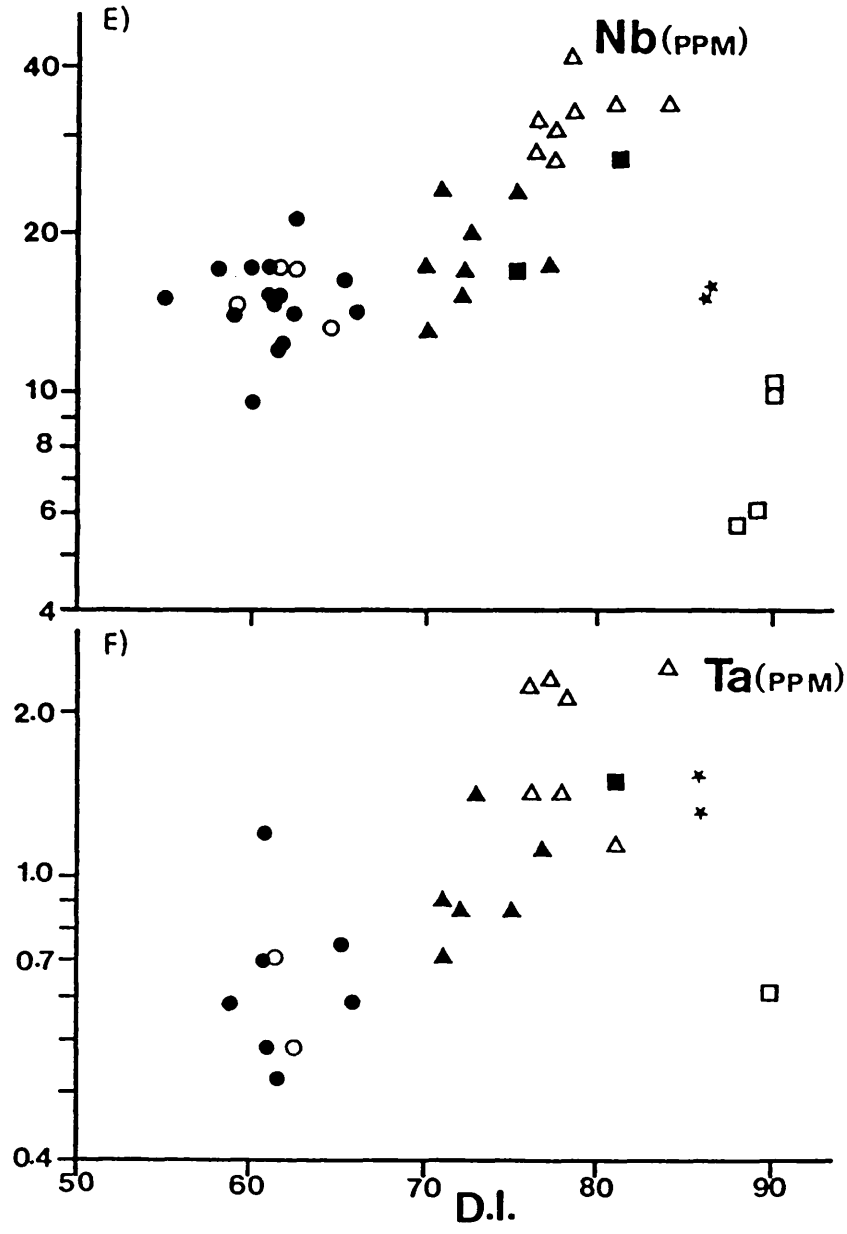


Figure 5.23 Continued

discussion so also has Sc. This group of elements is not easily transported in aqueous fluids, except when the fluids have high activities of certain complexing agents such as F^- (Pearce and Norry, 1979). As a consequence these elements are among the least mobile during any process of alteration. According to Winchester and Floyd (1977), P is perhaps the most mobile element in this group.

5.3.6.1 Zirconium

The distribution of Zr contents of rocks within the Bom Jardim complex shows a clear positive correlation with the differentiation index (see figure 5.23C). The members of the different major facies again appear to form separated clusters within the trend. The granites again plot away from the main monzonite-syenite trend.

The Kd values for Zr given in table 5.3 are all approximately ≤ 1.0, and clearly the element behaves in an incompatible fashion. Although zircon has been reported as a minor accessory phase, the low modal amounts have not substantially modified the Zr trend.

The Zr/TiO_2 ratio can be used as a sensitive differentiation index (Winchester and Floyd, 1977). Figure 5.24 shows a plot of this ratio versus wt% SiO_2 for the Bom Jardim complex.

Members of the alkaline rock suites generally have Zr contents greater than 400ppm, while rocks with distinct calc-alkaline affinities have lower Zr contents. The rocks from the PBAMS facies of the Bom Jardim complex have relatively low Zr contents (<300ppm) when compared to rocks of similar SiO_2 contents in the high-K plutonic complex of E. Greenland (Tarney and Saunders, 1979). However, the Zr contents of the Bom Jardim complex are higher than values quoted for the typical calc-alkaline suites from the Antarctica peninsula (Tarney and Saunders, 1979) and Coastal batholith, Peru (Atherton and Sanderson, 1985).

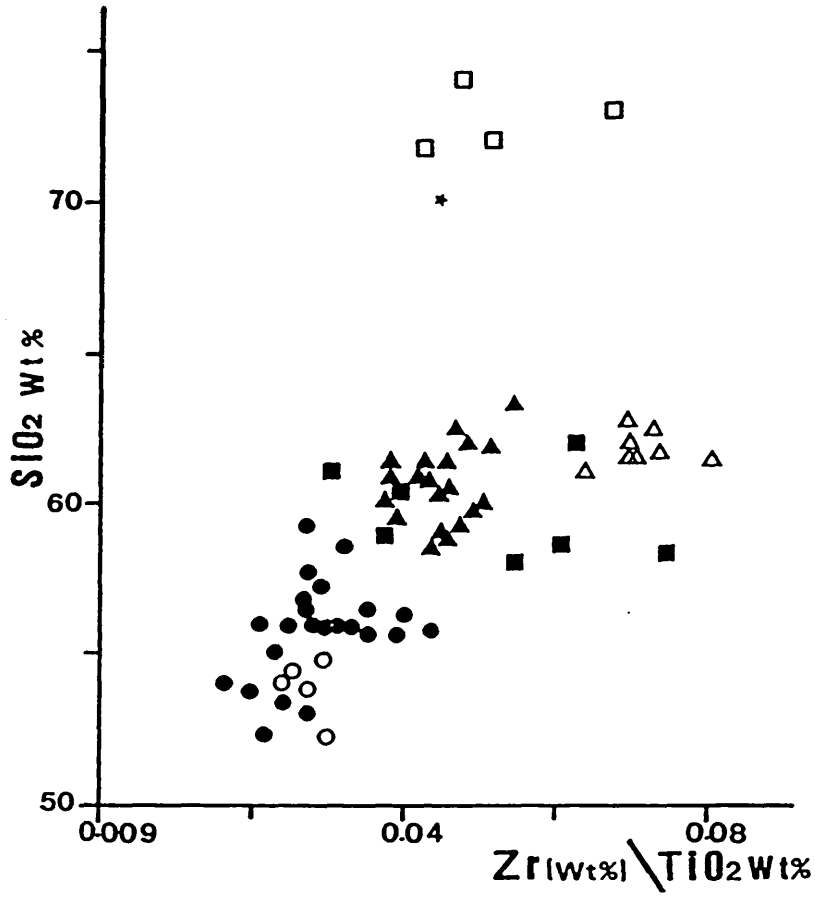


Figure 5.24 Zr(wt %)/TiO_2 ratios versus SiO_2 for the Bom Jardim granitoids. Simbols as in figure 5.12.

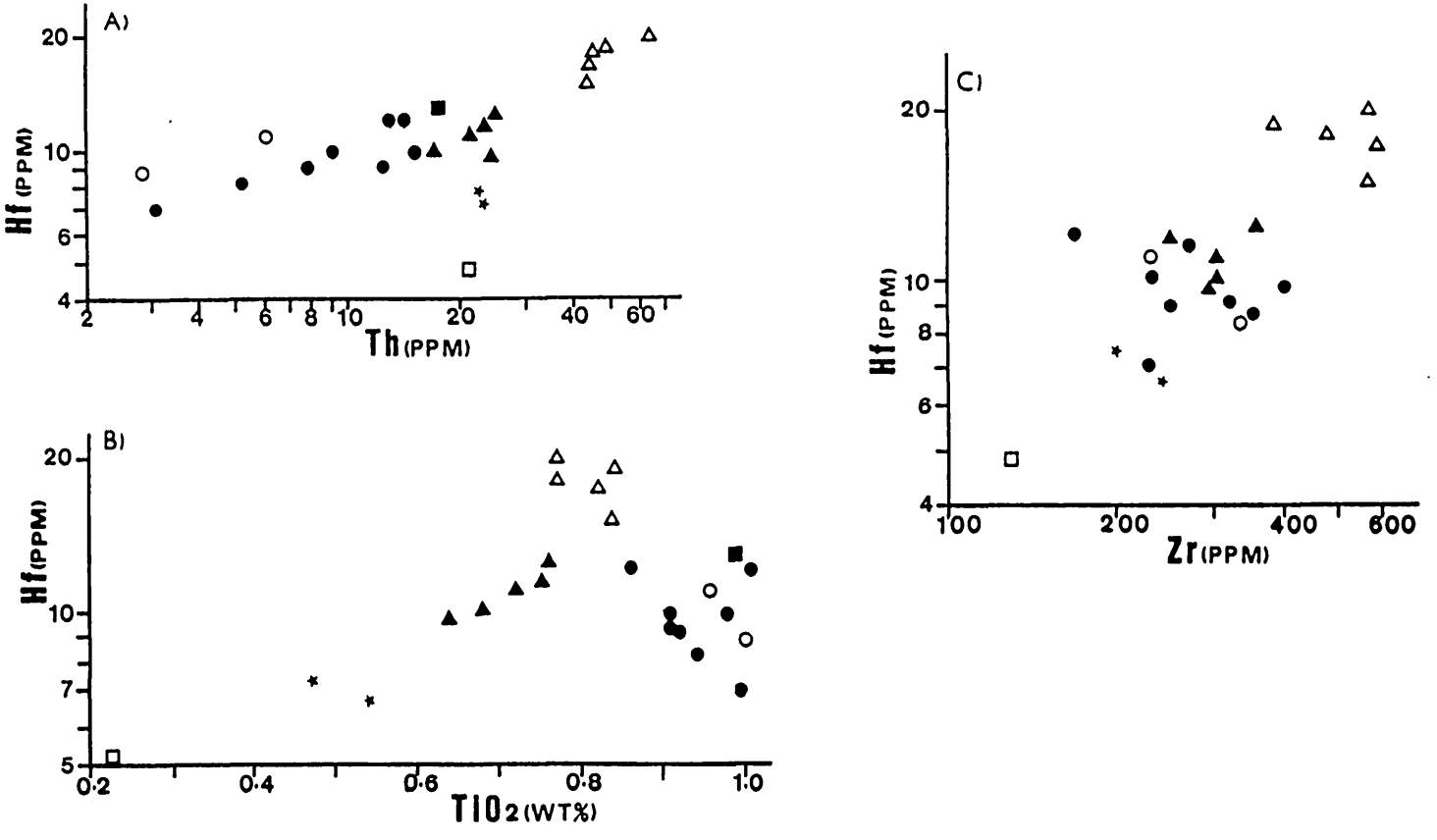


Figure 5.25 Bivariant plots of Hf-Th, Hf-TiO_2 and Hf-Zr for the Bom Jardim granitoids.
(open circles = PBM, closed circles = PBAMS, colsed triangles = MPBAS, open triangles = PBLS, closed squares = Cs, open squares = pink granites and stars = granites from the contact zone syenites - metasediments.

5.3.6.2 Hafnium

The Hf contents in the rocks of the monzonite-syenite suite of the complex display a poorly constrained, but overall, a positive correlation with the differentiation index (see figure 5.23D). The granites again form a distinct cluster away from the main trend.

There is a general paucity of Kd data for Hf in melts of intermediate composition in the literature. Of the modally important minerals present in the complex, biotite is the only phase with a Kd value just greater than 1.0, (Villement et al., 1981); all the other significant phases display a decided incompatible behaviour with respect to Hf. It is only the accessory phases, zircon and sphene which show Kd values significantly greater than 1.0. The mineral thorite could also be a host for Hf, but again the phase is modally insignificant.

In an attempt to relate the Hf distribution with the determined mineral chemistries, a series of bivariant plots have been used and are shown in figures 5.25 A-C. Hafnium shows a positive correlation with both Th (figure 5.25A) and Zr (figure 5.25C). Any substantial fractionation of either thorite or zircon would clearly have radically changed the trends shown in both diagrams. The relationship between Hf and TiO_2 (figure 5.25B) could be interpreted as the result of keilhauite fractionation; however, using the arguments already discussed, concerning the evolution of TiO_2 within the complex and the fact that the trend in figure 5.25A does not indicate any significant removal of Hf, the author believes that accessory phases crystallising in the more acidic melts of the leuco syenites, failed to fractionate to any marked degree.

5.3.6.3 Yttrium and scandium

The Y contents in the The Bom Jardim complex range from 14 to 23 ppm, and are comparable with the average values cited by (Morrison, 1980) for rocks belonging to the shoshonitic series. Yttrium does show a negative correlation with the differentiation index for the

early and intermediate stages of evolution of the complex (see figure 5.23B). The members of the leuco syenite suite (PBLS) however, show a slight enrichment in Y over the rocks of the MPBAS facies. The distribution coefficients of Y in intermediate melt compositions only exceed 1.0 in two phases, namely amphibole and apatite. The modal data clearly indicates that amphibole would be the major crystalline extract responsible for the Y distributions in the early stages of fractionation. The slight enrichment in Y in the PBLS facies is probably due to small concentrations of keilhauite, which according to the present investigation (see chapter 4) can contain up to 0.38 wt% Y_2O_3.

Lambert and Holland (1974) noted that the Ca/Y ratio generally decreases during the evolution of many common igneous rock series. Figure 5.26 shows the variation of CaO with Y for rocks of the Bom Jardim complex. The main point to note in the above diagram, is the marked "J" type curvature to the trend at low CaO contents. Lambert and Holland (1974) refer to this trend in subduction related calc-alkaline rocks, as the "J"-type or hornblendic series trend, and interpreted it as being the result of mainly amphibole and minor apatite fractionation. At first sight it is very tempting to adopt the same interpretation for the rocks in the Bom Jardim complex. Closer inspection of the rock types associated with the inflexion at low CaO contents reveals them to be granites. The present author has stressed on numerous occasions that both the major element chemistry and that of the trace elements discussed so far clearly point to the fact that the granites do not appear to be co-magmatic with the monzonite-syenite suite. Therefore, in the present case, although the linear part of the CaO versus Y trend can be attributed to such fractionation processes as discussed by Lambert and Holland (1974), the "J" type inflexion does not appear to be part of the same co-magmatic process. Such facts point to the inherent dangers of applying such fractionation discriminants without taking into consideration other geochemical evidence.

The Sc contents in the Bom Jardim complex range

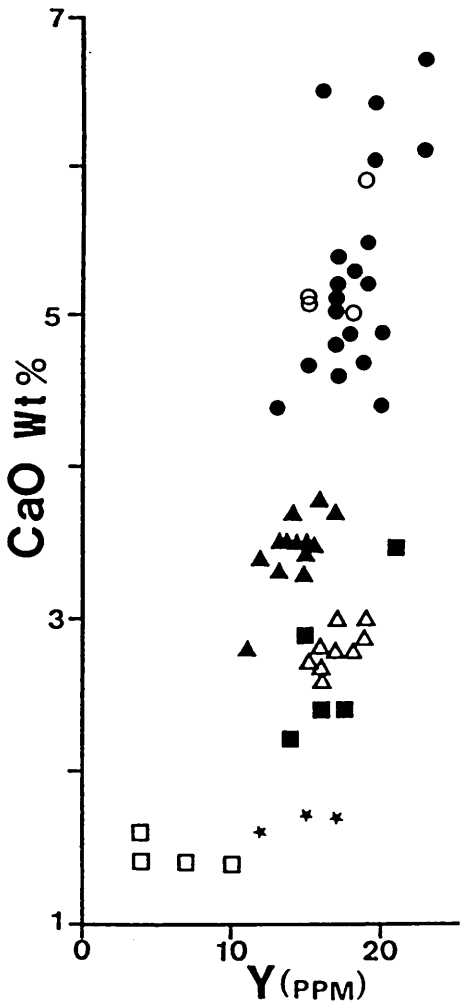


Figure 5.26 Variation of Y (ppm) with CaO (wt%) contents in granitoids of the Bom Jardim complex. (Note the "J" shape of the trend. Symbols as in figure 5.25.

from 4.2 to 18.7 ppm, and show a well defined negative correlation with the DI (see figure 5.23C). Using the Kd data for Sc in melts of intermediate composition cited by Gill (1978) and listed in table 5.3, the major phases which will behave in a compatible fashion with respect to Sc are amphibole, biotite and clinopyroxene. Such mineral phases have been recorded as being present in moderate to high modal abundance at various stages in the evolution of the complex, and their subsequent fractionation has had a significant control on the observed distribution of Sc.

5.3.6.5 Niobium and tantalum

The niobium contents within the monzonite-syenite suite vary from 12ppm to 42ppm; the granites generally contain less than 15 ppm Nb. Niobium shows a positive correlation with the differentiation index (see figure 5.23E). The available Kd data for Nb shown in table 5.3 indicates that amphibole and biotite are the only major phases with values greater than 1.0 (amphibole, 1.3 and biotite, 1.8). The slight compatible behaviour of these two phases has clearly reduced the general incompatibility nature of this element; this can be seen in the flatter part of the trend involving the PBAMS and MPBAS facies. With the reduction in the amount of amphibole and biotite being extracted, the rate of Nb retention within the melt is rapidly increased, i.e., in the PBLS facies. Within this latter facies, Nb appears to be mainly hosted in the LREE, Th enriched sphene, keilhauite.

Tatalum appears to behave in a more incompatible manner than Nb, judging by the differences in the slopes of the two elements in figures 5.23 E and F. The Ta contents within the monzonite syenite suite range from 0.42 to 2.4 ppm whereas the granites cover a much lower range of values (0.6 to 1.48 ppm). There are very few partition coefficient values available for Ta in the literature. As a consequence, it is very difficult to assign roles to the different phases in controlling the observed distribution of the element within the complex. However, a detailed investigation of some of the accessory phases has indicated

that the mineral keilhauite could act as an important host for Ta.

Tarney and Saunders (1979) observed that Nb and Ta along with other HFS elements, are strongly incompatible during the evolution of both alkali and tholeiitic basaltic suites, and as a consequence are strongly concentrated in the acid differentiates. In keeping with the evidence from other groups of trace elements, both the Nb and Ta contents for the granites within the Bom Jardim complex show a major reduction when compared to the rocks of the PBLS facies, again indicating that the granites are not co-magmatic with the other members of the complex.

5.3.7 Rare earth elements

The distribution of selected rare earth elements plotted as a function of the differentiation index (DI) are shown in figures 5.27 A-G. All the plots show some degree of scatter, but in general the REEs La, Ce, Nd and Sm show fairly flat trends. Europium shows a negative correlation with the differentiation index. Both the HREE Dy and Yb have scattered and flat trends. The REE data for the granites again indicates that they are unlikely to be the acid differentiates of the monzonite-syenite suite.

A series of chondrite normalized REE patterns for the individual major facies of the Bom Jardim complex is shown in figures 5.28 A-F. Members of the monzonite-syenite suite have patterns characterised by high total REE abundances (average total REE contents = 330ppm), high LREE\HREE ratios, general trends which are weakly concave upward, and lack of any significant Eu anomalies (apart from sample 10 in the PBLS facies and sample 54 in the CS facies). The chondrite normalized patterns for the granites are significantly different from the monzonite-syenite suite, with marked Eu anomalies in the patterns. The positive Eu anomalies show a variation in Eu^* from 1.3 to 2.7 (where Eu^* refers to normalized Eu abundance divided by the europium content determined from a straight line extrapolation between Sm and Gd).

The Ce contents of the monzonite-syenite suite

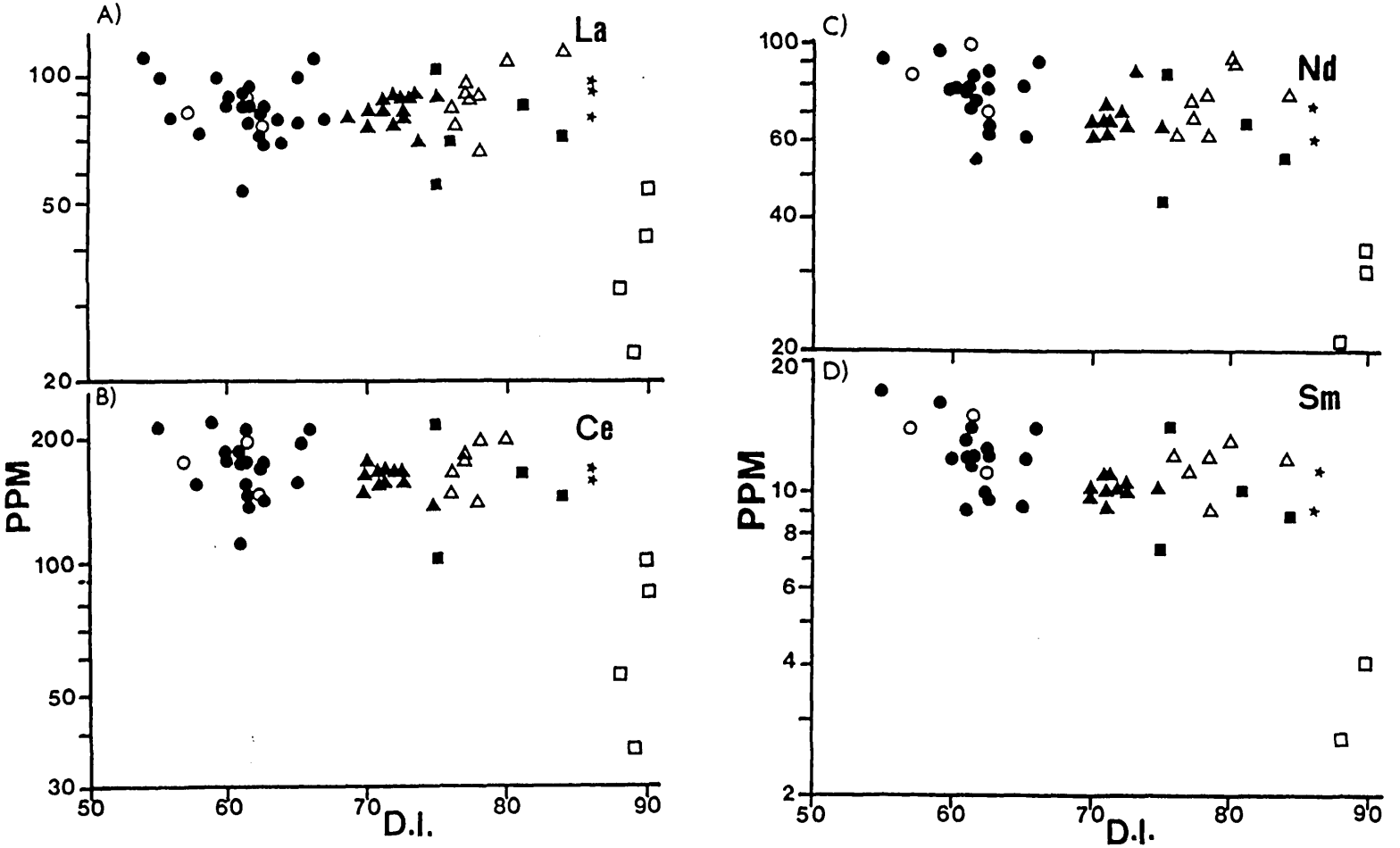


Figure 5.27 Plot of selected REE contents versus DI for members of the Bom Jardim complex. Symbols as indicated in figure 5.25.

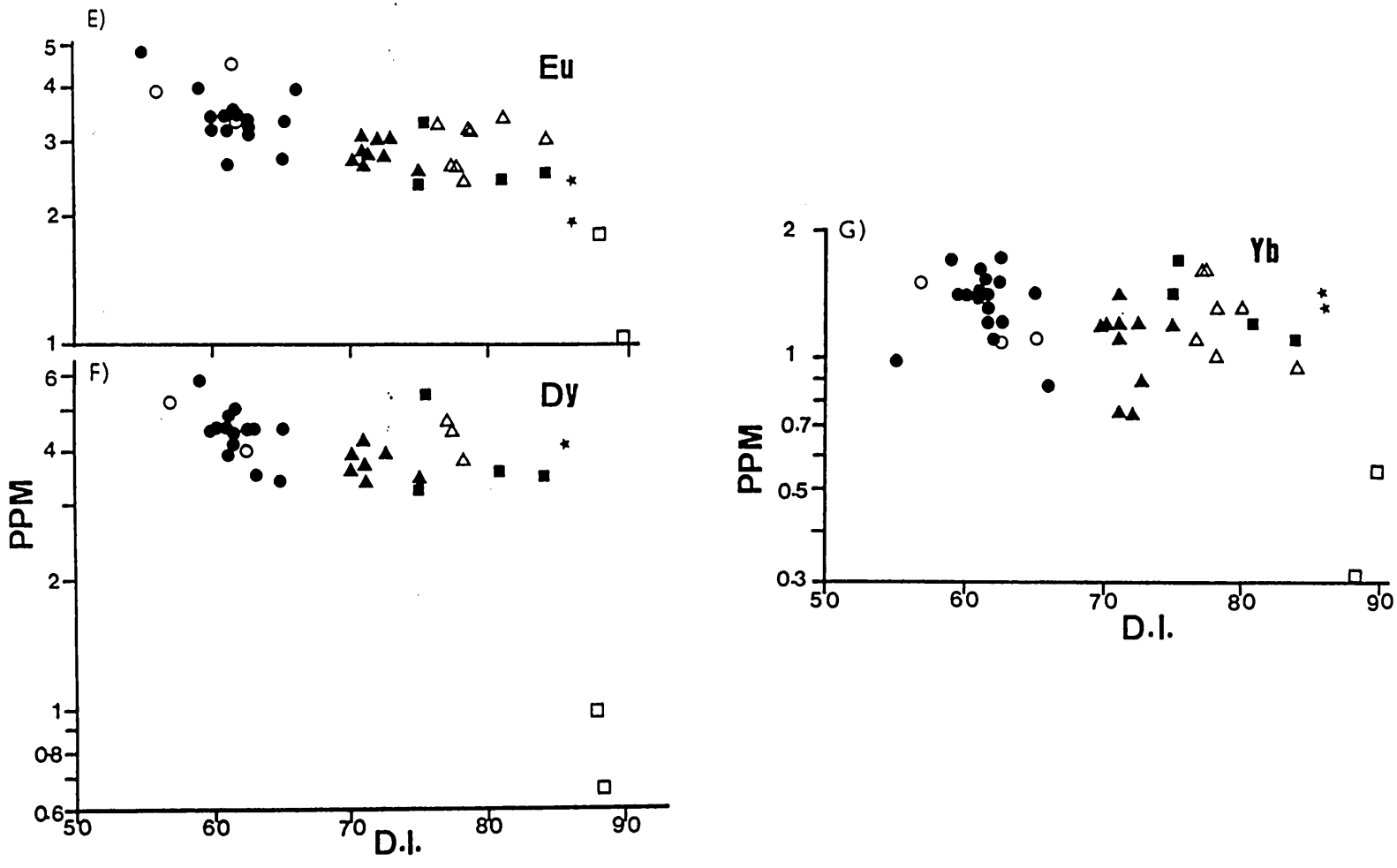


Figure 5.27 Continued

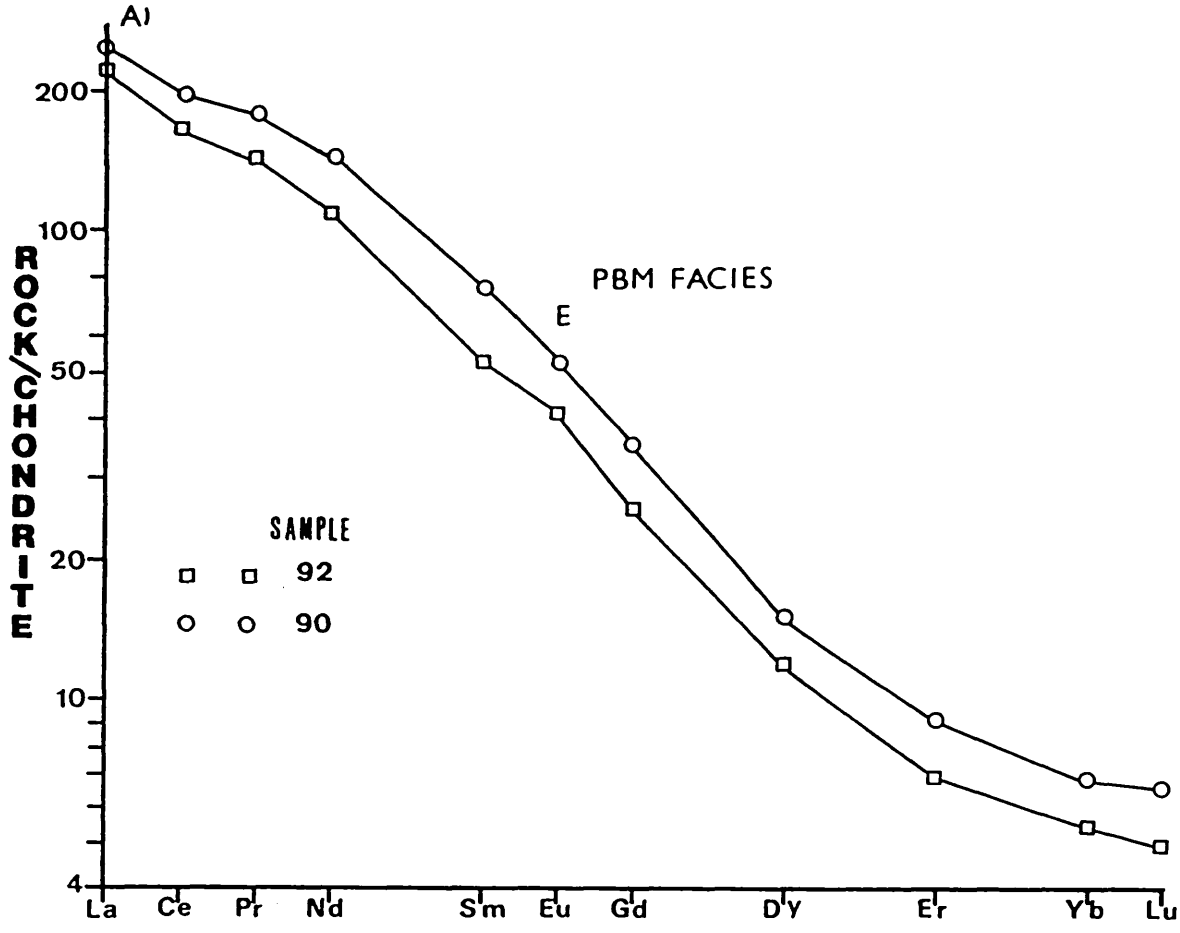


Figure 5.28 Chondrite normalized REE plots for the different lithologies of the Bom Jardim complex. Chondrite values are from Nakamura (1974).

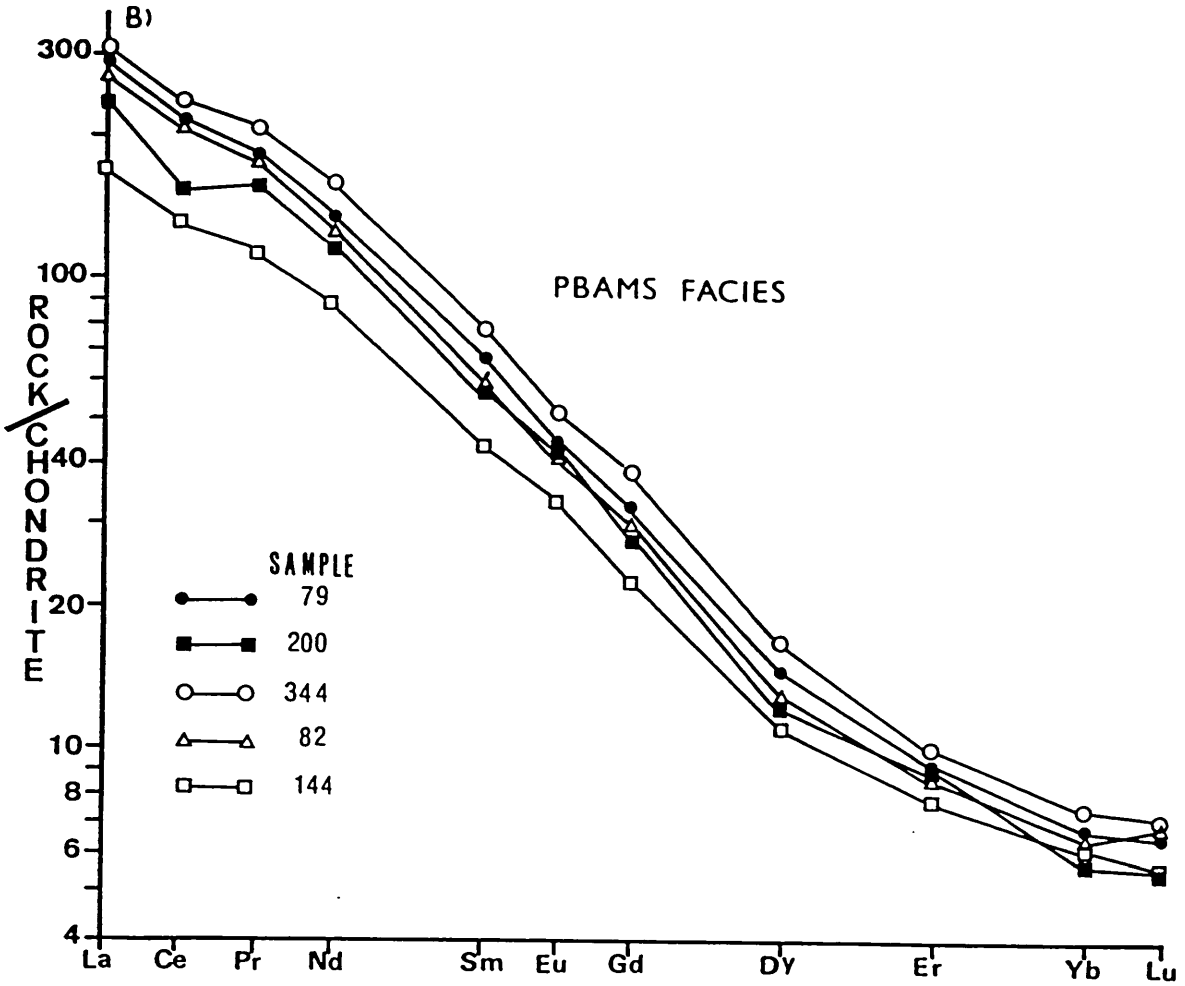


Figure 5.28 Continued

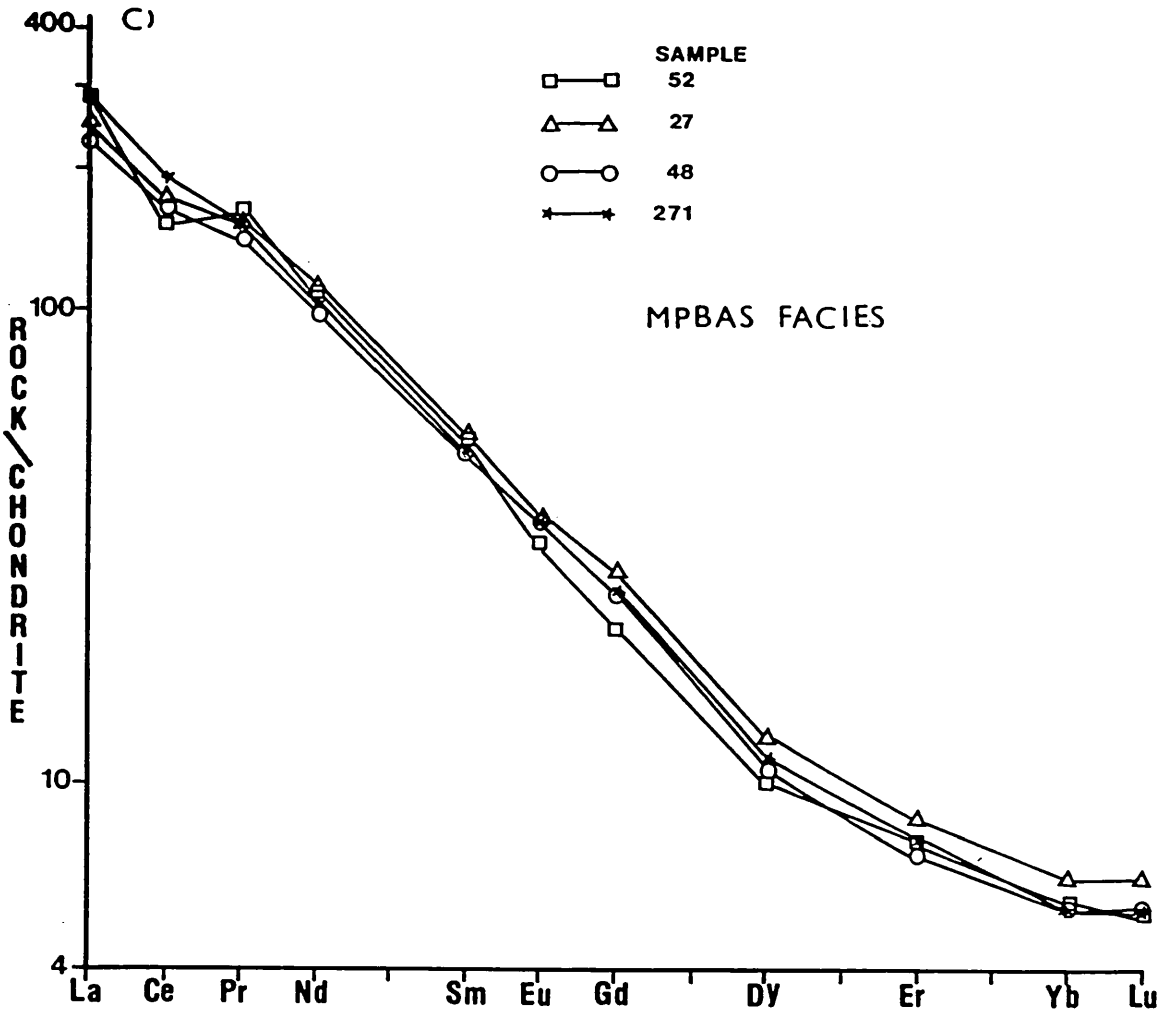


Figure 5.28 Continued

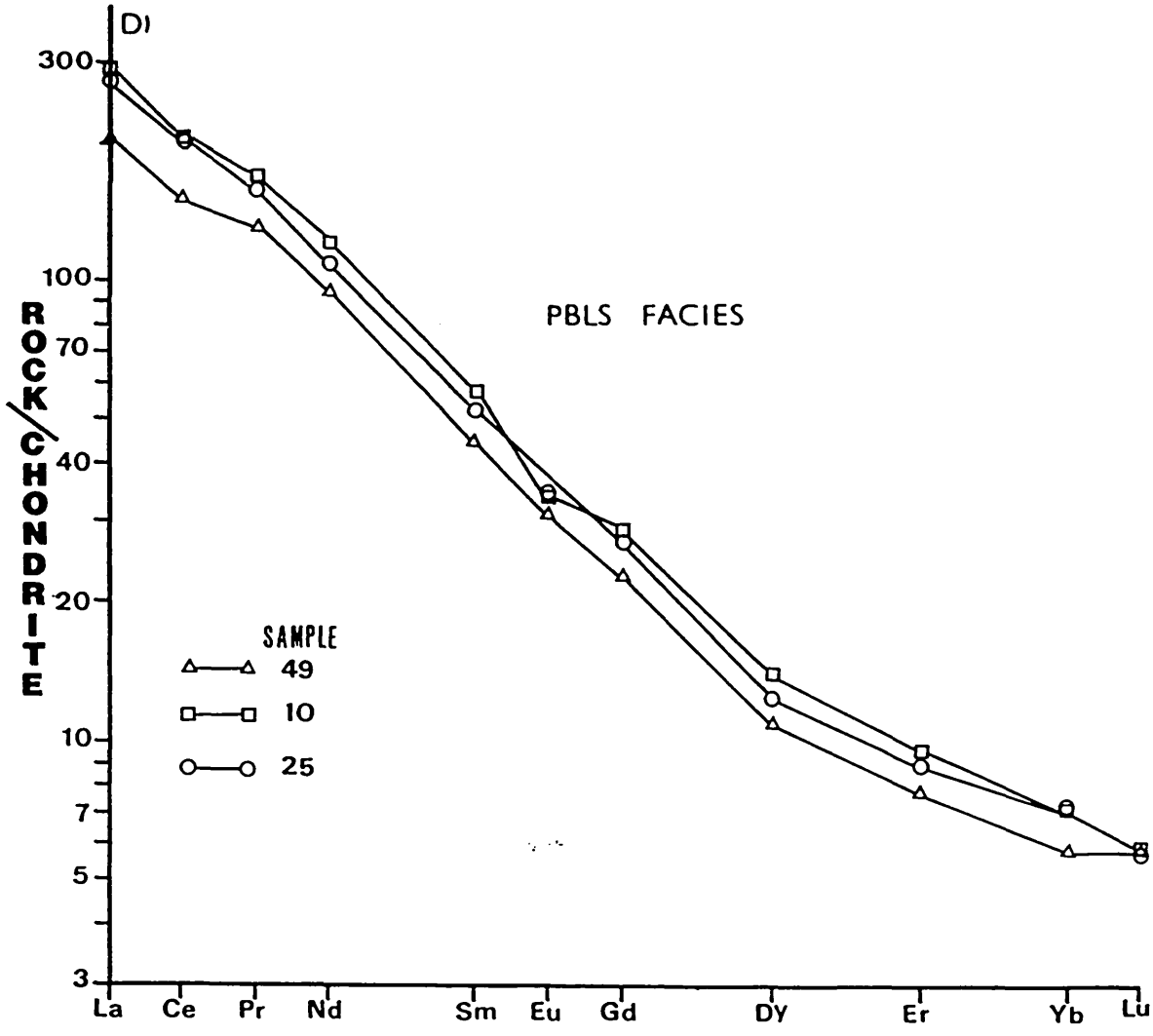


Figure 5.28 Continued

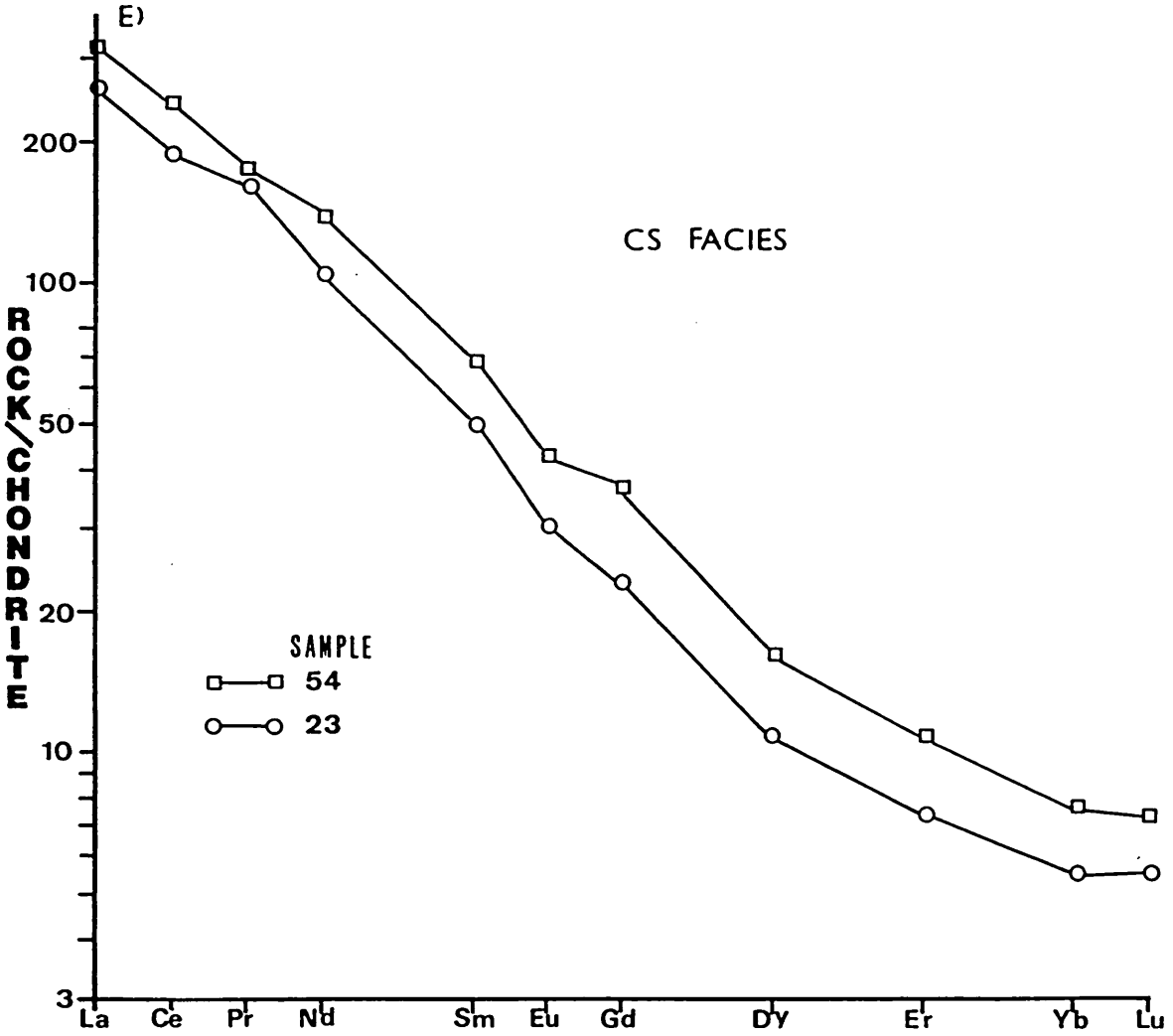


Figure 5.28 Continued

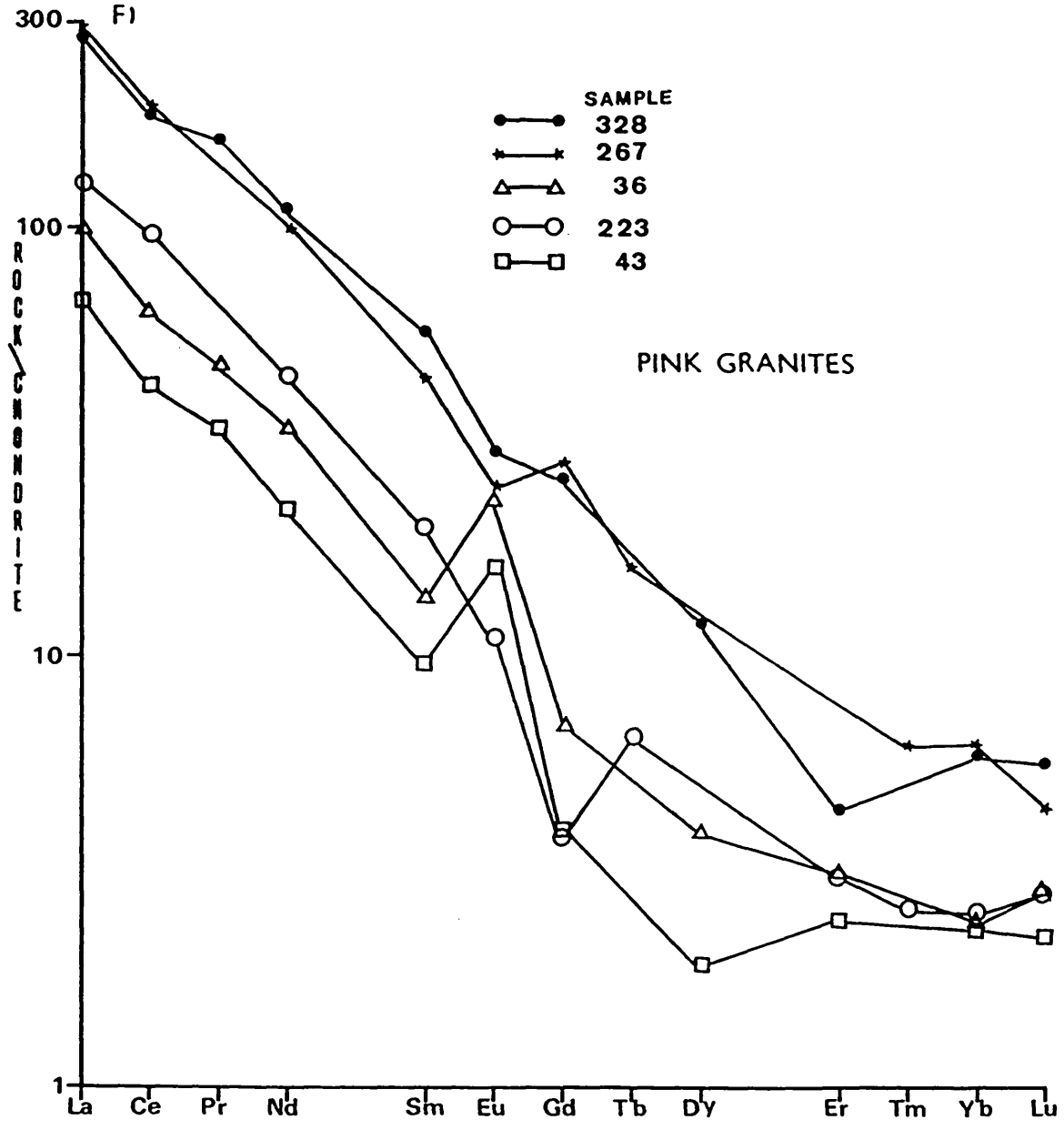


Figure 5.28 Continued

are high, greater than 150ppm, while the Yb contents are around 6ppm; the resultant Ce/Yb are high (approx 25) as shown by the slope of the chondrite normalized patterns. No significant variation in the Ce/Yb ratio has been observed between the individual major facies of the monzonite-syenite suite as a consequence of fractionation. Figure 5.29 shows a plot of the total REE contents versus the variation in silica for the rocks of the Bom Jardim complex; no obvious trend can be identified for the members of the monzonite-syenite suite. Many of the features of the REE trends displayed by the rocks of the complex are characteristic of rocks of shoshonitic affinity (Morrison, 1980 and Ewart, 1982).

Generally the decrease in intermediate (MREE) and heavy rare earth elements (HREE) contents during the evolution of an igneous rock suite requires the fractionation of such phases as amphibole, sphene, zircon and apatite (see table 5.3 for the appropriate Kd values).

Purified mineral separates of hornblende, clinopyroxene and biotite from the Bom Jardim complex were analysed for the rare earth elements by INAA techniques. Figure 5.30 shows their whole rock normalized REE patterns along with the Kd values cited by Hanson (1980). All three mineral phases show a marked negative Eu anomaly, but only the hornblende shows a Kd>1.0

The fractionation of apatite and sphene would deplete the melt in both light and heavy REE; zircon is also capable of reducing the melt in both HREE and MREE. However, in the present case zircon must be ruled out as a possible extract, because both Zr and Hf behave as incompatible elements throughout the differentiated facies of the Bom Jardim complex. Apatite fractionation would lead to a depletion in both the LREEs and MREEs in the melt (but it would also contribute to a possible negative anomaly in the chondrite normalized REE pattern). The fractionation of biotite would not significantly affect the REE patterns of the residual melt. The mineral vectors shown in figures 5.31 and 5.32, clearly indicate that both zircon and sphene were not involved in the fractionation of the major facies within the complex. It has been pointed out that none of

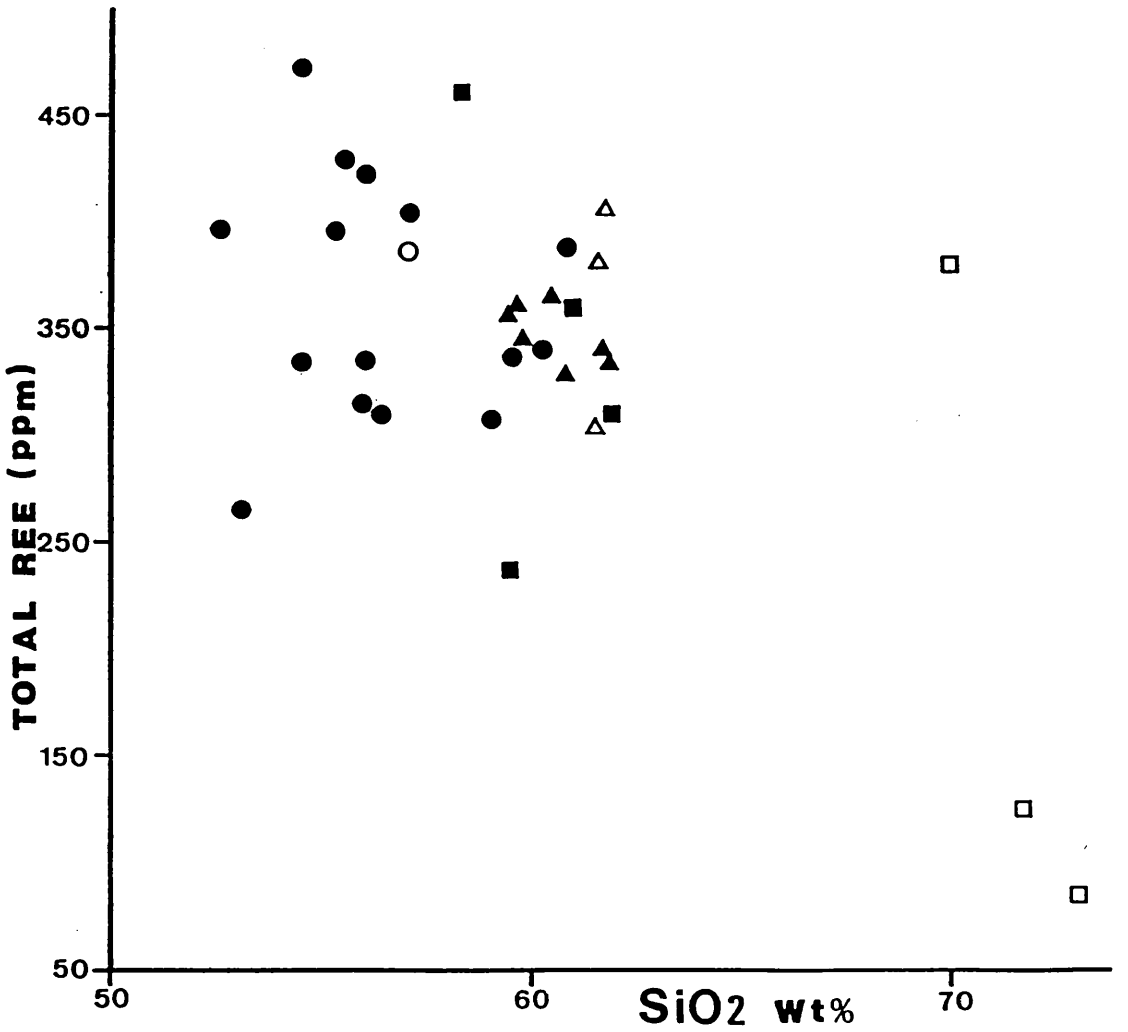


Figure 5.29 Variation of total REE content with SiO_2 for the Bom Jardim granitoids. Symbols as indicated in figure 5.25.

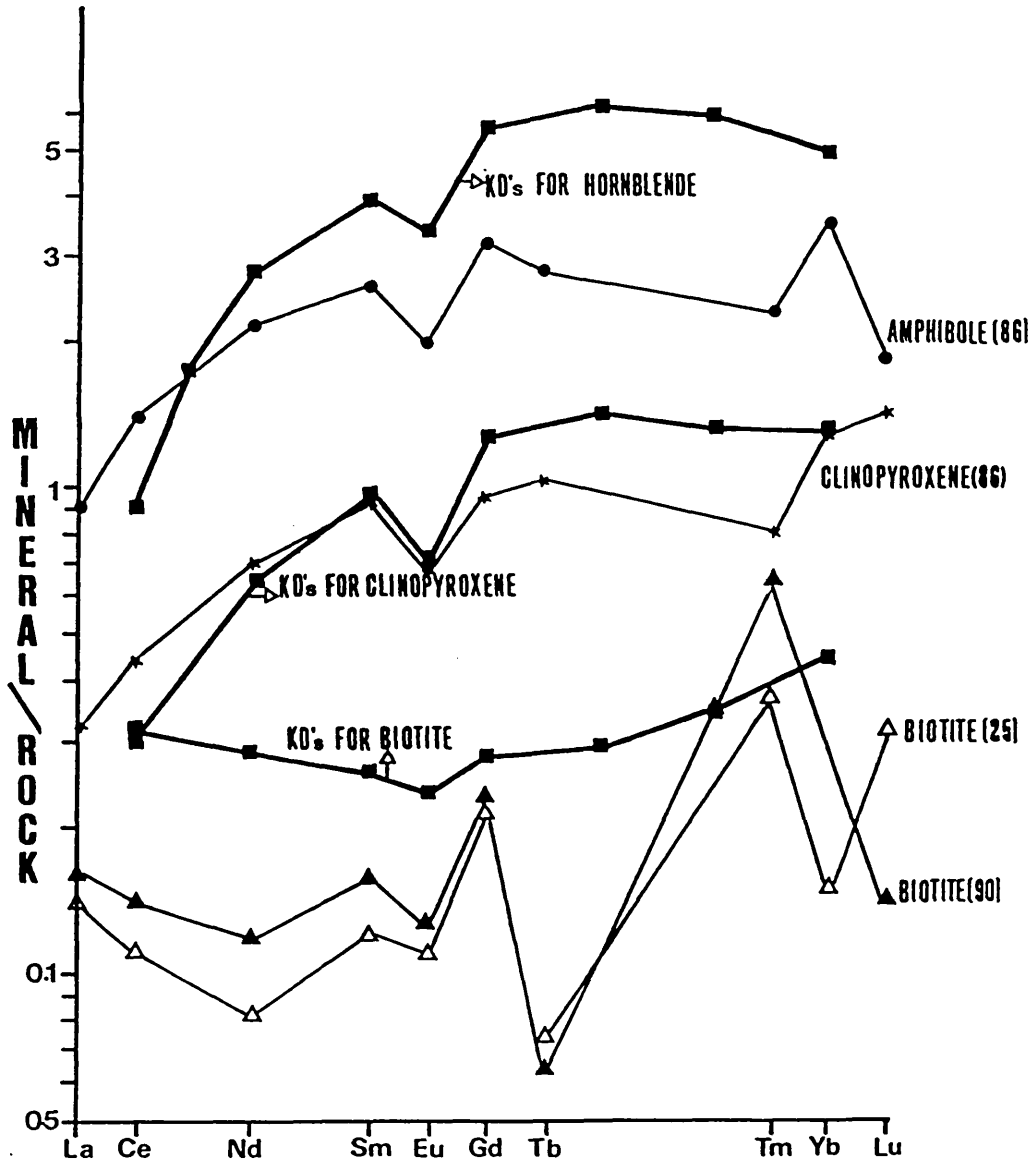


Figure 5.30 Whole rock normalized REE patterns of amphibole, clinopyroxene and biotite from the Bom Jardim complex. The thick lines are based on Kds from Hanson (1980).

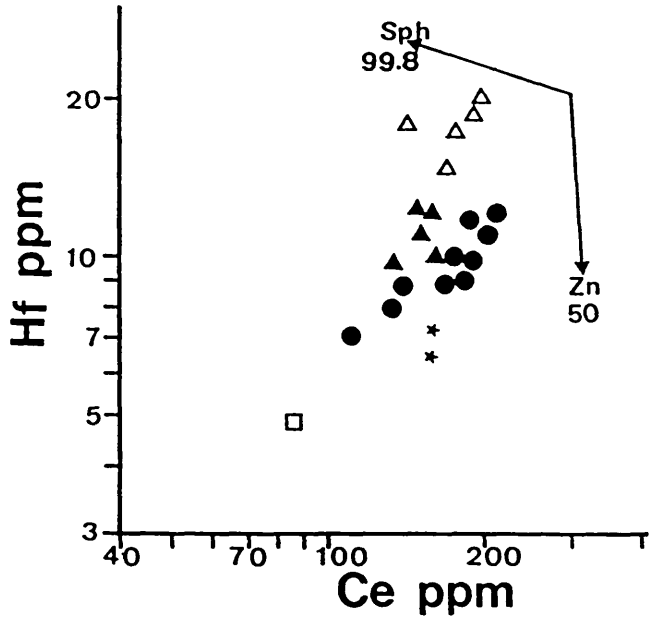


Figure 5.31 Logarithmic, bivariant plot of Hf versus Ce for the Bom Jardim granitoids. The mineral vectors were calculated using the Kd values from table 5.3. Symbols as in figure 5.25.

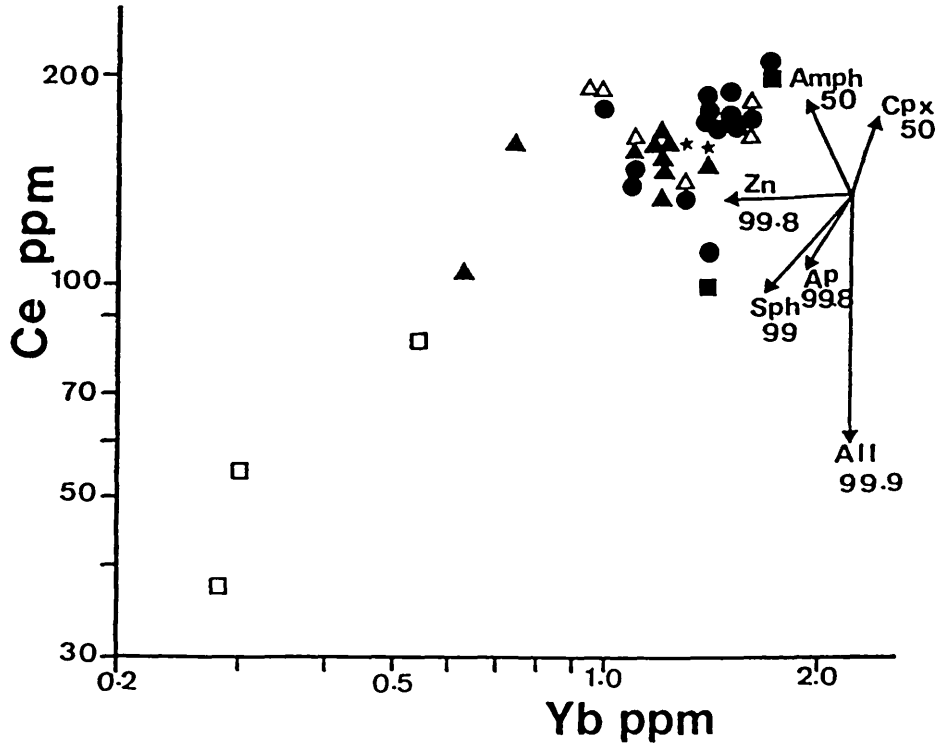


Figure 5.32 Logarithmic, bivariant plot of Ce versus Yb for the Bom Jardim granitoids. The mineral vectors were calculated using the Kds listed in the table 5.3.

the major facies within the monzonite-syenite suite displays Eu anomalies, even though the main phases being extracted clearly show negative Eu anomalies in their chondrite normalized REE patterns; this situation must be due to the off-setting action of feldspar fractionation which will tend to nullify the formation of Eu whole rock anomalies. However, the combined effects of fractionating, amphibole, feldspar and small amounts of apatite will be to progressively reduce the Eu contents in the successive melts, thereby explaining the negative correlation of Eu with the differentiation index shown in figure 5.27E. The lack of a Eu anomaly in the very coarse grained brown alkali feldspar syenite (CS), which is believed to have evolved in part by "feldspar cumulation", could be due to relatively high fO_2 conditions, which would negate the entry of Eu into the feldspar structure (Drake, 1975). The evidence for relatively high fO_2 values at this stage of evolution is rather sparse, although the ubiquitous presence of magnetite and the lack of ilmenite could be used in support of this hypothesis.

The general similarity of REE patterns for the different facies in the Bom Jardim complex suggests that the fractionation of the modally significant phases has had relatively little effect on the REE distributions, implying that the overall bulk REE partition coefficients were close to unity during the evolution of the complex.

Since the high LREE/HREE ratios for the different facies within the complex cannot be accounted for by major phase fractionation, and both petrographic and geochemical evidence rule out the possibility of fractionating the HREEs via accessory mineral extraction, the parental magma for the Bom Jardim complex must have evolved by the partial melting of a source already enriched in light rare earth elements.

5.3.8 Chondrite normalized incompatible element diagrams (spidergrams)

The interrelationships and characteristic features of the incompatible element trends both within and

between the major rock facies of the complex can be illustrated by adopting a series of chondrite normalized incompatible element plots (see figures 5.33 A-F). The normalizing factors are from Thompson (1982). A set of comparative patterns for the PBAMS, MPBAS and PBLS facies rocks is shown in figure 5.34.

All the constituent facies of monzonite-syenite suite within the Bom Jardim complex display similar patterns in their chondrite normalized incompatible element plots, i.e., deep troughs at Nb and Ta, and subordinate troughs of varying depth at Ti, P and U, together with peaks at K, La and Hf.

A close inspection of the individual spidergrams in figure 5.33 A to F, and the comparative patterns shown in figure 5.34 does show some subtle differences between the facies. For example the contents of Nb, Ta, Zr and Hf (HFSE) are consistently higher in the PBLS facies, indicating their overall incompatibility during this crystallisation interval. There is a constant increase in the Rb, Th and K contents in going from the PBAMS facies through the intermediate MPBAS to the PBLS facies. The Ti trough is deeper in the PBLS rock group than in any of the earlier evolved facies, reflecting the combined removal of amphibole, biotite and clinopyroxene. The fractionation of sphene cannot be considered to contribute to the deepening of the Ti trough, as no significant removal of Ce and Nd has been recorded (both elements occur in high concentration within this phase). The troughs at P show a progressive deepening from the PBAMS to the PBLS facies, indicating a continuous level of apatite fractionation during the evolution of the complex. The apatites from the Bom Jardim complex have low REE contents and therefore, moderate levels of apatite fractionation will not cause any significant change in the REE distribution patterns.

The individual sample patterns within a particular facies are generally concordant, although some minor differences do occur, for example the different concentration levels of U and Th in the PBAMS facies (figure 5. 33B). The patterns for both MPBAS (figure 5.33C) and the PBLS facies (figure 5.33D) are better constrained

and more uniform than those of the PBAMS. The single pattern representing the very coarse grained brown alkali feldspar syenite facies (CS) shows a slight departure in its pattern from all the other facies, in having a more noticeable peak at Rb. This latter feature could be a consequence of its suggested "feldspar cumulate" origin. The chondrite normalised REE plots for this facies however do not indicate any appreciable Eu anomaly. The fact that no Eu anomaly is seen does not preclude the idea of a "cumulate feldspar" origin, providing the range of fO_2 during this stage of evolution of the complex could be high.

The spidergrams for the group of granites within the complex are shown in figure 5.33F and are characterised by troughs at Nb, Ta, P, Sr and Ti, and a peak at La.

5.4 GEOCHEMICAL INTERACTIONS DURING THE INTRUSION OF THE COMPLEX, FENITISATION AND CONTAMINATION

The metasomatising action by fluids emanating from the crystallizing syenites into both the marginal metasediments and the metasedimentary xenoliths located within the PBAMS facies, have been recorded at several outcrops within the Bom Jardim complex.

Fowler (1988) identified and discussed the major changes in the trace element contents produced as a consequence of contamination during the emplacement of the Glen Dessary complex, Scotland. He recorded increases in Zr and HREE contents, decreases in Ba and Sr contents and the development of negative Eu anomalies within the contaminated syenites when compared to the uncontaminated rocks of the complex. Figure 5.35 shows a chondrite normalized REE plot for a series of country rock metasediments, xenoliths, fenitised rocks and contaminated syenites from the Bom Jardim complex; a sample of "uncontaminated" host syenite has also been included for comparison. The sample from the fenitised zone (sample 328) shows a higher LREE/HREE ratio than the country rocks

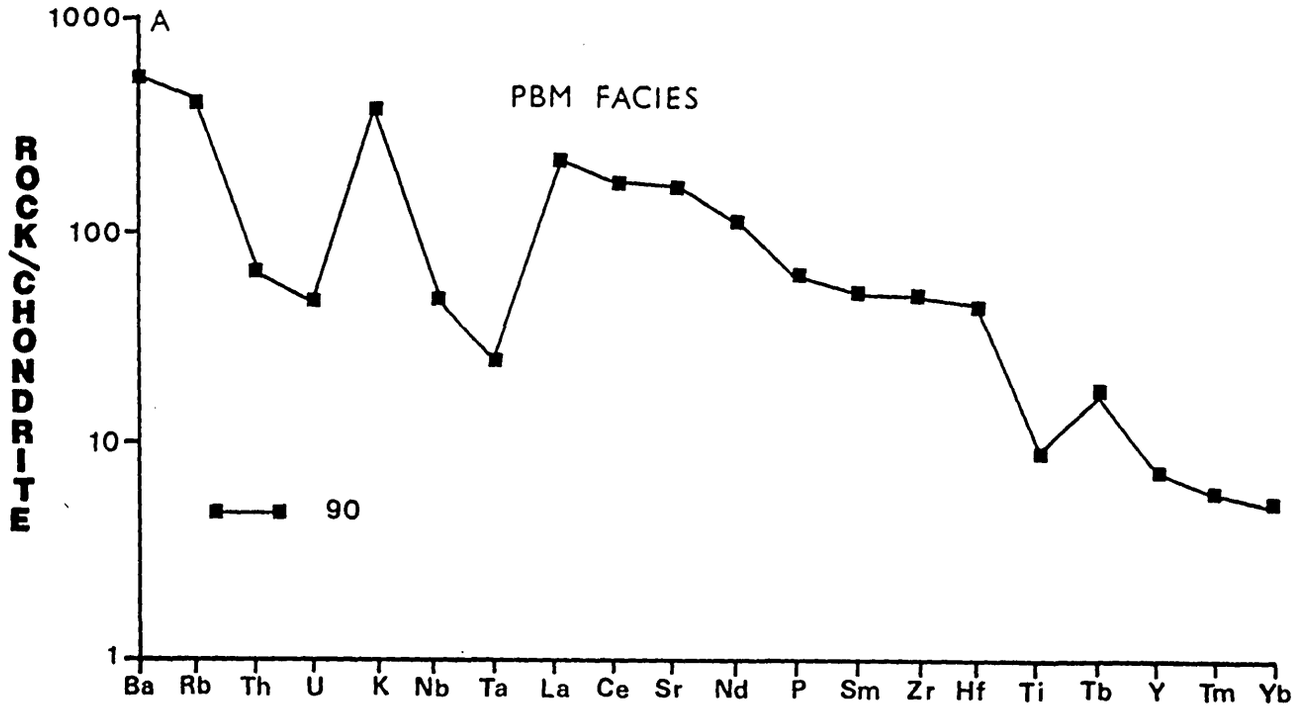


Figure 5.33 Chondrite normalized incompatible element patterns of the different facies of the Bom Jardim Complex.

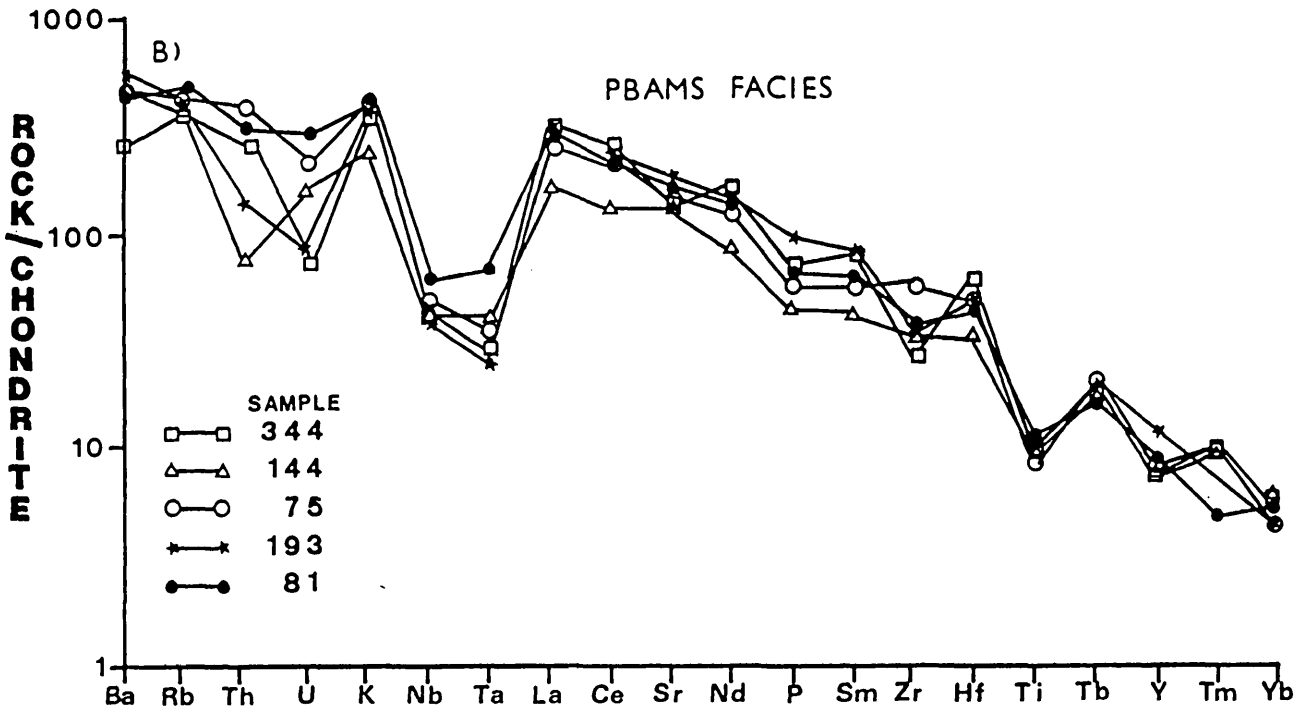


Figure 5.33 Continued

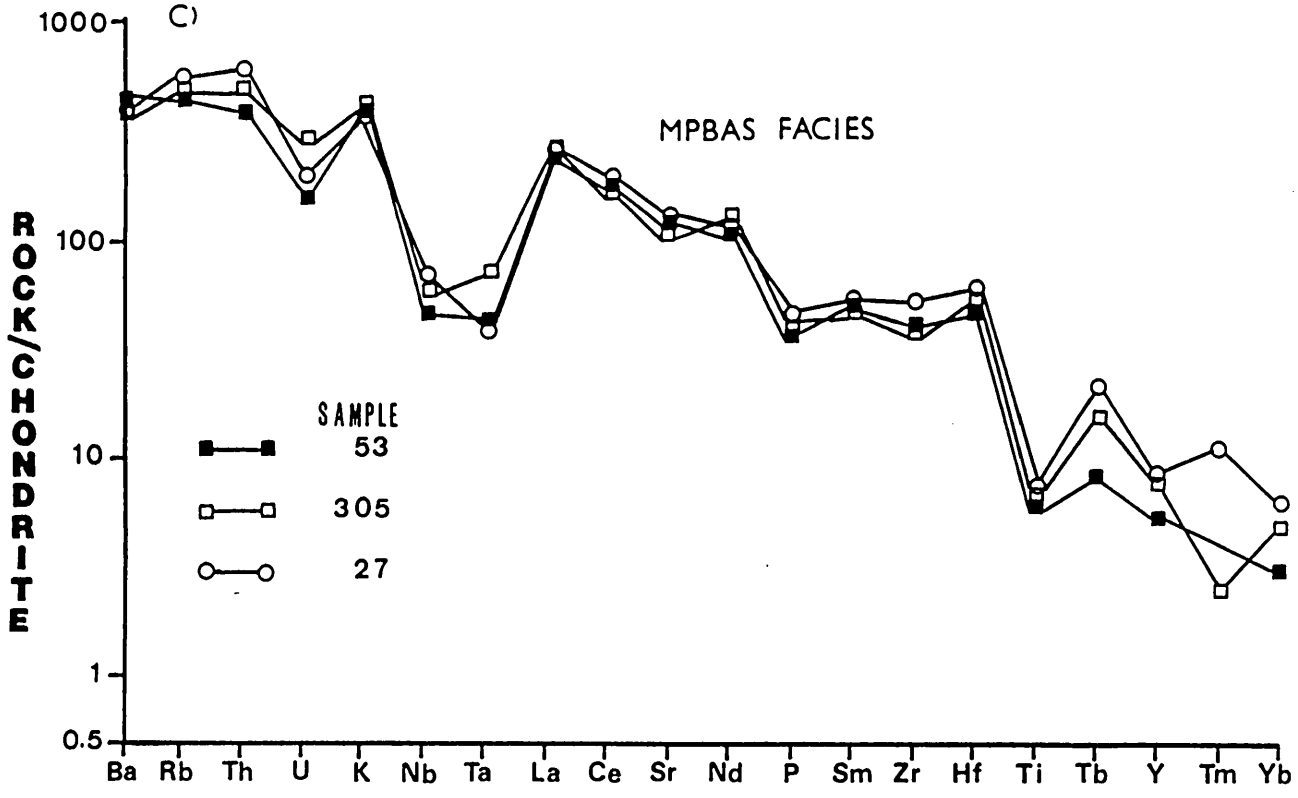


Figure 5.33 Continued

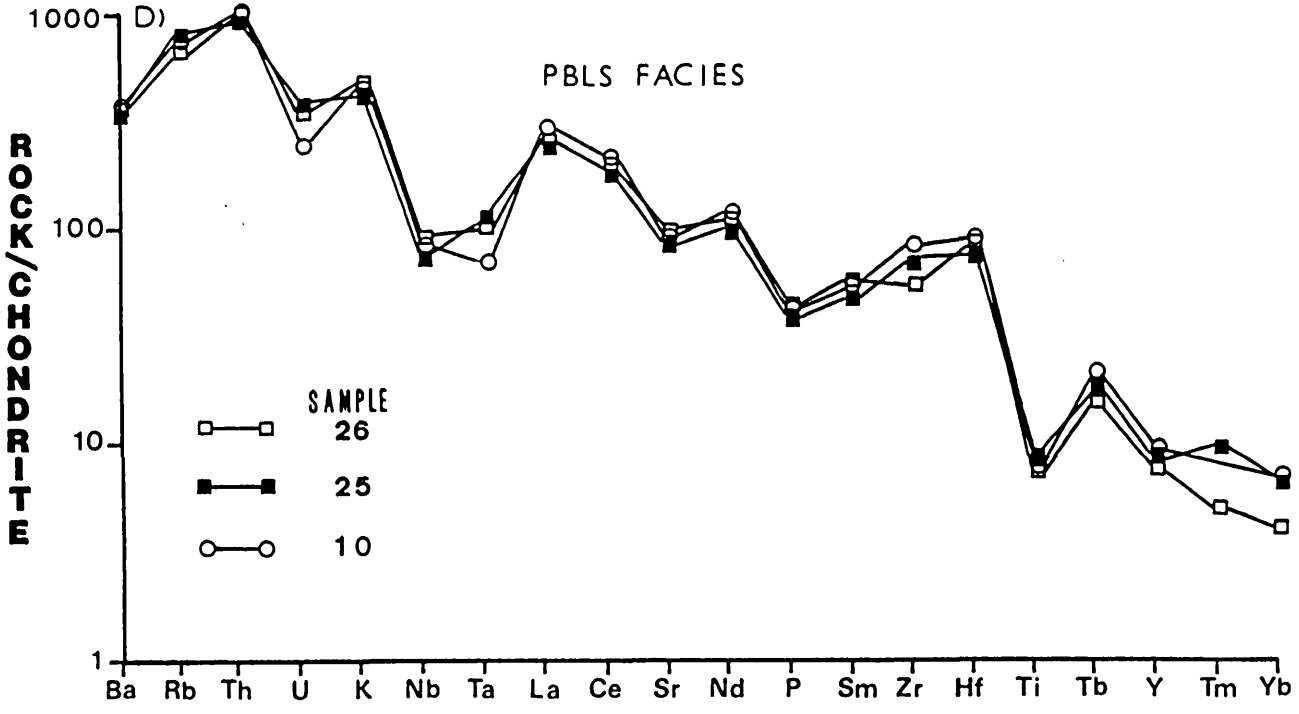


Figure 5.33 Continued

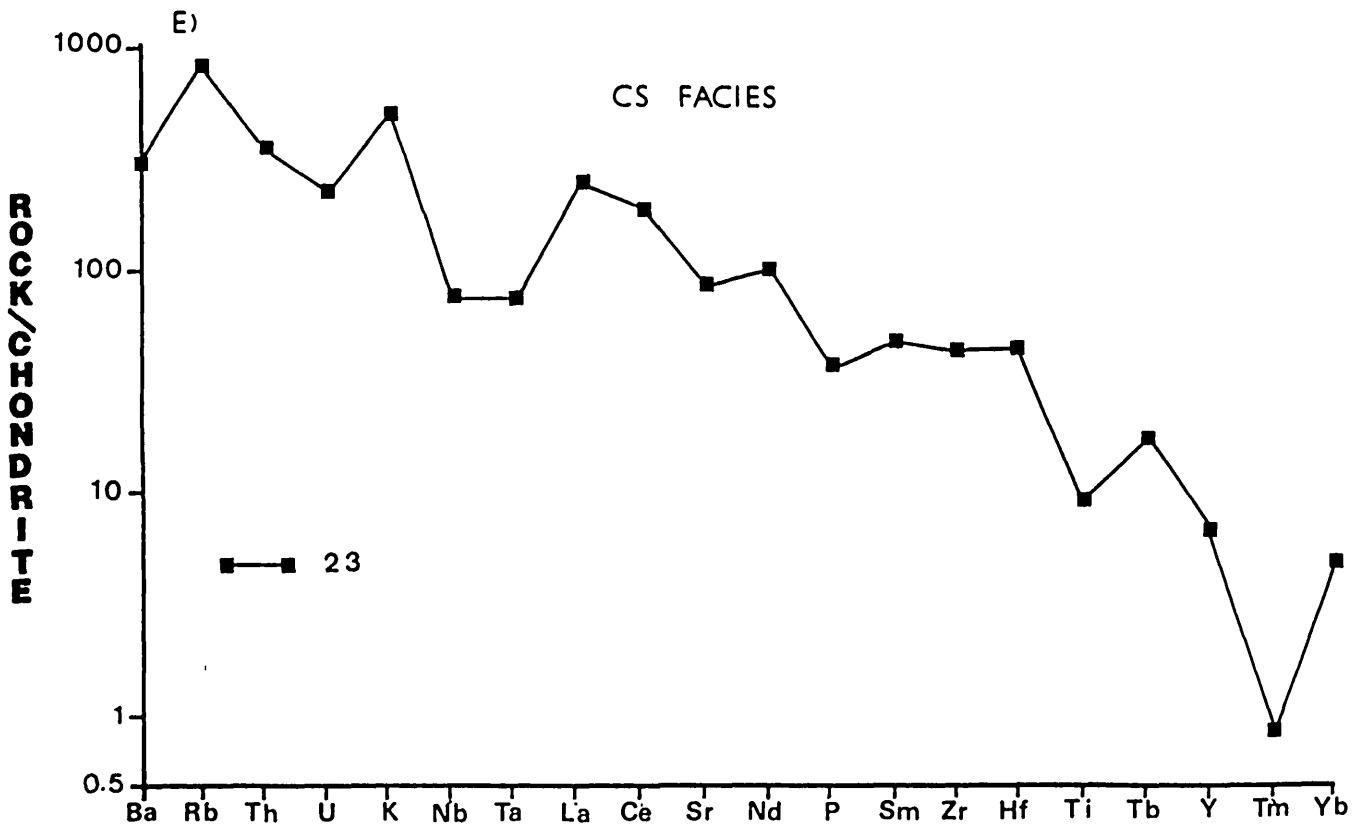


Figure 5.33 Continued

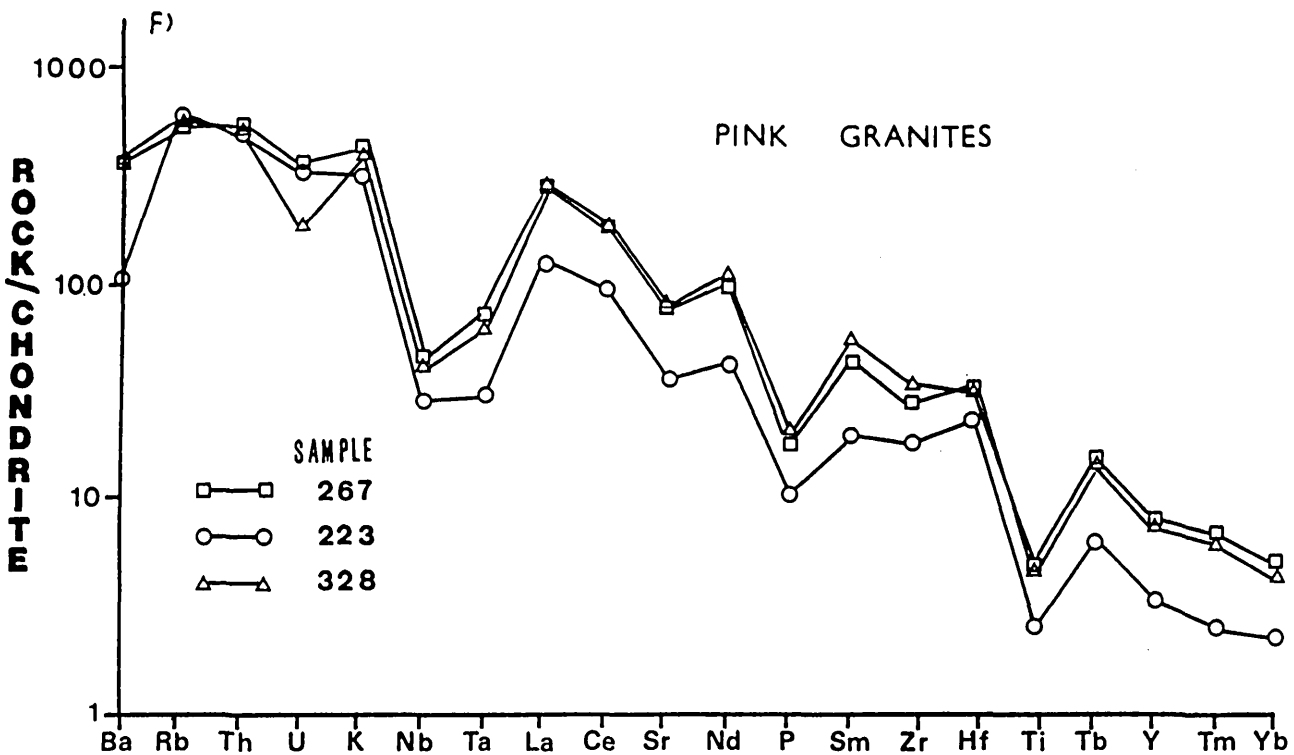


Figure 5.33 Continued

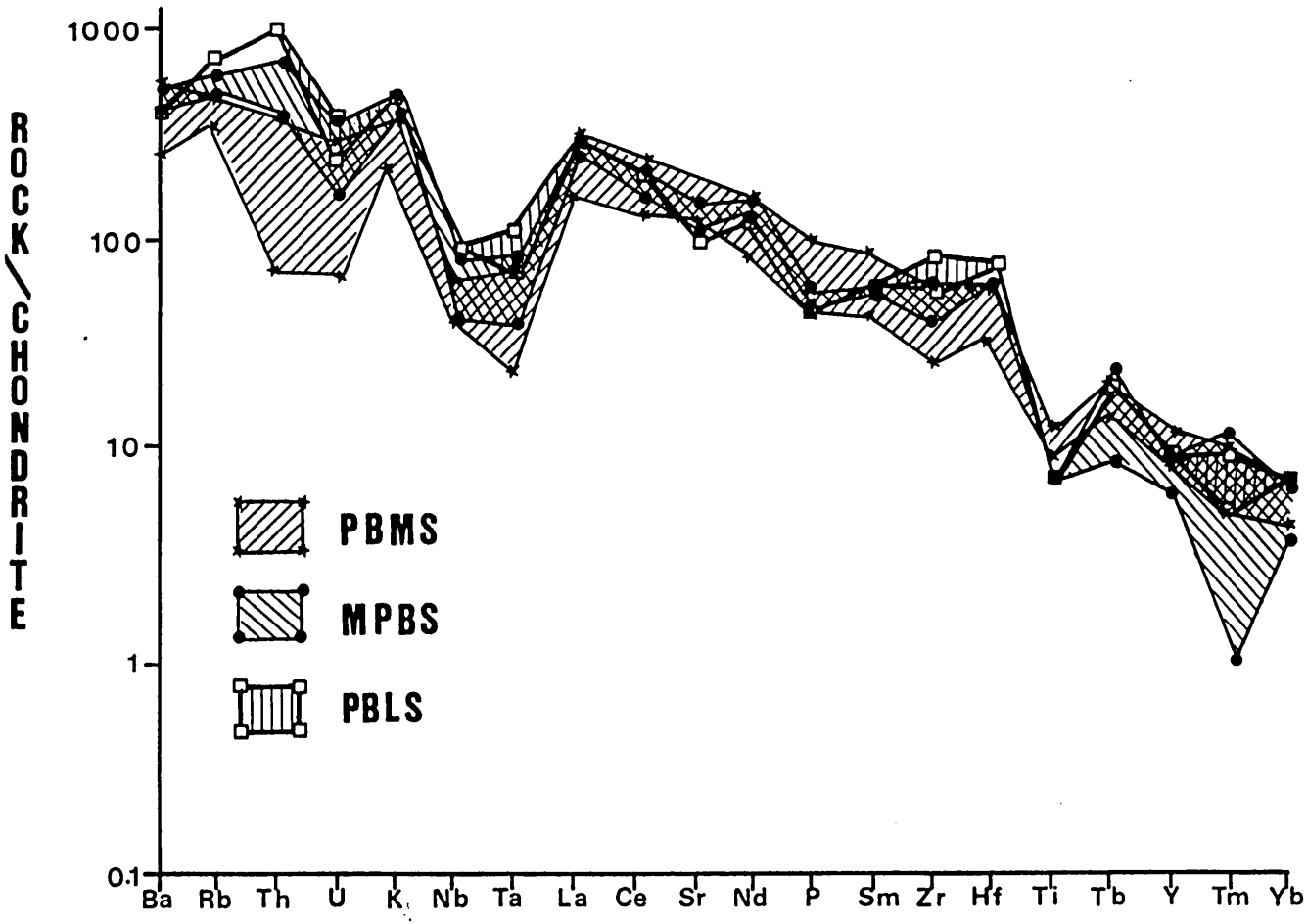


Figure 5.34 A comparison of the chondrite normalized incompatible element patterns for the PBAMS, MPBAS and PBLS facies of the Bom Jardim complex.

together with a slight negative Eu anomaly (Eu^* = 0.86).The metasedimentary xenoliths have low LREE contents comparable to those recorded in the "uncontaminated" syenite, a negative Eu anomaly (Eu^* = 0.75) and a lower LREE\HREE ratio. The contaminated syenite also displays a slight negative Eu anomaly (Eu^* = 0.82) and a lower LREE\HREE ratio. The country rocks show two distinct and contrasting Eu patterns, with the migmatites (samples 354 and 354B) showing significant negative Eu anomalies (Eu^* = 0.30-0.74 respectively), and the garnet biotite schist (sample 175) showing a slight positive Eu anomaly (Eu^* = 1.16).

The changes in magma chemistry (see figure 5.35 and table 5.4) produced as a consequence of contamination during the intrusion of the Bom Jardim complex can be summarized as follows: the contaminated syenites show lower LREE, Ba and Sr contents compared to the "uncontaminated" syenite. The elements Ba, Sr and the LREEs appear to have been tranferred to the country rocks by fluid processes (see sample 328 in table 5.4). The changes in trace element chemistry brought about by contamination are similar to those reported by Fowler (1988) for the Glen Dessary syenite, with the exception of the HREEs which do not appear to have been changed by contamination during the emplacement of the Bom Jardim complex.

The intrusion of the later granites also appears to have caused some localised changes to the host syenites. Table 5.5 lists the major oxide and selected trace element analyses of a series of syenite samples collected at 10m (125A) and 2m (125B) from the granite (125C) contact. Also included in the same table is a syenite (56) (collected from a different locality), sampled just a few centimetres away from the granite (56A). Sample 344 is again used to represent the "uncontaminated" host syenite. The syenite samples show an increasing in K_2O and Rb contents and a decrease in Fe_2O_3, MgO, CaO, P_2O_5, TiO_2, V, Cr, Ni, and Sr as one approaches the granite contact.

Table 5.4 Selected trace element analyses of metasediments (country rock and xenoliths), fenitised rock, and both contaminated and "uncontaminated" syenites.

	175	278	354	354B	328	207A	344	327A
La	22.0	40.5	28.3	34.6	93.0	60.1	102.6	102.1
Ce	43.2	84.0	79.3	80.5	161.0	113.9	206.3	211.7
Nd	15.7	38.3	27.5	43.1	71.6	47.2	98.2	93.4
Sm	2.4	7.3	6.0	8.5	11.4	7.8	15.8	16.3
Eu	0.8	1.8	0.6	2.2	2.3	1.7	4.0	3.5
Gd	2.0	4.7	0.6	9.5	4.1	5.5	10.9	12.3
Tb	0.3	1.1	1.2	0.9	n.d	n.d	n.d	n.d
Dy	n.d	n.d	n.d	n.d	4.1	3.8	5.9	9.3
Tm	0.4	0.8	0.5	0.4	n.d	n.d	n.d	n.d
Er	n.d	n.d	n.d	n.d	1.7	2.1	2.4	5.0
Yb	2.1	4.0	3.0	2.2	1.3	1.7	1.7	4.2
Lu	0.4	0.6	0.4	0.4	0.2	0.3	0.2	0.6
Rb	55	124	100	190	183	224	127	138
Ba	890	730	340	600	2410	2076	3475	2011
Sr	340	170	110	570	911	719	1810	675
Zr	110	260	160	145	240	270	170	490
Y	n.d	n.d	29.0	22.7	16.7	17.3	22.8	44.8

All elements in ppm. n.d = not determined

Key to samples: (175, 278, 354B and 354) are country rocks, (328) fenitisation zone, (327A) metasedimentary xenolith within PBAMS, (207A) "contaminated" syenite, (344) uncontaminated syenite.

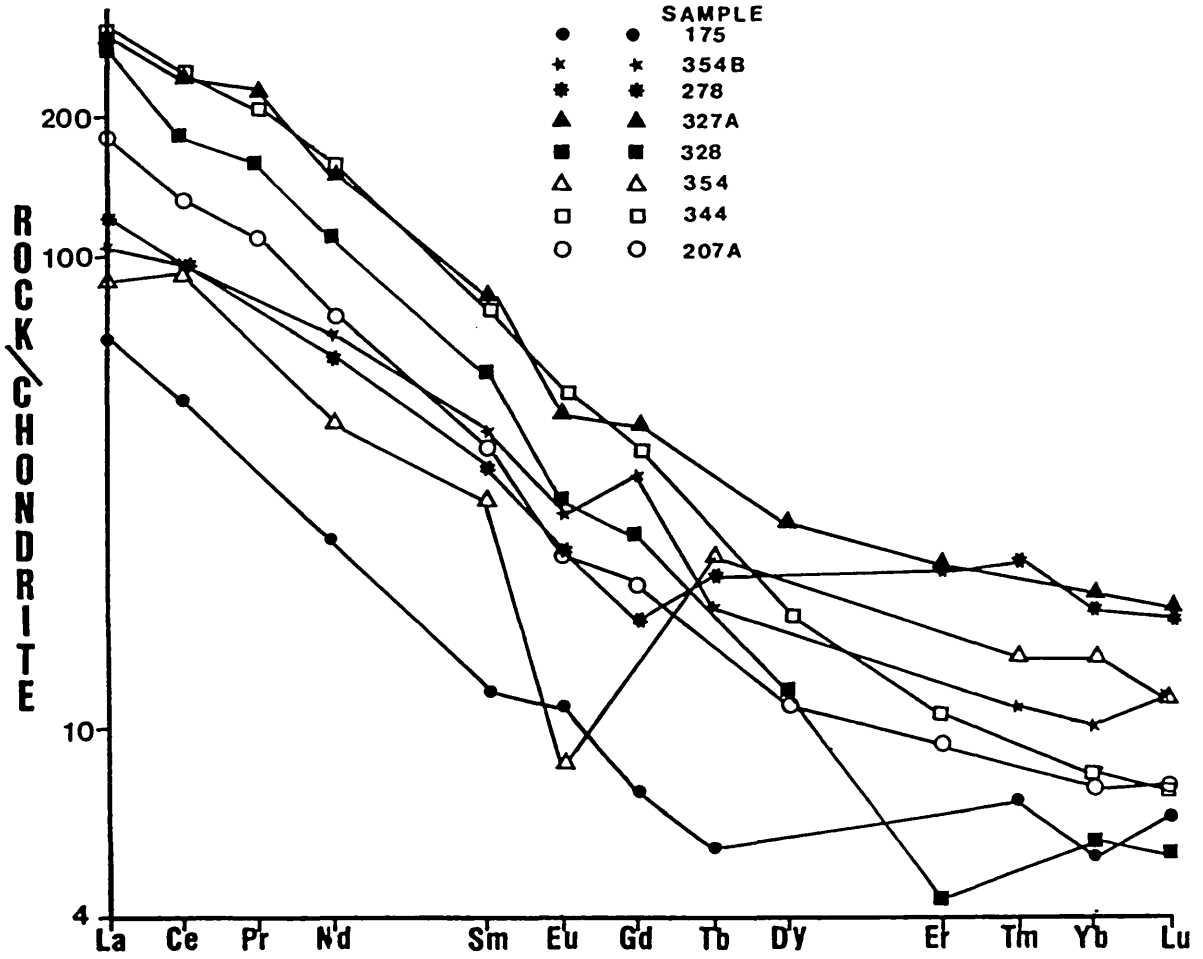


Figure 5.35 Chondrite normalized REE patterns of metasediments around the Bom Jardim complex (175, 354B, 354, 278), granite from the fenitisation zone (328), a metasedimentary enclave within the complex (327A), "uncontaminated" syenite (344) and, contaminated syenite (207A). See text for details.

Table 5.5 Analyses of granites and syenite host rocks from the Bom Jardim complex.

	125A	125B	125C	56	56A	344
SiO_2	57.59	58.32	72.06	59.49	74.23	54.35
Al_2O_3	15.64	15.73	14.44	14.71	13.71	14.96
Fe_2O_3*	6.26	5.26	1.94	5.39	1.29	6.64
MgO	5.16	4.28	0.58	3.10	0.25	6.12
CaO	5.13	4.25	1.44	3.01	1.04	6.12
Na_2O	3.89	3.80	3.79	3.74	3.80	3.65
K_2O	4.89	5.62	5.37	7.21	4.82	4.90
P_2O_5	0.65	0.53	0.13	0.54	0.05	0.74
TiO_2	0.96	0.80	0.35	1.02	0.17	1.05
MnO	0.09	0.09	0.03	0.07	0.02	0.10
LOI	0.46	0.67	0.39	0.46	0.20	0.88
Total	100.98	99.97	100.33	99.14	99.63	100.13
Rb	166	175	171	280	168	127
Ba	2984	3734	1776	2673	806	3475
Sr	1620	1685	693	935	338	1810
Cr	220	179	20	115	25	240
Ni	167	93	30	40	0	160
Zr	320	286	195	780	80	170
V	102	75	20	90	0	110

* All Fe reported as Fe_2O_3. BaO and SrO added to the total.

Oxides in weight percent, trace elements in ppm
key to samples: see text

5.5 SUMMARY AND CONCLUSIONS

The geochemistry of both the major and trace element components in the major facies of the Bom Jardim complex clearly indicates that the monzonite-syenite suite and the granites are not co-magmatic, and that one is dealing with two fundamentally different magma types derived from different sources. The granitic magmas have most probably originated by partial melting of the continental crust, the heat for which being generated during an episode of overthrusting (Brown, 1981). The case for overthrusting in the Borborema province is supported by geophysical evidence (see chapter 1). According to Vorma (1976) magmas are generated and dispersed in the lower part of the crust during collisional processes, and it is only when the compressional tectonic phase changes to one of distensional, that dispersed melts are collected together to form a magma resevoir.

The geochemical characteristics of the major facies of the complex, clearly indicate a shoshonitic affinity and the granites on the other hand appear to be part of a high-K calc-alkaline rock trend. The major and trace element distributions established for the complex, appear to be the result of mineral fractionation, mainly amphibole and biotite, with small contributions from the extraction of the clinopyroxene and apatite. The similarity of the REE patterns for the individual facies (i.e., high LREE/HREE and lack of Eu anomalies), precludes the fractionation of sphene and other accessory phases enriched in the LREEs. The evidence from both Zr and Hf distributions within the complex also rules out zircon as a major fractionating phase. In addition, the fractionation of any of the major mineral phases also fails to account for the high LILE contents (including the LREEs).

The similarity in the chondrite incompatible element patterns of the individual facies also indicates that the degree of fractionation, which occurred during the evolution of the complex, did not greatly modify either the incompatible element abundances or their ratios. Although evidence for contamination has been found within the

complex, it is both minor in amount and very localized in occurrence. The contaminated syenites generally show lower LREE, Ba and Sr contents, higher Rb values and negative Eu anomalies, when compared to the "uncontaminated syenites".

The granites occurring in the contact zone between the syenites and the metasedimentary country rocks appear to have been generated in situ by "metasomatic fluids" emanating from the syenite magma.

CHAPTER 6

GEOCHEMISTRY OF THE MAFIC DYKES AND ENCLAVES

Thirty samples representing the dykes and enclaves within the Bom Jardim complex have been analysed for the major elements and a selected number of trace elements (Ba, Sr, Zr, Zn, Cu, Cr and Ni). Smaller subsets of the above samples have also been analysed for Th, U, Hf, Nb, Y, Sc, Ta and REEs. The individual results together with their CIPW norms are presented in tables B.7 and B.8 in appendix B, and tables C.1.7, C.1.8, C.2.8 and C.2.9 in appendix C.

6.1 MAJOR ELEMENT GEOCHEMISTRY

The mafic enclaves and dykes have SiO_2 contents ranging from 48.6 to 59.4 wt%, together with high total alkali (K_2O + Na_2O) contents; These range widely from 5.97 to 9.15 wt%. As with the host syenites and monzonites the suite of dykes and enclaves show high K_2O contents (2.6% to 6.8 wt% K_2O) with K_2O > Na_2O. The sample of orthopyroxene-clinopyroxene diorite however is an exception with K_2O contents less than 2 wt%. The MgO contents of both groups are generally high ranging from 4.3 to 9.4 wt% and show no correlation with K_2O (see figure 6.1).

The normative compositions listed in tables 7 and 8 appendix B, and plotted in figure 6.2 show a wider distribution of the normative components Qz, Ab, Ne and Lc than the rocks of the major syenite and monzonite facies. The majority of the rocks are olivine and hypersthene normative and there is also a high proportion of nepheline normative.

The variations in the major element oxides are shown in a series of diagrams plotted as a function of the Thorton and Tutlle differentiation index, D.I. (see figures 6.3 [A-I]). Very few of the individual plots show a well constrained variation with respect to D.I. apart from FeO, CaO and perhaps MgO. The above oxides together with TiO_2, P_2O_5 and Fe_2O_3 are all negatively correlated with the

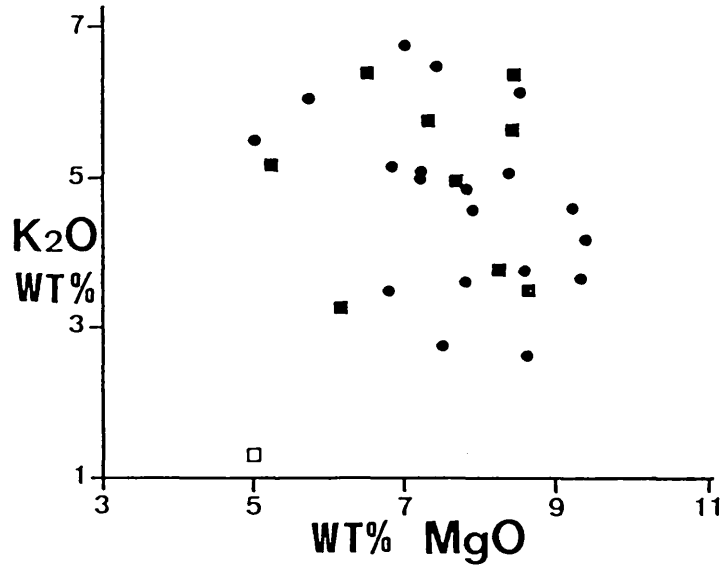


Figure 6.1 Variation of K_2O as a function of MgO for enclaves and dykes from the Bom Jardim complex. Closed circles = enclaves; closed square = dykes and open square = ortho-clinopyroxene diorite.

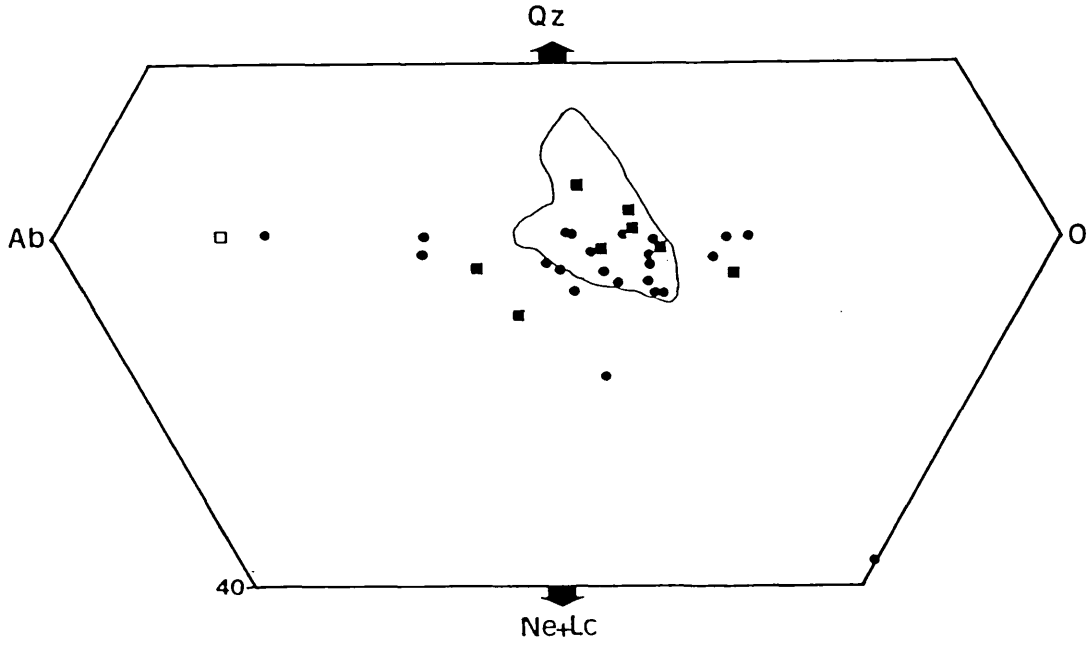


Figure 6.2 Normative data for Bom Jardim enclaves and dykes projected onto the Qz-Ab-Or-Feldspatoid quaternary diagram. The enclosed field represents normative composition of the Bom Jardim syenites and monzonites major facies. Symbols as in figure 6.1.

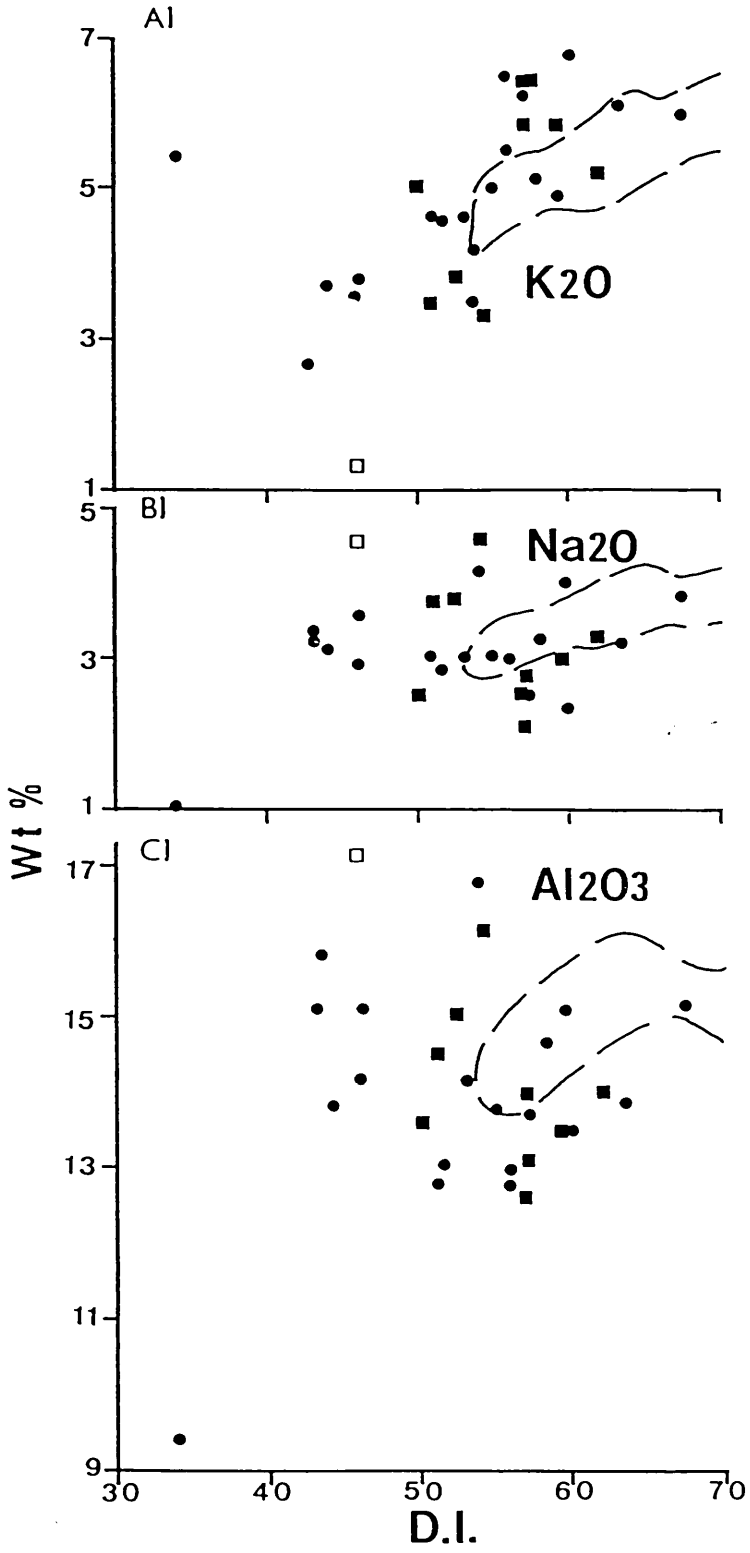


Figure 6.3 (A-I) Variation of the major element oxides as a function of D.I. for the dykes and enclaves of the Bom Jardim complex. Enclosed fields indicate the range of variation for the members of the major facies. Closed circles = enclaves; closed squares = dykes; open squares = two pyroxene diorite.

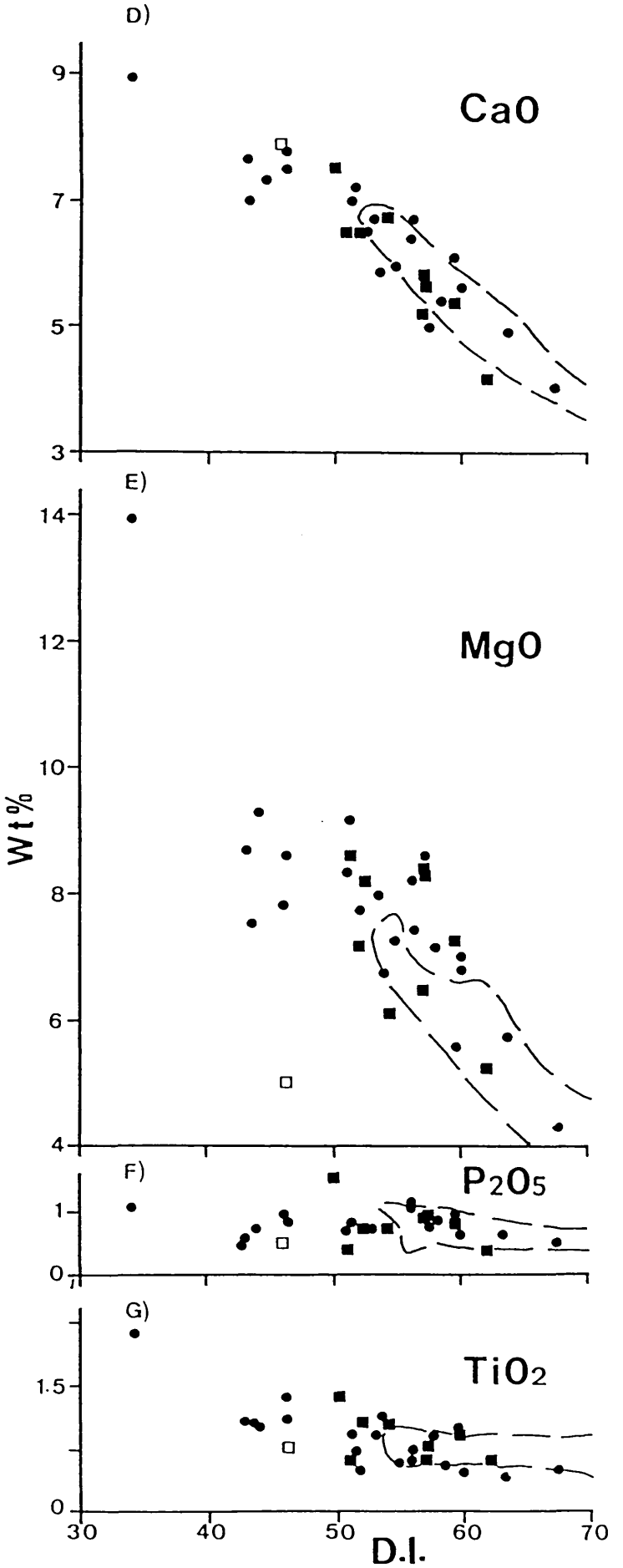


Figure 6.3 Continued

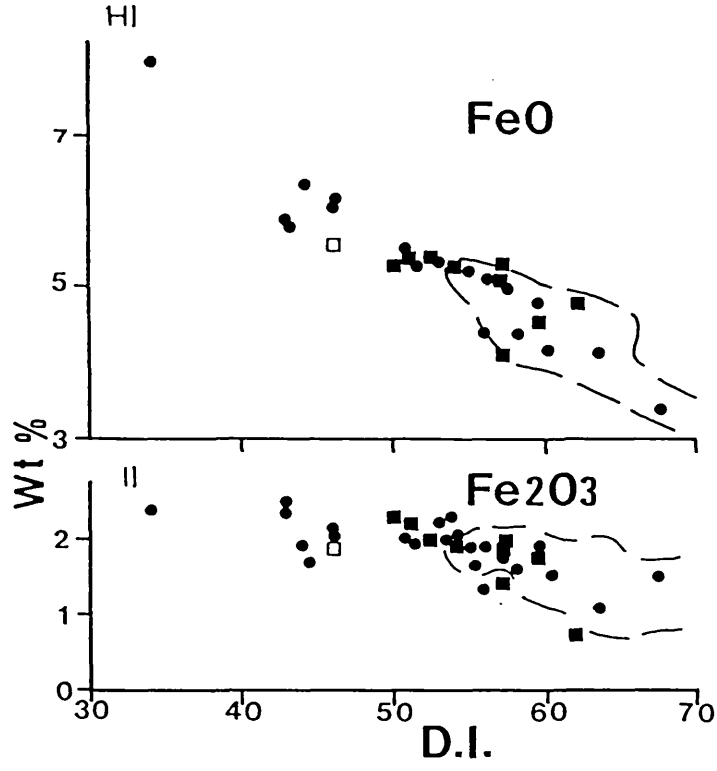


Figure 6.3 Continued

differentiation index. Potash on the other hand, shows a strong positive correlation whereas both Na_2O and Al_2O_3 show a very wide scatter with no obvious trends.

When one compares the ranges in element oxide variations between the minor and major facies it can be seen that there is a good deal of overlap in composition, especially when one considers the more mafic members of the major facies,i.e., the Pyroxene - biotite - amphibole mafic syenites (PBAMS) and pyroxene - biotite monzonites (PBM). Both the enclaves and dyke rocks however do contain members with significantly higher contents of MgO, FeO and CaO than either of the PBAMS or PBM major facies groups indicating a less evolved nature.

Using the K_2O versus SiO_2 plot of Peccerillo and Taylor (1976), it can be seen in figure 6.4 that all the dykes and enclaves (apart from the two pyroxene diorite) fall within the shoshonitic field. The other noticeable features of this diagram are firstly the strong positive correlation of K_2O with SiO_2 and the steep slope of the correlation at low SiO_2 contents (45 to 57 wt% SiO_2). This latter feature is especially common in suites with shoshonitic affinities (Morrison, 1980). The single sample of the two pyroxene diorite analysed falls well within the calc-alkaline field and clearly this rock type cannot be considered to be comagmatic with the others members of the minor facies. The restricted range in SiO_2 content for both the dykes and enclaves, together with their poorly constrained major element variation patterns precludes any attempt to model the petrogenetic evolution of the suite.

6.2 TRACE ELEMENT GEOCHEMISTRY

The variations of individual trace element contents with the differentiation index, D.I. are shown in a series of plots in figure 6.5. Most of the trace element variations are poorly constrained and show a wide scatter. Rb, Zr and Ba generally show a positive correlation with the differentiation index, Ni, Cr and Sr are negatively correlated, whereas both Nb and Y generally display rather flat trends.

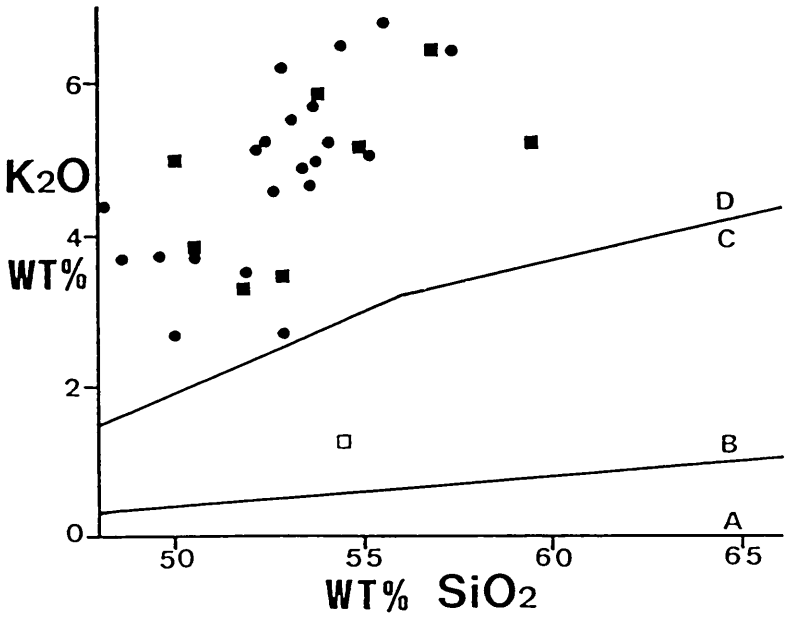


Figure 6.4 Plots of the Bom Jardim enclaves and dykes in the diagram of Peccerillo and Taylor (1976). Symbols as in figure 6.3. Fields: A = arc island tholeiitic series; B = normal calc-alkaline series; C = high K calc-alkaline series and D = shoshonitic series.

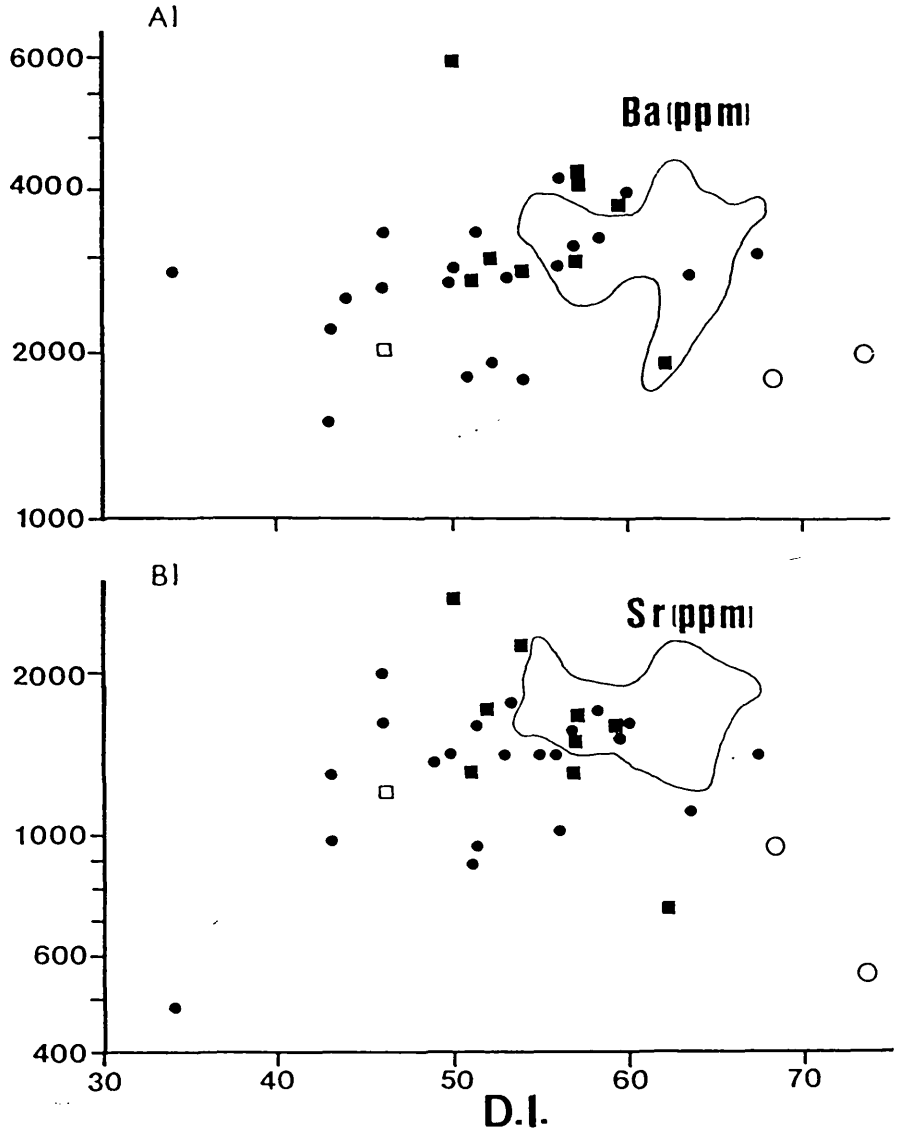


Figure 6.5 (A-H) Variation diagrams of analysed trace elements versus D.I.. Enclosed fields indicate the range of variation for the members of the PBAMS and the PBM facies. Symbols as in figure 6.3.

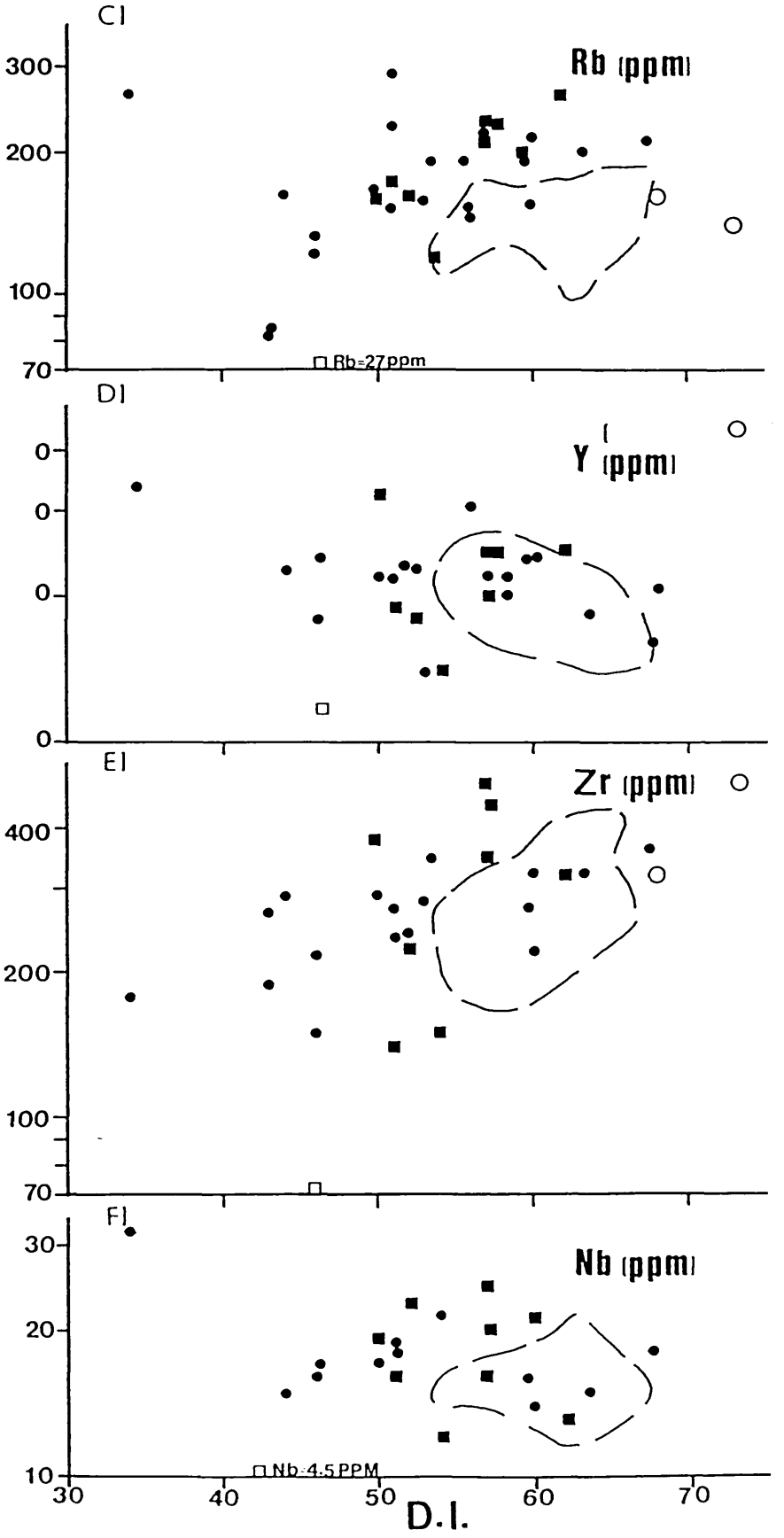


Figure 6.5 Continued

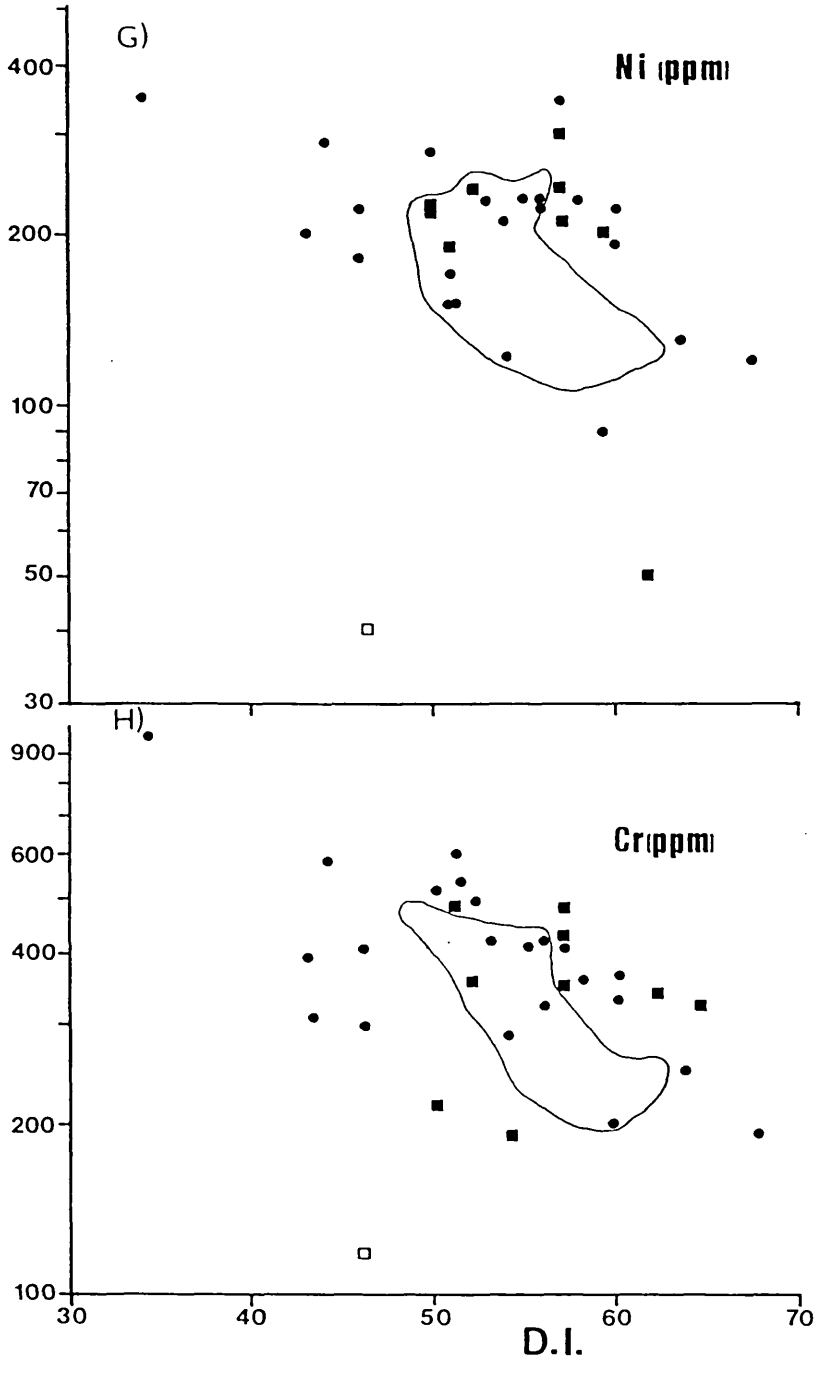


Figure 6.5 Continued

The transition elements Cr, Ni and V generally display high values, with Cr varying from 190 to 600 ppm, Ni from 120 to 340 ppm and V varying from 100 to 180 ppm.

Both the enclaves and dykes rocks show a marked enrichment in Ba (varying from 1500 to 6800 ppm) and Sr (722 to 2750 ppm). Rb shows a moderate enrichment (81 to 287ppm). Thorium values generally range from 1.8 to 23.3 ppm, however one particular dyke intruded within the syenite, close to the contact with the pink granite, shows much higher values of 35.9 ppm. The Cu contents of the minor facies show a wide variation reaching values of 5600 ppm in some enclaves; in such cases these high values of Cu can always be correlated with the presence of modal chalcopyrite in the samples.

The high field strength element (HFSE) concentrations within the minor facies are normally low, Nb contents are usually less than 25ppm (ranging from 12 to 25 ppm), this in contrast with the metasedimentry xenolith (327 A) with Nb values greater than 30 ppm. Tantalum values are all lower than 1ppm and Hf contents vary from 3.7 to 12.2 ppm. The overall trace element values leads to a general geochemical signature of low HSFE/LILE ratios for the group as a whole.

Sample 216 (see table C.1.8, appendix C) represents the only dyke recorded to have cut the metasedimentary country rocks. The only difference that can be established between it and the majority of dykes found cutting the syenitic rocks of the complex are the lower contents of Ba and Sr.

The trace element chemistry of the minor facies of the Bom Jardim complex in keeping with the major elements closely resembles that of the island arc shoshonitic series described by Morrison (1980).

6.3 RARE EARTH ELEMENTS

Eighteen samples of the minor facies rocks were analysed for the REEs, including one metasedimentary xenolith (sample 327 A). The individual analyses are listed

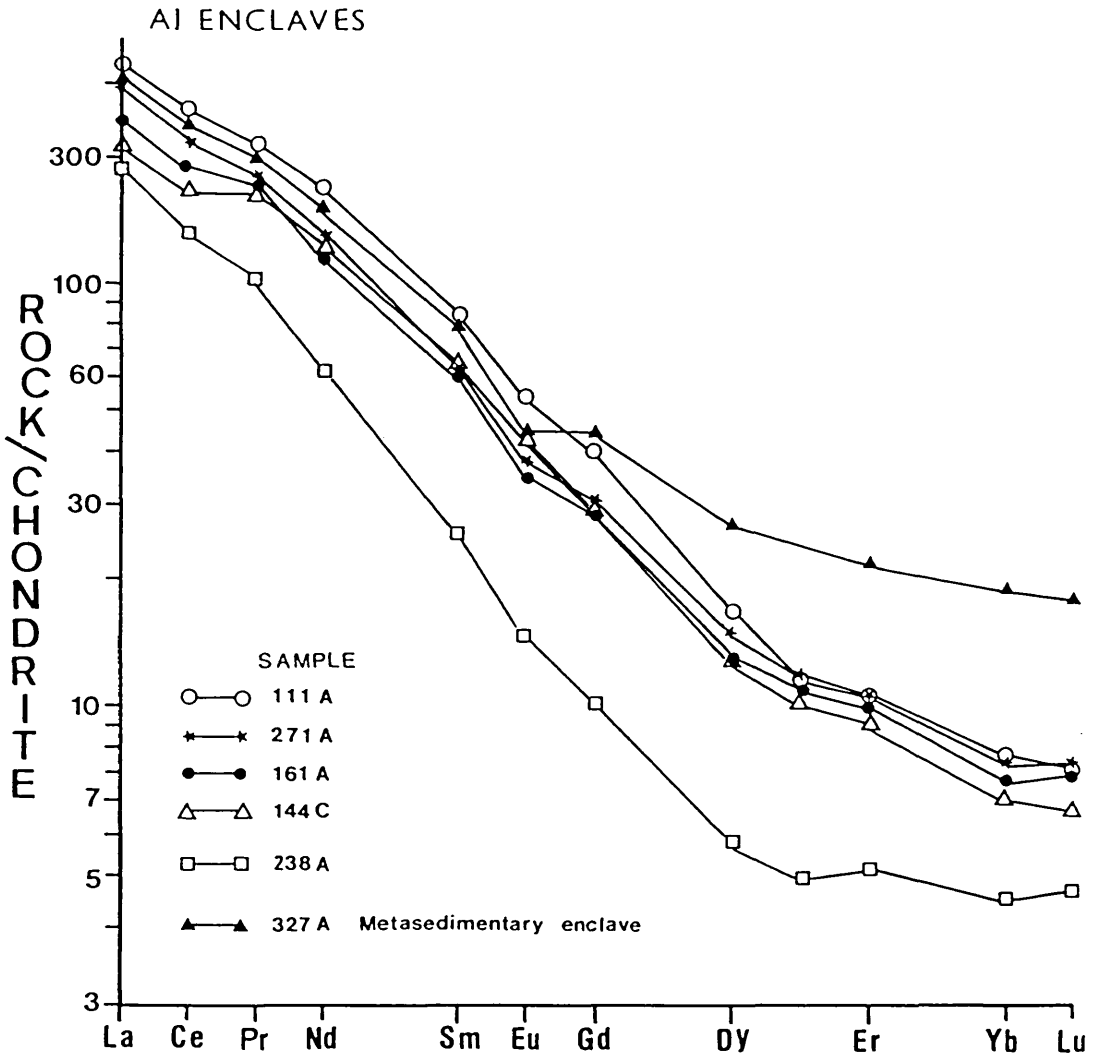


Figure 6.6 Chondrite normalized REE plots for the different enclaves (A and B) and dykes (C) lithologies. Chondrite values are from Nakamura (1974).

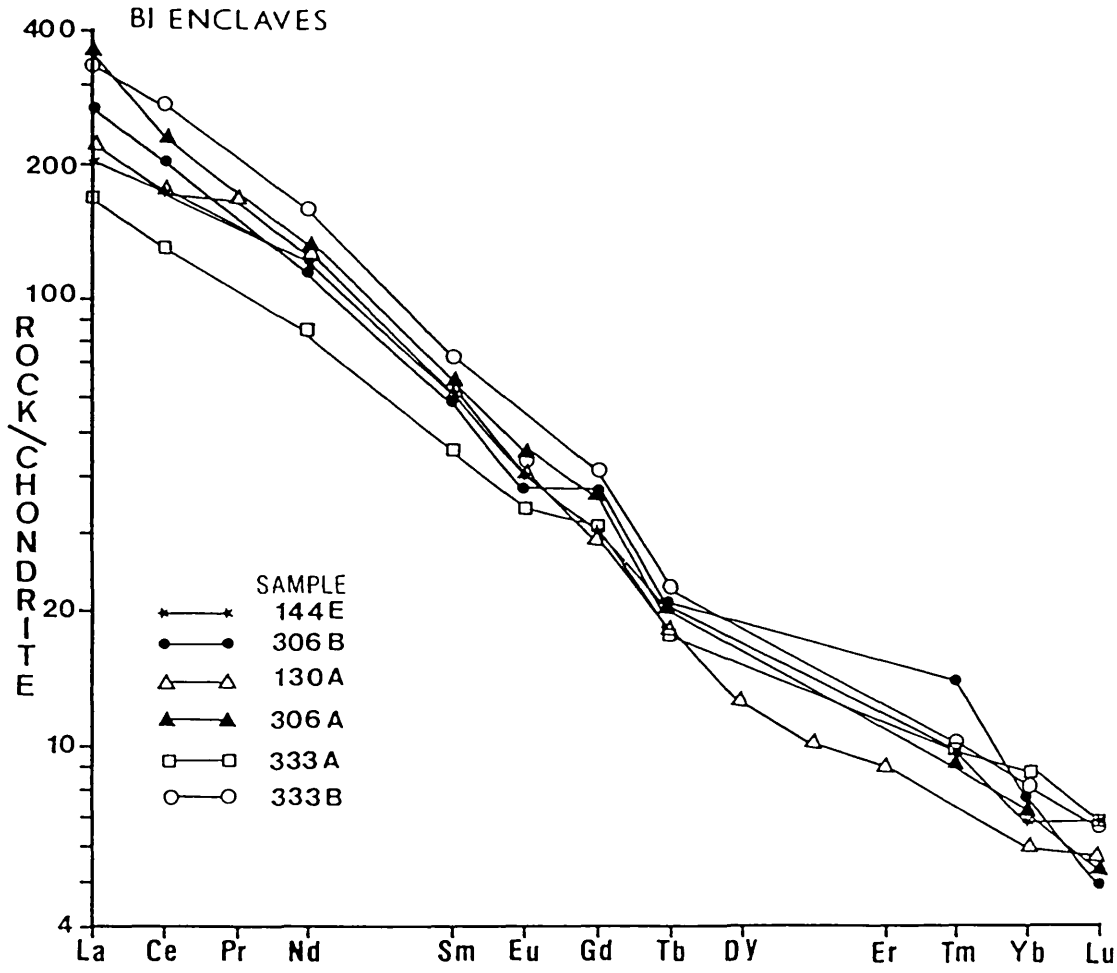


Figure 6.6 Continued

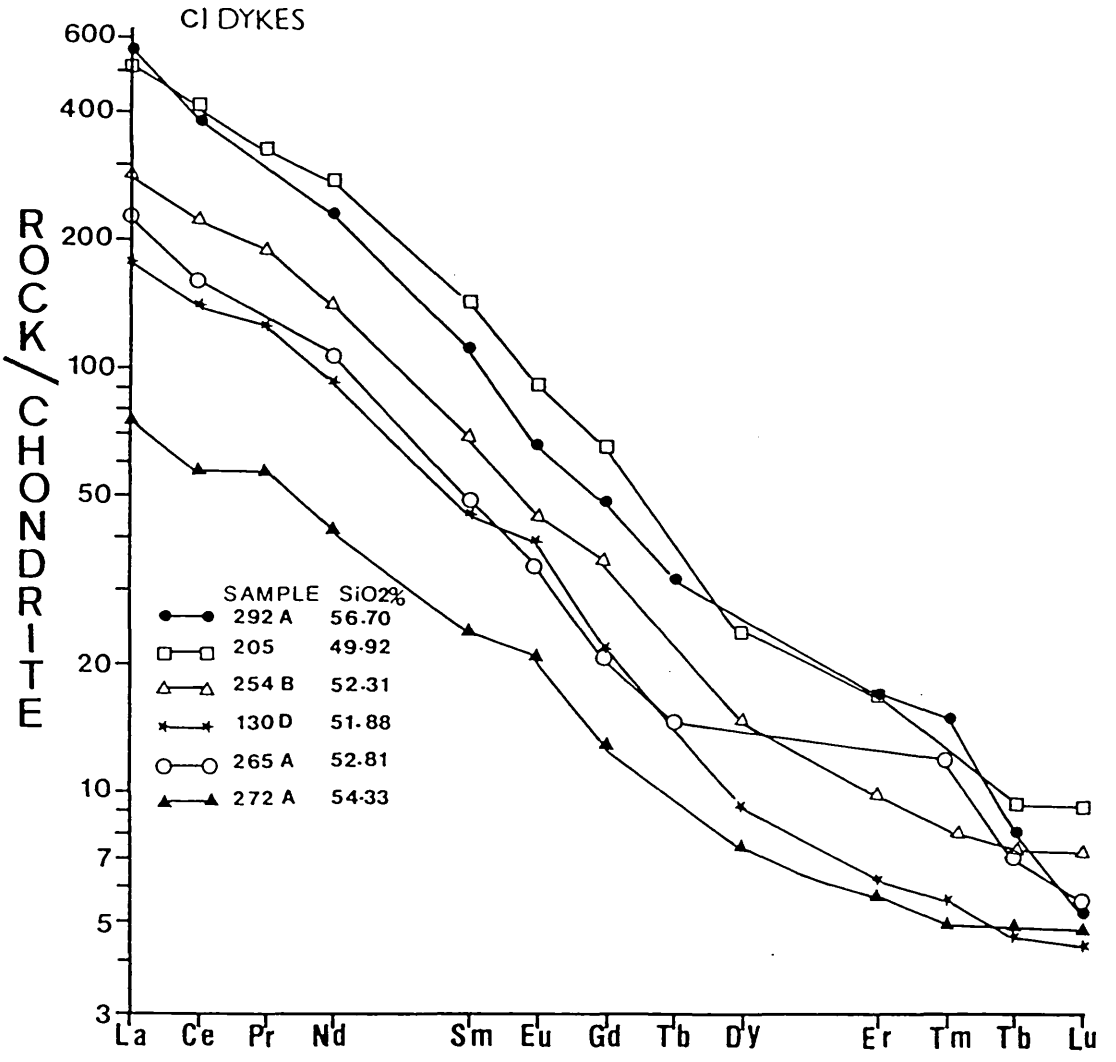


Figure 6.6 Continued

in table C.2.8 and C.2.9, appendix C and the data plotted in figures 6.6.A, B and C as a series of chondrite normalized patterns. The patterns are similar to those recorded for the host syenites and monzonites, i.e., they are characterised by high LREE/HREE ratios. However some of the enclaves do show small Eu anomalies, mainly negative, with Eu^* ranging from 0.79 to 0.95. Europium anomalies have also been detected within members of the dyke suite; in their case however, the anomalies are more variable with values of Eu^* ranging from 0.9 to 1.2. The two pyroxene diorite (sample 272 A, figure 6.6C) has a lower LREE/HREE ratio when compared to the others mafic dykes. The one metasedimentary enclave sample analysed (327 A) shows very similar LREE contents to the igneous enclaves but, is clearly very distinctive in being more enriched in the HREE than its igneous counterparts. The high LREE contents recorded in the minor facies of the Bom Jardim complex are characteristic of the geochemical signature of the shoshonitic rock series (Morrison, 1980 and Ewart, 1982).

6.4 CHONDRITE NORMALIZED INCOMPATIBLE ELEMENT DIAGRAMS (SPIDERGRAMS)

The chondrite normalized incompatible element plots presented in figures 6.7.A and B show that all dykes and igneous enclaves have significant troughs at Nb, Ta, P and Ti, and peaks at K and La. Some samples also show additional troughs at Sr, Th, U and Y. One enclave sample (86A, see figure 6.7.A) shows a marked departure from the normal patterns shown by both the dykes and igneous enclaves. This sample is an amphibolite enclave and probably represents the mafic members of the migmatitic country rocks series. The noticeable peaks at P, Zr and Ti and much lower LREE contents clearly singles this sample out as not being a member of the normal enclave\dyke suite of the minor facies of the complex.

The values of Th and U do not show a systematic behaviour, it would appear that their contents and distributions have been disturbed, probably by hydrothermal

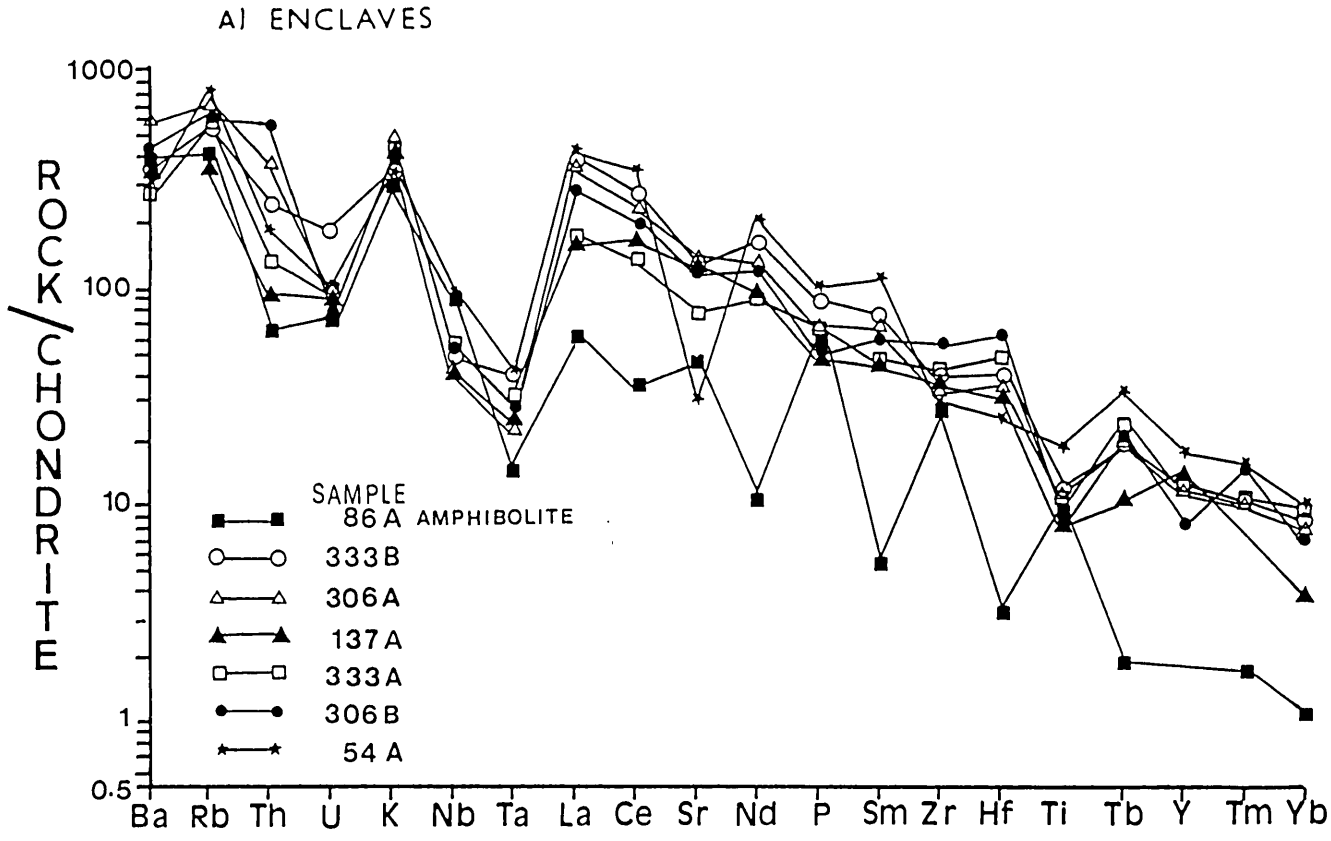


Figure 6.7 Chondrite normalized incompatible elements plots of Bom Jardim enclaves (A) and dykes (B). The normalizing factors are from Thompson (1982).

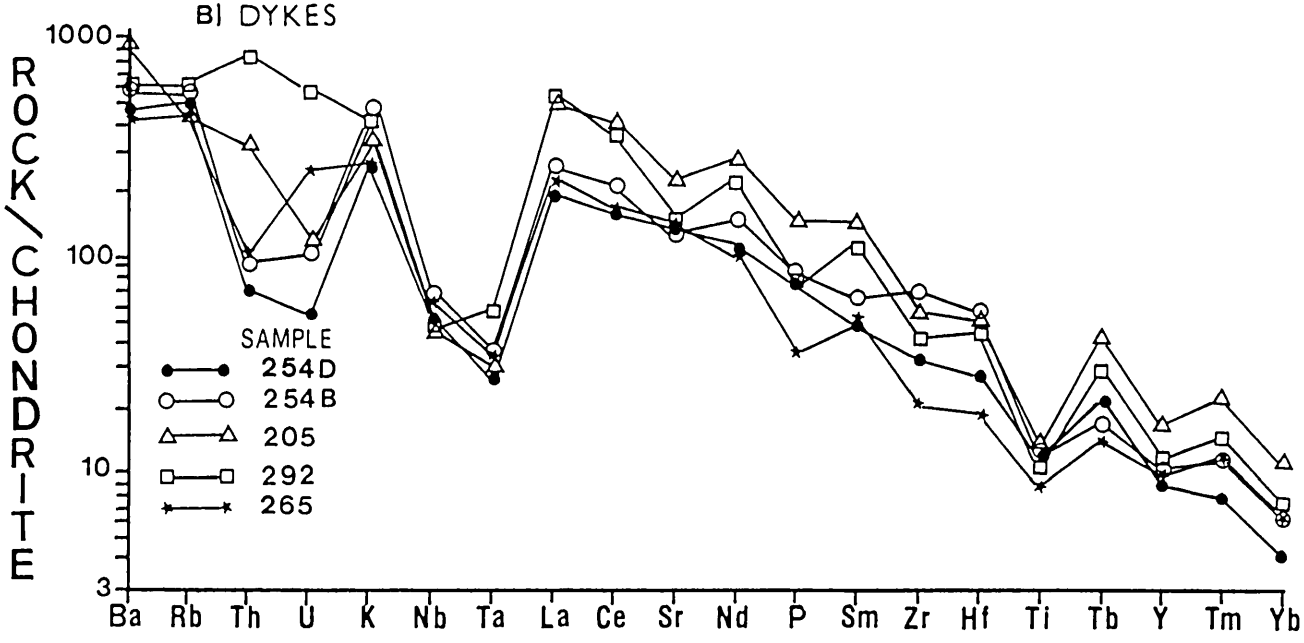


Figure 6.7 Continued

processes or by some earlier mixing by dyke disruption.

The troughs at Ti, Nb and Ta are probably related to residual Fe - Ti phases in the source, based on the partition coefficients of Nb and Ta for Fe oxides after Nash and Crecraft (1985), and Pearce and Norry (1979).

6.5 GENESIS OF THE ENCLAVES

Based on geochemical evidence of both major and trace element compositional overlaps and similar trace element signatures, coupled with the strong field evidence, the author is in very little doubt that the majority of the igneous enclaves are the result of synplutonic dyke intrusion and disruption. The spatial association of both rounded and elongated enclaves has been the subject of extensive dicussion in the literature. Some authors have interpreted the rounded shape of the enclaves as evidence of mixing (Kumar, 1988) while other authors believe that the rounded shape could be due to original "mingling" (Vernon 1983, 1984).

According to Bacon (1986) mafic inclusions in granitoids represent chilled blobs of basic magma intruded into a silic magma chamber. This is rather a dismissive conclusion which does not address the problem of the markedly different associated enclave shapes.

Vernon (1983, 1984) acknowledges neither the hybridisation, nor the reaction stages of microgranular enclave evolution. These findings are clearly in contradiction with the conclusions of Kumar (1988) who states that the final composition and texture of a microgranular enclave is often determined by reaction processes superimposed on earlier hybridisation mechanism.

Vernon et al. (1988) addressed the problem of differences in chemical composition between enclaves of different shape within the same host rock. He concluded that the differences in composition could be due to different batches of magma mingling with the host, and that the elongated enclaves were generally more deformed than the rounded varieties. The same author also stated that in

Table 6.1 A comparison of the compositions of elongated and rounded enclaves from the medium grained pyroxene biotite amphibole syenites (MPBAS).

	333-R	333-E	306-R	306-E
SiO_2	52.54	53.31	55.48	58.13
Al_2O_3	12.79	15.10	13.51	15.07
Fe_2O_3	8.07	7.28	6.15	5.27
MgO	9.20	5.60	7.01	4.31
CaO	7.03	6.13	5.63	3.96
Na_2O	3.01	3.96	2.34	3.83
K2O	4.61	4.93	6.81	5.98
P_2O_5	0.67	0.88	0.68	0.53
TiO_2	1.08	1.15	0.79	0.82
MnO	0.14	0.09	0.12	0.08
LOI	1.11	1.16	0.79	0.72
Total	100.54	100.05	100.02	99.41
Cr	600	200	360	190
Ni	150	90	220	120
V	140	140	100	90
Cu	70	320	240	30
Zr	270	270	220	360
Y	22.1	24.2	14.9	16.1
Nb	18.7	15.7	13.9	17.8
Hf	9.0	7.6	6.7	12.2
Th	5.5	9.9	14.9	23.3
Rb	225	189	212	208
Ba	1837	2612	3952	2968
Sr	860	1476	1568	1347

Total iron as Fe_2O_3. R = rounded and E = elongated enclaves. BaO and SrO added to the major oxide totals.

general the rounded enclaves have higher SiO_2 contents than the associated elongated types and, suggested that the loss of silica could be due to the pressing out of interstitial liquids during the deformation process, which gave rise to the elongate enclaves.

In order to evaluate these different hypotheses of enclave evolution in respect of those found within the Bom Jardim Complex, the chemistries of the rounded and elongated enclaves were studied from two different outcrops of the same host rock, namely the MPBAS facies. The analyses of both enclave types are presented in table 6.1. Inspection of the data shows that the rounded enclaves are enriched in MgO, CaO, Fe_2O_3, Cr, Ni and Rb, and show lower contents of Al_2O_3, SiO_2, TiO_2, Th, and Y, compared to the elongated types. The differences in silica content between the two types are clearly at odds with the findings of Vernon et al. (1988). The present author believes that the differences in shape largely reflect the different degrees of reaction with the host syenite, as indicated by the initial findings of the petrographic study of the different enclave types.

6.6 SUMMARY AND CONCLUSIONS.

The similarity between the chemistries of the dykes and many of the igneous enclaves together with the available field evidence suggests that such enclaves represent synplutonic disrupted dykes. It is possible that other enclaves could also represent samples of the margins of the magma chamber which have suffered some contamination and were later reabsorbed by the syenite magma.

The general overlap and similarities in chemistry between the mafic minor facies and the less evolved members of the major facies types, for example the pyroxene-biotite-amphibole mafic syenites (PBAMS) and pyroxene biotite monzonites (PBM), could also indicate that they shared the same source. If one continued this rather speculative argument, it is conceivable that the less differentiated magma could underplate the PBAMS (being

unable to rise due to density contrast), forming a layer probably vertically zoned in the roots of the chamber. The subsequent thrust tectonism then allowed the injection of the more mafic magma into the overlying cooler syenitic magma. Initially a small degree of magma mixing would be possible, but ultimately as the syenite magma rose any small amounts of the higher temperature mafic magma recharged into the system would be unable to mix (largely due to viscosity differences), and "magma mingling", i.e., incomplete mixing or failure to mix at all, would be the result. Deformation could have occurred during the mingling and\or mixing processes but, from the data available, it does not appear to be the main control in either the geochemical differences or in the the ultimate shape of the enclaves.

CHAPTER 7

A COMPARATIVE STUDY OF THE BOM JARDIM AND TORITAMA COMPLEXES

7.1 INTRODUCTION

The Toritama complex crops out in an area of about 50 sq km, around the village of Toritama, 30 km S.W. of the Bom Jardim complex. A geological sketch map of the Toritama complex based on the work of Mello (1971) and Mello and Mello (1969) is shown in figure 7.1. The general shape of the Toritama complex appears to indicate an emplacement controlled by faults as observed in the Bom Jardim complex. Both complexes in fact form elongate bodies emplaced within the thrust belt, which marks the contact zone between the Pernambuco-Alagoas massif and Pajeu Paraiba fold belt.

During a reconnaissance trip to the complex nine samples from the major facies and four enclave samples were collected along PE-104, a road which cuts the complex in a N.-S. direction. The location of the samples are shown in figure 7.1.

7.2 PETROGRAPHY AND MINERAL CHEMISTRY

The major rock type within the Toritama complex is syenite. Three major facies have been identified (Mello, 1972), namely; porphyritic syenites, equigranular syenites and pegmatoidal syenites. Petrographically all three facies type can be matched by equivalent rock types in the Bom Jardim complex (see table 7.1). Aplite granites have also been identified within the complex and are always found in association with the coarse grained alkali feldspar syenite (see plate 7.5). The classification and abbreviated nomenclature used in the following account of the Toritama complex will follow that adopted for the Bom Jardim complex.

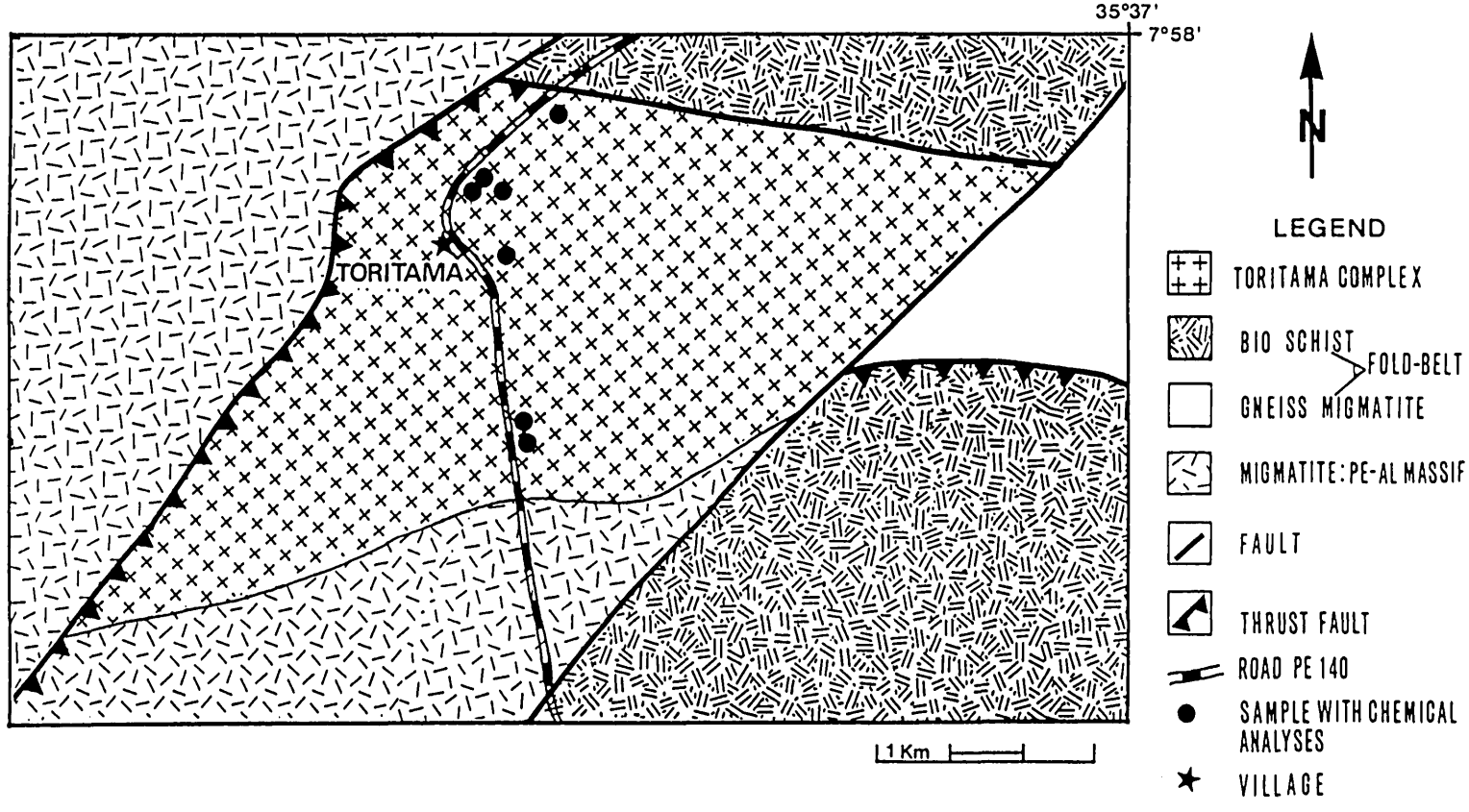


Figure 7.1 Geological sketch map of the Toritama complex. Source: Mello (1971) and Mello and Mello (1969).

Table 7.1 Equivalent rock types of the Toritama and Bom Jardim complexes.

TORITAMA COMPLEX	BOM JARDIM COMPLEX EQUIVALENT
Porphyritic syenite	Pyroxene biotite amphibole syenites (PBAMS) and Pyroxene biotite monzonite (PBM).
Equigranular syenite	Medium grained pyroxene biotite amphibole syenite (MPBAS).
Pegmatoidal syenite	Very coarse grained brown alkali feldspar syenite (CS).
No equivalent found	Pyroxene biotite alkali feldspar leuco syenite (PBLS).

Both the PBAMS and CS facies show a distinct porphyritic texture (see plates 7.1, 7.2 and 7.4) with zoned phenocrysts of mainly alkali feldspar and less frequently plagioclase. The matrix is generally medium grained and mafic in character. Members of the MPBAS facies are largely equigranular (see plate 7.3), although a few samples show a slight porphyritic texture. The coarse grained syenites (CS) consist mainly of large phenocrysts of coarse perthite (average modal content approximately 70%) set in a matrix of alkali feldspar (microcline microperthite), pyroxene, biotite, amphibole and quartz.

Alkali feldspars are modally the most important phase in the rocks of the Toritama complex, making up 40% of the PBAMS facies, 49% in the MPBAS facies and up to 70% in the CS facies. The dominant alkali feldspar is a microcline perthite which appears to have originally crystallised as orthoclase and inverted to microcline on cooling. X-ray determinations (Mello, 1972) have shown that the alkali feldspars are a mixture of microcline and orthoclase. The majority of the alkali feldspar phenocrysts contain abundant inclusions of quartz, plagioclase and



Plate 7.1 Mafic igneous enclave containing aligned alkali feldspar phenocrysts. The host rock is a mafic syenite (PBAMS).



Plate 7.2 A boudin shaped syn-plutonic dyke intruded into PBAMS.

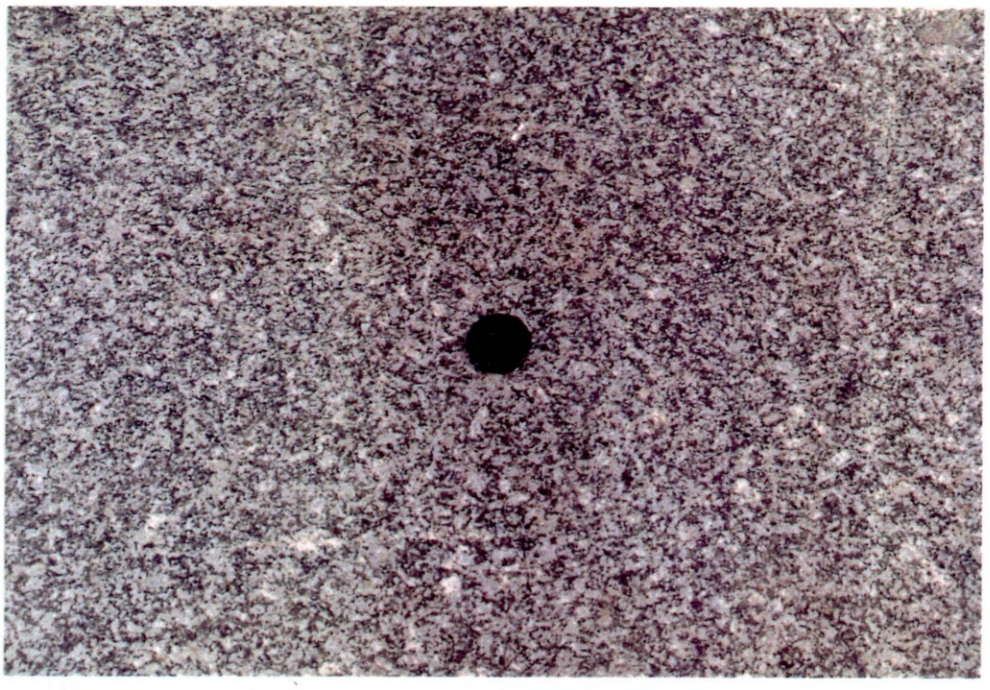


Plate 7.3 Typical surface exposure of the medium grained syenite (MPBAS).



Plate 7.4 Coarse grained syenite (CS) cut by a thin aplite vein.



Plate 7.5 Contact between aplite and the CS facies. The aplite shows both enclaves of coarse syenite and xenoliths of country rock. Alkali feldspar xenocrysts within the aplite appear to be disaggregated coarse syenite. A thin late aplite vein cuts both lithologies.

biotite. The large (4cm to 0.5cm) coarsely exsolved perthitic phenocrysts found in the very coarse brown alkali feldspar syenite (CS), display a concentric arrangement of euhedral to subhedral pyroxene, amphibole, biotite and opaque mineral inclusions. The coarsening of the perthite exsolution lamellae is generally considered to be related in part to the presence of magmatic fluids, as is the intricacy of the actual alkali feldspar grain boundaries (Parsons, 1978), both of which are a common feature of the alkali feldspars in the Toritama complex. Selected individual micropobe analyses of the alkali feldspars are listed in table 7.2. The feldspars show a range in composition which is very similar to that previously discussed for the Bom Jardim complex (Ab_7 Or_{93} An_0 to Ab_{15} Or_{85} An_0).

Modally plagioclase is subordinate to alkali feldspar in all the major rock types in the complex, constituting about 15% and 10% in PBAMS and MPBAS respectively . The plagioclase usually occurs as subhedral to anhedral crystals displaying a limited amount of normal zoning. Individual electron micropobe analyses of representative plagioclase grains are given in table 7.3. The plagioclases vary from An_{15} Ab_{84} Or_1 to An_{22} Ab_{77} Or_1. Within the very coarse syenites almost pure albite (An_2-An_1) has been recorded, forming myrmekitic intergrowths when in contact with alkali feldspar. Plagioclase partially replaced by alkali feldspar has been found occasionally.

Table 7.2 Representative micropobe analyses of the alkali feldspars from the Toritama complex.

	TO-6	TO-6	TO-3	TO-3
SiO_2	63.91	64.47	63.57	63.59
Al_2O_3	19.31	18.90	18.58	18.65
FeO	0.00	0.00	0.00	0.00
CaO	0.00	0.00	0.00	0.00
Na_2O	1.63	0.85	0.89	0.90
K_2O	13.84	15.01	15.37	15.44
BaO	1.45	1.10	0.53	0.41
Total	100.13	100.33	98.94	98.99
Si	2.946	2.971	2.897	2.899
Al	1.049	1.027	0.992	0.993
Fe	0.000	0.000	0.000	0.000
Ca	0.000	0.000	0.000	0.000
Na	0.146	0.079	0.071	0.071
K	0.814	0.886	0.891	0.993
Ba	0.026	0.022	0.008	0.007
Or	85	92	93	93
Ab	15	8	7	7
An	0	0	0	0

Table 7.3 Representative micropobe analyses of the plagioclases from the Toritama complex.

	TO-4	TO-6	TO-6	TO-6	TO-6
SiO_2	63.81	62.57	62.60	63.37	62.90
Al_2O_3	21.79	23.80	23.54	23.27	23.73
CaO	3.18	4.75	4.69	4.45	4.36
Na_2O	10.06	8.60	9.03	9.17	9.04
K_2O	0.15	0.20	0.12	0.00	0.23
Total	98.99	99.92	99.98	100.26	100.25
Si	2.802	2.764	2.769	2.788	2.771
Al	1.127	1.239	1.227	1.207	1.232
Ca	0.149	0.225	0.222	0.210	0.206
Na	0.854	0.736	0.775	0.782	0.772
K	0.007	0.011	0.007	0.000	0.013
Ab	84	77	77	79	78
An	15	22	22	21	21
Or	1	1	1	0	1

The amphiboles present in the major facies are mainly magnesio hornblende in composition with minor amount of edenitic amphiboles. Individual electron micropobe analyses of selected amphiboles are listed in table 7.4.

Table 7.4 Representative micropobe analyses of the amphiboles from the Toritama complex.

	TO-6	TO-6	TO-6	TO-2	TO-2	TO-2
SiO_2	46.77	47.10	48.20	47.19	47.52	47.41
Al_2O_3	7.12	7.82	6.72	6.20	5.60	6.27
TiO_2	1.42	1.45	1.09	0.92	1.13	1.15
FeO	11.34	8.90	12.70	9.95	11.41	11.35
Fe_2O_3	3.03	5.50	1.55	4.26	1.65	2.69
MgO	13.33	14.08	13.55	14.11	14.00	14.02
MnO	0.00	0.37	0.36	0.32	0.00	0.33
CaO	11.41	11.43	12.08	11.40	11.66	11.53
Na_2O	1.67	1.50	1.66	1.97	1.53	2.23
K_2O	0.89	0.80	0.81	0.69	0.57	0.73
Total	96.98	98.95	98.72	96.58	95.07	97.71
MINERAL FORMULA UNITS (BASED ON 23 OXYGENS)						
Si	6.920	6.777	7.023	6.970	7.132	6.976
Al^4	1.080	1.223	0.977	1.030	0.868	1.024
Al^6	0.162	0.104	0.177	0.049	0.123	0.063
Ti	0.158	0.159	0.119	0.102	0.128	0.127
Fe^{+2}	1.404	1.079	1.547	1.229	1.432	1.396
Fe^{+3}	0.337	0.596	0.170	0.473	0.187	0.298
Mg	2.939	3.018	2.942	3.106	3.131	3.074
Mn	0.000	0.045	0.044	0.040	0.000	0.041
Ca	1.809	1.765	1.885	1.804	1.875	1.818
Na_B	0.191	0.235	0.115	0.196	0.125	0.182
$(Na+K)_A$	0.456	0.441	0.266	0.497	0.234	0.591
$Mg/Mg+Fe^{+2}$	0.68	0.74	0.66	0.72	0.69	0.69

Their general petrographic associations and mineral chemistries are very similar to those described previously for the Bom Jardim complex. The empirical amphibole geobarometer (Hammarstron and Zen, 1986), previously described in detail (chapter 4, section 4.2.2.1) was again used to estimate the pressure range of the complex. The calculated pressures showed a range of 1.60 Kb to 2.75 Kb, well within the pressure range calculated for the Bom Jardim complex (see figure 7.2). The lower value of 1.6 Kb

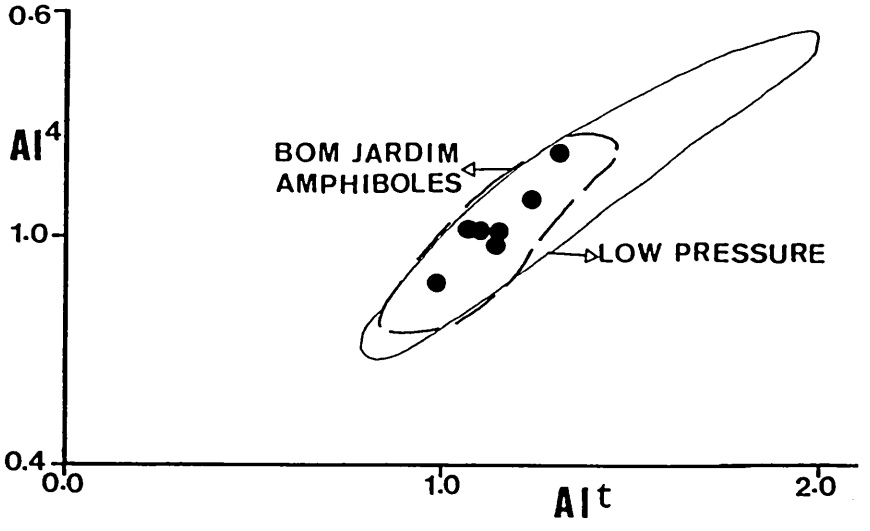


Figure 7.2 Al^4 and Al^t contents of amphiboles from the Toritama complex. The field of low pressure is from Hammarstron and Zen (1986).

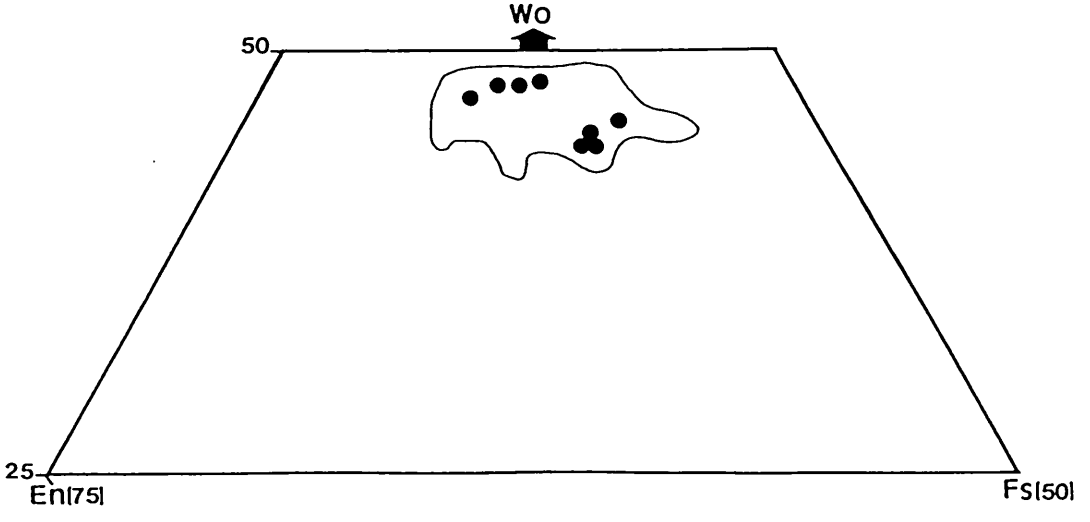


Figure 7.3 Pyroxene compositions from the Toritama complex. Enclosed field represents the range of pyroxene compositions in the Bom Jardim complex.

is probably the result of late stage hydrothermal alteration or re equilibration during reactivation along the Pernambuco lineament.

The modal distribution of clinopyroxene within the Toritama complex is extremely variable, with some of the rocks containing no pyroxene at all. When clinopyroxene is present it is invariably relict cores within amphibole. The pyroxenes are all Ca-rich and plot within the salite field, with compositions ranging from Wo_{48} En_{39} Fs_{13} to Wo_{44} En_{37} Fs_{19}. The pyroxenes from both the Toritama and Bom Jardim complexes have very similar mineral chemistries (see figure 7.3), characteristic of shoshonitic rocks (Morrison, 1980). A representative set of clinopyroxene analyses are given in table 7.5.

Table 7.5 Representative micropobe analyses of the pyroxenes from the Toritama complex.

	TO-3	**TO-3**	**TO-2**	**TO-6**	**TO-6**	**TO-6A**	**TO-6A**
SiO_2	52.63	52.42	52.42	53.09	53.05	53.36	53.70
Al_2O_3	0.91	0.90	0.57	0.69	0.98	0.89	1.09
FeO	8.45	8.39	11.23	8.56	8.30	7.23	7.27
TiO_2	0.00	0.00	0.00	0.22	0.00	0.23	0.00
CaO	22.79	22.15	20.70	23.25	22.83	22.86	23.30
MgO	13.21	13.51	12.20	13.51	13.37	13.89	13.90
MnO	0.32	0.52	0.38	0.35	0.32	0.44	0.41
Na_2O	1.37	1.19	1.66	1.03	0.83	0.70	0.83
Total	99.68	99.06	99.17	100.70	99.67	99.60	100.50
Si	1.969	1.945	1.993	1.975	1.983	1.987	1.980
Al	0.040	0.038	0.026	0.030	0.043	0.039	0.047
Fe	0.264	0.260	0.357	0.267	0.259	0.225	0.224
Ti	0.000	0.000	0.000	0.006	0.000	0.006	0.000
Ca	0.914	0.881	0.843	0.927	0.914	0.912	0.922
Mg	0.737	0.747	0.692	0.750	0.745	0.771	0.763
Mn	0.010	0.016	0.012	0.011	0.010	0.014	0.013
Na	0.099	0.086	0.122	0.074	0.060	0.050	0.060
Wo	48	47	44	48	48	48	48
En	38	39	37	38	39	40	40
Fs	14	14	19	14	13	12	12

Total iron expressed as FeO. Formula units based on 6 O.

Mello and Mello (1972) discussed what they described as " an intense replacement of clinopyroxene by

both amphibole and biotite". This replacement they considered was the result of intense metasomatism by external fluids. The present author can see no overwhelming evidence for the participation of any major amounts of an external fluid in the Toritama complex. Many of the late replacement amphiboles have in fact compositions more in keeping with late stage magmatic processes, brought about by increasing PH_2O, falling temperature and fO_2, than processes controlled by metasomatising fluids. Such magmatic reactions envolving pyroxene and others mafic silicates have been widely described in both alkaline and sub alkaline complexes (eg. Jones, 1984; Stephenson and Upton, 1982; Parsons, 1981; Sylvester et al., 1978 and Stephenson, 1972).

Biotite also shows a degree of modal variability within the complex (ranging from 4 to 13%). The biotites occur as large green/brown pleochroic isolate plates, as small flakes included within both plagioclase and alkali feldspar and as replacement rims around both pyroxene and amphibole. Chemically the biotites show very little variation (see table 7.6), with Fe/Fe+Mg ratios varying from 0.34 to 0.39.

Table 7.6 Representative micropobe analyses of the biotites from the Toritama complex.

	TO-3	**TO-3**	**TO-6**	**TO-6**	**TO-6**	**TO-2**	**TO-2**
SiO_2	37.49	37.32	38.27	38.55	38.29	39.10	38.56
Al_2O_3	13.68	13.58	14.70	14.93	14.81	12.01	11.89
FeO	16.26	16.78	15.96	15.79	16.14	14.90	15.30
MnO	0.24	0.00	0.00	0.00	0.24	0.26	0.00
MgO	15.15	14.64	14.26	14.55	14.68	16.34	15.60
TiO_2	1.24	2.02	1.65	1.85	1.83	2.23	2.81
K_2O	9.77	9.91	9.85	9.77	9.74	9.77	9.81
Na_2O	0.00	0.00	0.38	0.34	0.00	0.38	0.49
BaO	0.42	0.00	n.d	n.d	n.d	0.00	0.26
Total	94.25	94.25	95.06	96.04	95.49	94.99	94.72
Fe/Fe+Mg	0.38	0.39	0.39	0.38	0.38	0.34	0.35

Total iron expressed as FeO. n.d = not determined

The majority of the samples collected are quartz bearing with modal contents ranging from 0.5 to 5%. The quartz appears to be late in the crystallisation interval and, occurs primarily as anhedral crystals, showing undulose extinction.

Sphene is a ubiquitous accessory mineral occurring both as a primary phase where it forms late in the crystallisation interval and as a secondary phase. Sphene was separated from one sample of the PBAMS facies, carefully purified and analysed by INAA. The analysis is given in table 7.7.

Table 7.7 INAA data for sphene from the PBAMS facies of the Toritama complex.

	TO-6
Sc	5.74
Cr	47.43
Hf	30.77
Ta	106.12
Th	704.32
U	135.14
La	3195
Ce	10155
Nd	5215
Sm	895
Eu	229
Gd	455
Tb	67.86
Tm	19.89
Yb	97.04
Lu	8.29

All values in ppm.

The sphene contains high concentrations of Th and LREE (Ce = 10155ppm) and is very similar to those sphenes analysed from the Bom Jardim complex. Figure 7.4 shows a plot of the host rock normalized REE patterns of the separated sphene sample. In addition the Kd values of a comparable from Hanson (1980) are also shown. The determined normalized REE values are slightly lower than

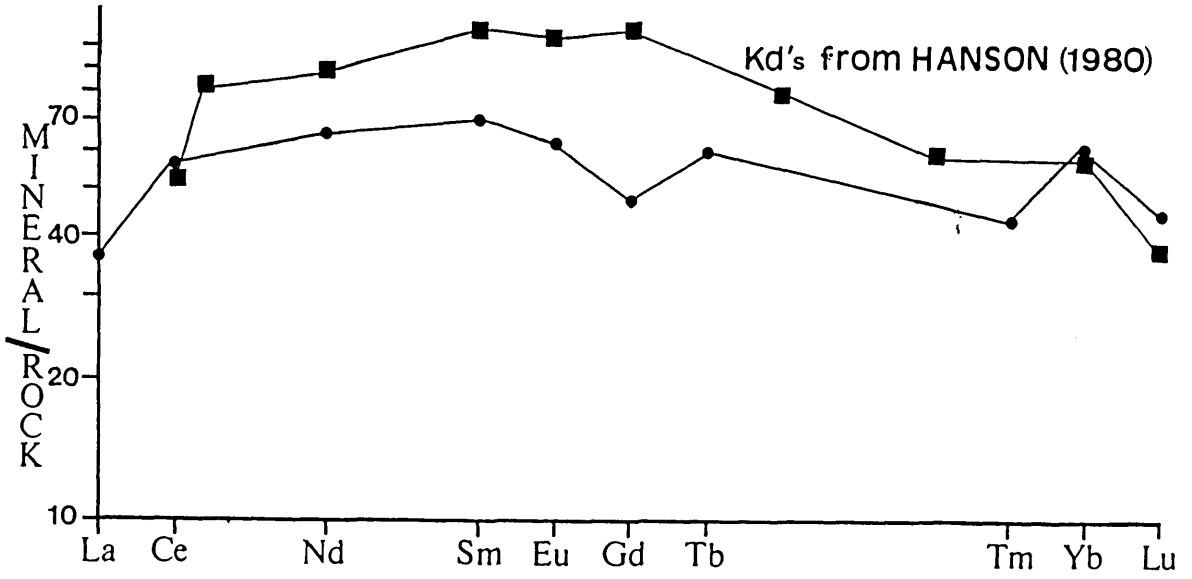


Figure 7.4 Whole rock normalized REE patterns of sphene from the Toritama complex.

those of Hanson (1980) data, but are 50 times greater than the REE concentrations in the whole rock. This data implies that the whole rock REE concentrations and signatures may largely reside in the sphene.

Apatite is by far the most abundant accessory mineral and is usually present as small early formed euhedral crystals. Acicular apatites with aspect ratios greater than 8:1 are observed in the hornblendite-pyroxenite enclaves.

Zircon is present as small early formed euhedral crystals, normally displaying pleochroic haloes when included by biotite. Allanite, as subhedral crystals included by amphibole, was observed in the PBAMS facies. Magnetite is the major opaque phase and, commonly occurs both as subhedral to anhedral grains in the matrix and as inclusions in both alkali feldspar and pyroxene.

7.3 GEOCHEMICAL CONSIDERATIONS OF THE TORITAMA COMPLEX

7.3.1 Introduction

Six samples representing the major facies and four representing the enclaves have been analysed for both the major oxides and trace elements. A smaller sample set have in addition been analysed for the REEs, Hf, Nb, Ta, Y, Sc, Th and U. Analyses of the individual samples together with their respective CIPW normative mineralogies are listed in tables 7.8 and 7.9.

7.3.2 Major element geochemistry

From the small sample set analysed, the Toritama complex appears to be largely intermediate in composition with silica values ranging from 56.38 to 61.19 wt%. The enclaves generally show much lower SiO_2 contents (50.42 to 54.4 wt%). The members of the major facies show MgO contents ranging from 2.94 (CS) to 5.16 (PBAMS) wt%, with higher values displayed by the enclaves (5.6 to 9.5 wt% MgO). The rocks generally have high total alkali contents

Table 7.8 Chemical analyses of the Toritama major facies

	TO-6	TO-5	TO-4	TO-3	TO-2	TO-1
SiO_2	56.38	56.28	57.31	60.52	61.19	74.08
Al_2O_3	15.48	16.04	15.88	15.17	14.96	13.47
Fe_2O_3	6.21	5.88	5.15	4.70	5.10	1.41
MgO	5.16	4.98	4.51	3.65	2.94	0.61
CaO	5.20	5.06	4.24	3.32	2.88	0.73
Na_2O	3.79	4.02	3.88	3.88	3.94	4.01
K_2O	5.17	4.88	6.05	6.19	7.26	5.51
P_2O_5	0.64	0.60	0.51	0.47	0.53	0.11
TiO_2	0.89	0.90	0.77	0.73	0.94	0.20
MnO	0.09	0.09	0.07	0.07	0.07	0.02
LOI	0.62	0.54	0.51	0.45	0.17	0.38
Total	100.16	100.11	99.51	99.58	100.37	100.53
			CIPW norm			
Qz	0.00	0.00	0.00	2.76	1.94	27.24
Or	30.62	28.95	35.63	36.74	42.87	32.29
Ab	31.99	34.09	33.04	33.04	33.57	34.09
An	10.02	11.13	8.07	5.56	1.67	2.50
Ne	0.00	0.00	0.00	0.00	0.00	0.00
Lc	0.00	0.00	0.00	0.00	0.00	0.00
Hy	5.90	4.50	2.88	9.58	6.94	2.49
Di	9.02	8.19	7.51	6.49	7.10	0.15
Ol	5.31	6.12	6.08	0.00	0.00	0.00
Mt	2.55	2.32	2.08	1.85	2.32	0.46
Il	1.67	1.67	1.52	1.37	1.82	0.46
Ap	1.53	1.24	1.24	0.93	1.24	0.31
DI	62.61	62.38	68.67	72.54	78.38	93.62
			Trace elements			
Cr	310	300	200	160	100	40
Ni	120	120	110	80	30	40
Cu	20	30	30	40	30	20
V	100	110	90	80	90	0
Ba	3126	3147	3628	2678	2393	750
Sr	1607	1657	1662	1295	995	390
Rb	140	148	151	216	330	173
Th	11.3	4.9	17.9	29.4	35.0	38
U	2.6	0.6	1.1	1.60	n.d	n.d
Zr	320	270	300	370	720	150
Ta	0.82	0.33	0.67	0.73	n.d	n.d
Hf	8.0	5.2	12.6	10.6	n.d	n.d
Nb	15.0	8.9	15.0		34.5	21.9
Sc	14.3	7.8	n.d	8.1	n.d	1.9
Y	18.0	16.3	15.7	13.6	19.4	9.2

Table 7.8 Continued

Rare earth elements

	TO-6	TO-5	TO-4	TO-3	TO-2	TO-1
La	89.55	82.45	96.33	82.54	97.90	32.20
Ce	182.39	159.71	162.16	149.14	184.91	52.10
Pr	n.d	18.84	20.11	17.45	20.11	n.d
Nd	83.17	69.92	70.74	61.16	72.67	17.40
Sm	12.98	11.17	10.95	9.39	11.63	n.d
Eu	3.65	3.04	2.91	2.47	2.67	n.d
Gd	9.39	7.31	7.12	6.10	7.66	n.d
Tb	1.13	n.d	n.d	n.d	n.d	n.d
Dy	n.d	3.97	3.87	3.30	4.61	n.d
Ho	n.d	0.72	0.70	0.61	0.85	n.d
Er	n.d	1.95	1.95	1.66	2.29	n.d
Tm	0.45	n.d	n.d	n.d	n.d	n.d
Yb	1.58	1.25	1.18	1.07	1.60	n.d
Lu	0.19	0.20	0.19	0.18	0.27	n.d

Major elements in % wt. Trace elements in ppm
Total Fe as Fe_2O_3. BaO and SrO added to the total.
n.d = not determined

Table 7.9 Chemical analyses of the Toritama enclaves

	TO-6B	TO-4A	TO-4B	TO-4C
SiO_2	50.42	54.92	54.43	54.47
Al_2O_3	14.34	13.46	15.14	15.10
Fe_2O_3	8.97	6.73	6.39	6.47
MgO	9.50	7.21	5.95	5.60
CaO	7.17	6.48	5.09	5.32
Na_2O	3.43	2.83	3.79	3.28
K_2O	3.14	5.54	5.14	6.10
P_2O_5	0.43	0.72	0.63	0.80
TiO_2	0.97	0.75	0.84	0.92
MnO	0.14	0.12	0.10	0.10
LOI	1.01	0.73	0.73	0.80
Total	99.82	100.11	98.75	99.64
		CIPW norm		
Qz	0.00	0.00	0.00	0.00
Or	18.37	32.84	30.62	36.18
Ab	23.47	24.13	29.63	25.24
An	14.75	7.51	8.90	8.35
Ne	2.91	0.00	1.28	1.39
Lc	0.00	0.00	0.00	0.00
Hy	0.00	2.13	0.00	0.00
Di	14.50	16.12	10.22	10.07
Ol	17.83	10.01	11.26	10.47
Mt	3.24	2.55	2.08	2.32
Il	1.82	1.37	1.67	1.82
Ap	0.93	1.55	1.24	1.86
DI	44.75	56.97	61.53	62.81
		Trace elements		
Cr	700	300	290	210
Ni	200	220	140	160
Cu	110	210	180	140
V	160	110	120	100
Ba	1650	3927	2917	4055
Sr	1056	1695	1575	1921
Rb	132	148	151	170
Th	7.4	n.d	7.8	n.d
U	0.7	n.d	1.0	n.d
Zr	190	210	290	350
Ta	0.98	n.d	0.81	n.d
Hf	13.2	n.d	9.0	n.d
Nb	12.0	11.8	15.8	n.d
Sc	n.d	n.d	n.d	n.d
Y	20.2	20.7	16.6	n.d

Table 7.9 Continued

	Rare earth elements			
	TO-6B	TO-4A	TO-4B	TO-4C
La	49.19	150.32	90.69	n.d
Ce	131.31	251.21	168.98	n.d
Pr	n.d	30.78	n.d	n.d
Nd	55.46	119.39	87.85	n.d
Sm	8.67	17.82	12.80	n.d
Eu	2.29	4.04	4.07	n.d
Gd	9.39	n.d	10.87	n.d
Tb	0.68	n.d	8.87	n.d
Dy	n.d	5.21	n.d	n.d
Er	n.d	2.57	n.d	n.d
Yb	1.04	1.65	1.13	n.d
Lu	0.28	0.24	0.24	n.d

Major elements in % wt. Trace elements in ppm
Total Fe as Fe_2O_3. BaO and SrO added to the total
n.d = not determined

with K_2O/Na_2O ratios greater than 1.0 (except in one enclave where $Na_2O > K_2O$). The data plotted in figure 7.5 (after Peccerillo and Taylor, 1976) again indicates strong shoshonitic affinities for the complex, as was the case for the Bom Jardim intrusion. The rocks are generally peraluminous ($Al_2O_3 > Na_2O+K_2O+CaO$), although some of the enclaves are metaluminous in character. Values of TiO_2 are consistently less than 1.0 wt%.

The AFM diagram shown in figure 7.6 indicates that the rocks of the Toritama complex follow a calc-alkaline high-K trend, similar to that discussed previously for the Bom Jardim complex. The individual major element oxide trends are shown in figure 7.7 as a series of variation diagrams. The oxides, MgO, CaO, Fe_2O_3, FeO and TiO_2 all show well constrained negative correlations with the differentiation index (D.I.). The trends shown by K_2O Na_2O and Al_2O_3 are more scattered, although the Na_2O and Al_2O_3 data for the major facies (shown as closed circles in figure 7.7) are much better constrained than that of the enclaves, with Na_2O showing a flat trend, and that of Al_2O_3 clearly negatively correlated with the D.I.. Overall K_2O shows a poorly constrained positive correlation. Both the abundances and individual trends of the major oxides are very similar to those already discussed for the Bom Jardim complex. The enclave samples again show all the characteristics of a less evolved suite. The similarity of the two complexes is clearly seen in the enrichment/depletion diagram shown in figure 7.8.

7.3.3 Trace element geochemistry

The individual trace element analyses of both the major facies and the enclave samples are listed in tables 7.8 and 7.9. The trace element contents of the rocks from the Toritama complex are characterized by high values of Ba (2364 to 4055 ppm), Sr(1001 to 1920 ppm) and Th (7.4 to 33.57ppm) and, medium values of Rb (132 to 330 ppm), typical of rocks with shoshonitic affinities (Morrison, 1980, Ewart, 1982). Of the high field strength elements

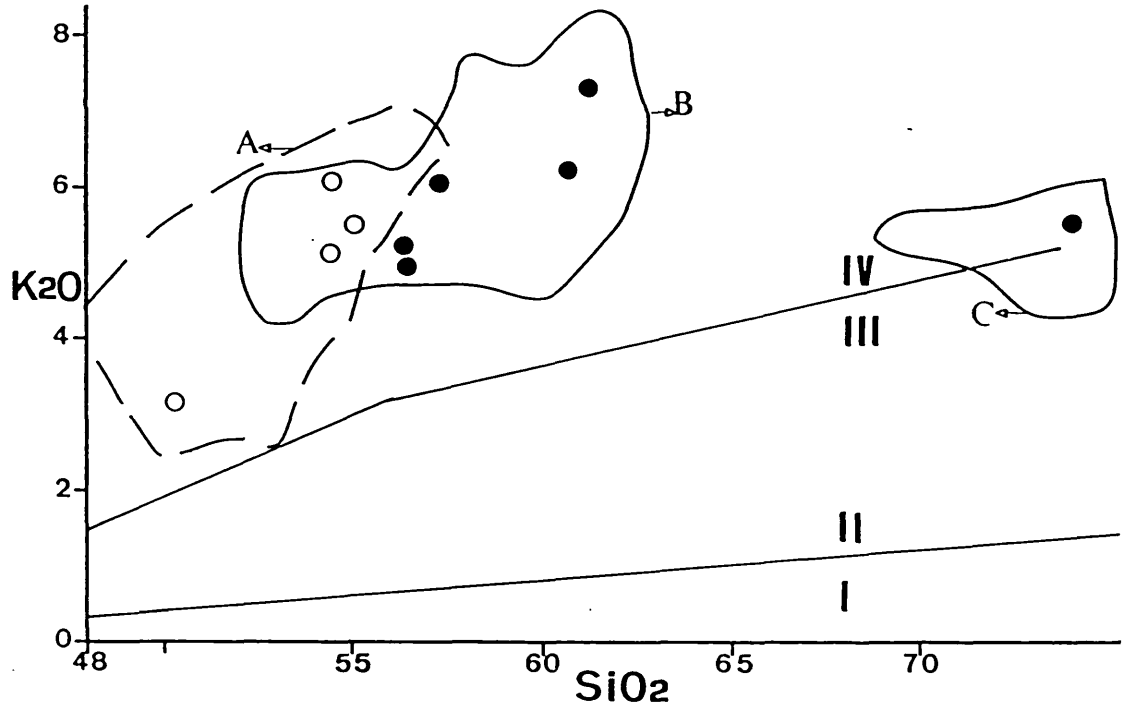


Figure 7.5 Variation of K_2O with SiO_2 content for the rocks of the Toritama complex. (Fields I-IV, after Peccerillo and Taylor, 1976).
I=Field of the arc island tholeiitic series, II=Field of the calc-alkaline series, III=Field of the high K calc-alkaline series and IV=Field of the shoshonitic series.
(A=Bom Jardim minor facies, B=Bom Jardim monzonites/syenites and C=Bom Jardim granite
Open circles=Toritama enclaves, closed circles Toritama major facies).

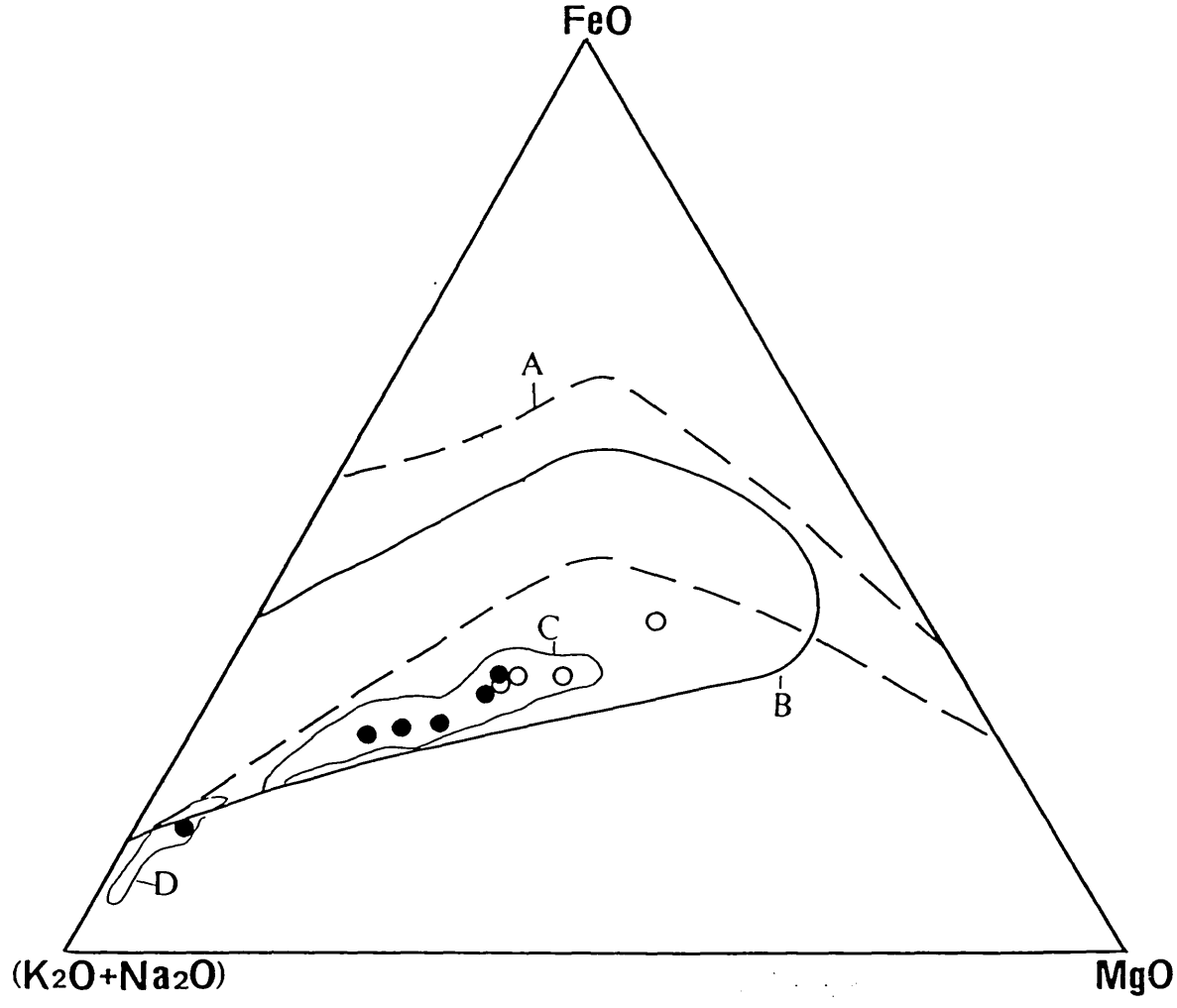


Figure 7.6 AFM diagrama of the Toritama granitoids. A = alkaline series; B = calc-alkaline series. Fields are from Morrison (1980). Symbols as in figure 7.5. C = Bom Jardim monzonites\syenites and D = Bom Jardim granites.

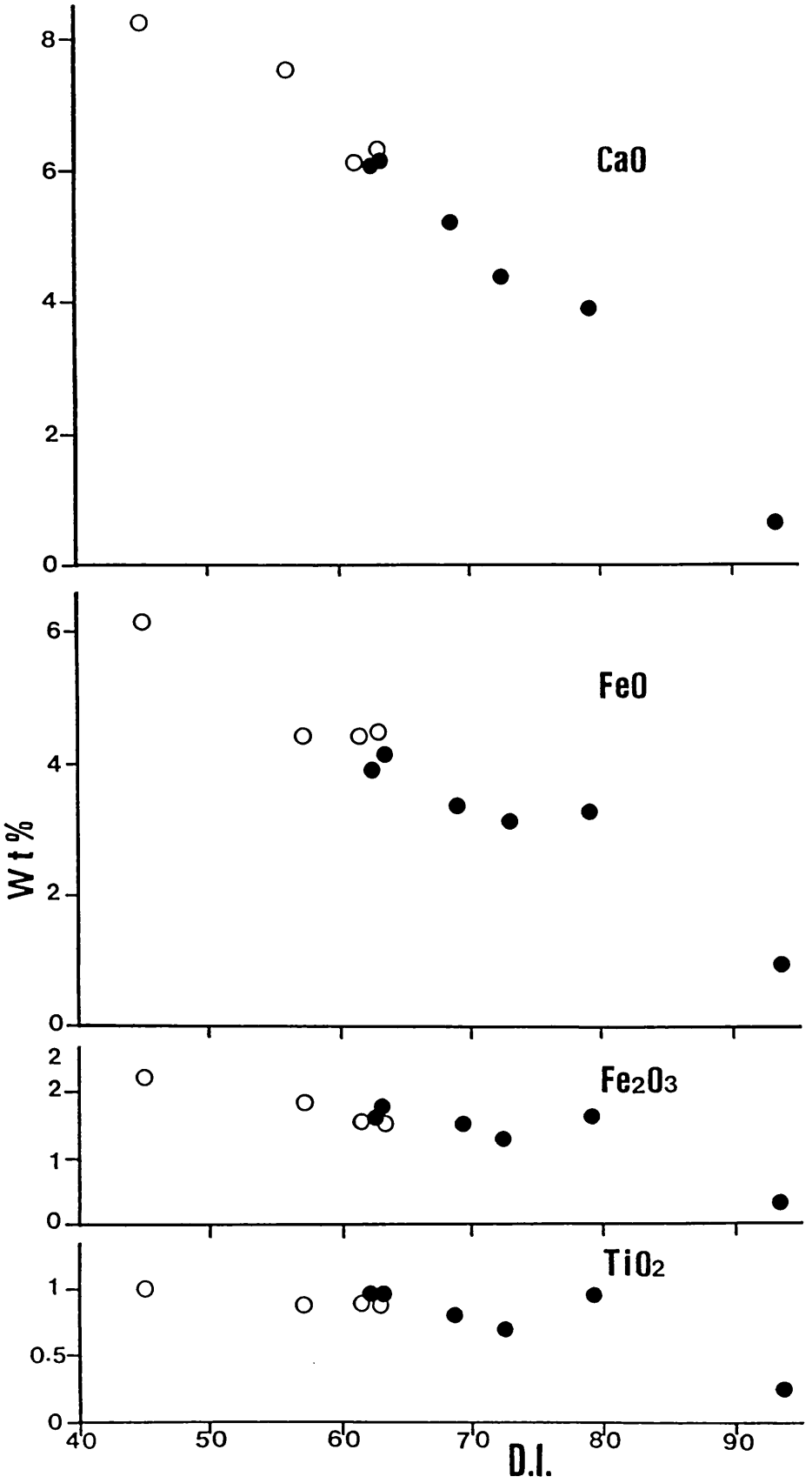


Figure 7.7 Major element oxide variation diagrams. The abscissa D.I. = Thornton and Tuttle differentiation index. (Closed circles = major facies, open circles = enclaves).

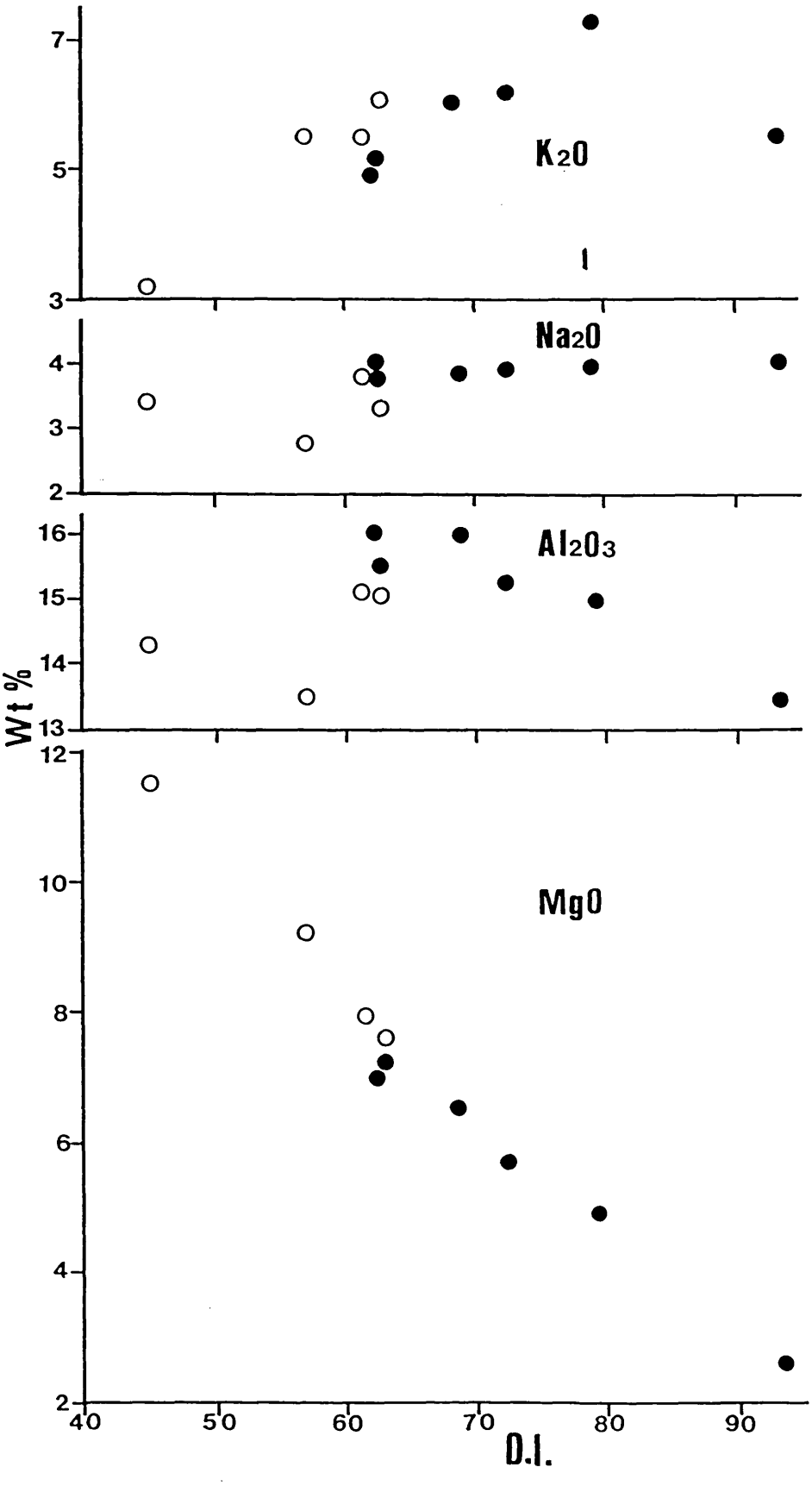


Figure 7.7 Continued

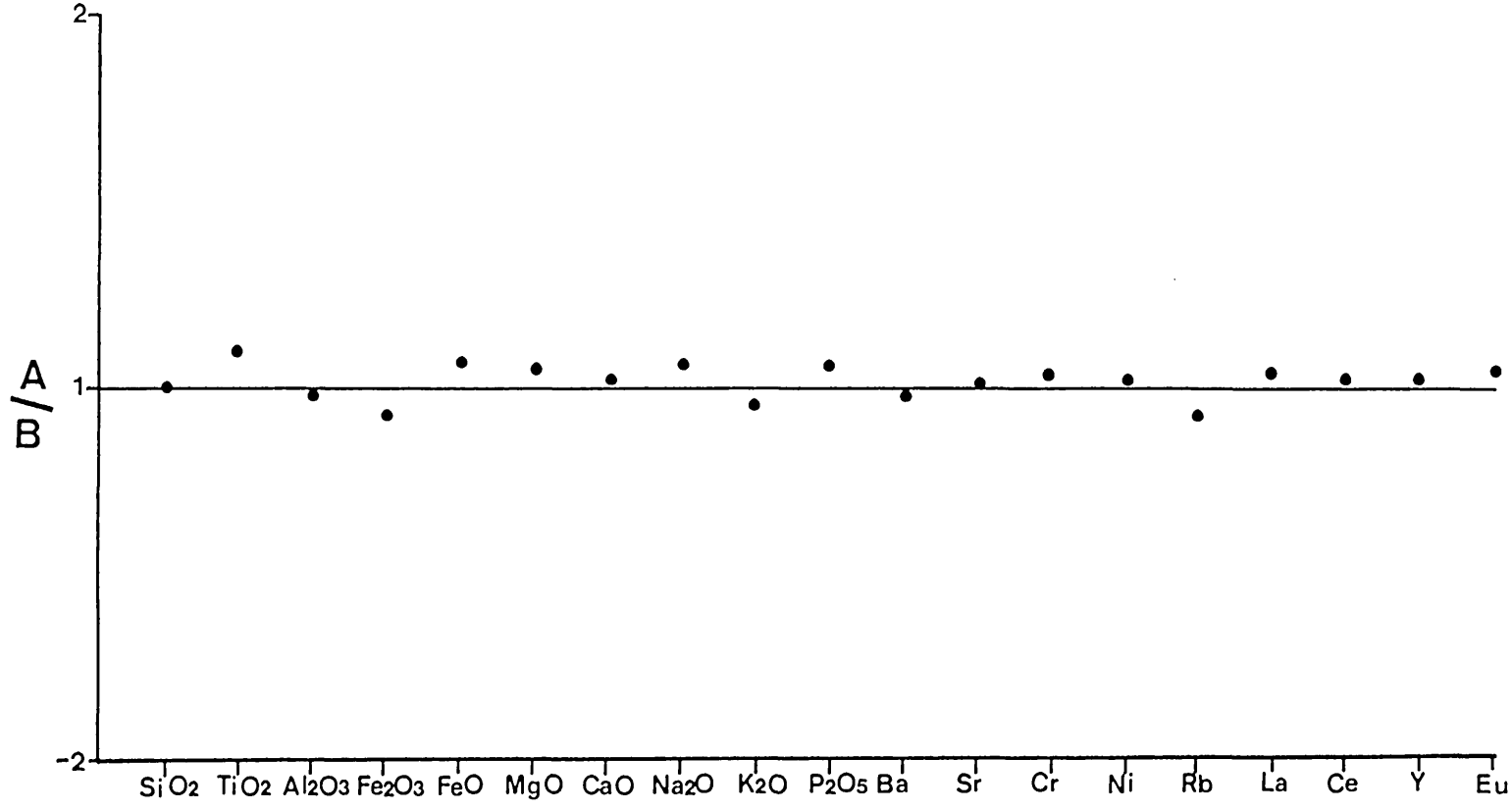


Figure 7.8 Enrichment/depletion pattern for PBAMS facies of both the Toritama and Bom Jardim complexes. A = element concentration in the Toritama PBAMS; B = element concentration in the Bom Jardim PBAMS.

(HFSE), Nb contents are generally lower than 20ppm (8.9 to 15.8ppm), apart from the CS facies and the pink granite (34.5ppm and 21.5ppm respectively). Ta values are also low, ranging from 0.33 to 0.98 ppm, Hf contents vary from 5.2 to 13.2 ppm and Zr from 150 to 720 ppm. The transition element contents are generally high with Cr values varying from 100 to 700 ppm, Ni from 30 to 220 ppm and V from 80 to 160 ppm. Such high values would appear to preclude the possibility of a crustal source for these rocks. Taylor and McLennan (1985) give lower crustal values for Cr, Ni and V as 235ppm, 135ppm and 285ppm respectively.

The Rb\Sr ratios determined for the Toritama complex are low, less than 0.25 (0.09 to 0.17), except in the CS facies where values of 0.33 have been recorded. As previously discussed in chapter 5, the determined values of Rb and Sr for the Toritama complex indicate source depths greater than 30 Km (see figure 7.9). Such a depth estimate is in agreement both with the evidence from the transition element data previously discussed and the geophysical data presented in chapter 1. Olade (1976) has also concluded that such low Rb\Sr ratios (< 0.1) as determined in the Toritama complex appear to reflect a mantle source.

The chondrite normalized REE patterns of rocks from the Toritama complex are shown in figure 7.10. They are characterized by high total REE abundances as follows:

Facies type	**Total REE abundance (ppm)**
PBAMS	349
MPBAS	314
CS	390

The trends lack any significant Eu anomaly and have high LREE/HREE ratios, characteristics which have previously been noted in the Bom Jardim complex. In fact the superposition of the Bom Jardim data in figure 7.10 demonstrates just how similar both complexes are in respect of their REE contents.

The general characteristics of the geochemical behaviour of the incompatible elements within the Toritama complex are displayed in a series of chondrite normalized incompatible element patterns in figure 7.11. The normalizing factors are those of Thompson (1982). All three

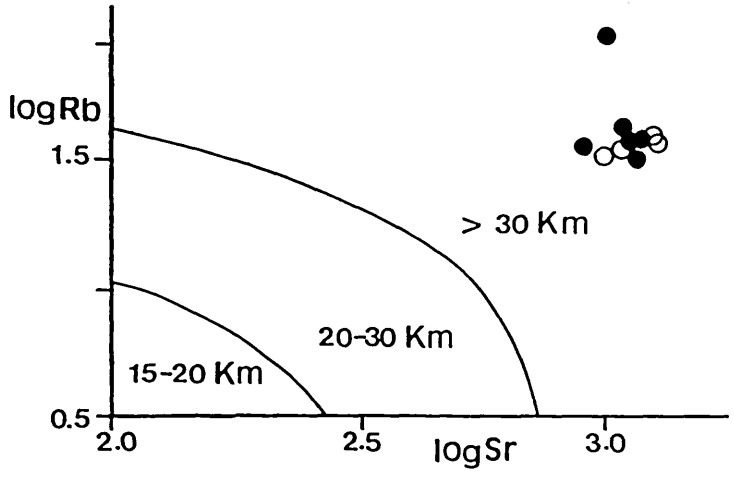


Figure 7.9 LogRb versus logSr diagram showing the distribution of the Toritama granitoids. Numbers in kilometer refer to crustal thicknesses (Condie 1973). Symbols as in figure 7.7.

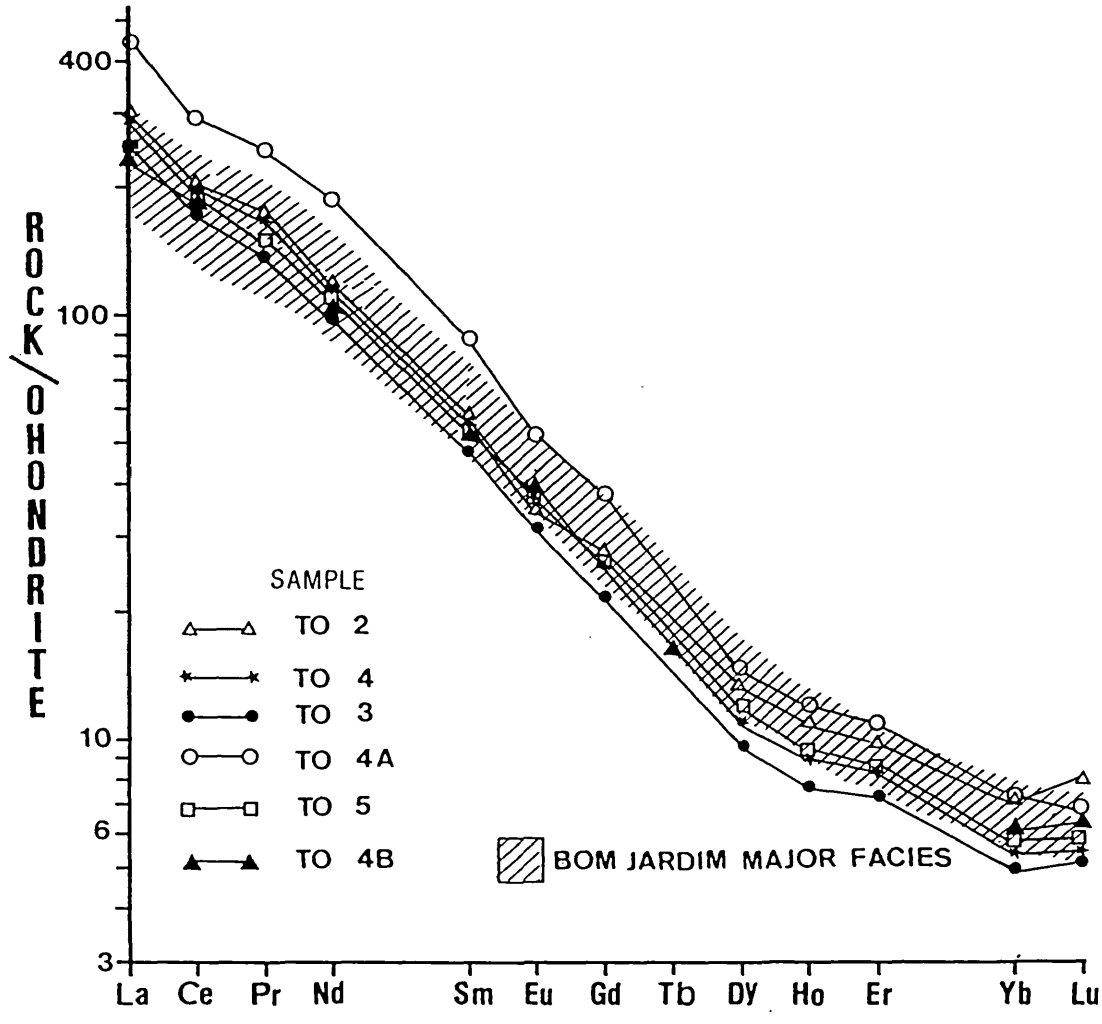


Figure 7.10 Chondrite normalized REE plots for the different lithologies of the Toritama complex. Chondrite values are from Nakamura (1974).

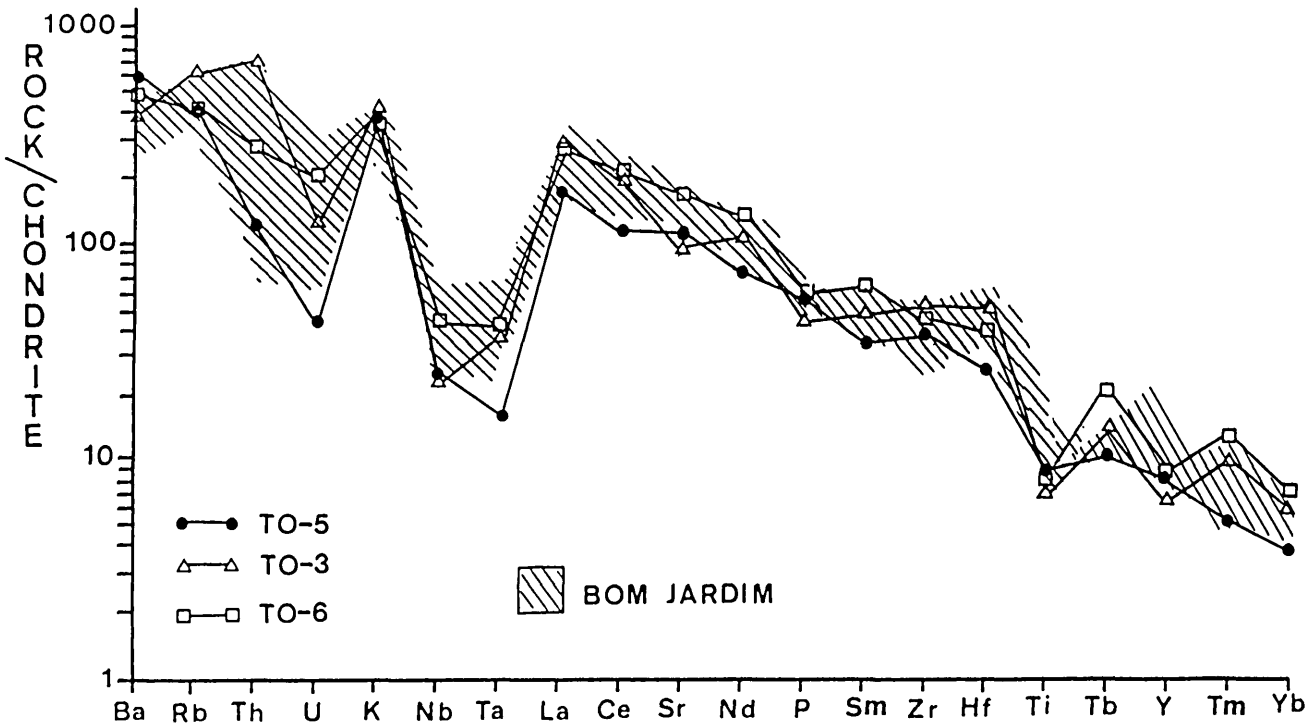


Figure 7.11 Chondrite normalized incompatible element patterns of the different major lithologies recorded in the Toritama complex. Normalizing factors are from Thompson (1982).

facies types plotted show a number of common features, i.e., significant troughs at Nb and Ta, together with troughs at variable depth at U, Ti and P, and peaks at K and La. An envelop showing the distribution of data from the Bom Jardim complex has been superimposed on the Toritama patterns. There is a close similarity in the incompatible element signatures between the two complexes.

7.4 SUMMARY AND CONCLUSIONS

Both the petrographic and geochemical data indicate a clear similarity between the Bom Jardim and Toritama complexes. The present author believes that the latter complex could easily represent an magmatic extension of the Bom Jardim complex.

The shoshonitic character of both complexes is of interest and importance, when one considers that they have a NE-SW alignment, following the strike of the main thrust in this part of the Borborema province. The tectonic implications of this magmatism will be discussed in chapter 8.

CHAPTER 8
TECTONIC SETTING

8.1 INTRODUCTION

The term "Pan African" is used widely to describe Precambrian (non - Archaean) tectono-thermal events in African terrains. There is however some disagreement among geologist as to the age range ascribed to such events. Some geologists restrict the term to rocks with an age span of 450 - 650 Ma., others to a longer period of 1200 - 450 Ma.. The "Pan-African", termed the Brasiliano event within Brazil, has been restricted to an age range of 510 to 710 Ma. by the Brazilian geologists (Jardim de Sa et al., 1984). This latter age range corresponds to the Upper Pan - African event of Gass (1982).

Within the Borborema province, the Brasiliano cycle is characterized by two intense phases of magmatism. The earlier phase occurring 550 to 670 Ma ago., resulted in the widespread development of I-type porphyritic granitoids of the Itaporanga type (Almeida et al., 1967, see table 8.1). The second phase of magmatism occurred between 510 and 570 Ma. ago, and resulted in the intrusion of S-type granitoids (Jardim de Sa et al., 1988, Jardim de Sa et al., 1987 and McMurry et al., 1987). The S-type granitoids have been recorded along the borders of the Pianco Alto Brigida fold belt (Sial, 1984) and along the southern border of the Pajeu Paraiba fold belt. According to Gass (1982), such intense phases of intrusive magmatism also appear to be characteristic of the Brasiliano cycle in N. Africa and Arabia. The same author considers that such calc-alkaline magmatism in both regions indicates the presence of a subduction zone. The end of the Brasiliano cycle in both the Borborema province (Da Silva Filho et al., 1987 and Sial, 1986) and in N. Africa (Gass, 1982) was marked by an intrusive phase of peralkaline magmatism.

Table 8.1 Granite-types in Northeast Brazil. After Almeida et al. (1967).

Granitoid type	Type; area of intrusion	Host rock	Petrographic Types
Itaporanga	Batholith;300Km^2	Migmatites	Porphyritic granodiorites and syenites
Conceiçao	Stocks; 35Km^2	Metasediment	Biotite-tonalites, porphiritic granites and granodiorites
Catingueira	Dykes;12 Km^2 and Batholith	Metasediments	Peralkalic syenites to Qz- syenites
Itapetim	Batholith; 200 Km^2	Migmatites	Granites and granodiorites

The isotopic ratios Rb^{87}/Sr^{86} and Sr^{87}/Sr^{86} have been determined (at the RHBNC Isotope laboratory) for both a series of whole rock samples (syenites and monzonites) and mineral separates (clinopyroxenes and biotites) from both the Bom Jardim and Toritama complexes. The results of the isotopic study are set out in table 8.2. An eleven point isochron (see figure 8.1A) which includes two samples from the Toritama complex and three clinopyroxene separates gave an age of 585$\pm$ 38 Ma., with an initial Sr^{87}/Sr^{86} ratio of 0.70714 $\pm$ 0.00001. Figure 8.1B shows a nine point isochron for the Bom Jardim complex (including both whole rock and clinopyroxene samples); this gave a age of 593$\pm$85 Ma. with an initial Sr^{87}/Sr^{86} ratio of 0.7071 $\pm$ 0.0003.

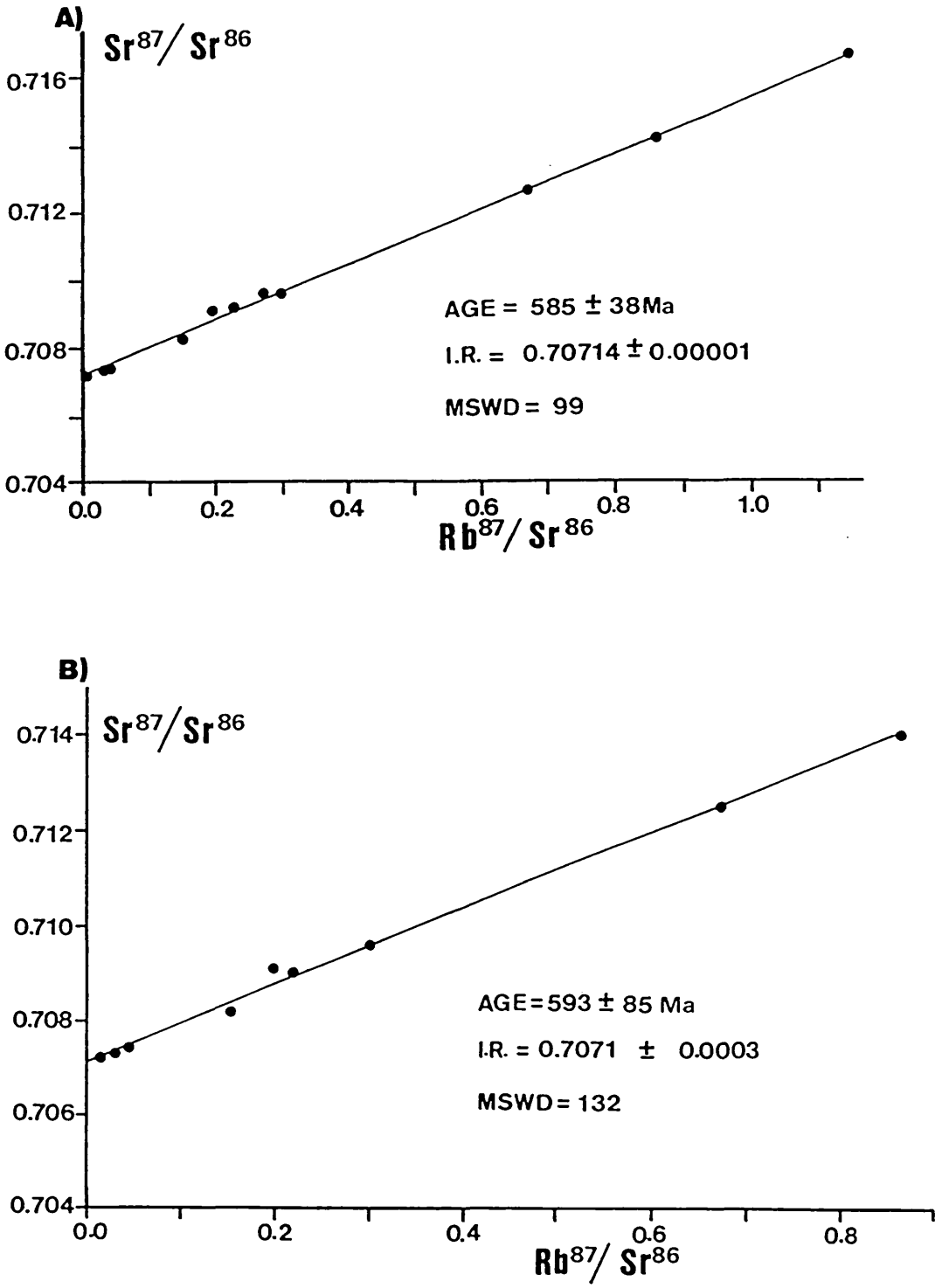


Figure 8.1(A-B) Rb - Sr whole rock clinopyroxene isochron. See text for detail.

Table 8.2 Rb-Sr data for the Bom Jardim and Toritama complexes.

SAMPLE	Rb(ppm)	Sr(ppm)	Sr^{87}/Sr^{86}	Rb^{87}/Sr^{86}
25	272±1	1162±5	0.712648±10	0.67443
23	298±1	995±1.5	0.714087±13	0.86456
53	164±0.4	1582±5	0.709645±31	0.29929
90	147±0.4	1954±5	0.708972±18	0.21630
144	112±0.4	1562±5	0.709102±10	0.19290
193	125±0.4	2422±5	0.708217±12	0.14916
TO-6	134±0.4	1683±5	0.709199±45	0.22889
TO-1	161±0.4	403±1.5	0.716705±27	1.15277
25cpx	1.05	77.45	0.707444±8	0.03908
53cpx	0.82	73.62	0.707367±13	0.03211
90cpx	0.35	93.99	0.707321±14	0.01067
90Bio	461.9	20±1	1.26744±2	70.1829
53Bio	596.3	35±4	1.10733±2	51.2568
25Bio	1056.8	29±1	1.63909±3	116.3714

Table 8.3 Mineral-whole rock and mineral-mineral Rb-Sr ages for the Bom Jardim complex.

53cpx - 53whole rock	T = 598±3 Ma	I.R.=0.70709±2
25cpx - 25whole rock	T = 574±8 Ma	I.R.=0.70712±1
25bio-25cpx-25whole rock	T = 568±12 Ma	I.R.=0.70713±1
53bio-53cpx-53whole rock	T = 563±44 Ma	I.R.=0.70712±9
90bio-90cpx-90whole rock	T = 561±6 Ma	I.R.=0.70724±1
25bio-25cpx	T = 562±8 Ma	I.R.=0.70713±1
53bio-53cpx	T = 548±7 Ma	I.R.=0.70712±1

The Rb-Sr isotopic data for clinopyroxene-whole rock pairs (see table 8.3) yielded ages ranging from 598± 3 Ma. (initial Sr^{87}/Sr^{86} ratio of 0.70709±0.00002) to 574±7 Ma. (initial Sr^{87}/Sr^{86} ratio of 0.70712±0.00001). The relatively younger age determined from biotite-clinopyroxene pairs and biotite - clinopyroxene - whole

rock assemblages (547±7 - 561±7Ma.) appears to reflect a re-set age caused by heating as a result of later movements along the Pernambuco lineament. Biotites in particular are well known to be highly susceptible to changes in their Rb/Sr ratios under such circumstances.

Although the data presented in figures 8.1 A and B do not permit high precision ages to be determined for the Bom Jardim and Toritama complexes, certain general conclusions can be made: both complexes are considered to be representatives of the Itaporanga type granitoid group (Almeida et al., 1967), similar type granitoids, for example the Fazenda Nova complex, intruded 10Km SW of the Toritama complex, have been dated (McMurry et al., 1987), giving an age of 630± 24 Ma. with an initial $Sr^{87}\backslash Sr^{86}$ ratio of 0.7065±0.0005. The age of the Fazenda Nova complex is similar to the determined clinopyroxene - whole rock ages (see table 8.3) and the ages determined from isochrons in figure 8.1A and B. The Rb and Sr contents of the clinopyroxenes are low, and any heating caused by later dynamo-thermal metamorphism will not have significantly affected them. Thus the age and initial $Sr^{87}\backslash Sr^{86}$ ratio of pyroxenes can be considered to reflect the age of the rock and not a re-set date. Consequently, using pyroxene-whole rock ages in table 8.3, the isochronic ages determined in figures 8.1A and B and the published age of the Fazenda Nova complex, an age of approximately 600 Ma. with an initial $Sr^{87}\backslash Sr^{86}$ ratio of 0.70709 appears to be a good estimate for both The Bom Jardim and Toritama complexes.

8.2 STRONTIUM ISOTOPE RATIOS AND THE MAGMA SOURCE

The initial $Sr^{87}\backslash Sr^{86}$ ratio of 0.70709 recorded for the Bom Jardim and Toritama complexes clearly indicates the contribution of a crustal component during the evolution of the magma. Most granitoids, especially those in subduction related regimes exhibit intermediate values of the initial $Sr^{87}\backslash Sr^{86}$ ratio, reflecting a mixing process between mantle and continental source material (Taylor and Silver, 1978 and De Paolo, 1981). Figure 8.2 indicates that

the initial $Sr^{87}\backslash Sr^{86}$ ratio for the Bom Jardim and Toritama complexes are similar to many intrusives in magmatic arcs with a Precambrian basement. Such examples include the well documented cases of the Californian granitoids (Kistler and Peterman, 1973), the Arequipa segment of the Peruvian Coastal batholith (Beckinsale et al., 1985), the Washington - Idaho granitoids (Armstrong et al. 1977) and Japanese granitoids (Shibata and Ishihara, 1979). In comparison with syn-collisional granitoids such ratios are much lower (see figure 8.2).

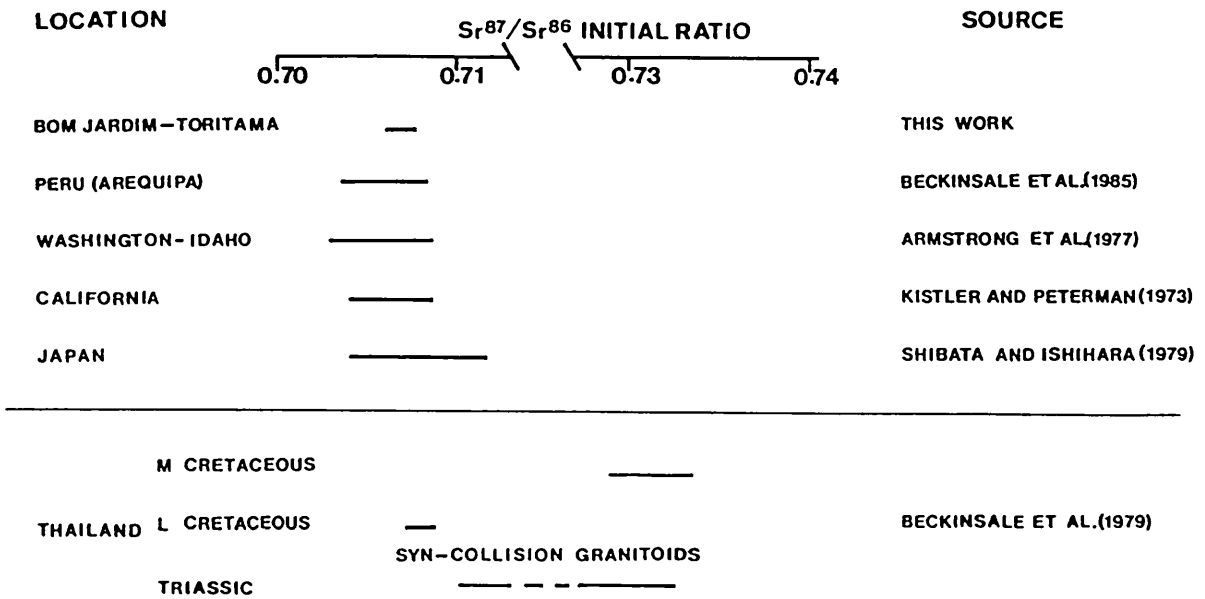


Figure 8.2 The ranges of Sr isotope ratios for intrusive suites from Mesozoic and Tertiary magmatic arcs, compared to those recorded in the Bom Jardim and Toritama complexes.

8.3 THE TECTONIC SETTINGS OF THE SHOSHONITIC ROCK SERIES

Geochemically and mineralogically the rocks of the Bom Jardim and Toritama complexes display all the general characteristics of an intrusive shoshonitic series (see chapters 4, 5 and 7). The tectonic setting of shoshonitic rocks has been the subject of several studies (Barberi et al., 1974; Morrison, 1980; Ewart, 1982;

Thompson et al., 1984; Thompson and Fowler, 1986; Zhou, 1987; Bloomer et al., 1989 and Gill and Whelan, 1989). Worldwide, the shoshonitic series are generally found above steep parts of active subduction zones, late in island arc development. These series may also characterize transitional stages between active subduction to other tectonic regimes (Thompson and Fowler, 1986). During the later stages of subduction, steeping of the Benioff zone can lead to failure or flipping of the subducted lithosphere and either renewed subduction with reverse polarity or extension takes place. Shoshonitic rocks are most commonly associated with these later stages of island arc evolution (Morrison, 1980).

Jakes and White (1972) and later Morrison (1980) have suggested that in well documented orogenic regions a spatial zonation of various associations can be recognized and that in unstable regions the shoshonites are normally associated with arc deformation during the termination of a subduction phase, or in some cases with oblique convergence of plates.

The occurrence of shoshonitic volcanism in response to reversals in arc polarity accompanying the development of thrust faults has been described in modern arcs, for example the Sunda arc, Indonesia (Foden and Varne, 1980), in the northern most Sangihe arc (Morrice et al., 1983) and N.W. Honshu (Honza and Tamaki, 1985).

Members of the shoshonitic rock series have also been cited as being developed during and after continental collision, following ocean basin closure (Zhou, 1985,1987; Thompson et al., 1984) and with early rifting of an oceanic island arc in Fiji (Gill and Whelan, 1989).

8.4 GEOCHEMICAL DISCRIMINANTS AND TECTONIC SETTING, THEIR IMPLICATIONS

Various authors (for example Brown, 1982; Harris et al., 1986; Pearce et al., 1984 and Pitcher, 1983) have recognized a range of different granitoids, many of which are the direct or indirect products of subduction related

processes. The geochemical characteristics of many of these intrusive rock suites from a range of different tectonic settings indicate that geochemical discriminant functions can be used to distinguish the tectonic setting in which the magmas were generated and intruded.

In order to assess the most likely tectonic setting for the Bom Jardim and Toritama complexes, a number of discriminant functions proposed by Pearce et al. (1984), Pearce (1982), Batchelor and Bowden (1985), Thorpe (1987), Harris et al. (1986) and Leat et al. (1986) have been used.

Figure 8.3 (after Batchelor and Bowden, 1985) shows a plot of two major element cation functions R_1 and R_2 for the rocks of the Bom Jardim and Toritama complexes, where R1 = [4Si - 11(Na+K) - 2Fe + Ti] and R2 = [6Ca + 2Mg + Al] (La Roche et al., 1980). Included in this diagram are the major tectonic fields for the granitoids, based on data from Pitcher (1979, 1982) and Harris (1983). The syenites and monzonites from the two complexes are largely constrained within two tectonic fields, namely the high-K calc-alkaline post-collisinal uplift field and the late orogenic sub-alkaline monzonitic field; both fields being associated with compressional regimes. However, some of the granite samples plot within the syn-collisional anatectic leuco-granite field and a few enclaves within the pre-collision granitoid field. Two important aspects concerning the use of R1 and R2 functions should be borne in mind: firstly their values can be significantly affected by fractional crystallisation processes, and secondly the rather scattered trend shown by the Bom Jardim and Toritama samples is broadly coincident with the predicted R1 - R2 trends as the rocks evolve through an orogenic cycle. The predicted trend in R1 - R2 values as a suite evolves through an orogenic cycle is largely based on the widespread tectonic relationship between K_2O content and depth of the subduction, i.e., K-h relationship (see Gill, 1981). Arculus (1987) however, has pointed out that the K_2O contents appear in reality to be the result of interactions between several processes and their relationship with the depth of Benioff zones is not very well understood.

The Nb - Y discriminant diagram (after Pearce et

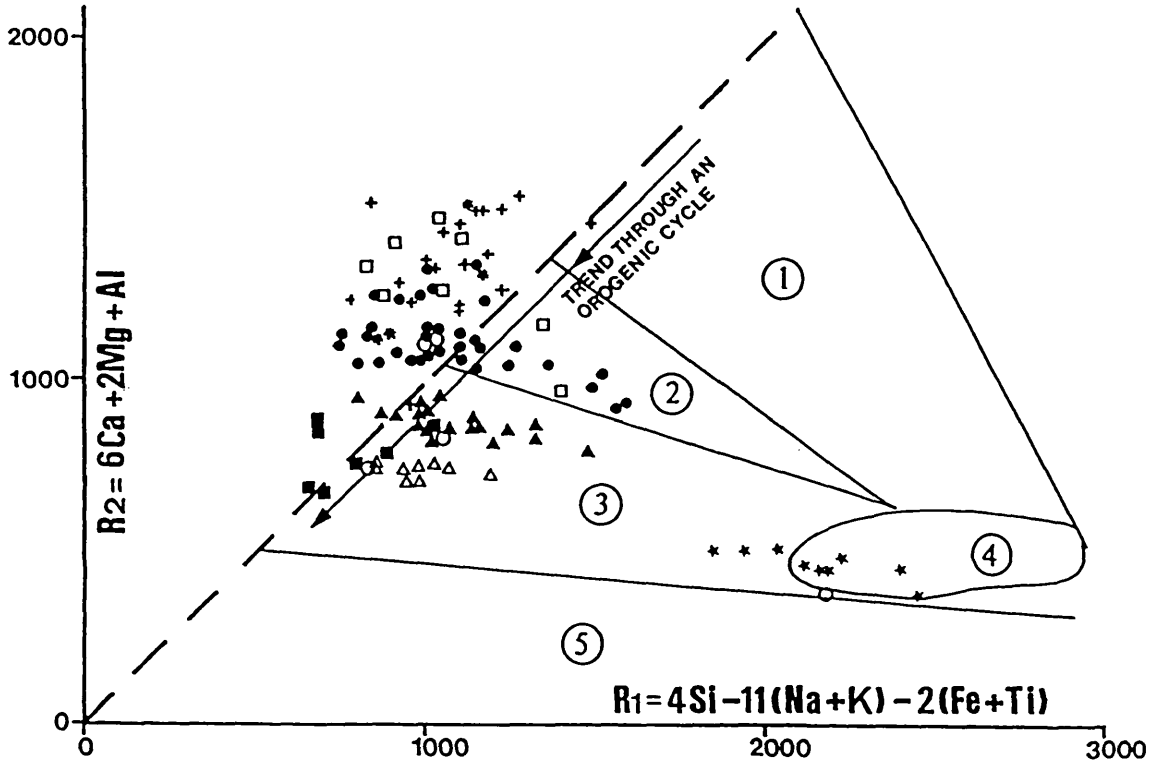


Figure 8.3 R1 versus R2 discriminant function diagram (Batchelor and Bowden, 1985) for the Bom Jardim and Toritama complexes. R1 and R2 from De La Roche et al. (1980). Tectonic fields FROM Pitcher (1979, 1982) and Harris (1983) and, petrological equivalents after Lameyre and Bowden (1982). 1 = Pre-plate collision - calc-alkaline and trondhjemitic; 2 = Post-collision uplift - high-K calc-alkaline; 3 = Late-orogenic - sub-alkaline monzonitic; 4 = syn-collision - anatetic two micas granites and 5 = anorogenic - alkaline and peralkaline.
(closed circles = PBAMS-Bom Jardim; closed triangles = MPBAS-Bom Jardim; open triangles = PBLS-Bom Jardim; closed squares = CS-Bom Jardim; stars = granites-Bom Jardim; crosses = enclave-Bom Jardim; open squares = dykes-Bom Jardim; open circles = Toritama major facies and roses = enclaves-Toritama)

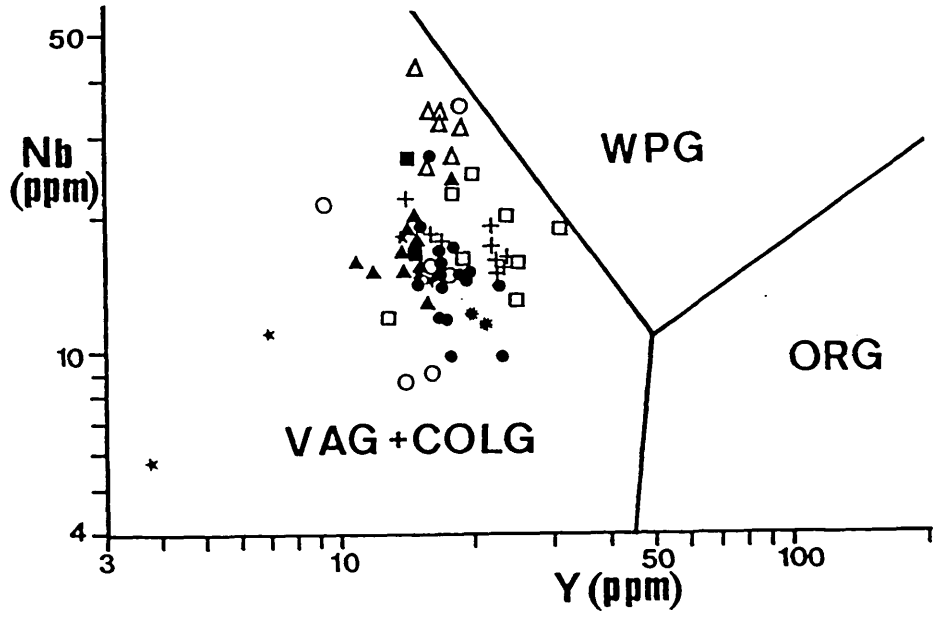


Figure 8.4 Variation of Nb versus Y for rocks from the Bom Jardim and Toritama complexes. WPG = within plate granitoids field; VAG = Volcanic arc granitoids field; COLG = syn-collision granitoids field and ORG = Ocean ridge granitoids after Pearce et al. (1984). Symbols as used in figure 8.3.

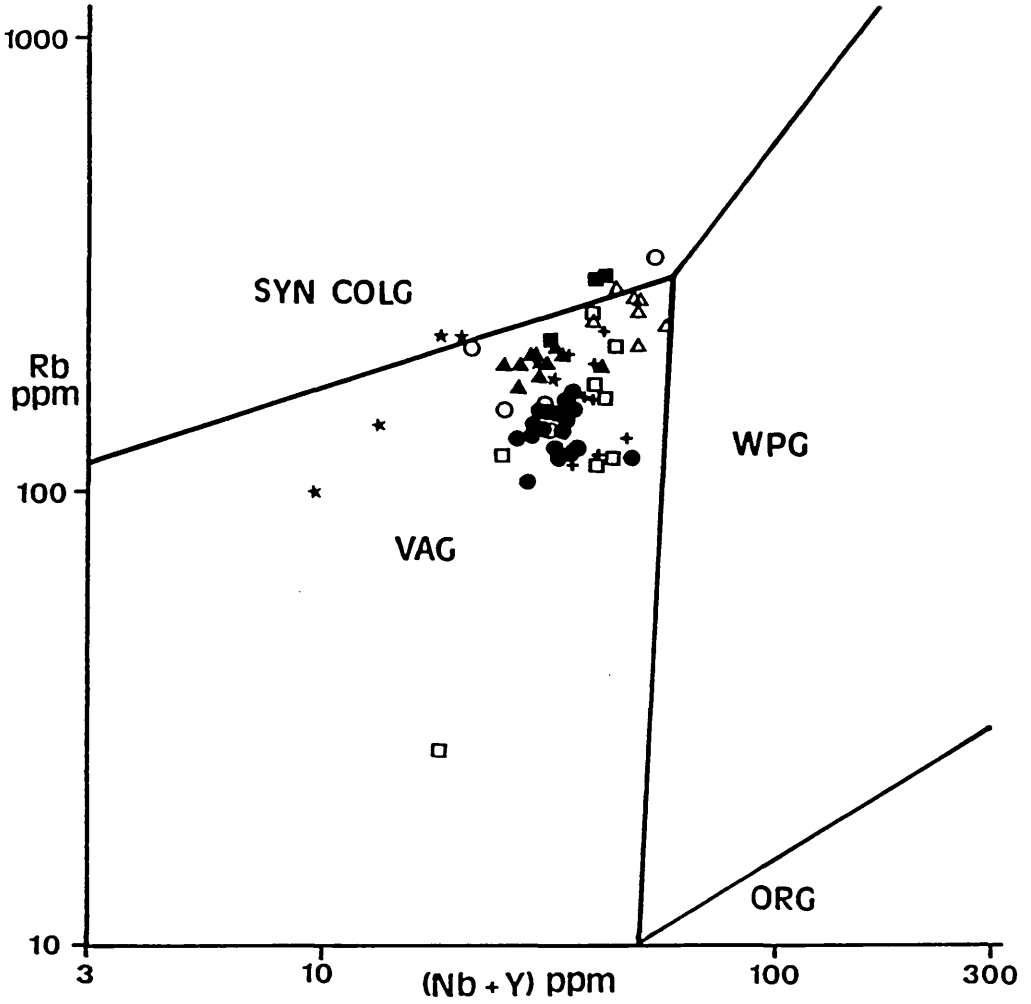


Figure 8.5 Rb versus (Y + Nb) discriminant diagram for syn-collision granitoids (SYN-COLG), within plate granitoids (WPG), volcanic arc granitoids (VAG) and ocean ridge granitoids (ORG), after Pearce et al. (1984). Symbols as in figure 8.3.

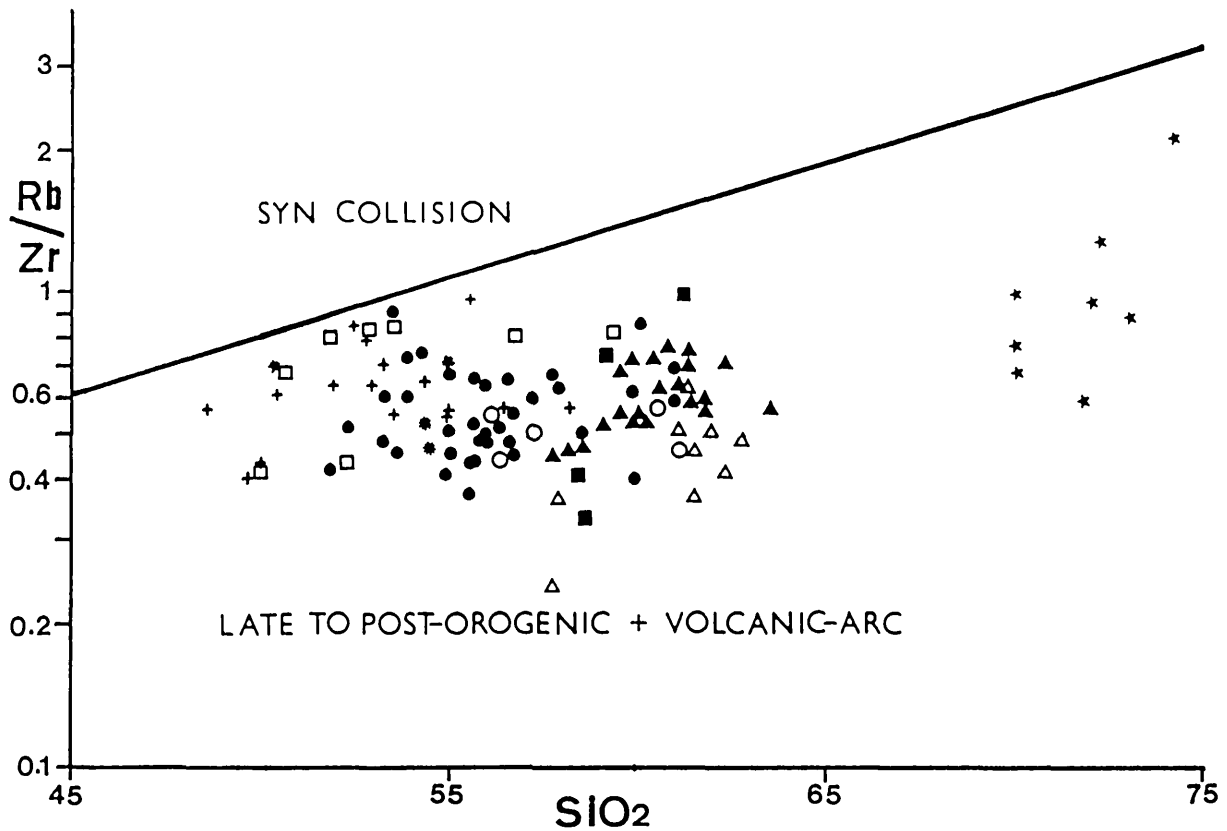


Figure 8.6 Rb/Zr ratios plotted versus SiO_2 for rocks from the Bom Jardim and Toritama complexes. Fields after Harris et al. (1986). Symbols as in figure 8.3.

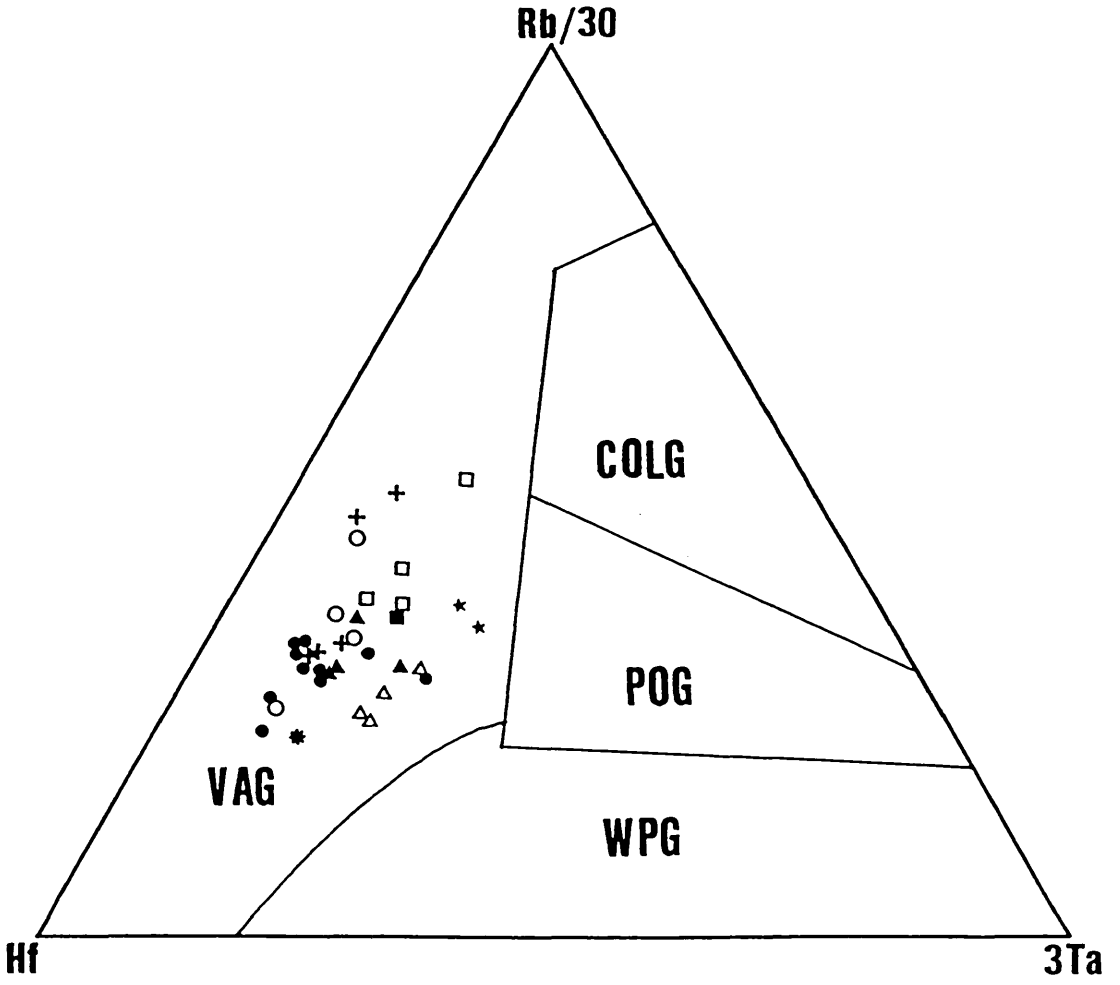


Figure 8.7 Rb-Hf-Ta plot for acid-intermediate intrusive magmatism from volcanic arc (VAG), within plate (WPG), post orogeny (POG) and syn-collision (COLG). Fields after Harris et al. (1986). Same symbol designations used as in figure 8.2.

al., 1984) shown in figure 8.4 shows that all the samples from both complexes fall within the field of volcanic arc and syn-collisional granitoids. Further tectonic discrimination is not possible using these two elements alone. However, when one considers the plot of Rb versus Nb+Y (see figure 8.5), further discrimination is possible and now, both the complexes fall solely within the field of volcanic arc granitoids.

According to Harris et al. (1986) syn- collision S-type granitoids (Chappel and White, 1974) can be distinguished from calc-alkaline pre-collision granitoids (volcanic arc granitoids) and post-collision granitoids by higher Rb\Zr ratio. Consequently, a plot of Rb\Zr ratio versus SiO_2 content can be used as a discriminant for syn-collision and volcanic arc granitoids (see figure 8.6). All the samples from the Bom Jardim and Toritama complexes, including both the granites and the members of the syenite - monzonite series, plot within the field of volcanic arc granitoids. However, no discrimination is made between volcanic arc and post orogenic granitoids. Some degree of discrimination between these latter granitoid groups, using a plot of Rb/30-3Ta-Hf (Harris et al., 1986) can be achieved and the results are shown in figure 8.7. Using such a discriminant diagram, all the samples from both complexes fall within the field of volcanic arc granitoids, but it does not permit such rocks to be temporally subdivided into post and pre collisional types (Harris et al., 1986).

Leat et al. (1986) have shown that for shoshonitic and ultrapotassic mafic rocks with SiO_2 contents < 60 wt%, a plot of Nb versus Zr is capable of distinguishing between both subduction related and post collisional suites and those far removed in both space and time from any subduction processes. Figure 8.8 shows such a plot and clearly, samples from the Bom Jardim and Toritama complexes fall within the field of subduction related K-rich suites.

The variation of the Th\Yb ratio with that of Ta\Yb has been proposed by Pearce (1982) as a tectonic discriminant for basalts. Yb is used as the denominator in

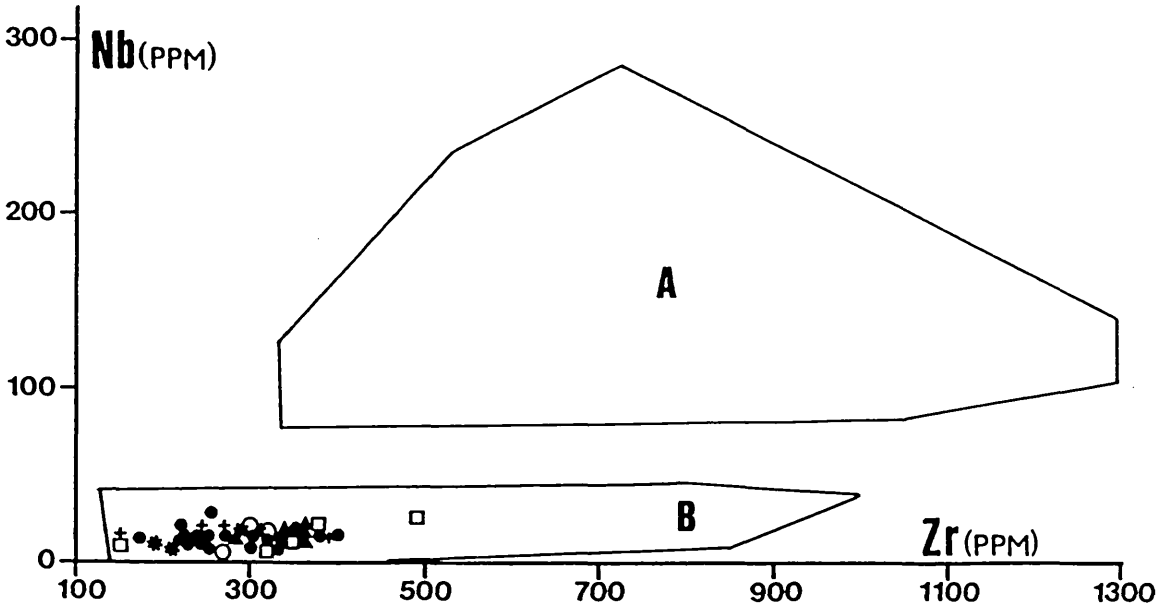


Figure 8.8 Variation of ppm Nb versus Zr for Bom Jardim and Toritama rocks with less than 60% SiO_2. Fields are from Leat et al.(1986). A = localities remote from subduction in space and time and B = localities closely related to subduction in space and\or time, including the first few million years following continental collision.
(Closed circles = PBAMS-Bom Jardim; closed triangles = MPBAS-Bom Jardim; open squares = mafic-dykes Bom Jardim; crosses = enclaves-Bom Jardim; open circles = Toritama and roses = enclaves-Toritama)

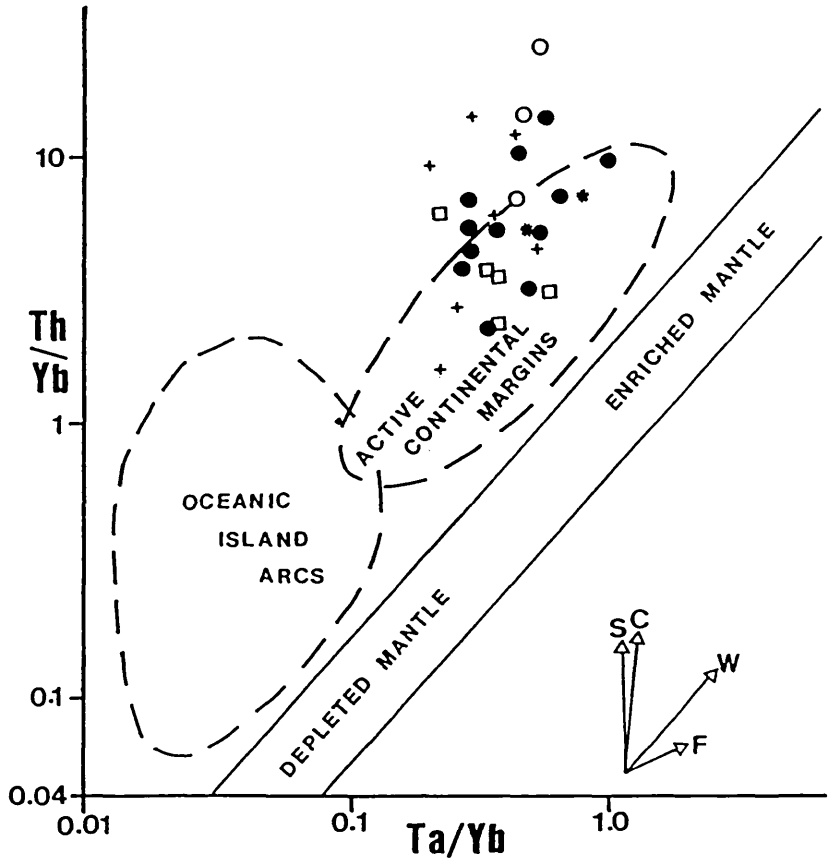


Figure 8.9 Variation of Th/Yb versus Ta/Yb for the Bom Jardim and Toritama rocks with less than 57% SiO_2. Vectors shown indicate the influence of subduction components (S), within plate enrichment (W), crustal contamination (C) and (F) fractional crystallization. After Pearce (1982).

both ratios because this has the effect of eliminating as far as possible differences due to partial melting and fractional crystallisation, thereby focusing the discriminant function primarily on the source composition. As a result, island arc and active continental margin basalts are displaced to higher Th\Yb ratios, reflecting the influence of fluids enriched in Th in subduction zones (Wilson, 1989). As this method of discrimination was primarily set up for basaltic rocks, only the more mafic PBAMS facies together with the dykes and enclaves (i.e., samples with SiO_2 contents < 57%) have been used in figure 8.9. The samples plot mainly in the field of active continental margins. The associated vectors indicate that both crustal contamination and a certain degree of fractional crystallisation have also influenced the evolution of these rocks.

Only two examples of shoshonitic rocks directly related to active continental margins are known to the present author, Yellowstone Park and in S. Peru (Morrison, 1980). The geochemistry of the shoshonitic rocks from Yellowstone Park is comparable in many ways to that of island arcs. On the other hand, the shoshonitic suite from S. Peru is composed predominantly of basaltic andesites and andesites with higher TiO_2, Na_2O, K_2O, P, Sr, Ba and LREE and lower CaO values than island arc suites with comparable SiO_2 contents. The rocks contain more modal orthopyroxene and biotite and less olivine than those recorded from island arcs. Similar differences are also recorded for shoshonitic rocks from island arcs resting on oceanic crust (eg. Fiji) and island arcs resting on deformed basement (Papua-New Guinea Highlands). Morrison (1980) emphasizes the importance of composition and thickness of the crust in promoting the chemical and mineralogical differences discussed above rather than just simply a crust margin versus island arc setting.

8.5 DISCUSSION AND CONCLUSIONS

The Bom Jardim and Toritama complexes show all the major characteristics of subduction related rock suites

i.e., enrichement in LIL elements, high LILE\HSFE ratios and distinct troughs at Nb-Ta, Ti and P in their chondrite normalized incompatible element patterns. The geochemical discriminants employed and discussed in this chapter and also in chapters 5 and 7, suggest that the intrusion of both complexes was associated with the late stages of island arc evolution.

Harris et al. (1986) employing plate tectonic modelling, suggest that if a large thickness of continental crust occurred above subducted oceanic lithosphere, magmatism with volcanic arc characteristics would result. On the other hand, magmatism with "within plate" characteristics would result within the continental crust in response to any overthrusting of continental lithosphere. The island arc geochemical signatures of both the Bom Jardim and Toritama complexes, suggest that the crustal thickness inferred from the strip of negative Bouger anomalies in the Toritama region (see chapter 1) could be related to the subduction of oceanic lithosphere.

An evolutionary model based on an initial Andean type margin in the NW part of the Borborema province, evolving later to an ensialic A-type subduction regime (Kroner, 1982) towards the SE., has been proposed by Jardim de Sa (1984). The determined island arc geochemical signatures for the Bom Jardim and Toritama complexes fundamentally disagree with the proposed model, as both Andean type and island arc magmatism are generally considered to be absent from such A-type subduction models.

Shackleton (1986) considers that much of the so-called evidence cited in support of A- type subduction is poor and, that most of the justification appears to be centred on the inability to substantiate the case for B-type subduction (i.e., negative evidence appears to be the main case for the existence of A-type subduction). The same author also emphasizes that, as no modern examples of A-type subduction have been observed, there seems to be very little justification to support its existence in the past geological record.

The apparent lack of a major suture zone has been used as the main argument in favour of A-type

subduction in the interior of the Borborema province. A strip of negative Bouger anomalies striking in a general SW-NE direction coincident with a major strike slip fault, which marks the northern boundary of the Pajeu Paraiba fold belt, has been recognised by Brito Neves et al. (1982). This major linear feature aligns the mafic and ultramafic complexes of Jabitaca, Itapetim and Floresta, with the eclogitic masses described by Beurlen (1988). Da Silva Filho (1989) suggests that the missing suture zone could in fact be coincident with the strip of negative Bouguer anomalies recorded in this region. However, there are ocurrences of eclogitic rocks in the Bodoco area (Beurlen, 1988), the Campina Grande area (Costa et al., 1979) and mafic and ultramafic rocks within the region of Limoeiro (Da Silva Filho and Guimaraes, 1979 and Farina et al., 1981) which show no alignment.

Geodynamic models for the province have up to now been somewhat speculative due to the lack of reliable geochronological, structural and petrological data in most parts of the Borborema Province. The present data, although only covering a small area of the province, does help to reduce some of the speculations. The irregular distribution of mafic and ultramafic rocks described as being probably ophiolitic by Beurlen (1988) and the widespread subduction related Brasiliano intrusive magmatism, based on compiled data from Sial (1987), Jardim de Sa et al. (1987) and Da Silva Filho and Guimaraes (in prep), suggest a succession of small collisional events involving both island arc-island arc regimes (eg. Pianco Alto da Brigida - Pajeu Paraiba fold belts) and island arc - continental regimes (eg. Pajeu Paraiba belt - PE-Al massif) within the Bom Jardim-Toritama region of the province. The evidence to date involving thrust direction, crustal thickness and the distribution of subduction related K-rich rocks suggests that the inferred subduction zone dips towards the SE..

CHAPTER 9
MAGMA GENESIS, CONSIDERATIONS AND FINAL CONCLUSIONS

The lack of any significant Eu anomalies within the recorded REE patterns of both the Toritama and Bom Jardim monzonites and syenites, points to a possible feldspar free source for the magmas. This would exclude the majority of potential crustal sources eg. the gneiss/migmatite complexes of the Pajeu Paraiba belt and the Pernambuco Alagoas massif. The high contents of the transition elements Ni and Cr in the more mafic members of the Toritama and Bom Jardim complexes could be generated by partial fusion of a lower crustal amphibolite source, but this would immediately give rise to a Eu anomaly, and therefore such a source has to be discounted. It is believed that the high Ni and Cr contents indicate a potential source within the mantle.

The chondrite normalized incompatible element patterns for the monzonite-syenite suites of both the Toritama and Bom Jardim complexes are very similar to certain isotopically well characterized primitive melts of mantle origin within the Scottish Caledonides. Figure 9.1 shows a comparison of two Lorne Plateau lavas (L54 and L8; Thirlwall, 1982), a shoshonitic picrite - kentallenite (MS 143; Thompson et al., 1984) and three samples from the Toritama and Bom Jardim complexes.

Sample L54, which represents an incompatible element rich lava, has a very similar pattern to those determined in the PBAMS facies of both the Toritama and Bom Jardim complexes. Slight differences between the patterns do occur but, they are mainly related to higher Rb contents in both the above complexes. Such higher Rb contents are probably due to small amounts of crustal contamination, as evidenced by higher initial $Sr^{87}\backslash Sr^{86}$ ratios (0.70709) recorded in the Toritama and Bom Jardim complexes. It is also possible that the parental syenite magma could have evolved from a basic melt with lower incompatible element abundances, similar in composition to shoshonitic picrite (MS 143), by the early fractionation of such mafic minerals

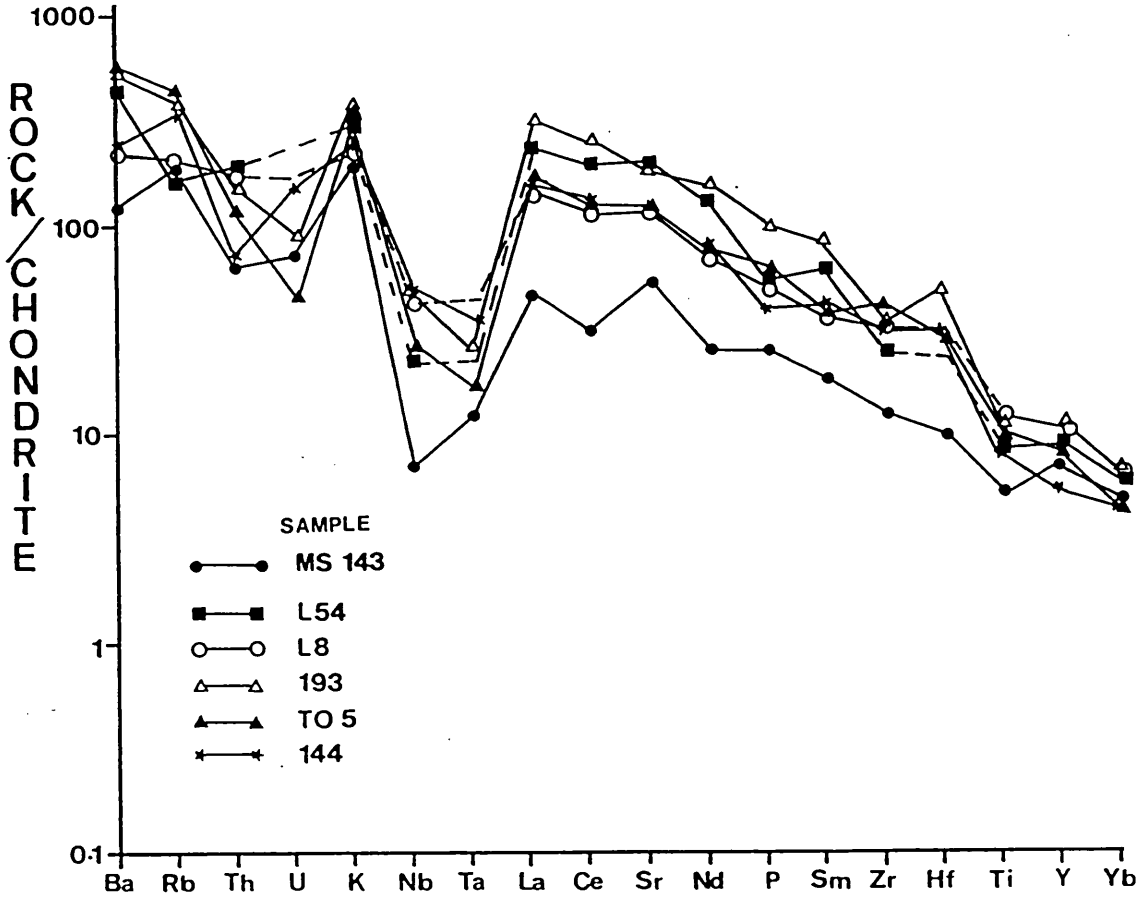


Figure 9.1 Chondrite normalized incompatible element plot comparing rocks from the PBAMS facies of the Toritama (TO-5) and the Bom Jardim complex (193 and 144), with samples from the Lorne plateau lavas (L54 and L8) and, a shoshonitic picrite (kentallenite, MS 143). See text for references.

as olivine and pyroxene. However the REE contents of the shoshonitic picrite display much lower La/Yb ratios (12.5) than those recorded in the Toritama and Bom Jardim complexes (>64.0). Therefore, if the shoshonitic picrite is taken as possible parental magma for the syenite-monzonite suite, abundant amphibole and\or garnet fractionation would be required to increase the La/Yb ratio in the magma (see Noyes et al., 1983). Fractionation of amphibole is supported to some extent by the widespread presence of amphibole-rich enclaves in both complexes (see chapter 6). This latter model for the evolution of the magmas associated with the development of both complexes is somewhat speculative as no rocks of shoshonitic picrite affinity have ever been recorded at outcrop within the Borborema province.

The details of the most probable tectonic setting for the emplacement of both the Toritama and Bom Jardim complexes within the Borborema province have been discussed in chapter 8. The genesis of the magmas can be summarized as follows: the parental melt was generated within the mantle above a Benioff zone. In such a situation it is possible for such a mantle to be metasomatized by fluids, rich in light REE and LIL elements, originated from the dehydration of a descending oceanic slab. It is also highly probable that mixing of different magmas could also have taken place, including magmas generated by lower continental crust melting under the influence of such uprising fluids (Wyllie, 1979, 1983 and Martin, 1987).

The fluids released from the dehydration of the descending slab would rise into the overlying mantle wedge and induce partial melting (Wyllie, 1983). Such fluids extracted at relatively high pressure from the subducted slab are likely to be enriched in the incompatible elements K, Rb and the light REE (Maysen, 1979). Experimental investigations have shown that metasomatized peridotite is capable of generating andesitic to dacitic calc-alkaline magmas (Kushiro, 1972; Green, 1973, 1976 and Wyllie, 1981, 1983). In such cases, olivine and pyroxene are the main fractionating phases, with garnet and spinel playing only minor roles. Such fractionation processes could generate a

magma geochemically similar to the most basic members of the Bom Jardim and Toritama complexes. This magma was probably accumulated later in a magma chamber within the lower crust, where it proceeded to fractionate amphibole, biotite and small amounts of clinopyroxene before the intrusion of the initial pulse of magma, which gave rise to the rocks of the PBAMS facies. This was followed by an upward accumulation of feldspar which developed into the very coarse syenite facies (CS), leaving a lower magma enriched in amphibole and biotite which formed the MPBAS facies. The late stage "crystal-liquid mush" is then believed to have formed the rocks of the leucocratic syenite facies (PBLS). The redox conditions during the later stages of the magma evolution are inferred to be relatively oxidising, thereby increasing the Eu^{3+}/Eu^{2+} ratio and negating the development of an Eu anomaly that would normally form under more reducing conditions. The effects of contamination during emplacement are minor and very localized.

The granites intruded at a later stage within the Bom Jardim complex show some of the characteristics of the leucogranites or so-called S-type granitoids of Chappell and White (1974). They show significant Eu anomalies. Many authors have suggested a simple crustal melting model for such granitoids. However, De Paolo (1981), Tindle and Pearce (1981) and Thompson et al. (1984) have put forward an alternative genetic model, involving fractional crystallization of a hydrous basic mantle derived magma, trapped in a relatively hot thick crust, which then undergoes progressive contamination by the sialic country rocks. The granites emplaced within the Bom Jardim complex have chondrite normalized incompatible element patterns very similar to those recorded for the metasedimentary country rocks (see figure 9.2). The author has interpreted the genesis of these granitic rocks as the result of partial melting whitin the continental crust during an episode of continental collision. The initial melt however was probably dispersed within the crust and unable to rise until the tectonic compressional regime gave way to one of distension (Vorma 1976). Such a scenario

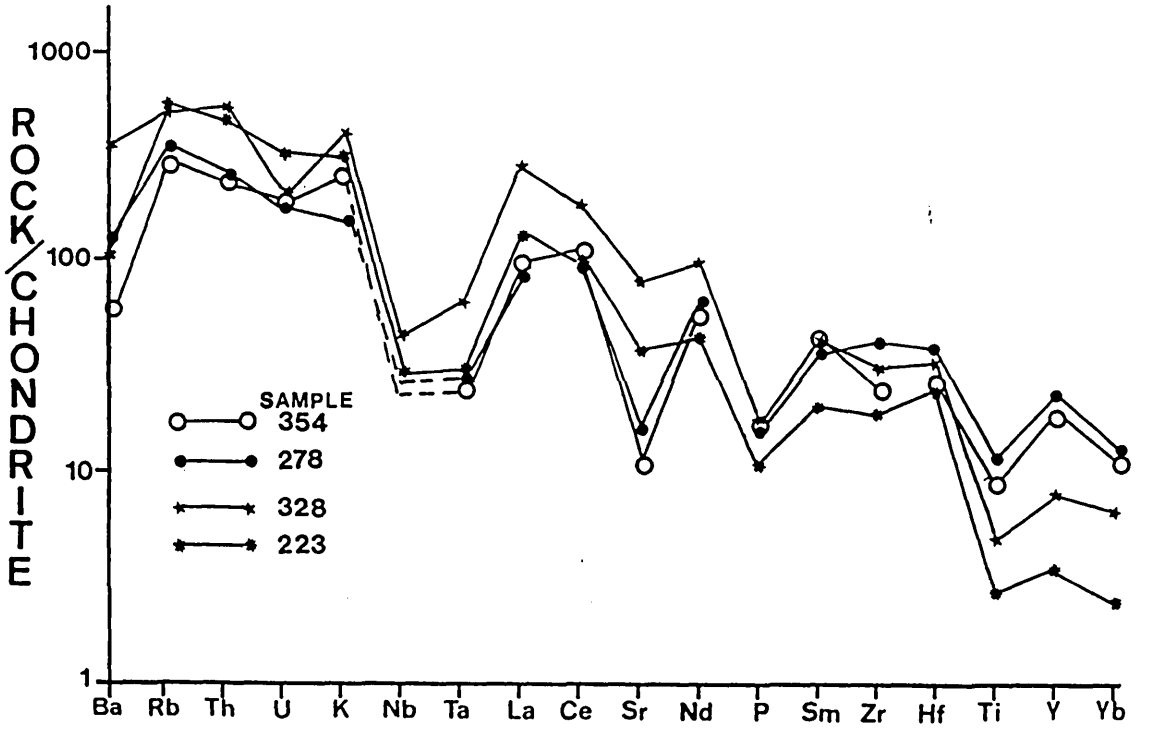


Figure 9.2 Chondrite-normalized incompatible-element plot comparing Bom Jardim granites (223 and 328) and country rocks (278 and 354).

could explain the collisional geochemical signature shown by this group of rocks. The determined age of 600Ma obtained for the monzonites and syenites of the Bom Jardim and Toritam complexes also agrees with the proposed tectonic evolution of the area. Jardim de Sa (1984) has estimated that the end of collisional regime in the Borborema province was approximately 600 Ma.

The fact that the granites are clearly later than the monzonite - syenite suite and their emplacement largely follows the trend of the strike slip faults associated with the Pernambuco lineament (extensional phase), suggests that the model proposed by Vorma (1976) appears to offer the best solution to the genesis and emplacement of the granites within the Bom Jardim complex.

REFERENCES

Albuquerque, C.A.R., 1973. Geochemistry of biotites from granitic rocks, northern Portugal. Geochem. et Cosmochim. Acta, 37; 1779-1802.

Al-Hashimi, A.R.K. and Brownlow, A.H., 1970. Cooper content of biotites from the Boulder batholith, Montana. Econ. Geology, 65; 985-982.

Almeida, F.F.M., Hasui, Y., Brito Neves, B.B. and Fuck, R.A., 1981. Brazilian structural provinces; an introduction. Earth Sci. Rev., 17; 1-29.

Almeida, F.F.M., Hasui, Y., Brito Neves, B.B. and Fuck, R.A., 1977. Provincias estruturais brasileiras. Atas do VIII Simp. Geol. Nordeste. p.363-391.

Almeida, F.F.M., Leonardos, O.H. and Valença, J., 1967. Granitic rocks of Northeast South America. In: Proceedings I.U.G.S. Symposium, Recife, pp.5-17.

Angel, M. and Riera, F., 1959. Report de la mission au Pernambouc. S.I. Bureau Minier Guyanais, Service Français de Cooperation Technique. 134p.

Arculus, R.J., 1987. The significance of source versus process in the tectonic controls of magma genesis. J. Volcanol. Geotherm. Res., 32; 1-12.

Armstrong, R.L., Taubeneck, W.H. and Hales, P.O., 1977. Rb-Sr and K-Ar geochemistry of Mesozoic granitic rocks and their Sr isotopic composition, Oregon, Washington and Idaho. Bull. Geol. Soc. of America, 88; 397-441.

Atherton, M.P. and Sanderson, L.M., 1985. The chemical variation and evolution of the Super-Units of the Coastal batholith. In: Magmatism at a plate edge- The Peruvian Andes. Pitcher, W.S., Atherton, M.P., Cobbing, E.J. and Beckinsale, A.W.(Eds.). Blackie Halsted, Glasgow. p.208-227.

Bacon, C.R., 1986. Magmatic inclusions in silic and intermediate volcanic rocks. J. Geophy. Research, 91; Nº B6 6091-6112.

Baker, P.E., 1982. Evolution and classification of orogenic volcanic rocks. In: Andesites. Thorpe, R.S. (Ed.). Wiley, London, p. 11-23.

Barberi, F., Innocenti, F., Ferrara, G., Keller, J. and

Villari, L., 1974. Evolution of the Eolian Arc volcanism. Earth Plant. Sci. Lett., 21; 269-276.

Batchelor, R.A. and Bowden, P. 1985. Petrogenetic interpretation of granitoid rock series using multicationic parameters. Chem. Geology, 48; 43-55.

Bateman, P.C. and Dodge, F.C.W., 1970. Variations of major chemical constituents across the Sierra Nevada batholith. Bull. Geol. Soc. of America, 81; 409-420.

Bateman, P.C., Clark, L., Huber, N.K., Moore, J.G. and Rinhehart, C.D., 1963. The Sierra Nevada batholith, a synthesis of recent work across the central part. U.S.G.S. Prof. Paper, 414D; 1-46.

Beckinsale, A.W., Sanchez-Fernandez, A.W., Brook, M., Cobbing, E. J., Taylor, W.P. and Moore, N.D., 1985. Rb-Sr whole-rock isochron and K-Ar age determinations for the Coastal batholith of Peru. In: Magmatism at a plate edge- The Peruvian Andes. Pitcher, W.S., Atherton, M.P., Cobbing, E.J. and Beckinsale, R.D. (Eds.). Blackie Hasted press, Glasgow. p.177-202.

Beckinsale, R.D., Suensilpong, S., Nakapadungrat, S. and Walsh, J.N., 1979. Geochronology and geochemistry of granite magmatism in Thailand in relation to a plate tectonic model. J. Geol. Soc. Lond., 136; 529-540.

Best, M.G. and Mercy, E.L., 1967. Composition and crystallization of mafic minerals in the Guadalupe igneous complex, California. The American Mineralogist, 52; 437-474.

Berthe, D., Choukroune, P. and Jegouzo, P., 1979. Orthogneiss, mylonite and non coaxial deformation of granites: The example of the South Armorican shear zone. J. Struct. Geol., 1, 1; 31-42.

Bertrand, J.M. and Caby, R., 1978. Geodynamic evolution of the Pan-African orogenic belt: a new interpretation of the Hoggar shield (Algerian Sahara). Geol. Runds., 67; 354-388.

Beurlen, H., 1988. Fazenda Esperança and Riacho da Posse: duas ocorrencias atipicas de Fe-Ti no estado de Pernambuco. Professor titular thesis, UFPE, Recife. 72p..

Black, R., 1980. Precambrian of West-Africa. Episodes, 4; 3-8.

Bloomer, S.H., Stern, R.J., Fisk, E. and Geschwind, C.H.,

1989. Shoshonitic volcanism in the northern Mariana arc 1. Mineralogic and major and trace element characteristics. J. Geophy. Research, 94, Nº B4; 4469-4496.

Brito Neves, B.B., 1983. O mapa geologico do nordeste oriental do Brasil, escala 1/1000000. Livre Docencia thesis. Inst. Geoc., Universidade de Sao Paulo. 177p..

Brito Neves, B.B., Sial, A.N., Rand, H. and Manso, V.A.V., 1982. The Pernambuco-Alagoas massif. Rev. Bras. Geoc., 12; 240-250.

Brito Neves, B.B., 1975. Regionalizaçao geotectonica do Precambrian Nordestino. Doctoral thesis, Universidade de Sao Paulo. 198p..

Brown, G.C., 1982. Calc-alkaline intrusive rocks; their diversity, evolution and relation to volcanic arcs. In: Andesites. Thorpe, R.S. (Ed.). Wiley London. p.437-461.

Brown, G.C., Cassidy, J., Locke, C.A., Plant, J. and Simpson, P.R., 1981. Caledonian plutonism in Britain : A summary. J. Geophy. Res., 86; 10502-10514.

Brown, G.C., 1981. Space and time in granite plutonism. Phil. Trans. R. Geo. Soc. London, A301; 321-336.

Burke, K. and Dewey, J.F., 1973. An outline of Precambrian plate development. In: Implications of continental drift to the earth sciences. Tarling, D.H. and Runcorn, S.K. (Eds.). 2, Academic Press. p. 1035-1044.

Caby, R., 1987. Precambrian terranes of Benin-Nigeria and Northeast Brazil and, the late Proterozoic South Atlantic fit. Abstract conference " Tectonothermal evolution of the west Africa orogens and circum-Atlantic terrane linkages". I.G.C.P, Project 233.

Caby, R., Bertrand, J.M. and Black, R., 1981. Pan-African closure and continental collision in the Hoggar-Iforas segment, central Sahara. In: Precambrian plate tectonics. Kroner, A. (Ed.). Elsevier, Amsterdam. p.407-434.

Caby,R., 1978. Paleodynamique d'une marge passive et d'une marge active au Precambrien Superieur: Leur collision dans la chaine Pan-African du Mali. Bull. Geol. Frac., 7; 857-862.

Chappell, B.W. and White, A.J.R., 1974. Two contrasting granite types. Pacific Geology, 8; 173-174.

Condie, K.C., 1973. Archean magmatism and crustal

thickening. Geol. Soc. Am. Bull., 43; 187-201.

Cook, N.D.J., 1988. Diorites and associated rocks in the Aglem complex at the Neck, northeastern Stewartisland, New Zealand: an example of magma mingling. Lithos, 21; 247-262.

Costa, A.C., Mendes, V.A., Rocha, D.E.G.A. and Andrade, D.A., 1979. Projeto extremo nordeste do Brasil. Relatorio final. 1, DNPM/CPRM (internal report).

Cox, K.G., Bell, J.D. and Pankhurst, R.J.,1979. The interpretation of igneous rocks. George Allen and Unwin, London. 450p..

Czamanske, G.K., Ishihara, S. and Atkin, S.A., 1981. Chemistry of rock-forming minerals of the Cretaceous-Paleocene batholith in southwestern Japan and implications of magma genesis. J. Geophy. Res., 86, Nº B11; 10431-10469.

Dantas, J.R.A. and Brito Neves, B.B., 1980. Mapa geologico do estado de Pernambuco-texto explicativo. DNPM/Minerios de Pernambuco, Recife. 112p..

Dantas, J.R.A., 1971. Levantamento dos estudos geologicos no Nordeste; resumo dos relatorios de graduaçao do curso de geologia da UFPE (1961-1970). Recife, DNPM (unpublished).

Da Silva Filho, A.F., 1989. Shoshonitic and ultrapotassic intrusive suites in the Pianco-Alto Brigida belt, Pernambuco state, Brazil. PhD thesis. University of London. 420p..

Da Silva Filho, A.F. and Guimaraes, I.P., 1989. Shoshonitic and ultrapotassic Proterozoic intrusive suites in the Pianco-Alto Brigida belt, NE Brazil; A transition from collision to post collision- related magmatism. J.Volc. Geother. Res. in press.

Da Silva Filho, A.F., Thompson, R.N. and Leat, P., 1987. Petrology of Terra Nova pluton, Brazil, and associated ultrapotassic dykes. Rev. Brasileira. Geoc., 7; 481-486.

Da Silva Filho, A. F. and Guimaraes, I.P., 1979. Petrologia e cadastramento das ocorrencias de Fe-Ti no municipio de Passira, Pernambuco. Atas do IX Symp. Geol. do Nordeste, Natal. 364-368.

Debon, F. and Le Fort, P., 1983. A chemical-mineralogical classification of common plutonic rocks and association. Trans. R. Soc. of Edinburgh: Earth Sciences, 73; 135-149.

Deer, W.A., Howie, R.A. and Zussman, J., 1980. An introduction to the rock forming minerals. Longman, London. 528p..

De La Roche, H., Leterrier, J., Grandclaude, P. and Marchall, M., 1980. A classification of volcanic and plutonic rocks using R_1R_2 diagrams and major element analyses - its relationships with current nomenclature. Chem. Geol., 29; 183-210.

De Paolo, D.J.,1981.A neodymium and strontium isotopic study of the Mesozoic calc-alkaline granitic batholith of the Sierra Nevada and Peninsular Ranges, California. J.Geophy. Res., 86; 10470-10488.

Dewey, J.F. and Burke, K.C., 1973. Tibetan, Variscan and Precambrian basement reactivation: products of continental collision. J. Geol. 81; 683-692.

Diddier, J., 1973. Granites and their enclaves. Elsevier Sci. Publ. Co. London. 393p..

Dodge, F.C.W., Smith, V.C. and Mays, R.E., 1969. Biotites from granitic rocks of the central Sierra Nevada batholith, California. J. Petrol., 10; 250-271.

Dodge, F.C.W., Papike, J.J. and Mays, R.E., 1968. Hornblendes from granitic rocks of the Sierra Nevada batholith, California. J. Petrology, 9; 378-410.

Drake, M.J. and Weill, D.F., 1975. Partition of Sr, Ba, Ca, Y, Eu^2, Eu^3 and other REE between plagioclase feldspar and magmatic liquid: an experimental study. Geochim. Cosmochim. Acta, 39; 687-712.

Drake, M.J., 1975. The oxidation state of europium as an indicator of oxygen fugacity. Geochim. Cosmochim. Acta, 39; 55-64.

Ernst, W.G., 1966. Synthesis and stability relations of ferrotremolite. Am. J Sci. 264; 37-65.

Ewart, A., 1982. The mineralogy and petrology of Tertiary-Recent orogenic volcanic rocks: with special reference to the andesite-basaltic range. In Andesites, Thorpe, R.S. (Ed.). Wiley, London. p.25-95.

Farina, M., Santos, E.J., Montenegro, C.B. and Zanini, L.F.P., 1981. Anortositos de Passira, Pernambuco. Atas do X Simp. Geol. Nordeste, Recife.

Foden, J.D. and Varne, R., 1980. The petrology and tectonic

setting of Quaternary-Recent volcanic centres of Lombok and Sumbawa, Sunda arc. Chem. Geology, 30; 201-226.

Fowler, M. B., 1988. Elemental evidence for crustal contamination of mantle-derived Caledonian syenite by metasediment anatexis and magma mixing. Chem. Geology, 69; 1-16.

Fowler, M.B., 1985. A geochemical and mineralogical investigation of the mobility of uranium and other lithophile elements during high-grade metamorphism. PhD thesis, Univ. London, 327p..

Gass, I.G., 1982. Upper Proterozoic (Pan-African) calc-alkaline magmatism in north-eastern Africa and Arabia. In Andesites, Thorpe, R.S.(Ed.), Wiley London. 591-609.

Gill, J.B. and Whelan, P., 1989. Early rifting of an oceanic island arc (Fiji), produced shoshonitic to tholeiitic basalts. J. Geophy. Res., 94; 4561-4578.

Gill, J.B., 1981. Orogenic andesites and plate tectonics. Spring-Verlag, Berlin, 390p..

Gill, J.B., 1978. Role of trace element partition coefficients in models of andesites genesis. Geochim. Cosm. Acta, 42; 709-724.

Green, D.H., 1976. Experimental testing of equilibrium partial melting of peridotite under water-saturated, high pressure conditions. Can. Mineral., 14; 255-268.

Green, D.H., 1973. Experimental melting studies on a model upper-mantle composition at high pressure under water-saturated and water-undersaturated conditions. Earth Planet. Sci. Lett., 19; 37-53.

Gromet, L.P. and Silver, L.T., 1983. Rare earth element distributions among minerals in a granodiorite and their petrogenetic implications. Geochim. Cosmoch. Acta, 47; 925-939.

Hammarstron, J.M. and Zen, E-An, 1986. Aluminium in hornblende: an empirical igneous geobarometer. Am. Mineral., 71; 1297-1313.

Hanson, G.N., 1980. Rare earth elements in petrogenetic studies of igneous systems. Ann. Rev. Earth Planet. Sci. Lett., 8; 371-406.

Hanson, G.N., 1978. The application of trace elements to the petrogenesis of igneous rocks of granitic composition.

Earth Planet. Sci. Lett., 38; 26-46.

Harris, N.B.W., Pearce, J.A. and Tindle, A.G., 1986. Geochemical characteristics of Collision zone magmatism. In: Collision Tectonics, Coward, M.P. and Ries, A.C. (Eds). Geol. Soc. London Spec. Public., Nº 19; 67-81.

Harris, N.B.W., Pearce, J.A. and Tindle, A.G.,1983. Geochemical characteristics of collision magmatism. Presented at R. Soc. London, meeting on Collision tectonics, London, April 26.

Hart, S.R. and Allegre, C.J., 1980. Trace element constraints on magma genesis. In: Physics of Magmatic Processes, Hargraves, R.B. (Ed), Princeton Univerty Press. p.121-159.

Helz, R.T., 1982. Phase relations and compositions of amphiboles produced in studies of melting behaviour of rocks. Min. Soc. Am. Rev. Min., 9B; 279-346.

Helz, R.T., 1973. Phase relations of basalts in their melt range at pH_2O = 5 Kb as a function of oxygen fugacity. Part I, Mafic Phases. J. Petrol., 14, 249-302.

Henderson, P., 1982. Inorganic geochemistry. Pergamon, Oxford, 353p..

Holliester, L.S., Grisson, G.C., Peters, E.K., Stowell, H.H. and Sisson, V.B., 1987. Am. Mineral., 72; 231-239.

Honza, E. and Tamaki, K., 1985. The Bonin arc. In: The ocean basis and margins, Nairn, F., Stehli, F. and Uyed, S. (Eds), 7A Pacific, Plenum, New York, p.459-502.

Hutton, D.H.W., 1987. Granite emplacement mechanism and tectonic controls. Inferences from deformation studies. Trans. R. Soc. Edinburgh, 79, part 2-3; 245-256.

Ishihara, S., 1977. The magnetite-series and ilmenite-series granitic rocks. Min. Geol., 27; 293-305.

Irving, A. J., 1978. A review of experimental studies of crystal/liquid trace element partitioning. Geochim. Cosmochim. Acta, 42; 743-770.

Jakes, P. and White, A.J.R., 1972. Major and trace element abundances in volcanic rocks of orogenic areas. Bull. Geol. Soc. Am., 83; 29-40.

Jardim de Sa, E.F., Macedo, M.H.F., Torres, H.H.F. and Kawashita, K., 1988. Geocronology of metaplutonics and the evolution of supracrustal belts in the Borborema province,

NE Brazil. Anais VII Congresso Latino Americano de Geologia, Belem, Para, 1; 49-62.

Jardim de Sa, E.F., Macedo, M.H.F., Legrand, J.M., McReath, I., Galindo, A.C. and Sa, J.M., 1987. Proterozoic granitoids in a policyclic setting; the Serido region, Northeast Brazil. In: I.S.G.A.M., extended abstract, Salvador, Brazil, p.103-110.

Jardim de Sa, E.F., 1984. A evoluçao Proterozoica da provincia Borborema. Anais Simp. Geol. do Nordeste, Natal, p.297-316.

Johan, Z., 1980. Mineralisation liees aux granitoides porphyres cupriferes dans leuer contexte magmatique. BRGM Mem. Nº 99; 326p..

Jones, A.P., 1984. Mafic silicates from the nepheline syenites of the Motzfeldt centre, South Greenland. Min. Magazine, 48; 1-12.

Kille, I., 1987. The minor Tertiary intrusions around Loch Scridain, Isle of Mull. PhD thesis, University of London, 364p..

Kistler, R.W. and Peterman, Z.E., 1973. Variation in Sr, Rb, K, Na, and initial Sr^{87}/Sr^{86} in Mesozoic granitic rocks and intruded wall rocks in central California. Geol. Soc. Am. Bull., 84; 3489-3512.

Kroner, A., 1982. Archaean to early Proterozoic tectonics and crustal evolution: a review. Rev. Bras. Geoc., 12, Nº 1-3; 15-31.

Kubach, I. and Wolgang, T., 1984. Sc, Y, La-Lu rare earth elements. Gmelin handbook of inorganic chemistry. A8, Nº 39, Spring-Verlag, Berlin.p.5-11.

Kumar, S.C., 1988. Microgranular enclaves in granitoids: agents of magma mixing. J. South. Asian Earth Sci., 2, Nº3/4; 109-121.

Kushiro, I., 1972. Effects of water on the composition of magmas formed at high pressure. J. Petrol., 13; 311-314.

Lambert, R.S.J. and Holland, J.G., 1974. Yttrium geochemistry applied to petrogenesis utilizing calcium-yttrium relationships in minerals and rocks. Geoch. Cosmochim. Acta, 38; 1393-1414.

Lameyre, J. and Bowden, P., 1982. Plutonic rock type series: discrimination of various granitoid series and

related rocks. J. Volcan. Geotherm. Res., 14, 169-186.

Leake, B.E., 1965. The relation between tetrahedral aluminum and the maximum possible octahedral aluminum in natural calciferous amphiboles. Am Mineralog., 50; 843-851.

Leake, B.E., 1978. Nomenclature of amphiboles. Canad. Mineralog., 16; 501-520.

La Maitre, R.W., 1981. GENMIX- a generalised petrological mixing model program. Comput. Geosc., 7; 229-247.

Leat, P., Thompson, R.N., Morrison, M.A., Hendry, G.L. and Trayhorn, S., 1986. Geodynamic significance of Post-Variscan intrusive and extrusive potassic magmatism in SW England. Trans. R. Soc. Edingurgh, 77; 349-360.

Loiselle, M.C. and Wones, D.R., 1979. Characteristics and origin of anorogenic granites. Geol. Soc. Am. Abstracts with Programs, 7; 468.

Long, P.E. and Luth, W.C., 1986. Origin of K feldspar megacrysts in granitic rocks: implications of a partitioning model of barium. Am. Mineralogist, 71; 367-375.

MacCarthy, T.S. and Hasty, R.A., 1976. Trace element distribution patterns and their relationship to the crystallisation of granitic melts. Geochem. Cosm. Acta, 40; 1351-1358.

Mackenzie, W.S., Donaldson, C.H and Guilford, C., 1982. Atlas of igneous rocks and their textures. Longman, Harlow, 148p..

Mahood, G. and Hildreth, W., 1983. Large partition coefficients for trace elements in high-silica rhyolites. Geochim. Cosm. Acta, 47; 11-30.

Maranhao, R.J.L., 1983. Projeto: Pesquisa regional para identificaçao de granitos para fins de utilizaçao como rochas ornamentais. Minerios de Pernambuco, internal report.

Maranhao, R.J.L., 1980. Relatorio de pesquisa da area de Bom Jardim-PE. Processo 840190/78 DNPM, Uniao de marmores e granitos do NE.

Martin, H., 1987. Archean and modern granitoids as indicators of changes in geodynamic processes. I.S.G.A.M. extended abstract, Salvador. p.23-24.

Mason, G.H., 1985. The mineralogy and textures of the

Coastal batholith, Peru. In Magmatism at a plate edge-The Peruvian Andes, Pitcher, W.S., Atherton, M.P., Cobbing, E.J. and Beckinsale, R.D. (Eds). Blackie Halsted Press, Glasgow, p.156-166.

Mason, B.O., 1978. Compositional variations in Ferromagnesian minerals from porphyry copper-generating and Barren intrusions of the Western Highlands, Papua-New Guinea. Econ. Geol., 73; 878-890.

Mysen, B.O., 1979. Trace-element partitioning between garnet peridotite minerals and water-rich vapor: experimental data from 5 to 30 kbar. Amer. Mineral.. 64; 274-287.

McMurry, J., Long, L.E. and Sial, A.N., 1987. Petrology and isotopic systematics of magma/crystal mushes: some porphyritic granitoids of northeastern Brazil. I.S.G.A.M. extended abstract, Salvador. p.173-176.

Mello, A.A., Costa, A.C., Mendes, V.A. and Hama, M., 1977. Elementos tectono-estruturais do nordeste meridional. Parte dos estados da Paraiba e Pernambuco. Atas do VIII Simpos. Geol. do Nordeste, Campina Grande, p.346-367.

Mello, A.A., 1972. Fazenda Nova: um exemplo de "modelo metassomatico". Revista Assoc. Geol. Pernambuco, Nº 1; 51-60.

Mello, A.A., 1971. Geologia e petrologia da regiao de Fazenda Nova, Pernambuco. Doctoral thesis, Inst. Geoc. Universidade de Sao Paulo, 101p.

Mello, A.A. and Mello, Z.F., 1969. Sienitizaçao de rocha basica em Toritama, Pernambuco. Anais do XXIII Congres. Brasil. Geol., Salvador, p.148-157.

Michot, P., 1961. Struktur der mesoperthite. NJMA 96; 213-216.

Miyashiro, A. and Shido, F., 1975. Tholeiitic and calc-alkalic series in relation to the behaviours of Ti, V, Cr and Ni. Am. J. Sci. 275; 265-277.

Mitchell, R.H. and Platt, R.G.,1978. Mafic mineralogy of ferroaugite syenite from the Coldwell alkaline complex, Ontario, Canada. J. Petrol., 19; 627-651.

Moore, N.D. and Hopson, C., 1961. The Independence dyke swarm in eastern California. Am. J. Sci., 259; 241-259.

Morrison, G.W., 1980. Characteristics and tectonic setting

of the shoshonite rock association. Lithos, 13; 97-108.
Morrice, M., Jezek, P.A., Gill, J.B., Whitford, D.J. and Monoarfa, M., 1983. An introduction to the Sangihe arc: volcanism accompanying arc-arc collision in the Molucca sea, Indonesia. J. Volc. Geoth. Res., 19; 135-165.
Nakamura, N., 1974. Determination of REE, Ba, Fe, Mg, Na and K in carbonaceous and ordinary chondrites. Geochim. Cosm. Acta, 38; 757-775.
Nash, W.P. and Crecraft, H.R., 1985. Partition coefficients for trace elements in silic magmas. Geochim. Cosm. Acta, 49; 2309-2322.
Nedelec, A. and Paquet, J., 1981. Biotite melting in high-grade metamorphic gneisses from the Haut Allier (French massif Central). Contrib. Mineral. Petrol., 77; 1-10.
Nockolds, S.R., 1947. The relation between chemical composition and paragenesis in the biotite micas of igneous rocks. American J. Sci., 245; 401p..
Noyes, H.J., Frey, F.A. and Wones, D.R., 1983. A tale of two plutons: geochemical evidence bearing on the origin and differentiation of the Red Lake and Eagle Peak plutons, central Sierra Nevada, California. J. Geol., 91; 487-509.
Olade, M.A., 1976. Geochemical evolution of copper-bearing granitic rocks of Guichon Creek batholith, British Columbia, Canada. Can. J. Erth Sci., 13; 199-209.
Pagel, M. and Leterrier, J., 1980. The subalkaline potassic magmatism of the Ballons massif (S.Voges. France): shoshonitic affinity. Lithos, 13; 1-10.
Parker, R. j., 1982. Single pass major element X-ray fluorescence analysis of silicate rock samples, using a Philips 1212 spectrometer. X-ray Spectrometry, 11; 100-108.
Parsons, I., 1981. The Klokken gabbro-syenite complex, S. Greenland: quantitative interpretation of mineral chemistry. J. Petrol., 22; 233-260.
Parsons, I., 1978. Feldspar and fluids in cooling plutons. Min. Mag., 42; 1-27.
Peacock, M.A., 1931. Classification of igneous rock series. J. Geol. 39; 54-67.
Pearce, N.J.G., 1988. The petrology and geochemistry of the Igaliho dyke swarm, South Greenland. Unpublished PhD thesis, Duhram University.

Pearce, J.A., Harris, N.B.W. and Tindle, A.G., 1984. Trace element discrimination diagrams for the tectonic interpretation of granitic rocks. J. Petrol., 25; 956-983.

Pearce, J.A., 1982. Trace element characteristics of lavas from destructive plate boundaries. In: Andesites, Thorpe, R.S. (ed.), Wiley, London.p. 525-548.

Pearce, J.A. and Norry, M.J., 1979. Petrogenetic implications of Ti, Zr, Y and Nb variations in volcanic rocks. Contrib. Mineral. Petrol., 69; 33-47.

Peccerillo, A. and Taylor, S.R., 1976. Geochemistry of Eocene calc-alkaline volcanic rocks from the Kastamanou area, northern Turkey. Contrib. Mineral. Petrol., 58; 63-81.

Pitcher, W.S., 1985. A multiple and composite batholith. In Magmatism at a plate edge-The Peruvian Andes, Pitcher, W.S., Atherton, M.P, Cobbing, E.J. and Beckinsale, R.D. (Eds), Blackie Halsted Press, Glasgow. p. 93-101.

Pitcher, W.S. and Bussel, M.A., 1985. Andean dyke swarms: andesite in synplutonic relationship with tonalite. In: Magmatism at a plate edge-The Peruvian Andes, Pitcher, W.S., Atherton, M.P., Cobbing, E.J. and Beckinsale, R.D. (Eds). Blakie Halsted Press, Glasgow. p.102-107.

Pitcher, W.S., 1983. Granite: typology, geological environment and melting relationships In: Migmatites, Melting and Metamorphism. Atherton, M.P. and Gribble, C.D. (Eds). Shiva publishing Ltd, Cheshire, p.277-285.

Pitcher, W.S., 1982. Granite type and tectonic environment. In: Mountain Building Processes. Hsu, K. (Ed), Academic Press. p.19-40.

Pitcher, W.S., 1979. The nature, ascent and emplacement of granitic magmas. J. Geol. Soc. Lond., 136; 627-662.

Pitcher, W.S. and Read, H.H., 1960. Early transverse dykes in the main Donegal granite. Geol. Mag., 97; 53-61.

Raase, P., 1974. Al and Ti contents of hornblende, indicators of pressure and temperature of regional metamorphism. Contrib. Mineral. Petrol., 45; 231-236.

Read, H.H., 1957. The granite controversy. Murby, London. 430p..

Roddick, J.A., and Armstrong, J.E., 1959. Relict dykes in the Coast mountains near Vancouver, B.C.. J. Geol. Chicago,

67; 603-613.

Rogers, J.J. and Greenberg, J.K., 1981. Trace elements in continental margin magmatism. Part III, Alkali granites and their relationship to cratonization. Bull. Geol. Soc. Am., 92; 6-9.

Rutter, M.J., 1985. Tertiary magmatism in northern Sardinia. PhD thesis, University of London, 322p..

Santos, E.J., Coutinho, M.G.N., Costa, M.P.A. and Ramalho, R., 1984. A regiao de dobramentos do nordeste e a bacia do Parnaiba, incluindo o craton de Sao Luis e as bacias marginais. In: Geologia do Brasil, Schobbenhaus, C., Almeida Campos,D., Derze, G.R. and Asmus, H.E. (Eds). DNPM, Brasilia. p. 131-189.

Santos, E.J., 1977. O modelo e evoluçao Precambriana da regiao de Arcoverde. Anais Simp. Geol. Nordeste, Campina Grande. p. 225-245.

Saunders, A.D., Tarney, J. and Weaver, S.D., 1980. Transverse geochemical variations across the Antartic peninsula; implications for the genesis of calc-akcaline magmas. Eart. Planet. Sci. Lett., 46; 344-360.

Sawka, W.N., 1988. REE and trace element variations in accessory minerals and hornblende from the strongly zoned McMurry Meadows pluton, California. Trans. R. Soc. Edinburgh: Earth Sci., 79; 157-168.

Sawkins, F.J., 1984. Metal deposits in relation to plate tectonics. Serie: Mineral and rocks, Spring Verlag, Chicago. p.163-166.

Shackleton, R.M., 1986. Precambrian collision tectonics in Africa. In: Collision tectonics, Coward, M.P. and Ries, A.C. (Eds.). Geol. Soc. London, Special Publ., Nº 17, p. 329-352.

Shand, S.J. 1951. The study of rock. Thomas Murby and Co., London. 236p..

Shibata, K. and Ishihara, S., 1979. Initial Sr87/Sr86 ratios of plutonic rocks from Japan. Contrib. Mineral. Petrol., 70; 381-390.

Sial, A.N.,1987. Granitic rocks of northeast Brazil. I.S.G.A.M., extended abstract, Salvador. p.61-69.

Sial, A.N., 1986. Granite-types in northeast Brazil: current knowledge. Rev. Bras.Geoc., 16; 54-72.

Sial, A.N. and Menor, E., 1973. Eulysite and associated mineralization of Fe-Ti, Passira district, Pernambuco, Brazil. In: P. Morin., Les Roches Plutoniques dans leurs Rapports avec les Gites Mineraux, Masson et Cie., Paris. p.239..

Silva Filho, M., Bonfin, L.F.C., Santos, R.A., Rodrigues, T.N. and Braz Filho, P.A., 1981. Projeto Caninde do Sao Francisco. Mapa geologico integrado 1/100.000. CPRM/DNPM, Salvador (unpublished).

Smith, J.V., 1974. Feldspar minerals, vol 2, chemical and textural properties. Springer Verlag, Berlin. 690p..

Sial, A.N. and Menor, E., 1969. Geologia de meia quadricula sul de Taquaritinga do Norte. Inst. Geoc. Univers. Federal Pernambuco, Recife, 1; 49p..

Smith, J.V., 1972. High-potassium intrusives from southeastern Papua New-Guinea. Contrib. Mineral. Petrol., 34; 167-176.

Spear, F.S., 1981. Ca-amphibole composition as a function of temperature, fluid pressure and oxygen fugacity in a basaltic system. Yearb. Carnegie. Inst., 75; 775-779.

Speer, J.A., 1980. The actinide orthosilicates. In: Reviews in Mineralogy, Ribbe, P.H. (Ed). Mineral. Soc. Am., 5; 113-132.

Spry, A., 1969. Metamorphic textures. Pergamon Press, Oxford.

Streckeisen, A., 1976. To each plutonic rock its proper name. Earth Sci. Rev., 12; 1-33.

Staaz, M.H., Adams, J.S. and Wahlberg (1976). Brown, yellow, orange, and grennish-black thorites from the Seerie pegmatite, Colorado. J. Res. U.S. Geol. Survey, 4; 575-582

Stephenson, D.C.N. and Upton, B.G.J., 1982. Ferromagnesian silicates in a differentiated alkaline complex: Kungnat Fjeld, South Greenland. Mineral. Mag., 46; 283-300.

Stephenson, D.C.N., 1972. Alkaline clinopyroxenes from nepheline syenites of the S. Qoroq centre, S. Greenland. Lithos, 5; 187-201.

Suarez, M., Herve, M. and Puig, A., 1985. Basic magmas in the early evolution of the southernmost Patagonian batholith, Chile. Geolg. Rundsch. 74/2; 337-342.

Sylvester, A.G., Miller, C.F. and Nelson, A., 1978.

Monzonites of the White-Inyo Range, California and their relation to the calc-alkalic Sierra Nevada batholith. Bull. Geol. Soc. Am., 89; 1677-1687.

Tarney, J. and Saunders, A.D., 1979. Trace element constraints on the origin of cordilleran batholiths. In: Origin of granite batholiths, Atherton, M.P. and Tarney, J. (Eds), Shiva Publishing Ltd., Cheshire. p. 90-105.

Taylor, S.R. and MacLennan, S.M., 1985. The continental crust: its composition and evolution. Blackwell, Oxford, 312p..

Taylor, H.P. and Silver, L.T., 1978. Oxygen isotope relationships in plutonic igneous rocks of the Peninsular Ranges batholith, southern and Baja California. USGS open file reprt Nº 78-701.

Thompson, R.N. and Fowler, M., 1986. Subduction-related shoshonite magmatism: a study of Siluro-Ordovician syenites from the Scottish Caledonides. Contrib. Mineral. Petrol. 94; 507-522.

Thompson, R.N., Morrison, M.A., Hendry, G.L. and Parry, S.J., 1984. An assessment of the relative roles of crust and mantle in magma genesis: an elemental approach. In: The relative contributions of mantle, oceanic crust and continental crust to magma genesis, Moorbath, S., Thompson, R.N. and Oxburgh, E.R.(Eds). Philos. Trans. R. Soc. London, A310; 549-589.

Thompson, R.N., 1982. Magmatism of the British Tertiary volcanic province. Scott. J. Geol., 18; 49-107.

Thirlwall, M.F., 1982. Nd-Sr isotopes across a Caledonian calc-alkaline volcanic arc: implications for source materials. Earth Planet. Sci. Lett., 58; 27-50.

Thorpe, R.S., 1987. Permian K-rich volcanic rocks of Devon: petrogenesis, tectonic setting and geological significance. Trans. R. Soc. Edinburgh: Earth Sci., 77; 361-366.

Thornton, C.P. and Tuttle, O.F., 1969. Chemistry of igneous rocks. I. Differentiation Index. Am. J. Sci., 258; 664-684.

Tindle, A.G. and Pearce, J.A., 1983. Assimilation and partial melting of continental crust: evidence from mineralogy and geochemistry of autholiths and xenoliths. Lithos, 16; 185-202.

Toth, M., 1987. Petrology and origin of the Bitterroot lobe

of the Idaho batholith. In: Geology of the Blue Mountains region of Oregon, Idaho, and Washington: The Idaho batholith and its border zone, U.S. Geol. Surv. Prof. Paper, 1436; 9-36.

Ussami, N., Karner,G. and Bott, M.H.P., 1986. Crustal detachment during S. Atlantic rifting and formation of Tucano-Gabon basin system. Nature, 322; 629-632.

Veronesse, V., 1985. Projeto ferro titanado de Floresta, Pe. Convenio RADAM Brasil-Metalogenia Salvador/Minerios de Pernambuco. Internal Report.

Vernon, R.H., Etheridge, M.A. and Wall, V.J., 1988. Shape and microstructure of microgranitoid enclaves: indicators of magma mingling and flow. Lithos, 22; 1-11.

Vernon. R.H., 1984. Microgranitoid enclaves in granites-globules of hybrid magma quenched in a plutonic environment. Nature, 309; 438-439.

Vernon, R.H., 1983. Restites, xenoliths and microgranitoid enclaves in granites. J. Proc. R. Soc. N.S.W. 116, 77-103.

Villemant, B., Jaffrezic, H., Joron, J.L. and Treuil, M. 1981. Distribution coefficients of major and trace elements, fractional crystallisation in the alkali basalt series of Chaine des Puys (Massif Central, France). Geochim. Cosm. Acta, 45; 1997-2016.

Vorma, A.1976. On the petrochemistry of rapakivi granites with special reference to the Laitila massif, southwestern Finland. Geol. Surv. Finland. 285; 98p..

Watson, E.B., 1976. Two-liquid partition coefficients: experimental data and geochemical implications. Contrib. Mineral. Petrol., 79; 252-257.

White, A.J.R. and Chappell, B.W., 1977. Ultrametamorphism and granitoid genesis. Tectonophysics, 43; 7-22.

Wiebe, R.A., 1980. Anorthositic magmas and the origin of Proterozoic anorthosite massifs. Nature, 286; 564-567.

Williams, C.T. and Wall, F., 1988. An INAA scheme for the routine determination of 27 elements in geological and archaelogical samples. BAR volume on "Neutron activation and ICP/DCP analyses in Archaelogy".

Wilson, M., 1988. Igneous petrogenesis. Unwin Hyman, London, 466p..

Wilson, J.T., 1968. Static or mobile earth: the current

scientific revolution. Proc. Am. Philos. Soc., 112; 309-320.

Winchester, J.A. and Floyd, P.A., 1977. Geochemical discrimination of different magma series and their products using immobile elements. Chem. Geol. 20; 325-343.

Wormer, G., Bensen, J.M., Duchateau, N., Gijbels, R. and Schimincke, H.V., 1983. Trace element abundances and mineral/melt distribution coefficients in phonolites from the Laacher See volcano (Germany). Contrib. Mineral. Petrol., 84; 152-173.

Wright, J.B., 1969. A simple alkalinity ratio and its application to questions of non-orogenic granite genesis. Geol. Mag. 20; 325-343.

Wyllie, P.J., 1983. Experimental and thermal constraints on the deepseated parentage of some granitoid magmas in subduction zones. In: Migmatites, melting and metamorphism, Atherton, M.P. and Gribble, C.D. (Eds). Shiva, Orpington. p.12-26.

Wyllie, P.J., 1981. Experimental petrology of subduction, andesites, and batholiths. Trans. Geol. S. Africa, 84; 281-291.

Wyllie, P.J., 1979. Magmas and volatile componentes. Amer. Mineral., 64; 469-500.

Wyllie, P.J., Cox, K.G. and Briggar, G.M., 1962. The habit of apatite in synthetic systems and igneous rocks. J. Petrol., 3 Nº2; 238-243.

Zhou, J.X., 1987. An occurrence of shoshonites near Kilmelford in the Scottish Caledonides and its tectonic implications. J. Geol. Soc. London, 144; 699-706.

Zhou, J.X., 1985. Geochemistry of the Kilmelford intrusives west Scotland in relation of the Caledonian orogeny. PhD thesis, University of London, 396p..

APPENDIX A

ANALYTICAL TECHNIQUES

A.1 WHOLE ROCK CHEMICAL ANALYSES

A.1.1 Sample preparation

A mechanical splitter was used to remove weathered surfaces from the rock samples, and they were then passed through a steel jaw crusher to reduce the size to about 1-2 cm chips. Inter-sample contamination was minimised by crushing rocks of similar bulk composition together, and by thorough cleaning of the jaw crusher with alcohol between samples. The samples were quartered, and representative portions of the crushed rock were powdered in a tema mill to a grain size of less than 200 mesh. Most of the samples were prepared using a tungsten carbide mill, as suitable grain sizes could be produced in about 30 seconds. However, significant Co and Ta contamination can be produced using a tungsten carbide mill (Rutter, 1985). Those samples which were analysed for Ta were ground in an agate tema mill.

A.1.2 Major elements analyses

The major elements were determined by inductively coupled plasma atomic emission spectometry (ICP-AES) using an ARL 3400C instrument, following the method of Watkins (pers. comm.). The analyses were done at the Department of Geology, Imperial College.

The method used was as follows: Exactly 0.2500g of sample powder (dried at 110°C) was thoroughly mixed with exactly 0.7500g of Spectroflux 100B (80% $LiBO_2$, 20% $Li_2B_4O_7$) (dried at 450°C). The mixture was transferred to a graphite crucible and fused at 1000°C for 20 minutes in an electric muffle furnace. The resulting melt was shattered by pouring into a 400 ml plastic beaker containing a

solution of 25 ml 2N HNO_3 and 150ml of deionised water, and dissolved by stirring with a magnetic stirrer for 30 minutes. Care was taken to ensure that the fused mixture was completely transferred to the nitric acid solution. The solution was diluted to 250 ml and, in order to remove any graphite particles, the solution was filtered into a plastic bottle. The bottles were then sealed using a piece of plastic placed under the cap. This solution is designated solution P.

Ten international reference materials were analysed with each batch of samples, these acting as calibration solutions and, a further reference material was analysed at regular intervals throughout the procedure to act as a monitor for instrumental drift. Blank solutions, in-house reference materials and duplicate sample preparations were used to monitor the accuracy of the determinations and 30 unknown samples were analysed in each batch. The data produced was processed using a computer programme (Kille, 1987). This programme corrects every reading with respect to a chosen drift value, thus compensating for long term machine drift, while short term machine drift is compensated by normalising each data set to an average Li value. A calibration line is set up using a group of standards, which correlates the mV output for a particular element to its recommended concentration. This line is then used to calculate the concentration of the element in the unknown samples. One duplicate and one in-house reference material were analysed with each group of eight unknown samples to check preparation and accuracy respectively. Tables A.1 and A.2 show the precision and accuracy of major element analyses by ICP-AES.

A.1.3 Trace element analysis

A.1.3.1 Ba, Cr, Cu, Ni, Sr, V, Zr, Pb, Y and Sc (and Rb)

Ba, Cr, Cu, Ni, Sr, V and Zr were analysed by ICP-AES simultaneously with the major elements. Their concentration was calculated using the same method already discussed in the previous section. Tables A.3 and A.4 show

the precision and accuracy of trace elements by ICP-AES. Y and Sc were analysed using solution P, on a Phil ips PV8060 ICP emission spectrometer at the Geology Department, Royal Holloway and Bedford New College.

The concentration of the same 7 elements plus Rb and Pb were determined using a Philips PW 1400 fully automated XRF spectometer at the Department of Geosciences, Durham University, using a rhodium tube operating at 80 kV and 35 mA. The data reduction was done using the programme "K-factor" (Pearce, 1988). The briquettes were prepared by mixing about 5.0g of dried (110^{o}C) sample powder with 6-8 drops of 2% polyvinyl alcohol (PVA) solution. Boric acid was used to form the supporting wall and backing of the briquettes, which were pressed under a hydraulic press at a pressure of 8 tons per square inch for 30 seconds. The briquettes formed were dried overnight at 50^{o}C before the analysis. Comparison between results obtained by XRF and ICP-AES can be seen in table A.5.

A.1.3.2 Rb analysis

Rb was determined in the study samples using an atomic absorption spectophotometer, Perkin-Elmer model 272, operating in the flame emission mode. 10.0 ml of solution P was mixed with 1.00ml of a 10000 ppm solution of Cs (as $CsNO_3$ in 0.2N HNO_3) in a 15ml glass beaker. The $CsNO_3$ solution was used as a radiation buffer solution. The machine was calibrated using 3 international standards. In-house reference materials and duplicate preparations were used to monitor the accuracy of the technique. Comparisons between Rb results from XRF and flame emission are shown in table A.6.

A.1.3.3 Nb analysis, by XRF.

Nb was analysed using a Phi lips PW1212 semi-automated XRF spectrometer at the Department of Geology, Imperial College, using a tungsten tube operating at 60 kV and 32mA. The data was reduced using programmes "TRANS and

PTRAC" (Parker, 1979).

A.1.3.4 REE and Y analysed by ICP-AES.

The REE and Y were analysed at the Geology Department, Royal Holloway and Bedford New College, using a Phi lips PV 8060 ICP emission spectometer.

The method used was as follows: 0.500g rock powder (dried at 110°C) was thoroughly mixed with 1.500g of lithium metaborate, $LiBO_2$, and fused in a platinum dish in an electric muffle furnace at 1000°C for 30 minutes. After cooling, the dish was placed in a 250 ml glass beaker containing a mixture of 70 ml 2N HCl and 40 ml of deionised water, and stirred magnetically for 1 hour to dissolve the glass fusion bead. This solution was loaded onto a glass chromatography column which contained 30 ml of Bio-Rad AG50W-X8 cation exchange resin, 200-400 mesh. Unwanted elements were eluted from the column using 200 ml 1.75N HCl followed by 200 ml 1.75N HNO_3. The REE and Y were eluted from the column using 100ml of 6N HNO_3 followed by 8N HNO_3. This eluate was carefully evaporated to dryness on a hot plate. Prior to analysis by ICP-AES, the evaporated salts were dissolved in 5.0 ml of 1.5N HNO_3. Comparison between REE results obtained by INAA and ICP-AES for 3 samples and also for an international reference material can be seen in table A.7.

A.1.3.5 REE, Sc, Hf, Ta, Th, U and Cs by INAA

The concentrations of the above elements were determined by instrumental neutron activation analysis (INAA), following the scheme of Williams and Wall (1988). The samples were irradiated for 5 days at Imperial College Reactor Center, Silwood Park. The counting and calculations were done at the British Museum (Natural History) using two counts each on an intrinsic Ge planar detector and a coaxial Ge(Li) detector, and a Nuclear Data ND6620 system.

The samples are prepared by accurately weighing

about 80mg (previously dried at 110^{o}C) directly into high purity polythene ampoules. The flux monitors were prepared by accurately micropipetting and weighing 50 ul of a standard solution of gold and sodium (20ppm Au, 20000ppm Na) onto a filter paper disc attached to a self adhesive paper. The filter papers were left to dry overnight and then a second label was placed on the top. Seven unknown samples, two in-house reference materials and three primary standards were analysed in each batch. The flux monitors were placed under each specimen and all twelve were loaded into a plastic tube which was then irradiated. The primary standards were two of STD 9 (for REEs and U) and STD 8 (for transition metals and other elements). Table A.8 shows the accuracy by INAA of the analysis of one international and two in-house reference materials. Comparisons between REE analysis by INAA and ICP-AES are shown in table A.7.

A.2 MINERAL ANALYSES

The majority of mineral analyses were performed on a Cambridge Instruments Microscan 5 electron microprobe, fitted with a Link System energy dispersive detector. Operating conditions were 15kV and a specimen current of 4.0 mA. Counting times of 100 seconds were used, with the electron beam focussed into a spot. Metal oxides, pure metals and end-member minerals were used in the calibration. Accuracy and precision were routinely checked by reference to standard minerals, and the results for 7 analyses of jadeite and olivine are given in table A.9.

Th-REE rich sphenes and monazites were analysed at the British Museum (Natural History) using a Cambridge Instruments Microscan 9 electron probe using a wavelength dispersive technique.

A.3 Rb-Sr ISOTOPIC METHOD.

The Rb-Sr isotopic determinations were performed at the Isotope Laboratory of the Geology Department, Royal Holloway and Bedford New College.

The separated mineral phases (biotite and clinopyroxene) were washed with ultra high quality (UHQ) water in an ultrasonic bath and the clinopyroxenes were lixiviated using sub boiled 6M HCl.

Seven grams of each well homogenised whole rock sample were selected for the determination of Rb and Sr concentrations by XRF, using a fully automated Phil ips PW 1400 instrument.

For determinations of Sr^{87}/Sr^{86}, and Rb (ppm) and Sr(ppm) concentrations in separated minerals, the method used was as follows: A portion of roughly 0.1g of whole rock powder (0.1000g of clinopyroxene and 0.1500g of biotite accurately weighed) was weighed using an electronic balance into a 50 ml teflon beaker. The mineral samples were accurately spiked with Sr^{84}. The samples were dissolved using 6-8 ml of 40% HF and evaporated to dryness under infra-red evaporators. 2 ml of sub-boiled HNO_3 was added to the residue and the samples were again evaporated dryness. Finally, 6ml of sub-boiled 6M HCl was added to the residue and the samples were evaporated to dryness for a third time, leaving a residue of soluble chlorides and perchlorates. The salts were now dissolved in 2.5M HCl, eg 5ml for the whole rock samples and 1ml for mineral samples. The solutions were tranferred to centrifuge tubes and centrifuged for 5 minutes at 1000 rpm. 1ml of each solution was passed through an ion exchange resin and elution was done using 2.5M HCl. The first 21 ml of the eluate were discarded. The next 6 ml were collected as this volume contained the Rb fraction. After discarding a further 18 ml of eluate, the next 14 ml were collected as this contained the Sr fraction. Each fraction retained was evaporated to dryness. Finally the Sr and Rb fractions were dissolved again with a few drops of UHQ water and carefully loaded into the turrets. One drop of H_3PO_4 was added to the turrets prior to Sr samples.

The samples were ignited under high voltage and analysed by a VG 354 mass spectometer. The accuracy of each run was monitored by a standard (SRM 987) loaded in the same way as the unknown samples (see table A.11). The data calculations were done with the aid of a Hewlett-Packard

desk computer. Rb^{87} was calculated from measured Rb-Sr. The radiometric date was calculated using the decay constant of $1.42\ 10^{-11}\ Yr^{-1}$. The estimated error for Rb/Sr is 0.7% and the estimated error for Sr and Rb concentration determined by XRF are 1.5% and 0.4% respectively for concentrations < 200ppm and 5% and 1% respectively for contents > 200ppm.

Table A.1 Precision of major element analysis by ICP-AES

Analyses of sample 263

SiO_2	55.44	55.82	55.77	55.52	54.96	55.85
TiO_2	0.99	0.99	1.00	0.99	1.01	1.00
Al_2O_3	18.02	17.96	18.02	17.97	17.99	18.08
Fe_2O_3t	7.84	7.88	7.92	7.78	7.82	7.83
MnO	0.11	0.11	0.11	0.11	0.11	0.11
MgO	4.26	4.29	4.27	4.20	4.25	4.22
CaO	7.39	7.57	7.49	7.30	7.62	7.34
Na_2O	3.95	3.84	3.77	3.75	3.94	3.77
K_2O	1.72	1.71	1.65	1.67	1.68	1.68
P_2O_5	0.24	0.25	0.24	0.23	0.22	0.23

	X	**S**
SiO_2	55.56	0.338
TiO_2	1.00	0.008
Al_2O_3	18.01	0.044
Fe_2O_3t	7.85	0.049
MnO	0.11	0.000
MgO	4.25	0.033
CaO	7.45	0.129
Na_2O	3.84	0.089
K_2O	1.69	0.026
P_2O_5	0.24	0.010

All values in percentage. Fe_2O_3t is total iron expressed as Fe_2O_3.
X = Average value
S = Standard deviation for all 6 analyses.

Table A.2 Accuracy of major element analysis by ICP-AES.

Analysis of in-house reference materials

	163		**2266**		**MV-01**	
	1	2	1	2	1	2
SiO_2	61.68	61.59	45.48	45.70	74.43	74.44
TiO_2	0.66	0.66	3.61	3.68	0.19	0.18
Al_2O_3	17.18	17.22	15.04	15.25	13.07	12.96
Fe_2O_3t	5.00	5.03	13.03	13.16	1.98	1.97
MnO	0.06	0.07	0.19	0.19	0.07	0.07
MgO	1.68	1.79	6.17	6.18	0.30	0.48
CaO	4.96	4.96	9.51	9.44	0.55	0.46
Na_2O	4.45	4.44	3.98	4.05	2.86	2.83
K_2O	2.65	2.68	1.78	1.83	4.93	4.96
P_2O_5	0.24	0.24	0.80	0.80	0.21	0.21

All values in percentage. Fe_2O_3t is total iron expressed as Fe_2O_3. 1 = This work, 2 = Recommended values.

Table A.3 Precision of trace element analysis by ICP-AES.

SAMPLE 263

							X	**S**
Ba	580	590	580	580	580	580	582	4.1
Cr	60	70	70	70	60	75	67	6.1
Cu	60	60	60	60	60	70	62	4.1
Ni	10	10	10	10	20	20	13	5.2
Sr	600	600	600	600	600	600	600	0.0
V	180	180	190	190	190	180	185	5.5
Zr	100	120	100	110	110	120	110	8.9

All values are in parts per million (ppm).
X= Average value
S= Standard deviation for 6 analyses.

Table A.4 Accuracy of trace element analysis by ICP-AES.

Analysis of in-house reference materials.

	MV-01		**2266**		**163**		**474**	
	1	2	1	2	1	2	1	2
Ba	85	80	735	725	900	850	820	830
Cr	10	10	100	100	25	15	64	50
Cu	0	0	65	65	35	30	15	15
Ni	0	0	40	40	0	10	10	30
Sr	30	25	1250	1240	760	750	415	415
V	0	0	300	265	95	100	60	75
Zr	100	95	560	370	160	160	150	140

1 = This work
2 = Recommended values.
All values in ppm.

Table A.5 Comparison of trace element data for 5 samples analysed by XRF and ICP-AES.

	23		**25**		**90**		**144**		**193**	
	1	2	1	2	1	2	1	2	1	2
Ba	1917	2094	2370	2441	3873	3786	1673	1764	4157	3786
Cr	61	80	84	90	239	240	451	420	220	215
Cu	52	50	27	30	14	20	34	40	84	90
Ni	31	20	51	40	143	130	236	250	155	150
Sr	995	978	1162	1133	1954	1853	1562	1429	2422	2236
V	73	90	75	65	118	110	137	140	113	110
Zr	372	310	630	530	353	330	232	230	330	240

1 = XRF data
2 = ICP-AES data
All values in ppm.

Table A.6 Comparison of Rb data for 5 samples analysed by XRF and Flame Emission Spectrometry (ES).

Sample	XRF	FES
144	112	122
193	125	125
90	147	150
25	272	276
23	298	300

All values in ppm.

Table A.7 Comparison of REE data for 3 samples analysed by INAA and ICP-AES.

	144		**90**		**200**	
	1	2	1	2	1	2
La	55.80	54.96	65.56	71.82	76.90	77.63
Ce	109.44	113.40	128.69	144.12	159.06	135.26
Nd	56.52	55.47	65.64	69.89	81.55	72.88
Sm	8.69	8.94	9.69	10.60	11.83	11.75
Eu	2.60	2.63	2.63	3.24	2.85	3.26
Gd	3.77	3.89	7.16	7.40	9.77	7.84
Yb	1.39	1.38	1.01	1.17	1.20	1.30
Lu	0.21	0.29	0.14	0.17	0.18	0.20

Comparison of REE data for an international reference material analysed by INAA an ICP-AES.

	BHVO-1		
	1	2	3
La	14.71	16.02	15.8
Ce	37.98	38.82	39.0
Nd	26.20	25.83	25.2
Sm	5.78	6.27	6.2
Eu	2.05	2.17	2.06
Gd	6.84	6.49	6.4
Yb	1.76	2.04	2.02
Lu	0.24	0.27	0.29

1 = INAA
2 = ICP-AES
3 = Recommended values
All values in ppm.

Table A.8 Accuracy of trace element analysis by INAA.

Analysis of 1 international and 2 in-house reference material.

	BHV01		**MV01**		**2266**	
	1	2	1	2	1	2
La	14.74	15.80	16.00	16.30	66.93	70.30
Ce	37.98	39.00	44.94	36.20	138.28	140.20
Nd	26.16	25.20	15.69	16.90	73.79	66.80
Sm	5.78	6.20	3.76	4.16	12.06	12.20
Eu	2.05	2.06	0.30	0.23	3.85	3.81
Gd	6.89	6.40	5.53	3.50	10.87	9.88
Yb	1.76	2.02	1.90	1.97	1.93	2.32
Lu	0.24	0.29	0.24	0.29	0.26	0.33
Th	1.07	1.00	13.44	-	5.32	-
U	0.27	0.40	28.20	-	1.09	-
Cs	0.15	0.15	64.91	-	0.23	-
Hf	4.54	4.40	3.22	-	8.16	8.9
Ta	1.13	1.10	4.40	-	4.73	5.0

1 = This work
2 = Recommended values
All values in ppm.

Table A.9 Analyses of jadeite and olivine by electron micropobe.

JADEITE

SiO_2	59.98	59.28	59.79	59.02	60.16	59.02	58.97
Al_2O_3	24.47	25.36	25.09	25.24	24.78	24.81	25.41
MgO	0.00	0.00	0.28	0.00	0.00	0.00	0.00
CaO	0.00	0.00	0.00	0.00	0.25	0.00	0.00
Na_2O	15.11	15.03	15.05	15.35	14.80	15.61	15.02
Total	99.56	99.67	100.21	99.61	99.99	99.44	99.40

OLIVINE

SiO_2	40.29	40.83	41.00	40.43	40.43	40.29	40.83
FeO	9.14	8.62	8.98	9.12	10.90	10.92	9.10
MnO	0.22	0.00	0.00	0.00	0.00	0.26	0.00
MgO	48.66	49.54	49.83	48.69	48.16	47.21	48.13
CaO	0.00	0.00	0.00	0.00	0.00	0.00	0.00
Na_2O	0.30	0.52	0.00	0.48	0.39	0.70	0.54
NiO	0.59	0.41	0.37	0.32	0.39	0.34	0.48
Total	99.20	99.92	100.18	99.04	100.27	99.72	99.08

Appendix B

Major element oxides, CIPW norm and modal data

Table B.1 - Bom Jardim Complex, PBAMS

Sample	02	16	28	75	79	80	81	82
SiO2	56.57	56.29	55.88	55.64	55.47	58.62	56.59	56.74
TiO2	.95	.87	.88	.91	.97	.87	.92	.93
Al203	15.39	15.42	15.98	15.72	15.25	14.86	15.43	15.24
Fe203	1.67	1.54	1.17	1.59	1.73	1.82	1.72	1.80
FeO	4.23	3.97	4.15	3.85	4.21	3.62	3.85	4.10
MnO	.09	.08	.07	.08	.10	.08	.09	.09
MgO	5.32	5.37	5.16	5.06	5.54	4.74	5.02	5.24
CaO	5.14	4.50	4.81	4.58	5.20	4.87	5.06	5.10
Na20	3.64	3.78	3.85	3.77	3.55	3.50	3.86	3.58
K20	4.93	6.09	5.12	5.71	5.37	4.92	5.11	4.95
P205	.66	.61	.61	.59	.62	.62	.63	.67
LOI	.64	.87	.79	.56	.76	.44	.50	.42
SUM*	99.76	100.01	99.28	99.01	98.77	99.50	99.38	99.45
CIPW Norms								
Qz	.00	.00	.00	.00	.00	4.17	.00	.04
Or	28.29	36.16	30.06	33.96	31.73	28.95	30.06	29.50
Ab	30.94	29.96	32.52	31.40	29.90	29.37	32.52	30.42
An	11.13	6.96	11.41	8.90	10.02	10.57	9.74	10.57
Ne		1.10		.32				
Hy	12.24		4.32		3.10	11.87	7.47	13.78
Di	7.91	9.30	7.10	8.19	9.75	7.95	9.29	8.12
Ol	1.60	9.72	7.60	9.43	7.84		3.48	
MT	2.32	2.32	1.62	2.32	2.55	2.55	2.55	2.55
Il	1.82	1.67	1.67	1.67	1.82	1.67	1.82	1.82
Ap	1.55	1.24	1.24	1.24	1.24	1.24	1.24	1.55
R1	1138.00	802.00	1000.00	848.00	996.00	1360.00	1038.00	1150.00
R2	1118.00	1048.00	1086.00	1050.00	1132.00	1050.00	1092.00	1104.00
DI	59.23	67.24	62.58	65.36	61.60	62.49	62.58	59.92

* Totals include BaO and SrO

Table B.1 - Bom Jardim Complex, PBAMS (contd)

Sample	83	86	105	109	134	144	177	187
SiO2	56.04	56.04	53.06	55.95	55.83	53.02	57.35	53.39
TiO2	.98	.98	.90	.91	1.06	.99	.86	1.03
Al2O3	15.22	15.22	14.34	15.35	14.16	14.84	15.69	13.67
Fe2O3	1.91	1.91	1.74	.94	1.67	1.48	.87	1.78
FeO	4.16	4.16	5.02	3.84	4.63	5.54	4.44	5.11
MnO	.10	.10	.13	.08	.10	.12	.08	.13
MgO	5.52	5.52	7.46	5.21	6.50	8.08	4.95	7.89
CaO	5.34	5.34	5.86	4.69	6.01	6.48	4.69	6.40
Na2O	3.60	3.60	3.41	3.70	3.34	3.71	3.91	2.84
K2O	5.03	5.03	4.85	5.50	4.97	3.36	5.52	5.11
P2O5	.70	.70	.43	.57	.71	.47	.57	.72
LOI	.61	.61	.63	1.01	.95	.57	.61	.76
SUM*	99.89	99.89	99.45	99.27	100.40	99.03	100.11	99.40
CIPW Norms								
Qz	.00	.00	.00	.00	.00	.00	.00	.00
Or	30.06	29.50	28.39	32.29	29.50	36.18	32.84	30.06
Ab	31.47	30.42	26.22	31.47	28.32	22.02	33.04	24.13
An	10.85	10.57	9.74	9.18	8.90	8.07	8.90	9.46
Ne			1.42			2.84		
Hy	5.03	9.50	.00	3.76	7.27		3.27	.74
Di	9.09	9.00	13.18	8.43	13.02	9.34	8.72	14.12
Ol	6.12	3.28	13.56	7.23	5.90	12.64	8.02	13.39
MT	2.55	2.78	2.55	1.39	2.32	2.08	1.16	2.55
Il	1.82	1.82	1.67	1.67	1.97	1.52	1.67	1.97
Ap	1.24	1.55	.93	1.24	1.55	1.55	1.24	1.55
R1	1026.00	1100.00	1026.00	974.00	1166.00	742.00	964.00	1140.00
R2	1126.00	1142.00	1276.00	1064.00	1242.00	1096.00	1058.00	1344.00
DI	61.53	59.92	56.03	63.76	57.82	61.04	65.88	54.19

* Totals include BaO and SrO

Table B.1 - Bom Jardim Complex, PBAMS (contd)

Sample	188	193	200	207	283	344	190
SiO2	56.56	52.38	55.62	55.72	55.03	54.35	57.80
TiO2	.92	1.13	.94	.97	.98	1.05	.84
Al2O3	15.37	14.50	15.46	15.24	15.06	14.96	15.25
Fe2O3	1.11	1.74	1.63	1.27	1.64	1.62	.93
FeO	4.51	4.99	4.13	4.27	4.44	4.52	4.23
MnO	.09	.10	.09	.09	.10	.10	.09
MgO	5.10	6.51	5.35	5.47	5.51	6.12	4.73
CaO	5.05	6.74	5.40	4.81	5.50	6.12	4.68
Na2O	3.64	3.41	3.59	3.53	3.79	3.65	3.71
K2O	5.09	4.65	5.23	5.81	4.93	4.90	5.19
P2O5	.66	.98	.71	.64	.68	.74	.59
LOI	.58	.90	.49	.91	.75	.88	.72
SUM*	99.20	99.28	99.26	99.34	99.43	99.61	99.27
CIPW Norms							
Qz	.00	.00	.00	.00	.00	.00	.44
Or	30.06	27.28	31.17	34.51	28.95	28.95	30.62
Ab	30.94	26.35	30.42	29.90	31.99	28.97	31.47
An	90.57	10.57	10.57	8.35	9.74	10.02	9.74
Ne		1.35				1.07	
Hy	10.54		4.17	1.29	2.04		13.65
Di	7.95	13.12	9.23	8.80	10.38	12.58	7.80
Ol	3.04	11.38	6.84	9.67	8.75	10.53	
MT	1.62	2.55	2.32	1.85	2.32	2.32	1.39
Il	1.82	2.12	1.82	1.82	1.82	1.97	1.67
Ap	1.55	2.17	1.55	1.55	1.55	1.55	1.24
R1	1098.00	988.00	1016.00	914.00	988.00	980.00	1152.00
R2	1094.00	1326.00	1146.00	1086.00	1158.00	1252.00	1.32
DI	61.00	54.98	61.59	64.41	60.94	58.99	62.53

* Totals include BaO and SrO

Table B.2 - Bom Jardim Complex, PBM

Sample	90	92	111	258	252
SiO2	54.04	52.21	53.75	54.89	53.94
TiO2	1.00	1.17	1.12	.94	.96
Al2O3	16.08	15.01	15.05	15.52	14.75
Fe2O3	1.54	1.93	2.01	1.64	1.54
FeO	4.21	4.90	4.66	4.05	4.28
MnO	.07	.10	.10	.09	.09
MgO	5.53	6.64	6.23	5.50	6.51
CaO	5.14	5.89	5.89	5.15	5.07
Na2O	3.87	3.31	3.60	3.70	3.49
K2O	5.55	5.34	5.02	5.74	5.70
P2O5	.65	.75	.80	.69	.66
LOI	.65	.63	.77	.63	.53
SUM*	99.22	98.57	99.80	99.64	98.57
CIPW Norms					
Qz	.00	.00	.00	.00	.00
Or	32.84	31.73	29.50	33.96	33.96
Ab	26.55	21.83	28.45	27.93	27.93
An	10.29	10.29	10.29	8.62	7.79
Ne	3.23	3.23	1.07	1.92	1.99
Hy					
Di	8.56	11.45	10.70	9.89	10.10
Ol	10.45	11.95	11.20	9.73	11.83
MT	SiO2	2.78	3.01	2.32	2.32
Il	1.97	2.28	2.12	1.82	1.82
Ap	1.55	1.55	1.86	1.55	1.55
R1	748.00	8.40	922.00	812.00	832.00
R2	1142.00	1254.00	1236.00	1128.00	1152.00
DI	62.63	56.79	59.02	63.81	61.65

* Totals include BaO and SrO

Table B.3 - Bom Jardim Complex, MPBAS

Sample	01	03	06	07	27	44	47
SiO2	59.92	59.21	61.79	59.63	59.18	61.44	61.69
TiO2	.75	.78	.68	.74	.76	.76	.69
Al2O3	15.45	15.49	15.10	15.46	15.59	15.07	15.10
Fe2O3	1.59	1.66	1.22	1.43	1.65	1.21	1.24
FeO	3.17	3.22	2.99	3.04	3.04	3.02	3.12
MnO	.07	.07	.06	.06	.07	.07	.06
MgO	4.07	3.98	3.55	3.92	3.98	3.96	3.76
CaO	3.69	3.52	3.13	3.50	3.69	3.58	3.40
Na2O	3.90	3.79	3.87	3.84	3.95	3.82	3.65
K2O	6.34	6.19	6.04	6.17	6.28	5.49	6.14
P2O5	.46	.47	.42	.45	.50	.46	.41
LOI	.69	.93	.68	.28	.49	.58	.39
SUM*	100.61	99.82	100.12	99.07	99.73	100.00	100.05
CIPW Norms							
Qz	.72	1.20	5.41	1.56	.14	5.71	5.35
Or	37.30	36.74	35.63	36.74	37.30	32.52	36.18
Ab	33.02	31.99	32.52	32.52	33.57	32.29	30.94
An	6.12	6.96	6.12	6.68	6.12	7.79	6.68
Ne							
Hy	9.94	10.37	9.68	10.04	9.71	10.61	9.87
Di	7.59	6.25	5.37	6.25	6.83	5.81	6.04
Ol							
MT	2.32	2.32	1.85	2.08	2.32	1.85	1.85
Il	1.37	1.52	1.37	1.37	1.52	1.37	1.37
Ap	.93	.93	.93	.93	1.24	.93	.93
R1	980.00	994.00	1204.00	1012.00	912.00	1310.00	1244.00
R2	902.00	880.00	808.00	870.00	900.00	876.00	848.00
DI	71.10	69.90	73.56	70.82	71.01	70.52	72.47

* Totals include BaO and SrO

Table B.3 - Bom Jardim Complex, MPBAS (contd)

Sample	48	52	53	62	65	66	99
SiO2	60.17	60.37	60.37	61.48	62.47	58.43	58.60
TiO2	.72	.73	.68	.66	.71	.91	.81
Al2O3	15.25	15.53	15.42	14.85	15.25	15.20	15.34
Fe2O3	1.50	1.50	1.41	.98	1.29	1.42	1.46
FeO	3.25	2.97	2.68	3.01	2.91	3.45	3.13
MnO	.07	.06	.06	.06	.08	.07	.06
MgO	4.21	3.81	3.73	3.50	3.39	4.55	4.27
CaO	3.67	3.50	3.44	3.34	3.03	4.05	3.91
Na2O	3.72	3.97	4.01	3.74	3.61	3.87	3.78
K2O	6.06	6.30	5.90	5.52	5.61	5.67	6.15
P2O5	.49	.45	.44	.37	.43	.55	.50
LOI	.39	.38	.50	.89	.52	.76	1.00
SUM*	100.02	100.12	99.17	98.87	99.64	99.42	99.65
CIPW Norms							
Qz	2.64	1.68	3.00	6.97	9.01	.68	.38
Or	35.63	37.30	35.07	32.84	33.40	33.40	36.18
Ab	31.47	33.57	34.09	31.47	30.42	32.52	31.99
An	7.23	5.84	6.40	7.51	8.62	7.51	6.68
Ne							
My	11.03	9.29	9.01	10.07	10.07	11.79	10.59
Di	6.48	6.92	6.22	5.16	2.91	7.07	7.28
Ol							
MT	2.08	2.08	2.08	1.39	1.85	2.08	2.08
Il	1.37	1.37	1.37	1.21	1.67	1.67	1.52
Ap	.93	.93	.93	.93	.93	1.24	1.24
R1	1130.00	1000.00	1074.00	1348.00	1494.00	1044.00	982.00
R2	898.00	864.00	854.00	826.00	792.00	956.00	932.00
DI	69.70	72.55	72.16	71.28	72.83	66.60	68.55

*Totals include BaO and SrO

Table B.3 - Bom Jardim Complex, MPBAS (contd)

Sample	162	268	271	272	305	306
SiO2	59.47	60.85	61.30	60.43	61.11	60.62
TiO2	.75	.69	.64	.70	.72	.72
Al2O3	15.24	15.08	15.54	15.36	14.62	15.72
Fe2O3	1.60	1.12	1.07	.47	1.49	1.48
FeO	3.01	3.00	2.74	3.75	3.00	2.86
MnO	.07	.07	.06	.06	.07	.06
MgO	4.17	3.75	3.19	3.48	3.93	3.56
CaO	3.77	3.52	3.31	3.10	3.44	3.49
Na2O	3.84	3.84	4.03	4.07	3.77	4.24
K2O	6.37	6.03	6.48	6.29	6.18	6.15
P2O5	.49	.42	.39	.45	.46	.43
LOI	.36	.68	.71	.39	.42	.59
SUM*	100.01	99.82	99.92	99.11	99.66	100.38
CIPW Norms						
Qz	.42	3.72	2.76	1.08	3.97	1.62
Or	37.85	35.63	38.41	37.30	36.74	36.18
Ab	32.52	32.52	34.09	34.62	31.99	35.66
An	5.29	6.12	5.01	5.01	4.45	5.84
Ne						
Hy	9.47	9.57	7.76	11.06	9.30	8.55
Di	8.46	6.94	6.94	6.12	7.81	6.92
Ol						
MT	2.32	1.62	1.62	.69	2.08	2.08
Il	1.37	1.37	1.21	1.37	1.37	1.37
Ap	.93	.93	.93	.93	.93	.93
R1	956.00	1148.00	1010.00	962.00	1134.00	974.00
R2	906.00	860.00	816.00	804.00	846.00	856.00
DI	70.79	71.87	75.29	73.00	72.70	73.46

* Totals include BaO and SrO

Table B.4 - Bom Jardim Complex, PBLS

Sample	10	25	26	49	159	163	209D	323	330
SiO2	61.54	61.10	61.30	61.52	61.87	62.71	62.38	61.61	61.83
TiO2	.82	.84	.84	.80	.71	.77	.74	.67	.77
Al2O3	14.96	14.99	15.11	16.04	14.93	15.16	15.65	14.77	15.28
Fe2O3	1.65	1.56	1.47	1.65	1.53	1.63	1.50	1.46	1.39
FeO	3.01	2.94	2.94	3.00	2.89	2.72	2.57	2.96	2.80
MnO	.07	.07	.07	.06	.06	.06	.06	.06	.07
MgO	2.89	2.79	2.75	2.71	2.89	2.38	2.25	3.11	2.53
CaO	2.86	2.78	3.00	2.69	2.98	2.66	2.58	2.83	2.77
Na2O	3.96	3.99	4.14	4.32	4.06	4.11	4.36	3.75	3.71
K2O	6.65	6.80	6.96	6.67	6.49	6.85	6.58	6.71	6.33
P2O5	.47	.43	.48	.42	.42	.44	.38	.41	.50
LOI	.20	.15	.23	.21	.26	.31	.24	.30	.08
SUM*	99.60	98.89	100.01	100.64	99.80	100.59	99.97	99.40	99.89
CIPW Norms									
Qz	3.97	3.60	2.04	2.04	4.33	5.11	4.45	4.69	7.47
Or	39.52	40.08	41.20	39.52	38.41	40.64	38.97	39.52	37.30
Ab	33.57	33.57	35.14	36.71	34.62	34.62	36.71	31.99	31.47
An	3.34	3.06	1.95	4.45	3.06	2.78	3.62	3.62	6.40
Ne									
Hy	7.13	6.57	5.84	7.37	6.68	5.51	5.64	8.11	7.72
Di	6.50	6.50	8.08	4.49	7.17	6.06	5.17	6.06	2.85
Ol									
MT	2.32	2.32	2.08	2.32	2.32	2.32	2.08	2.08	2.08
Il	1.52	1.67	1.67	1.52	1.37	1.52	1.37	1.21	1.52
Ap	.93	.93	.93	.93	.93	.93	.93	.93	1.24
R1	980.00	930.00	836.00	848.00	1010.00	980.00	944.00	1060.00	1186.00
R2	744.00	732.00	750.00	736.00	754.00	698.00	694.00	744.00	720.00
DI	77.10	77.25	78.38	78.27	77.36	80.37	80.13	76.20	76.24

* Totals include BaO and SrO

Table B.5 - Bom Jardim Complex, CS

Sample	23	31	40	54	104
SiO2	61.12	58.64	61.90	58.44	60.45
TiO2	.99	1.01	.80	1.06	1.01
Al2O3	15.90	15.34	16.29	14.91	15.67
Fe2O3	1.46	2.00	1.44	1.90	1.87
FeO	2.78	3.23	1.79	3.51	3.16
MnO	.06	.08	.04	.08	.07
MgO	2.29	3.50	1.81	3.45	2.75
CaO	2.43	3.41	2.18	3.55	3.10
Na2O	4.35	3.64	3.92	3.74	3.61
K2O	7.45	7.53	8.25	7.41	7.37
P2O5	.39	.57	.34	.63	.55
LOI	.32	.40	.30	.26	.52
SUM*	99.99	99.94	99.55	99.44	100.58
CIPW Norms					
Qz	.42	.00	1.84	.00	2.54
Or	43.98	44.54	48.99	43.98	43.42
Ab	36.71	30.94	33.04	31.47	30.42
An	1.95	3.06	2.50	1.95	5.01
Ne					
Hy	5.41	2.44	3.00	2.25	6.92
Di	5.84	8.16	5.15	8.80	5.30
Ol		3.61		3.93	
MT	2.08	3.01	2.08	2.78	2.78
Il	1.82	1.97	1.52	1.97	1.97
Ap	.93	1.24	.62	1.55	1.24
R1	650.00	676.00	690.00	660.00	868.00
R2	684.00	840.00	644.00	842.00	774.00
DI	81.11	75.48	83.87	75.45	76.38

* Totals include BaO and SrO

Table B.6 - Bom Jardim Complex, Pink Granites

Sample	08	36	43	66	223	238	266	267	328
SiO2	71.99	71.77	72.96	73.37	72.56	72.23	69.38	69.19	69.88
TiO2	.35	.40	.24	.28	.27	.28	.53	.47	.54
Al2O3	14.52	14.65	14.00	14.07	14.52	14.32	14.75	15.35	14.55
Fe2O3	.96	.96	.85	.85	.56	.75	1.05	.84	1.38
FeO	1.02	1.20	.94	.79	1.06	.91	1.58	1.33	1.38
MnO	.01	.01	.01	.03	.04	.02	.03	.03	.04
MgO	.66	.68	.52	.41	.53	.45	.85	.74	.95
CaO	1.24	1.56	1.42	1.26	1.43	1.44	1.61	1.66	1.74
Na2O	3.75	3.68	3.72	3.62	4.39	3.90	3.58	3.80	3.41
K2O	5.16	5.09	4.57	5.08	4.49	5.40	5.67	5.76	5.65
P2O5	.13	.14	.12	.09	.11	.10	.20	.19	.21
LOI	.29	.41	.54	.28	.34	.61	.30	.39	.39
SUM*	100.09	100.90	100.19	100.40	100.41	100.71	100.07	100.28	100.64
CIPW Norms									
Qz	26.72	26.66	29.96	30.02	25.82	25.50	22.03	20.41	23.41
Co	.75	.65	.65	.75	.14	.00	.14	.24	.03
Or	30.62	30.06	27.28	30.06	26.72	31.73	33.40	33.96	33.40
Ab	31.99	30.94	31.47	30.42	37.24	33.04	30.42	31.99	28.85
An	5.19	6.86	6.03	5.19	6.03	5.56	7.14	7.42	7.70
Hy	2.13	2.50	1.97	1.27	2.36	1.34	3.16	2.86	2.94
Di						.60			
Ol									
MT	1.39	1.39	1.16	1.16	.93	1.16	1.62	1.16	2.08
Il	.61	.76	.46	.61	.46	.61	1.06	.91	1.06
Ap	.31	.31	.31	.31	.31	.31	.31	.31	.31
R1	2180.00	2222.00	2406.00	2370.00	2162.00	2114.00	1938.00	1850.00	2032.00
R2	448.00	490.00	450.00	428.00	460.00	458.00	506.00	518.00	520.00
DI	89.33	87.66	88.71	90.50	89.72	90.27	86.03	86.36	85.66

* Totals include BaO and SrO

Table B.7 - Bom Jardim Complex, Igneous Enclaves

Sample	03A	28A	74A	75A	130A	130G
SiO2	51.88	50.50	54.29	54.89	48.64	53.14
TiO2	1.26	1.19	.93	.85	1.41	.97
Al2O3	16.68	14.17	12.97	14.56	15.06	12.79
Fe2O3	2.27	2.05	1.93	1.63	2.08	1.33
FeO	5.31	6.12	4.40	4.40	6.15	5.09
MnO	.10	.13	.11	.10	.13	.12
MgO	6.76	8.55	7.42	7.12	7.80	8.24
CaO	5.88	7.48	6.67	5.43	7.83	6.39
Na2O	4.15	2.95	2.03	3.32	3.58	3.00
K2O	3.49	3.78	6.54	5.12	3.64	5.51
P2O5	.54	.84	1.13	.67	.89	1.02
LOI	1.01	.88	.77	.54	1.31	.81
SUM*	100.14	99.11	99.93	99.21	9.79	99.55
CIPW Norms						
Qz						
Or	20.60	22.27	38.41	30.06	21.71	32.29
Ab	30.55	22.75	17.31	28.32	16.84	21.76
An	16.69	14.19	6.96	9.74	14.19	5.29
Ne	2.49	1.32			7.35	1.85
LC						
Hy			6.03	3.82		
Di	7.07	13.86	14.96	10.09	15.44	15.99
Ol	13.97	16.14	7.49	10.43	14.04	14.24
MT	3.24	3.01	2.78	2.32	3.01	1.85
Il	2.43	2.28	1.82	1.67	2.73	1.82
Ap	1.24	1.86	2.48	1.55	1.86	2.17
R1	926.00	1168.00	1170.00	1090.00	838.00	1002.00
R2	1294.00	1500.00	1336.00	1222.00	1522.00	1342.00
DI	53.64	46.34	55.72	58.38	45.90	55.90

* Totals include BaO and SrO

Table B.7 - Bom Jardim Complex, Igneous Enclaves (contd)

Sample	137A	144E	54A	83A	323A	249A
SiO2	54.97	49.63	45.63	53.57	53.56	50.01
TiO2	.85	1.19	1.88		.82	1.21
Al2O3	13.77	13.82	9.40	14.15	12.77	15.09
Fe2O3	1.91	1.91	2.41	2.23	1.28	2.46
FeO	5.16	6.35	7.96	5.30	5.97	5.89
MnO	.15	.14	.16	.15	.14	.09
MgO	7.24	9.30	13.93	7.90	7.77	8.74
CaO	5.99	7.31	8.86	6.67	6.48	7.65
Na2O	3.00	3.08	.89	3.03	3.36	3.32
K2O	4.99	3.70	5.42	4.60	4.87	2.65
P2O5	.50	.68	1.05	.73	.48	.53
LOI	.88	.64	.94	.86	.67	.86
SUM*	100.48	99.17	99.79	100.77	100.15	98.88
CIPW Norms						
Qz						
Or	29.50	21.71	21.56	27.28	28.95	15.59
Ab	25.18	19.99		25.70	22.62	26.75
An	9.46	13.63	5.56	11.41	5.29	18.36
Ne		2.52	3.98		3.09	.85
LC			8.41			
Hy	7.73					
Di	13.34	14.18	25.48	13.67	19.55	12.63
Ol	7.69	18.30	23.11	13.09	13.58	16.33
MT	2.78	2.70	3.47	3.24	1.85	3.47
Il	1.67	1.37	3.64	1.97	1.52	2.28
Ap	1.24	1.55	2.17	1.55	.93	1.24
R1	1220.00	1154.00	1118.00	1174.00	1010.00	1268.00
R2	1270.00	1504.00	1822.00	1384.00	1332.00	1546.00
DI	54.68	44.22	33.95	52.98	51.66	43.19

* Totals include BaO and SrO

Table B.8 - Bom Jardim Complex, Mafic Dykes

Sample	130D	133A	205	216	254B	254D	265A	272A	292A
SiO2	51.88	53.57	49.92	59.37	52.31	50.46	52.81	54.33	56.70
TiO2	1.21	.89	1.38	.83	1.35	1.23	.88	.98	.08
Al2O3	16.17	12.58	13.56	13.96	13.95	15.04	14.54	17.12	13.08
Fe2O3	1.95	1.41	2.29	.75	1.81	2.02	2.20	1.90	1.81
FeO	5.29	5.04	5.31	4.82	5.30	5.42	5.42	5.59	4.10
MnO	.10	.11	.12	.10	.11	.10	.13	.13	.11
MgO	6.13	8.40	7.71	5.25	8.37	8.21	8.61	5.01	6.51
CaO	6.67	5.76	7.45	4.15	5.20	6.50	6.54	7.81	5.56
Na2O	4.57	2.75	2.48	3.28	2.53	3.78	3.75	4.52	2.11
K2O	3.26	5.74	5.03	5.16	6.42	3.81	3.49	1.31	6.44
P2O5	.67	.89	1.53	.35	.89	.75	.38	.46	.77
LOI	1.03	.93	.71	.43	.91	1.82	.91	.59	.73
SUM*	99.51	99.10	98.56	98.76	100.41	100.26	100.74	100.00	100.02
CIPW Norms									
Qz				3.65					1.60
Or	19.48	33.96	29.50	30.62	37.85	22.27	20.60	7.79	37.85
Ab	29.70	22.75	19.73	27.80	16.98	25.53	28.71	38.29	17.83
An	13.91	5.01	11.13	8.07	7.79	13.08	12.52	22.54	7.23
Ne	4.94	.18	.68		2.45	4.58	1.78		
Hy				15.85				12.78	14.93
Di	11.43	14.46	12.55	8.65	10.02	11.65	13.81	10.87	12.53
Ol	11.53	14.95	13.72		16.09	15.25	15.61	1.28	
MT	2.78	2.08	3.24	1.16	2.55	3.01	3.24	2.78	2.55
Il	2.28	1.67	2.58	1.52	2.58	2.28	1.67	1.82	1.82
Ap	1.55	1.86	3.41	.62	1.86	1.55	.93	.93	1.55
R1	826.00	1052.00	1036.00	1400.00	856.00	904.00	1128.00	1470.00	1346.00
R2	1336.00	1280.00	1446.00	978.00	1248.00	1400.00	1416.00	1418.00	1172.00
DI	54.12	56.89	49.91	62.07	57.28	52.37	51.09	46.09	57.28

* Totals include BaO and SrO

Table B.9 - Bom Jardim Complex, Country Rocks

Sample	175	278	349A	349B	290	348
SiO2	67.71	59.22	62.61	56.11	74.39	63.41
TiO2	.32	1.21	.83	.82	.25	.87
Al2O3	16.24	17.04	15.58	14.44	14.07	15.75
Fe2O3*	2.93	8.93	7.46	8.74	2.59	7.06
MnO	.07	.18	.15	.14	.11	.11
MgO	1.02	3.11	3.52	6.22	.46	3.61
CaO	4.25	2.55	2.37	5.74	2.35	2.48
Na2O	3.92	3.09	2.88	3.03	5.12	2.96
K2O	2.06	3.30	2.91	2.21	.52	2.99
P2O5	.11	.15	.17	.52	.06	.19
LOI	.92	.89	.82	2.10	.53	.89
SUM	99.56	99.66	99.29	100.08	100.45	100.34

*Total Fe expressed as Fe2O3

Table B.10 - Modal Analysis of the Bom Jardin Complex, PBMAS

Sample	16	28	29	35	86
Quartz	3.70	1.70		1.00	2.90
Alk. Felds.	56.70	23.00	36.00	39.10	28.00
Plagioclase	10.60	24.40	4.40	17.10	30.00
Biotite	11.50	18.20	25.00	16.40	15.40
Amphibole	13.40	28.80	27.00	24.00	16.50
Clinopyrox.	2.60	.30	4.10	.20	.30
Zircon		.30	.20	.20	.50
Sphene	.80	2.00	2.20	.80	.70
Apatite	.80	1.00	1.00	1.20	1.70
Opaques	Trace	Trace	Trace	.07	Trace
Allanite	Trace				
Monazite					

Sample	87	144	193	200	287
Quartz	.40	.90			2.00
Alk. Felds.	50.30	21.60	37.00	31.00	14.00
Plagioclase	14.70	33.50	10.70	22.00	40.00
Biotite	15.90	14.90	30.90	21.00	16.00
Amphibole	11.70	27.40	12.00	18.00	14.00
Clinopyrox.	4.10		7.80	4.00	.90
Zircon	.10	.30	.10	.30	.60
Sphene	1.50	.30	.60	1.40	2.00
Apatite		.80	.80	1.70	1.50
Opaques	Trace	.20	.10	.20	Trace
Allanite		.10	Trace	Trace	
Monazite					Trace

Table B.11 - Modal Analysis of the Bom Jar

Sample	91	111	252
Quartz	.60	1.00	1.00
Alk. Felds.	17.10	30.00	35.00
Plagioclase	30.80	18.50	14.00
Biotite	32.80	24.10	26.00
Amphibole	1.60		4.10
Clinopyrox.	15.50	21.80	17.50
Zircon	.08	.30	.10
Sphene			
Apatite	.80	2.40	1.70
Opaques	1.60	1.90	.40
Allanite			
Monazite	Trace		

Table B.12 - Modal Analysis of the Bom Jardin Complex, MPBAS

Sample	48	51	52	62	65	78	124	248
Quartz	.80	2.80	5.00	7.00	6.50	6.70	4.60	2.00
Alk. Felds.	56.00	59.00	57.60	44.50	41.50	63.30	46.90	63.00
Plagioclase	17.00	12.10	13.60	23.00	28.60	11.70	13.90	8.90
Biotite	13.00	14.20	12.20	11.50	14.50	6.40	17.50	13.20
Amphibole	1.00	1.60	2.80	8.70	8.50	7.60	9.70	4.20
Clinopyrox.	14.00	9.30	6.30		.20	3.00	4.10	6.60
Zircon	Trace	.30	.10	.20	Trace	.08	.20	Trace
Sphene		.10	.20	1.60	.50	.30	1.40	.30
Apatite	.60	.50	1.00	.50	.80	.80	1.60	.70
Opaques	.30	.90	1.40	.10	.50	1.00	1.30	1.00
Allanite								
Monazite				Trace				

Table B.13 - Modal Analysis of the Bom Jardin Complex, PBLS

Sample	10	24	163
Quartz	5.30	1.20	7.30
Alk. Felds.	73.40	7.30	68.80
Plagioclase	3.30	2.00	4.60
Biotite	9.70	11.00	10.10
Amphibole		.90	1.00
Clinopyrox.	6.00	9.00	5.20
Zircon	Trace	.60	.10
Sphene	.20	1.10	.10
Apatite	.60	.70	.60
Opaques	1.50	Trace	1.50
Allanite			
Monazite	Trace		

Table B.14 - Modal Analysis of the Bom Jardin Complex, Granite

Sample	36	43	110	267	292
Quartz	16.90	25.00	33.00	24.40	19.00
Alk. Felds.	46.80	44.00	40.50	48.30	43.00
Plagioclase	28.40	25.60	17.00	15.90	31.00
Biotite	5.40	3.40	6.00	7.90	4.40
Amphibole					
Clinopyrox.		.08	.30		
Zircon	.60	.10	1.30	1.70	.07
Sphene	.80	.80	.80	.40	.70
Apatite	.40	.70	1.10	1.20	.30
Opaques	1.00	Trace		.20	
Allanite					.40
Monazite					

Table B.15 - Modal Analysis of the Bom Jardin Complex, Enclave

Sample	249A	130F	28A	75A	83A
Quartz	1.00				.20
Alk. Felds.	3.90	2.00	14.30	18.80	24.20
Plagioclase	3.52	46.10	21.00	33.50	17.40
Biotite	22.30	36.70	28.80	18.00	24.90
Amphibole	36.00	12.40	31.00	25.40	29.60
Clinopyrox.	.20	2.00	2.90	.50	1.40
Zircon		.20	.10		.20
Sphene			.80	2.30	1.30
Apatite	.80		.20	.20	.80
Opaques	.70	.60		.30	
Allanite					
Monazite			Trace		

Table B.15 - Modal Analysis of the Bom Jardin Complex, Enclave

Sample	323A	124A	207B	54A
Quartz				1.30
Alk. Felds.	36.60	40.50	36.70	8.20
Plagioclase	18.50	7.30	12.00	.10
Biotite	21.70	19.60	21.10	58.10
Amphibole	11.40	24.90	12.00	5.10
Clinopyrox.	10.70	3.10	7.57.5	26.00
Zircon			.30	
Sphene		3.70	.10	
Apatite	.30	.40	.30	1.10
Opaques	.80	.30		
Allanite				
Monazite				

Table B.16 - Modal Analysis of the Bom Jardin Complex, Mafic Dykes

Sample	130D	133A	205	254B	254D	272A
Quartz	.40	2.90	.40	1.20	.20	.50
Alk. Felds.	12.40	14.50	33.10	25.00	13.30	
Plagioclase	33.10	45.60	4.50	3.20	29.00	66.10
Biotite	36.90	27.50	25.50	41.10	21.80	5.90
Amphibole	9.80		29.90	25.80	30.50	
Orthopyrox						9.50
Clinopyrox.	5.00	4.90			.40	16.20
Zircon	.20		.10			
Sphene			5.30	2.10	3.50	
Apatite	.80	.70	1.10	1.20	1.00	.20
Opaques	1.50	3.70	Trace		.40	2.20
Allanite			.20			
Monazite						

APPENDIX C

TRACE ELEMENT DATA

C.1 TRACE ELEMENTS

Table C.1.1 - Bom Jardim Complex, PBAMS

Sample	02	16	28	75	79	80	81
Sr	1 608.00	1 765.00	2 092.00	1 711.00	1 513.00	1 488.00	1 572.00
Ba	2 985.00	3 700.00	4 281.00	3 367.00	3 161.00	2 907.00	2 976.00
Rb	138.00	180.00	105.00	150.00	160.00	141.00	162.00
Cs	nd	nd	nd	2.19	nd	nd	5.85
U	nd	nd	nd	2.14	1.90	nd	3.61
Th	nd	nd	9.00	15.20	11.00	nd	12.40
Pb	nd	nd	25.00	nd	32.00	nd	nd
Zn	300.00	350.00	220.00	400.00	380.00	280.00	250.00
Nb	nd	nd	14.00	16.00	15.00	nd	21.00
Y	nd	nd	17.00	16.90	19.10	17.70	nd
Sc	nd	nd	nd	11.40	12.50	nd	11.60
Hf	nd	nd	nd	9.90	nd	nd	9.10
Ta	nd	nd	nd	.75	nd	nd	1.48
Cr	240.00	250.00	220.00	225.00	280.00	210.00	205.00
Ni	130.00	130.00	130.00	120.00	140.00	100.00	110.00
V	105.00	30.00	50.00	80.00	95.00	40.00	110.00
Cu	20.00	20.00	40.00	10.00	60.00	40.00	40.00

Sample	82	83	86	105	134	177	187
Sr	1 685.00	1 633.00	1 729.00	1 607.00	1 472.00	1 685.00	1 592.00
Ba	3 058.00	3 230.00	3 401.00	2 780.00	2 693.00	3 286.00	3 432.00
Rb	140.00	138.00	133.00	165.00	146.00	150.00	123.00
Cs	nd	nd	nd	nd	nd	nd	nd
U	nd	nd	nd	nd	nd	1.57	1.11
Th	nd	nd	nd	nd	6.90	12.90	7.00
Pb	nd	nd	nd	nd	20.00	nd	nd
Zn	250.00	300.00	270.00	180.00	220.00	250.00	250.00
Nb	17.00	12.00	10.00	nd	17.00	14.00	15.00
Y	17.40	17.30	17.70	nd	19.30	15.40	19.50
Sc	nd	nd	nd	nd	16.60	12.00	18.70
Hf	nd	nd	nd	nd	nd	12.10	nd
Ta	nd	nd	nd	nd	nd	.58	.48
Cr	220.00	225.00	230.00	455.00	360.00	220.00	4.70
Ni	140.00	120.00	120.00	200.00	180.00	140.00	220.00
V	120.00	110.00	100.00	110.00	120.00	90.00	120.00
Cu	30.00	20.00	30.00	115.00	80.00	30.00	70.00

nd = Not Determined

Table C.1.1 - Bom Jardim Complex, PBAMS (contd)

Sample	188	193	200	207	283	344	144
Sr	1 489.00	2 236.00	1 799.00	3 700.00	1 625.00	1 810.00	1 429.00
Ba	3 084.00	3 786.00	3 700.00	1 690.00	3 167.00	2 475.00	1 764.00
Rb	150.00	125.00	144.00	170.00	154.00	127.00	122.00
Cs	2.00	nd	2.02	nd	nd	nd	2.90
U	.59	1.08	.82	nd	1.11	.91	1.29
Th	8.00	5.80	5.10	nd	9.00	10.40	3.10
Pb	30.00	28.00	30.00	nd	38.00	nd	22.00
Zn	320.00	140.00	330.00	320.00	230.00	170.00	230.00
Nb	15.00	15.00	12.00	nd	15.00	14.00	17.00
Y	17.20	22.60	17.20	20.00	19.20	22.80	18.70
Sc	12.90	16.50	12.60	13.00	15.00	16.30	17.10
Hf	9.20	nd	8.30	nd	10.10	12.30	7.00
Ta	.45	nd	.42	nd	.70	.58	.83
Cr	280.00	320.00	240.00	250.00	220.00	240.00	420.00
Ni	130.00	150.00	110.00	120.00	120.00	160.00	250.00
V	110.00	110.00	110.00	100.00	100.00	110.00	140.00
Cu	50.00	90.00	40.00	20.00	50.00	50.00	40.00

Table C.1.2 - Bom Jardim Complex, PBM

Sample	90	92	111	258	252
Sr	1 853.00	1 815.00	2 794.00	1 248.00	1 695.00
Ba	3 789.00	3 606.00	3 280.00	3 774.00	3 368.00
Rb	150.00	148.00	138.00	137.00	167.00
Cs	1.93	nd	nd	nd	nd
U	.61	nd	nd	nd	1.31
Th	2.80	nd	nd	nd	5.90
Pb	31.00	nd	nd	nd	nd
Zn	350.00	350.00	300.00	270.00	230.00
Nb	17.00	nd	14.00	13.00	17.00
Y	15.00	19.40	nd	17.10	18.20
Sc	11.30	nd	nd	13.40	15.00
Hf	8.80	nd	nd	nd	11.10
Ta	.48	nd	nd	nd	.70
Cr	240.00	330.00	280.00	250.00	340.00
Ni	130.00	150.00	150.00	150.00	180.00
V	100.00	125.00	125.00	100.00	100.00
Cu	20.00	50.00	30.00	50.00	50.00

nd = Not Determined

Table C.1.3 - Bom Jardim Complex, MPBAS

Sample	01	03	06	07	27	44	47
Sr	1413.00	1418.00	1221.00	1494.00	1457.00	1331.00	1238.00
Ba	3071.00	3050.00	2548.00	3041.00	3074.00	2804.00	2572.00
Rb	202.00	184.00	206.00	200.00	190.00	216.00	184.00
Cs	nd	nd	nd	nd	4.07	nd	nd
U	nd	nd	nd	nd	2.33	nd	nd
Th	nd	nd	nd	nd	25.80	nd	nd
Pb	nd	nd	nd	nd	nd	nd	nd
Zn	280.00	350.00	350.00	360.00	360.00	290.00	330.00
Nb	nd	nd	nd	15.00	24.00	nd	nd
Y	nd	15.20	nd	14.60	16.70	nd	nd
Sc	nd	nd	nd	nd	10.30	nd	nd
Hf	nd	nd	nd	nd	12.40	nd	nd
Ta	nd	nd	nd	nd	.90	nd	nd
Cr	190.00	200.00	170.00	180.00	165.00	200.00	180.00
Ni	80.00	90.00	90.00	100.00	90.00	110.00	100.00
V	80.00	75.00	55.00	80.00	65.00	85.00	60.00
Cu	70.00	20.00	20.00	20.00	20.00	10.00	20.00

Sample	48	52	53	62	65	66	99
Sr	1492.00	1361.00	1538.00	1296.00	1003.00	1677.00	1741.00
Ba	3073.00	2814.00	3030.00	2650.00	1996.00	3176.00	3524.00
Rb	193.00	210.00	166.00	135.00	220.00	184.00	179.00
Cs	nd	nd	nd	nd	nd	nd	nd
U	nd	nd	2.15	nd	nd	nd	nd
Th	nd	nd	16.70	nd	nd	nd	nd
Pb	nd	nd	45.00	nd	nd	nd	nd
Zn	360.00	340.00	300.00	280.00	390.00	390.00	370.00
Nb	17.00	18.00	17.00	nd	nd	nd	nd
Y	14.40	14.70	12.00	13.30	nd	nd	16.00
Sc	nd	nd	9.40	nd	nd	nd	nd
Hf	nd	nd	10.10	nd	nd	nd	nd
Ta	nd	nd	.86	nd	nd	nd	nd
Cr	210.00	160.00	165.00	165.00	160.00	185.00	150.00
Ni	110.00	90.00	90.00	80.00	110.00	110.00	110.00
V	70.00	75.00	80.00	50.00	50.00	80.00	70.00
Cu	30.00	15.00	20.00		15.00	30.00	40.00

nd = Not Determined

Table C.1.3 - Bom Jardim Complex, MPBAS (contd)

Sample	162	268	271	262	305	306
Sr	1595.00	1274.00	1304.00	1187.00	1248.00	1331.00
Ba	3236.00	2741.00	2872.00	2503.00	2741.00	2728.00
Rb	183.00	201.00	204.00	188.00	190.00	190.00
Cs	nd	nd	3.29	nd	7.24	nd
U	2.33	nd	2.93	2.32	4.08	nd
Th	23.20	22.00	24.30	16.70	21.10	nd
Pb	nd	38.00	45.00	44.00	51.00	nd
Zn	27.00	260.00	290.00	270.00	300.00	310.00
Nb	13.00	15.00	19.00	16.00	20.00	nd
Y	16.30	14.10	14.50	11.30	14.80	13.30
Sc	9.60	902.00	6.80	6.40	9.20	8.60
Hf	11.60	nd	9.60	nd	10.70	nd
Ta	.70	nd	.86	1.08	1.34	nd
Cr	170.00	170.00	130.00	150.00	180.00	160.00
Ni	100.00	100.00	70.00	70.00	100.00	100.00
V	80.00	70.00	70.00	60.00	70.00	80.00
Cu	40.00	15.00	20.00	50.00	30.00	40.00

nd = Not Determined

Table C.1.4 - Bom Jardim Complex, PBLS

Sample	10	25	26	49	159	163	209D	323	330
Sr	1199.00	1133.00	1125.00	1189.00	1083.00	1331.00	1139.00	1238.00	1242.00
Ba	2558.00	2441.00	2379.00	2477.00	2288.00	2744.00	2305.00	2627.00	2624.00
Rb	270.00	276.00	248.00	235.00	250.00	260.00	225.00	250.00	268.00
Cs	8.34	10.51	nd	nd	nd	nd	nd	nd	nd
U	3.07	4.55	4.61	3.00	nd	3.67	6.35	5.90	3.67
Th	44.50	40.20	47.10	nd	nd	64.60	63.20	61.40	64.60
Pb	52.00	60.00	nd	nd	nd	55.00	nd	59.00	55.00
Zn	570.00	530.00	390.00	640.00	490.00	560.00	530.00	3.60	470.00
Nb	31.00	27.00	33.00	42.00	nd	34.00	34.00	28.00	32.00
Y	19.00	18.00	17.30	14.80	18.80	16.20	16.20	15.70	17.10
Sc	7.10	14.90	9.00	8.20	8.40	6.80	8.00	9.00	8.30
Hf	17.60	14.90	18.60	nd	nd	20.20	nd	nd	18.00
Ta	1.38	1.48	2.10	1.40	nd	2.40	2.10	2.40	2.20
Cr	110.00	90.00	80.00	90.00	110.00	60.00	50.00	120.00	60.00
Ni	40.00	40.00	40.00	40.00	50.00	50.00	30.00	60.00	50.00
V	75.00	65.00	70.00	75.00	70.00	70.00	60.00	80.00	79.00
Cu	40.00	30.00	40.00	30.00	40.00	40.00	40.00	40.00	40.00

nd = Not Determined

Table C.1.5 - Bom Jardim Complex, CS

Sample	23	31	40	54	104	163	209D
Sr	978.00	1316.00	1186.00	1226.00	1067.00	1331.00	1139.00
Ba	2094.00	2905.00	3008.00	2785.00	2707.00	2744.00	2305.00
Rb	300.00	247.00	285.00	265.00	207.00	260.00	225.00
Cs	7.48	nd	nd	nd	nd	nd	nd
U	2.93	nd	nd	nd	nd	3.67	6.35
Th	17.40	nd	nd	nd	nd	64.60	63.20
Pb	48.00	nd	nd	nd	nd	55.00	nd
Zn	310.00	750.00	500.00	640.00	390.00	560.00	530.00
Nb	27.00	nd	nd	nd	nd	34.00	34.00
Y	14.50	18.00	14.10	21.10	nd	16.20	16.20
Sc	7.10	nd	nd	nd	nd	6.80	8.00
Hf	10.00	nd	nd	nd	nd	20.20	nd
Ta	1.53	nd	nd	nd	nd	2.40	2.10
Cr	80.00	130.00	55.00	110.00	110.00	60.00	50.00
Ni	20.00	60.00	40.00	60.00	40.00	50.00	30.00
V	90.00	120.00	40.00	120.00	100.00	70.00	60.00
Cu	100.00	30.00	40.00	50.00	15.00	40.00	40.00

nd = Not Determined

Table C.1.6 - Bom Jardim Complex, Pink Granites

Sample	36	43	223	238	266	267	328
Sr	854.00	735.00	445.00	670.00	921.00	908.00	2410.00
Ba	2173.00	1489.00	760.00	1619.00	2444.00	2448.00	183.00
Rb	100.00	140.00	218.00	226.00	173.00	194.00	2.88
Cs	nd	nd	3.27	nd	nd	7.24	2.38
U	nd	nd	4.36	6.00	nd	4.59	22.00
Th	7.70	4.80	19.70	29.00	nd	22.70	35.00
Pb	37.00	38.00	45.00	42.00	nd	nd	240.00
Zn	170.00	168.00	130.00	200.00	260.00	200.00	15.00
Nb	6.00	6.00	10.00	10.00	nd	15.00	16.70
Y	3.80	4.20	7.00	10.00	12.00	15.00	4.70
Sc	2.50	1.00	4.00	4.00	4.40	4.00	6.70
Hf	nd	nd	4.80	nd	nd	7.30	1.26
Ta	nd	nd	.61	nd	nd	1.48	20.00
Cr	30.00	30.00			15.00	10.00	15.00
Ni		20.00					40.00
V	20.00	15.00	15.00	20.00	40.00	30.00	15.00
Cu	15.00	60.00		20.00	10.00	10.00	

nd = Not Determined

Table C.1.7 - Bom Jardim Complex, Enclaves

Sample	03A	28A	54A	74A	75A	83A
Sr	1573.00	1642.00	478.00	1009.00	1719.00	1401.00
Ba	1782.00	2663.00	2807.00	4175.00	31.76	2695.00
Rb	192.00	133.00	264.00	187.00	145.00	155.00
Cs	nd	nd	nd	nd	nd	nd
U	nd	nd	nd	nd	nd	nd
Th	1.80	4.60	5.10	nd	nd	nd
Pb	17.00	17.00	6.00	nd	nd	nd
Zn	170.00	220.00	180.00	29.00	260.00	280.00
Nb	21.00	16.00	31.00	nd	nd	nd
Y	14.40	24.20	33.90	30.90	20.10	23.00
Sc	17.70	22.20	26.40	15.90	14.60	19.40
Hf	nd	nd	nd	nd	nd	nd
Ta	nd	nd	nd	nd	nd	nd
Cr	290.00	410.00	968.00	325.00	360.00	420.00
Ni	170.00	220.00	353.00	230.00	230.00	230.00
V	145.00	160.00	220.00	110.00	105.00	160.00
Cu	210.00	80.00	120.00	20.00	230.00	630.00

Sample	130A	130C	137A	144E	249A	323A
Sr	1947.00	1389.00	1416.00	1345.00	1280.00	959.00
Ba	3371.00	2873.00	2861.00	2625.00	2220.00	1882.00
Rb	123.00	154.00	124.00	156.00	81.00	287.00
Cs	nd	nd	nd	3.27	nd	nd
U	nd	nd	1.19	.79	nd	2.40
Th	3.10	nd	3.90	3.00	nd	16.10
Pb	16.10	nd	nd	19.00	nd	47.00
Zn	220.00	250.00	220.00	390.00	190.00	240.00
Nb	17.00	nd	16.00	15.00	nd	18.00
Y	17.80	nd	23.80	23.20	nd	22.80
Sc	21.90	nd	19.70	22.70	nd	20.30
Hf	nd	nd	6.70	9.00	nd	7.70
Ta	nd	nd	.53	.48	nd	.69
Cr	590.00	420.00	410.00	480.00	400.00	500.00
Ni	300.00	220.00	230.00	290.00	200.00	150.00
V	150.00	1210.00	120.00	160.00	180.00	140.00
Cu	130.00	180.00	120.00	110.00	60.00	5610.00

nd = Not Determined

Table C.1.8 - Bom Jardim Complex, Mafic Dykes

Sample	130D	133A	205	216	254B	254D	265A	272A	292A
Sr	2196.00	1275.00	2747.00	722.00	1469.00	1696.00	1300.00	1269.00	1655.00
Ba	2853.00	2894.00	6792.00	1892.00	4336.00	2961.00	2717.00	1040.00	4126.00
Rb	120.00	225.00	156.00	261.00	212.00	158.00	173.00	27.00	224.00
Cs	1.34	nd	3.56	nd	6.36	8.00	8.66	nd	5.62
U	.69	nd	1.65	nd	1.35	.69	3.17	nd	7.39
Th	1.90	17.00	14.90	6.00	3.90	2.90	4.70	1.80	35.10
Pb	nd	31.00	24.00	44.00	21.00	23.00	nd	11.00	34.00
Zn	150.00	260.00	380.00	320.00	484.00	229.00	140.00	70.00	280.00
Nb	12.00	20.00	19.00	13.00	25.00	23.00	16.00	4.00	16.00
Y	13.10	24.50	32.20	24.80	19.80	18.30	18.60	12.20	24.50
Sc	18.20	nd	15.90	nd	13.70	14.20	18.90	nd	12.20
Hf	5.20	nd	9.00	nd	10.70	5.60	3.70	ndf	9.10
Ta	.42	nd	.45	nd	.68	.63	.60	nd	1.13
Cr	190.00	480.00	215.00	340.00	430.00	360.00	490.00	120.00	350.00
Ni	120.00	240.00	220.00	50.00	300.00	240.00	190.00	40.00	210.00
V	150.00	110.00	140.00	120.00	120.00	140.00	140.00	200.00	100.00
Cu	200.00	20.00	50.00	40.00		170.00	100.00	20.00	

nd = Not Determined

C.2 REE ELEMENTS

Table C.2.1 - Bom Jardim Complex, PBAMS

Sample	79	83	75	86	28
La	95.50	85.90	100.20	91.40	70.60
Ce	188.10	169.40	185.90	179.10	138.10
Pr	22.50	19.80	21.70	21.00	16.50
Nd	85.30	74.50	81.20	79.10	63.10
Sm	13.60	12.10	12.30	12.80	9.60
Eu	3.50	3.30	3.30	3.40	3.20
Gd	9.30	8.30	8.40	8.80	6.60
Dy	5.00	4.40	4.50	4.50	3.60
En	2.20	1.95	1.90	2.00	1.60
Yb	1.50	1.40	1.40	1.40	1.10
Lu	.23	.20	.20	.20	.17

Table C.2.1. - Bom Jardim Complex, PBAMS (contd)

Sample	144	344	283	200
La	55.00	102.60	86.20	77.60
Ce	133.40	206.30	173.20	135.30
Pr	14.00	25.20	20.80	19.30
Nd	55.50	98.20	79.40	72.88
Sm	8.90	15.80	12.90	11.70
Eu	2.60	4.00	3.40	3.30
Gd	6.40	10.90	8.90	7.80
Dy	3.90	5.90	4.80	4.20
En	1.80	2.40	2.10	2.10
Yb	1.40	1.70	1.60	1.30
Lu	.20	.25	.24	.20

Table C.2.2 - Bom Jardim Complex, PBM

Sample	90	92
La	71.80	83.30
Ce	144.10	167.30
Pr	17.70	21.70
Nd	69.90	85.90
Sm	10.60	14.10
Eu	3.20	3.90
Gd	7.40	9.70
Dy	4.00	5.20
En	1.60	2.10
Yb	1.20	1.50
Lu	.17	.22

Table C.2.3 - Bom Jardim Complex, MPBAS

Sample	03	07	48	52	62	271
La	84.00	96.30	75.80	90.00	83.70	90.00
Ce	157.40	160.70	145.30	161.50	152.80	135.00
Pr	18.30	18.30	16.60	18.30	17.10	20.10
Nd	67.10	67.20	61.20	65.00	62.50	65.10
Sm	10.20	10.00	9.80	10.10	9.10	9.90
Eu	2.70	2.80	2.70	2.70	2.60	2.50
Gd	7.10	6.90	6.90	7.00	6.20	6.00
Dy	3.90	3.70	3.60	3.80	3.40	3.40
En	1.70	1.80	1.60	1.70	1.50	1.70
Yb	1.20	1.20	1.20	1.20	1.10	1.20
Lu	.19	.18	.18	.18	.15	.18

Table C.2.4 - Bom Jardim Complex, PBLS

Sample	10	25	49
La	99.10	92.30	67.00
Ce	176.30	171.70	132.50
Pr	20.60	19.40	16.20
Nd	74.30	67.50	60.80
Sm	11.40	10.60	9.00
Eu	2.60	2.60	2.40
Gd	8.20	7.70	6.50
Dy	4.70	4.30	3.80
En	2.20	2.10	1.80
Yb	1.60	1.60	1.30
Lu	.20	.20	.20

Table C.2.5 - Bom Jardim Complex, CS

Sample	23	40	54
La	86.80	72.90	105.80
Ce	162.66	141.90	205.80
Pr	19.10	15.90	24.10
Nd	66.00	55.30	86.20
Sm	10.00	8.70	14.00
Eu	2.40	2.50	3.30
Gd	6.50	6.40	10.00
Dy	3.60	3.50	5.40
En	1.70	1.60	2.50
Yb	1.20	1.10	1.70
Lu	.19	.17	.25

Table C.2.6 - Bom Jardim Complex, Pegmatites

Sample	150	156
La	24.20	2.25
Ce	40.10	5.73
Pr		
Nd	14.20	1.81
Sm	2.30	.25
Eu	1.50	.19
Gd		.39
Tb	.14	.05
Tm		.07
Yb	.21	.33
Lu	.03	.06

Table C.2.7 - Bom Jardim Complex, Pink Granites

Sample	36	43	223	267
La	32.90	22.71	44.21	93.70
Ce	55.30	37.20	84.26	159.90
Pr	5.90	4.10		
Nd	21.40	13.70	28.00	62.40
Sm	2.70	1.90	4.10	9.10
Eu	1.80	1.30	.80	1.90
Gd	1.90	1.10	.80	7.90
Tb			.34	.80
Dy	1.00	.70		
En	.50	.30		
Tm			.09	.21
Yb	.30	.28	.54	1.37
Lu	.06	.04	.06	.15

Table C.2.8 - Bom Jardim Complex, Enclaves

Sample	306A	306B	333A	333B	130A	144E	327A*
La	115.20	93.40	55.70	119.20	95.80	67.00	102.10
Ce	200.70	174.90	113.30	231.50	213.90	150.00	211.70
Pr					21.10		24.70
Nd	81.90	72.20	54.00	100.00	78.70	73.60	93.40
Sm	13.10	11.80	9.30	14.90	12.70	12.40	16.30
Eu	3.50	2.90	2.60	3.50	3.40	3.10	3.50
Gd	10.40	10.60	8.70	11.40	8.30	6.30	12.30
Tb	1.09	1.08	.94	1.19		1.10	
Dy					4.40		9.30
En					2.10		5.00
Tm	.31	.49	.35	.36		.33	
Yb	1.60	1.50	1.94	1.77	1.30	1.80	4.20
Lu	.18	.17	.23	.23	.19	.24	.63

* Metasedimentary Enclave

Table C.2.9 - Bom Jardim Complex, Mafic Dykes

Sample	130D	205	272A	254B	254D	292A
La	66.20	169.40	25.00	93.40	65.70	182.20
Ce	126.40	369.10	49.80	191.10	131.50	333.30
Pr	15.30	40.30	6.90	23.10		
Nd	64.10	176.00	26.60	86.80	143.80	69.60
Sm	9.10	28.60	4.80	13.80	22.40	9.40
Eu	3.20	7.10	1.60	3.50	5.10	2.70
Gd	6.00	18.20	3.50	9.50	13.70	5.60
Tb					1.65	.93
Dy	3.20	8.20	2.60	5.00		
En	1.60	3.80	1.30	2.30		
Tm					.51	.27
Yb	1.20	2.00	1.10	1.60	1.70	.90
Lu	.15	.31	.16	.24	.18	.13

Table C.2.10 - Bom Jardim Complex, Country Rocks

Sample	175	278	349B	354
La	22.00	40.50	34.60	28.30
Ce	43.20	84.00	80.50	79.30
Nd	15.70	38.30	43.10	27.50
Sm	2.40	7.30	8.50	6.00
Eu	.80	1.80	2.20	.60
Gd	2.00	4.70	9.50	.60
Tb	.29	1.09	.93	1.19
Tm	.24	1.04	.85	.48
Yb	1.20	4.00	2.10	3.00
Lu	.22	.59	.37	.36

APPENDIX D
MINERAL CHEMISTRY DATA

Table D.1.1 - Bom Jardim Complex, PBAMS, Pyroxenes

Sample	200	200	200	200	288	288	249	249
Point	Rim	Core	Core	Rim	Core	Rim	Core	Core
SiO2	52.330	53.170	53.040	52.780	51.620	52.940	52.390	52.880
TiO2	.190	.000	.230	.000	.270	.000	.250	.000
Al2O3	1.040	.940	.720	.890	1.250	.790	.930	.920
Cr2O3	.000	.000	.000	.000	.160	.000	.000	.000
FeO	9.010	9.070	8.340	9.450	9.350	9.120	8.640	8.800
MnO	.490	.380	.430	.440	.450	.640	.220	.700
NiO	.000	.000	.000	.000	.000	.000	.000	.180
MgO	13.690	13.600	14.040	13.470	12.480	12.480	14.030	14.330
CaO	21.900	22.470	22.300	22.740	22.320	22.530	21.860	21.980
Na2O	.960	.940	.790	.830	1.180	.860	.910	.990
Total	99.610	100.570	99.890	100.600	99.080	99.360	99.230	100.780
FORMULA UNITS (Based on 6 Oxygens)								
Si	1.967	1.977	1.981	1.967	1.961	1.985	1.969	1.962
Al4	.033	.023	.019	.033	.039	.015	.031	.038
Al6	.013	.018	.013	.006	.047	.035	.010	.002
Ti	.005	.000	.006		.008		.007	
Cr								
Fe	.286	.282	.260	.295	.297	.289	.271	.273
Mn	.016	.012	.014	.014	.014	.020	.007	.022
Ni								
Mg	.767	.754	.782	.748	.706	.706	.786	.792
Ca	.882	.896	.892	.908	.908	.916	.880	.874
Na	.070	.068	.057	.065	.087	.063	.067	.071
Fe/Fe+Mg	.272	.272	.249	.283	.296	.290	.256	.256
WO	46.000	46.000	46.000	46.000	47.000	48.000	45.000	45.000
EN	40.000	39.000	40.000	38.000	37.000	37.000	41.000	41.000
FS	14.000	15.000	14.000	16.000	16.000	15.000	14.000	14.000

Table D.1.1 - Bom Jardim Complex, PBAMS, Pyroxenes (contd)

Sample	193	193	187	187	287	287
Point	Core	Core	Core	Core	Core	Core
SiO2	52.550	52.750	53.480	52.880	52.830	53.310
TiO2	.000	.170	.240	.000	.000	.200
Al2O3	1.050	1.150	1.250	1.170	.740	1.040
Cr2O3	.370	.580	.000	.230	7.970	.260
FeO(T)	8.250	8.480	6.380	7.840	.400	5.810
MnO	.220	.330	.260	.260	.000	.350
NiO	.000	.000	.000	.000	14.110	.190
MgO	13.380	13.460	15.380	13.600	22.450	14.940
CaO	22.760	22.110	21.300	22.660	.760	23.130
Na2O	1.130	.940	.890	.880		1.090
Total	99.710	99.970	99.180	99.520	99.260	100.320

FORMULA UNITS (Based on 6 Oxygens)

Si	1.969	1.971	1.977	4.978	1.977	1.968
Al4	.031	.029	.023	.024	.023	.032
Al6	.015	.021	.031	.028	.010	.013
Ti	.000	.005	.007			.006
Cr	.011	.017		.007		.008
Fe	.259	.265	.197	.245	.247	.179
Mn	.007	.010	.008	.008	.013	.011
Ni						
Mg	.747	.750	.847	.757	.787	.822
Ca	.914	.885	.843	.907	.900	.915
Na	.082	.068	.064	.064	.055	.078
Fe/Fe+Mg	.257	.261	.198	.244	.239	.179
WO	48.000	47.000	45.000	47.000	46.000	48.000
EN	39.000	39.000	45.000	40.000	41.000	43.000
FS	13.000	14.000	10.000	13.000	13.000	9.000

Table D.1.2 - Bom Jardim Complex, PBM, Pyroxenes

Sample	258	258	258	258	258	252	252	252	252
Point	Rim	Rim	Core	Core	Rim	Core	Core	Rim	Core
SiO2	52.500	52.910	52.490	53.020	52.460	52.750	52.930	53.170	52.820
TiO2	.000	.000	.000	.000	.000	.000	.000	.000	.180
Al2O3	1.270	1.420	.730	1.160	1.140	1.160	.720	.860	.510
Cr2O3							.180		
FeO(T)	8.310	8.730	8.370	8.300	8.740	8.210	7.680	7.920	8.140
MnO	.510	.400	.460	.310		.490	.250	.230	.330
NiO						.220	.000		
MgO	13.190	13.640	13.040	13.760	13.670	13.880	13.600	13.470	13.410
CaO	22.270	21.870	23.020	22.970	22.510	21.920	23.030	22.890	22.740
Na2O	.930	1.230	.900	1.080	1.190	1.070	.770	1.000	.850
Total	99.000	100.200	99.010	100.600	99.710	99.700	99.160	99.540	99.380

FORMULA UNITS (Based on 6 Oxygens)

Si	1.979	1.968	1.983	1.972	1.962	1.972	1.978	1.985	1.979
Al4	.210	.320	.017	.028	.038	.028	.022	.015	.021
Al6	.035	.030	.016	.023	.012	.023	.010	.018	.019
Ti									.005
Cr							.005		
Fe	.262	.272	.264	.258	.272	.257	.240	.247	.255
Mn	.016	.013	.015	.010		.016	.008	.007	.011
Ni						.007			
Mg	.741	.756	.734	.763	.762	.773	.758	.749	.749
Ca	.900	.872	.932	.904	.902	.878	.922	.915	.913
Na	.067	.089	.066	.078	.086	.078	.056	.073	.062
Fe/Fe+Mg	.261	.265	.264	.253	.263	.249	.240	.248	.254
WO	47.000	46.000	48.000	47.000	47.000	46.000	48.000	48.000	48.000
EN	39.000	40.000	38.000	40.000	39.000	41.000	39.000	39.000	39.000
FS	14.000	14.000	14.000	13.000	14.000	13.000	13.000	13.000	13.000

Table D.1.3 - Bom Jardim Complex, MPBAS, Pyroxenes

Sample	272	272	272	272	172	172
Point	Core	Core	Core	Core	Core	Core
SiO2	53.460	52.140	52.890	52.970	53.080	52.100
TiO2	.000	.270	.000	.000	.220	1.450
Al2O3	1.580	1.350	.920	1.230	1.140	.840
Cr2O3	.000	.340	.000	.000	.210	.000
FeO	9.300	8.490	8.450	8.390	8.390	8.390
MnO	.290	.520	.350	.260	.330	.270
NiO	.000	.180	.230	.000	.000	.000
MgO	14.540	12.900	12.870	13.600	13.170	13.110
CaO	18.850	21.880	22.730	22.140	22.690	22.460
Na2O	1.020	1.380	1.330	1.130	1.140	.930
Total	99.040	99.450	99.770	99.720	100.370	99.550

FORMULA UNITS (Based on 6 Oxygens)

Si	1.994	1.972	1.982	1.977	1.959	1.953
Al4	.006	.028	.018	.023	.041	.037
Al6	.064	.032	.023	.031	.010	.010
Ti		.008			.008	.040
Cr		.010			.008	
Fe	.290	.268	.265	.262	.258	.265
Mn	.009	.017	.011	.008	.011	.010
Ni		.005	.001			
Mg	.808	.724	.719	.757	.733	.734
Ca	.753	.886	.913	.885	.903	.898
Na	.074	.100	.097	.082	.084	.071
Fe/Fe+Mg	.264	.270	.269	.257	.260	.265
WO	41.000	47.000	48.000	46.000	48.000	47.000
Em	44.000	39.000	38.000	40.000	39.000	39.000
FS	16.000	14.000	14.000	14.000	13.000	14.000

Table D.1.3 - Bom Jardim Complex, MPBAS, Pyroxenes (contd)

Sample	27	27	07	07	07	07
Point	Core	Core	Core	Core	Core	Rim
SiO2	52.760	52.560	52.560	53.350	52.540	53.100
TiO2	.000	.190	.210	.000	.210	.000
Al2O3	.910	1.160	1.190	.770	.820	1.080
Cr2O3	.000	.200	.530	.190	.180	.200
FeO	8.730	8.460	8.060	8.420	7.830	8.620
MnO	.370	.540	.380	.350	.430	.450
NiO	.000	.000	.000	.000	.000	.260
MgO	13.220	12.900	13.220	13.020	13.570	13.770
CaO	23.370	22.230	22.360	22.820	22.470	20.570
Na2O	1.470	1.110	1.070	1.160	1.190	1.220
Total	100.830	99.350	99.580	100.080	99.240	99.270
FORMULA UNITS (Based on 6 Oxygens)						
Si	1.978	1.978	1.971	1.992	1.976	1.989
Al4	.022	.022	.029	.008	.024	.011
Al6	.018	.030	.024	.026	.012	.037
Ti		.005	.006		.006	
Cr		.006	.016	.006	.005	.006
Fe	.274	.266	.253	.263	.246	.270
Mn	.012	.017	.012	.011	.014	.014
Ni						.008
Mg	.739	.724	.739	.725	.761	.769
Ca	.899	.896	.898	.913	.906	.826
Na	.107	.081	.078	.084	.087	.088
Fe/Fe+Mg	.270	.269	.255	.266	.244	.260
WO	47.000	48.000	48.000	48.000	47.000	44.000
Em	39.000	38.000	39.000	38.000	40.000	41.000
FS	14.000	14.000	13.000	14.000	13.000	15.000

Table D.1.4 - Bom Jardim Complex, PBLS, Pyroxenes

Sample	49	49	49	49	10	10
Point	Core	Core	Core	Rim	Core	Rim
SiO2	52.150	52.540	52.030	52.210	51.670	52.570
TiO2	.210	.000	.330	.210	.190	.000
Al2O3	.940	1.050	.960	1.040	1.210	.660
Cr2O3	.000	.000	.000	.000	.000	.000
FeO	10.660	10.550	10.720	10.830	10.420	9.940
MnO	.290	.330	.460	.450	.290	.340
NiO	.000	.000	.000	.000	.000	.000
MgO	12.370	12.370	12.370	12.250	11.840	11.980
CaO	22.380	22.490	21.420	21.410	22.410	23.190
Na2O	1.190	1.100	1.260	1.310	1.150	1.280
Total	100.190	99.380	99.550	99.710	99.180	99.960
FORMULA UNITS (Based on 6 Oxygens)						
Si	1.964	1.969	1.973	1.975	1.964	1.975
Al4	.036	.031	.027	.025	.036	.025
Al6	.006	.016	.016	.015	.018	.004
Ti	.006	.000	.010	.008	.005	
Cr						
Fe	.336	.331	.340	.327	.331	.312
Mn	.009	.011	.015	.014	.009	.011
Ni						
Mg	.695	.691	.699	.695	.671	.671
Ca	.903	.903	.870	.869	.913	.934
Na	.087	.080	.093	.094	.085	.093
Fe/Fe+Mg	.326	.324	.327	.320	.330	.317
WO	46.000	46.000	45.000	45.000	47.000	48.000
En	36.000	36.000	36.000	36.000	35.000	35.000
FS	18.000	18.000	19.000	19.000	18.000	17.000

Table D.1.4 - Bom Jardim Complex, PBLS, Pyroxenes (contd)

Sample	10	10	10	10
Point	Core	Core	Core	Rim
SiO2	51.830	52.200	52.520	51.750
TiO2	.000	.190	.320	.000
Al2O3	1.220	1.020	.930	.730
Cr2O3	.000	.000	.000	.000
FeO	10.820	10.500	10.910	11.350
MnO	.410	.360	.490	.470
NiO	.000	.000	.000	.000
MgO	11.600	11.790	12.600	12.110
CaO	22.070	22.640	20.140	21.800
Na2O	1.330	1.170	1.420	1.120
Total	99.280	99.870	99.330	99.330
FORMULA UNITS (Based on 6 Oxygens)				
Si	1.971	1.975	1.979	1.965
Al4	.029	.025	.031	.033
Al6	.026	.021	.011	
Ti		.005	.009	
Cr				
Fe	.344	.332	.344	.360
Mn	.013	.012	.016	.015
Ni				
Mg	.658	.665	.708	.685
Ca	.899	.918	.813	.887
Na	.098	.086	.104	.082
Fe/Fe+Mg	.343	.333	.327	.344
WO	47.000	48.000	43.000	46.000
En	34.000	34.000	38.000	35.000
FS	19.000	18.000	19.000	19.000

Table D.1.5 - Bom Jardim Complex, CS, Pyroxenes

Sample	23	23	23	23
Point	Core	Core	Core	Core
SiO2	52.010	52.010	52.160	51.470
TiO2		.240		.200
Al2O3	.740	.820	.730	.510
Cr2O3			.290	
FeO	11.520	12.470	12.600	13.190
MnO	.190	.320	.270	.430
NiO		.330		.290
MgO	11.330	10.890	10.980	10.530
CaO	21.250	20.650	21.150	20.750
Na2O	1.700	2.000	1.960	1.980
Total	98.740	99.730	100.140	99.350
FORMULA UNITS (Based on 6 Oxygens)				
Si	1.991	1.982	1.980	1.890
Al4	.009	.018	.020	.110
Al6	.024	.019	.013	
Ti		.007		
Cr		.000	.009	
Fe	.369	.397	.400	.399
Mn	.005	.010	.009	.014
Ni		.010		.010
Mg	.647	.619	.621	.593
Ca	.872	.843	.860	.844
Na	.126	.147	.144	.147
Fe/Fe+Mg	.363	.394	.392	.402
WO	46.000	45.000	46.000	46.000
En	34.000	33.000	33.000	32.000
FS	20.000	22.000	21.000	22.000

Table D.1.6 - Bom Jardim Complex, Igneous Enclaves, Pyroxenes

Sample	1306	1306	1306	1306	1306	323A
Point	Core	Rim	Core	Rim	Core	Core
SiO2	53.590	53.400	52.770	53.700	53.020	51.310
TiO2			.210		.200	.600
Al2O3	1.050	2.050	1.070	.960	.690	3.110
Cr2O3		.520	.490			
FeO	8.630	6.650	8.000	8.690	8.570	10.890
MnO	.220	.210	.410	.270	.650	.370
NiO						
MgO	15.460	16.100	13.630	14.290	14.360	13.090
CaO	18.710	19.070	21.610	21.960	21.760	18.970
Na2O	1.230	1.180	1.050	1.080	.640	1.760
Total	99.030	99.280	99.450	100.950	99.830	100.100

FORMULA UNITS (Based on 6 Oxygens)

Si	1.992	1.968	1.972	1.978	1.978	1.920
Al4	.008	.032	.028	.022	.021	.080
Al6	.038	.057	.019	.020	.009	.057
Ti			.006			.017
Cr		.015	.014			
Fe	.268	.205	.250	.267	.268	.341
Mn	.007	.006	.013	.008	.021	.012
Ni						
Mg	.857	.885	.759	.782	.799	.730
Ca	.745	.753	.865	.864	.870	.761
Na	.088	.085	.076	.077	.046	.128
Fe/Fe+Mg	.238	.188	.248	.254	.251	.318
WO	30.700	40.870	46.140	45.470	45.000	41.000
Em	46.140	47.960	40.770	41.370	41.000	40.000
FS	23.160	11.170	13.090	13.160	14.000	19.000

Table D.1.6 - Bom Jardim Complex, Igneous Enclaves, Pyroxenes (contd)

Sample	130E	130E	130E	130E	130E	130E
Point	Core	Rim	Core	Rim	Core	Rim
SiO2	52.340	52.540	52.260	53.150	53.030	53.600
TiO2						.230
Al2O3	.360	.970	.930		.920	1.520
Cr2O3	.170	.370				.340
FeO	7.490	7.750	7.710	8.300	7.790	7.150
MnO	.290		.300	.340	.390	.280
NiO						
MgO	14.380	13.920	13.880	14.490	14.360	14.670
CaO	21.990	22.370	21.690	21.810	21.900	21.960
Na2O	.770	1.080	.870	1.100	.870	.900
Total	98.080	99.390	98.890	99.630	99.100	100.650
FORMULA UNITS (Based on 6 Oxygens)						
Si	1.986	1.974	1.976	1.963	1.986	1.971
Al4	.014	.026	.024	.037	.014	.029
Al6	.002	.017	.018	.016	.027	.037
Ti						.007
Cr	.005	.011				.010
Fe	.238	.244	.242	.259	.244	.220
Mn	.009		.013	.013	.012	.009
Ni						
Mg	.813	.780	.794	.802	.801	.810
Ca	.894	.900	.885	.866	.879	.887
Na	.057	.079	.062	.085	.063	.061
Fe/Fe+Mg	.226	.238	.233	.244	.233	.214
WO	46.000	47.000	46.000	45.000	45.000	46.000
EN	42.000	41.000	41.000	42.000	42.000	42.000
FS	12.000	13.000	13.000	13.000	13.000	120.000

Table D.1.7 - Bom Jardim Complex, Mafic Dykes, Pyroxenes

Sample	216	216	216	216	205
Point	Rim	Core	Core	Rim	Core
SiO2	52.140	51.720	52.160	47.810	56.200
TiO2	.390	.300		4.630	
Al2O3	1.870	.940	1.140	2.100	1.960
Cr2O3		.500		.270	
FeO	10.490	10.470	10.340	13.530	10.150
MnO	.500	.400	.620	.580	
NiO					
MgO	13.970	13.180	13.230	12.770	17.680
CaO	18.960	21.690	21.220	17.450	12.800
Na2O	.770	.860	1.010	1.000	.580
Total	99.400	100.500	99.830	100.160	99.370
FORMULA UNITS (Based on 6 Oxygens)					
Si	1.960	1.952	1.962	1.823	2.041
Al4	.040	.042	.038	.095	
Al6	.043		.013		.084
Ti	.011	.009		.133	
Cr		.015		.008	
Fe	.330	.330	.326	.431	.308
Mn	.016	.013	.020	.019	
Ni					
Mg	.783	.741	.742	.726	.957
Ca	.764	.877	.855	.713	.498
Na	.056	.063	.074	.074	.041
Fe/Fe+Mg	.296	.308	.305	.372	.243
WO	41.000	45.000	44.000	38.000	28.000
Em	42.000	38.000	39.000	39.000	54.000
FS	17.000	17.000	17.000	23.000	18.000

Table D.1.7 - Bom Jardim Complex, Mafic Dykes, Pyroxenes (contd)

Sample	130D	133A	133A	133A	133A
Point	Core	Core	Core	Rim	Core
SiO2	51.560	52.560	52.800	53.020	52.520
TiO2				.370	.350
Al2O3	1.660	1.100	.930	1.650	1.090
Cr2O3			.260		
FeO	9.350	7.870	7.530	8.560	9.250
MnO	.260	.310	.330	.280	.250
NiO					
MgO	13.220	14.060	14.470	14.970	13.810
CaO	21.660	21.970	22.150	19.540	21.850
Na2O	1.350	1.260	1.030	1.040	1.140
Total	99.060	99.130	99.510	99.450	100.260

FORMULA UNITS (Based on 6 Oxygens)

Si	1.943	1.970	1.970	1.970	1.962
Al4	.056	.030	.030	.030	.038
Al6	.018	.019	.011	.042	.010
Ti					
Cr			.008		
Fe	.295	.247	.235	.266	.289
Mn	.008	.010	.011	.009	.008
Ni					
Mg	.743	.786	.805	.829	.769
Ca	.875	.883	.886	.778	.874
Na	.099	.091	.075	.075	.082
Fe/Fe+Mg	.284	.239	.226	.243	.273
WO	46.000	46.000	46.000	42.000	45.000
Em	39.000	41.000	42.000	44.000	40.000
FS	15.000	13.000	12.000	14.000	15.000

Table D.2.1 - Bom Jardim Complex, PBAMS, Amphiboles

Sample	88	88	88	88	81	81	200	200
Point	Rim	Core	Rim	Core	Core	Core	Core	Core
SiO2	47.280	46.770	47.720	48.330	47.140	47.610	46.810	47.490
Al2O3	6.340	6.810	6.440	6.630	6.990	6.060	7.350	6.300
TiO2	1.340	1.050	.970	1.240	1.130	1.190	1.510	1.200
FeO	10.040	9.720	7.940	9.170	11.750	11.370	12.110	12.610
Fe2O3	2.090	3.480	5.220	3.460	2.090	1.560	3.330	1.870
MgO	14.810	14.670	15.180	15.560	13.240	13.770	13.350	13.290
MnO	.000	.000	.330	.000	.000	.430	.000	.230
CaO	11.630	11.730	11.330	11.950	11.370	11.730	11.970	12.040
Na2O	1.930	2.000	2.210	2.230	1.700	1.500	1.750	1.480
K2O	.620	.710	.570	.590	.740	.630	.810	.590
Total	96.080	96.940	97.910	98.980	96.150	95.850	98.990	97.100
MINERAL FORMULA UNITS (Based on 23 Oxygens)								
Si	7.000	6.894	6.930	6.933	7.015	7.097	6.827	7.033
Al4	1.000	1.106	1.070	1.069	.985	.903	1.173	.967
Al6	.106	.077	.032	.055	.241	.162	.090	.133
Ti	.146	.116	.106	.135	.126	.133	.166	.134
Fe+2	1.243	1.198	.964	1.099	1.462	1.417	1.477	1.562
Fe+3	.233	.386	.571	.374	.234	.175	.495	.209
Mg	3.268	3.223	3.286	3.322	2.936	3.059	2.902	2.933
Mn	.000	.000	.041			.054	.000	.029
Ca	1.845	1.853	1.763	1.834	1.813	1.874	1.870	1.911
NaB	.155	.147	.237	.166	.187	.126	.130	.089
(Na+K)A	.521	.556	.488	.557	.441	.424	.516	.441
Mg/Mg+Fe+2	.720	.730	.770	.750	.670	.680	.600	.650

Table D.2.1 - Bom Jardim Complex, PBAMS, Amphiboles (contd)

Sample	193	193	249	249	29	29	287	287
Point	Rim	Core	Core	Core	Core	Core	Core	Core
SiO2	46.540	46.720	47.840	47.880	47.450	48.840	48.320	48.550
Al2O3	6.890	6.900	6.610	6.490	6.560	6.210	6.260	6.310
TiO2	1.350	1.010	.950	1.200	1.090	1.060	.960	.990
FeO	12.850	13.430	10.270	8.530	8.380	10.780	8.740	9.210
Fe2O3	1.850	1.910	2.470	4.440	4.680	.950	3.100	2.510
MgO	13.160	12.450	14.230	14.660	15.040	15.060	15.250	15.030
MnO	.240	.000	.290	.360	.330	.000	.240	.350
CaO	11.910	11.670	11.430	11.220	11.500	12.130	11.550	11.450
Na2O	1.820	1.560	1.570	1.860	1.990	1.500	1.790	1.900
K2O	.890	.810	.650	.630	.760	.720	.720	.640
Total	97.500	96.460	96.610	97.280	97.780	97.250	96.870	96.940
MINERAL FORMULA UNITS (Based on 23 Oxygens)								
Si	6.905	6.994	7.047	6.989	6.913	7.123	7.062	7.090
Al4	1.095	1.006	.953	1.011	1.087	.877	.938	.910
Al6	.110	.211	.195	.106	.039	.190	.140	.176
Ti	.151	.114	.105	.132	.119	.116	.099	.109
Fe+2	1.594	1.682	1.266	1.041	1.021	1.315	1.069	1.125
Fe+3	.206	.215	.274	.488	.514	.104	.341	.276
Mg	2.910	2.778	3.124	3.189	3.266	3.273	3.322	3.271
Mn	.030		.036	.045	.041		.030	.043
Ca	1.899	1.872	1.851	1.755	1.795	1.896	1.809	1.792
NaB	.111	.128	.149	.245	.205	.104	.191	.208
(Na+K)A	.582	.478	.420	.393	.503	.458	.451	.447
Mg/Mg+Fe+2	.650	.620	.710	.750	.760	.760	.760	.740

Table D.2.1 - Bom Jardim Complex, PBAMS, Amphiboles (contd)

Sample	187	187	144	144	112	112
Point	Core	Core	Core	Core	Core	Core
SiO2	48.060	48.430	48.580	48.600	45.870	45.170
Al2O3	6.520	6.650	6.400	6.790	7.670	8.050
TiO2	1.290	1.220	.970	.710	1.720	1.490
FeO	10.350	10.920	10.450	8.540	12.850	11.280
Fe2O3	2.800	2.170	1.820	4.290	2.360	4.220
MgO	14.220	14.490	14.700	14.770	12.360	12.120
MnO	.300	.210	.000	.300	.250	.240
CaO	11.720	11.760	11.750	11.570	11.700	11.260
Na2O	1.480	1.940	1.570	1.580	1.510	1.420
K2O	.760	.710	.760	.590	.980	.990
Total	97.500	98.500	97.000	97.740	97.270	96.180
MINERAL FORMULA UNITS (Based on 23 Oxygens)						
Si	7.026	7.017	7.106	7.038	6.826	6.776
Al4	.974	.983	.894	.962	1.174	1.224
Al6	.149	.153	.209	.197	.171	.199
Ti	.142	.133	.107	.077	.193	.168
Fe+2	1.265	1.323	1.279	1.034	1.599	1.415
Fe+3	.308	.236	.200	.468	.264	.477
Mg	3.098	3.129	3.205	3.188	2.741	2.710
Mn	.037	.026	.000	.037	.032	.030
Ca	1.836	1.826	1.842	1.795	1.866	1.810
NaB	.164	.174	.158	.205	.134	.190
(Na+K)A	.402	.506	.427	.353	.492	.401
Mg/Mg+Fe+2	.710	.700	.710	.780	.630	.660

Table D.2.2 - Bom Jardim Complex, MPBAS, Amphiboles

Sample	07	07	27	27	268
Point	Core	Core	Core	Core	Core
SiO2	47.840	46.840	46.290	46.550	47.460
Al2O3	6.200	6.280	7.070	6.940	6.110
TiO2	1.260	1.170	1.230	1.390	1.370
FeO	12.050	9.180	11.280	12.590	8.570
Fe2O3	1.040	4.860	3.510	1.690	5.610
MgO	14.040	13.790	13.650	12.990	13.390
MnO	.200	.410	.000	.560	.310
CaO	11.490	10.770	11.410	11.710	11.160
Na2O	2.130	1.640	2.220	1.880	.550
K2O	.820	1.280	.920	.860	.720
Total	97.070	96.220	97.580	97.160	95.250
MINERAL FORMULA UNITS (Based on 23 Oxygens)					
Si	1.063	6.971	6.841	6.923	7.067
Al4	.937	1.029	1.159	1.077	.933
Al6	.142	.073	.072	.139	.134
Ti	.140	.131	.137	.155	.153
Fe+2	1.488	1.143	1.394	1.566	1.067
Fe+3	.116	.544	.390	.189	.629
Mg	3.089	3.059	3.006	2.879	2.972
Mn	.025	.052	.000	.071	.039
Ca	1.818	1.717	1.807	1.866	1.781
NaB	.182	.283	.193	.134	.219
(Na+K)A	.584	.436	.619	.575	.246
Mg/Mg+Fe+2	.670	.730	.680	.650	.650

Table D.2.2 - Bom Jardim Complex, MPBAS, Amphiboles (contd)

Sample	272	272	01	01	107	107
Point	Core	Core	Core	Core	Core	Core
SiO2	47.870	48.070	45.960	46.670	47.660	49.460
Al2O3	6.340	6.260	6.600	7.150	6.590	5.070
TiO2	1.420	1.100	1.230	1.310	1.300	.720
FeO	12.160	12.430	12.110	12.940	10.710	9.640
Fe2O3	1.360	.820	2.800	1.300	3.510	3.960
MgO	13.870	13.990	12.760	12.950	13.780	14.510
MnO	.260	.000	.300	.350	.290	.660
CaO	11.520	11.560	11.530	11.700	11.530	11.890
Na2O	2.120	2.190	1.680	1.920	1.720	1.060
K2O	.770	.620	.740	.840	.680	.580
Total	97.690	97.040	95.710	97.130	97.770	97.550

MINERAL FORMULA UNITS (Based on 23 Oxygens)

Si	7.032	7.090	6.934	6.936	6.978	7.208
Al4	.968	.910	1.066	1.064	1.022	.792
Al6	.130	.178	.108	.188	.115	.079
Ti	.157	.122	.140	.146	.143	.079
Fe+2	1.494	1.534	1.528	1.608	1.312	1.175
Fe+3	.151	.091	.318	.145	.387	.434
Mg	3.036	3.075	2.869	2.868	3.007	3.152
Mn	.032		.038	.044	.036	.081
Ca	1.813	1.827	1.864	1.863	1.809	1.857
NaB	.187	.173	.136	.137	.191	.143
(Na+K)A	.558	.573	.493	.572	.425	.268
Mg/Mg+Fe+2	.670	.670	.650	.640	.650	.730

Table D.2.3 - Bom Jardim Complex, Enclaves, Amphiboles

Sample	112A	112A	145	145	145
Point	Core	Core	Core	Core	Core
SiO2	46.840	46.040	44.960	45.500	45.220
Al2O3	6.510	7.380	7.550	8.030	8.160
TiO2	1.140	1.060	1.280	1.410	1.510
FeO	13.450	11.950	13.580	12.700	13.530
Fe2O3	.930	3.740	2.770	3.760	2.780
MgO	13.180	12.400	11.640	11.890	11.980
MnO	.000	.340	.330	.500	.390
CaO	12.090	11.830	11.560	11.420	11.700
NiO					
Na2O	1.590	1.270	1.620	1.910	1.980
K2O	.800	.800	1.090	.950	1.080
Total	96.530	96.810	96.380	98.070	98.330

MINERAL FORMULA UNITS (Based on 23 Oxygens)

Si	7.003	6.870	6.805	6.750	6.714
Al4	.997	1.130	1.195	1.250	1.286
Al6	.150	.168	.152	.154	.142
Ti	.128	.119	.146	.157	.169
Fe+2	1.681	1.492	1.718	1.526	1.679
Fe+3	.104	.420	.316	.420	.311
Mg	2.937	2.758	2.626	2.629	2.651
Mn		.043	.042	.063	.049
Ca	1.937	1.892	1.875	1.815	1.861
NaB	.063	.108	.125	.185	.139
(Na+K)A	.554	.411	.560	.544	.636
Mg/Mg+Fe+2	.640	.650	.600	.630	.610

Table D.2.3 - Bom Jardim Complex, Enclaves, Amphiboles (contd)

Sample	144C	144C	306A	265B	265B	265B
Point	Core	Core	Core	Core	Core	Core
SiO2	47.940	48.020	47.880	56.230	51.720	53.150
Al2O3	5.810	6.360	6.020	.000	4.060	3.230
TiO2	1.290	1.190	.880	.000	.440	.000
FeO	11.680	10.690	10.190	14.000	8.530	6.100
Fe2O3	1.620	3.090	2.510	.000	.000	2.120
MgO	14.180	14.320	14.550	22.380	18.270	18.480
MnO	.000	.240	.370	1.030	.250	.000
CaO	11.490	11.340	11.820	2.030	11.330	12.280
NiO				.410		
Na2O	1.990	2.240	1.680	.000	1.410	.980
K2O	.650	.710	.630	.000	.630	.300
Total	96.650	98.230	96.530	96.080	96.640	96.340

MINERAL FORMULA UNITS (Based on 23 Oxygens)

Si	7.092	6.997	7.069	8.002	7.431	7.576
Al4	.908	1.003	.931	.000	.569	.424
Al6	.105	.089	.117		.119	.119
Ti	.144	.130	.098		.047	
Fe+2	1.445	1.302	1.259	1.667	1.025	.727
Fe+3	.181	.339	.279			.228
Mg	3.126	3.110	3.202	4.747	3.914	3.926
Mn		.030	.046	.124	.031	
Ca	1.821	1.770	1.870	.309	1.745	1.876
NaB	.179	.230	13.000	.000	.255	.124
(Na+K)A	.515	.543	.470	.000	.254	.202
Mg/Mg+Fe+2	.680	.700	.720	.740	.790	.840

Table D.2.4 - Bom Jardim Complex, Mafic Dykes, Amphiboles

Sample	254B	254B	205	205	205	205
Point	Core	Core	Core	Core	Core	Core
SiO2	48.720	48.770	48.180	47.590	47.310	47.360
Al2O3	5.030	5.660	7.320	7.310	6.910	6.780
TiO2	1.090	1.110	1.290	1.540	1.440	1.660
FeO	8.210	10.720	10.700	11.530	12.500	11.550
Fe2O3	2.780	.820	2.930	2.440	1.940	2.390
MgO	16.190	15.270	14.190	13.760	13.500	13.720
MnO	.260	.000	.000	.400	.250	.240
CaO	11.770	12.240	11.890	11.950	12.120	11.870
Na2O	1.770	1.530	1.610	1.810	1.670	1.570
K2O	.650	.500	.660	.720	.770	.770
Total	96.470	96.620	98.770	99.050	98.410	97.910
MINERAL FORMULA UNITS (Based on 23 Oxygens)						
Si	7.134	7.154	6.954	6.898	6.928	6.941
Al4	.866	.846	1.046	1.102	1.072	1.059
Al6	.002	.133	.199	.147	.121	.112
Ti	.120	.122	.140	.168	.159	.183
Fe+2	1.006	1.315	1.291	1.398	1.531	1.415
Fe+3	.307	.091	.318	.267	.213	.264
Mg	3.533	3.338	3.052	2.972	2.946	2.997
Mn	.032			.049	.031	.030
Ca	1.847	1.924	1.839	1.856	1.902	1.864
NaB	.153	.076	.161	.144	.098	.136
(Na+K)A	.471	.453	.412	.498	.520	.454
Mg/Mg+Fe+2	.780	.720	.700	.680	.660	.680

Table D.3.1 - Bom Jardim Complex, PBAMS, Biotites

Sample	35	35	29	29	200	144
Point	Core	Core	Core	Core	Core	Core
SiO2	37.880	38.220	37.640	37.480	38.310	38.650
TiO2	1.700	1.630	2.190	2.150	2.230	1.950
Al2O3	14.280	14.970	14.110	13.610	14.100	15.010
Cr2O3				.240		
FeO	16.910	15.940	16.990	15.790	16.970	14.940
MnO						
MgO	14.380	14.890	14.620	15.360	14.210	15.620
Na2O	.320	.340	.360	.500	.460	.400
K2O	10.170	10.230	10.350	10.330	10.110	9.960
BaO				.420		
Total	95.640	96.130	94.400	96.070	96.390	95.560

FORMULA UNITS (Based on 22 Oxygens)

Si	5.685	5.651	5.623	5.634	5.711	5.679
Ti	.191	.181	.246	.243	.250	.216
Al	2.525	2.608	2.485	2.411	2.478	2.600
Cr				.028		
Fe	2.122	1.972	2.123	1.985	2.116	1.836
Mn						
Mg	3.215	3.283	3.255	3.442	3.159	3.420
Na	.093	.097	.105	.148	.130	.116
K	1.978	1.930	1.974	1.982	1.923	1.867
Ba				.025		
Fe/Fe+Mg		.370	.390	.370	.400	.350

Table D.3.1 - Bom Jardim Complex, PBAMS, Biotites (contd)

Sample	249	112	112	258	258	86	193	193
Point	Core	Core	Core	Core	Core	Core	Core	Core
SiO2	37.430	37.490	37.600	37.590	37.550	37.790	37.890	37.870
TiO2	2.610	1.850	3.340	2.490	3.130	2.270	1.600	1.520
Al2O3	13.770	15.080	15.440	13.640	13.810	14.050	15.190	14.620
Cr2O3			.260					
FeO	15.410	16.900	15.220	14.920	15.430	16.350	16.260	16.080
MnO			.380	.300		.300	.260	.300
MgO	15.410	13.320	13.440	15.120	14.830	14.060	14.230	14.400
Na2O	.420	.370	.390	.440	.440	.490		.280
K2O	9.700	9.850	9.880	9.560	9.790	9.790	10.140	8.840
BaO			.250	.270				.370
Total	94.390	94.860	96.220	94.330	95.050	95.110	95.580	95.270

FORMULA UNITS (Based on 22 Oxygens)

Si	5.6.296	5.673	5.595	5.688	5.647	5.676	5.661	5.709
Ti	2.451	.211	.373	.283	.354	.256	.180	.172
Al		2.690	2.708	2.433	2.448	5.488	2.676	2.597
Cr	1.945		.030					
Fe		2.139	1.894	1.889	1.940	2.054	2.032	2.028
Mn	3.385		.049	.038		.039	.034	.038
Mg	.124	3.004	2.982	3.411	3.325	3.148	3.171	3.235
Na	1.868	.107	.114	.129	.129	.144		.083
K		1.901	1.875	1.845	1.878	1.877	1.934	1.892
Ba			.015	.016				.022
Fe/Fe+Mg	.360	.420	.390	.360	.370	.390	.390	.380

Table D.3.2 - Bom Jardim Complex, PBM, Biotites

Sample	91	91	251	251	111	252
Point	Core	Core	Core	Core	Core	Core
SiO2	37.420	37.110	38.000	37.900	37.120	37.410
TiO2	4.300	3.820	3.760	3.790	4.070	3.130
Al2O3	13.670	13.620	13.520	13.570	13.080	13.790
Cr2O3		.290	.230	.210		.240
FeO	15.430	13.240	14.820	14.730	14.720	15.080
MnO	.230				.260	
MgO	15.080	15.390	14.240	14.850	14.230	14.630
Na2O	.390	.340			.440	.360
K2O	9.670	9.590	9.790	9.960	9.320	9.950
BaO	N.D.	N.D.	.650			.320
NiO		.470				
Total	95.300	93.880	95.000	95.010	93.240	94.910

FORMULA UNITS (Based on 22 Oxygens)

Si	5.603	5.613	5.726	5.655	5.614	5.639
Ti	.484	.435	.426	.425	.467	.355
Al	2.413	2.428	2.396	2.387	2.349	2.450
Cr		.035	.028	.025		.029
Fe	1.819	1.675	1.864	1.837	1.877	1.901
Mn	.029				.035	
Mg	3.367	3.470	3.191	3.304	3.235	3.286
Na	.114	.099			.133	.104
K	1.846	1.850	1.869	1.895	1.814	1.913
Ba	N.D.	N.D.	.038			.019
Fe/Fe+Mg	.350	.330	.370	.360	.370	.370

Table D.3.3 - Bom Jardim Complex, MPBAS, Biotites

Sample	272	272	107	07	07	268	124	162	162
Point	Core	Core	Core	Core	Core	Core	Core	Core	Core
SiO2	37.920	38.280	38.100	38.190	37.800	38.260	37.910	37.670	38.090
TiO2	2.200	1.850	1.800	2.200	2.660	1.600	1.770	2.500	2.060
Al2O3	13.340	13.650	14.410	13.480	13.430	13.480	13.600	14.280	14.070
Cr2O3					.230		.320		
FeO	16.430	15.600	16.160	15.850	15.960	15.820	15.690	15.550	15.110
MnO	.220	.230							.270
MgO	14.740	15.330	14.240	14.990	14.320	14.120	15.010	14.010	14.350
Na2O		.500		.470	.430		.450	.340	.220
K2O	9.850	10.230	9.840	9.920	9.690	9.900	10.140	9.930	9.860
BaO					.420	.680			
Total	94.610	95.670	94.560	95.100	94.950	94.120	94.900	94.280	94.030

FORMULA UNITS (Based on 22 Oxygens)

Si	5.748	5.735	5.731	5.733	5.716	5.842	5.706	5.700	5.778
Ti	.251	.208	.204	.248	.303	.184	.201	.285	.234
Al	2.383	2.411	2.555	2.385	2.394	2.426	2.413	2.546	2.514
Cr					.027		.038		
Fe	2.083	1.954	2.033	1.990	2.018	2.020	1.975	1.968	1.916
Mn	.029	.029				.035			.033
Mg	3.271	3.424	3.192	3.355	3.228	3.212	3.368	3.160	3.244
Na		.145		.137	.127		.130	.099	.062
K	1.908	1.955	1.889	1.900	1.869	1.926	1.947	1.917	1.907
Ba					.025	.041			
Fe/Fe+Mg	.390	.360	.390	.370	.380	.390	.370	.380	.370

Table D.3.4 - Bom Jardim Complex, PBLS, Biotites

Sample	49	49	49	10	10	10	209	209
Point	Core	Core	Core	Core	Core	Core	Core	Core
SiO2	38.880	38.460	37.870	37.980	38.070	38.360	38.490	38.070
TiO2	3.680	3.460	3.720	3.730	3.450	3.620	4.200	3.280
Al2O3	13.210	12.900	12.830	12.590	12.410	12.510	13.440	13.170
CrO3								
FeO	16.800	16.640	15.360	16.570	16.540	17.110	16.480	15.890
MnO							.280	.250
MgO	15.100	14.380	14.220	13.970	14.210	14.300	14.420	13.340
Na2O		.480	.400	.500	.580	.740	.420	.370
K2O	10.430	10.000	10.300	9.860	10.030	10.150	9.861	9.780
BaO			.400	.340	.330		.320	
Total	98.090	96.380	95.100	95.580	95.630	96.790	97.920	94.130

FORMULA UNITS (Based on 22 Oxygens)

Si	5.648	5.728	5.729	5.691	5.735	5.719	5.648	5.768
Ti	.402	.387	.424	.421	.391	.406	.463	.373
Al	2.262	2.264	1.288	2.225	2.204	2.198	2.325	2.353
Cr								
Fe	2.041	2.072	1.943	2.077	2.084	2.133	2.023	2.012
Mn							.035	.032
Mg	3.270	3.192	3.208	3.121	3.190	3.177	3.154	3.012
Na		.140	.119	.145	.170	.213	.120	.108
K	1.933	1.900	1.987	1.885	1.928	1.930	1.846	1.891
Ba			.023	.020	.019		.018	
Fe/Mg+Fe	.380	.390	.380	.400	.390	.400	.390	.400

Table D.3.5 - Bom Jardim Complex, CS, Biotites

Sample	23	23	23	23	23	23	31	31
Point	Core	Core	Core	Core	Core	Core	Core	Core
SiO2	39.050	39.320	39.050	39.070	39.200	39.610	38.780	38.070
TiO2	3.050	3.760	3.420	2.530	3.660	3.420	3.600	3.240
Al2O3	10.810	11.210	11.210	11.200	11.430	11.580	12.840	12.340
CrO3				.260				
FeO	17.370	18.360	18.910	17.650	17.580	17.250	16.910	17.120
MnO								
MgO	14.030	13.430	13.960	14.830	13.720	14.410	14.690	14.120
Na2O	.310	.520	.510	.460	.440	.440	.490	.510
K2O	10.020	10.190	10.020	10.240	11.430	10.200	9.870	9.810
BaO	.270							
Total	94.910	96.780	97.090	96.250	96.110	96.910	97.190	95.200
FORMULA UNITS (Based on 22 Oxygens)								
Si	5.942	5.868	5.845	5.867	5.881	5.865	5.735	5.764
Ti	.349	.422	.385	.286	.413	.381	.400	.369
Al	1.939	1.972	1.977	1.982	2.021	2.020	2.238	2.202
Cr				.031				
Fe	2.211	2.291	2.367	2.216	2.206	2.136	2.091	2.168
Mn								
Mg	3.184	2.987	3.114	3.320	3.069	3.180	3.239	3.186
Na	.091	.151	.150	.134	.128	.128	.142	.150
K	1.946	1.941	1.913	1.961	1.630	1.927	1.861	1.894
Ba	.016							
Fe/Fe+Mg	.410	.430	.430	.400	.420	.400	.390	.400

Table D.3.6 - Bom Jardim Complex, Pink Granites, Biotites

Sample	43	292A	292B	292C	292
Point	Core	Core	Core	Core	Core
SiO2	37.830	38.360	37.310	37.190	37.960
TiO2	3.510	2.260	2.850	2.250	3.120
Al2O3	15.490	15.570	15.180	15.280	15.400
CrO3					
FeO	18.510	18.070	18.760	18.860	19.030
MnO	.290	.310	.260		
MgO	10.690	11.970	11.200	10.740	10.800
Na2O	.430	.380	.540	.230	
K2O	10.270	9.690	9.790	8.980	10.040
BaO				.380	
Total	97.030	96.600	95.890	93.920	96.350

FORMULA UNITS (Based on 22 Oxygens)

Si	5.624	5.722	5.653	5.725	5,696.000
Ti	.392	2.530	.325	.260	.352
Al	2.716	2.738	2.710	2.772	2.723
Cr					
Fe	2.302	2.254	2.377	2.428	2.388
Mn	.037	.039	.033		
Mg	2.370	2.662	2.529	2.465	2.414
Na	.430	.109	.160	.070	
K	10.270	1.844	1.892	1.764	1.922
Ba					
Fe/Fe+Mg	.490	.460	.480	.500	.500

Table D.3.7 - Bom Jardim Complex, Igneous Enclaves, Biotites

Sample	130G	130G	130G	130E	323A	133
Point	Core	Core	Core	Core	Core	Core
SiO2	38.800	38.600	38.160	37.990	38.110	36.790
TiO2	2.570	3.110	3.340	3.840	3.140	3.470
Al2O3	13.150	12.700	13.180	12.720	12.680	13.820
CrO3			.350			
FeO	14.440	14.030	15.480	14.510	15.380	15.670
MnO	.250			.270	.340	
MgO	15.340	15.920	14.740	15.190	15.040	14.370
Na2O		.300	.440	.590	.330	.700
K2O	10.110	9.820	10.260	10.090	9.670	9.550
BaO	.730				NA	.290
Total	95.460	94.460	95.950	95.210	94.870	94.650

FORMULA UNITS (Based on 22 Oxygens)

Si	5.782	5.574	5.698	5.702	5.736	5.587
Ti	.288	.348	.375	.433	.356	.397
Al	2.310	2.232	2.319	2.250	2.249	2.474
Cr			.041			
Fe	1.799	1.750	1.933	1.822	1.936	1.987
Mn	.031			.035	.043	
Mg	3.407	3.538	3.280	3.398	3.375	3.252
Na		.048	.128	.172	.096	.206
K	1.922	1.868	1.955	1.932	1.857	1.850
Ba	.042					.017
Fe/Mg+Fe	.350	.330	.370	.350	.360	.380

Table D.3.7 - Bom Jardim Complex, Igneous Enclaves, Biotites (contd)

Sample	265B	265B	265B	145	145	54	54
Point	Core	Core	Core	Core	Core	Core	Core
SiO2	39.620	39.620	39.700	37.460	37.500	36.600	37.910
TiO2	1.320	2.080	1.860	1.990	1.740	3.500	3.620
Al2O3	13.430	13.800	13.520	14.180	14.090	12.910	13.140
CrO3	.290		.320				
FeO	10.630	10.750	11.500	17.510	17.480	13.690	14.860
MnO	.320			.260			
MgO	18.660	17.860	18.090	13.730	13.570	16.260	15.420
Na2O		.280	.350	.340	.490	.530	.470
K2O	9.740	9.980	10.000	9.700	9.950	9.820	9.540
BaO	.280		.320			.700	.650
Total	94.300	94.370	95.650	95.090	94.830	96.130	95.690

FORMULA UNITS (Based on 22 Oxygens)

Si	5.859	5.830	5.814	5.674	5.707	5.714	5.658
Ti	.147	.232	.205	.227	.199	.390	.407
Al	2.342	2.393	2.333	2.532	2.527	2.253	2.311
Cr	.034		.036				
Fe	1.315	1.323	1.408	2.218	2.224	1.695	1.854
Mn	.034			.033			
Mg	4.115	3.918	3.950	3.100	3.077	3.589	3.432
Na		.080	.101	.101	.145	.153	.135
K	1.838	1.874	1.869	1.875	1.931	1.855	1.816
Ba	.016		.019			.041	.038
Fe/Mg+Fe	.240	.250	.260	.420	.420	.320	.350

Table D.3.8 - Bom Jardim Complex, Mafic Dykes, Biotites

Sample	205	205	133	133	133	216
Point	Core	Core	Core	Core	Core	Core
SiO2	38.670	38.320	37.430	37.670	37.630	37.640
TiO2	2.070	1.760	3.680	3.430	3.670	2.650
Al2O3	15.090	15.140	13.030	12.840	12.810	14.390
CrO3					.260	
FeO	15.350	15.310	13.470	13.690	13.530	17.390
MnO	.300	.270			.280	
MgO	15.150	15.030	15.620	15.270	15.730	13.290
Na2O	.480		.330	.240	.400	.520
K2O	10.000	9.770	9.510	9.610	9.920	9.620
BaO		.470	1.550	1.530	.310	.260
Total	97.120	96.070	94.620	94.270	94.540	95.760
FORMULA UNITS (Based on 22 Oxygens)						
Si	5.679	5.680	5.666	5.712	5.681	5.659
Ti	.228	.196	.419	.391	.417	.299
Al	2.613	2.646	2.324	2.296	2.280	2.550
Cr					.031	
Fe	1.885	1.899	1.706	1.737	1.709	2.186
Mn	.038	.034			.035	
Mg	3.317	3.322	3.524	3.452	3.541	2.978
Na	.138		.097	.069	.118	.152
K	1.873	1.847	1.838	1.860	1.911	1.845
Ba		.027	.092	.091	.018	.015
Fe/Mg+Fe	.360	.360	.330	.330	.320	.420

Table D.3.8 - Bom Jardim Complex, Mafic Dykes, Biotites (contd)

Sample	130D	130D	254B	254B	272A	272A
Point	Core	Core	Core	Core	Core	Core
SiO2	37.260	37.570	37.890	37.920	37.650	36.900
TiO2	4.480	4.070	2.440	2.470	4.680	4.770
Al2O3	13.620	13.900	14.290	13.880	14.750	14.030
CrO3				.350		
FeO	18.030	17.850	14.810	15.150	16.750	17.280
MnO			.260			
MgO	12.300	12.670	14.570	14.560	13.940	12.690
Na2O			.450	.420	.450	
K2O	9.780	10.010	9.820	10.140	9.560	9.790
BaO	.740	.490		.410	.610	.730
Total	96.210	96.560	94.540	95.310	98.400	96.180

FORMULA UNITS (Based on 22 Oxygens)

Si	5.612	5.620	5.710	5.710	5.508	5.554
Ti	.508	.458	.276	.280	5.140	.540
Al	2.417	2.451	2.538	2.464	2.542	2.489
Cr				.042		
Fe	2.271	2.233	1.867	1.907	2.049	2.176
Mn			.034			
Mg	2.761	2.825	3.274	3.268	3.039	2.846
Na			.131	.124	.127	
K	1.880	1.910	1.888	1.948	1.784	1.879
Ba	.044	.029		.024	.035	.043
Fe/Mg+Fe	.450	.440	.360	.370	.400	.430

Table D.3.9 - Bom Jardim Complex, Country Rocks, Biotites

Sample	348	348	348	350	350	350
Point	Core	Core	Core	Core	Core	Core
SiO2	36.180	35.790	36.510	36.600	36.920	36.740
TiO2	2.450	3.000	2.640	2.510	2.230	2.390
Al2O3	18.450	18.670	18.750	16.430	16.720	15.930
CrO3						
FeO	17.680	17.970	17.870	18.930	19.200	19.890
MnO				.280	.460	.360
MgO	10.970	10.530	10.680	11.020	11.030	10.650
Na2O	.610	.360	.300		.370	.480
K2O	9.690	9.980	10.040	9.780	10.100	9.740
BaO						
Total	96.030	96.290	96.790	65.560	97.030	96.190

FORMULA UNITS (Based on 22 Oxygens)

Si	5.406	5.361	5.420	5.555	5.542	5.578
Ti	.275	.338	.295	.287	.252	.273
Al	3.296	3.295	3.280	2.939	2.958	2.851
Cr						
Fe	2.209	2.251	2.218	2.402	2.411	2.525
Mn				.037	.058	.046
Mg	2.442	2.350	2.364	2.494	2.468	2.410
Na	.177	.103	.086		.107	.142
K	1.847	1.907	1.901	1.893	1.935	1.887
Ba						
Fe/Mg+Fe	.470	.490	.480	.490	.490	.510

Table D.3.9 - Bom Jardim Complex, Country Rocks, Biotites (contd)

Sample	358	239	239	239
Point	Core	Core	Core	Core
SiO2	36.740	36.840	36.490	36.880
TiO2	2.390	2.650	3.050	2.650
Al2O3	15.930	15.460	15.950	16.500
CrO3				
FeO	19.890	19.020	20.260	17.760
MnO	.360	.250	.230	.320
MgO	10.650	11.530	11.150	11.170
Na2O	.480	.630	.560	
K2O	9.740	9.880	9.710	9.900
BaO				
Total	96.190	96.260	97.410	95.170
FORMULA UNITS (Based on 22 Oxygens)				
Si	5.578	5.569	5.483	5.588
Ti	.273	.302	.345	.302
Al	2.851	2.754	2.825	2.947
Cr				
Fe	2.525	2.405	2.456	2.251
Mn	.046	.031	.030	.041
Mg	2.410	2.599	2.498	2.522
Na	.142	.185	.163	
K	1.887	1.906	1.861	1.914
Ba				
Fe/Mg+Fe	.510	.480	.500	.470

Table D.4.1 - Bom Jardim Complex, PBAMS, Plagioclases

Sample	81	81	35	35	112	112	29
Point	Core	Rim	Core	Core	Core	Rim	Core
SiO2	62.070	61.990	63.130	63.400	59.880	61.120	62.050
Al2O3	23.450	23.100	23.090	22.790	24.190	23.650	23.360
FeO	.230	.300			.470	.290	
CaO	4.770	4.840	4.360	4.310	6.100	5.430	4.790
Na2O	8.660	8.810	9.120	9.190	7.820	8.250	8.860
K2O	.330	.220	.110	.150	.580	.220	.310
Total	99.600	99.330	99.810	99.840	99.040	99.040	99.380
FORMULA UNITS (Based on 8 Oxygens)							
Si	2.763	2.767	2.792	2.801	2.696	2.737	2.760
Al	1.230	1.215	1.204	1.187	1.283	1.249	1.225
Fe	.009	.011			.017	.011	
Ca	.228	.231	.207	.204	.293	.260	.228
Na	.748	.762	.782	.787	.680	.716	.764
K	.019	.013	.006	.008	.033	.011	.018
Ab	75.000	76.000	78.000	79.000	68.000	73.000	76.000
An	23.000	23.000	21.000	20.000	29.000	26.000	22.000
Or	2.000	1.000	1.000	1.000	3.000	1.000	9.000

Table D.4.1 - Bom Jardim Complex, PBAMS, Plagioclases (contd)

Sample	29	249	249	144	144	200	200
Point	Core	Core	Core	Core	Rim	Rim	Core
SiO2	62.010	62.030	62.550	60.700	62.090	62.380	62.050
Al2O3	23.210	23.170	23.500	24.980	24.030	23.560	23.030
FeO		.260				.210	.230
CaO	4.900	4.920	4.780	5.960	5.090	4.940	4.790
Na2O	8.630	8.580	8.830	8.210	8.640	8.630	8.810
K2O	.190	.340	.150	.160		.280	.290
Total	98.940	99.310	99.810	99.980	100.190	100.030	99.220
FORMULA UNITS (Based on 8 Oxygens)							
Si	2.767	2.768	2.769	2.685	2.741	2.762	2.775
Al	1.226	1.218	1.226	1.302	1.250	1.230	1.214
Fe		.100				.008	.009
Ca	.236	.235	.227	.282	.241	.234	.229
Na	.744	.742	.758	.704	.740	.741	.769
K	.011	.010	.009	.009	.019	.016	.010
Ab	75.000	74.000	76.000	71.000	74.000	75.000	76.000
An	24.000	24.000	23.000	28.000	24.000	24.000	23.000
Or	1.000	2.000	1.000	1.000	2.000	1.000	1.000

Table D.4.2 - Bom Jardim Complex, PBM, Plagioclases

Sample	91	91	252	252	251	258	258
Point	Rim	Core	Rim	Core	Core	Core	Core
SiO2	62.150	62.600	63.130	63.030	63.610	62.470	62.560
Al2O3	23.200	23.050	22.970	22.660	22.460	23.150	23.110
FeO	.370	.220		.190	.310	.210	
CaO	4.320	4.760	4.050	3.980	3.380	4.380	4.280
Na2O	9.010	8.530	9.160	9.130	9.320	9.000	8.960
K2O	.180	.450	.200	.260	.310	.200	.270
Total	99.230	99.610	99.510	99.250	99.390	99.200	99.180
FORMULA UNITS (Based on 8 Oxygens)							
Si	2.773	2.776	2.799	2.798	2.825	2.779	2.780
Al	1.220	1.217	1.200	1.186	1.176	1.214	1.210
Fe	.014	.008		.007	.012		
Ca	.207	.228	.193	.189	.161	.209	.204
Na	.779	.713	.787	.786	.803	.776	.772
K	.010	.025	.011	.015	.018	.011	.016
Ab	78.000	74.000	79.000	79.000	82.000	78.000	78.000
An	21.000	24.000	20.000	19.000	16.000	21.000	20.000
Or	1.000	2.000	1.000	1.000	2.000	1.000	2.000

Table D.4.3 - Bom Jardim Complex, MPBAS, Plagioclases

Sample	62	62	62	107	107	107
Point	Core	Core	Rim	Core	Rim	Core
SiO2	63.270	62.940	63.220	64.700	63.460	63.620
Al2O3	22.490	22.690	22.570	21.850	22.610	22.540
FeO	.350		.230		.260	
CaO	3.760	3.970	3.440	2.800	3.120	2.940
Na2O	9.550	9.350	9.350	10.040	10.240	9.870
K2O	.270		.360	.130		.180
Total	99.690	99.180	99.170	99.520	99.690	99.150

FORMULA UNITS (Based on 8 Oxygens)

Si	2.808	2.799	2.810	2.850	2.819	2.817
Al	1.176	1.189	1.182	1.136	1.164	1.176
Fe	.013		.009		.009	
Ca	.179	.189	.164	.133	.146	.140
Na	.822	.806	.806	.859	.868	.847
K	.015		.020	.007		.010
Ab	81.000	81.000	81.000	86.000	86.000	85.000
An	18.000	19.000	17.000	13.000	14.000	14.000

Table D.4.3 - Bom Jardim Complex, MPBAS, Plagioclases (contd)

Sample	48	48	268	268	07	07
Point	Core	Core	Core	Rim	Core	Core
SiO2	64.790	65.350	63.940	64.610	64.160	64.450
Al2O3	21.150	20.710	22.060	22.120	22.070	21.470
FeO		.290			.270	
CaO	3.300	2.540	3.710	3.510	3.450	3.170
Na2O	9.580	9.900	9.530	9.420	9.550	9.540
K2O	.300	.210		.130	.330	.330
Total	99.120	99.000	99.240	99.790	99.960	99.210
FORMULA UNITS (Based on 8 Oxygens)						
Si	2.875	2.900	2.827	2.841	2.836	2.863
Al	1.106	1.083	1.150	1.146	1.150	1.124
Fe		.011			.012	
Ca	.157	.120	.176	.166	.164	.151
Na	.820	.850	.817	.803	.819	.822
K	.017	.011		.007	.021	.019
Ab	82.000	87.000	82.000	82.000	82.000	83.000
An	16.000	12.000	18.000	17.000	16.000	15.000

Table D.4.4 - Bom Jardim Complex, PBLS, Plagioclases

Sample	49	49	49	49	10	10	10	10	10
Point	Core	Core	Core	Core	Core	Core	Rim	Core	Core
SiO2	65.130	65.540	66.390	66.990	68.480	66.170	65.760	65.580	65.750
Al2O3	21.610	20.650	20.580	20.990	19.360	20.820	20.840	21.350	20.820
FeO		.230				.220			
CaO	2.840	2.100	1.630	2.490	.130	1.820	1.700	2.240	2.420
Na2O	9.610	10.480	10.410	9.770	11.500	10.210	10.460	9.830	10.140
K2O	.250	.340	.300				.240	.320	.240
Total	99.440	99.340	99.350	100.270	99.570	99.240	99.000	99.330	99.190
FORMULA UNITS (Based on 8 Oxygens)									
Si	2.873	2.903	2.920	2.912	2.998	2.918	2.912	2.886	2.894
Al	1.124	1.078	1.067	1.076	.999	1.082	1.088	1.107	1.097
Fe		.009				.008			
Ca	.134	.098	.077	.116	.006	.086	.081	.106	.107
Na	.822	.900	.888	.823	.976	.873	.898	.839	.879
K	.014	.019	.017				.013	.018	.014
Ab	85.000	88.000	90.000	87.000	99.000	91.000	91.000	87.000	88.000
An	14.000	10.000	8.000	12.000	1.000	9.000	8.000	11.000	11.000
Or	1.000	2.000	2.000	1.000			1.000	2.000	1.000

Table D.4.5 - Bom Jardim Complex, Igneous Enclaves, Plagioclases

Sample	28A	28A	130G	130G	133
Point	Rim	Core	Rim	Core	Core
SiO2	61.790	61.730	62.690	61.950	59.950
Al2O3	23.460	23.570	23.000	23.790	25.450
FeO			.280		
CaO	5.520	5.560	4.690	5.170	7.430
Na2O	8.270	8.400	8.580	8.170	7.070
K2O	.280	.170	.320	.480	
Total	99.320	99.440	99.560	99.560	99.560
FORMULA UNITS (Based on 8 Oxygens)					
Si	2.755	2.748	2.784	2.750	2.654
Al	1.233	1.237	1.204	1.245	1.339
Fe			.010		
Ca	.263	.265	.223	.246	.356
Na	.715	.725	.738	.703	.609
K	.016	.010	.018	.027	.011
Ab	72.000	72.000	75.000	72.000	62.000
An	26.000	27.000	23.000	25.000	36.000
Or	2.000	1.000	2.000	3.000	2.000

Table D.4.5 - Bom Jardim Complex, Igneous Enclaves, Plagioclases (contd)

Sample	133	133	133	112A	112A
Point	Rim	Core	Rim	Rim	Core
SiO2	61.560	58.130	60.160	60.200	59.910
Al2O3	23.570	26.240	24.770	24.610	24.720
FeO					.430
CaO	5.320	8.030	6.380	6.230	6.820
Na2O	8.430	6.950	7.970	8.020	7.310
K2O	.210	.220	.180	.120	.150
Total	99.090	99.570	99.170	99.180	99.340
FORMULA UNITS (Based on 8 Oxygens)					
Si	2.746	2.604	2.677	2.694	2.683
Al	1.239	1.385	1.299	1.298	1.305
Fe					.016
Ca	.254	.386	.304	.299	.327
Na	.729	.604	.688	.696	.635
K	.012	.012	.010	.007	.008
Ab	73.000	60.000	69.000	69.000	65.000
An	26.000	39.000	30.000	30.000	34.000
Or	1.000	1.000	1.000	1.000	1.000

Table D.4.6 - Bom Jardim Complex, Mafic Dykes, Plagioclases

Sample	130D	254B	254B	216	216	216
Point	Core	Core	Core	Core	Core	Rim
SiO2	63.390	63.040	63.420	61.560	59.060	62.600
Al2O3	23.410	22.870	22.840	23.490	24.400	22.720
FeO					.280	.210
CaO	4.500	3.800	3.630	5.590	6.680	4.570
Na2O	8.550	9.340	9.710	8.490	7.850	8.920
K2O		.170	.180	.250	.480	.160
Total	99.850	99.220	99.780	99.380	98.750	99.180
FORMULA UNITS (Based on 8 Oxygens)						
Si	2.792	2.795	2.798	2.745	2.668	2.794
Al	1.215	1.195	1.188	1.234	1.299	1.195
Fe					.011	.008
Ca	.212	.181	.172	.267	.324	.219
Na	.730	.805	.831	.734	.688	.772
K		.010	.010	.014	.028	.009
Ab	77.000	80.000	82.000	72.000	66.000	77.000
An	23.000	18.000	17.000	26.000	31.000	22.000
Or		1.000	1.000	2.000	3.000	1.000

Table D.4.6 - Bom Jardim Complex, Mafic Dykes, Plagioclases (contd)

Sample	272A	272A	272A	205	205
Point	Core	Core	Core	Core	Core
SiO2	55.110	59.710	58.960	63.920	62.890
Al2O3	27.810	24.680	25.680	23.200	23.850
FeO					
CaO	10.720	6.930	7.510	8.850	4.580
Na2O	4.970	7.780	6.870	3.880	8.610
K2O	.210	.250	.220	.740	.200
Total	98.950	99.350	99.250	100.590	100.130
FORMULA UNITS (Based on 8 Oxygens)					
Si	2.506	2.676	2.645	2.803	2.764
Al	1.490	1.304	1.358	1.199	1.236
Fe					
Ca	.524	.333	.361	.182	.216
Na	.437	.676	.598	.752	.734
K	.015	.015	.013	.042	.011
Ab	45.000	66.000	62.000	77.000	76.000
An	54.000	33.000	37.000	19.000	23.000
Or	1.000	1.000	1.000	4.000	1.000

Table D.5.1 - Bom Jardim Complex, PBMAS, Alkali Feldspars

Sample	29	29	29	88	88
Point	Rim	Core	Core	Rim	Core
SiO2	63.280	63.150	63.510	63.320	63.910
Al2O3	18.550	18.880	19.040	18.890	19.390
FeO					.400
CaO					
Na2O	1.230	1.160	1.020	1.470	2.150
K2O	14.700	15.020	15.390	14.120	13.060
BaO	1.500	1.830	1.500	1.740	1.450
Total	99.260	100.040	100.760	99.540	100.360
FORMULA UNITS (Based on 8 Oxygens)					
Si	2.963	2.944	2.947	2.951	2.936
Al	1.024	1.037	1.042	1.038	1.050
Fe					.015
Ca					
Na	.111	.105	.091	.133	.192
K	.878	.893	.911	.840	.765
Ba	.028	.033	.027	.032	.026
Or	89.000	89.000	91.000	86.000	80.000
Ab	11.000	11.000	1.000	14.000	10.000
An					

Table D.5.1 - Bom Jardim Complex, PBMAS, Alkali Feldspars (contd)

Sample	187	35	35	81	81
Point	Core	Core	Rim	Core	Core
SiO2	63.220	62.610	63.400	64.770	64.020
Al2O3	18.950	18.850	18.660	18.200	18.840
FeO					
CaO	.230			.240	
Na2O	.750	.810	1.480	2.850	2.610
K2O	15.250	15.530	14.360	12.340	12.900
BaO	1.430	1.560	1.280	1.000	1.030
Total	99.830	99.360	99.180	99.340	99.400
FORMULA UNITS (Based on 8 Oxygens)					
Si	2.951	2.938	2.961	2.977	2.959
Al	1.043	1.043	1.027	.986	1.026
Fe					
Ca	.011			.012	
Na	.068	.074	.134	.255	.234
K	.908	.930	.856	.724	.761
Ba	.026	.029	.023	.018	.019
Or	92.000	93.000	86.000	73.000	77.000
Ab	7.000	7.000	14.000	26.000	23.000
An	1.000			1.000	

Table D.5.2 - Bom Jardim Complex, MPBAS, Alkali Feldspars

Sample	107	107	48	48	268
Point	Core	Rim	Core	Core	Core
SiO2	63.660	63.500	64.140	64.750	63.480
Al2O3	18.670	18.510	18.020	18.540	19.370
FeO			.250		
CaO				.400	.220
Na2O	1.030	.630	.810	3.770	2.420
K2O	15.010	15.410	15.350	10.800	13.050
BaO	.680	1.040	1.410	.630	1.220
Total	99.050	99.090	99.980	98.890	99.760
FORMULA UNITS (Based on 8 Oxygens)					
Si	2.965	2.975	2.990	2.977	2.935
Al	1.025	1.023	.990	1.004	1.055
Fe			.010		
Ca				.020	.011
Na	.093	.054	.074	.336	.217
K	.892	.922	.913	.633	.770
Ba	.012	.018	.026	.011	.022
Or	91.000	94.000	92.000	64.000	77.000
Ab	9.000	6.000	8.000	34.000	22.000
An				2.000	1.000

Table D.5.2 - Bom Jardim Complex, MPBAS, Alkali Feldspars (contd)

Sample	268	162	27	272	272
Point	Rim	Core	Core	Core	Rim
SiO2	63.770	63.410	63.450	63.780	66.200
Al2O3	17.970	18.460	18.820	18.240	19.530
FeO					
CaO	.220		.250		.400
Na2O	.930	.800	1.460	1.020	6.830
K2O	15.190	15.320	14.590	15.500	6.630
BaO	.930	1.140	.770	1.000	
Total	99.010	99.130	99.340	99.540	99.590
FORMULA UNITS (Based on 8 Oxygens)					
Si	2.984	2.971	2.949	2.979	2.965
Al	.991	1.019	1.031	1.004	1.031
Fe					
Ca	.011		.012		.019
Na	.084	.073	.131	.093	.593
K	.907	.916	.865	.924	.379
Ba	.017	.021	.014	.018	
Or	91.000	92.000	86.000	91.000	38.000
Ab	8.000	8.000	13.000	9.000	60.000
An	1.000		1.000		2.000

Table D.5.3 - Bom Jardim Complex, PBLS, Alkali Feldspars

Sample	10	10	10	49	49	49
Point	Core	Core	Core	Core	Core	Core
SiO2	63.830	65.690	63.910	64.640	64.880	63.970
Al2O3	18.900	19.210	18.490	18.590	18.820	18.490
FeO						
CaO	.300	.490	.180	.290		
Na2O	1.470	5.370	1.030	1.900	1.110	.900
K2O	14.310	8.850	15.330	14.190	15.470	15.310
BaO	.910	.230	.940	.550	.440	.500
Total	99.720	99.840	99.880	100.160	100.810	99.170
FORMULA UNITS (based on 8 oxygens)						
Si	2.950	2.968	2.967	2.970	2.963	2.977
Al	1.029	1.023	1.012	1.007	1.013	.999
Fe						
Ca	.015	.024	.009	.014		
Na	.132	.470	.093	.170	.099	.080
K	.844	.510	.908	.832	.901	.915
Ba	.016	.004	.017	.010	.008	.007
Or	85.000	51.000	90.000	82.000	90.000	92.000
Ab	13.000	47.000	9.000	17.000	10.000	8.000
An	2.000	2.000	1.000	1.000		

Table D.5.4 - Bom Jardim Complex, CS, Alkali Feldspars

Sample	23	23	23	23	31	31	31
Point	Core	Core	Rim	Core	Rim	Core	Core
SiO2	63.960	66.050	64.180	64.410	63.630	63.740	66.090
Al2O3	17.920	18.630	18.170	18.610	18.480	18.330	19.260
FeO	.230						
CaO							
Na2O	.820	2.040	.510	1.280	1.090	1.000	7.210
K2O	16.120	13.070	16.270	15.160	15.070	15.390	6.400
BaO			.380	.430	.940	.550	
Total	99.050	99.790	99.510	99.890	99.210	99.010	98.960
FORMULA UNITS (Based on 8 Oxygens)							
Si	2.988	2.993	2.984	2.968	2.964	2.973	2.974
Al	.986	.995	.996	1.011	1.015	1.007	1.022
Fe	.009						
Ca							
Na	.072	.262	.046	.115	.099	.090	.630
K	.962	.755	.965	.891	.896	.916	.368
Ba			.007	.008	.017	.010	
Or	93.000	74.000	95.000	89.000	90.000	91.000	37.000
Ab	7.000	26.000	5.000	11.000	10.000	9.000	63.000
An							

Table D.5.5 - Bom Jardim Complex, Igneous Enclaves, Alkali Feldspars

Sample	130G	130G	144C	144C	144C
Point	Core	Core	Core	Core	Core
SiO2	63.810	63.450	63.930	64.130	63.590
Al2O3	18.930	18.350	18.640	18.440	18.370
FeO		.390			
CaO	.380	.280	.350	.270	.220
Na2O	2.550	.650	.680	.660	.840
K2O	12.210	15.250	15.050	15.700	15.170
BaO	1.140	1.690	.430	.980	.910
Total	99.020	100.060	99.080	100.180	99.110

FORMULA UNITS (Based on 8 Oxygens)

Si	2.937	2.957	2.968	2.973	2.970
Al	1.027	1.008	1.020	1.007	1.012
Fe		.015			
Ca	.019	.014	.017	.014	.011
Na	.227	.059	.062	.059	.076
K	.717	.906	.891	.929	.907
Ba	.028	.031	.008	.018	.017
Or	74.000	94.000	92.000	93.000	91.000
Ab	24.000	6.000	6.000	6.000	8.000
An	2.000		2.000	1.000	1.000

Table D.5.5 - Bom Jardim Complex, Igneous Enclaves, Alkali Feldspars (contd)

Sample	112A	112A	28A	28A
Point	Rim	Rim	Rim	Core
SiO2	63.100	63.320	62.700	62.870
Al2O3	18.320	18.340	18.190	18.260
FeO	.310		.260	
CaO				.140
Na2O	.520	1.380	1.200	1.000
K2O	16.190	15.050	14.430	14.390
BaO	1.070	1.090	2.350	2.340
Total	99.510	99.180	99.130	99.000
FORMULA UNTIS (Based on 8 Oxygens)				
Si	2.962	2.964	2.962	2.969
Al	1.014	1.012	1.013	1.016
Fe	.012		.010	
Ca				.007
Na	.047	.126	.110	.090
K	.970	.899	.870	.867
Ba	.020	.020	.044	.043
Or	95.000	88.000	89.000	90.000
Ab	5.000	12.000	11.000	9.000
An				1.000

Table D.5.6 - Bom Jardim Complex, Mafic Dykes, Alkali Feldspars

Sample	205	130D	254B	254B	254B	254B	133A	133A
Point	Core	Core	Core	Rim	Core	Core	Core	Core
SiO2	63.210	63.620	62.440	63.830	62.800	63.370	63.570	64.060
Al2O3	19.630	19.420	19.350	18.600	18.350	19.000	19.150	18.500
FeO			.300					
CaO		.360					.380	
Na2O	1.610	2.070	1.120	.810	.960	.730	1.670	1.550
K2O	13.530	12.570	14.580	15.140	14.960	14.870	13.890	13.880
BaO	2.840	2.400	1.380	1.050	2.050	1.990	.670	1.150
Total	100.820	100.440	99.170	99.430	99.120	99.960	99.330	99.140
FORMULA UNITS (Based on 8 Oxygens)								
Si	2.925	2.932	2.919	2.966	2.966	2.940	2.947	2.983
Al	1.071	1.055	1.066	1.019	1.019	1.039	1.046	1.016
Fe			.012					
Ca		.018					.019	
Na	.145	.185	.102	.073	.079	.066	.150	.140
K	.799	.739	.869	.897	.898	.880	.821	.825
Ba	.052	.043	.025	.019	.038	.036	.012	.021
Or	85.000	78.000	89.000	92.000	92.000	93.000	83.000	85.000
Ab	15.000	20.000	11.000	8.000	8.000	7.000	15.000	15.000
An		2.000					2.000	

Table D.6.1 - Bom Jardim Complex, PBAMS, Magnetites

Sample	117	200	200	91
SiO2	.26	.54	.55	255.00
TiO2		.22		
Al203				
Cr203	1.09	2.93	4.02	.60
Fe203	66.66	63.14	61.15	66.98
FeO	30.89	31.25	29.89	31.81
MnO			.26	
MgO			.22	
CaO	.19		.14	
NiO		.25		
Total	99.09	98.35	96.23	99.82
Si	.01	.02	.02	.02
Ti		.01		
Al				
Cr	.03	.09	.13	.02
Fe+3	1.95	1.85	1.83	1.94
Fe+2	1.00	1.02	.99	1.02
Mn			.01	
Mg			.01	
Ca	.01		.01	
Ni		.01		
O	4.00	4.00	4.00	4.00

Table D.6.2 - Bom Jardim Complex, MPBAS, Magnetites

Sample	306	306	306	1q107	209a	07
SiO2	.39	1.20	.35	.38	.33	.22.22
TiO2		.21				
Al2O3		.26				
Cr2O3	.21	.91	.23	.81	.48	1.68
Fe2O3	66.87	64.55	66.91	66.51	67.23	65.14
FeO	31.12	32.38	30.82	31.00	31.03	30.63
MnO			.23	.21		
MgO		.39				
CaO						
NiO					.24	
Total	98.59	99.90	98.53	98.91	99.32	99.67
Si	.02	.05	.01	.01	.01	.01
Ti		.01				
Al		.01				
Cr	.01	.03	.01	.02	.01	.05
Fe+3	1.96	1.85	1.97	1.95	1.96	1.93
Fe+2	1.02	1.03	1.01	1.01	1.01	1.01
Mn			.01	.01		
Mg		.00				
O	4.00	4.00	4.00	4.00	4.00	4.00

Table D.6.3 - Bom Jardim Complex, PBLS, Magnetites

Sample	163	163	163	163
SiO2	.46	.45	.46	.37
TiO2			.25	
Al2O3		.29	.23	
Cr2O3	.34	.42	.33	.36
Fe2O3	67.02	67.17	66.91	67.48
FeO	31.40	31.36	31.60	31.33
MnO				.23
MgO				
CaO	.42			
NiO				
Total	99.64	99.69	99.78	99.77
Si	.02	.02	.02	.01
Ti			.01	
Al		.01	.01	
Cr	.01	.01	.01	.01
Fe+3	1.94	1.94	1.93	1.95
Fe+2	1.01	1.00	1.01	1.01
Mn				.01
Mg				
Ca	.02			
Ni				
O	4.00	4.00	4.00	4.00

Table D.7 - Bom Jardim Complex - Other Accessory Minerals

Allanites

Sample	112	112	144	144	144
Point	Rim	Core	Core	Core	Core
SiO2	32.71	31.21	31.57	32.10	31.45
TiO2	1.01	1.70	.82	.82	.68
Al2O3	14.85	12.85	15.57	15.69	15.75
La2O3	7.72	7.50	8.08	7.97	8.18
Ce2O3	10.32	10.92	9.33	9.70	9.30
Nd2O3	1.35	1.62	1.69	1.46	1.36
FeO	11.10	9.46	12.77	12.91	12.29
MgO	.69	1.44	.96	.75	1.31
CaO	11.34	9.58	12.77	12.14	12.38
ThO2	.74	.81	1.00	nd	nd
Total	92.03	87.35	94.56	94.07	92.72

Sphenes

Sample	112	163	162	162	272	267
SiO2	29.33	29.24	30.04	30.17	29.21	29.21
TiO2	37.22	34.80	36.89	36.94	35.91	34.25
CaO	28.22	26.78	27.42	27.85	26.19	26.02
Ce2O3	1.41	1.81	1.09	1.47	1.91	1.72
Nd2O3		.93	.60	1.05	.77	1.02
Al2O3	1.20	.44	.95	1.05	1.14	1.75
FeO	1.38	2.83	1.97	1.40	1.90	2.18
Total	98.76	96.83	98.96	98.88	97.03	96.15

nd = Not Determined

Table D.7 - Bom Jardim Complex - Other Accessory Minerals (contd)

Monazites - Thorites

Sample	91	91	10	10	162	162	287	159
La2O3	24.66	24.76	20.18	10.54	21.54	3.50	22.98	.44
Ce2O3	30.48	32.42	26.00	13.79	26.93	4.29	29.25	3.05
Pi2O3	nd	nd	nd	nd	nd	nd	nd	.55
Nd2O3	6.60	6.21	6.00	3.55	4.91	1.03	6.40	.56
Gd2O3	nd	nd	nd	nd	nd	nd	nd	
ThO2	4.45	2.98	19.13	45.93	15.85	5.90	4.28	66.75
UO2	nd	nd	nd	nd	nd	nd	nd	2.83
PbO	nd	nd	nd	nd	nd	nd	nd	1.44
CaO	1.30	1.07		.27	.56	42.95	1.25	2.40
P2O5	30.39	30.17	24.50	13.50	23.77	37.02	28.23	2.29
SiO2	1.02	.99	3.90	9.48	3.92	1.67	1.09	15.41
Total	99.90	99.36	99.71	97.06	97.55	96.36	96.00	95.72

Apatites

Sample	10	163	163	268	35
CaO	55.26	54.46	54.59	53.96	55.10
P2O5	44.16	44.93	44.15	44.29	43.70
SiO2	.60	.56	.68	.54	.46
Na2O		nd		.42	
Total	100.02	99.95	99.42	99.21	99.26

nd = Not Determined